A PHYSIOLOGIC MODEL OF GLUCOSE METABOLISM IN MAN AND ITS USE TO DESIGN AND ASSESS IMPROVED INSULIN THERAPIES FOR DIABETES

VOL. 1

by

JOHN THOMAS SORENSEN

B.S., University of California, Berkeley

(1978)

SUBMITTED TO THE DEPARTMENT OF
CHEMICAL ENGINEERING IN PARTIAL
FULFILLMENT OF THE
REQUIREMENTS FOR THE
DEGREE OF

DOCTOR OF SCIENCE

at the

MASSACHUSETTS INSTITUTE OF TECHNOLOGY

April 1985

Signature of Author .....
Department of Chemical Engineering
April 18, 1985

Certified by .....
Clark K. Colton
Thesis Supervisor

Accepted by .....
William M. Deen
Chairman, Department Graduate Committee

A PHYSIOLOGIC MODEL OF GLUCOSE METABOLISM IN MAN AND ITS USE TO DESIGN AND ASSESS IMPROVED INSULIN THERAPIES FOR DIABETES

by

JOHN THOMAS SORENSEN

Submitted to the Department of Chemical Engineering
on April 18, 1985 in partial fulfillment of the
requirements for the Degree of Doctor of Science

ABSTRACT

A physiologic model using anatomical organ and tissue compartments was developed for simulating glucose metabolism and its regulation by insulin and glucagon in normal (nondiabetic) man. Mass balance equations were written to account for blood flow, exchange between compartments, and metabolic processes causing addition or removal of glucose, insulin, and glucagon, yielding simultaneous differential equations which were solved numerically. Physiologic parameters were selected to represent a 70 kg adult male. Metabolic processes were quantified from clinical data in the literature. Model predictions of plasma concentrations, hepatic glucose output, and muscle glucose uptake agreed well (±10%) with clinical data for a wide variety of glucose and insulin inputs using a single set of model parameters. The model's unique design gave better physiologic correspondence and accuracy than prior models.

The model pancreas was removed from the normal model to create a "controlled" Type I (insulin-dependent) diabetic model; because this model represented the idealized end state apparently achievable with improved therapies, it was employed for subsequent insulin therapy design and assessment. An "uncontrolled" Type I diabetic model incorporating the reversible diabetes-related abnormalities secondary to pancreatic dysfunction (insulin resistance, insulin antibody binding, and impaired glucose counterregulation) was demonstrated to yield good predictions of response data for typical Type I diabetics.

Internal Model Control (IMC) was employed to design an optimal glucose-controlled (closed-loop) insulin delivery system using the controlled Type I diabetic model to predict in vivo response. Optimal IMC analysis yielded a mathematically simple control system that provided for blood glucose regulation comparable to that resulting from normal pancreatic response in the nondiabetic. Analysis was extended to explore the quality of IMC blood glucose control achievable in the presence of the following glucose sensor measurement nonidealities: sensor dead time, sensor response time, variation in the sampling interval used for digital control, and introduction of systematic measurement error. Measurement noise and its filtering were also investigated. Results demonstrated that IMC control loop compensation methods provided a powerful approach to realizing effective blood glucose control in the presence of glucose sensor measurement nonidealities.

Thesis Supervisor: Dr. Clark K. Colton

Title: Professor of Chemical Engineering

ACKNOWLEDGEMENTS

First and foremost, I would like especially to thank my family for their understanding, encouragement, and support through the years of my academic pursuits. This thesis is dedicated to my family with love.

The author wishes to thank his thesis advisor Clark K. Colton and the members of his thesis committee: J. Stuart Soeldner, George Stephanopoulos, Thomas Aoki, William Deen, and Lawrence Evans. Also, I would like to acknowledge my appreciation for Bob Reid's humanistic approach to academics and to thank him for his support and understanding.

In addition, thanks are due to American Hospital Supply Corporation for their enthusiasm toward and financial support of this work. I look forward to our continued collaboration in the future and hope that our efforts will indeed impact on improving the outlook for diabetics.

Finally, I wish to thank the many people whose friendship and encouragement helped me to endure through the long hours of work and the less than ideal times. Thanks to Gail for the late nights on the word processor and for maintaining a sense of humor through it all. Thanks also to Jean, Lynne, and Barbara for making MIT a brighter place to be. Special thanks to my close friends and colleagues for their support, both technical and personal: Karen, Hsueh-Rong, Mohan, and especially Naomi. I hope that neither time nor distance will weaken our friendship, and my sincerest wishes for their continued success and good fortune in the future.

TABLE OF CONTENTS

I. INTRODUCTION

Considering all causes of death by disease, diabetes mellitus is responsible for the third largest toll of life, after cardiovascular disease and cancer (Ganda, 1983). In the United States, diabetes mellitus affects 5% of the population, and the number of diabetics is increasing at a rate of about 6% per year, or double the population growth rate (Crofford, 1975). In general, diabetes mellitus is caused by an insufficiency of insulin relative to the requirements of the tissues for this hormone, the major manifestation of which is an excessive level of glucose in the circulation. Since the discovery of insulin in 1921, the overt symptoms of diabetes have been controllable and the risk of death by diabetic coma substantially reduced. The traditional therapies, such as insulin injection and dietary management, however, have proven inadequate in preventing the chronic complications, including kidney disease, blindness, and various cardiovascular and nervous system disorders, that are responsible for the severe morbidity and mortality associated with diabetes today (Matas et al., 1976). The life expectancy of the diabetic is currently about one-third less than that of the general population (Crofford, 1975), and the total health costs due to diabetic morbidity alone have been estimated at over $15 billion a year in the United States (National Diabetes Advisory Board, 1981).

In normal (nondiabetic) man, glucose metabolism is controlled by precise minute-to-minute pancreatic insulin response to changes in circulating glucose levels, resulting in the regulation of blood glucose concentration within a narrow range of about 80-120 mg/dl during the daily transitions between the fed and fasted metabolic states (Service et al., 1970). In

contrast, such precise control is not realized in the diabetic since conventional therapy, typically consisting of a single daily injection of intermediate-acting insulin, only provides a gross compensation for diabetic insulin deficiency by simply maintaining relatively constant in vivo insulin levels over the course of a 24 h day (Soeldner et al., 1973); as a result, blood glucose concentration varies over a characteristic range of about 100-300 mg/dl in the diabetic on conventional injection therapy (Service et al., 1970). Increasing clinical evidence suggests that the inability to maintain blood glucose within normal physiologic ranges by conventional means of treatment may contribute to the development of the chronic complications associated with diabetes (National Diabetes Data Group, 1979). Thus, a great deal of effort is being directed toward development of new diabetic therapies that could provide for better glycemic control through more physiologic patterning of insulin delivery (Soeldner, 1981).

Because of the analogy to the physiologic control offered by the normal pancreas, treatment of diabetes by glucose-controlled insulin delivery will probably represent the ultimate approach to effective therapy. Potentially implantable devices for glucose-controlled insulin delivery are currently under development (Soeldner, 1981), but inherent in potential designs will be various factors, such as lag times and measurement nonidealities, that will tend to degrade performance. Considering the precise minute-to-minute regulation of blood glucose resulting from normal pancreatic insulin response, serious questions arise concerning tolerable performance limits for improved therapy systems. Although the efficacies of new therapies will ultimately be established by clinical studies, animal and human experimentation is extremely expensive and must be limited in

scope for ethical reasons. An alternative and complementary approach involves use of physiologic models of glucose metabolism (Figure 1) to predict the theoretical responses of a diabetic to a wide variation of insulin input specifications; a physiologic model of glucose metabolism can thus be used as a powerful tool for designing and assessing the effectiveness of potential therapy systems.

The potential usefulness of glucose metabolism models has fostered the appearance of numerous formulations in the literature. Upon review, however, all of the literature models of glucose metabolism were found subject to one or more of the following drawbacks: 1) selection of model design resulting in poor correspondence between important physiology and its mathematical modeling, 2) lack of direct quantification of metabolic processes within respective models, 3) insufficient testing of model performance to establish general predictive capacity over a wide range of inputs, and 4) errors in mathematical documentation resulting in nonfunctional equation systems.

Because of problems associated with the existing literature models, the first thesis objective was to develop a new model for the distribution and metabolism of glucose and its regulation by insulin and glucagon in normal man. Using the model of glucose metabolism in normal man as a foundation, the second thesis objective was to develop a model of glucose metabolism in the insulin-dependent diabetic suitable for insulin therapy assessment. Finally, employing the model of glucose metabolism in the insulin-dependent diabetic, the third thesis objective was to design an optimal scheme for glucose-controlled insulin delivery and to assess how the presence of glucose sensor measurement limitations affect the quality of achievable blood glucose control.

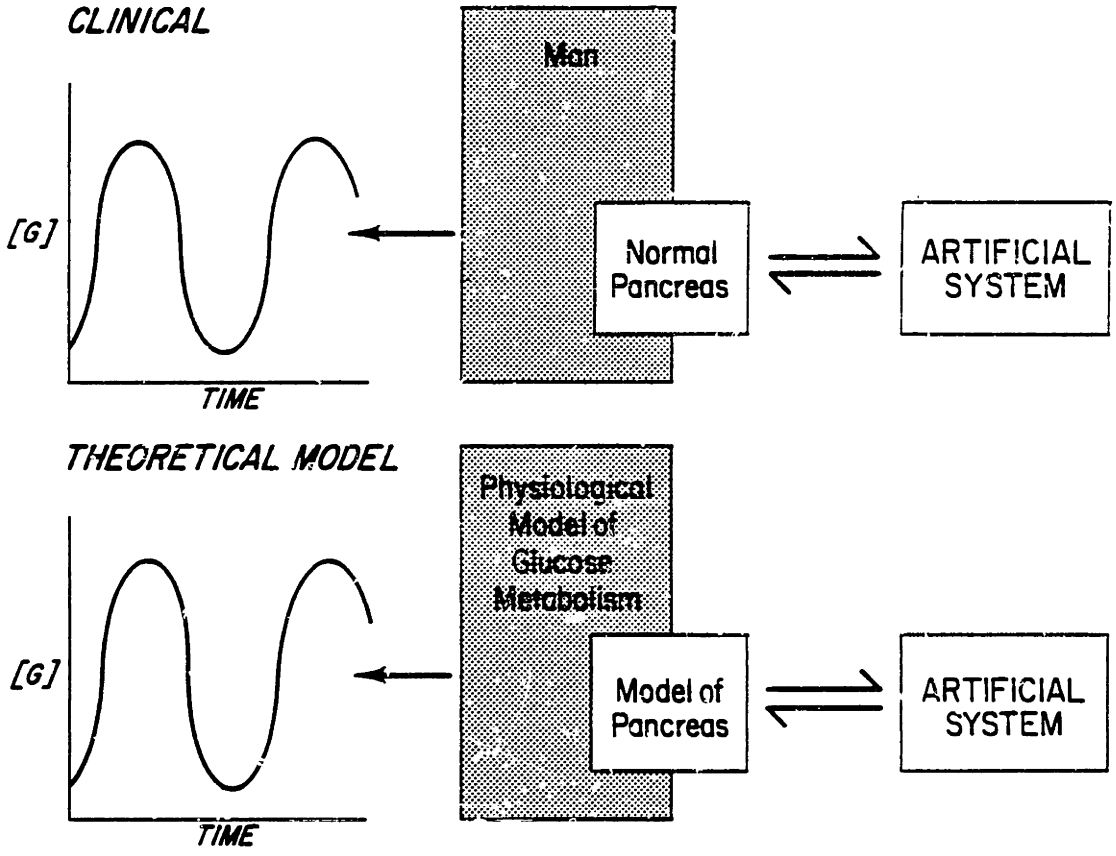

Fig. 1 Comparison of clinical experimentations and theoretical modeling approaches for determining the efficacy of artificial systems for blood glucose control.

II. MODELING OF GLUCOSE METABOLISM IN NORMAL MAN

A) General Overview

Model formulations vary in form and detail as primarily determined by their intended purpose. The recent trend in modeling glucose metabolism has been toward development of explanatory physiological system models. An explanatory model (Finkelstein and Carson, 1979) provides a description of the ways in which different features of system structure and behavior depend upon each other. Models of this type are extremely useful, as they can promote insight and understanding, be used for hypothesis testing, and may possibly define quantitative interactions which are normally inaccessible to measurement. An explanatory model, if valid, must describe not only those specific features of structure and detail which entered into its formulation, but also correctly predict all relevant system behavior over a general spectrum of inputs.

The present modeling effort has been directed toward development of an explanatory physiologic model of glucose metabolism in the human body. In general, development of explanatory mathematical representations requires independent knowledge of the component unit metabolic processes involved. This is because complex physiologic systems generally encompass a number of nonlinear processes, and conventional identification and parameter estimation techniques neither guarantee structural nor parametric uniqueness (Carson and Finkelstein, 1973). Thus, models which are valid explanatory representations, and which must therefore mirror structurally and parametrically the component regulatory processes, generally require independent validation of the functional aspects of these component processes.

With respect to modeling glucose metabolism, experimental techniques

which provide a means of independently varying and maintaining glucose and insulin levels in vivo (known as clamping) have recently been developed. Such procedures have been coupled with measuring arterial-venous glucose and insulin concentration differences across organ and tissue regions of the body; results of such studies have given a direct measure of tissue and organ responses to local changes in glucose and insulin concentrations over a wide spectrum of conditions. Within the last few years, a wealth of experimental data of this type has appeared in the literature, thus providing a unique opportunity to formulate and validate component metabolic processes of the model on the whole organ and tissue level. It was decided to structure the present model using a tissue and organ compartmentalization approach such that one-to-one correspondence was maintained between quantifiable features of the glucose metabolic processes and their mathematical representations in the model.

The model has been formulated by techniques similar to those originally developed for simulating drug distribution (Teorell, 1937; Bischoff and Brown, 1966; Dedrick, 1973; Himmelstein and Lutz, 1979). For this physiologic modeling approach, the body is divided into a number of physiologic compartments that represent the capillary beds of various organs and tissues. A general representation for such a compartment (Figure 2) includes three well-mixed spaces throughout which the solute concentration is assumed to be uniform. The capillary blood space is fed by arterial blood inflow and drained by venous blood outflow. The interstitial fluid space may exchange mass with the capillary blood space by diffusion of solute through the capillary wall. The intracellular space may exchange mass with the interstitial fluid space through transport of solute across the cell membrane. For the purpose of modeling glucose metabolism, however, at most

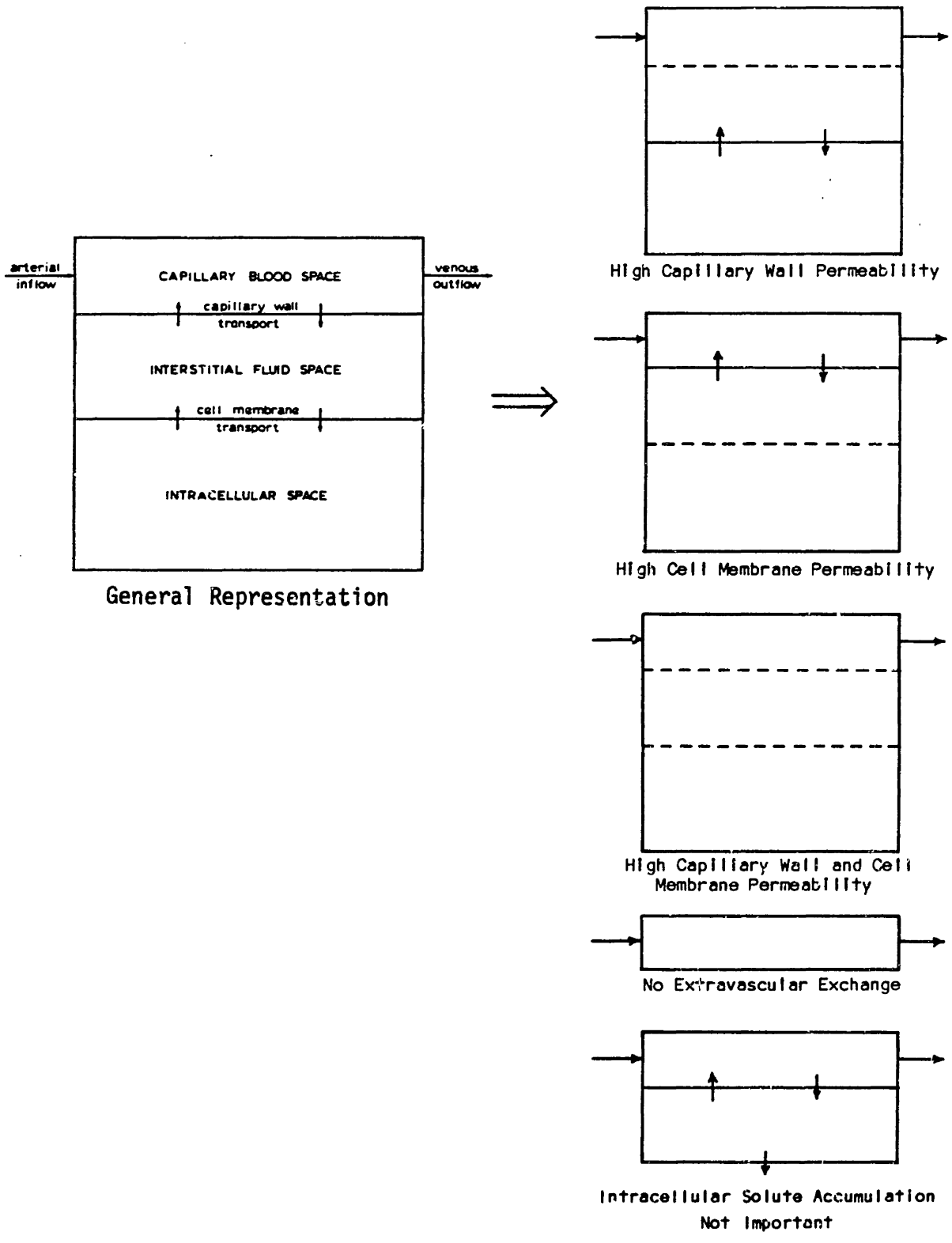

Fig. 2 General representation of a physiologic organ or tissue compartment and various factors leading to simplified representations.

only two spaces are required to represent any given physiologic compartment. In some cases (see Figure 2), the capillary wall permeability is sufficiently high that rapid equilibration occurs between the capillary blood and interstitial fluid spaces, in which case these two spaces may be combined into a single space of uniform concentration. Likewise, solute transport across the cell menbrane is sufficiently rapid in some cases that the interstitial and intracellular spaces may be combined into a single space of uniform concentration. Another possibility is that both the capillary wall and cell membrane permeabilities are high such that all fluid spaces may be combined into a single space of uniform concentration. For regions in which no extravascular solute exchange occurs, the extravascular fluid spaces may be excluded from the formulation. Finally, when the rate of solute transport across the cell membrane is not limited by a significant buildup of solute within the intracellular fluid, the intracellular fluid space may be omitted.

Mass balances are written for each physiologic compartment. As an example, illustrated in Figure 3 is a typical physiologic compartment with capillary wall resistance and negligible intracellular solute accumulation limitations. The mass balances for this compartment may be written

Capillary Blood

$$V_B \frac{dC_{Bo}}{dt} = Q_B (C_{Bi} - C_{Bo}) + PA (C_I - C_{Bo}) - r_{RBC} \qquad (1)$$

accumulation — convection — diffusion — metabolic sink

Interstitial Fluid

$$V_I \frac{dC_I}{dt} = PA (C_{Bo} - C_I) - r_T \qquad (2)$$

accumulation — convection — metabolic sink

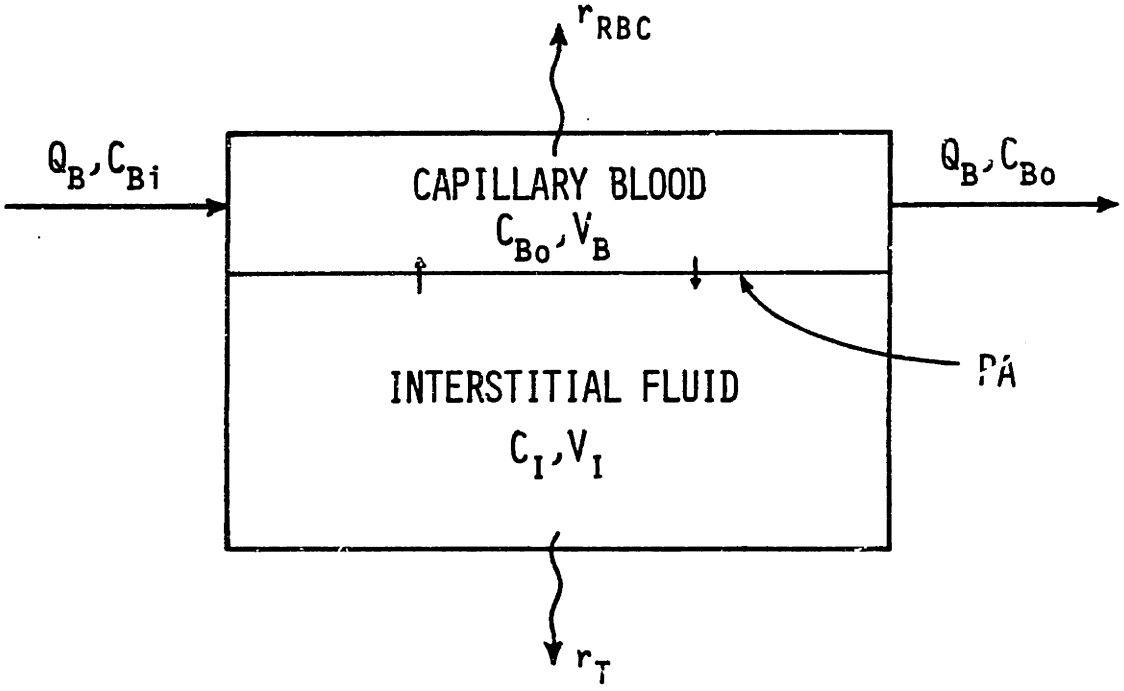

Fig. 3 Schematic representation of a typical physiologic compartment with capillary wall resistance and no intracellular solute limitations.

where: V_B = capillary blood volume
V_I = interstitial fluid volume
Q_B = volumetric blood flow rate
PA = permeability-area product
C_{Bi} = arterial blood solute concentration
C_{Bo} = capillary blood (and venous) solute concentration
C_I = interstitial fluid solute concentration
r_{RBC} = rate of red blood cell uptake of solute
r_T = rate of tissue cellular removal of solute through the cell membrane

Since the capillary blood space is represented by a well-mixed volume, the rate of mass accumulation in the capillary blood is equal to the capillary blood volume multiplied by the time rate of change of the solute concentration in the capillary blood. This rate of mass accumulation is the net additive resultant of contributions by convection, diffusion, and any metabolic sources or sinks which add or remove mass from the capillary blood space. An example of a metabolic sink for capillary blood solute is the rate of red blood cell uptake. A similar mass balance is written for the interstitial fluid space, except in this case there is no convective contribution. Thus, the rate of mass accumulation is the result of contributions from diffusion and any metabolic sources and sinks which add or remove mass from the interstitial fluid, an example being the rate of tissue cellular removal of solute across the cell membrane.

The permeability-area product which characterizes diffusive resistance of the capillary walls is often expressed in terms of an alternate parameter, the transcapillary diffusion time T, as

$$PA = \frac{V_I}{T} \tag{3}$$

The transcapillary diffusion time may be interpreted as the characteristic

time for diffusion between two well-mixed regions of uniform concentration. This may be illustrated as follows (Figure 4); for diffusion

$$\frac{dC_I}{dt} = \frac{1}{T}(C_{Bo} - C_I) \tag{4}$$

Imposing a step change in capillary blood solute concentration at time equals zero

$$C_{Bo} = \begin{cases} C(0) & t<0 \\ C(\infty) & t>0 \end{cases} \tag{5}$$

the resulting interstial fluid solute concentration as a function of time may be written

$$C_I(t) = [C(\infty) - C(0)][1 - \exp(-\frac{t}{T})] + C(0) \tag{6}$$

Thus, when time is equal to the transcapillary diffusion time

$$C_I(T) = [C(\infty) - C(0)](0.63) + C(0) \tag{7}$$

Therefore, the transcapillary diffusion time represents the time required for interstitial solute concentration to reflect 63% of a capillary blood solute step change. In addition,

$$C_I(0.69T) = [C(\infty) - C(0)](0.50) + C(0) \tag{8}$$

Thus, the transcapillary diffusion time multiplied by 0.69 is the time required for interstitial fluid solute concentration to reflect 50% of a capillary blood solute concentration step change.

Physical parameters such as blood flow rates and distribution volumes were selected to represent a normal 70 kg adult male. Hormonal regulation by insulin and glucagon were included in the model formulation. The baseline initial conditions were defined as basal postabsorptive metabolism. The model is a physiologically structured explanatory representation of the

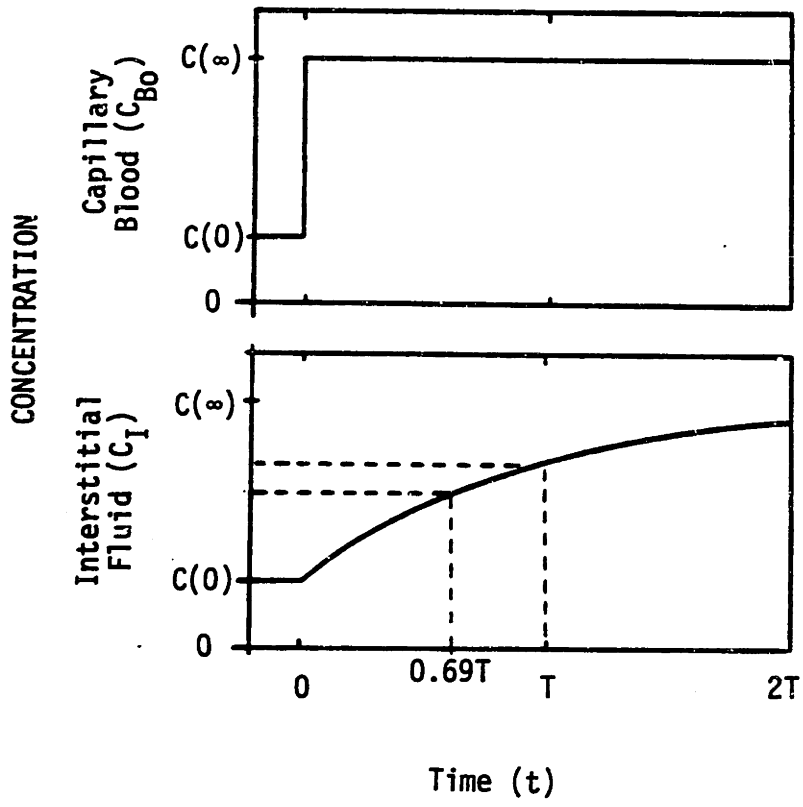

Fig. 4 Interstitial fluid solute concentration in response to a step change in capillary blood solute concentration.

glucose regulatory system and is used for generating predictions of response to a wide spectrum of glucose and insulin inputs. Because of the basis of parameter selection, model simulations predict mean response of a 70 kg male population.

With respect to limitations of the model, a few comments are in order. First, hormonal effects of epinephrine (adrenalin), cortisol, and growth hormone have been neglected. In a recent review, Gerich et al. (1981) have shown that the normal daily variations of these agents are unlikely to cause quantitative effects on glucose regulation; these potent insulin antagonistic hormones, however, can induce hyperglycemia (stimulation of liver glucose output and inducement of peripheral insulin resistance) at levels associated with various diseased states, stress, and trauma. Second, physiology related to changes in amino acid and free fatty acid substrate levels has not been considered. Following ingestion of a mixed meal, postprandial variations in the circulating levels of these substrates could interact with the glucose regulatory system by altering pancreatic hormonal secretion and influencing hepatic metabolism. During glucose loading alone, however, effect of these substrate level variations are generally assumed to be second order with respect to glucose regulation. Third, initial conditions for the model reflect normal basal postabsorptive metabolism, and changes in fuel utilization associated with prolonged fasting and starvation (Cahill and Soeldner, 1969), such as hepatic glycogen depletion and displacement of brain glucose utilization, have not been incorporated into the model formulation. Finally, the physiologic modeling approach employed here uses fixed parameters representative of a 70 kg man to predict average responses to a wide variety of inputs. This may be distinguished from the modeling efforts of Bergman et al. (1982) in which

individual responses to an intravenous glucose tolerance test are used to fit model parameters, thus providing diagnostic information about the insulin (Bergman et al., 1979) and beta cell (Toffolo et al., 1980) sensitivities of the individual.

A general overview of the model will now be presented. Detailed discussion of parameter selection and unit metabolic process formulation will be deferred until later in the text.

A schematic representation of the glucose model is shown in Figure 5. The body has been divided into six physiologic compartments: 1) brain, which represents the central nervous system; 2) heart and lungs, which represents the rapidly mixing vascular volumes of the heart, lungs, and arteries; 3) periphery, which includes skeletal muscle and adipose tissue; 4) gut; 5) liver; and 6) kidney. Arrows connecting the physiologic compartments represent the direction of blood flow. This physiologic compartmentalization is similar to that employed by Tiran et al. (1975) and gives the minimal set of physiologic compartments required to isolate the unit metabolic processes on the organ and tissue level. The heart and lungs compartment serves to close the circulatory loop, representing simply the blood volume of the cardiopulmonary system and the major arteries; the small contribution of arteriovenous blood flow through capillaries of these tissues has been lumped into the periphery. For reasons which will be discussed later, blood contained in the major veins has been distributed on the basis of relative regional blood flow rates among the remaining organ and tissue blood volume spaces.

The physiologic processes that lead to metabolic sources and sinks in the glucose model are summarized in Table 1. In general, these physiologic processes occur at a constant rate or at a rate which is mediated in a

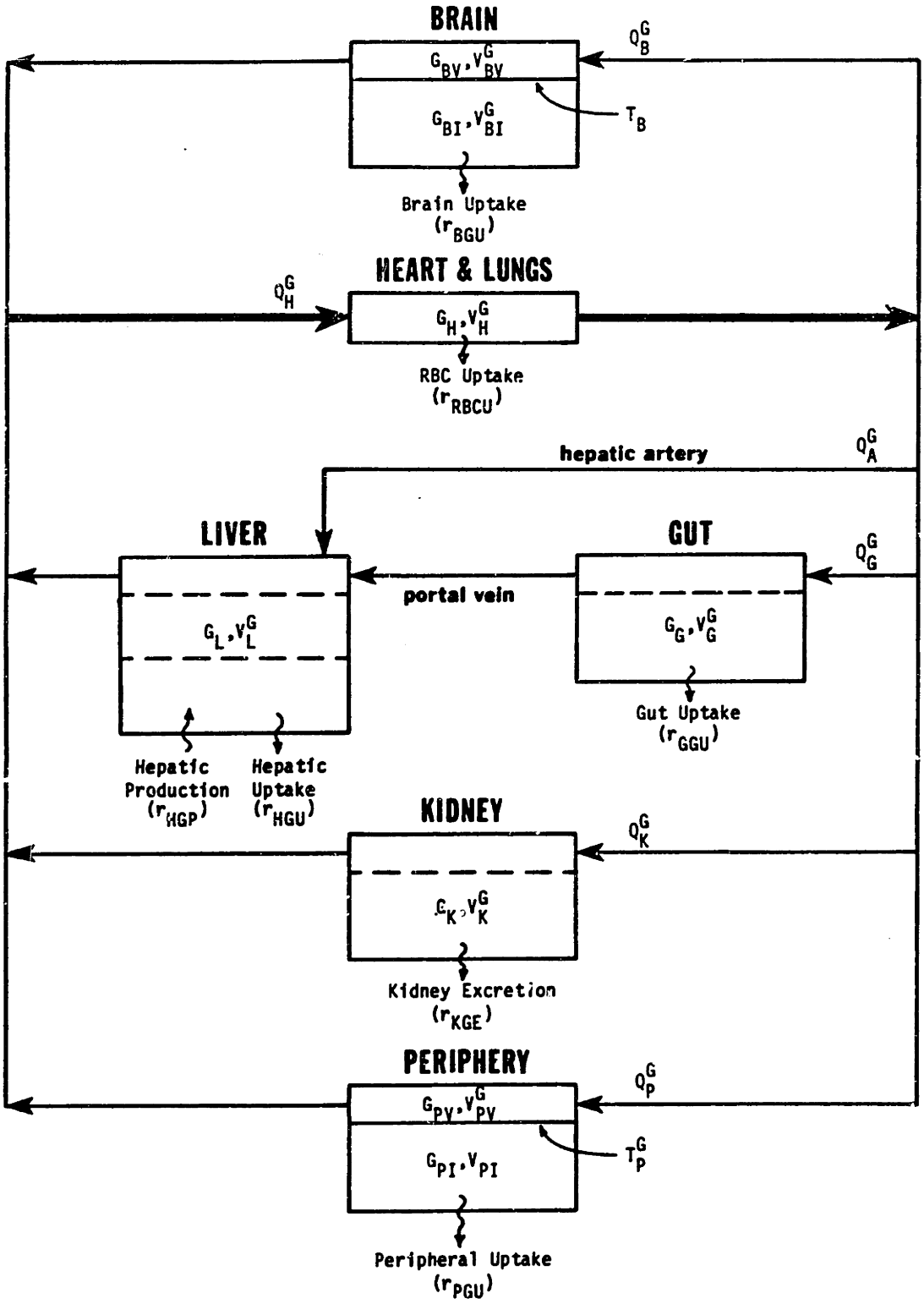

Fig. 5 Schematic representation of the glucose model.

TABLE 1. Summary of physiologic processes leading to metabolic sources and sinks in the glucose model.

Physiologic Process	Rate is Function of	Process is
Sinks		
Red Blood Cell Uptake	Constant	-
Brain Uptake	Constant	-
Gut Uptake	Constant	-
Peripheral Uptake	Peripheral Interstitial Glucose Peripheral Interstitial Insulin	Linear Nonlinear
Urinary Excretion	Kidney Plasma Glucose	Nonlinear
Hepatic Uptake	Liver Glucose Liver Insulin (first-order response time)	Nonlinear Nonlinear
Sources		
Hepatic Production	Liver Glucose Liver Insulin (first-order response time) Plasma Glucagon (first-order response time)	Nonlinear Nonlinear Nonlinear

nonlinear manner by relevant local changes in glucose, insulin, and glucagon concentrations. As indicated, hormonal effects of insulin and glucagon on hepatic glucose metabolism were formulated to include the time dependence associated with their mediatory action.

The mass balance equations for the glucose model are given in Table 2. The mathematical nomenclature is defined in Table 2 and corresponds to the symbols used in the glucose model schematic of Figure 5. In general, subscripts distinguish physiologic compartments and, if required, a second subscript is included to indicate fluid spaces within compartments. Superscripts indicate respective models (glucose, insulin, or glucagon) and are used to distinguish those variables for which different numerical values are employed for the different models. Mass balances for the glucose model result in a set of 8 simultaneous ordinary differential equations which are nonlinear as a result of the metabolic source and sink rates. In addition, it is through those metabolic rates which depend on insulin and glucagon concentrations that the glucose model is coupled to the insulin and glucagon models, respectively. The mass unit of milligrams was employed for glucose modeling since glucose concentrations are generally expressed in these terms. Mathematical equations for the metabolic rates of glucose addition and removal are summarized in Section II.S. These rate formulations, as well as selection of physiologic parameter values, will be discussed in detail in the body of the text.

A schematic diagram of the insulin model is presented in Figure 6. The body was divided into the same physiologic compartments described for the glucose model. Differences arise, however, with respect to extravascular fluid space access in the brain and liver compartments. Studies have shown (Davson and Spaziani, 1959; Mahon et al., 1962) that the blood-brain

TABLE 2. Glucose model mass balance equations.

$$\text{BRAIN:}\quad V_{BV}^{G}\frac{dG_{BV}}{dt} = Q_{B}^{G}(G_{H} - G_{BV}) - \frac{V_{BI}}{T_{B}}(G_{BV} - G_{BI}) \tag{9}$$

$$V_{BI}\frac{dG_{BI}}{dt} = \frac{V_{BI}}{T_{B}}(G_{BV} - G_{BI}) - r_{BGU} \tag{10}$$

$$\text{HEART AND LUNGS:}\quad V_{H}^{G}\frac{dG_{H}}{dt} = Q_{B}^{G}G_{BV} + Q_{L}^{G}G_{L} + Q_{K}^{G}G_{K} + Q_{P}^{G}G_{PV} - Q_{H}^{G}G_{H} - r_{RBCU} \tag{11}$$

$$\text{GUT:}\quad V_{G}^{G}\frac{dG_{G}}{dt} = Q_{G}^{G}(G_{H} - G_{G}) - r_{GGU} \tag{12}$$

$$\text{LIVER:}\quad V_{L}^{G}\frac{dG_{L}}{dt} = Q_{A}^{G}G_{H} + Q_{G}^{G}G_{G} - Q_{L}^{G}G_{L} + r_{HGP} - r_{HGU} \tag{13}$$

$$\text{KIDNEY:}\quad V_{K}^{G}\frac{dG_{K}}{dt} = Q_{K}^{G}(G_{H} - G_{K}) - r_{KGE} \tag{14}$$

$$\text{PERIPHERY:}\quad V_{PV}^{G}\frac{dG_{PV}}{dt} = Q_{P}^{G}(G_{H} - G_{PV}) - \frac{V_{PI}}{T_{P}^{G}}(G_{PV} - G_{PI}) \tag{15}$$

$$V_{PI}\frac{dG_{PI}}{dt} = \frac{V_{PI}}{T_{P}^{G}}(G_{PV} - G_{PI}) - r_{PGU} \tag{16}$$

Variables:

G = glucose concentration (mg/dl)
Q = vascular blood water flow rate (dl/min)
r = metabolic source or sink rate (mg/min)
T = transcapillary diffusion time (min)
V = volume (dl)
t = time (min)

First Subscript: Physiologic Comparment

B = brain
G = gut
H = heart and lungs
L = liver
P = periphery
(A = hepatic artery)

Second Subscript: Physiologic Subcompartment (if required)

I = interstitial fluid space
V = vascular blood water space

Metabolic Rate Subscripts:

BGU = brain glucose uptake
GGU = gut glucose utilization
HGP = hepatic glucose production
HGU = hepatic glucose uptake
KGE = kidney glucose excretion
PGU = peripheral glucose uptake
RBCU= red blood cell glucose uptake

Superscript:

G = glucose model

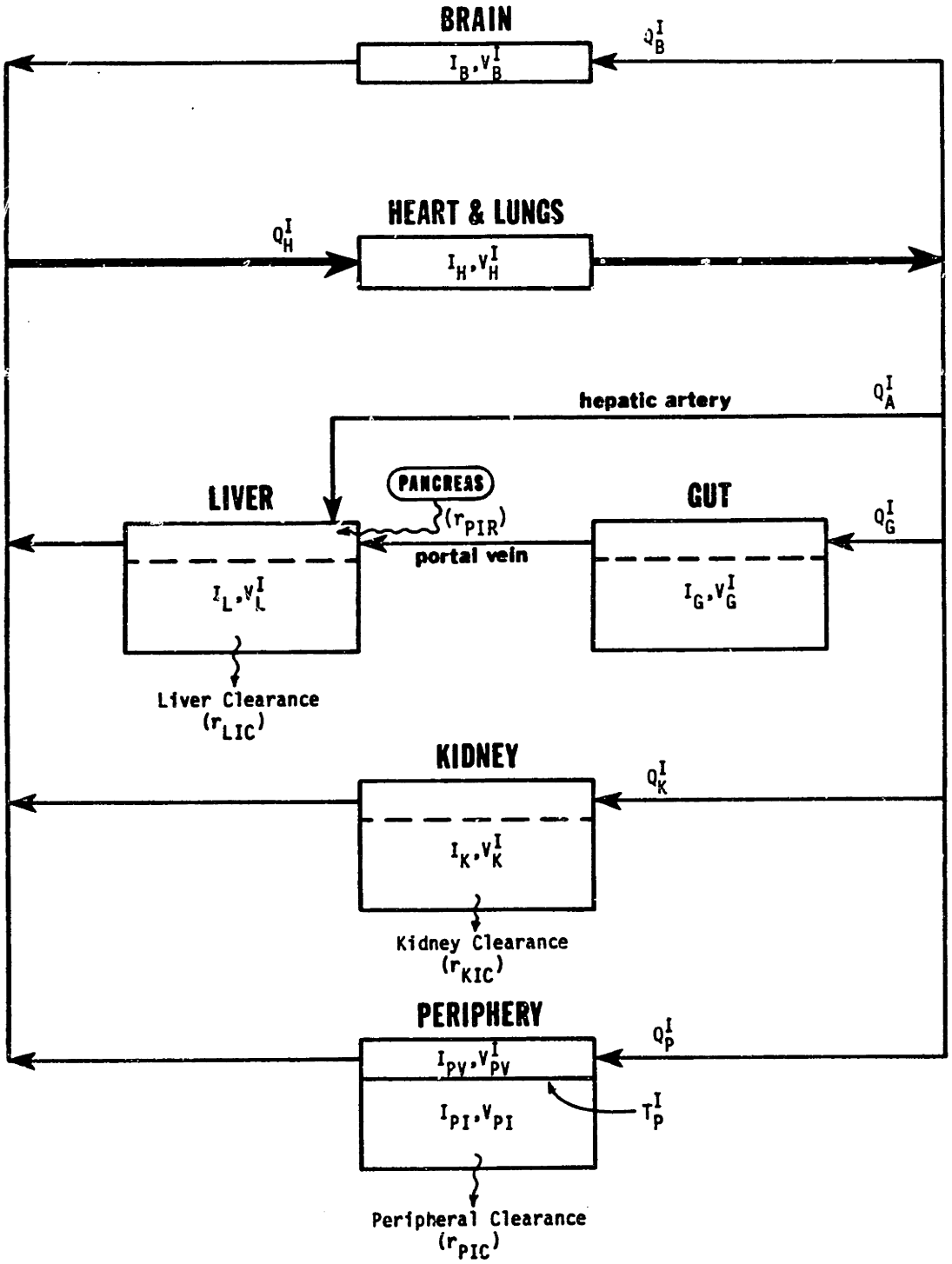

Fig. 6 Schematic representation of the insulin model.

barrier capillary structure is impermeable to insulin passage into cerebrospinal fluid; thus, the brain interstitial fluid space (cerebrospinal fluid) has been omitted from the insulin formulation. Also, unlike the case for glucose, the liver cell membrane is not freely permeable to insulin and the intracellular fluid volume has thus been omitted as insulin is degraded via binding to cell membrane receptors.

Physiologic processes leading to metabolic sources and sinks for insulin are summarized in Table 3. Since pancreatic insulin is released into the portal vein which perfuses the liver, and since separate compartments have not been included in the model for vessel blood volumes, pancreatic insulin release appears as a source term in the liver insulin compartment. A separate compartmental model for pancreatic insulin release is used to predict insulin release rates; the pancreas model, which is an adaptation of that developed by Landahl and Grodsky (1982), relates insulin release rate to arterial (heart and lung compartment) glucose concentration via a system of three simultaneous nonlinear ordinary differential equations.

Mass balance equations and mathematical nomenclature for the insulin model are given in Table 4. Mass balances for the insulin formulation result in a set of 7 simultaneous ordinary differential equations which are linear except for the liver (Equation 20) where the rate of pancreatic insulin release as an insulin source term is computed from an additional set of three nonlinear ordinary differential equations which constitute the model pancreas formulation (a nonlinear coupling to the glucose model). For insulin modeling, the mass unit of milliunits of insulin was selected as this choice is convenient for expressing insulin concentrations. Mathematical equations for calculating metabolic rates of insulin addition and removal are summarized in Section II.S. Details of the model of

TABLE 3. Summary of physiologic processes leading to metabolic sources and sinks in the insulin model.

Physiologic Process	Rate is Function of	Process is
Sinks		
Liver Clearance	Liver Insulin	Linear
Kidney Clearance	Kidney Insulin	Linear
Peripheral Clearance	Peripheral Interstitial Insulin	Linear
Sources		
Pancreatic Insulin Release	Heart and Lung Glucose (time dependent)	Nonlinear

TABLE 4. Insulin model mass balance equations.

$$\text{BRAIN:} \quad V_B^I \frac{dI_B}{dt} = Q_B^I(I_H - I_B) \tag{17}$$

$$\text{HEART AND LUNGS:} \quad V_H^I \frac{dI_H}{dt} = Q_B^I I_B + Q_L^I I_L + Q_K^I I_K + Q_P^I I_{PV} - Q_H^I I_H \tag{18}$$

$$\text{GUT:} \quad V_G^I \frac{dI_G}{dt} = Q_G^I(I_H - I_G) \tag{19}$$

$$\text{LIVER:} \quad V_L^I \frac{dI_L}{dt} = Q_A^I I_H + Q_G^I I_G - Q_L^I I_L + r_{PIR} - r_{LIC} \tag{20}$$

$$\text{KIDNEY:} \quad V_K^I \frac{dI_K}{dt} = Q_K^I (I_H - I_K) - r_{KIC} \tag{21}$$

$$\text{PERIPHERY:} \quad V_{PV}^I \frac{dI_{PV}}{dt} = Q_P^I (I_H - I_{PV}) - \frac{V_{PI}}{T_P^I} (I_{PV} - I_{PI}) \tag{22}$$

$$V_{PI} \frac{dI_{PI}}{dt} = \frac{V_{PI}}{T_P^I} (I_{PV} - I_{PI}) - r_{PIC} \tag{23}$$

Variables:

I = insulin concentration (mU/dl)
Q = vascular plasma flow rate (l/min)
r = metabolic source or sink rate (mU/min)
T = transcapillary diffusion time (min)
V = volume (l)
t = time (min)

First Subscript: Physiologic Compartment

B = brain
G = gut
H = heart and lungs
L = liver
P = periphery
(A = hepatic artery)

Second Subscript: Physiologic Subcompartment (if required)

I = interstitial fluid space
V = vascular plasma space

Metabolic Rate Subscripts:

KIC = kidney insulin clearance
LIC = liver insulin clearance
PIC = peripheral insulin clearance
PIR = pancreatic insulin release

Superscript:

I = insulin model

pancreatic insulin release, selection of physiologic parameter values, and metabolic rate formulations are included later in the text.

The glucagon model is presented in Figure 7. Here, a simple one-compartment formulation was employed, representing the whole-body fluid distribution volume for glucagon. As summarized in Table 5, glucagon is cleared from the body at a rate which is a linear function of its plasma level, and glucagon is released from the pancreas as a nonlinear function of arterial glucose and insulin concentrations. The glucagon model mass balance equation is given by

$$V^{\Gamma} \frac{d\Gamma}{dt} = r_{P\Gamma R} - r_{P\Gamma C} \tag{24}$$

where: Γ = glucagon concentration (pg/ml)
V^{Γ} = glucagon distribution volume (ml)
$r_{P\Gamma R}$ = pancreatic glucagon release rate (pg/min)
$r_{P\Gamma C}$ = plasma glucagon clearance rate (pg/min)
t = time (min)

Details of the metabolic rate formulations are included in the text and summarized in Section II.S.

With respect to modeling of the various metabolic processes, a major consideration in formulating mathematical representations concerns selecting an appropriate level at which to scrutinize these biological processes. At the molecular level, typical enzyme reactions involved in glucose metabolism are very complex. For example, reactions associated with phosphofructokinase, an enzyme in the pathway of glycolysis, would require at least a system of 15 nonlinear differential equations for an accurate representation (Finkelstein and Carson, 1979). Even if sufficient information were available, incorporation of enzymatic reactions into a complete system model of glucose metabolism is obviously not feasible. Acknowledg-

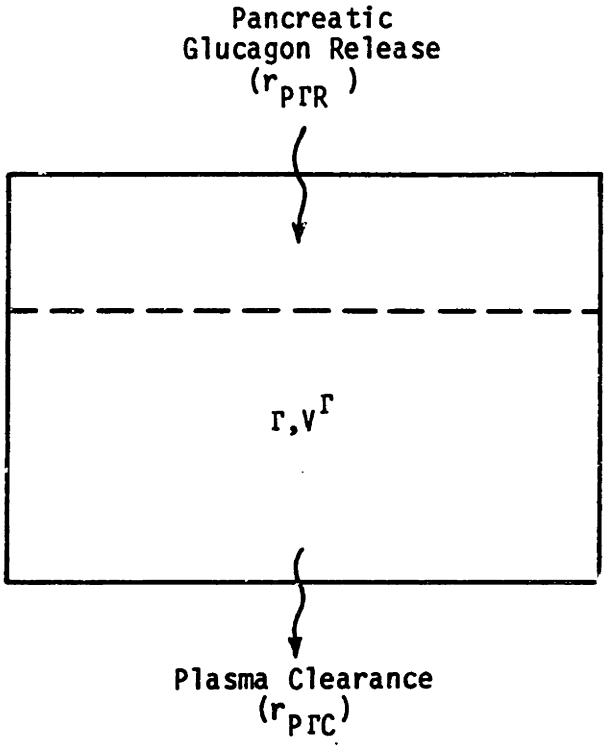

Fig. 7 Schematic diagram of glucagon model.

TABLE 5. Summary of physiologic processes leading to metabolic sources and sinks in the glucagon model.

Physiologic Process	Rate is Function of	Process is
Sinks		
Plasma Clearance	Plasma Glucagon	Linear
Sources		
Pancreatic Glucagon Release	Heart and Lung Glucose Heart and Lung Insulin	Nonlinear Nonlinear

ing the importance of being able to quantify the component metabolic processes which add or remove mass from the system, available data in the literature strongly supported characterizing these metabolic processes on the whole-organ or tissue level. This may be considered a grey box approach. Formulations for organ and tissue responses were quantified directly from experimental data compiled from the literature. Consideration of underlying mechanisms, at least in a qualitative sense, however, was often important for insuring proper interpretation.

The general approach employed for the modeling of physiologic processes was as follows. Metabolic rates causing addition or removal of mass were assigned methematical equations of the general form

$$r = M^{\Gamma}(\Gamma,t)\ M^{I}(I,t)\ M^{G}(G)\ r_{basal} \tag{25}$$

where r = metabolic rate of mass addition or removal (mass/time)
M^{Γ} = multiplicative effect of glucagon (dimensionless)
M^{I} = multiplicative effect of insulin (dimensionless)
M^{G} = multiplicative effect of glucose (dimensionless)
r_{basal} = basal metabolic rate (mass/time)

This method of representing regulatory effects in terms of separable multiplicatives functions is commonly utilized in the modeling of biological processes (Carson et al., 1983). As indicated in Equation 25, the hormonal effects of glucagon and insulin could in general incorporate time dependence. The form of the above equation is particularly suited to correlating experimental data. Normalizing with respect to the basal rate yields

$$r^{N}(\Gamma,I,G,t) = \frac{r}{r_{basal}} = M^{\Gamma}M^{I}M^{G} \tag{26}$$

Since hyperbolic tangent functions have been found to be readily suitable

for representing the sigmoidal nonlinearities commonly observed in biological data correlation, the rate multiplier functions were generally given the mathematical form

$$M^i(i) = A + B \tanh[C(i-D)] \tag{27}$$

where the i^{th} multiplier function was fit to clinical data by adjustment of the four constants A, B, C and D. In cases where sufficient data was available for the metabolic process being modeled, experimental data for normalized rates was compliled from the literature over a wide variation in the relevant local concentrations of glucose, insulin, and glucagon, and least squares techniques were employed to fit the multiplier functions to the data. For some processes, however, excessive scatter in the data required assuming appropriate shapes of curves. Finally, for metabolic processes that were time dependent, the above procedures were applied to fitting initial value or steady state rate data, and the time dependence was incorporated via first order response time dynamics in the rate multiplier functions. Use of these methods to model metabolic rates will be further detailed in the text with respect to quantification of each respective physiologic process.

A problem which was often encountered in attempting to correlate experimental data was that results in the literature were not always reported directly in terms of variable of interest in the model. For example, rates of organ glucose uptake were generally reported as a function of arterial glucose concentration, whereas the local organ glucose concentration is actually reflected by the venous effluent concentration. In such cases, variables of interest were estimated from reported values by simply using steady state mass balance relationships as employed in the model formulation.

B) Distribution and Flow Parameters for a 70 kg Man

Estimated distribution volumes and blood flow rates for an average 70 kg man are summarized in Table 6. Organ massses (total wet masses including contained blood) were compiled from Altman and Dittmer (1974). Values for regional blood flow rates and total cardiac output were representative of those found in the literature (Spector, 1956; Mapleson, 1963; Bischoff and Brown, 1966; Mountcastle, 1974; Tiran et al., 1975; Guyton, 1976), where the peripheral blood flow rate was taken as the difference between total cardiac output and the sum of the blood flow rates to the remaining tissues.

Anatomic volumes were estimated using methods described by Bischoff and Brown (1966). A 70 kg man has a total blood volume of about 5.60 l (Gibson and Evans, 1937) which is roughly distributed as shown in Table 7. The total capillary (plus arteriole and venule) blood volume is about 0.56 l. This was distributed among the tissue regions by assuming that the ratio of capillary blood volumes between the i^{th} and j^{th} organs is given by (Bischoff and Brown, 1966)

$$\frac{V_{Ci}}{V_{Cj}} = \left(\frac{M_i}{M_j}\right)^{\frac{1}{3}} \left(\frac{Q_{Bi}}{Q_{Bj}}\right) \tag{28}$$

where V_C is capillary blood volume and M and Q_B represent organ mass and blood flow rate, respectively. Equation 28 was based on the postulate that capillary flow rates are about the same in every body region and that the average capillary length is related to the total size of the region (Bischoff and Brown, 1966). Capillary blood volumes calculated in this manner are presented in Table 8.

In order to reduce computing costs, capillary blood volumes were not

TABLE 6. Estimated distribution volumes and blood flow rates for an average 70kg man.

Organ or Tissue	Mass[d] (kg)	Blood Flow Rate[e] (l/min)	Blood Equilibration Volume (l)	Interstitial Fluid Volume (l)	Intracellular Fluid Volume (l)
Brain	1.35	0.70	0.41	0.45	8.60
Heart and Lungs	a	(5.20)	1.64	a	a
Liver	1.85	1.50	0.90	0.60	1.15
Gut	1.60	(1.20)	0.71	0.52	1.01
Kidney	0.32	1.20	0.68	0.09	0.18
Periphery	29.84[b]	1.80	1.26	6.74	19.65
(Hepatic Artery)	-	(0.30)	-	-	-
TOTAL	34.96[b]	5.20	5.60	8.40[c]	22.05

[a]Tissue (Extravascular) spaces of the heart and lungs have been lumped into periphery

[b]Based on total fluid volume (see Table 9)

[c]Connective tissue fluid volume of 3.15 l assumed inaccessible and thus excluded from volume (see text)

[d]Total wet mass including contained blood

[e]Entries in parenthesis represent branch flows or branch flow summations and thus do not contribute to the total blood flow rate summation value

TABLE 7. Total blood volume distribution.

	% Blood Volume[a]	Volume (l)
Capillaries, Arterioles, and Venules	10	0.56
Heart, Lungs, and Arteries	30	1.64
Veins	60	3.40
TOTAL	100	5.60[b]

[a]Guyton, 1976; Bischoff and Brown, 1966

[b]Gibson and Evans, 1937

TABLE 8. Regional distribution of blood volume.

Organ or Tissue	% Blood Flow	Venous Equilibration Volume (l)	Capillary Volume (l)	Blood Equilibration Volume (l)
Brain	10.9	0.370	0.040	0.41
Heart and Lungs	-	-	-	1.64
Liver	23.4	0.800	0.100	0.90
Gut	18.8	0.635	0.075	0.71
Kidney	18.8	0.635	0.045	0.68
Periphery	28.1	0.960	0.300	1.26
TOTAL	100.0	3.400	0.560	5.60

directly employed in modeling. Instead, regional blood volumes were represented in terms of blood equilibration volumes (Table 8). At any given time, the majority of blood is contained in the venous vessels (see Table 7). For modeling, it was assumed that a certain fraction of the venous pool is essentially in equilibrium with the capillary blood of the region from which it flows (Mapleson, 1963). Thus, venous equilibration volumes were computed by distributing the total venous volume among the body regions on the basis of their respective fractional blood flows. Regional blood equilibration volumes were then obtained by summing the respective venous equilibration and capillary blood volumes. These calculations are summarized in Table 8. Blood contained in the arterial vessels was lumped with cardiopulmonary blood volume of 1.64 l (see Tables 7 and 8). The alternative to using regional blood equilibration volumes would be to use the actual capillary blood volumes with additional blood volume compartments inserted into the circulatory loop to account for the venous vessel blood volumes. There are two major disadvantages to this alternative: 1) addition of venous blood volume compartments increases the number of mass balance differential equations to be solved, and 2) since the capillary blood volumes are about an order of magnitude smaller than respective blood equilibration volumes, their use in model formulation would increase computing time by roughly a factor of ten.

Interstitial and intracellular fluid volumes were estimated using the approximate whole-body fluid distribution volumes tabulated in Table 9. These values are representative of estimates reported in the literature from results of various in vivo tracer dilution studies. In general, total body fluid volume is measured using a small tracer such as D_2O, extracellular fluid volume is determined by measuring distribution of saccharides

TABLE 9. Approximate body fluid distribution of 70kg man.

	Volume (l)	
Extracellular Fluid	14.91	
Blood Plasma		3.36[b]
Interstitial-Lymph		8.40[a]
Dense Connective Tissue, Cartilage		3.15[a]
Intracellular Fluid	25.09	
Blood Cells		2.24[b]
Extravascular		22.85
TOTAL	40.00[c]	

[a]Edelman and Leibman, 1959
[b]Based on total blood volume of 5.60 l and hematocrit of 0.40
[c]Guyton, 1976

such as inulin which are excluded from cells, and intracellular fluid volume is taken as the difference between these volumes (for review see Edelman and Leibman, 1959). For modeling, it was assumed that the ratio of interstitial fluid to cellular fluid volume is the same for all body regions (Bischoff and Brown, 1966) since more detailed information is not available. Thus, from Table 9,

$$\frac{V_{interstitial}}{V_{intracellular}} = \frac{8.40 + 3.15}{22.85} = 0.51 \tag{29}$$

Using this expression, and noting that for each body region

$$V_{total} = V_{capillary} + V_{interstitial} + V_{intracellular} \tag{30}$$

where total volume is approximated by equating with total organ or tissue mass, the interstitial and intracellular fluid volumes were approximated for each body region, and these values are given in Table 6. It has been reported (Edelman and Leibman, 1959) that a portion of the extravascular extracellular fluid volume, associated with the deep connective tissues and cartilage, is relatively inaccessible to normal solute penetration; whereas insulin equilibrates within about 6 h with an extravascular fluid volume of 8.40 l, an additional fluid volume of about 3.15 l apparently equilibrates much more slowly (see Table 9). For modeling, the peripheral interstitial fluid volume calculated from Equations 29 and 30 was corrected to account for this inaccessible region such that the interstitial fluid volumes of Table 6 sum to 8.40 l. Although intracellular volumes calculated for regions other than the liver were not utilized for glucose homeostasis modeling, these values have been included in Table 6 for completeness.

C) Glucose Distribution in the Blood

In blood, glucose is distributed in plasma water and erythrocyte intracellular water. Plasma protein displacement represents about 7 to 7.5 percent of plasma volume (Harper et al., 1979). Under isotonic conditions, the water content of normal red cells is approximately 71 volume percent (Harris, 1965); the displacement volume in red cells is primarily attributed to the large intracellular hemoglobin content. Based on the above relationships and a normal hematocrit of 0.40, the distribution volume for glucose equals 84.2% of whole blood volume with a ratio of intracellular glucose concentration to plasma glucose concentration of 0.76. This ratio is in good agreement with the average value of 0.73 reported by Clauvel et al. (1965) for blood samples for 46 normal subjects.

It can be further calculated that under equilibrium conditions about 33.7% of the glucose in whole blood is inside erythrocytes; thus, it is important to consider the rate at which glucose equilibrates across the red cell membrane. Measurements in human erythocytes have indicated that red cell permeability to glucose is relatively insensitive to insulin (Wilbrandt, 1961; Zipper and Mawe, 1972). Glucose is transported across the erythrocyte membrane by facilitated rather than simple diffusion (Widdas, 1954; Britton, 1964; Widdas, 1968). Although all aspects of the facilitated diffusion process are not fully understood, it has been experimentally verified that rates of glucose diffusion across red cell membranes can be accurately predicted using the carrier system model of Widdas (1954):

$$\frac{dG_{cw}}{dt} = K\left[\frac{G_{pw}}{G_{pw} + \phi} - \frac{G_{cw}}{G_{cw} + \phi}\right] \qquad (31)$$

where: G_{cw} = Glucose concentration in RBC water (mg/dl RBC water)
G_{pw} = Glucose concentration in plasma water (mg/dl plasma water)
K = Transfer constant (mg/dl RBC water•s)
ϕ = Half-saturation concentration (mg/dl system water)

For human erythrocytes, Sen and Widdas (1962) have reported values of K and ϕ measured at 37°C and pH 7.4 as 1.06 isotonic units/min and 72 mg/dl, respectively. Since these measurements were made in 342 milli-osmolar saline solutions, and assuming a red blood cell water content of 71 volume percent, the value of K converted to the units used herein equals 153.2 mg/dl RBC water•s.

The Widdas model was used to simulate red blood cell water glucose concentration response to step changes in plasma water glucose concentration between 100 and 200 mg/dl (Figure 8). Red blood cell water glucose equilibrated within about 20 s following the 100 mg/dl step increase in plasma water glucose concentration, and equilibrated within about 15 s following the step decrease; the longer response time required for glucose entry into the red blood cell results from intracellular glucose accumulation (Zipper and Mawe, 1972). For the purpose of modeling glucose dynamics and distribution in the human body, the most extreme change in plasma glucose occurs during the infusion period of an intravenous glucose tolerance test when plasma glucose concentration may rise at a rate of 100 mg/dl per minute. Since the 100 mg/dl step change equilibration time is only about 20 s, it is safe to assume that red blood cell water glucose is essentially equilibrated with plasma water glucose even during the rapid dynamics of an intravenous glucose infusion.

For the glucose model, it was assumed that glucose equilibration exists across the red cell membrane, and thus glucose is uniformly distri-

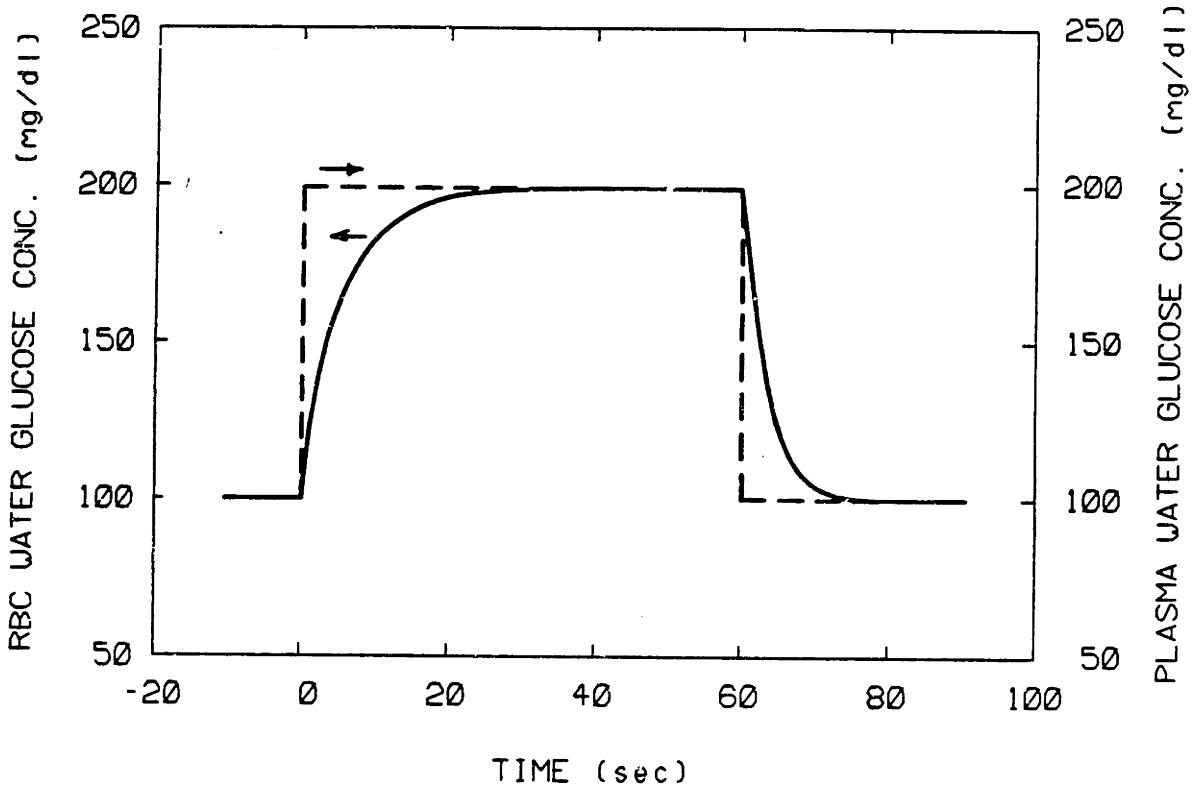

Fig. 8 Prediction of Widdas model (1954) for RBC water glucose concentration response to step changes in plasma water glucose concentration between 100 and 200 mg/dl.

buted throughout the entire water volume in whole blood. Since the water content of whole blood is roughly 84 volume percent, the blood volumes and flow rates as estimated for a 70 kg man (Table 6) were reduced by 16% for glucose modeling. The resulting vascular parameter values as incorporated into the glucose model are included in Table 10. Using whole blood water content as the volume basis for modeling vascular distribution of glucose, the vascular glucose concentrations in the glucose model mass balance equations represent whole blood water glucose concentrations. Thus, in order to compare model predictions with clinical data, the following conversions are required: 1) plasma glucose concentration is 92.5% of whole blood water glucose concentration, and 2) blood glucose concentration is 84% of whole blood water glucose concentration.

Although protein displacement of water in whole blood is significant (about 16%), protein displacement is only about 2% in interstitial fluids (Pitts,1963). This small correction for glucose distribution in the interstitial fluid volumes has been neglected.

D) Kidney Glucose Excretion

In the kidney, the rate of glucose excretion is equal to its rate of glomerular filtration minus its rate of tubular reabsorption (Pitts, 1974; Vander, 1975; Robinson, 1967). Presented in Figure 9 is experimental data for the rates of glucose filtration, reabsorption, and excretion as functions of kidney plasma glucose concentration in humans (Brod, 1973). Glucose is transported against a concentration gradient by the epithelial cell layer of the kidney tubules; thus, glucose is not normally excreted into the urine but is reabsorbed from the glomerular filtrate back into the blood. The maximum tubular reabsorption rate for glucose, however, is

TABLE 10. Vascular volumes and flow rates used in glucose model. (based on whole blood water)

Organ or Tissue	Vascular Flow Rate[a] (l/min)	Vascular Equilibration Volume (l)
Brain	0.59	0.35
Heart and Lungs	(4.37)	1.38
Liver	1.26	0.76
Gut	(1.01)	0.60
Kidney	1.01	0.57
Periphery	1.51	1.04
(Hepatic Artery)	(0.25)	-
TOTAL	4.37	4.70

[a]Entries in parentheses represent redundant flows and are thus excluded in total sum value

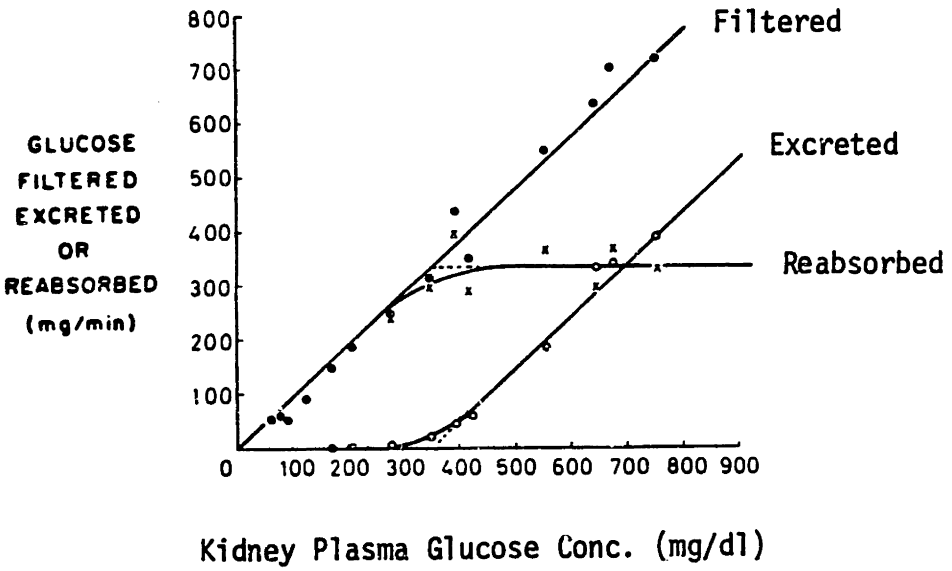

Fig. 9 Experimental data for the mean rates of glucose filtration, reabsorption, and excretion as a function of kidney plasma glucose concentration in 8 normal subjects. (Adapted from Brod, 1973.)

approximately 361 mg/min, and any amount in excesss of this load is excreted rather than reabsorbed. The maximum reabsorption rate is approached somewhat gradually, along a curve (see Figure 9); this behavior probably results from a gradual saturation of the glucose "carrier" associated with the active transport mechanism of glucose reabsorption.

The data in Figure 9 was used to quantify the rate of kidney glucose excretion:

$$r_{KGE}(\text{mg/min}) = \begin{cases} 71 + 71 \tanh[0.011(G_K - 460)] & 0 < G_K < 460 \text{ mg/dl} \\ -330 + 0.872\, G_K & G_K > 460 \text{ mg/dl} \end{cases} \quad (32)$$

where G_K represents whole blood water glucose concentration. The kidney excretion data of Figure 9 has been replotted and compared with the model function fit of Equation 32 in Figure 10.

E) Red Blood Cell Uptake

Red blood cells derive energy from anaerobic glycolysis of intracellular glucose to lactate. As with other glycolytic tissues, glucose utilization is relatively insensitive to changes in glucose and insulin concentration (Bishop and Surgenor, 1964). The rate of glucose consumption by human erythrocytes has been measured by a number of investigators. A summary of their results is presented in Table 11. Also included in the table are extrapolations of total red blood cell uptake for an average 70 kg man based on these results. The rate of human leukocyte glucose consumption has been measured at 7.24 $\mu g/10^6$ cells·h (Guest et al., 1953). Although this rate is much greater per cell than that observed for erythrocytes, the density of leukocytes is only about 1.5×10^5 cells/ml whole blood (Guest et al., 1953); thus, assuming a total blood volume of 5600 ml for an average 70 kg man, white cell glucose uptake only totals about 0.1

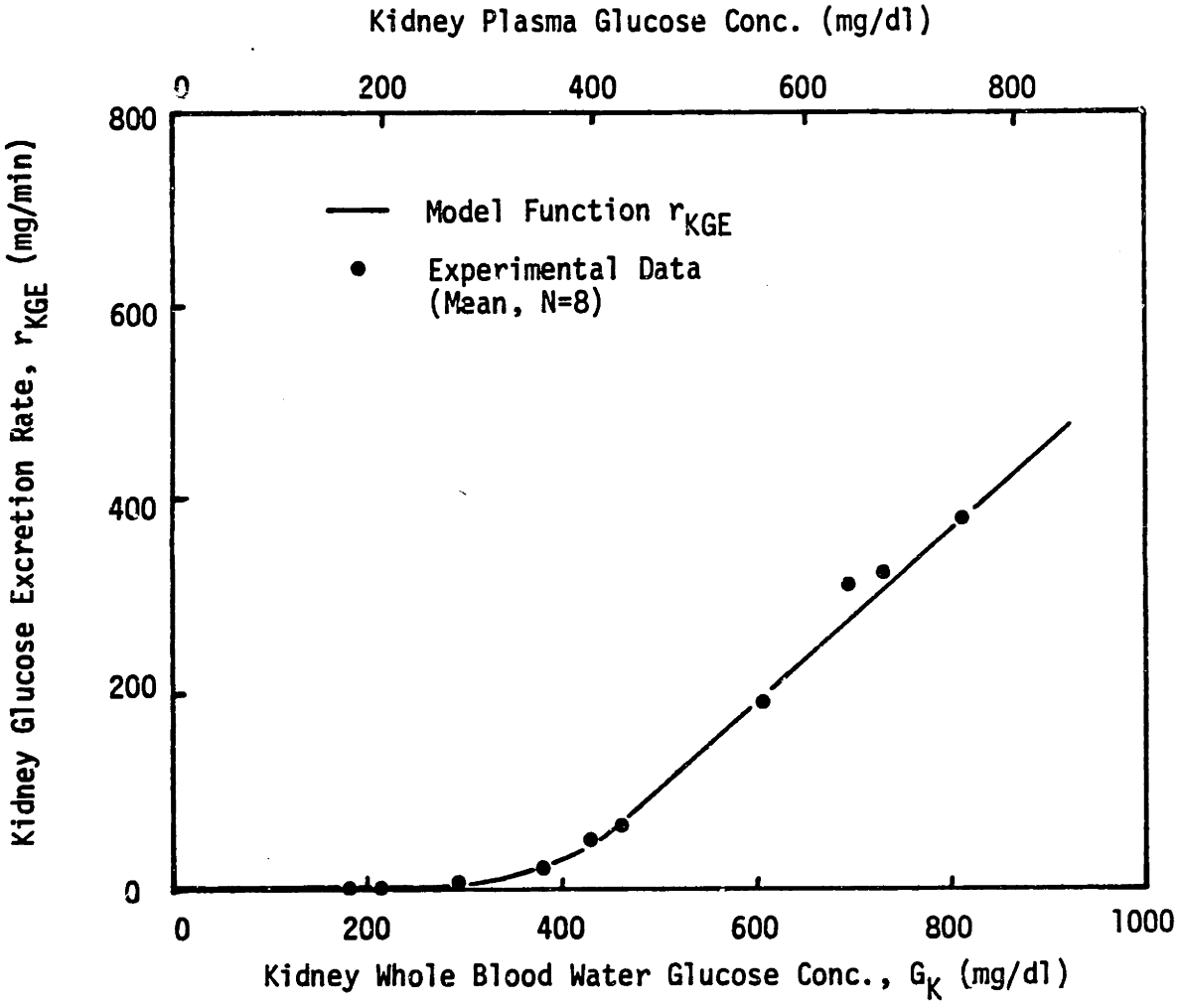

Fig. 10 Comparison of model function and experimental data of Brod (1973) for rate of kidney glucose excretion as a function of the kidney glucose level.

TABLE 11. Literature values for the rate of rbc glucose uptake and extrapolated total rbc glucose uptake for a 70 kg man based on these values.

Reference	Rate of RBC Glucose Uptake	Estimated Rate of RBC Glucose Uptake for 70 kg Man† (mg/min)
Guest et al. 1953	0.019 µg/10^6 cells/h	8.9 ††
Murphy, 1960	2.10 µg/ml blood/min*	9.4
DeLoecker and Prankerd, 1961	2.05 µmol/ml cells/h	13.8
Jacob and Janol, 1964; Janol, 1965	360 µg/ml cells/h	13.4
Brewer et al., 1970	0.80 ±.12 mg/ g hemoglobin/h	11.9 †††

* Hematocrit = 0.50 in cellular suspensions of this experiment
Assuming: † Total Blood Volume = 5600 ml; Hematocrit = 0.40

†† 5 x 10^9 RBC/ml whole blood

††† 16 g hemoglobin/100 ml whole blood

mg/min.

Red blood cell uptake of glucose was assigned a constant rate of 10 mg/min in the glucose model. Although an exacting approach would require uniform volumetric distritbution of red cell uptake throughout all of the vascular compartments of the glucose model, it has been assumed for simplicity that the total red blood cell uptake can be assigned to the large vascular volume of the heart and lungs with little error. Red cell uptake is a relatively small metabolic sink for glucose in the model, never accounting for more than about 5% of the total rate of glucose uptake.

F) Brain Glucose Uptake

Under normal conditions, the brain derives its entire fuel requirement from glucose. Of the glucose consumed, about 8% is glycolized to lactic and pyruvic acid, and 92% is oxydized to CO_2 (Gottstein et al., 1963). The brain contains only 0.1 weight percent glycogen (Fenn and Rahn, 1965) and thus must rely on a minute-to-minute supply of glucose from the blood.

Estimates of cerebral glucose consumption in man have been obtained by measuring cerebral blood flow together with arterial and jugular glucose concentrations. In a review, Sokolov (1960) has reported that normal adult brain glucose metabolism figures in the literature range from 4.9 to 6.2 mg/100 g brain·min. In a study of 45 subjects having no known brain disease, Gottstein et al. (1963) reported a mean cerebral glucose consumption of 5.3 mg/100 g brain·min.

The rate of glucose entry into cerebral tissue is not affected by insulin (Sokolov, 1960; Crone, 1965). In addition, brain glucose uptake remains constant with respect to changes in blood glucose concentration except in the case of severe hypoglycemia. Experiments on dogs by Himwich

and Fazikas (1937) indicated that cerebral glucose and oxygen uptake remained essentially unchanged over a blood glucose range of 25 to 245 mg/dl, but that both glucose and oxygen consumption dropped significantly when blood glucose was reduced from 25 to 7 mg/dl. Intravenous injection of glucose during hypoglycemia restored normal brain metabolism. Cerebral metabolism in humans during hypoglycemia has been studied during treatment of schizophrenia by insulin shock (Kety et al., 1948; Porta et al., 1964). During insulin-induced hypoglycema in schizophrenic patients, Kety et al. (1948) reported that when arterial glucose fell from 74 to 19 mg/dl, glucose and oxygen metabolism decreased from normal values. At a mean arterial glucose concentration of 8 mg/dl, deep coma developed, and glucose metabolism decreased further. Since brain cells are relatively permeable to glucose, brain hexokinase is the rate-limiting factor in glucose metabolism (Fromm, 1981). When circulating glucose levels fall below a critical level, usually accepted to be about 40 to 50 mg/dl in humans, glucose uptake begins to decrease because of an inadequate gradient for normal rates of facilitated transport of glucose across the blood-brain barrier (Cahill, 1981).

Another case in which brain glucose uptake may change is during starvation. Partial oxidation of fatty acids in the liver provides circulating ketone bodies, namely acetoacetate and β-hydroxybutyrate. During a prolonged fast, the vascular concentration of these water-soluble fuels rises due to diminuation of their utilization by peripheral tissues. These circulating concentrations become sufficient to provide a gradient for transport across the blood-brain barrier. Ketone body utilization thus displaces about two-thirds of the cerebral glucose requirement. This adaptation in man is important to survival because it conserves body protein by

reducing the amount of glucose required from hepatic gluconeogenesis (Cahill and Owen, 1968; Cahill and Soeldner, 1969).

For the glucose model, brain glucose uptake was assumed to occur at a constant rate of 5.3 mg/100 g brain·min. Assuming the brain of a normal 70-kg adult has an average mass of 1350 g (Altman and Dittmer, 1974), the total rate of brain glucose uptake was estimated to equal about 70 mg/min.

G) Peripheral Glucose Uptake

1) Pathways of Glucose Metabolism in Muscle and Adipose Tissue

The peripheral compartment represents the lumped contributions of skeletal muscle and adipose tissue to glucose metabolism. In these tissues, the rate of glucose transport across the cell membrane is enhanced by insulin and is most likely the rate-limiting step for all subsequent intracellular glucose metabolism (Levine et al., 1950).

In muscle tissue, the main pathways for glucose meatbolism are illustrated in Figure 11. Under basal conditions, resting muscle derives the major portion of its energy from oxidation of circulating fatty acids and ketone bodies. The balance of energy is obtained from uptake of plasma glucose which undergoes aerobic glycolysis and oxidation to carbon dioxide via the citric acid cycle. During exercise, the capacity of these oxidative pathways to supply energy becomes limited due to lack of tissue oxygen availability; NADH produced by the citric acid cycle accumulates as its rate of usage for ATP production becomes limited by oxygen availability, and thus the available NADH is instead utilized in the conversion of pyrurate to lactate. Under these conditions, the primary source of energy is thus derived from the anaerobic conversion of glucose 6-phosphate to lactate. Since glucose transport across the muscle cell membrane does not

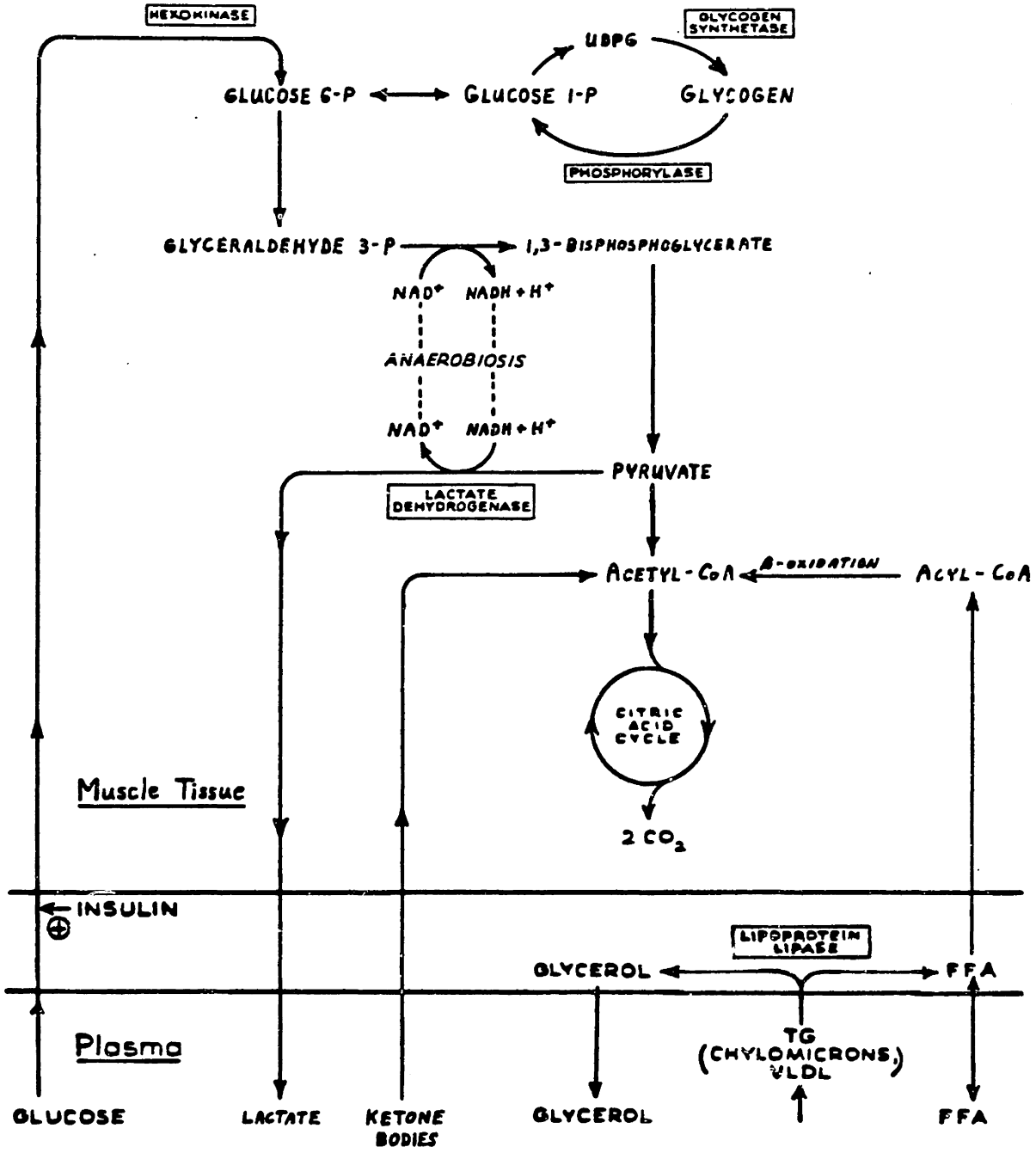

Fig. 11 Pathways of glucose metabolism in muscle tissue.

increase as a direct result of exercise, glucose 6-phosphate is provided by the breakdown of muscle glycogen stores.

The major pathways for glucose metabolism in adipose tissue are shown in Figure 12. Upon entry into the adipose cell, glucose is irreversibly phosphorylated by hexokinase enzyme. The subsequent conversion of glucose 6-phosphate to fructose 6-phosphate may occur either directly, or indirectly via the hexose monophospate shunt; this alternate pathway is important because it provides fat cells with the NADPH required for the synthesis of long-chain fatty acids. The main pathways for fructose 6-phosphate metabolism are oxidation to carbon dioxide via the citric acid cycle and incorporation of the skeletal carbons into triglyceride, either in the glycerol moiety via glycerol 3-phosphate, or in the fatty acids via lipogenesis. Under normal conditions, the major source of energy for adipose tissue is derived from oxidation of fatty acids.

2) Glucose Disposal in Peripheral Tissues

When circulating levels of glucose and insulin increase, such as in the postprandial state, glucose uptake in peripheral tissues increases. In view of the above discussion, glucose entering muscle may be oxidized to carbon dioxide, converted to lactate, or stored as glycogen, whereas glucose taken up by adipose tissue may be oxidized to carbon dioxide or incorporated into triglyceride. The relative contributions of these different pathways are important to consider in interpreting the role of peripheral tissues in overall glucose tolerance.

The capacity of adipose cells to convert glucose to triglyceride has been extensively investigated in rat (Mehlman and Hanson, 1971), which can incorporate large quantities of glucose carbon into fatty acids (Jeanrenaud

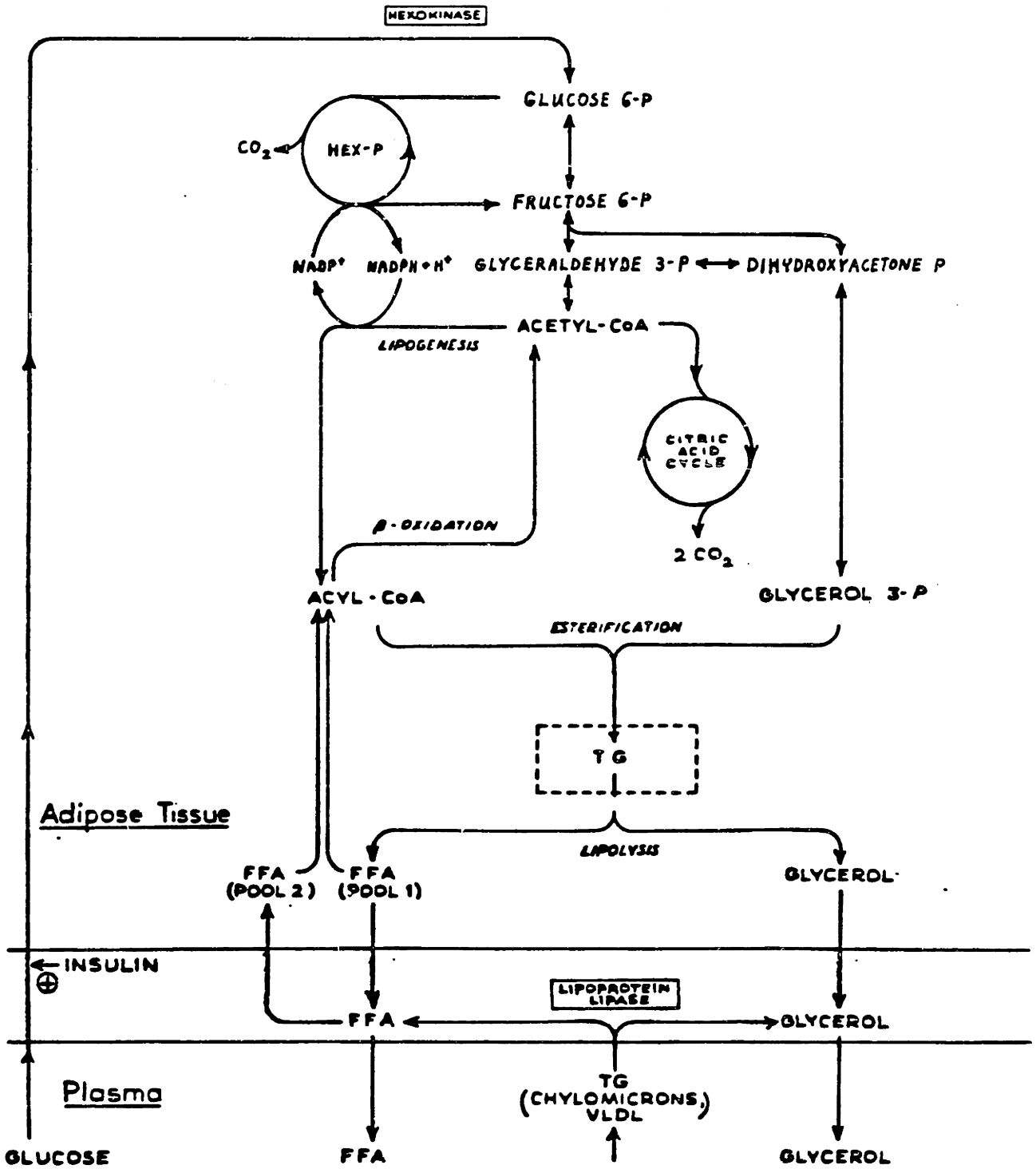

Fig. 12 Pathways of glucose metabolism in adipose tissue.

and Renold, 1959). Mounting evidence would suggest, however, that the rat is a poor experimental model for studying the regulation of human lipid metabolism (Shrago et al., 1971). In contrast to the rat, it has been reported that the ability of human adipose cells to synthesize fatty acids (Sjøstrøm, 1973; Patel et al., 1975) and glycerol (Bjørntorp et al, 1968) from glucose is extremely limited, and that certain key enzymes in the lipogenic pathway are present at negligible levels (Shrago et al., 1971). Based on a comprehensive review of data obtained from in vitro and in vivo studies of human adipose tissue metabolism, Bjørntorp and Sjøstrøm (1978) have concluded that conversion to triglyceride is a quantitatively insignificant route for glucose disposal, totaling at most 1-2 g/day in nonobese subjects.

With respect to the importance of anaerobic glycolysis in muscle, Jackson et al.(1973), Aoki et al. (1982), and Radziuk and Inculet (1983) have reported no significant increase in measured lactate production across human forearm during a 100g OGTT in normal subjects. Similar results have been obtained from lactate balance measurements across human leg (DeFronzo et al., 1981a) and forearm (Rabinowitz and Zierler, 1962) during insulin-induced stimulation of peripheral glucose uptake and across human forearm during intravenous glucose (Radziuk and Inculet, 1983). In addition, Aoki et al. (1983) have recently made extremely precise measurements of carbon dioxide production across human forearm using volumetric blood gas analysis methods (Peters and Van Slyke, 1932) to elucidate the importance of glucose oxidation. During a 100g OGTT in normal subjects, mean carbon dioxide production did not rise above a maximum value of 7.3 ± 1.1 μmol/100 ml forearm•min, representing an insignificant increase from the basal value of 6.2 ± 1.1.

Glycogen storage in human skeletal muscle has been studied in relation to exercise physiology by a number of investigators (Morgan et al., 1971; Hultman et al., 1971; Bergstrom et al., 1967). Using needle biopsy studies on 228 normal subjects, Hultman et al. (1970) have reported a mean resting muscle glycogen content of 13.9 g/kg wet muscle (range 9.2 - 24.9). In non-exercised muscle, fasting over a period of 10 days only results in about a 30% reduction in muscle glycogen content (Hultman et al., 1971). Heavy exercise combined with a carbohydrate-rich diet, however, can elevate glycogen levels significantly above normal (Morgan et al., 1971), increasing muscle content by 200% within a period of several days (Hultman et al., 1971). Assuming skeletal muscle constitutes 40 percent of total body weight (Andres et al., 1956; Heymsfield et al., 1982; Yki-Jarvinen and Koivisto, 1983), the normal muscle glycogen stores of a 70 kg man would average about 400 g, increasing to a kilogram or more with exercise and carbohydrate availability. Thus, skeletal muscle has a large buffering potential for storage of glucose. Larner et al. (1981) have demonstrated that both insulin and glucose 6-phosphate stimulate activation of glycogen synthetase, a key enzyme in the regulation of muscle glycogenesis (see Figure 11).

The above results would suggest two important conclusions. First, glucose storage as muscle glycogen represents the only quantitatively significant metabolic pathway for insulin-mediated glucose uptake by peripheral tissues. Second, adipose tissue does not significantly contribute to the disposal of glucose in nonobese humans. This general interpretation of peripheral glucose metabolism is further supported by the recent studies of Finebereg and Schneider (1982) in which glucose uptake was simultaneously measured across both superficial (mainly adipose tissue) and

deep (mainly muscle, with a small amount of intramuscular adipose tissue) beds in the human forearm. During insulin perfusion, no significant increase in superficial tissue uptake was observed, whereas deep tissue uptake increased significantly. In studies relating insulin sensitivity to body composition, Yki-Jarvien and Koivisto (1983) have recently reported that the rate of glucose metabolism in normal man is directly related to muscle mass and inversely proportional to adiposity.

3) Basal Metabolism of Peripheral Tissues

Studies of human forearm glucose metabolism provide a basis for modeling peripheral glucose uptake. Forearm uptake is determined experimentally by measuring arterial-venous differences in glucose concentration coupled with forearm blood flow. Values for the basal rate of forearm uptake calculated from data in the literature are presented in Table 12. Also included in the table are total rates of basal peripheral glucose uptake for a 70 kg man. These values were extrapolated from the forearm data using following assumptions: 1) muscle and adipose account for respectively 89 and 11 percent of basal forearm uptake (Jackson et al., 1973); 2) in nonobese subjects muscle and adipose tissues constitute respectively 64 and 8 percent of total forearm volume (Cooper et al., 1955); 3) a normal 70 kg man has a total muscle mass of 30 kg and a total adipose tissue mass of 10 kg (Dole, 1965; Yki-Jarvinen and Koivisto, 1983; Anyan, 1978). The values from Table 12 yield a mean ± sd basal rate of peripheral glucose uptake of 47.7 ± 27 mg/min. The wide range of values (22.7 - 88.8 mg/min) and large scatter are attributed to the uncertainty in determining forearm blood flow and the difficulty in measuring small arterial-venous concentration differences. Additional uncertainty is

TABLE 12. Basal forearm glucose uptake rates compiled from the literature and estimated total rates of basal peripheral (muscle and adipose) glucose uptake based on these values.

Reference	Subjects	Basal Rate of Glucose Uptake† (mg/dl forearm/min)	Estimated Basal Rate of Peripheral Glucose for 70 kg man†† (mg/min)
Rabinowitz and Zierler, 1962	5	.047*	26.1
Pozefsky et al., 1969	16	.083*	46.0
Razio et al., 1972	9	.139	77.1
Jackson et al., 1979	25	.044	24.4
Kalant et al., 1979	7	.048	26.6
Fineberg and Schneider, 1982	17	.16*	88.8
Aoki et al., 1983	5	.072	39.9

* Assuming Ratio of Deep Venous to Superficial Venous Blood Flow Equals 4:1 (Cooper et al., 1962)

† Glucose Uptake Calculated as Product of Forearm Blood Flow and Arterial-Venous Difference in Glucose Concentration

†† See text for assumptions

introduced in extrapolation of forearm to whole-body values. Under steady state basal conditions, however, the rate of liver glucose production must balance the rate of glucose uptake by the remaining tissues of the body. In order to close this balance on the basis of available data for the rate of basal liver glucose production, a basal peripheral glucose uptake rate of 35 mg/min was used for the glucose model. Although this value falls below the mean extrapolated rate of 47.7 mg/min, it is well within the standard deviation of the available data. Additional discussion of closing the basal glucose uptake and production balance will be deferred to the section of the text on basal liver glucose metabolism.

4) Mediation of Peripheral Glucose Uptake

The rate of glucose uptake by peripheral tissues is mediated by changes in the interstitial insulin and glucose concentrations that bathe these tissue cells. For modeling, it was assumed that these effects are multiplicative, and the rate of peripheral glucose uptake was is expressed

$$r_{PGU} = M^{I}_{PGU} M^{G}_{PGU} r^{B}_{PGU} \tag{33}$$

or, normalizing with respect to basal uptake

$$r^{N}_{PGU} = M^{I}_{PGU} M^{G}_{PGU} \tag{34}$$

where basal state values are denoted by superscript B and normalization of values through division by basal values is indicated by superscript N.

Compiled in Table 13 are data of forearm studies of glucose uptake taken from the literature. Normalized uptake rates were computed directly from reported steady state and basal values. Since interstitial fluid measurements of glucose and insulin concentration were not available, these quantities required estimation from reported arterial and venous con-

TABLE 13. Peripheral glucose uptake rates based on forearm glucose studies from the literature.

Reference	Sub-jects	Basal Forearm Glucose Uptake Rate (mg/min/dl forearm)	Steady Forearm Glucose Uptake Rate (mg/min/dl forearm	Normalized Peripheral Glucose Uptake Rate [b] r^N_{PGU}	Arterial Plasma Insulin Conc. (mU/l)		Normalized Peripheral Interstitial Insulin Conc., [c] I^N_{PI}	Arterial Plasma Glucose Conc. (mg/dl)		Normalized Peripheral Interstitial Glucose Conc. [e] G^N_{PI}
					Basal	Steady		Basal	Steady	
Razio et al., 1972	9	0.139	0.181	1.3	10	30	3.0	86	86	0.9
Jackson et al., 1973	25	0.044	0.55	12.5	10	72[f]	7.2	85	150[f]	1.4
Kalant et al., 1979	4	0.034	0.041	1.2	8	8	1.0	106	206	1.3
	4	0.041	0.155	3.8	7	17	2.4	170	264	1.5
	6	0.045	0.321	7.1	6	29	4.8	99	130	1.7
Fineberg and Schneider, 1982	5	0.20	0.40	2.0	10[a]	43[a]	4.3[d]	93	93	0.8
	5	0.10	0.75	7.5	8[a]	74[a]	9.4[d]	93	93	0.6
Aoki et al, 1982	4	0.09	0.60	6.7	10	60	6.0	95	95	0.7
	7	0.09	0.65	7.2	10	110	11.0	95	95	0.6

[a] Venous Plasma Insulin Concentration
[b] Diabetic Subjects
[c] Calculated from Equation 42
[d] Calculated from Equation 44
[e] Calculated from Equation 49
[f] Quasi-Steady Values obtained from mean data 45-75 min after OGTT administration

centrations. For insulin, the mass balance equations for the peripheral compartment (Equations 22 and 23) at steady state give

$$0 = Q_P^I (I_H - I_{PV}) - \frac{V_{PI}}{T_P^I} (I_{PV} - I_{PI}) \tag{35}$$

$$0 = \frac{V_{PI}}{T_P^I} (I_{PV} - I_{PI}) - r_{PIC} \tag{36}$$

Addition of these equations yields

$$0 = Q_P^I (I_H - I_{PV}) - r_{PIC} \tag{37}$$

which states that the rate of insulin removal from the vascular space equals its rate of tissue clearance at steady state. Solving Equation 36 for peripheral vascular insulin concentration

$$I_{PV} = r_{PIC} \left(\frac{T_P^I}{V_{PI}}\right) + I_{PI} \tag{38}$$

and substituting into Equation 37 gives

$$I_{PI} = I_H - r_{PIC} \left[\frac{T_P^I}{V_{PI}} - \frac{1}{Q_P^I}\right] \tag{39}$$

It will be shown later in the text that the rate of peripheral insulin clearance is proportional to the rate of insulin presentation to peripheral tissues, or

$$r_{PIC} = F\, Q_P^I\, I_H \tag{40}$$

where F is a constant of proportionality. Equation 39 may thus be rewritten

$$I_{PI} = I_H \left[1 - F \left(\frac{T_P^I\, Q_P^I}{V_{PI}} - 1\right)\right] \tag{41}$$

It can be seen from this expression that

$$I^N_{PI} = \frac{I_{PI}}{I^B_{PI}} = \frac{I_H}{I^B_H} = I^N_H \tag{42}$$

and therefore normalized peripheral interstitial insulin concentration equals normalized arterial insulin concentration at steady state. In a similar manner to the above, it can be shown that

$$I_{PI} = I_{PV}\left[1 - \left(\frac{F}{1-F}\right)\frac{T^I_P\, Q^I_P}{V_{PI}}\right] \tag{43}$$

and thus

$$I^N_{PI} = I^N_{PV} \tag{44}$$

and the normalized peripheral interstitial insulin concentration also equals the normalized peripheral venous insulin concentration at steady state. Since the normalized interstitial, arterial, and venous insulin concentrations are equal at steady state, the peripheral interstitial insulin concentrations in Table 13 were computed directly from reported arterial or venous data in the literature. For glucose, the peripheral compartment mass balance equations (15 and 16) at steady state give

$$0 = Q^G_P\,(G_H - G_{PV}) - \frac{V_{PI}}{T^G_P}\,(G_{PV} - G_{PI}) \tag{45}$$

$$0 = \frac{V_{PI}}{T^G_P}\,(G_{PV} - G_{PI}) - r_{PGU} \tag{46}$$

Solving Equation 46 for peripheral vascular glucose concentration

$$G_{PV} = G_{PI} + r_{PGU}\left(\frac{T^G_P}{V_{PI}}\right) \tag{47}$$

and substituting into Equation 45 yields

$$G_{PI} = G_H - r_{PGU}\left(\frac{T_P^G}{V_{PI}} + \frac{1}{Q_P^G}\right) \tag{48}$$

The values for normalized peripheral interstitial glucose concentration in Table 13 were estimated from the steady state relationship

$$G^N = \frac{G_{PI}}{G_{PI}^B} = \frac{G_H - r_{PGU}\left(\frac{T_P^G}{V_{PI}} + \frac{1}{Q_P^G}\right)}{G_H^B - r_{PGU}^B\left(\frac{T_P^G}{V_{PI}} + \frac{1}{Q_P^G}\right)} \tag{49}$$

where uptake rates and arterial concentrations were taken as those reported in the respective studies.

Presented in Figure 13 is a plot of normalized peripheral glucose uptake rate as a function of normalized interstitial insulin concentration. Data points in the figure represent results of forearm studies tabulated in Table 13. Examination of the data indicates that peripheral glucose uptake is a strong function of the interstitial insulin level as the rate of uptake varies over an order of magnitude within a physiologic range of insulin concentration. In addition, there is indicated a secondary mediation of peripheral uptake by interstitial glucose. In order to fit the insulin and glucose multiplier functions of Equation 34 to the data, each of the functions was assumed to have the hyperbolic tangent from of Equation 27. Parameter adjustment using a Levenberg-Marquardt algorithm (IMSL library computer subroutine ZXSSQ) was employed to obtain a least squares fit of the multiplier functions; for n adjustable parameters, the routine utilizes a finite-difference (derivative free) method to search for

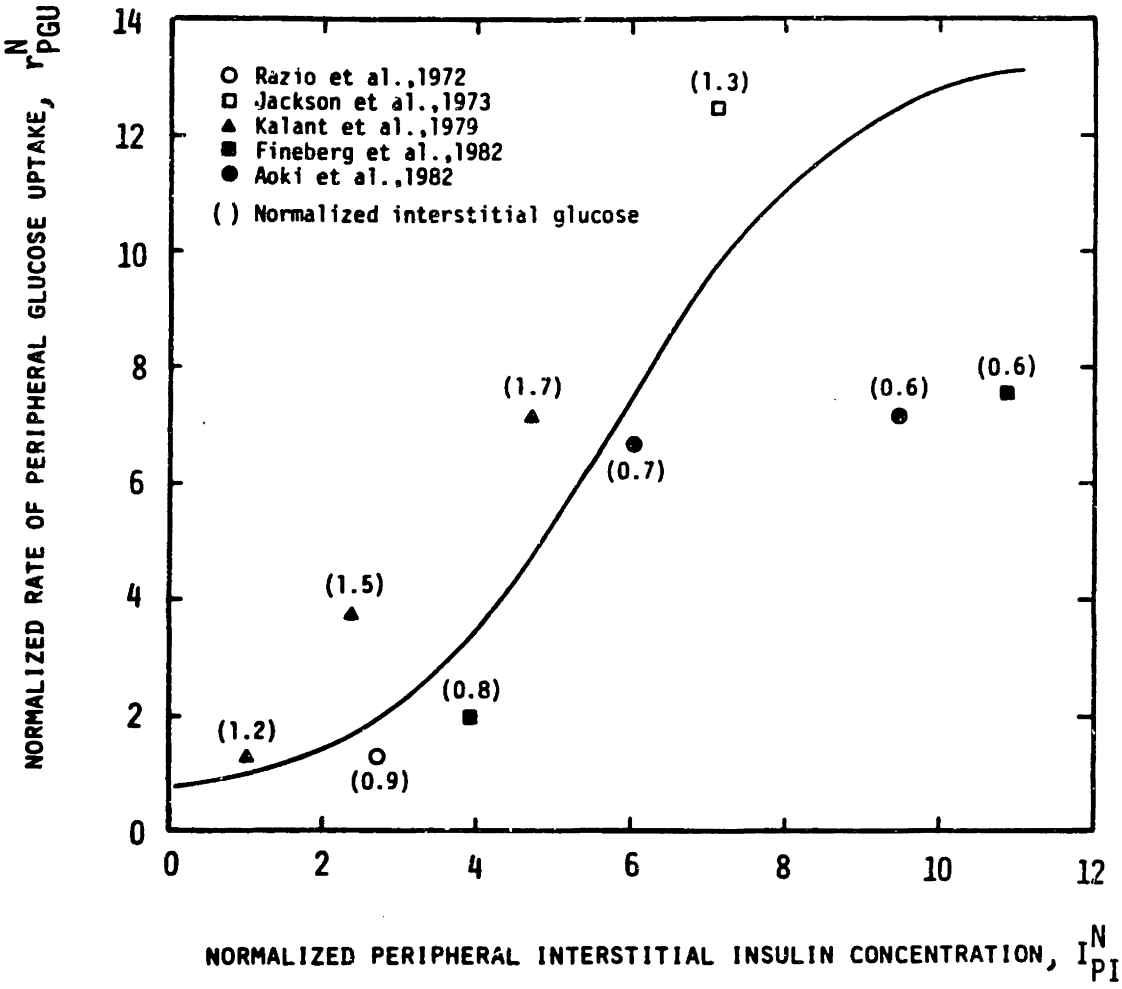

Fig. 13 Plot of normalized peripheral glucose uptake rate as a function of normalized peripheral interstitial insulin concentration. The solid curve indicates the model function for the isolated effect of interstitial insulin on glucose uptake rate.

a minimum in the n-dimensional least squares error space. Results of initial fitting yielded an effect of interstitial glucose on glucose uptake that was essentially a linear function passing through the origin; therefore, the glucose hyperbolic tangent fitting function was simply replaced by

$$M^{G}_{PGU} = G^{N}_{PI} \tag{50}$$

subsequent parameter adjustment of the insulin multiplier function then yielded

$$M^{I}_{PGU} = 7.03 + 6.52 \tanh[0.338(I^{N}_{PI} - 5.82)] \tag{51}$$

This function, shown as the curve in Figure 13, represents the rate at which glucose uptake would occur at a normalized interstitial glucose concentration of unity ($M^{G}_{PGU} = 1$ in Equation 34). Using the insulin multiplier function of Equation 50, values of the glucose multiplier for each of the forearm data points were calculated from Equation 34

$$M^{G}_{PGU} = \frac{r^{N}_{PGU}}{M^{I}_{PGU}} \tag{52}$$

and these values are plotted as a function of interstitial glucose concentration in Figure 14. The data plotted in this manner shows the isolated effect of interstitial glucose concentration on the rate of glucose uptake, the line in the figure illustrating the glucose multiplier function of Equation 50. As shown in Figure 15, the model multiplier functions for the effects of interstitial glucose and insulin yield accurate predictions for the rate of peripheral glucose uptake over the range of available data.

Although the action of insulin in promoting peripheral glucose uptake has long been recognized, the extent to which the mass action of glucose

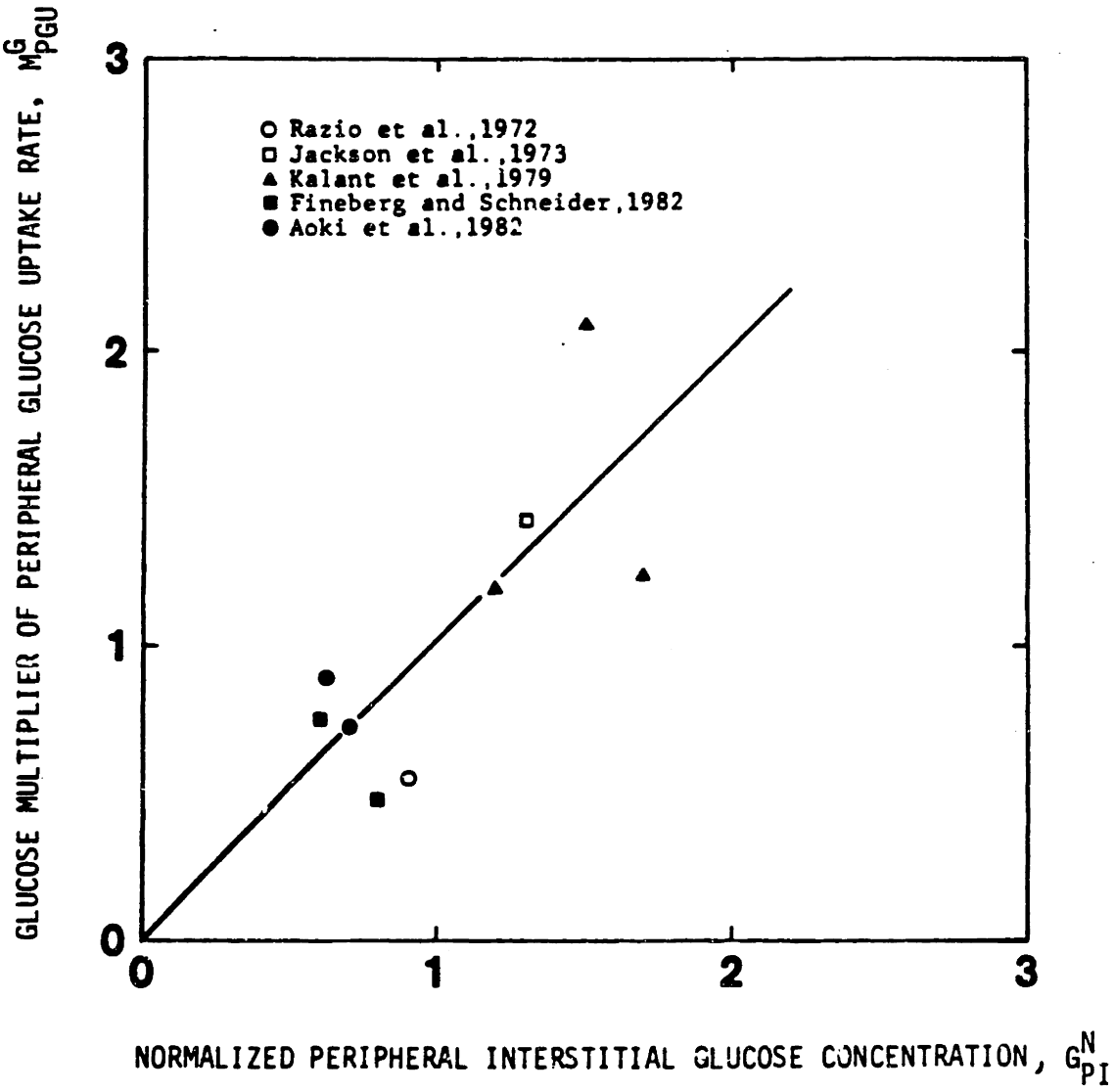

Fig. 14 Plot of glucose multiplier of peripheral glucose uptake rate as a function of normalized peripheral interstitial glucose concentration. The line represents the model function for the isolated effect of interstitial glucose on glucose uptake rate.

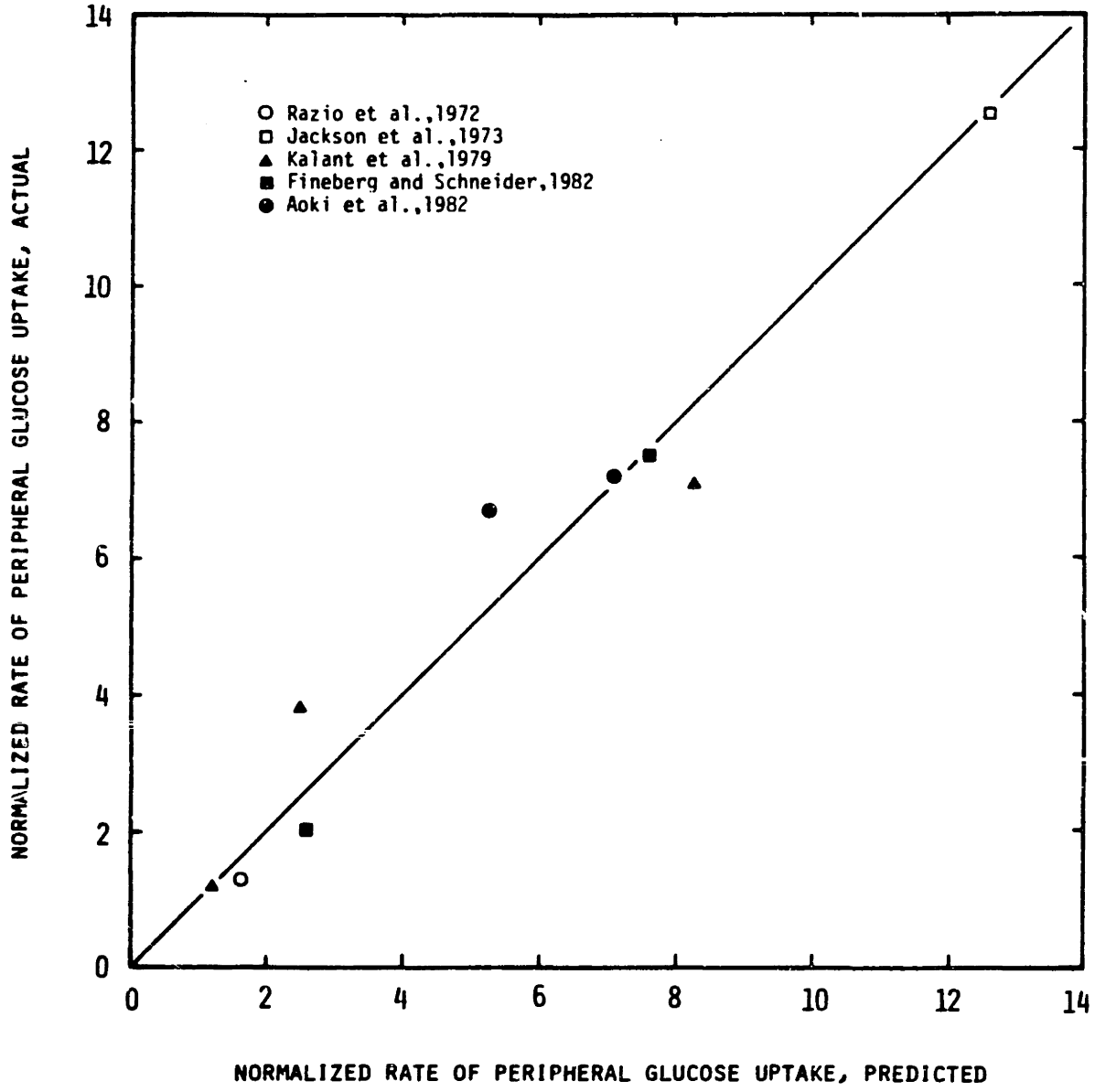

Fig. 15 Plot of actual versus predicted values for normalized rate of peripheral glucose uptake.

alone affects peripheral uptake has remained controversial. In vitro studies on isolated perfused cat hind limb (Lundsguard et al., 1939) and rat heart (Morgan et al. 1961) have demonstrated dependence of muscle glucose uptake on glucose concentration over a physiologic range. The applicability of these studies to human physiology has been questioned on the basis of an early dye dilution forearm study in which Adres and Zierler (1958) reported "stability" of glucose uptake during local arterial hyperglycemia. To date, however, definitive experiments using glucose perfusions to change forearm glucose concentrations in the presence of fixed insulin levels have never been performed. Human forearm data as correlated in Figure 14 suggests that increasing glucose concentration over a physiologic range can roughly double the rate of peripheral glucose uptake. This is in good agreement with results of in vivo studies on eviscerated rabbits (Wick and Drury, 1953) in which elevating blood glucose concentration in the presence of fixed insulin levels increased glucose disappearance by a factor of two.

Since insulin binds to specific cell membrane receptors to affect increases in cell membrane glucose transport, it is the quantity of bound insulin that should reflect insulin enhancement of peripheral glucose uptake. With this in mind, it might seem reasonable that the rate of peripheral tissue glucose uptake would correlate with the rate of removal of insulin from plasma by these tissues. In the early forearm studies of Rasio et al. (1972) and Jackson et al. (1973), however, simultaneous measurements of glucose uptake and insulin clearance showed no significant correlation between these factors. The high degree of correlation that has been demonstrated between glucose uptake rate and peripheral insulin concentration suggests that the sigmoidal curve of Figure 13 may represent a rapid equilibrium binding curve relating interstitial insulin concentration

to the relative quantity of bound insulin on the tissue cell membranes.

H) Hepatic Glucose Metabolism

1) Pathways of Glucose Metabolism in the Liver

The liver displays tremendous metabolic flexibility with respect to glucose processing. The major pathways of hepatic glucose metabolism are illustrated in Figure 16. Disposal routes for glucose entering the liver cell are similar to those discussed for muscle and adipose tissue. Following intracellular phosphorylation, glucose may be 1) stored as glycogen, 2) oxidized to carbon dioxide via the hexose monophosphate shunt and/or the citric acid cycle, or 3) converted to triglyceride, either in the glycerol moiety via glycerol 3-phosphate, or in the fatty acids (acyl-CoA) via lipogenesis. An important feature of liver cells is the presence of glucose-6-phosphatase enzyme (Nordlie, 1981) which catalyzes the conversion of glucose 6-phosphate to glucose (see Figure 16). This enzyme gives liver cells the capacity to release glucose into the blood. Metabolic pathways contributing to hepatic glucose release include glycogen breakdown and gluconeogenesis. The major precursors available as substrates for gluconeogenesis include circulating lactate (from RBC and gut glucose metabolism), glycerol (from adipose triglyceride breakdown), and glycogenic amino acids (from muscle protein breakdown). The amino acids, after deamination or transamination, may enter the gluconeogenic pathway as citric acid cyle intermediates or via conversion to pyruvate (see Figure 16).

2) Experimental Measures of Splanchnic Glucose Metabolism

Before discussing liver glucose metabolism, it will be helpful to define various terms with respect to measurement of hepatic processes and

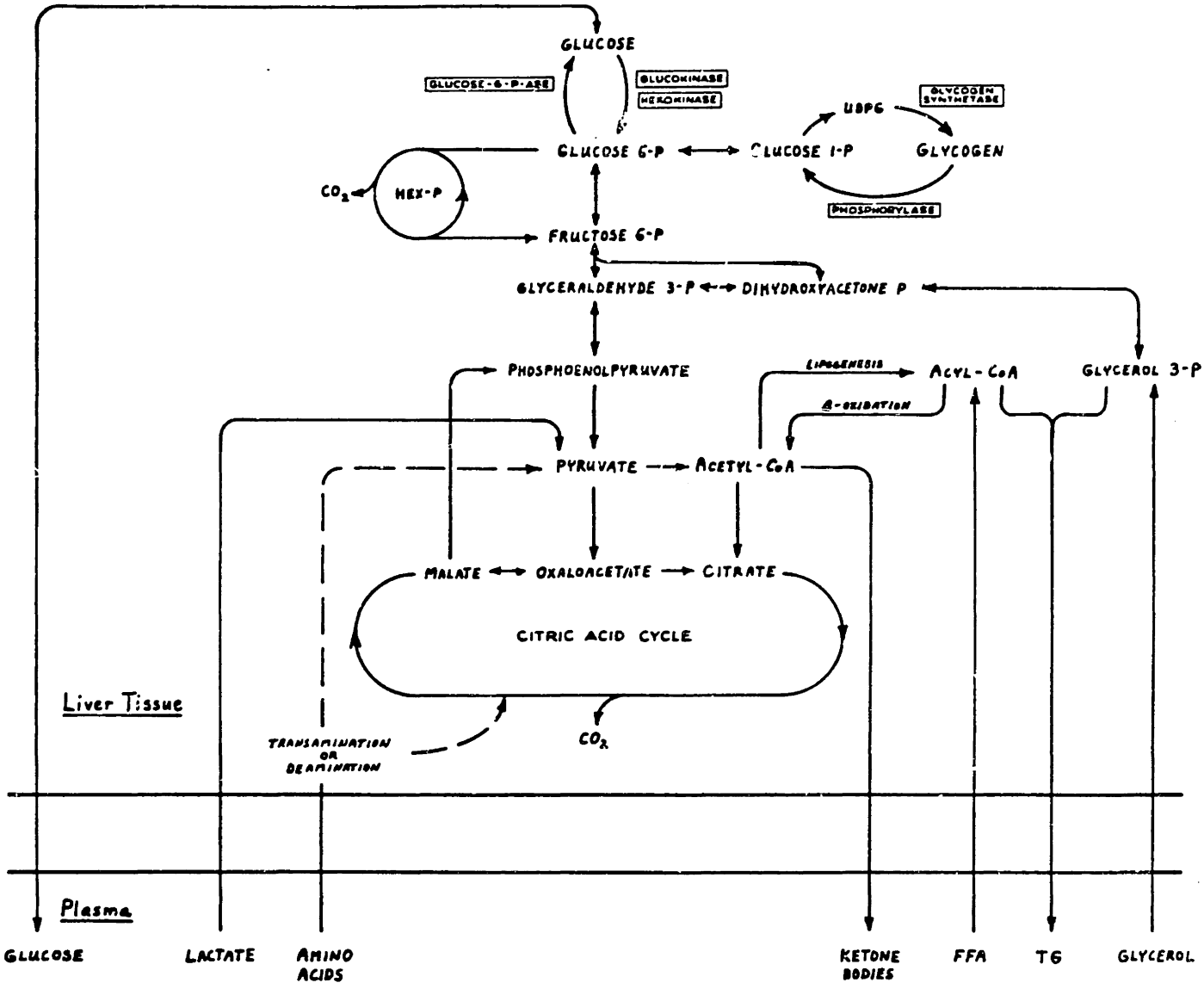

Fig. 16 Major pathways of glucose metabolism in the liver.

how these quantitities are determined from experimental studies. A schematic diagram of the splanchnic bed is shown in Figure 17. Anatomical positioning of the liver and gut tissues with respect to blood flow is the same as that illustrated for the glucose model in Figure 5. Also indicated are the metabolic processes which add or remove glucose from the spalanchnic organs; these processes are the same as those employed in the glucose model except for the inclusion of a glucose input from gut absorption following oral glucose. There are two experimental methods that are commonly employed for study of splanchnic glucose metabolism, the hepatic venous catheterization technique and the tritiated glucose infusion method. In the hepatic venous catheterization technique (Wahren et al., 1976), arterial and hepatic venous glucose concentrations are measured together with hepatic blood flow rate. These values permit calculation of the rate of net splanchnic glucose appearance r_{NSGA}, given by

$$r_{NSGA} = Q_L(G_L - G_H) \tag{53}$$

which represents the net rate at which the splanchnic metabolic processes simultaneouly add and remove glucose (see Figure 16)

$$r_{NSGA} = r_{HGP} - r_{HGU} + r_{OGA} - r_{GGU} \tag{54}$$

The hepatic venous catheterization technique thus provides an experimental measure of the net glucose release rate from the splanchnic bed as a result of the four simultaneous metabolic processes indicated in Equation 54 and Figure 17. The rate of hepatic glucose production r_{HGP} can be determined experimentally using isotope dilution methods (Hentenyl and Norwich, 1974). In general, a glucose tracer such as [^{3}H-3]-glucose is infused at a constant rate and both labeled and cold vascular glucose concentrations are measured over the duration of the experiment. The rate of glucose turnover

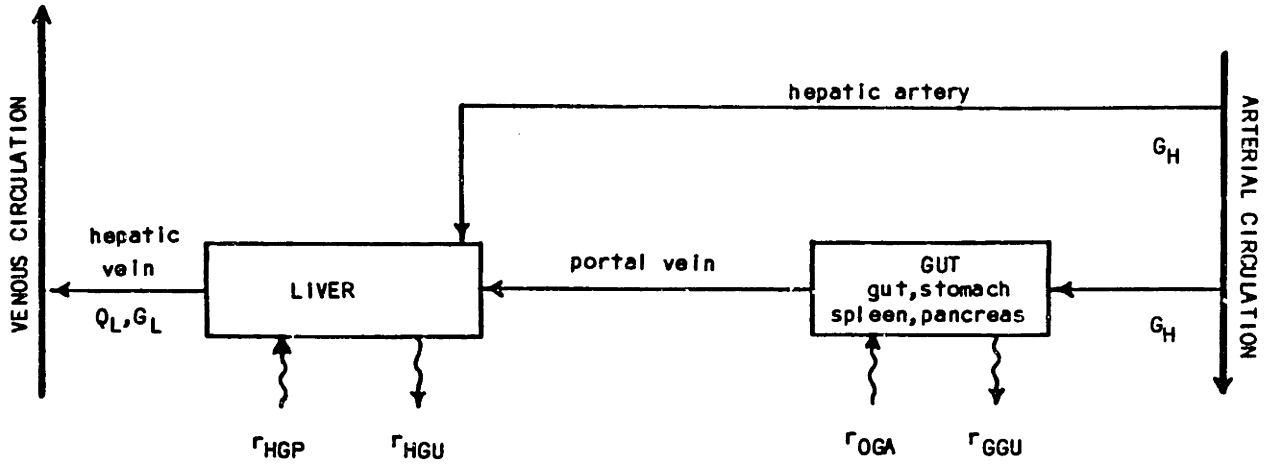

G_H = Arterial Glucose Concentration

G_L = Liver Effluent (Hepatic Venous) Glucose Concentration

Q_L = Hepatic Blood Flow Rate

r_{HGP} = Rate of Hepatic Glucose Production

r_{HGU} = Rate of Hepatic Glucose Uptake

r_{OGA} = Rate of Oral Glucose Absorption

r_{GGU} = Rate of Gut Glucose Uptake

Fig. 17 Schematic diagram of the splanchnic bed illustrating anatomical positioning of the liver and gut tissues with respect to blood flow and the metabolic processes which add or remove glucose from the splanchnic organs. The gut compartment represents primarily the gut tissues, but includes lumping of the remaining nonhepatic splanchnic organs.

under steady (Wall et al., 1957) or nonsteady (Radziuk et al., 1974) conditions is calculated from consideration of isotope dilution relative to the rate of tracer infusion. Simultaneous application of hepatic venous catheterization and tritiated glucose infusion provides an experimental measure of the rate of net splanchnic glucose uptake r_{NSGU}, defined by

$$r_{NSGU} = r_{NSGA} - r_{HGP} \tag{55}$$

which according to Equation 54 and Figure 17 represents

$$r_{NSGU} = r_{HGU} + r_{GGU} \; (- r_{OGA}) \tag{56}$$

The contribution of oral glucose absorption has been included in parentheses for completeness in Equation 56. For experiments in which glucose is administered orally (and thus r_{OGA} is nonzero), the oral glucose is labeled with a tracer such as [D-1^{14}C]-glucose such that a double tracer analysis can be employed to distinguish between liver glucose production and gut absorption of oral glucose (Radziuk et al., 1978; Ferrannini et al., 1981).

Unfortunately, portal vein measurements are not available for humans. From the above discussion, it is thus apparent that clinical studies do not distinguish between liver and gut contributions to splanchnic metabolism. As will be shown, quantification of hepatic glucose metabolism required assumptions with respect to gut glucose metabolsm in order to estimate liver contributions to observed splanchnic response reported in the literature.

3) Basal Liver Metabolism

Based on over 200 studies using [^{3}H-3]-glucose infusions to quantitate hepatic glucose production, DeFronzo et. al. (1981a) have reported a mean basal rate of 2.2 ± 0.1 mg/kg (body weight)·min. In 45 subject (DeFronzo

et al., 1979a; 1981a), hepatic venous catheterization techniques were simultaneously employed. In these studies, arterial-hepatic venous glucose concentration differences multiplied by hepatic blood flow rates indicated a net basal rate of splanchnic glucose appearance (r_{NSGA} in Equations 53 and 54) of 1.6 ± 0.1 mg/kg·min. Thus, of the total amount of glucose produced by the liver (2.2 mg/kg·min), 1.6 mg/kg·min is available for use by the nonsplanchnic tissues of the body, and the remaining 0.6 mg/kg·min is taken up by tissues in the splanchnic bed. Based on studies in dogs using combined portal and hepatic catheterizations (Barrett et al., 1980), it can be estimated that the liver accounts for approximately half of the basal splanchnic glucose utilization, while extrahepatic splanchnic tissues (primarily the gut) account for the other half. Presented in Table 13A and Figure 18 is a summary of glucose metabolism in a 70 kg man during the basal postabsorptive state. As previously discussed, due to difficulties in determining the basal rate of peripheral tissue glucose uptake directly from extrapolations of experimental forearm studies, this value was determined from the difference between the basal hapatic glucose production rate and the sum of the basal glucose uptake rates of the remaining tissues.

From studies examining the splanchnic balance of gluconeogenic substrates (Wahren et al., 1972; Nilsson et al., 1973; Dietze et al., 1976), it can be estimated that in the basal state approximately 70 to 80 percent of hepatic glucose release results from glycogen breakdown and the remaining 20 to 30 percent is due to gluconeogenesis. A summary of these studies is presented in Table 14. These results are in good agreement with studies of liver glycogen content. Nilsson and Hultman (1973) have reported that measurements of glycogen in serial liver biopsy specimens obtained over a 4 h period in postabsorptive humans indicate a glucose

TABLE 13A. Summary of basal glucose balance in a 70kg man.

	RATE (mg/min)	
Hepatic Glucose Production	155	(2.2 mg/kg. min)
Total Glucose Uptake	155	
Brain	70	
†Peripheral (Muscle and Adipose)	35	
Liver	20	(0.3 mg/kg. min)
Gut	20	(0.3 mg/kg. min)
Red Blood Cells	10	

†The rate of peripheral tissue glucose uptake determined from the difference between the rate of hepatic glucose production and the sum of the remaining tissue uptake rates.

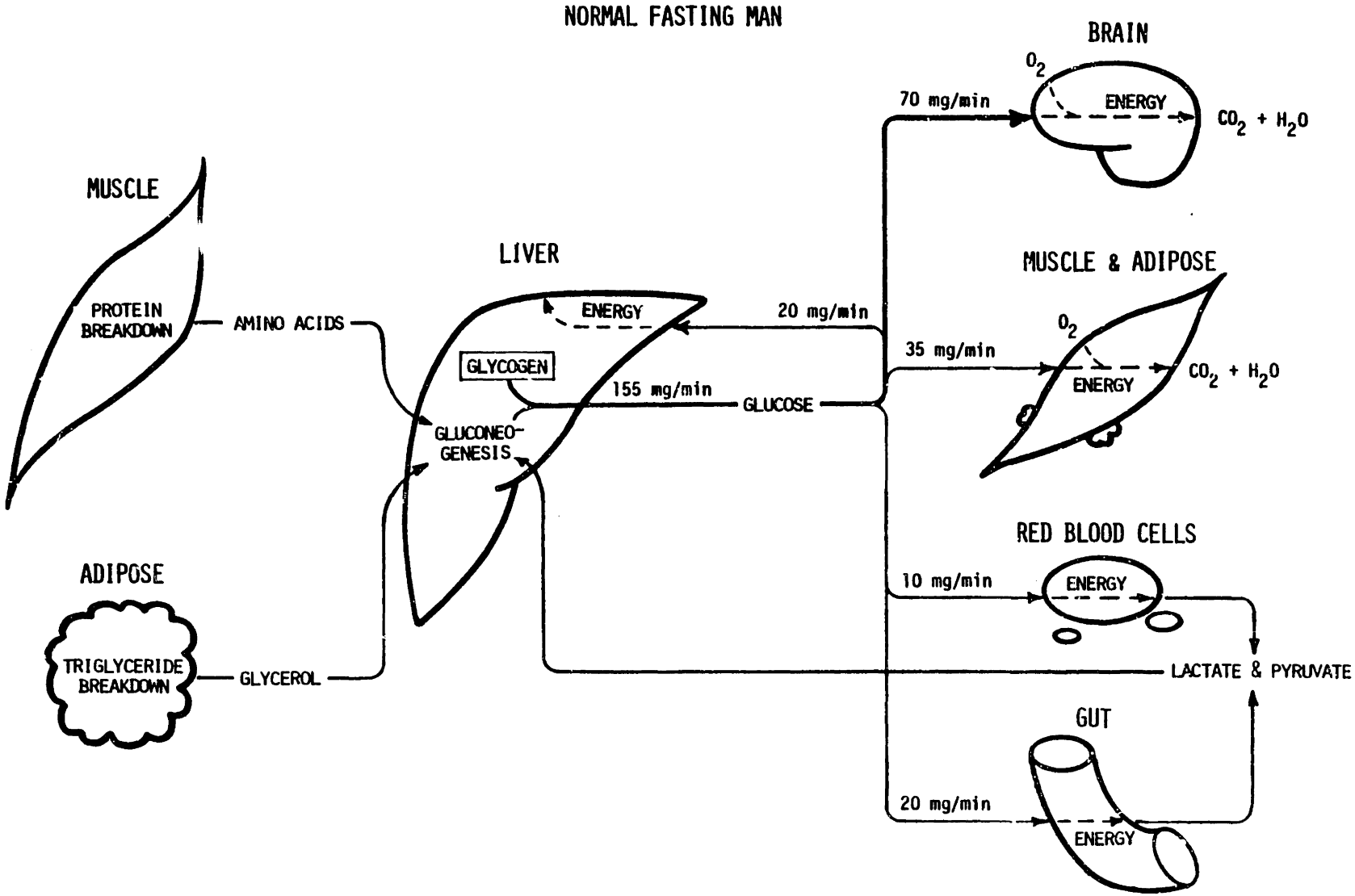

Fig. 18 Basal glucose metabolism in a normal 70 kg man.

TABLE 14. Relative contributions of glycogenolysis and gluconeogensis to hepatic glucose output in normal postabsorptive man. (adapted from Gerich et al., 1981)

	Wahren et al., 1972	Nilsson et al., 1973	Dietze et al., 1976
Net Splanchnic Uptake (mg/min glucose equivalents)			
Lactate	23	22	21
Glycerol	2.8	7.2	6.5
Amino Acids	9.6	16	11
Pyruvate	1.4	-	1.6
Sum of Uptake (mg/min glucose equivalents)	36	45	41
Glucose Production (mg/min)	171	157	162
Gluconeogenic Contribution	21%	29%	25%
Glycogenolysis (mg/min)	135	112	121
Glycogenolysis Contribution	79%	71%	75%

release of 1.49 mg/kg·min. If total hepatic glucose output is assumed to be 2.2 mg/kg·min, this corresponds to a 68 percent contribution from glycogenolysis.

Based on the splanchnic balance data presented in Table 14, the relative contributions of gluconeogenic substrates to hepatic glucose output are compiled in Table 15. Data indicate that the lactate released from extrahepatic tissues as a product of anaerobic glycolysis is quantitatively the most important gluconeogenic precursor, the remaining glucose production resulting from glycerol uptake and conversion of amino acids.

Since lactate and pyruvate resulting from anaerobic glycolysis are reincorporated into glucose (the Cori cycle), amino acids represent the most important de novo source of carbon for hepatic glucose production (see Figure 18). Alanine is the primary amino acid precursor for hepatic gluconeogenesis, accounting for roughly 50 percent of the glucose production from amino acid conversion. The primary source for circulating amino acids is proteolysis in skeletal muscle. Muscle tissues release large proportions of glutamine and, to a lesser extent, alanine relative to release of other amino acid entities; however, glutamine removal and conversion to alanine by the nonhepatic splanchnic bed (Wahren et. al., 1972) results in the liver primarily seeing alanine as a gluconeogenic precursor. The net quantitative importance of alanine to total hepatic glucose production is similar to that of circulating glycerols.

4) Time Dependence of Hormonal Action in the Liver

Insulin binds to specific receptor molecules on the plasma membranes of target cells, forming a hormone-receptor complex which stimulates cellular activation (Goldfine, 1978; Roth et al., 1979; Olefsky, 1981). The

TABLE 15. Relative contributions of gluconeogenic precursors to gluconeogenesis and total hepatic glucose production

	% of Gluconeogenesis	% of Total Hepatic Glucose Production
Lactate	54	13
Pyruvate	4	1
Glycerol	13	4
Amino Acids	29	7
(Alanine)	(15)	(4)

effects of insulin on cells are diverse and occur over different characteristic time scales. In general, the effects of insulin may be characterized as follows (Goldfine, 1978): 1) rapid alteration of plasma membrane transport properties that occur within seconds to minutes; 2) intermediate effects on cytoplasmic enzyme activation and protein synthesis that occur within minutes to hours; and 3) delayed mediation of RNA and DNA synthesis that occurs after hours to days. In peripheral tissues, the dominant effect of insulin is to increase glucose transport across the cell membrane (Levine et al., 1950). The liver cell membrane, however, is highly permeable to glucose, resulting in free equilibrium of glucose between plasma and liver intracellular water (Cahill et al., 1958). Thus, insulin mediation of hepatic glucose metabolism must result from alteration of intracellular enzyme functions. The liver is also the site of glucagon action. Like insulin, glucagon binds to specific liver cell membrane receptors (Rodbell, 1972) and exerts its action through effects on intracellular enzyme function (Harper et al., 1979). In view of the above discussion, it would be expected that, whereas insulin action on peripheral tissues is rapid, hormonal effect of insulin and glucagon on the liver are more time dependent. As will be shown, such time dependence is supported by experimental data, and this time dependence of hepatic hormonal action has been included in the model formulation.

5) Hepatic Glucose Production

Hepatic glucose production is mediated by changes in insulin, glucagon, and glucose. These effects were modeled in a multiplicative manner, expressed

$$r_{HGP} = M^{I}_{HGP}\, M^{\Gamma}_{HGP}\, M^{G}_{HGP}\, r^{B}_{HGP} \tag{57}$$

a) Insulin Mediation of Hepatic Glucose Production

Presented in Table 16 are literature data establishing the steady state effects of insulin on the rate of endogenous hepatic glucose production. Data were correlated from literature studies in which tritiated glucose infusions were used to measure endogenous glucose production during euglycemic hyperinsulinemia in normal subjects (Gerich et al., 1981; DeFronzo et al., 1983) and following insulin withdrawal in Type I diabetics (Miles et al., 1980). Normalized rates of glucose production were computed directly from reported basal and steady state values. Liver insulin concentrations were estimated from reported arterial values. For this purpose, the insulin model equations (17-23) were solved at steady state using reported arterial insulin concentrations, correcting basal pancreatic insulin release to account for insulin feedback inhibition observed during euglycemic hyperinsulinemia (Liljenquist et al., 1978; Beischer et al., 1979; DeFronzo et al., 1981c). Data from the euglycemic clamp studies directly reflect the isolated effects of insulin on hepatic glucose production, because plasma glucagon and liver glucose concentrations remained essentially normal in these experiments. The data for insulin withdrawal was more difficult to interpret since arterial glucose and glucagon levels initially increased to roughly 1.5 times their basal levels; nevertheless, the data indicated that hypoinsulinemia roughly doubled the rate of liver glucose production since the effects of increasing glucose and glucagon levels would tend to counteract each other.

Presented in Figure 19 is a plot of normalized rate of hepatic glucose production as a function of normalized liver insulin concentration. Data points in the figure represent results of the clinical studies listed in Table 16. Since the data essentially reflect the isolated effects of

TABLE 16. Literature studies establishing the steady state effects of insulin on the rate of endogenous hepatic glucose production.

Reference	Subjects	Rate of Hepatic Glucose Production (mg/kg/min)		Normalized Rate of Hepatic Glucose Production r^N_{HGP}	Arterial Plasma Insulin Conc. (mU/l)		†Normalized Liver Plasma Insulin Conc, I^N_L
		Basal	Steady		Basal	Steady	
Miles, et al., 1980	7[a]	2.38	4.3[b]	1.81	19	10[b]	0.53
Gerich et al., 1981	6	2.0[c]	0.80	0.40	11[c]	27	1.3
			0.50	0.25		42	1.9
			0.03	0.02		96	4.0
DeFronzo et al., 1983	4	2.27[c]	0.73	0.32	12[c]	37	1.6
	3		0.31	0.14		53	2.2
	6		0.05	0.02		101	3.8

[a]Type I Diabetics
[b]Mean Response over 2 h Quasisteady Period Following Insulin Withdrawal
[c]Mean Basal Value for all Subjects

†Estimated on the basis of changes in arterial plasma insulin concentration as predicted by solution of the insulin model equations at steay state (see text).

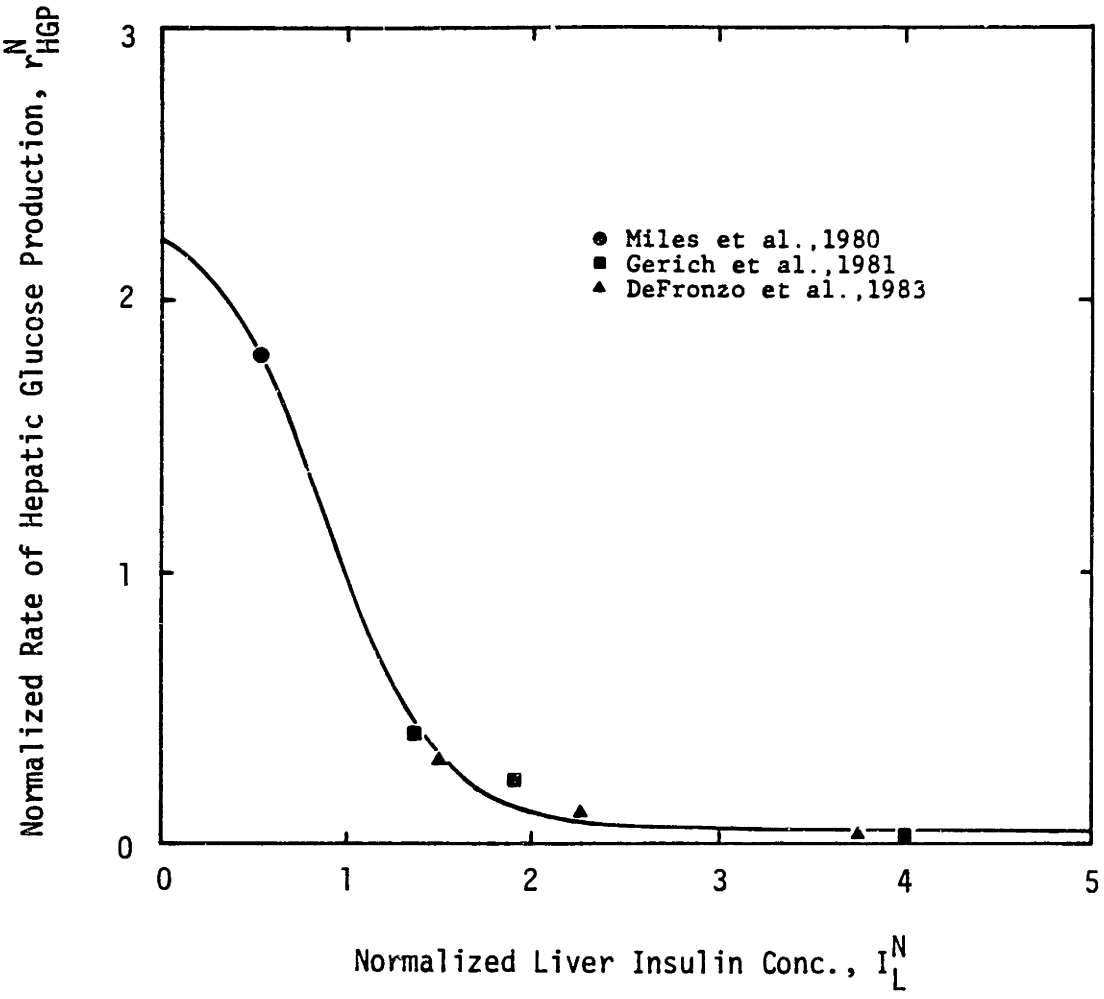

Fig. 19 Plot of normalized rate of hepatic glucose production as a function of normalized liver insulin concentration. The solid curve shows the model function for the steady state effect of liver insulin concentration on glucose production rate (Equation 58).

changes in liver insulin concentration on the rate of hepatic glucose production ($M^{\Gamma}_{HGP} = M^{G}_{HGP} = 1$ in Equation 57), the steady state insulin multiplier function of hepatic glucose production rate was determined by assuming a hyperbolic tangent form and adjusting the function parameters to obtain a least squares fit to the data in Table 16 and Figure 19. The resulting function

$$M^{I\infty}_{HGP} = 1.21 - 1.14 \tanh[1.66(I^{N}_{L} - 0.89] \tag{58}$$

is shown by the solid curve in Figure 19. The superscript ∞ has been included in Equation 58 to indicate that this the steady state effect of insulin. The shape of the curve below a normalized liver insulin concentration of about 0.5 is somewhat arbitrary, but the data of Miles et al. (1980) is the only hypoinsulinemic data available for quantification in this region. A rough approximation over hypoinsulinemic ranges is adequate for modeling purposes, however, since hypoinsulinemia is never observed to any appreciable extent in normal man.

The data presented in Figure 19 indicate the steady state effect of insulin on hepatic glucose production. The time course of insulin action will now be considered. Application of the euglycemic insulin clamp technique results in a very rapid step increase in arterial insulin concentration (DeFronzo et al., 1979b). Presented in Figure 20 is data of DeFronzo et al. (1983) for the time course of the rate of net splanchnic glucose appearance r_{NSGA} (hepatic venous catheterization technique) following graded euglycemic hyperinsulinemia. Since the net splanchnic glucose uptake rate r_{NSGU} remained approximately constant in these studies (about 0.5 mg/kg·min), the dynamic changes in r_{NSGA} as shown in Figure 20 are a direct indication of the time course of insulin suppression of the

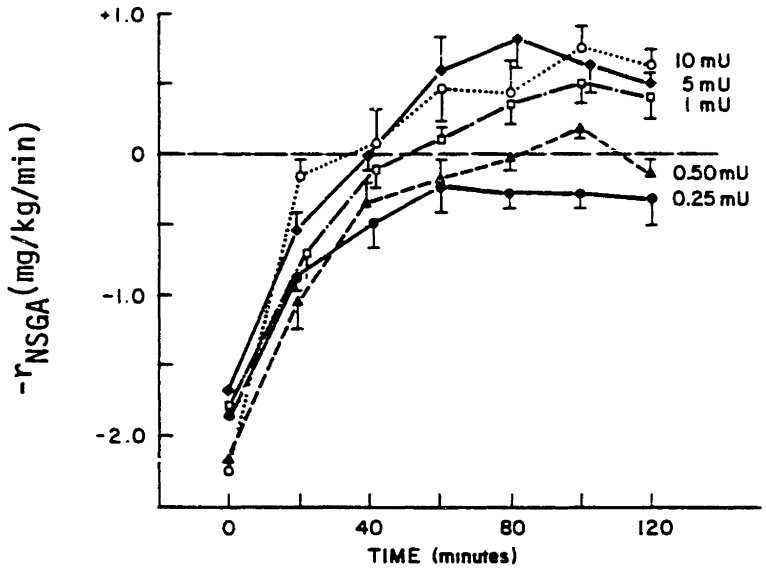

Fig. 20 Data of DeFronzo et al. (1983) for the time course of the rate of net splanchnic glucose appearance, r_{NSGA} (hepatic venous catheterization technique) following graded euglycemic hyperinsulinemia. Numbers annotating curves indicate insulin infusion rates in units of mU/kg/min.

hepatic glucose production rate r_{HGP} following step increases in insulin concentration (see Equation 55). It may be noted that the "steady state" data points presented in Figure 19 are the 60 to 120 min average values following initiation of the euglycemic insulin clamps.

From the time course data of Figure 20 it was inferred that following a step change in insulin concentration, the rate of hepatic glucose production changes from its basal to its steady state value in an exponential manner with time. To test the validity of this hypothesis, it was assumed that the data of Figure 20 could be represented by

$$\frac{r_{NSGA}(t) - r_{NSGA}(\infty)}{r_{NSGA}(0) - r_{NSGA}(\infty)} = \exp[-\frac{t}{\tau_I}] \tag{59}$$

where τ_I is the time constant for the first order process, and the data of Figure 20 was replotted in semilog form as shown in Figure 21. The resulting plot was linear within the scatter of the data, and the slope of the best fit line yielded the time constant as given by

$$\tau_I = -\frac{1}{(\text{slope})} = \frac{1}{(-0.040\ \text{min}^{-1})} = 25\ \text{min} \tag{60}$$

For step changes in liver insulin concentration, Equation 59 is the solution to

$$r_{NSGA}(t) = r_{NSGA}(0) \qquad t < 0 \tag{61}$$

$$\frac{d}{dt}[r_{NSGA}(t)] = \frac{1}{\tau_I}[r_{NSGA}(\infty) - r_{NSGA}(t)] \qquad t > 0 \tag{62}$$

or, normalizing with respect to basal rate

$$r^N_{NSGA}(t) = 1 \qquad t < 0 \tag{63}$$

$$\frac{d}{dt}[r^N_{NSGA}(t)] = \frac{1}{\tau_I}[r^N_{NSGA}(\infty) - r^N_{NSGA}(t)] \qquad t > 0 \tag{64}$$

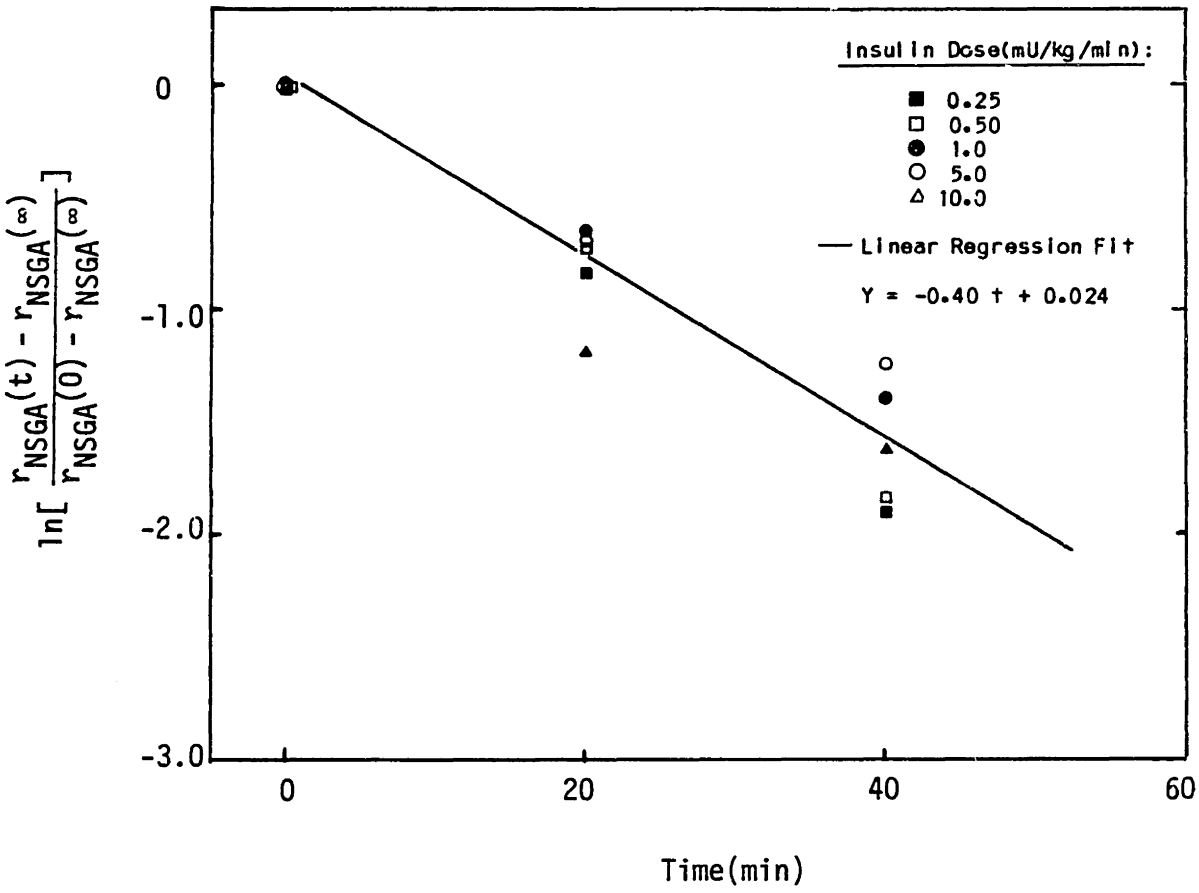

Fig. 21 Replotting of the data of DeFronzo et al. (1983) from Figure 20 in a semilog form for determination of the first order time constant associated with the time dependent effect of insulin step changes on the rate of net splanchnic glucose appearance.

Since the data in Figures 20 and 21 essentially reflect the isolated effects of step changes in liver insulin concentration on the rate of hepatic glucose production ($M^{\Gamma}_{HGP} = M^{G}_{HGP} = 1$ in Equation 57), the above is equivalent to

$$M^{I}_{HGP}(t) = 1 \qquad t < 0 \qquad (65)$$

$$\frac{d}{dt}\left[M^{I}_{HGP}(t)\right] = \frac{1}{\tau_I}\left[M^{I}_{HGP}(\infty) - M^{I}_{HGP}(t)\right] \qquad t \geq 0 \qquad (66)$$

This expression was generalized from step changes to arbitrary changes in liver insulin concentration as a function of time by

$$\frac{d}{dt}\left[M^{I}_{HGP}(I^{N}_{L},t)\right] = \frac{1}{\tau_I}\left[M^{I\infty}_{HGP}(I^{N}_{L}) - M^{I}_{HGP}(t)\right] \qquad (67)$$

subject to the initial condition

$$M^{I}_{HGP}(0) = 1 \qquad (68)$$

where $M^{I\infty}_{HGP}$ from Equation 58 can vary with time as liver insulin levels (I^{N}_{L}) change. Equation 67 together with Equation 58 for $M^{I\infty}_{HGP}(I^{N}_{L})$ give the relationship between liver insulin concentration and its dynamic effect on the rate of hepatic glucose production.

b) Glucagon Mediation of Hepatic Glucose Production

Glucagon is the primary hormone of glucose counterregulation. When blood sugar drops to hypoglycemic levels, circulating glucagon concentration increases, which in turn stimulates hepatic glucose production. Glucagon directly stimulates both glycogen breakdown and gluconeogenesis in the liver (Cherrington et al., 1981). The differential time course of glucagon's effect on these pathways (a rapid transient increase in glycogen breakdown followed by a slow steady increase in the rate of gluconeogenesis) results in a rapid hepatic response which wanes with time. The time course of hepatic glucose production in response to an isolated step change in

liver glucagon concentration has been most definitively studied in the dog where intraportal access is experimentally acceptable. Cherrington et al. (1982) have given somatostatin (to block endogenous pancreatic insulin and glucagon release) plus basal intraportal replacement amounts of insulin and glucagon to conscious dogs. After 2 h, arterial glucose concentrations were raised and maintained constant (hyperglycemic clamp technique). After an hour of hyperglycenic stabilization, the glucagon infusion rate was increased fourfold. Infusion of ^{3}H-glucose was used to measure hepatic glucose production. Mean results for six studies are presented in Figure 22. Of interest here is the data for the time course of hepatic glucose production from 0-240 min, where an isolated step increase in glucagon concentration was introduced at 60 min. Following the glucagon step increase there was a rapid increment in hepatic glucose production, and this incremental effect decreased to roughly half its initial value within 180 min. The reason for introduction of hyperglycemia prior to increasing the glucagon level was to eliminate the changes in glucose concentrations which would have otherwise resulted from the increase in liver glucose production, as the glucose infusion rate could be adjusted so as to maintain steady arterial glucose levels under the chosen experimental conditions (see Figure 22). Together with the ability to independently adjust and maintain liver insulin and glucagon levels, the experiment was carefully designed so as to isolate the singular effects of a glucagon step increase on the in vivo rate of hepatic glucose production.

The time course of the hepatic glucose production rate following a step increase in glucagon concentration in the above studies suggested use of the general mathematical step response representation shown in Figure 23. The step response function was modeled in terms of two component func-

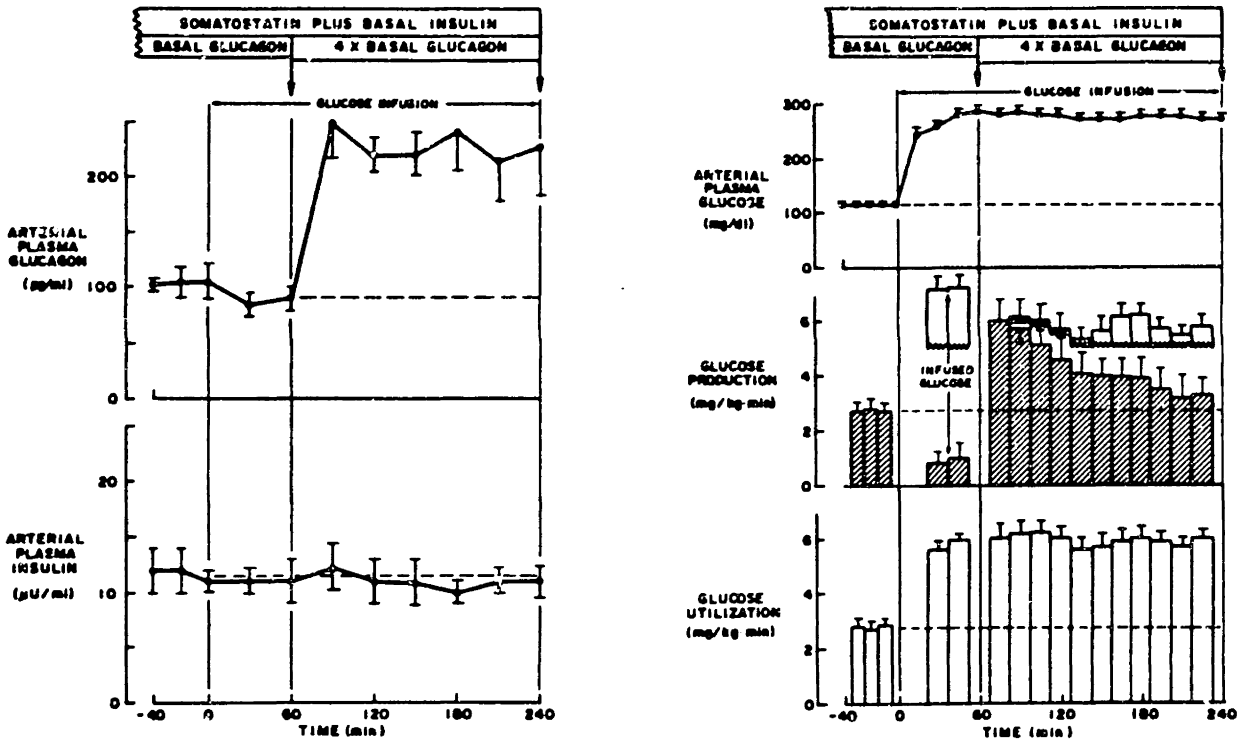

Fig. 22 Data of Cherrington et al. (1982) showing time course of hepatic glucose production in dogs following an isolated step increase in plasma glucagon concentration.

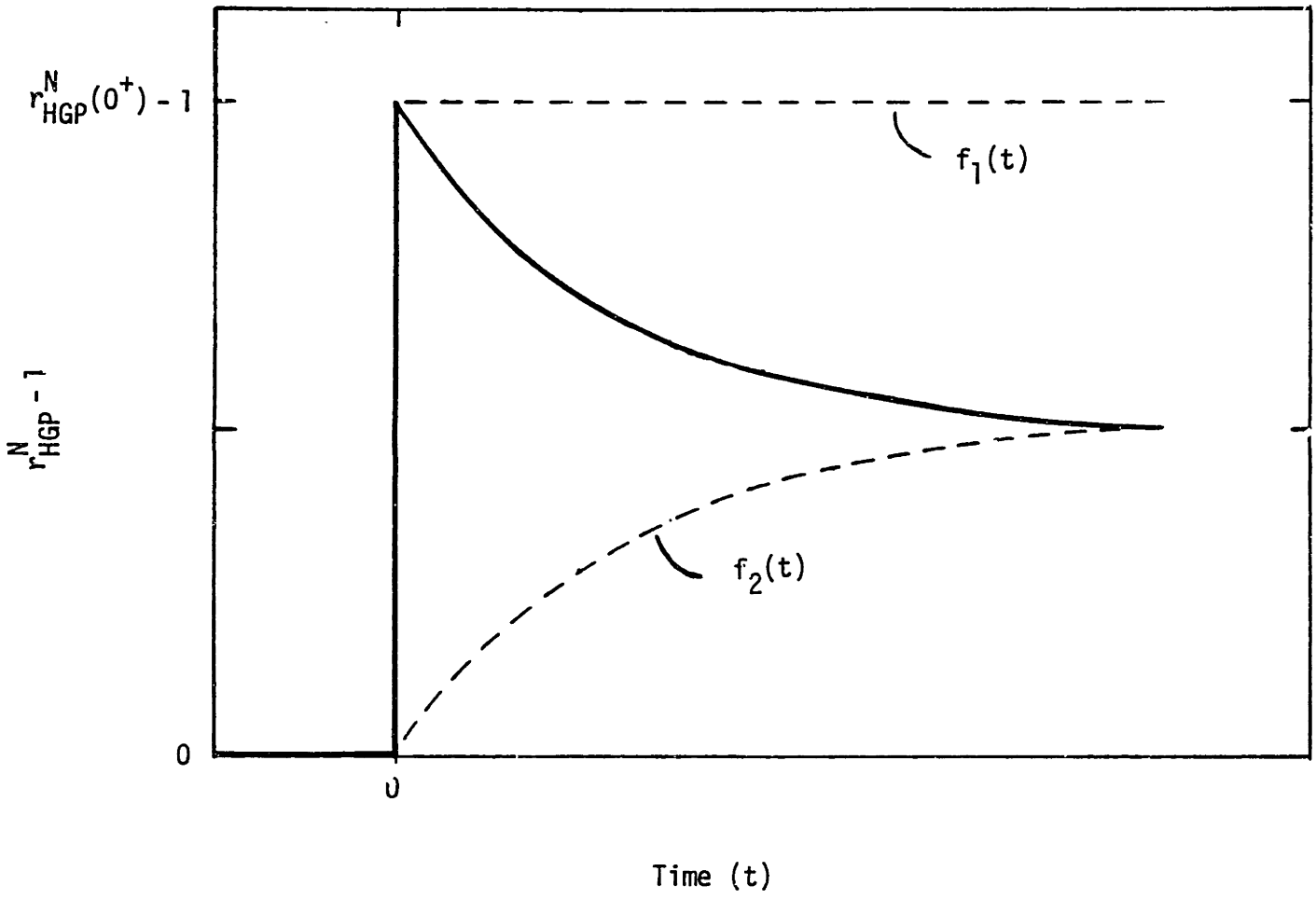

Fig. 23 Normalized time course of hepatic glucose production rate following a step change in glucagon concentration represented by the difference in component functions, $f_1(t)$ and $f_2(t)$.

tions $f_1(t)$ and $f_2(t)$ where, as shown in the figure

$$r^N_{HGP}(t) = 1 \qquad t < 0 \tag{69}$$

$$r^N_{HGP}(t) = f_1(t) - f_2(t) + 1 \qquad t > 0 \tag{70}$$

and

$$f_1(t) = r^N_{HGP}(0^+) - 1 \tag{71}$$

$$\frac{d}{dt}[f_2(t)] = \frac{1}{\tau_\Gamma}\left[\left(\frac{r^N_{HGP}(0^+) - 1}{2}\right) - f_2(t)\right] \tag{72}$$

In these equations, $r^N_{HGP}(0^+)$ equals the initial normalized rate of hepatic glucose production resulting from the glucagon step change. Thus, function $f_1(t)$ provides for the initial maximal effect of glucagon action, and $f_2(t)$ serves to degrade the maximal response to half its initial impact at a rate proportional to the inverse of the first order time constant τ_Γ. Since the solution to Equation 72 is given by

$$\frac{r^N_{HGP}(t) - \left(\frac{r_{HGP}(0^+)-1}{2}\right)}{\left(\frac{r^N_{HGP}(0^+) + 1}{2}\right)} = \exp\left[-\frac{t}{\tau_\Gamma}\right] \tag{73}$$

the data in Figure 22 was replotted in semilog form as presented in Figure 24 for determination of the time constant; linear regression fitting of the data in Figure 24 yielded

$$\tau_\Gamma = -\frac{1}{(\text{slope})} = -\frac{1}{(-0.015\ \text{min}^{-1})} = 65\ \text{min} \tag{74}$$

Since the data of Cherrington et al. (1982) reflect the isolated effects of a step change in liver glucagon concentration on the rate of hepatic glucose production ($M^I_{HGP} = M^G_{HGP} = 1$ in Equation 57), Equations 69-72

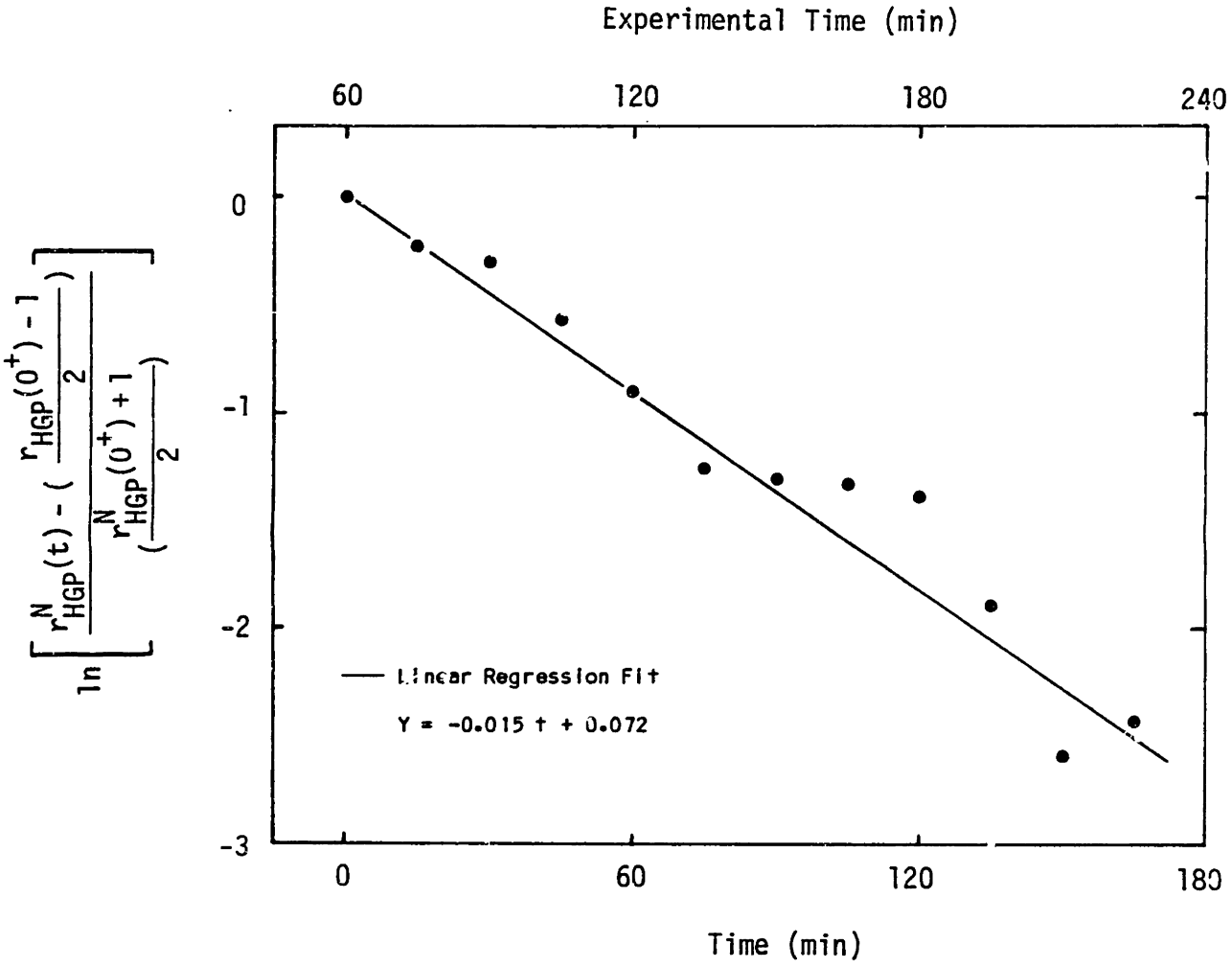

Fig. 24 Semilog replotting of the data of Cherrington et al. (1982) for the time course of the rate of hepatic glucose production following an isolated step increase in plasma glucagon concentration. Upper scale indicates experimental time corresponding to data as presented in Figure 22.

are equivalent to

$$M^{\Gamma}_{HGP}(t) = 1 \qquad t < 0 \tag{75}$$

$$M^{\Gamma}_{HGP}(t) = M^{\Gamma}_{HGP}(0^+) - f_2(t) \qquad t > 0 \tag{76}$$

where

$$\frac{d}{dt}[f_2(t)] = \frac{1}{\tau_\Gamma}\left[\left(\frac{M^{\Gamma}_{HGP}(0^+) - 1}{2}\right) - f_2(t)\right] \tag{77}$$

In the general case, however, plasma glucagon concentration varies as an arbitrary function of time; thus, generalizing the above step change formulations yielded

$$M^{\Gamma}_{HGP}(\Gamma^N,t) = M^{\Gamma o}_{HGP}(\Gamma^N) - f_2(\Gamma^N,t) \tag{78}$$

$$\frac{d}{dt}[f_2(\Gamma^N,t)] = \frac{1}{\tau_\Gamma}\left[\left(\frac{M^{\Gamma o}_{HGP}(\Gamma^N) - 1}{2}\right) - f_2(\Gamma^N,t)\right] \tag{79}$$

subject to the initial condition

$$f_2(0^+) = 0 \tag{80}$$

where the initial effect of glucagon on the rate of hepatic glucose production $M^{\Gamma o}_{HGP}$ has become an arbitrary function of time as plasma glucacon levels Γ^N vary. Equations 78-79 give the relationship between plasma glucagon concentration and its dynamic effect on the rate of hepatic glucose production.

The glucagon formulation was completed by quantifying the initial normalized response of hepatic glucose production rate $M^{\Gamma o}_{HGP}$ as a function of plasma glucagon concentration. This relationship was formulated on the basis of data from various human studies as correlated from the literature in Table 17. Data points in the table were taken from studies of normal subjects in which hepatic glucose production was measured during acute step

TABLE 17. Literature studies relating initial response of hepatic glucose production rate to acute changes in arterial plasma glucagon level.

Reference	Subjects	Rate of Hepatic Glucose Production (mg/min)		Normalized Rate of Hepatic Glucose Production $r^N_{HGP}(0^+)$	Arterial Plasma Glucagon Conc. (pg/ml)		Normalized Liver Plasma Glucagon Concentration r^N
		Basal	Initial Response		Basal	Post Basal	
Felig et al., 1976	6	155	385	2.5	102	403	3.9
Bomboy et al., 1977	4	95	219	2.3	100	450	4.5
Gerich, et al., 1981	8	130[a]	84[a]	0.65	110	70	0.65
	8	126[a]	161[a]	1.3	120	165	1.4

[a]Assuming 70 kg body weight

changes in arterial glucagon concentration induced by glucagon infusion alone (Felig et al., 1976; Bomboy et al., 1977) or glucagon infusion combined with somatostatin and basal replacement of insulin (Gerich et al., 1981). Normalized hepatic glucose production rates were computed from the basal values and the initial peak response following the glucagon step changes. Normalized plasma glucagon concentrations were computed directly from the arterial data. In all of these studies, the initial increments in hepatic glucose production preceded significant changes in the arterial concentrations of either glucose or insulin; thus, the data as presented reflect isolated responses to glucagon changes.

Results of the clinical studies listed in Table 17 are plotted in Figure 25. Since the data reflect the isolated initial effects of acute glucagon changes on the rate of hepatic glucose production at constant normal liver insulin and glucose levels ($M^{I}_{HGP} = M^{G}_{HGP} = 1$ in Equation 57), the glucagon multiplier $M^{\Gamma o}_{HGP}$ was determined by assuming a hyperbolic tangent functionality and adjusting the parameters to obtain a least squares fit to the data in Table 17 and Figure 25. The resulting function

$$M^{\Gamma o}_{HGP} = 2.7 \tanh[0.39\ \Gamma^{N}] \qquad (81)$$

is shown by the curve in Figure 25. Equations 78-79 and 81 give the overall analytical formulation relating plasma glucagon concentration to its dynamic effect on hepatic glucose production rate.

c) Glucose Mediation of Hepatic Glucose Production

The degree to which glucose alone mediates hepatic glucose production is difficult to interpret, especially during hypoglycemia. Presented in Table 18 are data correlated from various human studies reported in the literature. Normalized rates were computed from values of glucose produc-

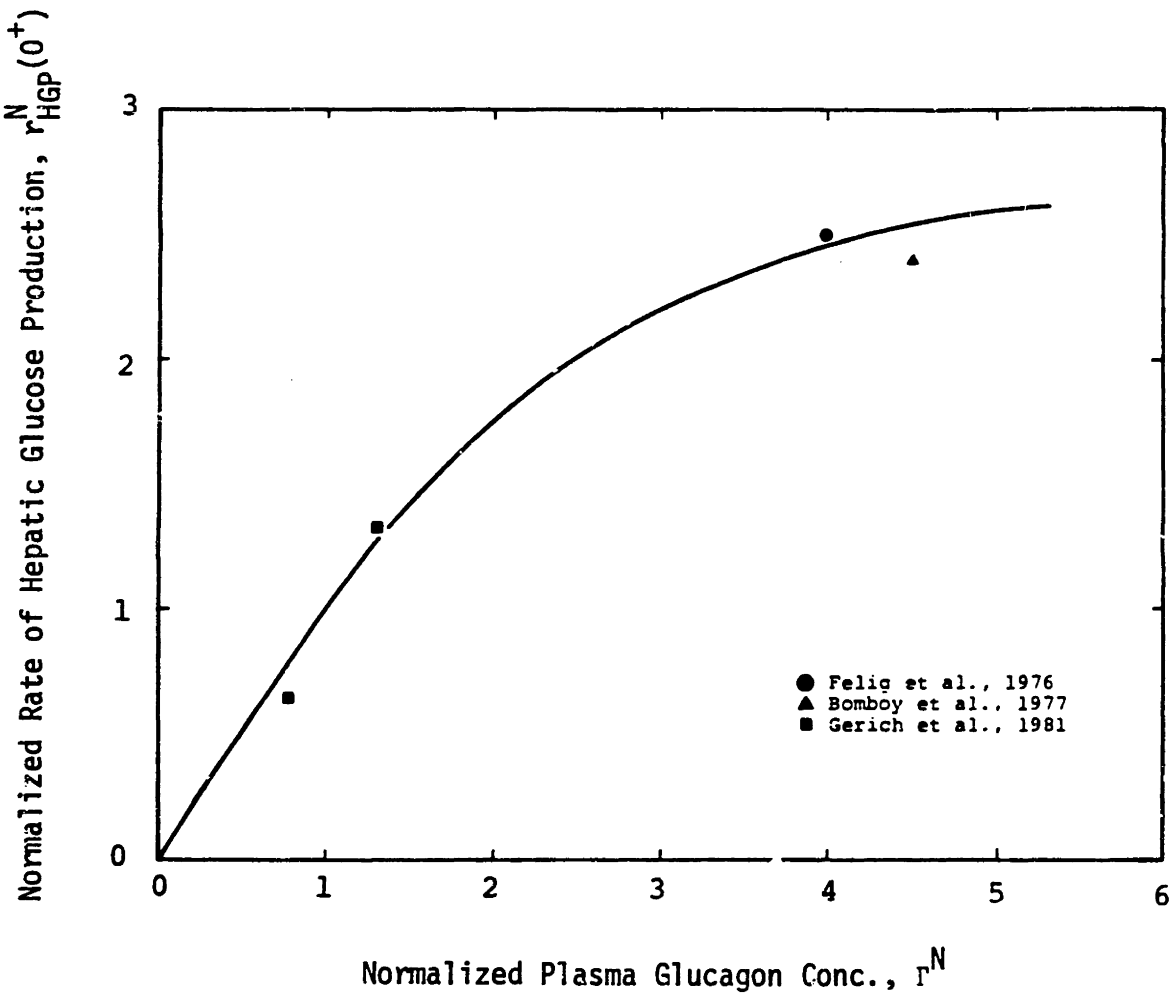

Fig. 25 Plot of normalized initial rate of hepatic glucose production as a function of normalized plasma glucagon concentration. The curve shows the model function for the initial effect of acute plasma glucagon changes on the rate of hepatic glucose production (Equation 81).

TABLE 18. Literature data used to quantify the effect of liver glucose concentration on the rate of hepatic glucose production. Data at hypoglycemic levels have been correlated to account for the effects of simultaneous insulin and glucagon changes which resulted at steady state in these studies.

Reference	Subjects	Rate of Hepatic Glucose Production (mg/kg/min)		Normalized Rate of Hepatic Glucose Production	Arterial Plasma Insulin Conc. (mU/dl)		†Normalized Liver Glucose Concentration
		Basal	Steady	r^N_{HGP}	Basal	Steady	G^N_L
Sacca et al., 1978	6[a]	1.9	0.40	0.21	77[b]	200[b]	2.6
Liljenquist et al., 1979	4	1.8[c]	0.64	0.36	110	225[c]	2.1
Gerich et al., 1981	8	1.8	1.5	0.83	90	65	0.72
	8	1.5[d]	1.8	1.20	90	80	0.89

[a]Type I diabetics receiving constate rate of insulin infusion
[b]Venous plasma glucose values
†Estimated from change in arterial glucose concentration
[c]Mean vlaue for euglycemic control group (N=7)
††Estimate from insulin model steady state mass balances
[d]Reference value taken at stabilized insulin levels

TABLE 18. (Continued) Literature data used to quantify the effect of liver glucose concentration on the rate of hepatic glucose production. Data at hypoglycemic levels have been correlated to account for the effects of simultaneous insulin and glucagon changes which resulted at steady state in these studies.

Reference	Arterial Plasma Insulin Conc. (mU/l)		††Normalized Liver Insulin Conc., I_L^N	Insulin Multiplier of Hepatic Glucose Production Rate M_{HGP}^I	Plasma Glucagon Conc. (pg/ml)		Normalized Plasma Glucagon Conc. Γ^N	Glucagon Multiplier of Hepatic Glucose Production Rate M_{HGP}^Γ
	Basal	Steady			Basal	Steady		
Sacca et al., 1978	-	-	-	-	-	-	-	-
Liljenquist et al., 1979	-	-	-	-	-	-	-	-
Gerich et al., 1981	14	16	1.1	0.81	110	70	0.64	0.83
	18	18	1.0	1.00	110	120	1.2	1.09

tion (measured by hepatic venous catheterization or tritiated glucose infusion) before and after changes in glycemia. Hyperglycemic data was taken from studies in which glycemic levels were acutely elevated in the presence of fixed insulin and glucagon levels by 1) infusion of glucose into Type I diabetics stabilized by constant basal insulin infusion (Sacca et al., 1978), or 2) by infusion of glucose into normals following blockage of endogenous insulin and glucagon secretion with somatostatin infusion (Liljenquist et al., 1979). "Isolated" hypoglycemia cannot be observed directly, because low blood sugar levels must be induced by hypoglucagonemia or hyperinsulinemia. However, relative effects of glucose could be estimated by using the previously determined multiplying factors to correct for the glucagon or insulin contributions to the steady state hepatic glucose production rates. The hypoglycemic data points in the table were correlated from studies in which somatostatin infusion was combined with either basal insulin replacement or basal glucagon replacement with mild hyperinsulinemia (Gerich et al., 1981). It was assumed for all studies that the normalized liver glucose concentration was roughly reflected by the reported changes in systemic arterial glucose concentration; rigorous preliminary analysis using steady state glucose mass balances for the liver indicated that liver glucose concentration seldom varies by more than a few percent from inflowing arterial glucose concentration independent of the rate of endogenous hepatic glucose production.

A plot of the glucose multiplier of hepatic glucose production rate as a function of normalized liver plasma glucose concentration is presented in Figure 26. Data points in the figure were based on the tabulated values in Table 18, where the isolated effects of liver glucose concentration have been estimated for the hypoglycemic data by correcting the normalized hepa-

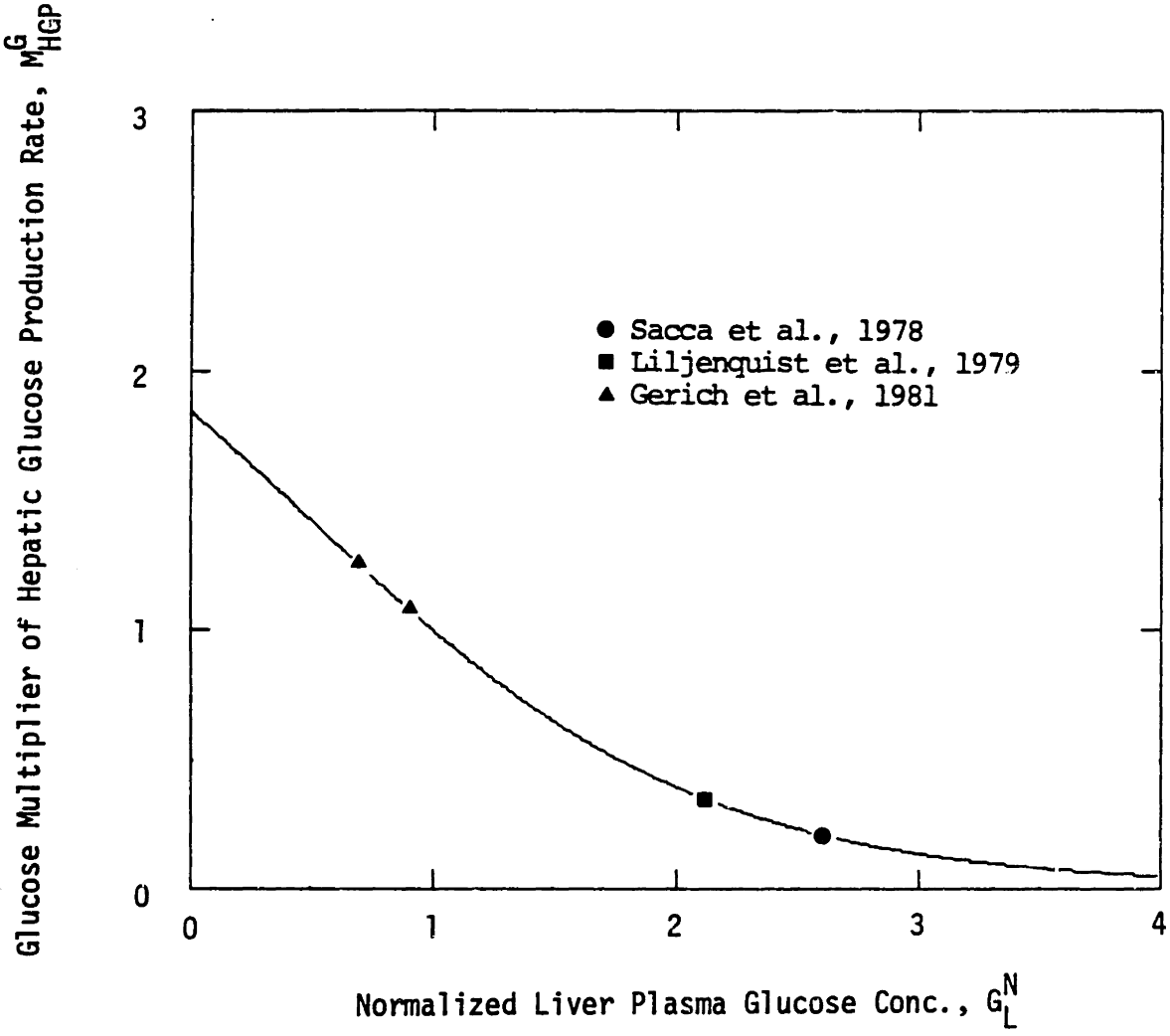

Fig. 26 Plot of glucose multiplier of hepatic glucose production rate as a function of normalized liver plasma glucose concentration. The curve indicates the model function (Equation 82) resulting from a least squares fitting of the data.

tic glucose production rates by the proper insulin and glucagon multipliers (M^{I}_{HGP} and M^{Γ}_{HGP} in Equation 57). A hyperbolic tangent functionality for M^{G}_{HGP} was fit to the data of Figure 26 by least squares optimization, yielding

$$M^{G}_{HGP}\ (G^{N}_{L}) = 1.42 - 1.41\ \tanh[0.620(G^{N}_{L} - 0.497)] \qquad (82)$$

which is shown by the curve in the figure. Although there was insufficient data available for characterizing the precise shape of the curve in the hypoglycemic range, the function fitting procedure gave essentially a linear relationship in this region; this would seem like the most reasonable guess in view of the limited data and should yield acceptable extrapolated predictions down to a hypoglycemic level of about one-half normal. The general validity of the glucose model is questionable at hypoglycemic levels lower than this level anyway because of exclusion of factors such as changes in brain glucose uptake rates and regulation by stress-induced hormones such as epiniphrine which would become imporant at extremely low glycemia.

Presented in Figure 27 is a plot of actual versus predicted values for normalized rate of hepatic glucose production. Date points in the figure represent experimental values employed for quantification of the insulin, glucagon, and glucose mediation effects, and predicted values were calculated from Equation 57 using the model multiplier functions. Good agreement was obtained between model predictions and experimental data over the entire range of normalized hepatic glucose production rates.

6) Hepatic Glucose Uptake

Liver is the only site of mediated glucose uptake aside from muscle. Thus, hepatic glucose uptake is important to overall glucose tolerance, especially following oral ingestion. Hepatic uptake of glucose is mediated

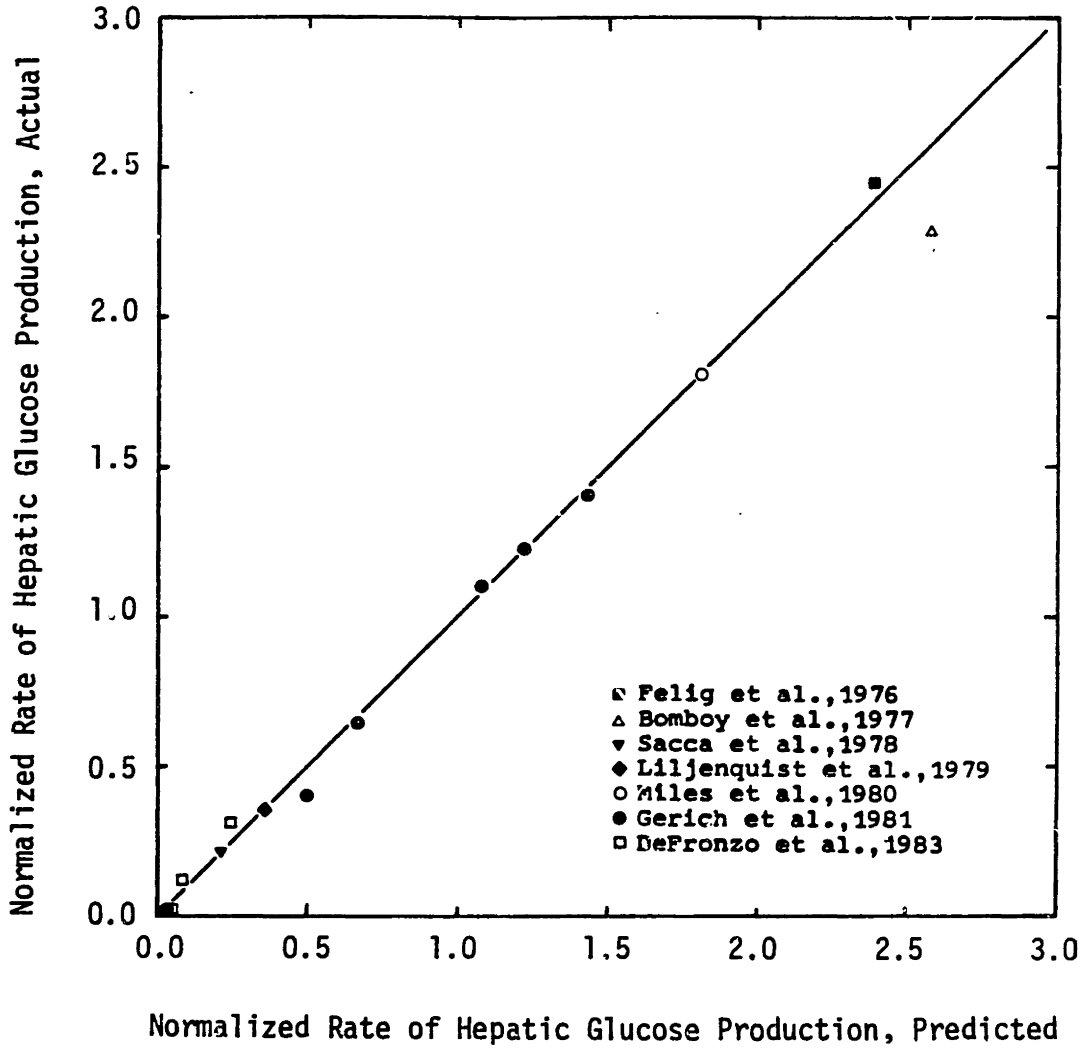

Fig. 27 Plot of actual versus predicted values for normalized rate of hepatic glucose production.

by changes in liver insulin and glucose concentration, modeled

$$r_{HGU} = M^{I}_{HGU} M^{G}_{HGU} r^{B}_{HGU} \tag{83}$$

where, as previously discussed, the basal rate of uptake is 20 mg/min.

The interactions of glucose and insulin in regulating liver uptake of glucose have been extensively studied. Considerable controversy has arisen over the relative importance of portal vein insulin in the control of hepatic glucose uptake. Some investigators (Madison, 1969; Felig and Wahren, 1971) have promoted the view that insulin rather than glucose provides the dominant stimulus for hepatic uptake of glucose. This opinion has been formulated on the basis of studies demonstrating the inability of glucose infusions to induce hepatic glucose uptake in portacaval shunted diabetic dogs (Madison et al., 1963) and the observation that hyperglycemic diabetics maintain normal or elevated hepatic glucose output which, during infusion of glucose, is not suppressed as in normal subjects (Wahren et al., 1972). It should be noted that dogs used in the former study were rendered diabetic (by partial pancreatectomy and alloxan) at least three weeks prior to investigation (Madison et al., 1960). Thus, the evidence cited above reflects the response of livers subjected to the diabetic state for prolonged periods of time prior to study. This is an important consideration in view of the mounting evidence that hepatic response to glucose is impaired by chronic insulin deficiency. Bishop (1970) has reported that glucose administration fails to activate glucose synthetase in pancreatectomized dogs. In studies of extracts from alloxan diabetic rats, Gold (1970) has demonstrated that several hours of insulin exposure can reverse impairment of glucose synthetase phosphatase activity and increase glycogen formation. Diminished response to glucose has also been observed in the

perfused liver (Whitton and Hems, 1975) and isolated hepatocytes (Katz et al., 1979) of alloxan diabetic rats. Insulin is also required for the maintenance of normal intracellular glucokinase levels (Sols et al., 1964). In addition, recent studies have shown that intensive insulin therapy can restore normal glucose tolerance in Type I diabetics (Foss et al., 1982) through reactivation of the hepatic component of the glucose disposal system (Aoki et al., 1983).

More than 40 years ago Soskin et al. (1938) observed a reciprocal relationship between hepatic glucose output and blood glucose concentration following dextrose administration in dogs, thus establishing the classical view that glucose provides the major stimulus for liver glucose uptake (Soskin, 1940). By the early 1970's, results of extensive studies with animal livers had clearly demonstrated the capacity of insulin to inhibit hepatic glucose release, but definitive evidence suggesting any significant effect of insulin on hepatic glucose uptake remained elusive (for review, see Mortimore, 1972). A series of systematic studies (Bergman and Bucolo, 1973; Bucolo et al., 1974; Bergman and Bucolo, 1974) has since been undertaken to determine the relative contributions of glucose and insulin in the control of hepatic glucose balance. In these experiments, isolated puppy livers were cross-perfused with blood from large adult dogs (pilot-liver technique of Urquhart and Keller, 1971). In this system, source dogs provided blood with constant basal levels of glucose and insulin, to which additional quantities were added to produce controlled increments in the portal concentrations perfusing the isolated livers. A summary of results from these studies is presented in Table 19. Reported values for the rate of net hepatic glucose appearance r_{NHGA} were determined by measurements of flow rates and glucose concentration differences across the perfused

TABLE 19. Effects of portal glucose and insulin levels on the steady state glucose balance across the isolated, blood-perfused canine liver. (Data taken from Bucolo et al., 1972 and Bergman and Bucolo, 1972)

Number of Studies	Portal Vein Increment		Steady State NHGB (mg/min/100 g Liver)
	Glucose (mg/dl)	Insulin (mU/l)	
6	0	0	+ 3.6 ± 2.0
5	70	0	- 5.0 ± 1.3
7	140	0	-10.3 ± 1.6
2	210	0	-14.1 ± 0.5
4	0†	500	- 1.0 ± 1.5
6	140	500	- 9.5 ± 2.6
7	140	200††	-20.8 ± 2.3

†Portal glucose decreased due to hyperglycemia in source dog.

††Insulin preinfused for 90 min.

livers; since measurements were made across the liver,

$$r_{NHGA} = r_{HGP} - r_{HGU} \quad (84)$$

and the contributions of gut metabolsm as reflected by in vivo splanchnic balances were excluded (compare Equation 54 for r_{NSGA}). In control studies (no glucose or insulin infusion), livers released glucose at a mean output rate of 3.6 mg/min•100g liver. Incrementing portal glucose over a range of 70 to 210 mg/dl in the presence of basal insulin resulted in rapid suppression of glucose output and stimulation of uptake, demonstrating direct glucose autoregulation. In the reverse situation, however, raising portal insulin by 500 mU/l in the presence of basal glucose suppressed hepatic production but failed to stimulate any significant uptake. Finally, the effects of insulin on glucose-stimulated uptake were examined. When portal glucose was incremented 140 mg/dl together with a simultaneous insulin increment of 500 mU/l, hepatic uptake was not significantly different than that observed for the glucose stimulation alone. However, when insulin was incremented 200 mU/l for 90 min prior to addition of a 140 mg/dl glucose increment, glucose uptake was almost exactly double that observed for the isolated glucose stimulation.

Results of the canine liver perfusion studies suggest that glucose provides the primary signal for glucose uptake, and that insulin serves to modulate the glucose-stimulated response. Furthermore, the insulin mediation appears to be time dependent and can be quantitatively significant, capable of doubling the glucose-stimulated response within physiologic portal insulin levels.

Since portal measurements are not available in human studies, the hepatic glucose uptake rate cannot be determined directly. Instead, com-

bined application of hepatic vein catheterization and isotope dilution techniques provides an experimental measure of the rate of net splanchnic glucose uptake r_{NSGU} as previously discussed (see Equation 55), and from Equation 56

$$r_{HGU} = r_{NSGU} - r_{GGU} + r_{OGA} \tag{85}$$

The rate of hepatic glucose uptake can thus be determined from Equation 85 given appropriate estimates for the contributions of gut to the net splanchnic glucose uptake rate. As discussed earlier with respect to basal liver metabolism, the rate of gut glucose uptake constitutes about 50% of the net rate of splanchnic glucose uptake in the basal state,

$$r^B_{GGU} = 0.5\ r^B_{NSGU} \tag{86}$$

and, as will be shown later, the rate at which gut tissues remove glucose for utilization as fuel remains essentially constant. Therefore, substituting the above expression into Equation 85,

$$r_{HGU} = r_{NSGU} - 0.5\ r^B_{NSGU} + r_{OGA} \tag{87}$$

For intravenous studies, the rate of oral glucose absorption is zero, and Equation 87 was normalized to yield

$$r^N_{HGU} = \frac{r_{NSGU} - 0.5\ r^B_{NSGU}}{r^B_{NSGU} - 0.5\ r^B_{NSGU}} = 2\ (r^N_{NSGU}) - 1 \tag{88}$$

which was employed to calculate normalized hepatic glucose uptake rates from net aplanchnic glucose uptake rate data in the literature. For correlation of data from oral glucose studies, Equation 87 was averaged over the total time required for gut absorption of the oral glucose load (T_A),

$$\frac{1}{T_A}\int_0^{T_A} r_{HGU}(t)dt = \frac{1}{T_A}\int_0^{T_A} [r_{NSGU}(t) - 0.5\, r^B_{NSGU} + r_{OGA}(t)]\, dt \quad (89)$$

$$\text{or} \quad \bar{r}_{HGU} = \bar{r}_{NSGU} - 0.5\, r^B_{NSGU} + \bar{r}_{OGA} \quad (90)$$

where overbars have been used to indicate time-averaged values. The reason for time averaging was to allow estimation of the oral glucose absorption rate term by

$$\bar{r}_{OGA} = \int_0^{T_A} r_{OGA}(t)\, dt = \frac{\text{Oral Glucose Dose}}{T_A} \quad (91)$$

Substituting into Equation 90 and normalizing with respect to basal uptake yielded

$$\bar{r}^N_{HGU} = \frac{\bar{r}_{NSGU} - 0.5\, r^B_{NSGU} + \dfrac{\text{Oral Glucose Dose}}{T_A}}{r^B_{NSGU} - 0.5\, r^B_{NSGU}} \quad (92)$$

and this expression was used to calculate mean normalized rates of hepatic glucose uptake following oral glucose administration.

Presented in Tables 20 and 21 are human data correlated from various intravenous and oral studies, respectively. For intravenous studies, Equation 88 was employed to calculate normalized rates of hepatic glucose uptake from reported net splanchnic glucose uptake rate data. Liver glucose concentrations were estimated using arterial concentrations and splanchnic glucose appearance data; under quasi-steady conditions (see Equation 53)

$$G_L = G_H - \left(\frac{r_{NSGA}}{Q^G_L}\right) \quad (93)$$

which upon normalization yields

TABLE 20. Correlation of hepatic glucose uptake data taken from intravenous glucose loading studies in the literature.

Reference	Subjects	Rate of Net Splanchnic Glucose Uptake, r_{NSGU} (mg/kg/min)		Normalized Rate of Hepatic Glucose Uptake † r^N_{HGU}	Arterial Plasma Glucose Conc. (mg/dl)		Normalized Liver Glucose Conc. †† G^N_L	Arterial Plasma Insulin Conc. (mU/l)		Normalized Liver Insulin††† Conc., I^N_L
		Basal	Steady		Basal	Steady		Basal	Steady	
DeFronzo et al., 1978	2[a]	0.5[a]	1.1	3.4	96	223	2.1	11	191	16
DeFronzo et al., 1983	3[b]	0.52	0.47	0.81	97	137	1.3	11	20	1.8
	5[b]	0.52	1.27	3.9	99	224	2.0	11	55	5
	3[b]	0.52	0.63	1.4	99	224	2.1	15	10	0.6
	6[b]	0.52	0.46	0.77	94	92	0.86	15	101	6.3
	3[b]	0.52	1.02	2.9	97	222	2.0	15	40	1.2

[a]Based on data for r_{NSGA} assuming r^B_{HGP} = 2.2 mg/kg/min (DeFronzo et al., 1981) and r_{HGP} = 0 at steady state due to insulin suppression

†Calculated from Equation 88

††Calculated from Equation 94

†††Estimated on the basis of changes in arterial plasma insulin concentration as predicted by solution of the insulin model equations at steady state.

[b]Mean basal value for entire study group

TABLE 21. Correlation of hepatic glucose uptake data taken from oral loading studies in the literature.

Number of Studies	Oral Glucose Load (g)	Absorption Time, T_A (min)	r^B_{HSU} (mg/min)	Average Values Over Absorption Time				$\bar{r}^N_{HGU}$	Total Splanchnic Uptake (% Oral Load)	Reference
				$\bar{r}_{NSGA}$ (mg/min)	$\bar{r}_{HGP}$ (mg/min)	$\bar{r}^*_{OGA}$ (mg/min)	$\bar{r}^{**}_{HGU}$ (mg/min)			
10	100	180	22	- 220	0	555	312	14.2	60	Felig et al., 1975
3	95.5	217	13†††	- 273	40	440	194	14.9	47	Radziuk et al., 1978
10	100	180	18	- 287	0	555	251	13.9	48	Ferrannini et al., 1980
4	70†	210	19†††	- 198	67	333	183	9.6	61	Pilo et al., 1981
22	100	240	18	- 285	0	416	113	6.3	31	Katz et al., 1983

† Oral Load of 1 g/kg body weight

†† r^B_{HGU} = 15 percent of r^B_{NSGA} (DeFronzo et al., 1981)

††† r^B_{HGU} = 11 percent of r^B_{HGP} (DeFronzo et al., 1981)

* $r_{GGA} = \frac{\text{oral glucose load}}{\text{absorption time}}$

** Computed from Equation 90, and noting that $\bar{r}_{NSGU} = \bar{r}_{NSGA} - \bar{r}_{HGP}$

TABLE 21. Correlation of hepatic glucose uptake data taken from oral loading studies in the literature. (Continued)

Reference	Arterial Plasma Glucose Conc. (mg/dl)		Normalized Liver Glucose Conc.,†	Arterial Plasma Insulin Conc. (mU/l)		Normalized Liver Insulin Conc.,††
	Basal	Time Averaged	$\bar{G}_L^N$	Basal	Time Averaged	$\bar{I}_L^N$
Felig et al., 1975	95[a]	150[a]	1.7	6	35	6
Radziuk et al., 1978	100	140	1.6	b	b	-
Ferrannini et al., 1980	100	147	1.5	b	29	-
Pilo et al., 1981	100	150	1.6	b	b	-
Katz et al., 1983	90[a c]	135[a c]	1.5[c]	14	70	5

[a]Assuming: (Plasma Glucose Conc) = (1.10)(Blood Glucose Conc.)

[b]Insulin Data not Reported

[c]Computed directly from reported heptatic venous glucose concentrations

†Computed from time averaging Equation 94 over absorption time T_A

††Estimated on basis of changes in arterial plasma insulin concentration as predicted by solution of insulin model equations at steady state.

$$G_L^N = \frac{G_H - \left(\frac{r_{NSGA}}{Q_L^G}\right)}{G_H^B - \left(\frac{r_{NSGA}^B}{Q_L^G}\right)} \qquad (94)$$

Normalized liver insulin concentrations were estimated from reported arterial plasma values using the steady state insulin model equations as previously described for correlation of the hepatic glucose production rate data of Table 16. For oral glucose studies, normalized hepatic glucose uptake rates averaged over the time required for absorption of the oral load were computed from Equation 92. Values of normalized liver glucose concentration were approximated by averaging Equation 94 over the absorption time, except for the study of Katz et al. (1983) for which hepatic venous glucose concentrations were reported and could be averaged directly. Normalized liver insulin concentrations were estimated as for the case of intravenous studies except that the arterial plasma insulin concentrations were time averaged over the absorption period. No insulin data were reported by Radziuk et al. (1978), Ferrannini et al. (1980), and Pilo et al. (1981), but, based on similar studies, normalized values of about 5 were assumed.

Presented in Figure 28 is a plot of normalized rate of hepatic glucose uptake as a function of normalized liver glucose concentration. Data points in the figure correspond to results of the intravenous (solid symbols) and oral (open symbols) studies correlated in Tables 20 and 21, respectively. Values in parentheses indicate normalized liver insulin concentrations.

The data of Figure 28 are difficult to interpret and demonstrate the

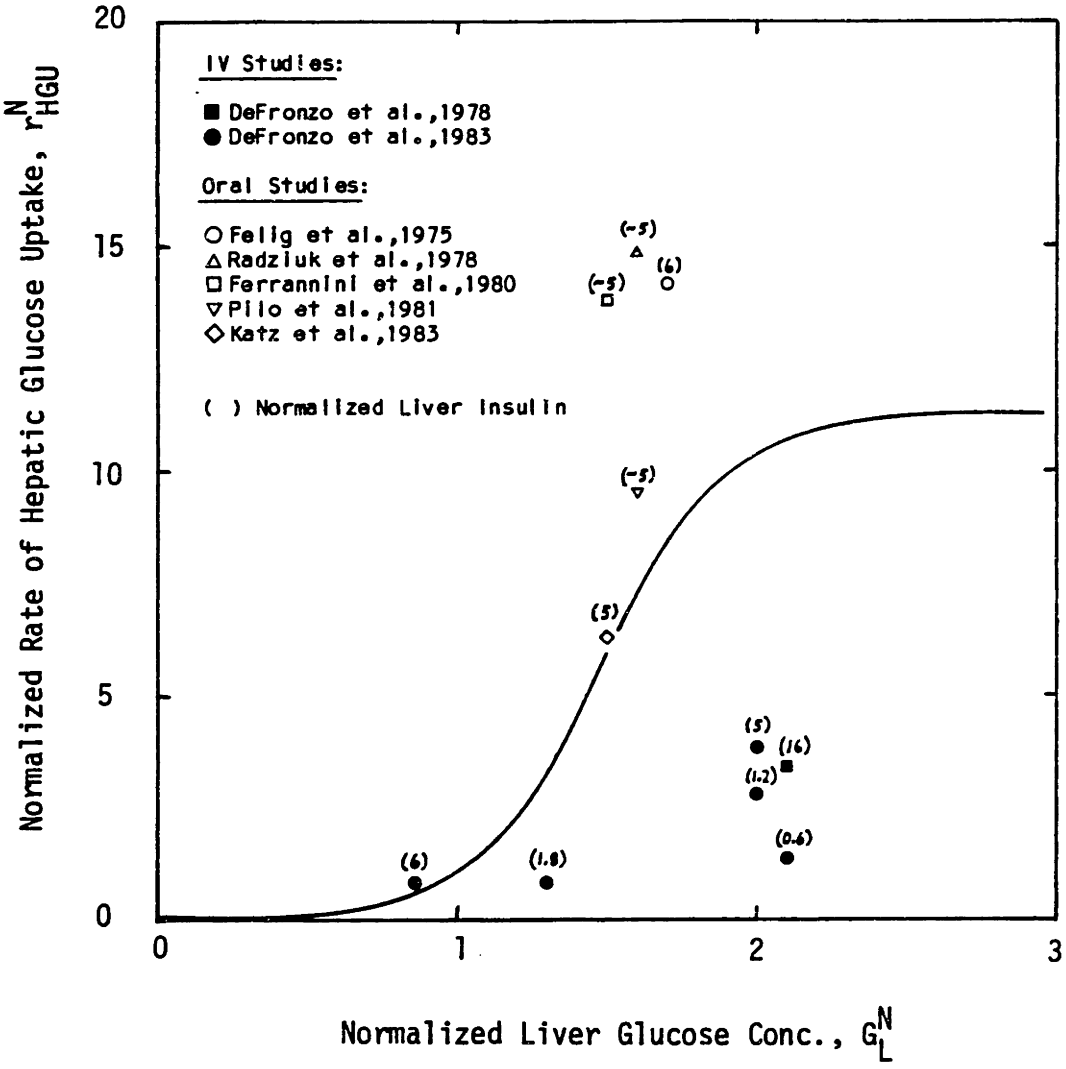

Fig. 28 Plot of normalized hepatic glucose uptake rate as a function of normalized liver glucose concentration. The curve indicates the model function for the effect of liver glucose on uptake rate of glucose (Equation 97).

reasons why much controversy has surrounded discussion of hepatic glucose uptake. First, scatter in the human data has not provided a basis for assessing the direct effect of insulin on hepatic glucose uptake. Second, reported values of total splanchnic uptake following oral glucose have ranged from about 30 to 60 percent of the ingested load (see Table 21). Further complicating the situation is the observation that measured rates of hepatic glucose uptake in response to intravenous glucose have been significantly lower than those reported during oral loading.

In order to model hepatic glucose uptake, it was first assumed on the basis of the isolated canine liver perfusion studies that insulin exposure doubles the rate of hepatic glucose uptake within a physiologic range of insulin concentrations. Since this effect is time dependent, it was formulated in a manner similar to that of insulin mediation of hepatic glucose production. The asymptotic effect of liver insulin concentration on the rate of hepatic glucose uptake was given by

$$M_{HGU}^{I\infty} = 2 \tanh[0.55\ I_L^N] \tag{95}$$

and the time dependent insulin multiplier was obtained by substituting this expression into (see Equation 67)

$$\frac{d}{dt}\left[M_{HGU}^{I}(I_L^N,t)\right] = \frac{1}{\tau_I}\left[M_{HGU}^{I\infty}(I_L^N) - M_{HGU}^{I}(t)\right] \tag{96}$$

Equation 95 states that elevating the liver insulin concentration above about three times normal will eventually double the rate of hepatic glucose output according to the time dependence of Equation 96.

Having established a formulation for mediated glucose uptake in peripheral tissues, preliminary model simulations were run to investigate quantification of hepatic glucose uptake. The standard 0.5 g/kg body

weight Intravenous Glucose Tolerance Test (IVGTT) was employed for these simulation studies. The IVGTT was selected for two reasons: 1) following the rapid (3 min) infusion which acutely increases plasma glucose levels, mediated glucose uptake by muscle and liver quickly disposes of the exogenous glucose, and thus the time course for the decrease in plasma glucose concentration is sensitive to these uptake rates; and 2) because of the rapid insulin dynamics, the time dependent effect of insulin on hepatic glucose uptake (Equations 95 and 96) is minimal, and thus the hepatic contribution disposal is dominated by the effects of glucose mediation. For these simulations, pancreatic insulin release as a function of time was adjusted and fixed such that plasma insulin concentrations predicted by the model agreed closely with experimental data over the time course of the IVGTT; in this manner it could be assumed that all insulin concentrations were at their proper levels independent of changes in glycemia resulting from adjustment of metabolic functions in the glucose model. Finally, a hyperbolic tangent functionality was assumed for the effect of liver glucose concentration on hepatic glucose uptake rate, and parameters in the function were adjusted by least squares fitting of model predictions to experimental data for peripheral blood glucose concentrations following IVGTT administration. The resulting function,

$$M^{G}_{HGU} = 5.66 + 5.66 \tanh[2.44(G^{N}_{L} - 1.48)] \qquad (97)$$

is shown by the curve in Figure 28. This equation, together with the insulin multiplier function of Equation 95 predict the hepatic glucose uptake data of Tables 20 and 21 and Figure 28 as shown in Figure 29.

To date, the discrepancy between data for orally and intravenously stimulated hepatic glucose uptake has not been explained. Noting the dif-

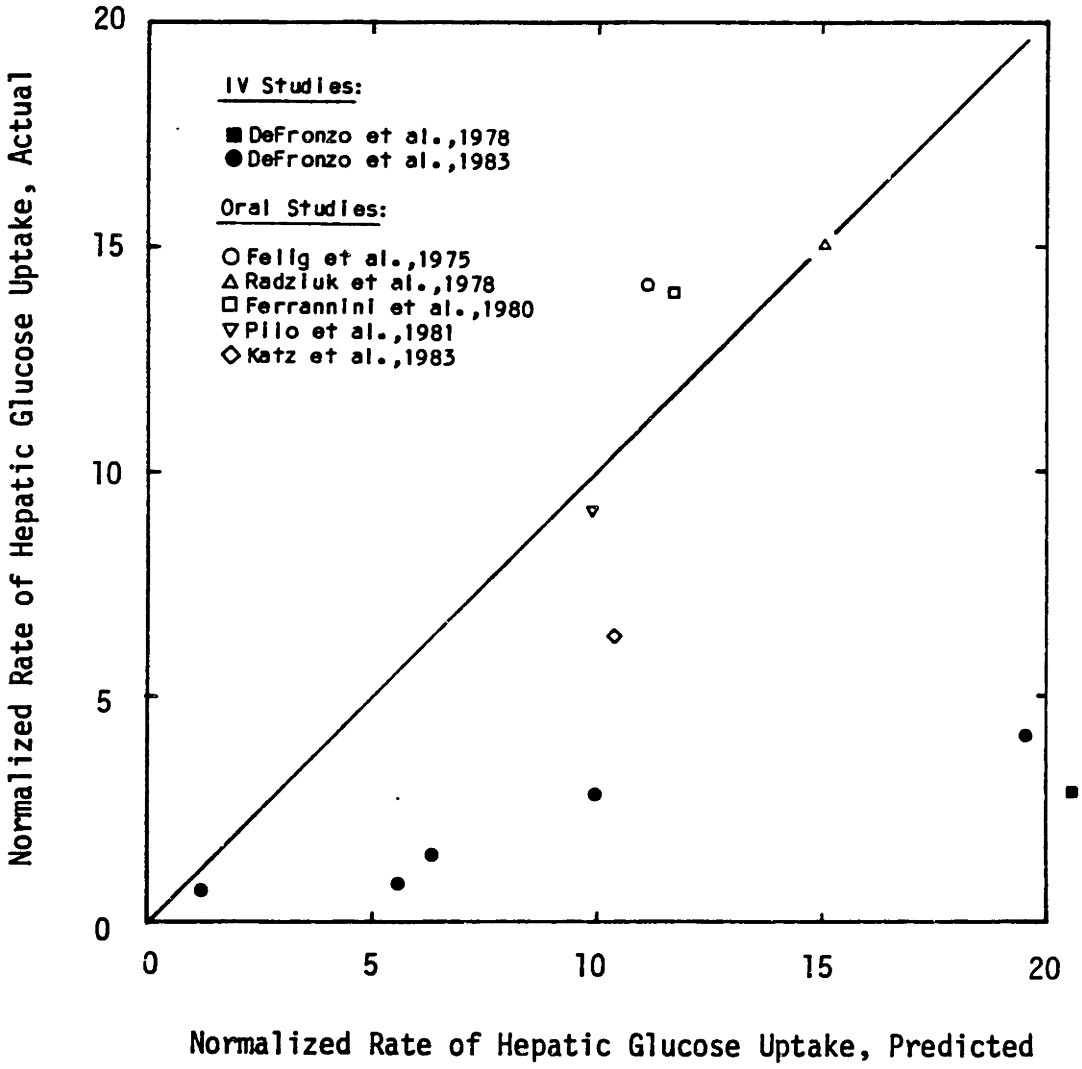

Fig. 29 Plot of actual versus predicted values for the rate of hepatic glucose uptake.

ference resulting from the route of glucose administration, DeFonzo et al. (1978) first suggested that orally consumed glucose may cause release of a gastrointestinal factor that enhances insulin-mediated glucose uptake by the liver. This idea has been challenged on the basis of results obtained in the dog (Bergman et al., 1982); when intraportal glucose and insulin infusions were used to match the temporal patterns observed in the portal vein during oral loading, there was no significant difference between the uptake of intravenous and oral glucose. It is interesting to note from Figure 29 that fitting of intravenous data (IVGTT) resulted in a model function which yielded predicted liver glucose uptake rates of various glucose and insulin levels that corresponded to data from the oral loading studies in the literature, supporting the notion that intravenous and oral glucose are processed by the liver in the same way. However, it should be emphasized that the model liver functions cannot predict the low levels of glucose uptake that have been reported during intravenous stimulation. It is worth mentioning that if such low uptake rates actually occur in response to intravenous glucose, some form of oral gut factor augmentation would be required on the basis of normal daily liver glycogen turnover considerations. During postabsorptive periods, the liver releases glucose at a rate of about 155 mg/min to provide for the fuel requirements of the extrahepatic tissues (primarily brain). Since glycogen breakdown accounts for roughly 80% of basal hepatic glucose output, or 124 mg/min, liver glycogen stores are depleated at a rate of about 7.5 g/hr during fasting. The highest total splanchnic uptake rate reported during intravenous stimulation was about 1.3 mg/kg·min (DeFronzo et al., 1983), or 90 mg/min, and thus even total conversion of this glucose to liver glycogen (an overestimate) would only provide about 5.5 g/hr. These estimates clearly

indicate that hepatic glycogen deposition during postprandial periods (about 10 h/day) must normally occur at a much higher rate than suggested by intravenous data in the literature.

The disposal of glucose is dominated by liver and muscle uptake when glycemia exceeds its normal level. Furthermore, it is the effect of peripheral interstitial insulin concentration that predominantly regulates the rate of peripheral tissue glucose uptake, and it is the changes in liver glucose concentration that primarily regulate the hepatic glucose uptake rate. Thus, there is a balance between the model functions for these glucose disposal processes (M^{I}_{PGU} for periphery and M^{G}_{HGU} for liver) such that their underlying contributions sum to produce observed glucose tolerance. Having established a function for peripheral glucose uptake sensitivity on the basis of forearm studies, hepatic glucose uptake rate sensitivity was quantified by parameter adjustment during simulation of an IVGTT because human data for the liver contained to much scatter for direct assessment. The model is quite sensitive to changes in either of the dominant glucose uptake functions, but there is a compensating symmetry between the peripheral and liver uptake functions which can always combine to give the observed glucose tolerance during an IVGTT. This is shown in the simmulation studies of Figures 30 and 31. In these studies, the parameter adjustment methods employed for fitting of the liver glucose uptake rate formulation on the basis of IVGTT simulations were repeated, but the peripheral glucose uptake rate was arbitrarily increased and decreased from normal sensitivity to insulin as shown in the upper panel of Figure 30. These changes in peripheral glucose uptake sensitivity when combined with the normal liver glucose uptake function caused deviations between model predictions and clinical data for blood glucose levels during an IVGTT as

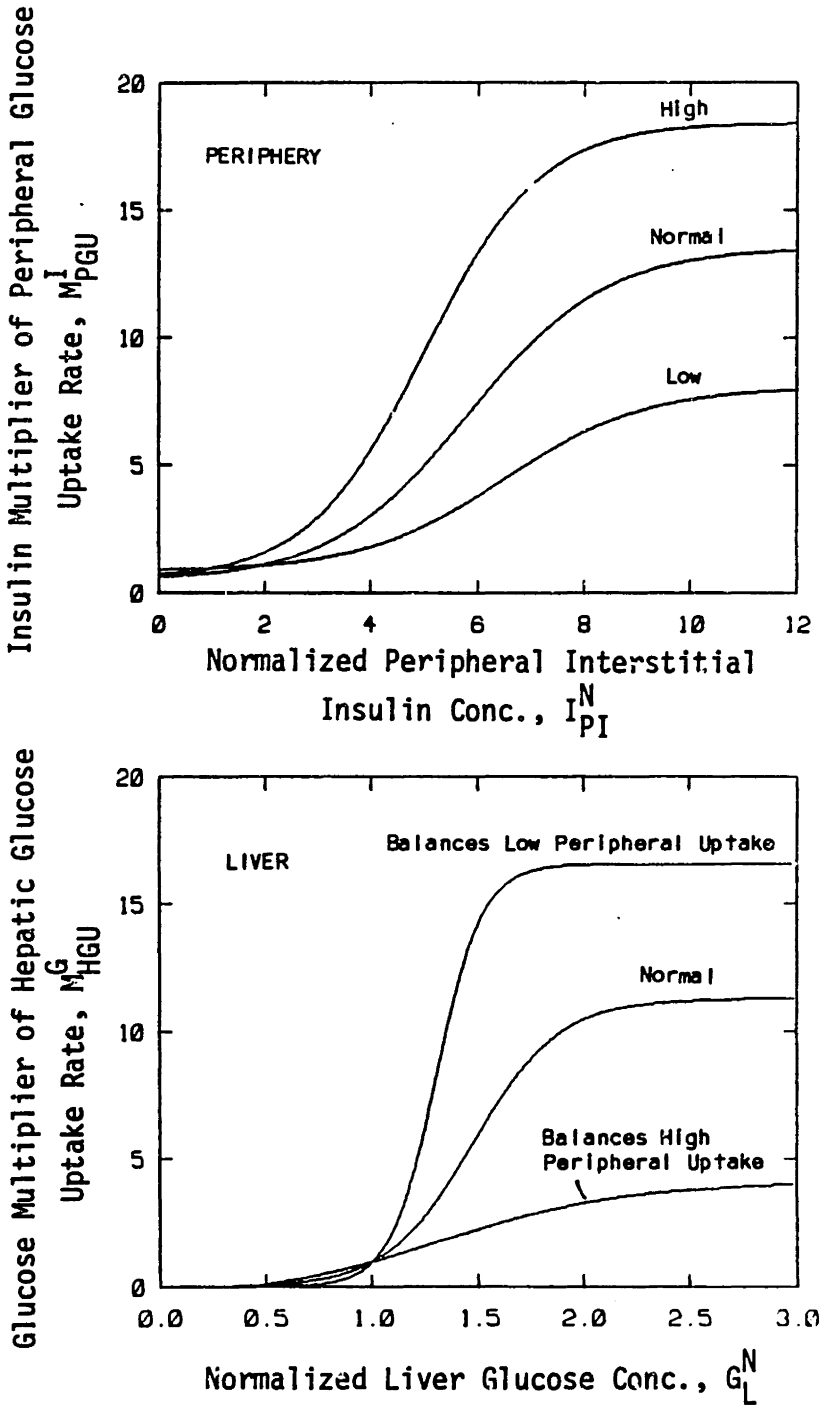

Fig. 30 Symmetry between peripheral and liver glucose uptake rate functions required to produce observed glycemic levels during a standard 0.5 g/kg body weight 3-min IVGTT (see Figure 31).

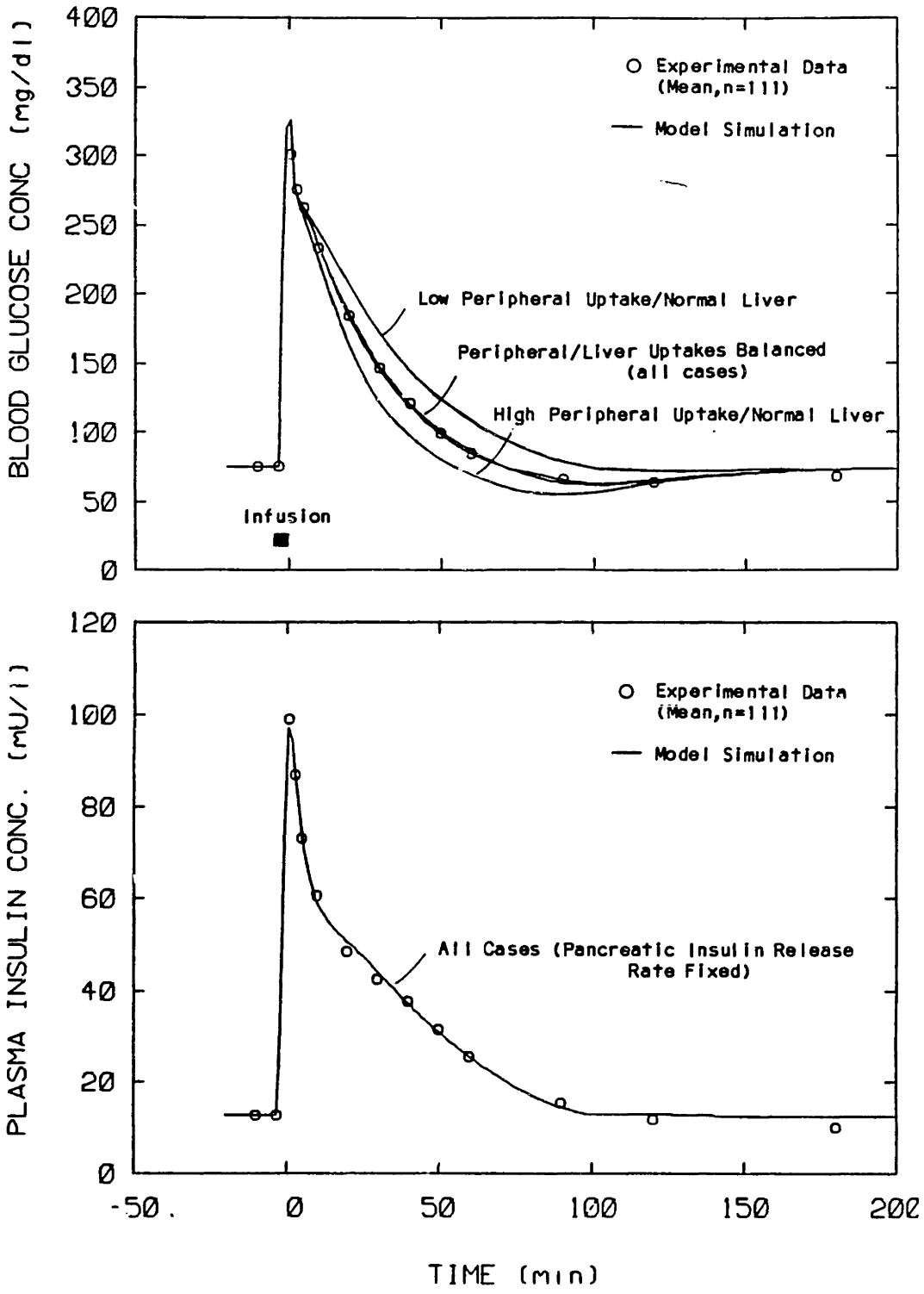

Fig. 31 Plots of peripheral venous blood glucose and plasma insulin concentrations as a function of time for a standard 0.5 g/kg body weight 3-min IVGTT. Upper panel shows effects of raising and lowering peripheral glucose uptake sensitivity of model with and without compensation of liver glucose uptake sensitivity (see Figure 30). (Data from Joslin Research Laboratory for normal adult males.)

shown in the upper plot in Figure 31; however, readjustments of the liver uptake function (least squares refitting of Equation 97) to compensate for changes in the peripheral sensitivity restablished agreement between model predictions and the IVGTT data. The liver glucose uptake functions that reestablished the balance between peripheral and hepatic glucose uptake are shown in the lower plot of Figure 30. Results of these simulation studies clearly demonstrate the nonuniqueness problems that occur in attempting to quantify nonlinear metabolic processes by fitting data that reflect simultaneous balances in their respective contributions. In the glucose model, the relative roles of liver and peripheral glucose uptake were uniquely established only because peripheral glucose uptake rate could be quantified independently from forearm studies, although the resulting liver formulation yielded good predictions of the available data for hepatic glucose uptake following oral glucose administration. In the model, however, there is a relatively delicate balance between the normal liver and peripheral uptake functions, and model performance quickly degrades if either of these functions is altered without appropriate compensation in the conjugate function.

Since peripheral glucose uptake is dominated by changes in insulin levels and liver glucose uptake is primarily regulated by liver glucose levels, the in vivo interplay between these modes of glucose disposal are interesting to examine. Because ingested glucose must pass through the liver prior to entering the systemic circulation, the efficiency of the liver in disposing of the incoming glucose is inversely related to elevation of circulating glucose levels. As arterial glucose concentration rises, however, insulin is released by the pancreas and the subsequent rise in circulating insulin levels signals the peripheral tissues in turn to

dispose of the excess glucose which has escaped from the liver.

I) Gut Glucose Uptake

As previously discussed, under basal conditions the extrahepatic splanchnic tissues (gastrointestinal tract, pancreas, and spleen), primarily the gut, metabolize glucose at a rate of about 20 mg/min. In the fasted state, the primary fuel requirements of gut tissues are derived from glutamine and ketone body metabolism (Windmueller and Spaeth, 1980). Portal catheterization studies in dogs (Barrett et al., 1980) have shown a significant step increase in alanine and lactate from artery to portal vein, suggesting that a large fraction of the glucose taken up by gut tissues is converted to three carbon compounds. Results from in vivo studies of rat small intestine metabolism (Windmueller and Spaeth, 1980) have supported this conclusion, indicating that only about 10 percent of the glucose extracted under basal conditions is oxidized.

Glucose utilization by gut tissues appears to be relatively insensitive to postprandial stimulations. In the fed state, both gut lumenal and arterial glucose becomes available to gut tisues, and circulating insulin levels increase. Windmueller and Spaeth (1980) have shown that arterial glutamine remains the most important energy source for gut tissues in the fed rat, and that only about 3 percent of the gut lumenal glucose is metabolized during transport across the intestine. For modeling, gut glucose utilization was assumed insensitive to changes in glucose and insulin levels, and the rate of gut glucose uptake r_{GGU} was assigned a constant value of 20 mg/min.

J) Glucose Transcapillary Diffusion Time Constants

Since reliable values of glucose concentration in cerebrospinal fluid

were available in the literature, the transcapillary diffusion time constant for the brain compartment was estimated directly. The brain compartment glucose mass balance equations (9 and 10) at steady state give

$$0 = Q_B^G (G_H - G_{BV}) - \frac{V_{BI}}{T_B} (G_{BV} - G_{BI}) \tag{98}$$

$$0 = \frac{V_{BI}}{T_B} (G_{BV} - G_{BI}) - r_{BGU} \tag{99}$$

Solving Equation 99 for brain vascular glucose concentration

$$G_{BV} = G_{BI} + \frac{T_B \, r_{BGU}}{V_{BI}} \tag{100}$$

and substituting into Equation 98 yields upon rearrangement and simplification

$$T_B = \frac{V_{BI}}{r_{BGU}} (G_H - G_{BI}) - \frac{V_{BI}}{Q_B^G} \tag{101}$$

Pryce et al. (1970) have correlated measurements of cerebrospinal fluid glucose concentrations for 89 normal males and reported a mean fasting value of 55.9 mg/dl. Assuming a fasting arterial plasma glucose concentration of about 90 mg/dl and substituting values into Equation 101 yielded an estimated brain transcapillary diffusion time constant of 2.1 min.

Direct, reliable measurements of peripheral interstitial glucose concentrations are not available, thus the transcapillary diffusion time constant required estimation by indirect means. This was done by model simulation. For a rapid intravenous infusion of glucose, the initial time course of vascular glucose is determined by the balance between 1) the rate at which glucose enters the circulation by infusion, and 2) the rate

at which glucose leaves the circulation by dispersion into the peripheral interstitial fluids. Presented in Figure 32 is a plot of peripheral blood glucose concentration as a function of time for the initial period of a standard IVGTT (0.5 g glucose per kg body weight infused over 3 min). Data points represent mean ± SEM values correlated from 111 studies of normal males performed at the Joslin Research Laboratory. Lines in the figure illustrate the effect of varying the peripheral transcapillary diffusion time constant on the simulated time course of blood glucose concentration. The solid lines result from fixing all glucose metabolic rates at their basal values in the glucose model. The dashed lines result from elevating all of the mediated glucose metabolic uptake rates to their maximum values upon initiation of the glucose infusion. It can be seen from the figure that the initial simulated time course was sensitive to changes in the value of the peripheral transcapillary diffusion time constant, and comparison between solid and dashed lines shows the relative insensitivity of these results to changes in the rate of metabolic clearance of glucose. Based on the simulation studies presented in Figure 32, a value of 5 min was selected for the peripheral transcapillary diffusion time constant T_P^G. This value is in good general agreement with results of studies on the rate of glucose diffusion from blood into dog hind limb lymph following IVGTT administration (Rasio et al, 1968); these results were difficult to interpret due to the transient nature of the experiment but suggested an equilibration time constant on the order of 5 min.

K) Insulin Distribution in the Blood

The red blood cell membrane is impermeable to insulin; thus, unlike glucose, insulin is only distributed thoughout the plasma volume of whole

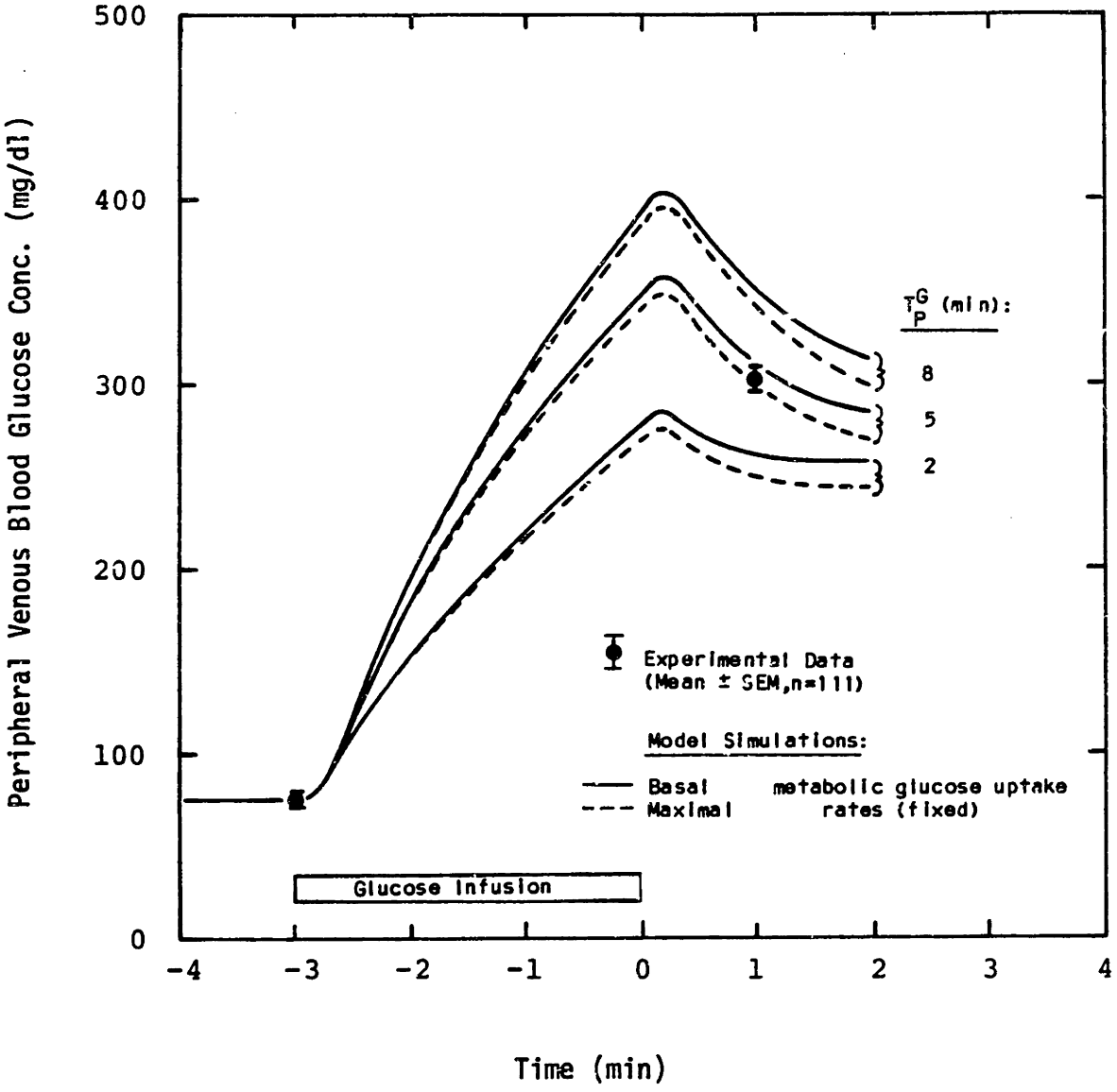

Fig. 32 Simulation studies showing the effect of varying the peripheral glucose transcapillary diffusion time constant (T_P^G) on model predictions for the initial time course of blood glucose concentration during a standard 0.5 g/kg body weight 3-min IVGTT. (Data from Joslin Research Laboratory for normal adult males.)

blood. The measured hematocrit of normal male blood, based on the volume of packed red cells, is 0.45 liters per liter of whole blood (Harper et al., 1979). The average body hematocrit is approximately 87 percent of the measured hematocrit (Guyton, 1976) because: 1) packed red blood cell volume is a nonideal measure of hematocrit as a small quantity of plasma becomes entrained in the interstices of the packed cell matrix, and 2) axial streaming of red blood cells during flow through the smaller vessels would reduce the total average in vivo hematocrit value. Therefore, the average body hematocrit for a normal male is about 0.40 liters per liter.

Although red blood cells are insulin insensitive with respect to glucose metabolism, insulin binds to specific plasma membrane receptors of erythrocytes (Kappy and Plotnick, 1979). It is thus important to consider the extent to which RBC receptor binding may act as a reversible buffer for insulin storage and release. The buffering capacity of red blood cells can be estimated from the binding data reported by Kappy and Plotnick (1979); presented in Figure 33 is a plot of insulin bound to RBC's as a function of plasma insulin concentration. The ordinate has been normalized with respect to the number of RBC's normally contained in 1 ml whole blood (about 3.6×10^9 RBC's/ml). For a fasting plasma insulin concentration of 15 μU/ml, one milliliter of whole blood would contain roughly 9 μU of free insulin in plasma and 1.1 μU of insulin bound to RBC's. During a standard intravenous or oral glucose tolerance test, plasma insulin concentration peaks at about 100 μU/ml; at this maximum, one milliliter of whole blood would contain roughly 60 μU plasma insulin and 4.4 μU bound insulin. Therefore, to increase plasma insulin concentration from 15 μU/ml to 100 μU/ml would require the addition of 54.3 μU/ml whole blood, of which only 3.3 μU (6%) would bind to RBC's. Based on this estimation, neglect of RBC

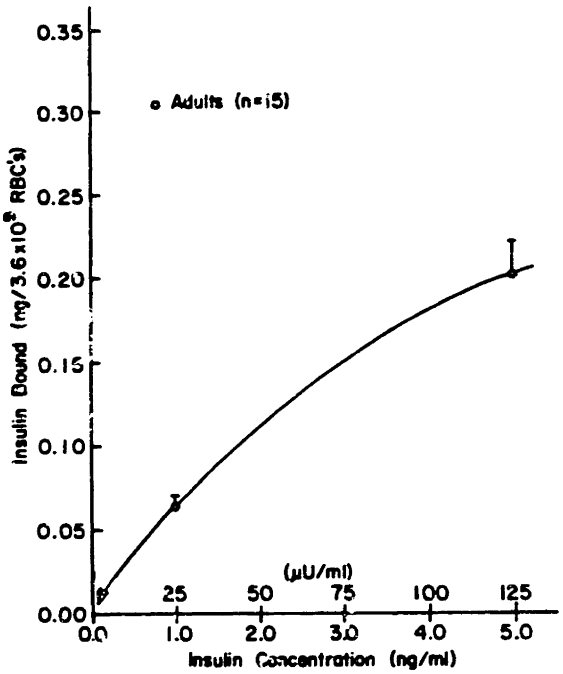

Fig. 33 Total insulin specifically bound to red blood cells as a function of insulin concentration in surrounding medium. (Adapted from Kappy and Plotnick, 1979.)

buffering capacity in the model introduces at most a 6% error into calculaion of plasma insulin concentration. Since no data is available for determining the time course of reversible RBC binding (data points in Figure 33 represent steady state values), and since the maximum error is quantitatively small, no correction for RBC binding was introduced into the model.

For the insulin model, it was assumed that insulin is uniformly distributed in the plasma volume of whole blood. Since the average red blood cell content of whole blood is about 40 volume percent, the blood volumes and flow rates as estimated for a 70 kg man (Table 6) were reduced by 40 percent for insulin modeling. The resulting vascular parameter values as incorporated into the insulin model are included in Table 22.

L) Insulin Clearance

The primary sites of insulin clearance are the liver and kidney, with a smaller contribution by peripheral tissues. Insulin clearance results from a degradation process that occurs at the target tissue plasma membrane and is associated with binding of insulin to a degrative enzyme complex (Kahn, 1979). It is possible that degradation is linked in some manner to insulin receptor binding, but this relationship is unclear at present (Terris and Steiner, 1975; Duckworth, 1979).

1) Liver Insulin Clearance

Harding et al. (1975) have studied hepatic insulin clearance in anesthetized dogs using intraportal insulin infusions. In 14 dogs, basal clearance averaged 42 ± 20 percent of the insulin presented to the liver, and the percentage of insulin cleared did not change when intraportal insulin infusions were increased tenfold, elevating the portal insulin con-

TABLE 22. Vascular volumes and flow rates used in insulin model. (Based on whole blood plasma)

Organ or Tissue	Vascular Flow Rate† (l/min)	Vascular Equilibration Volume (l)
Brain	0.42	0.25
Heart and Lungs	(3.12)	0.98
Liver	0.90	0.54
Gut	(0.72)	0.43
Kidney	0.72	0.41
Periphery	1.08	0.75
(Hepatic Artery)	(0.18)	-
TOTAL	3.12	3.36

†Entries in parentheses represent redundant flows and are thus excluded in total sum value

centration from 50 to 500 mU/l. Madison and Kaplan (1958) have injected insulin-I^{131} into the portal veins of 15 patients undergoing abdominal surgery. Based on arterial insulin concentrations measured 10 seconds later, they have estimated that about 50 percent of the insulin presented to the liver is cleared during a single transhepatic passage. Samols and Ryder (1961) have studied the hepatic clearance of insulin in humans by measuring the arteriohepatic insulin concentration differences in patients with portal-systemic shunts. In four subjects, basal hepatic insulin clearance averaged 41 percent, and in two subjects, elevation of arterial insulin levels to 250 mU/l by infusion of exogenous insulin did not result in any significant change in the percentage of insulin clearance.

Both glucagon and glucose may affect hepatic insulin clearance (Field et al., 1980). Rojomark et al. (1978) have reported that simultaneous infusion of insulin and glucagon into dogs results in a significant decrease in the fraction of insulin cleared by the liver. Studies of insulin clearance in the perfused rat liver (Terris and Steiner, 1976; Honey and Price, 1979), however, have shown no effect of glucagon variation. Kadcn et al. (1973) have reported that intraduodenal glucose administration significantly increases the percentage of insulin cleared in the dog liver. This conflicts with the rat liver perfusion results of Honey and Price (1979) which indicate a significant drop in insulin clearance as a result of increasing glucose concentration. To date, results of animal studies are inconclusive, and further experimentation will be required to characterize the effects, if any, of glucagon and glucose on hepatic insulin clearance.

For the insulin model formulation it was assumed that, within physiologic limits, the liver clears 40 percent of the insulin presented to it

independent of plasma insulin levels. This was expressed

$$r_{LIC} = F_{LIC}[Q_A^I I_H + Q_G^I I_{GV} + r_{PIR}] \quad (102)$$

where the fractional clearance of insulin by the liver F_{LIC} equals 0.40.

2) Kidney Insulin Clearance

Chamberlain and Stimmler (1967) have studied the renal handling of insulin by comparing insulin levels in arterial blood, renal venous blood, and urine in normal subjects before and after an oral glucose load. Their results indicate that the kidney clears about 30 percent of the insulin presented to it independent of the arterial insulin concentration, and that less than 2 percent of the insulin filtered at the glomerulus is excreted into the urine.

In the insulin model, the kidney was assumed to clear 30 percent of the insulin presented to it independent of the arterial insulin level. This was given by

$$r_{KIC} = F_{KIC}[Q_K^I I_H] \quad (103)$$

where the fractional clearance of insulin by the kidney F_{KIC} equals 0.30.

3) Peripheral Insulin Clearance

The clearance of insulin by peripheral tissues has been studied by measuring arteriovenous insulin concentration differences across human forearm and leg. Presented in Table 23 is a summary of results compiled from the literature. Included in the table for each study is a value for the percentage of insulin cleared which is representative of the data collected over the indicated arterial insulin concentration range. A

TABLE 23. Peripheral tissue insulin clearance data compiled from the literature.

Reference	Study	Arterial Insulin Concentration Range (mU/l)	% Insulin Clearance
Butterfield et al., 1963	Forearm	100 - 1400	13
Samols & Ryder, 1961	Leg	15 - 230	10
Razio et al., 1972	Forearm	5 - 60	30
Jackson et at., 1973	Forearm	10 - 80	15
Kalant et al., 1979	Forearm	5 - 250	23
Fineberg & Schneider, 1982	Forearm	80 - 330	43

review of the available literature indicates that peripheral tissues are observed to clear a relatively constant percentage of the insulin presented to them, but that the reported value for this percentage varies over a wide range from study to study. Whether this is an artifact of experimental technique or an indication of large individual variability is uncertain.

For the insulin model, it was assumed that 15 percent of the insulin presented to peripheral tissues is cleared, which was expressed

$$r_{PIC} = F_{PIC}\, Q_P^I\, I_H \tag{104}$$

where the fractional clearance of insulin by peripheral tissues F_{PIC} equals 0.15. From a physiologic standpoint, however, it was desirable to formulate peripheral insulin clearance as a function of the peripheral interstitial fluid insulin concentration, since insulin is actually removed from the interstitial fluid space by binding and subsequent degradation on the tissue cell membrane. Under psuedo-steady conditions, the peripheral insulin mass balance formulations (Equations 22 and 23) give

$$0 = Q_P^I\,(I_H - I_{PV}) - \frac{V_{PI}}{T_P^I}\,(I_{PV} - I_{PI}) \tag{105}$$

$$0 = \frac{V_{PI}}{T_P^I}\,(I_{PV} - I_{PI}) - r_{PIC} \tag{106}$$

It thus follows from these expressions and Equation 104,

$$r_{PIC} = 0.15\, Q_P^I\, I_H = Q_P^I(I_H - I_{PV}) = \frac{V_{PI}}{T_P^I}\,(I_{PV} - I_{PI}) \tag{107}$$

from which the arterial and peripheral vascular insulin concentrations were eliminated to yield the desired relationship,

$$r_{PIC} = \frac{I_{PI}}{\left[\left(\frac{1 - F_{PIC}}{F_{PIC}}\right)\left(\frac{1}{Q_P^I}\right) - \left(\frac{T_P^I}{V_{PI}}\right)\right]} \qquad (108)$$

M) Peripheral Insulin Transcapillary Diffusion Time Constant

Diffusion is the most important process by which solutes are exchanged between the blood and interstitial fluids. The rate of diffusion is primarily dependent upon the size of the solute and the permeability of the capillary wall. Insulin is less readily accessible to peripheral extravascular fluids than glucose, due in part to its large size (MW~5800) relative to glucose (MW 180) (Rasio, 1982). In addition, insulin diffusion is restricted by the continuous capillaries of skeletal muscle and adipose tissue which are less permeable than the sinusoids of liver or the fenestrated capillaries of kidney and gut (Yoffey and Courtice, 1970). Studies in dogs (Rasio et al., 1968; Camu and Rasio, 1972) and humans (Rasio et al., 1967) have shown rapid equilibration of glucose and insulin between blood plasma and thoracic duct lymph. Since thoracic duct lymph drains the extravascular fluid spaces of the liver and gastrointestinal tissues, these results provide direct confirmation that the capillaries of these viscera are highly permeable. Similar measurements of insulin diffusion into the hind leg lymph of dogs (Rasio et al., 1968), however, indicate that the capillaries of peripheral tissues are much less permeable to insulin; following an acute increase in arterial insulin concentration, insulin measured in leg lymph rose to 60 percent of its equilibrium concentration in about 20 min. Based on these results, a transcapillary diffusion time constant of 20 min was selected to characterize diffusional

exchange of insulin in the peripheral compartment of the insulin model.

N) Pancreatic Insulin Release

Insulin is produced by beta cells located in the islets of Langerhans of the pancreas. Here, insulin is synthesized and stored in a labile form that can be rapidly released in response to stimulatory factors. In humans, the islets are about 100 - 200 μ in size and are distributed throughout the exocrine pancreas, constituting only 1 to 2% of the total pancreatic tissue (Steiner et al., 1972). The high vascularity and fenestrated endothelial structure of the pancreatic islet microcirculation (Lacy and Greider, 1972) provide for rapid transfer of newly secreted insluin into the blood stream. Measurements of insulin in venous effluent of the perfused rat pancreas (Curry et al., 1968) have demonstrated insulin response within 30 s after a stimulating concentration of glucose reached the pancreas. Because of anatomical positioning in the circulation, insulin released by the pancreas in vivo enters the portal vein and thus traverses the liver prior to entry into the systemic circulation.

1) Biosynthesis and Storage of Insulin in the Beta Cell

The insulin biosynthetic mechanism of the pancreatic beta cell (Steiner et al., 1974) is summarized in Figure 34. The sequence of events is initiated with the synthesis of proinsulin by ribosomes associated sith the rough endoplasmic reticulum; proinsulin (see Figure 35), the biosynthetic precursor of insulin, is a single-chain polypeptide (MW 9600) consisting of C-peptide and the disulfide linked A- and B-chains of insulin (MW 5800). Proinsulin is next transferred by an energy-dependent process, possibly within microvesicles, to the Golgi complex. Within the Golgi apparatus of the cell, early storage granules form as proinsulin is incor-

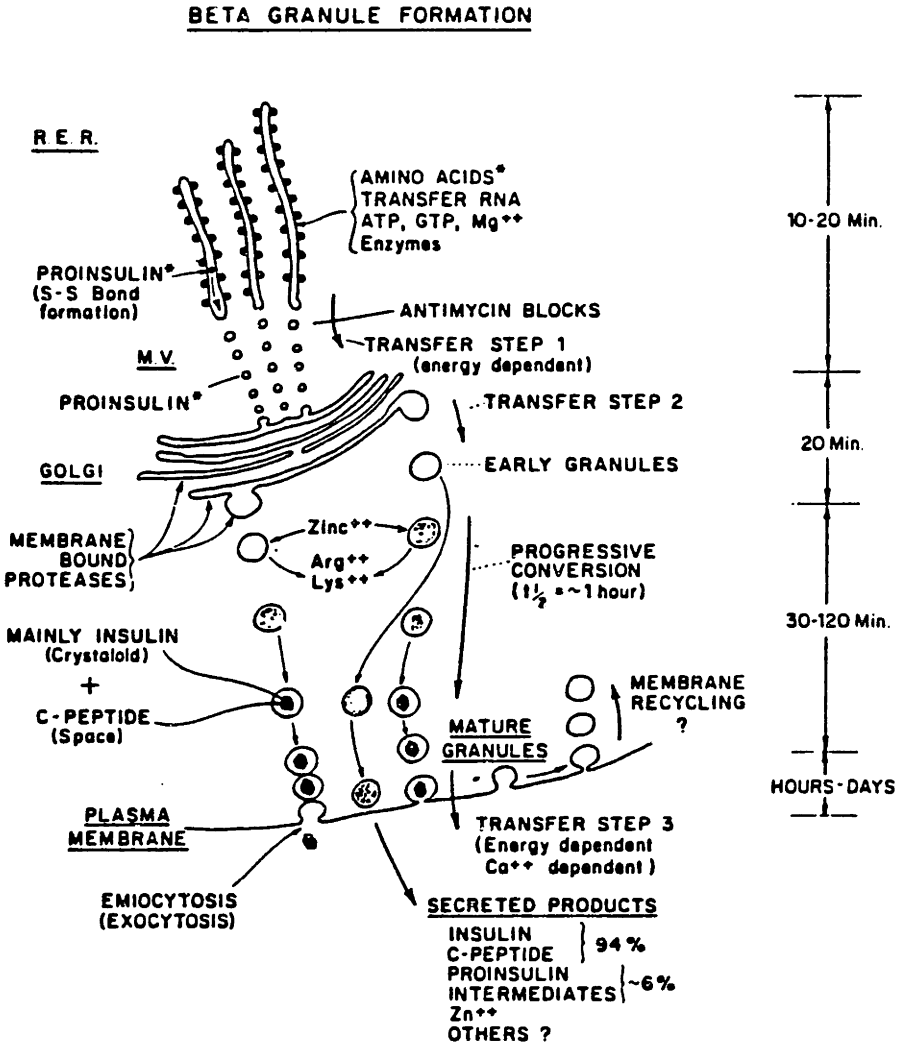

Fig. 34 Schematic representation of beta cell insulin biosynthesis. (Steiner et al., 1974)

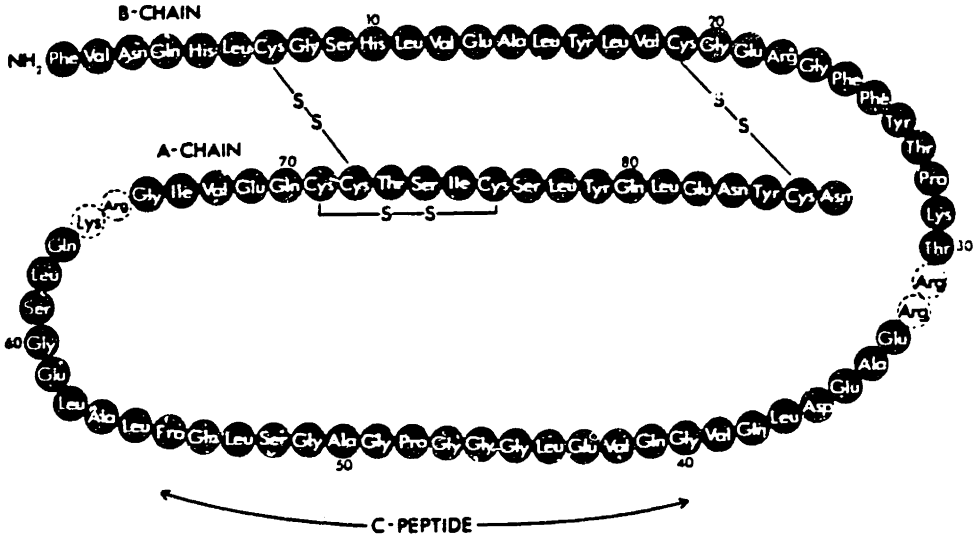

Fig. 35 The structure of human proinsulin. (Steiner et al., 1972)

porated into membranous sacs derived from the Golgi tubules. As the storage granules move away from the Golgi region and collect in the cytoplasm, proinsulin is converted to insulin through cleavage of the C-peptide segment by proteolytic enzymes. As insulin is liberated from proinsulin, it forms a dense crystalline matrix with zinc (beta granule). With electron microscopy, the process of granule maturation is evidenced by appearance of the beta granule surrounded by a fluid region (presumably containing C-peptide) within the membranous sac. Finally, insulin release occurs by the process of emiocytosis; the sacs fuse with the plasma membrane of the beta cell, and the mature granules are extruded into the extracellular space. Upon release, the crystalline granules undergo rapid dissolution due to the high concentration of sodium in the extracellular fluid (Lacy and Greider, 1972; Howell et al., 1969).

The times required for each of the major stages in the biosynthetic sequence are indicated in the time scale on the right side of Figure 34. These values refect experimental results obtained by introducing radioactive amino acids into beta cells (primarily of rats) and monitoring the movement of label through the synthesis sequence. Although label can be detected in proinsulin within 1-2 min of incubation, 10-15 min are required before small amounts of labeled insulin begin to accumulate in granules (Steiner et al., 1972). The conversion of proinsulin to insulin behaves like a first-order reaction with a half-life of about 1 hour (Steiner, 1967). Overall, there is an observed time delay of about 1 hour before newly made insulin begins to appear as a secretary product (Steiner, 1967; Sando and Grodsky, 1973; Howell and Taylor, 1967). In rabbit pancreas slices (Howell and Taylor, 1967), newly synthesized insulin was maximally released 2.5-3.5 hour after start of a 20-min incubation with ^{3}H-leucine

label. The above evidence suggests that newly synthesized insulin does not significantly contribute to short-term pancreatic response.

2) Factors Regulating Release of Insulin

a) Glucose

Glucose provides the primary stimulus for insulin release (Wilson, 1983; Gerich et al., 1976). A step change in glucose concentration elicits a biphasic insulin response (see Figure 36) characterized by an initial rapid release lasting about 5-10 min. (first phase) followed by a more sustained and gradual increase in the rate of release (second phase)(Curry et al., 1968; Grodsky et al., 1969; Bergman and Urquhart, 1971). Dose-response relationships in humans (Figure 37)(Cerasi et al., 1974) have shown that the response of insulin to glucose is sigmoidal, with little stimulation of release by glucose concentrations below normal fasting levels, and the most sensitive secretory response induced by glucose concentrations just above fasting levels. The relatively high threshold for glucose-stimulated insulin release (about 80-100 mg/dl)(Malaisse, 1972; Cerasi et al., 1974; Grodsky, 1972) suggest that glucose alone does not regulate fasting insulin levels. An important action of fasting glucose is most likely its modification of insulin release in response to other stimuli, such as gut hormones, glucagon, fatty acids, arginine, and neuronal factors that elicit little insulin secretion alone but are effectively potentiated by the presence of low glucose concentrations (Gerich et al., 1976).

b) Amino Acids

A variety of amino acids stimulate insulin secretion in man (Fajans and Floyd, 1972; Gerich et al., 1976). The most potent stimulator is argi-

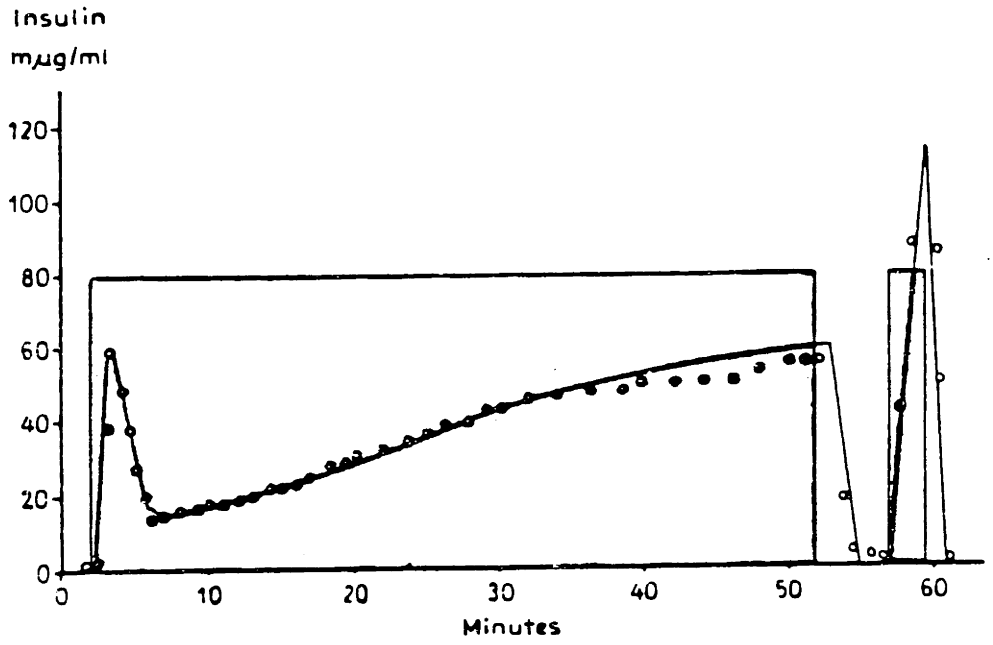

Fig. 36 Effect of 300 mg/dl glucose step changes on insulin secretion from the perfused rat pancreas. (Grodsky et al., 1969)

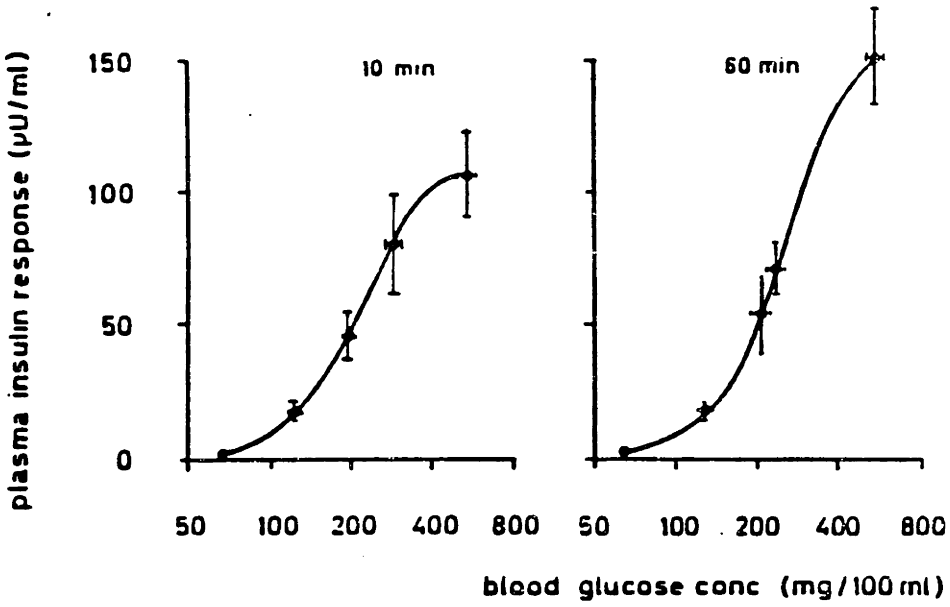

Fig. 37 Dose-response relationship between blood glucose concentration and plasma insulin increment early (10 min) and late (60 min) during glucose infusions in normal subjects. Data represent mean ± SEM values for 8 healthy subjects. (from Cerasi et al., 1974)

nine, followed by lysine and leucine (Fajans et al., 1967; Floyd et al., 1966b). Amino acids cause a monophasic release of insulin in the absence of glucose, whereas biphasic release is restored upon addition of small quantities of glucose (Gerich et al., 1974). Results of studies comparing the effects of various combinations of glucose and amino acid stimulations of insulin release suggest that amino acids mimic but do not potentiate glucose-induced secretion (Malaisse, 1972). Postprandial increases in plasma levels of amino acids following protein feeding have been shown to cause physiological stimulation of insulin release in man (Floyd et al., 1966a; Berger and Vongaraya, 1966; Rabinowitz et al. 1966). It is unlikely, however, that the changes in plasma amino acid levels observed during oral or intravenous glucose (Cahill et al., 1966; Wahren et al., 1972; Felig et al., 1975) would cause quantitative effects on beta cell secretion.

c) Free Fatty Acids

Although the possible role of lipid ingestion in augmenting insulin release in man has been studied, results have been inconsistent and would at best suggest a minor interaction (Fajans and Floyd, 1972). Plasma insulin does not increase when the concentration of plasma free fatty acids (FFA) is increased by intravenous administration of lipid emulsions (Felber and Vannotti, 1964). Furthermore, plasma insulin response to oral (Thorell et al., 1966) and intravenous (Thorell et al., 1966; Pelkonen et al., 1968) glucose is not enhanced by elevation in the concentraion of FFA.

d) Hormones

A number of hormones can directly affect pancreatic insulin release (Gerich et al., 1976; Unger et al., 1978). Whether insulin exerts feedback

regulation of its own secretion has generated much controversy. While studies using the prefused canine pancreas (Iverson and Miles, 1971) and pancreatic islets of mice (Loreti et al., 1974) demonstrated inhibition of insulin release with increased perfusate insulin levels, results of investigations using the perfused rat pancreas (Grodsky et al., 1968) and isolated rat islet preparations (Malaisse et al., 1967) indicated no such inhibitory action. Recent studies have used C-peptide assay to determine if exogenous insulin inhibits insulin secretion in man. DeFonzo et al. (1981c) have shown that elevation of plasma insulin levels by about 24 μU/ml or more in the presence of basal glucose concentrations causes rougly a 50% reduction in the rate of endogenous insulin release. Liljenquist et al. (1978) have reported that exogenous insulin does not result in inhibition of the pancreatic insulin response to hyperglycemic stimulus unless prolonged (60 min) euglycemic hyperinsulinemia is maintained prior to induction of elevated glucose. Since euglycemic hyperinsulinemia does not occur under natural conditions, it can be concluded from the above that insulin feedback inhibtion does not play an important role in the normal regulation of pancreatic insulin release.

In additon to insulin, two other hormones are produced in the islets of Langerhans, glucagon (by the alpha, or A_2 cells) and somatostatin (by the delta, or A_1 cells). In physiologic doses, each of these hormones influences the secretion of at least one of the other pancreatic hormones. Glucagon stimulates both insulin (Samols et al., 1965) and somatostatin (Patton et al., 1977; Weir et al., 1977) release. Somatostatin inhibits both insulin and glucagon secretion (Mortimore et al., 1974; Reichlin, 1983). Insulin inhibits glucagon release (Samols et al., 1972; Raskin et al., 1975) and may inhibit somatostatin release (Reichlin, 1983b). Because

of the complex interactions of these hormonal influences, Unger et al. (1978) have hypothesized that a "paracrine" system may exist within islets in which regulatory action is exerted through hormonal communication between neighboring islet cells via the interstitial spaces of the islets. Although increasing evidence suggests that some form of an intraislet regulatory mechanism may exist (Kohen et al., 1983; Orci et al., 1975; Reichlin, 1983b), its relative significance in the overall mediation of insulin release has not been determined.

Gastrointestinal hormones cause a significant quantitative enhancement of insulin release. Perley and Kipnis (1967) observed that the plasma insulin response to oral glucose was about 3 times greater than that resulting from intravenous glucose causing comparable glycemic levels. Similar results have been reported by Elrick et al. (1964) and McIntyre et al. (1965). In the presence of glucose, the gastointestinal hormones gastrin, secretion, and pancreozymin, which are primarily involved with regulating the motor and secretory functions of the splanchnic organs, can elicit insulin release in vitro (Grodsky, 1970). Studies with humans, however, have suggested that these hormones do not exert significant regulatory action on insulin release in vivo (Dupre et al., 1969; Hayes et al., 1975; Grayburn et al., 1975). One of the more recently identified gastrointestinal hormones, gastric inhibitory polypeptide (GIP), is secreted by the mucosal K-cells in the upper part of the small intestine (Solcia et al., 1978). GIP has been shown to be a potent stimulator of insulin release in the perfused rat pancreas (Pederson and Brown, 1978). Evidence suggests that endogenous GIP secretion is an important stimulator of insulin release in man (Morgan, 1979). Elahi et al. (1979) have demonstrated that GIP infusions elevating plasma levels within physiologic ranges can inducce a

significant plasma insulin response in the presence of hyperglycemia in normal subjects.

e) Autonomic Nervous System

Both the sympathetic and parasympathetic nervous systems may play important roles in the modulation of insulin release (Wilson, 1983). The islets of Langerhans are enervated by sympathetic fibers from the greater and lesser splanchnic nerves (Gerich et al., 1976). The sympathetic nervous system may affect islet function in two ways: 1) by local release of the adrenergic neurotransmitter norepinephrine, and 2) through adrenomedullary release of epinephrine. Both norepinephrine (Porte, 1966a) and epiniphrine (Porte, 1966b; Karem et al., 1966) inhibit insulin secretion in man through simulation of the α-adrenergic receptor (Porte, 1967). β-adrenergic stimulation by isoproternol (a synthetic agent), however, elevates circulating insulin levels (Porte 1967; Gerich et al., 1974) and enhances glucose-induced insulin release (Malaisse et al., 1967). Because of the opposing actions of α- and β-adrenergic stimulation, it has been proposed that adrenergic tone may be important in the modulation of basal pancreatic hormone secretion (Gerich et al., 1976), since both norepinephrine and epinephrine stimulate β-adrenergic receptors to some degree. In addition, events such as surgical stress (Allison et al., 1967) and exercise (Hunter et al., 1968) are associated with decreased insulin response to hyperglycemia, suggesting inhibition of insulin secretion through sympathetic nervous system activation (Porte, 1969).

With respect to the parasympathetic nervous system, the pancreatic islets are enervated by fibers originating from the vagus nerve (Wilson, 1983). The parasympathetic neurotransmitter, acetylcholine, augments insu-

lin release in vitro (Iversen, 1973; Malaisse et al., 1967; Sharp et al., 1974), and stimulation of the vagus nerve has been shown to cause an increase in insulin secretion in the dog (Frohman et al., 1967). Vagal denervation, however, has been reported to result in a marked decrease in insulin response to oral and intravenous glucose in rats, although basal insulin levels were not significantly affected (Hakanson et al., 1971). Even though the role of parasympathetic regulation of insulin release has not been clearly determined, these findings suggest the involvement of such a mechanism in normal response to glucose.

3) Insulin Release Mechanism

The mechanism of insulin release from the beta cell has been extensively studied (Malaisse, 1972; Randle and Hales, 1972). A model summarizing the release process is shown in Figure 38. Glucose (acting through a product of its cellular metabolism), leucine, and perhaps tolbutamide (an insulin-inducing drug) stimulate cellular uptake and/or intracellular redistribution of calcium ion. Amino acids which do not stimulate insulin release by themselves, such as arginine, probably act by potentiating Ca^{2+} flux through cotransport with Na^{+}. Although Ca^{2+} probably plays a primary role in excitation of the release process, cyclic AMP most likely plays a secondary or reinforcing role. It is through stimulation of the adenyl cyclase receptor system that agents like glucagon could enhance insulin release by elevating intracellular cyclic AMP levels. Likewise, inhibition of insulin secretion by α-adrenergic effectors could involve inhibition of cyclic AMP formation (not shown in Figure 38). Excitation of the release process is depicted as involving a coupling system which mediates the effects of Ca^{2+}(and perhaps cyclic AMP). Even though the

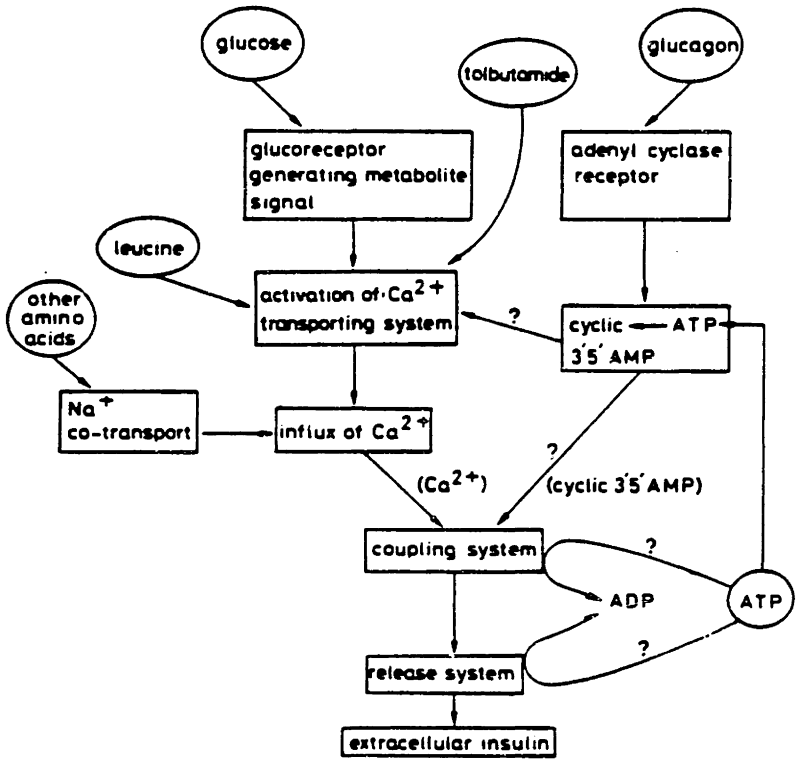

Fig. 38 Schematic depiction of the mechanisms for insulin release from the beta cell. (Randle and Hales, 1972)

release process involves ATP turnover, it is not known whether ATP is utilized directly for energy needs (as shown by its conversion to ADP) or if ATP plays an indirect role through formation of cyclic AMP.

Irrespective of the stimulus, the molecular basis of the release system which constitutes the final common pathway of release is not known. Lacy et al. (1968) have postulated that some of the insulin secretion granules are attached to a microtubule system, the microtubules of which contract or change their physical conformation in response to stimulatory factors, resulting in transport of granules to the cell surface where they are liberated.

4) Models of Glucose-Stimulated Insulin Release

Release of insulin from the pancreas is complicated, involving synthesis and release mechanisms in the beta cell which are not clearly understood, and subject to a complex array of regulatory factors. Since glucose is the primary stimulus of insulin secretion, mathematical models to date have primarily focused on glucose-induced release. Within the context of in vivo homeostasis modeling, such pancreatic insulin release models thus provide a quantitative relationship between glycemia and insulin release. Although this a useful and meaningful approach, it is important to recognize the range of physiologic situations for which such a simplified relationship is invalid. First, glycemia related to oral glucose must be distinguished, since insulin response is substantially augmented by gastointestinal hormones. Additional situations which would be anticipated to alter quantitatively the insulin response in normal man include: 1) inhibited response caused by euglycemic hyperinsulinemia or catichol intervention during stress, and 2) enhanced response resulting

from protein ingestion. Finally, the degree of modulation exerted by paracrine and/or other nervous system mechanisms remains to be determined, but such influences could be important. In view of the above discussion, glucose-induced insulin release models are strictly valid only for clinical studies in which in vivo arterial glucose concentrations are varied as a result of glucose infusions, such as intravenous glucose tolerance tests and hyperglycemic clamps. In addition, there are a number of clinical situations in which endogenous insulin release provides a small contribution to circulating insulin levels, such as intravenous insulin tolerance tests, euglycemic insulin clamps, and continuous insulin infusions; for such cases, the errors associated with omitting the effects of insulin feedback inhibition on pancreatic insulin release would not be of any quantitative significance.

In an early series of papers, Grodsky et al. (1969, 1970a, 1970b) proposed a single two-compartment model of insulin release. A small labile compartment (containing a few percent of the total stored insulin) was assumed in slow exchange with a large storage compartment such that a rapid stimulation of insulin release caused a partial depletion of the small compartment. This provided a mathematical description of the biphasic response which had been observed experimentally in the perfused rat pancreas (Curry et al., 1968). Subsequent perfusion studies using continuous staircase stimulations indicated that the initial spike of insulin release was not due to depletion of a single labile compartment since more insulin was elicited by each higher glucose step (Grodsky, 1970c). Grodsky (1972) thus hypothesized that insulin in the labile compartment was nonhomogenous, stored in insulin packets that varied sigmoidally in their glucose-threshold for release; this concept was incorporated into the

mathematical model depicted in Figure 39. Here, m is a time constant controlling the release rate of insulin from the labile compartment for packets whose thresholds have been exceeded. The exchange of insulin between the large and small compartments is controlled by rate parameters $K_1(P)$ and K_2. A postulated "provisionary factor" P, which is a function of glucose concentration, regulates the value of $K_1(P)$, thus controlling the refill rate of the labile compartment. The model produces first phase secretion by rapid depletion of the threshold-exceeded labile insulin packets, and the slowly rising second phase secretion by refilling from the large compartment as controlled by the value of P, which reaches steady state in approximately 1 hr. Since insulin synthesized de novo would not significantly contribute to insulin release for 1-2 hr following glucose stimulation, no representation of the synthesis process was included in the mathematical formulation. Licko and Silvers (1975) subsequently used regression analysis of the intravenous glucose tolerance test in normal humans to readjust parameter of the threshold distribution model for predicting insulin response in man.

Bergman and Urquhart (1971) formulated a model based upon contemporary views of the biosynthesis and release mechanisms of beta cell insulin secretion (Figure 40) to simulate results of canine pancreas perfusion studies. Granular insulin (I_g) was postulated to form via a relatively slow combination of "source" molecules into a precursor molecule (I_p), which is then transformed (via intermediate "b") into I_g. The granular insulin is subsequently transformed to a labile form (I_m) which is present at the cell membrane. Glucose was assumed to stimulate insulin synthesis through production of an intermediate "a" which increases the rate of combination of source molecules into I_p. The conversion of granular insulin to labile

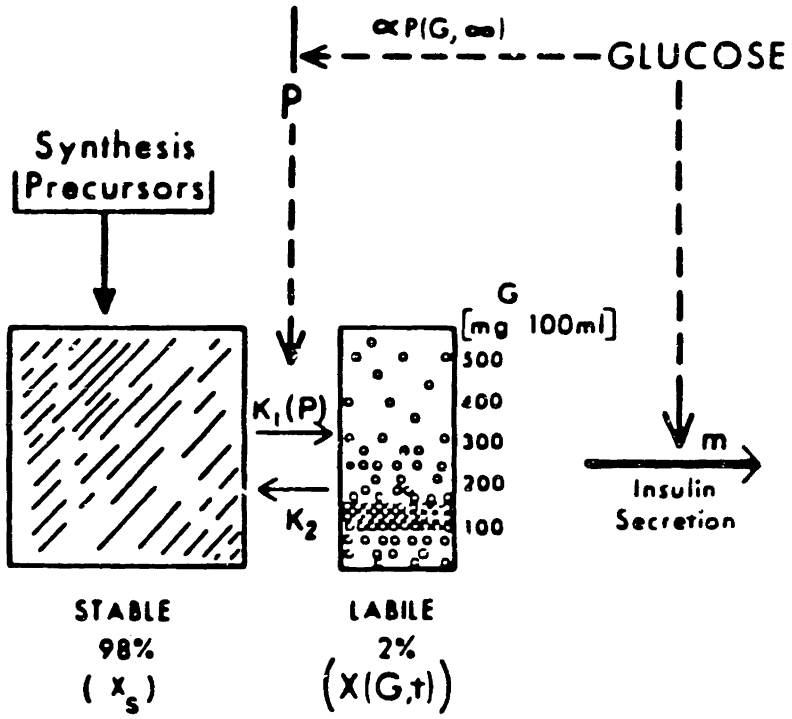

Fig. 39 Schematic diagram of the threshold distribution model of pancreatic insulin release of Grodsky (1972). (O'Connor et al., 1980)

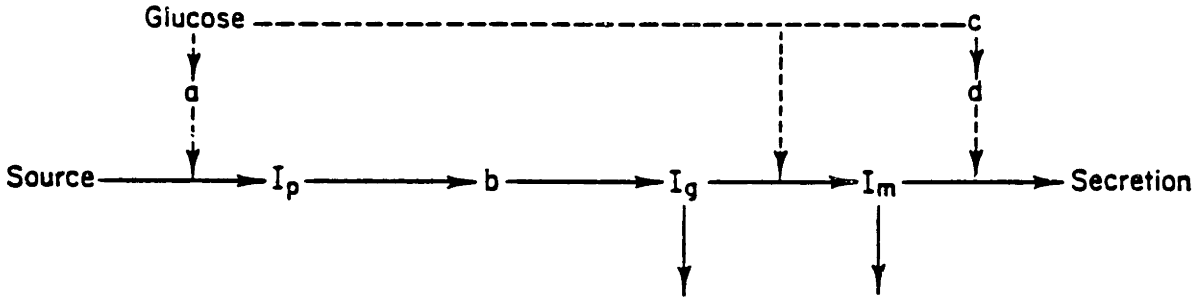

1) $\dot{a} = G - 0.025\,a$
2) $\dot{I}_p = 0.01\,a - 0.089\,I_p$
3) $\dot{b} = 0.021\,I_p - 0.11\,b$
4) $\dot{I}_g = 0.021\,b - I_g(0.065 + 0.020\,G) + 0.021$
5) $\dot{I}_m = I_g(0.015 + 0.015\,G) - I_m(1.45 + 0.75\,d)$
6) $\begin{cases} c = 4.1\,G & 0 \le G \le 0.25 \\ c = 2.3\,G + 0.59 & G > 0.25 \end{cases}$
7) $\dot{d} = 1.6\,c - 8.0\,d$
8) Secretion $= I_m(1.45 + 0.75\,d)$

Initial conditions $I_m(0) = 0.00331$, $I_a(0) = 0.319$

Fig. 40 Glucose-stimulated insulin secretory model of Bergman and Urquhart (1971).

insulin was also assumed to be glucose dependent. Finally, glucose triggered release of labile insulin through mediating intermediates "c" and "d", where production of "c" by glucose was assumed to follow saturation kinetics. The model was later modified (Bergman and Bucolo, 1973) to include effects of amino acids.

Guyton et al. (1978) formulated a heterogeneous fast pool model of human pancreatic insulin release (Figure 41) on the basis of plasma insulin responses to various glucose infusion experiments. Insulin is synthesized and stored in a large compartment (slow pool) which is in exchange with a small capacity system of compartments (heterogeneous fast pool) consisting of sites for the holding and releasing of labile insulin. The process of insulin synthesis was postulated to follow a sequence of steps similar to those assumed in the model of Bergman and Urquhart (1971). Glucose in the beta cell (GBC) acts through a metabolite (GMET) to stimulate the formulation of messenger RNA (MRNA) from "source" molecules (i.e. amino acids). Proinsulin (PROI) is produced from the MRNA and is transfered to the Golgi complex (IGOL), where insulin is cleaved from the proinsulin. Insulin formed in the Golgi complex is converted to granular form and transfered to the slow pool where it is stored (insulin in slow pool, ISP). The heterogeneous fast pool consists of a set of four distinct compartments (releasing sites with insulin, RSI; releasing sites that are empty, RSE; holding sites with insulin, HSI; and holding sites that are empty, HSE). Insulin is rapidly released at a rate which is proportional to the quantity of releasing site insulin (RSI). The heterogeneous fast pool is basically an alternative mathematical representation of the threshold distribution model of Grodsky (1972). Whereas Grodsky employed a single inhomogenous "compartment" of labile insulin packets with a sigmoidal glucose threshold

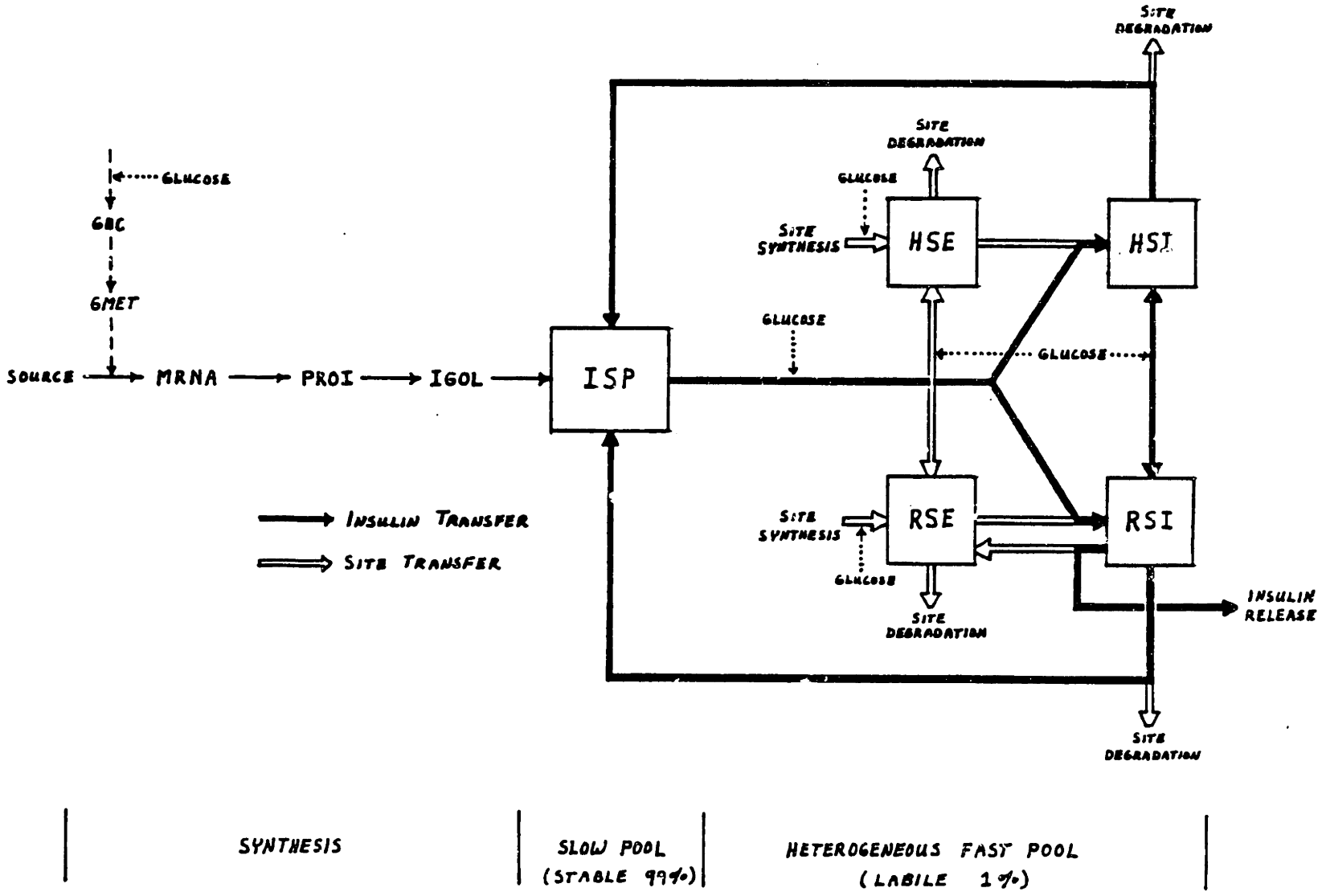

Fig. 41 Schematic representation of the heterogenous fast pool insulin release model of Guyton et al. (1978).

distribution, Guyton et al. used a system of homogenous compartments with a sigmoidal function relating glucose concentration to the quantity of sites whose thresholds had been exceeded (releasing sites) relative to the quantity of sites whose thresholds had not been exceeded (holding sites). Thus, first phase insulin release from the heterogeneous fast pool results from a rapid glucose-induced shift of holding site insulin (HSI) to releasing site insulin (RSI). The second phase of release results from a glucose-related increase in the rate of transfer of slow pool insulin (ISP) to fill empty sites in the fast pool. In addition, glucose slowly augments the number of fast pool sites (site synthesis) causing a potentiation of insulin response following glucose exposure. The mathematical equations for insulin synthesis and storage were given by

$$\frac{d}{dt}(GBC) = \left[G_A - \frac{(GBC)}{(VBC)}\right](GDC) + (FMG)(GMET) - (FGMPM)(GBC) \tag{109}$$

$$\frac{d}{dt}(GMET) = (FGMPM)(GBC) - [(FMMPM) + (FMG)](GMET) \tag{110}$$

$$\frac{d}{dt}(MRNA) = (EGMET)\, r^{B}_{MRNA} - \frac{(MRNA)}{T_{MRNA}} \tag{111}$$

$$\frac{d}{dt}(PROI) = (MRNA)\, r^{B}_{PIR} - \frac{(PROI)}{T_{PROI}} \tag{112}$$

$$\frac{d}{dt}(IGOL) = \frac{(PROI)}{T_{PROI}} - \frac{(IGOL)}{T_{IGOL}} \tag{113}$$

$$\frac{d}{dt}(M^{D}_{C}) = \frac{M_C - M^{D}_{C}}{T_C} \tag{114}$$

$$\frac{d}{dt}(ISP) = \frac{(IGOL)}{T_{IGOL}} + \frac{(HSI) + (RSI)}{T_{SD}} - r_{ISTF} \tag{115}$$

where: GBC = Glucose in Beta Cell (mg)
GMET = Glucose Metabolite in Beta Cell (mg)

MRNA = Messenger RNA Molecules (normalized)

PROI = Proinsulin (mU insulin equivalents)

IGOL = Insulin in Golgi Complex (mU)

M_C^D = Delayed Effect of Glucose on Rate of Insulin Transfer from Slow to Fast Pool (dimensionless)

ISP = Insulin in Slow Pool (mU)

G_A = Arterial Blood Glucose Concentration (mg/dl)

VBC = Beta Cell Volume = 0.01 dl

GDC = Beta Cell Glucose Diffusion Coefficient = 0.01 mg/(mg/dl)·min

FMG = Fraction of GMET Converted Back into Glucose per Minute = 0.5 min^{-1}

FGMPM = Fraction of GBC Metabolized per Minute = 2.0 min^{-1}

FMMPM = Fraction of GMET Metabolized per minute = 1.0 min^{-1}

EGMET = Nonlinear Effect of GMET on MRNA synthesis (dimensionless)

r_{PIR}^B = Basal Rate of Pancreatic Insulin Release (mU/min)

T_{MRNA} = MRNA Time Constant = 20 min

r_{MNRA}^B = Basal Rate of MNRA Synthesis (min^{-1})

T_{PROI} = Time Required for PROI Transfer to Golgi Complex = 20 min

T_{IGOL} = Time Required for Insulin Transfer to Slow Pool = 20 min

T_C = Time Constant for Delayed Effect of Glucose on r_{ISTF} = 45 min

T_{SD} = Time Constant For Site Degradation = 45 min

r_{ISTF} = Rate of Insulin Transfer From Slow to Fast Pool (mU/min)

and the nonlinear function EGMET is shown in Figure 42. The nonlinear insulin transfer rate r_{ISTF} was expressed

$$r_{ISTF} = M_A \left[M_B\, M_C^D\, r_{PIR}^B \left(\frac{(ISP)}{(ISP)_{basal}}\right) + \left(\frac{(HSI) + (RSI)}{T_{SD}}\right)_{basal}\right] \qquad (116)$$

where the multiplier functions M_i are presented in Figure 43 (the delayed effect M_C^D is determined from Figure 43 and Equation 114).

The fast pool insulin dynamics were given by

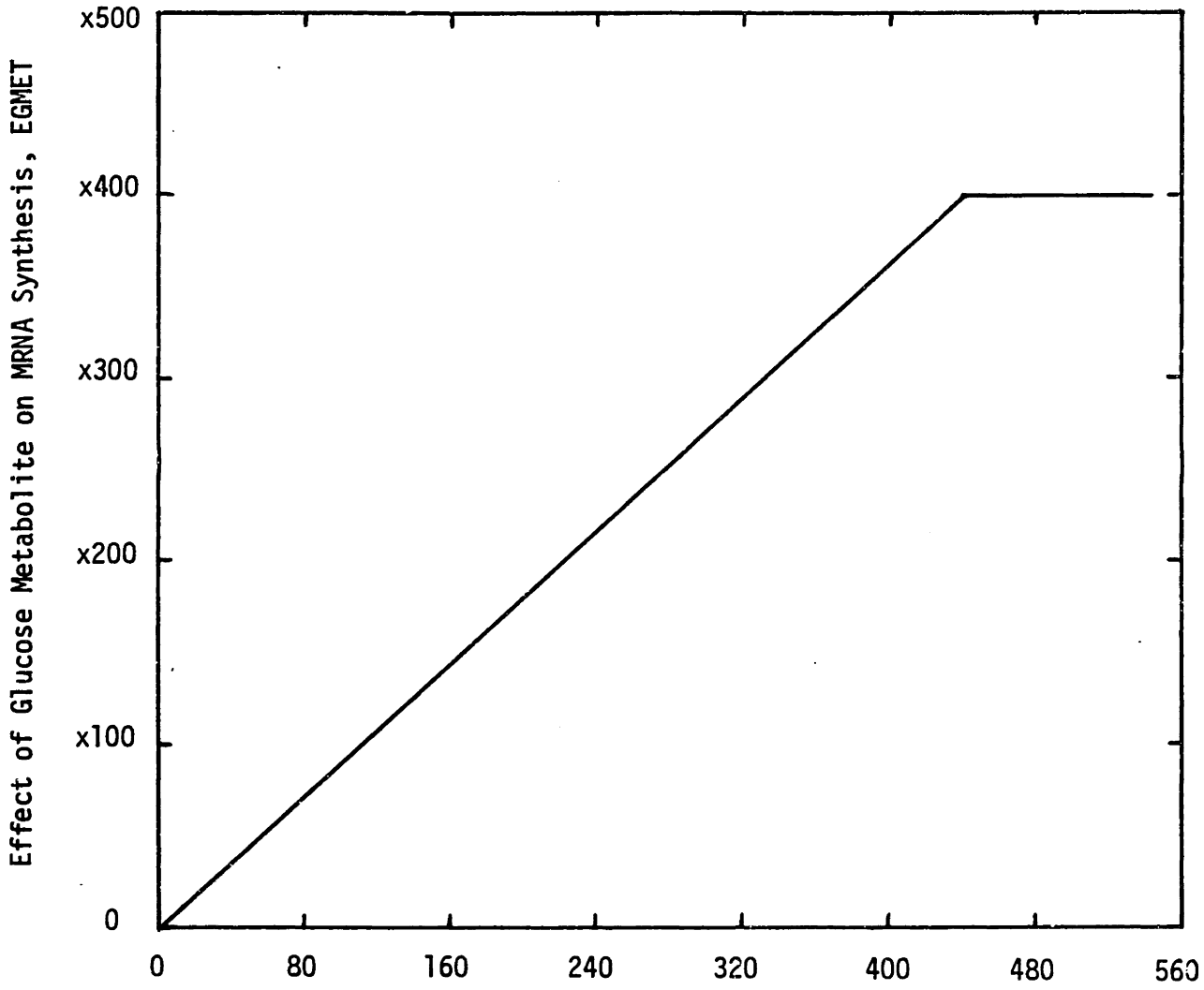

$$GMETC = 80 \text{ mg/dl } \left(\frac{GMET}{GMET_{basal}}\right)$$

Fig. 42 Effect of glucose metabolite in the beta cell on the rate of MRNA synthesis.

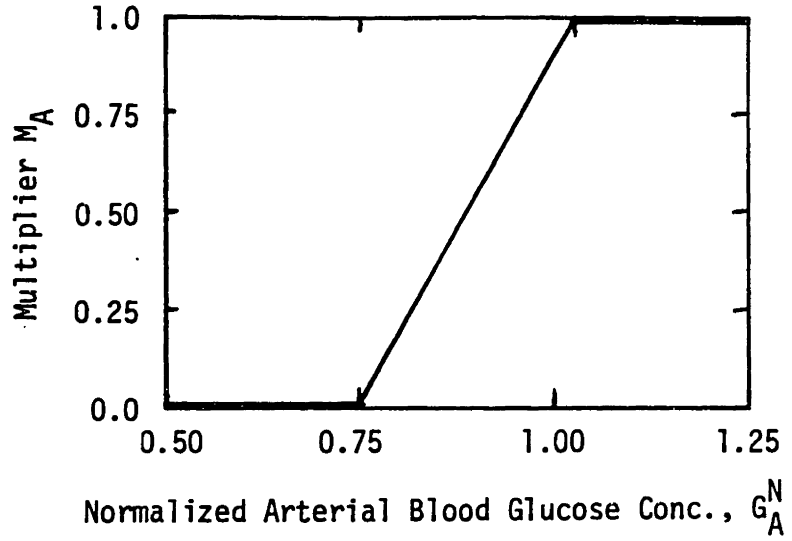

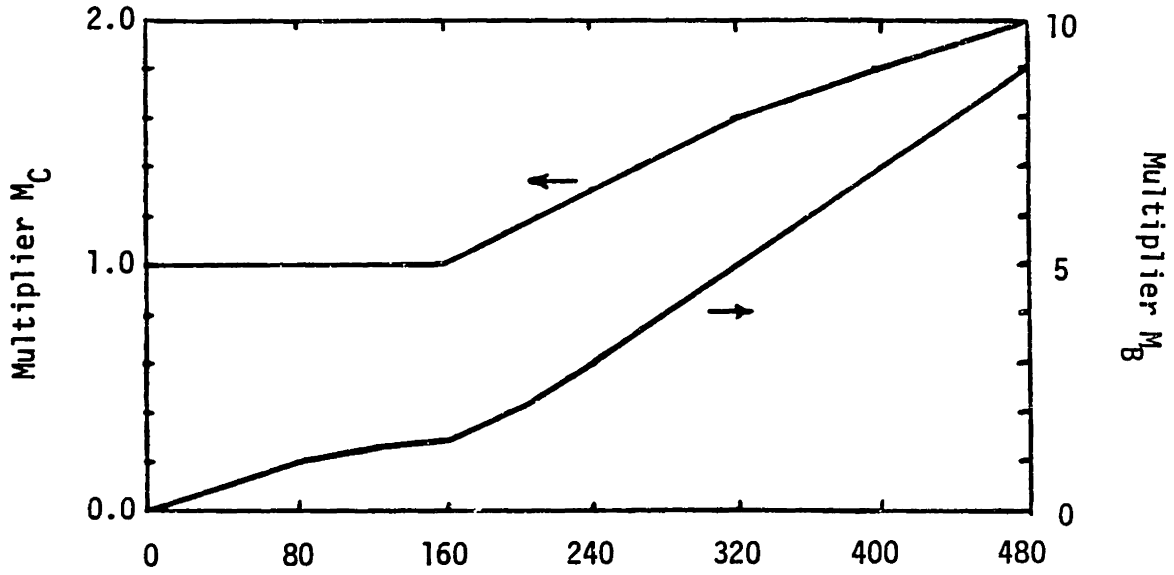

$$GMETC = 80\ mg/dl\left(\frac{GMET}{GMET_{basal}}\right)$$

Fig. 43 Multipliers M_i for computing effects of glucose on the rate of insulin transfer from the slow to fast pool (r_{ISTF}).

$$\frac{d}{dt}(HSI) = \left(\frac{(HSE)}{(HSE) + (RSE)}\right) r_{ISTF} + \left[\left(\frac{(RSI)}{(RSE) + (RSI)}\right) r_{\theta}\right]^{0^+}$$

$$+\left[\left(\frac{(HSI)}{(HSE) + (HSI)}\right) r_{\theta}\right]^{0^-} - \frac{(HSI)}{T_{SD}} \tag{117}$$

$$\frac{d}{dt}(HSE) = -\left(\frac{(HSE)}{(HSE) + (RSE)}\right) r_{ISTF} + \left[\left(\frac{(RSE)}{(RSE) + (RSI)}\right) r_{\theta}\right]^{0^+}$$

$$+\left[\left(\frac{(HSE)}{(HSE) + (HSI)}\right) r_{\theta}\right]^{0^-} - \frac{(HSE)}{T_{SD}} + (EGSS)\, r^{B}_{HSS} \tag{118}$$

$$\frac{d}{dt}(RSI) = \left(\frac{(RSE)}{(HSE) + (RSE)}\right) r_{ISTF} + \left[\left(\frac{(HSI)}{(HSE) + (HSI)}\right) r_{\theta}\right]^{0^+}$$

$$+\left[\left(\frac{(RSI)}{(RSE) + (RSI)}\right) r_{\theta}\right]^{0^-} - \frac{(RSI)}{T_{SD}} - \frac{(RSI)}{T_{IR}} \tag{119}$$

$$\frac{d}{dt}(RSE) = -\left(\frac{(RSE)}{(HSE) + (RSE)}\right) r_{ISTF} + \left[\left(\frac{(HSE)}{(HSE) + (HSI)}\right) r_{\theta}\right]^{0^+}$$

$$+\left[\left(\frac{(RSE)}{(RSE) + (RSI)}\, r_{\theta}\right]^{0^-} - \frac{(RSE)}{T_{SD}} + (EGSS)\, r^{B}_{RSS} \tag{120}$$

where:
- HSI = Holding Sites with Insulin (mU equivalents)
- HSE = Holding Sites Empty (mU equavalents)
- RSI = Releasing Sites with Insulin (mU equavalents)
- RSE = Releasing Sites Empty (mU equivalents)
- EGSS = Nonlinear Effect of Glucose on Site Synthesis (dimensionless)
- r^{B}_{HSS} = Basal Rate of Holding Site Synthesis (mU/min)
- r^{B}_{RSS} = Basal Rate of Releasing Site Synthesis (mU/min)
- r_{θ} = Rate of Site Redistribution (mU/min)
- T_{IR} = Insulin Release Time Constant = 0.4 min

and the superscripts 0^+ and 0^- mean that the arguments in brackets assume a value of zero unless they are greater or less than zero, respectively. The nonlinear effect of glucose on site synthesis augmentation EGSS is shown in

Figure 44. The rate of site redistribution r_θ was expressed

$$r_\theta = \frac{[(RSE)+(RSI)] - [(HSE)+(HSI)+(RSE)+(RSI)]\theta}{T_{DIS}} \quad (121)$$

where: T_{DIS} = Site Redistribution Time = 0.2 min

and θ represents the fraction of sites that are releasing sites,

$$\theta = \frac{(RSE)+(RSI)}{(HSE)+(HSI)+(RSE)+(RSI)} \quad (122)$$

The value of θ was given as a nonlinear function of the beta cell glucose metabolite concentration as presented in Figure 45. Since θ was calculated from the glucose metabolite concentration, the numerator in Equation 121 yielded the error in the number of releasing sites at any given time, thus providing the driving force for site redistribution. The rate of pancreatic insulin release (the last term in Equation 119) was given by

$$r_{PIR} = \frac{(RSI)}{T_{IR}} \quad (123)$$

By setting all of the time derivatives equal to zero at steady state, initial conditions were uniquely calculated from specification of the fasting arterial blood glucose concentration (G_A) and the assumption (arbitrary) that the total quantity of sites was 2323 mU equivalents. For example, a fasting arterial blood glucose concentration of 80 mg/dl yields the following initial conditions:

GBC = 0.349 mg
GMET = 0.465 mg
MRNA = 1.00 (normalized molecules)
PROI = 437 mU insulin equivalents
IGOL = 437 mU
ISP = 200,000 mU

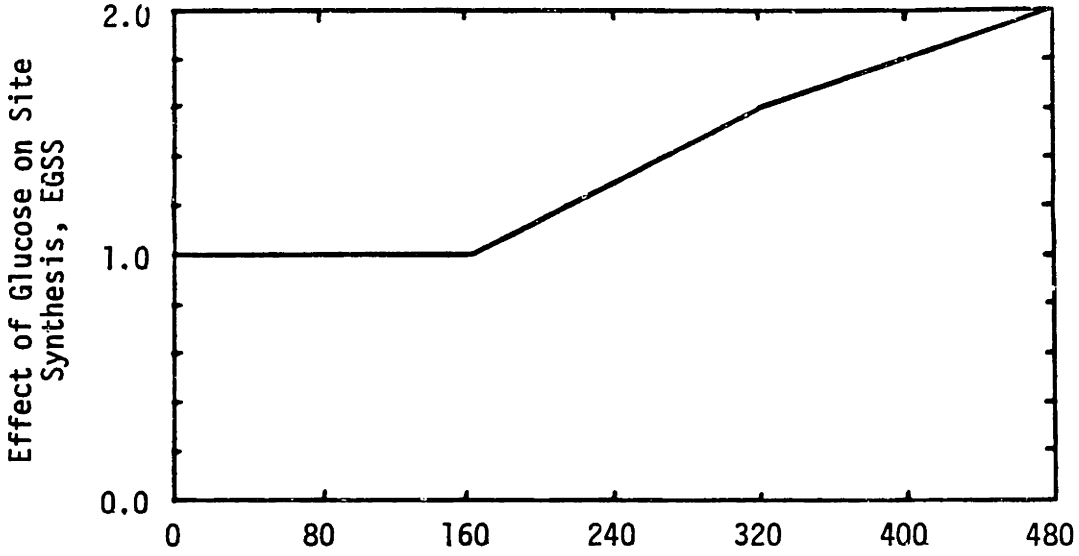

$$GMETC = 80\ mg/dl\left(\frac{GMET}{GMET_{basal}}\right)$$

Fig. 44 The effect of glucose metabolite concentration in the beta cell on the rate of site synthesis.

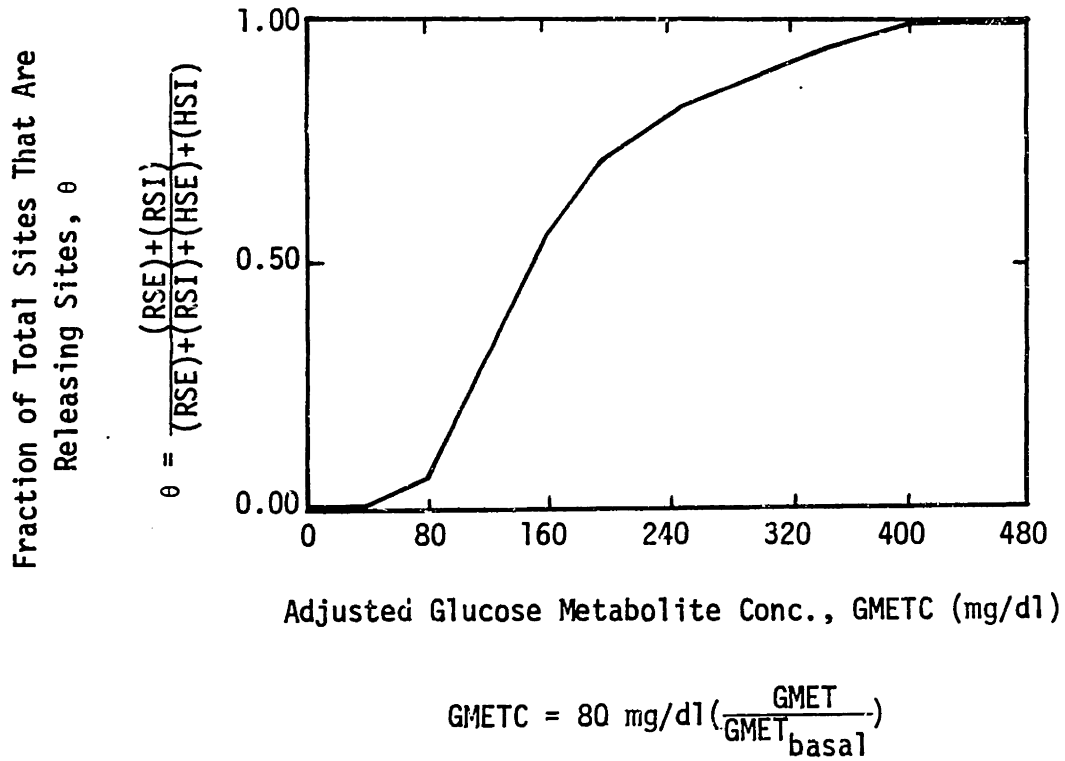

$$GMETC = 80\ mg/dl\left(\frac{GMET}{GMET_{basal}}\right)$$

Fig. 45 The effect of glucose metabolite concentration in the beta cell on the distribution of fast pool sites.

$$HSI = 1990 \text{ mU equivalents}$$
$$HSE = 217 \text{ mU equivalents}$$
$$RSI = 8.75 \text{ mU equivalents}$$
$$RSE = 107 \text{ mU equivalents}$$
$$M_C^D = 1.0$$

and
$$r_{PIR}^B = 21.9 \text{ mU/min}$$
$$r_{MRNA}^B = 0.05 \text{ min}^{-1}$$
$$r_{HSS}^B = 49 \text{ mU/min}$$
$$r_{RSS}^B = 2.6 \text{ mU/min}$$

In the models of Grodsky (1972) and Guyton et al. (1978), the rate of insulin release was determined by the quantity of available insulin within a small labile compartment; such formulations are referred to as storage-limited models. Based on studies of glucose-insulin interactions during intravenous glucose administration in man, Cerasi et al. (1974) assumed that insulin is stored in a single large compartment and that insulin release is directly associated with changes in glucose-induced signals (Figure 46). This is an example of a signal-limited model. Glucose was postulated to cause an instananeous multiplicative augmentation of insulin release; this was expressed in terms of a sigmoidal function of glucose concentration (f(g) in the figure) derived from dose-response studies. In addition, glucose was assumed to enhance levels of a potentiator (p) through an intermediate (p_1), and insulin release to increase levels of an inhibitor (b) through an intermediate (b_1). The exponential difference between the potentiator (p) and inhibitor (b) levels was also assigned a multiplicative effect on the rate of insulin release. In this model, first phase release is caused by an instantaneous glucose-induced augmentation signal followed by a rapid increase in the level of inhibitor b. Second

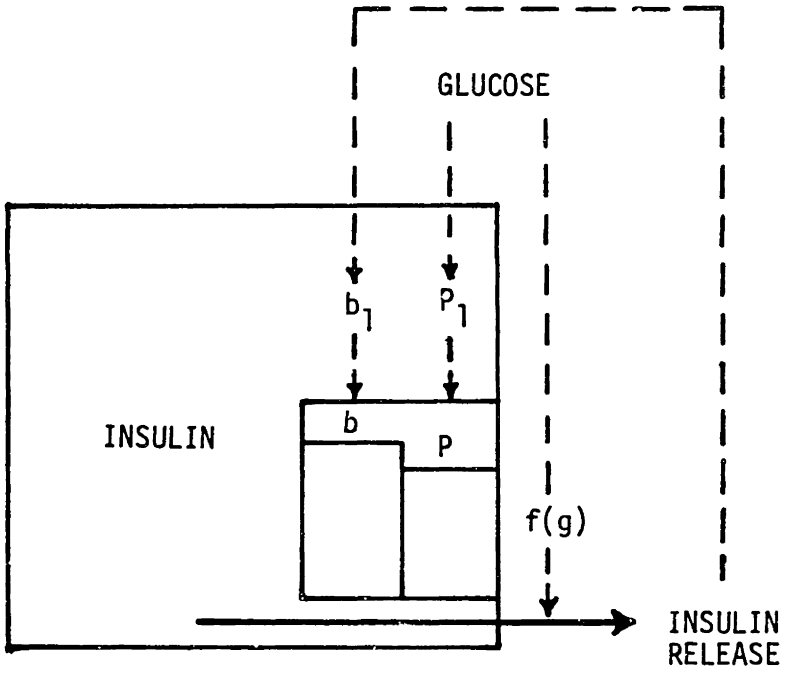

Fig. 46 Schematic diagram of signal-limited insulin release model of Cerasi et al. (1974).

phase release results form a gradual rise in the level of potentiator p with prolonged glucose exposure. The effects of glucose on insulin synthesis were not considered. The mathematical equations for this model were given by

$$\frac{dp_1}{dt} = (-\frac{1}{\tau_{p1}})\ p_1 + k_p\ f(g) \tag{124}$$

$$\frac{dp}{dt} = -\frac{1}{\tau_p}\ (p - p_1) \tag{125}$$

$$\frac{db_1}{dt} = (-\frac{1}{\tau_{b1}})\ b_1 + k_b\ i_r \tag{126}$$

$$\frac{db}{dt} = \frac{1}{\tau_b}\ (b - b_1) \tag{127}$$

$$i_r = e^{(p-b)} f(g) \tag{128}$$

$$r^*_{PIR} = V_{ip} k_i i_r \tag{129}$$

where: p = Potentiator Variable (dimensionless)
p_1 = Intermediate Potentiator Variable (dimensionless)
b = Inhibitory Variable (dimensionless)
b_1 = Intermediate Inhibitory Variable (dimensionless)
τ_{p1} = Time Constant = 30 min
τ_p = Time Constant = 30 min
τ_{b1} = Time Constant = 20 min
τ_b = Time Constant 5 min
k_p, k_b = Parameters (min^{-1})
V_{ip} = Distribution Volume for Secreted Insulin (ml)
$f(g)$ = Nonlinear Effect of Blood Glucose Concentration on Initiating Insulin Secretion (dimensionless)
k_i = Parameter ($\mu U/ml \cdot min$)
i_r = Abstraction Representing Dynamics of Insulin Secretion (dimensionless)
r^*_{PIR} = Insulin Release Rate Above Basal ($\mu U/min$)

and the nonlinear function f(g) is shown in Figure 47. Values for the parameters k_p, k_b, and k_i were adjusted to obtain fits of individual plasma insulin profiles following intravenous glucose administration in normal, prediabetic, and diabetic subjects. Additional signal-limited mathematical models (the excitor-inhibitor and delta-signal models) have been developed by O'Connor et al. (1980) to describe pancreatic insulin release from the perfused rat pancreas.

Cobelli et al. (1980) conbined both storage- and signal-limited features into a relatively simple model of insulin secretion (Figure 48). The model consists of two linearly connected compartments of stored (X_1) and labile (X_2) insulin. Insulin is synthesized and transfered to the insulin storage compartment at a rate which is determined by glucose concentration. The rate of insulin release from the labile compartment is dependent on both the quantity of labile insulin and the concentration of glucose. The model is described by the following equations:

$$\frac{dX_1}{dt} = k_{21} X_2 - k_{12} X_1 + r_{SYN}(G) \tag{130}$$

$$\frac{dX_2}{dt} = k_{12} X_1 - k_{21} X_2 - r_{PIR}(X_2,G) \tag{131}$$

$$r_{SYN}(G) = 0.5\ a\ \{ 1 + \tanh[b(G - G^B + c)\} \tag{132}$$

$$r_{PIR}(G,X_2) = 0.5\ d\ \{ 1 + \tanh[e(G - G^B + f)]\} \tag{133}$$

where: X_1 = Quantity of Stored Insulin (mU/kg body weight)
X_2 = Quantity of Labile Insulin (mU/kg body weight)
r_{SYN} = Rate of Insulin Synthesis (mU/min/kg body weight)
r_{PIR} = Rate of Insulin Release (mU/min/kg body weight)
G = Glucose Concentration (mg/dl)
G^B = Basal Glucose Concentration (mg/dl)

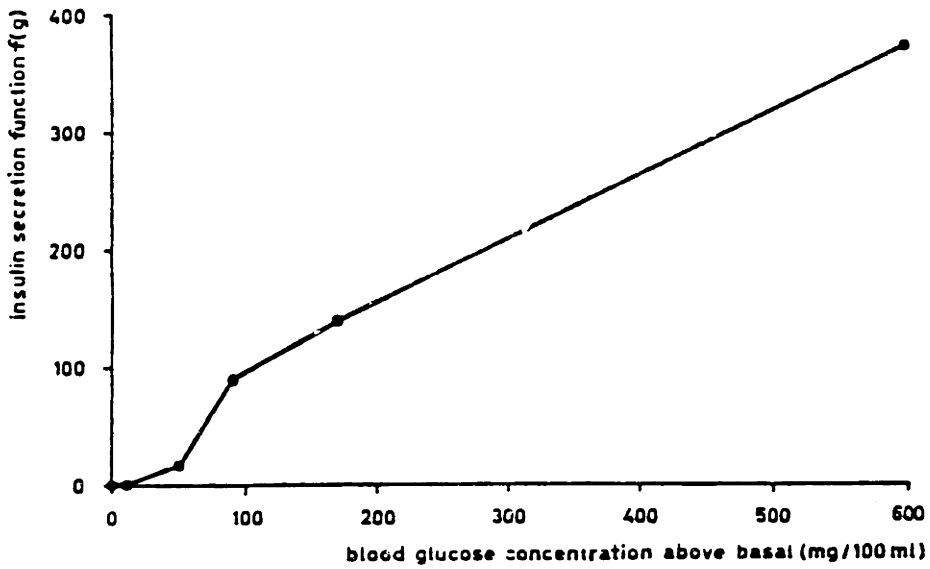

Fig. 47 Nonlinear function f(g) relating blood glucose concentration to activation of insulin secretion in the model of Cerasi et al. (1974).

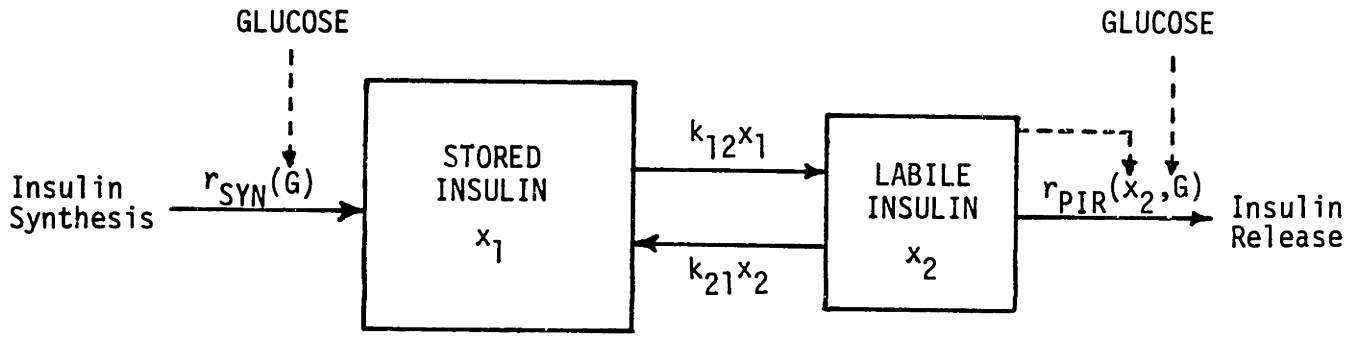

Fig. 48 Insulin secretion model of Cobelli et al. (1980).

with parameter values

$k_{21} = 0.01\ min^{-1}$
$k_{12} = 4.34 \times 10^{-3}\ min^{-1}$
$a = 4.1$ mU/min/kg body weight
$b = 1.51 \times 10^{-2}$ dl/mg
$c = -92.3$ mg/dl
$d = 1.3\ min^{-1}$
$e = 9.23 \times 10^{-2}$ dl/mg
$f = -19.68$ mg/dl

and initial conditions

$X_1(0) = 75$ mU/kg body weight
$X_2(0) = 7.5$ mU/kg body weight

Numerical values for the parameters and initial conditions were obtained from the experimental data of Bergman and Urquhart (1971) and Grodsky (1972), although details of the quantification process were not reported. Cobelli et al. normalized the model with respect to body weight (values of X_1, X_2, and a were expressed per kg of body weight) and assumed the validity of interspecies extrapolation on the basis of simple linear body weight proportionality.

Landahl and Grodsky (1982) modeled insulin secretion by combining storage and signal models from previous papers (Grodsky et al., 1969; O'Connor et al., 1980). The resulting "mixed model" of pancreatic insulin release is shown in Figure 49. As with the threshold distribution model (see Figure 39), a small labile insulin compartment was assumed in exchange with a large storage compartment, with a glucose-stimulated provisionary factor P regulating the rate of labile compartment filling. The labile compartment, however, was assumed to be homogenous, while the insulin secretion rate (S) was modified to incorporate signal-limited charac-

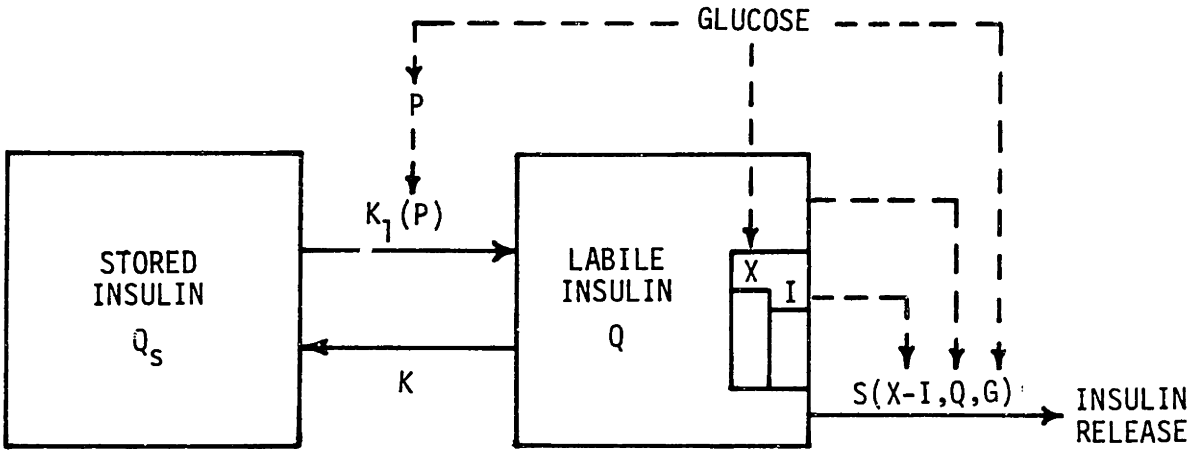

Fig. 49 Pancreatic insulin release model of Landahl and Grodsky (1982).

teristics. The rate of insulin release S is dependent on glucose concentration, the quantity of labile insulin (Q), and the difference in the instantaneous levels of a glucose-enhanced excitation moiety (X) and its inhibitor (I). The quantity of labile insulin (Q) available for release at any given time was determined by the rate of exchange between the storage compartments, an incremental rate of insulin transfer due to glucose-stimulated provision, and the rate of loss resulting from insulin secretion. This was expressed by the mass balance equation

$$\frac{dQ}{dt} = K' Q_S - KQ + \gamma P - S \tag{134}$$

where K' and K are rate constants and γP represents the incremental rate of transfer due to provision ($K_1(P)$ in Figure 49 thus corresponds to the sum of $K' Q_S$ and γP). The mass balance formulation for the insulin storage compartment was given by

$$\frac{dQ_S}{dt} = KQ - K' Q_S - \gamma P \tag{135}$$

Because of the large capacity of stored insulin, the quantity of insulin in the storage compartment (Q_S) was assumed constant. For a glucose concentration of zero, γP was set to zero, and from Equation 135 at steady state,

$$Q_S = \left(\frac{K}{K'}\right) Q_0 \tag{136}$$

where Q_0 represents the quantity of labile insulin (Q) when the glucose concentration is zero. Equation 136 was used to eliminate Q_S from the mass balance Equation 134, and the complete system of equations for the pancreatic insulin release model was given by

$$\frac{dp}{dt} = \alpha \left(P_\infty(G) - P\right) \tag{137}$$

$$\frac{dI}{dt} = \beta\,(X(G) - I) \tag{138}$$

$$\frac{dQ}{dt} = K\,(Q_0 - Q) + \gamma P - S(X-I, Q, G) \tag{139}$$

$$S = [M_1 Y(G) + M_2 (X-I)^{0^+}]\,Q \tag{140}$$

where
- P = Provisionary Factor (dimensionless)
- I = Inhibitor (dimensionless)
- Q = Quantity of Labile Insulin (μg)
- α, β = Inverse Time Constants (min^{-1})
- K, M_1, M_2 = Rate Constants (min^{-1})
- γ = Rate Constant ($\mu g/min$)
- S = Rate of Pancreatic Insulin Release ($\mu g/min$)
- Q_0 = Quantity of Labile Insulin For G=0 ($\mu g/min$)
- $X(G)$ = Nonlinear Effect of Glucose on Early Insulin Release (dimensionless)
- $Y(G)$ = Secretory Effect of Glucose (dimensionless)
- $P_\infty(G)$ = Nonlinear Effect of Glucose on Late Insulin Release (dimensionless)
- G = Glucose Concentration ($\mu g/dl$)

The model parameters and nonlinear input functions were established from dose-step response studies of the glucose perfused rat pancreas (Grodsky, 1972). For a step increase in glucose concentration from 0 to G at t=0: 1) at early times, the second term in Equation 140 dominates such that first phase insulin release rate tends to be proportional to X(G); 2) at late times or steady state, from Equations 139 and 140 (noting that X=I and P=P∞)

$$0 = K(Q_0 - Q) + \gamma P_\infty - S(G, \infty) \tag{141}$$

$$S(G, \infty) = M_1 Y(G) Q \tag{142}$$

and solving Equation 141 for Q and substituting into Equation 142 yields

$$S(G,\infty) = \frac{(\gamma P_\infty(G) + KQ_0)M_1 Y(G)}{K + M_1 Y(G)} \tag{143}$$

It can be seen from this expression that if the value of the parameter K is small enough, the late phase insulin secretion rate is proportional to $P_\infty(G)$. Thus, the functions X(G) and $P_\infty(G)$ could have been obtained purely by fitting empirical approximations of the early and late secretion data of Grodsky (1972). Landahl and Grodsky, however, showed that the same results could be achieved on the basis of theoretical assumptions. First, it was postulated that two entities X must associate with some receptor system in order that P can be produced or that the second component of insulin secretion can occur, such that

$$X^2(G) = P_\infty(G) = Y(G) \tag{144}$$

Secondly, it was assumed that if four molecules of G (or its metabolite in proportion to G) combine in the presence of Ca^{2+}, and if X(G) is the fraction with four associations with G, then X(G) would be expressed by G^4 divided by a fourth degree polynomial in G. For a high degree of cooperativity, a function of the form

$$X(G) = \frac{G^4}{G_0^4 + G^4} \tag{145}$$

would be representative, where G_0 is the value of G for which X = 1/2. For G_0 = 150 mg/dl, Equations 144 and 145 yielded good approximations of the data of Grodsky (1972) as shown in Figure 50. The remaining parameters were estimated by comparing model predictions with experimental data:

$K = 0.035\ min^{-1}$

$\alpha = 0.05\ min^{-1}$

$\beta = 0.6\ min^{-1}$

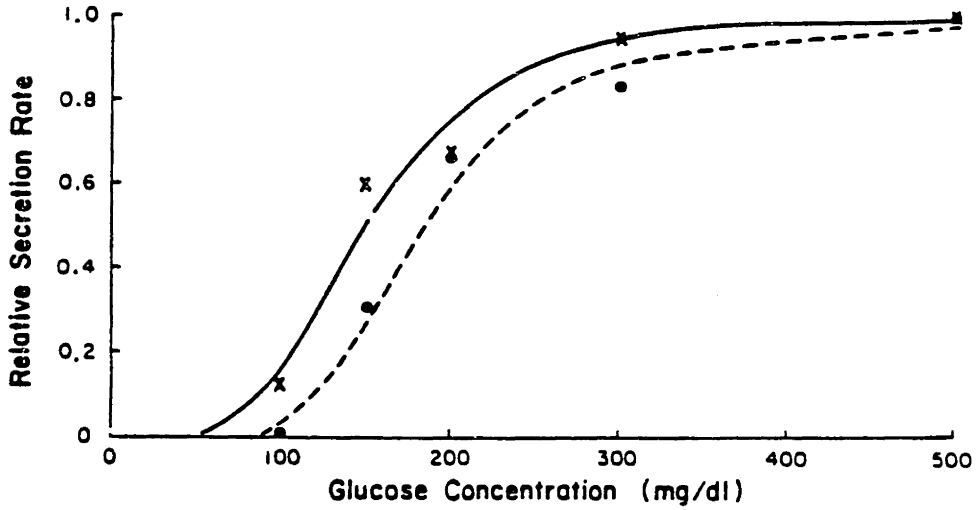

Fig. 50 Early (x) and late (●) secretion data (Grodsky, 1972) measured relative to the maximum value for various glucose concentrations. Plotted for comparison are X(G) (solid) and $P_\infty(G) = X^2(G)$ (dashed) for G_0 = 150 mg/dl. (Landahl and Grodsky, 1982).

$M_1 = 0.27 \text{ min}^{-1}$

$M_2 = 0.9 \text{ min}^{-1}$

$\gamma = 0.45$ μg/min

$Q_0 = 1.2$ μg

Two mathematical representations of pancreatic insulin release have directly incorporated the concept that insulin response is both sensitive to glucose concentration and its rate of change with time. Foster et al. (1973) assumed that each of these factors had a nonlinear effect on insulin secretion which when multiplied together times the basal insulin release rate yielded the pancreatic rate of insulin release. An additional multiplicative effect of free fatty acid concentration was also included in the formulation. In a more recent model, Carson and Cramp (1976) have employed an additive relationship of the following form:

$$r_{PIR} = r^B_{PIR} + C_1 [G-G^B]^{0^+} + C_2 \left[\frac{dG}{dt} \right]^{0^+} \quad (146)$$

where: r_{PIR} = Pancreatic Insulin Release Rate (mU/min)

r^B_{PIR} = Basal Insulin Release Rate = 4 mU/min

G = Glucose Concentration (mg/dl)

G^B = Basal Glucose Concentration = 90 mg/dl

C_1 = Constant = 1.0 (mU/min)(mg/dl)$^{-1}$

C_2 = Constant = 2.0 (mU/min)(mg/dl·min)$^{-1}$

With the above models, first phase release results from the terms that are sensitive to the rate of change of glucose with time, and second phase release is generated by the terms that are sensitive to the glucose concentration level.

A summary comparison of literature models of glucose-stimulated insulin release is presented in Table 24. General mathematical features of each model have been included in the table to provide a basic index for

TABLE 24. Summary comparison of insulin release models.

MODEL	TYPE	INSULIN SYNTHESIS	COMPLEXITY			BASIS
			Differential Equations	Parameters	Nonlinear Input Functions	
Grodsky, 1972	Storage	No	3	15	2	Perfused rat pancreas
Bergman and Urquhart, 1971	Storage & Signal	Yes	6	23	1	Perfused dog pancreas
Foster et al., 1973	G, $\frac{dG}{dt}$ sensitive	No	0	2	3	Plasma appearance in man
Cerasi et al., 1974	Signal	No	4	9	1	Plasma appearance in man
Guyton et al., 1978	Storage	Yes	11	14	6	Plasma appearance in man
Cobelli et al., 1980	Storage & Signal	Yes	2	10	2	Perfused dog/rat pancreas
O'Connor et al., 1980	Signal	No	3	9	2	Perfused rat pancreas
Cramp and Carson 1981	G, $\frac{dG}{dt}$ sensitive	No	0	3	0	Plasma appearance in man
Landahl and Grodsky 1982	Storage & Signal	No	3	8	2	Perfused rat pancreas

comparing relative model complexities. Although attractive because of their simple forms, the models of Foster et al. (1973) and Cramp and Carson (1981), which are sensitive to glucose concentration and its rate of change, bear the least physiologic correspondence to beta cell function. In addition, the formulation of Cramp and Carson (see Equation 146) yields basal insulin release for all degrees of hypoglycemia and generates a linear dose-response to hyperglycemia. Since human glucose dose-response is highly nonlinear (sigmoidal) (Cerasi et al., 1974), the general predictive power of this model is questionable. Bergman and Urquhart (1971) and Guyton et al. (1978) included physiologic representations of the insulin biosynthesis pathway in their models; this increased the relative mathematical complexities of these models, and since the mechanisms of insulin synthesis are not fully characterized, increased the number of parameters requiring estimation. Furthermore, the contribution of newly formed insulin to short term (~1-2 h) response is probably not important. Due to the use of four compartments to represent storage-limited release of labile insulin, the model of Guyton et al. encompasses an extra degree of complexity with respect to the complicated filling and redistribution dynamics of these compartments, and also employs a large number of nonlinear irput table functions in the formulation. Cerasi et al. (1974) demonstrated that a relatively simple signal model could predict the important features of biphasic insulin response to intravenous square-wave glucose stimuli in man. Cobelli et al. (1980) combined storage and signal aspects to develop a relatively simple mathematical formulation which included input from glucose-stimulated synthesis of insulin, although details of the synthesis pathway were omitted. The model, based on dog and rat data, was normalized with respect to body weight and used to predict

insulin release in the perfused canine pancreas and in man without parameter readjustment (Cobelli et al., 1980). Since the relative glucose dose-response curves of the rat (Grodsky, 1972) and man (Cerasi et al., 1974) appear to be significantly different (the sigmoidal glucose dose-response curve in man saturates at a much higher glucose concentration), direct interspecies extrapolation on the basis of body weight may be an oversimplification. Over the years, Grodsky and his coworkers have studied response of the perfused rat pancreas to a wide variety of glucose patterns, including step, staircase, multiple square wave, and slow and fast ramp stimuli. Cumulative results form these studies have provided a broad basis upon which to elucidate the important characteristics of pancreatic insulin response to glucose. Although the storage (Grodsky, 1972) and signal (O'Connor et al., 1980) models were partially successful in predicting the experimental data, the recent combined model (Landahl and Grodsky, 1982) is the only model that can predict in a semiquantitative manner all of the regularly appearing dynamic features of insulin response over this wide range of glucose simuli. In addition, the model of Landahl and Grodsky is of simple mathematical complexity, while incorporationg a reasonably high degree of physiologic correspondence with respect to relevant aspects of insulin storage and release.

5) Modeling of Glucose-Stimulated Insulin Release in Man

The pancreatic insulin release model of Landahl and Grodsky (1982) was selected as the basis for modeling in vivo pancreatic insulin secretion in man. Although simple in form, the model's mathematical structure has proven to generate accurate predictions of dynamic insulin response over a very wide range of glucose stimuli in the perfused rat pancreas. In addi-

tion to its demonstrated performance, the model encompasses a reasonable degree of physiologic correspondence. For example, in man the normal adult pancreas contains about 250 U of extractable insulin (Wrenshall et al., 1951). Since this quantity of stored insulin represents about 5 to 10 times the total normal daily insulin requirement, exclusion of the insulin synthesis process and the assumption that the quantity of stored insulin in the pancreas remains quasisteady is well justified. It should be mentioned, however, that even though newly synthesized insulin does not begin to appear in secreted insulin for about 1-2 h following glucose stimulation of the beta cell, experimental evidence has suggested that, once formed, new insulin granules may be secreted preferentially (Gold et al., 1982); thus, during prolonged hyperglycemia, release of newly formed insulin could conceivably be important even though its relative contribution to the total quantity of pancreatic insulin remains small. The labile compartment of the model, which constitutes only a few percent of the total pancreatic insulin, could represent those insulin storage granules in the cytoplasm of the beta cell that are associated with the microtubule system. Besides its apparent physiologic correspondence, antoher advantage of the model is its direct use of a glucose dose-response relationship as a primary input function, since such a relationship may be determined experimentally.

The model of Landahl and Grodsky (Figure 49, Equations 137-140) was modified for human applications by first considering the importance of basal insulin release in vivo. In normal subjects, basal plasma insulin concentrations range between about 10-20 mU/l. Bagdade et al. (1967) studied the relationship between fasting insulin levels and insulin response to glucose in nondiabetic males. Results indicated that insulin responses could not be evaluated without consideration of fasting insulin

levels because there was a highly significant linear correlation between basal insulin and insulin response to glucose. In addition, basal insulin levels did not significantly correlate with fasting glucose concentrations. The above evidence suggests that pancreatic insulin release should be modeled in terms of a multipliative scaling of the basal secretion rate, with the basal release rate being decoupled from the precise fasting level of arterial glucose concentration. This was achieved by letting

$$r_{PIR}(G_H) = S^N(G_H) \quad r^B_{PIR} \tag{147}$$

where

$$S^N(G_H) = \frac{S(G_H)}{S(G^B_H)} \tag{148}$$

and

$$r^B_{PIR} = f \text{ (basal plasma insulin levels)} \tag{149}$$

Here, the insulin secretion rate $S(G_H)$ from Equation 140 is normalized with respect to its basal value $S(G_H = G^B_H)$. The rate of pancreatic insulin release $r_{PIR}(G_H)$ is then computed from multiplying the resulting normalizing secretion rate $S^N(G_H)$ by the basal pancreatic release rate r^B_{PIR}. As denoted by Equation 149, the basal release rate is determined by factors external to the pancreas. Specification of fasting insulin levels gives the basal rates of insulin degradation in the liver, kidney, and periphery by solving the steady state insulin model mass balance equations (17-23). For steady basal conditions, the rate of pancreatic insulin release must equal the total rate of body insulin degradation, and thus r^B_{PIR} can be determined from specification of the basal insulin levels.

The second major consideration in adapting the pancreatic release model

was specification of the nonlinear glucose dose-response relationship $X(G_H)$. The functional relationship used by Landahl and Grodsky for the rat (Figure 50, Equation 145) was obtained from graded glucose step-response data with the isolated perfused pancreas. The ideal in vivo analog for humans would require measurement of peak portal plasma insulin responses to step increases in arterial plasma glucose concentration. Since such data is not available, the sigmodial shape of the insulin response curve was instead determined from relative peak plasma insulin concentrations following rapid intravenous glucose infusions of varying doses. Presented in Table 25 is data for IVGTT experiments in which 3-min glucose infusions were administered at doses ranging from 0.05-0.75 g/kg body weight. As indicated by the data, the graded glucose infusions caused acute increases in venous glucose levels and elicited rapid plasma insulin responses. Since arterial rather than venous plasma glucose concentration stimulates pancreatic insulin release in vivo, it was desired to correlate peak insulin responses against arterial glucose concentration instead of the reported venous quantities. Because of its physiologic design, the glucose model was used for the purpose of predicting the peak arterial glucose concentrations induced by each of the respective glucose dose levels. As shown previously (see Figure 32), such simulations of plasma glucose levels immeidately following rapid intravenous glucose administration are insulin insensitive. Model predictions for peak arterial plasma glucose concentrations are listed in Table 25. Also included in the table are simulated values for peripheral venous blood glucose concentrations 1 min post-infusion; comparison of these values with the actual experimental data demonstrates the extreme accuracy with which the model predicted the observed venous glucose levels during these simulations. A plot of peak insulin response as a function

TABLE 25. Tabulation of experimental data and model simulations for variable-dose IVGTT studies. (Experimental data measured in 15 normal subjects at the Joslin Research Laboratory, Boston)

DOSE (g/kg body weight)	EXPERIMENTAL DATA (N=15 normal subjects)					MODEL SIMULATION	
	Venous Blood Glucose Concentration (mg/dl)		Venous Plasma Insulin Concentration (μU/ml)			Venous Blood Glucose Concentration (mg/dl)	Arterial Plasma Glucose Concentration (mg/dl)
	Basal	1 min	Basal	1 min.	% Change	1 min.	0 min.
0.05	76	109	18	57	217	113	159
0.1	76	130	17	78	359	128	220
0.2	77	180	19	106	458	177	340
0.33	75	242	19	116	511	246	495
0.5	76	318	19	134	605	315	695
0.75	72	380	21	162	671	371	991

of peak arterial plasma glucose concentration is presented in the upper panel of Figure 51. The relative insulin response curve was obtained by linearly rescaling the peak insulin response data such that basal and maximal responses corresponded to relative responses of 0.2 and 0.9, respectively; although this was an arbitrary scaling from a mathematical standpoint, it resulted in a realistic representation in a physiologic sense. The model function for $X(G)$ was then determined by fitting the relative insulin response data in the lower plot of Figure 51 to a function of the form

$$X(G_H) = \frac{(G_H)^A}{(G_o)^A + B(G_H)^C} \tag{150}$$

where parameters A,B,C, and G_o(mg/dl) were adjusted to obtain a least squares fit (IMSL library computer subroutive ZXSSQ). The resulting empirical functional fit, given by

$$X(G_H) = \frac{(G_H)^{3.27}}{(132)^{3.27} + 5.93(G_H)^{3.02}} \tag{151}$$

is shown by the curve in the lower plot of Figure 51. Comparison of the sigmoidal functions $X(G_H)$ for the rat (Equation 145 and Figure 50) and the human (Equation 151 and Figure 51) indicates that the human insulin response curve does not saturate at the low glucose levels (about 300 mg/dl) observed to cause saturation of the rat pancreas response. Such behavior is also suggested by the human insulin secretion function f(g) derived by Cerasi et al. (Figure 47).

The final step in adapting the insulin release model involved

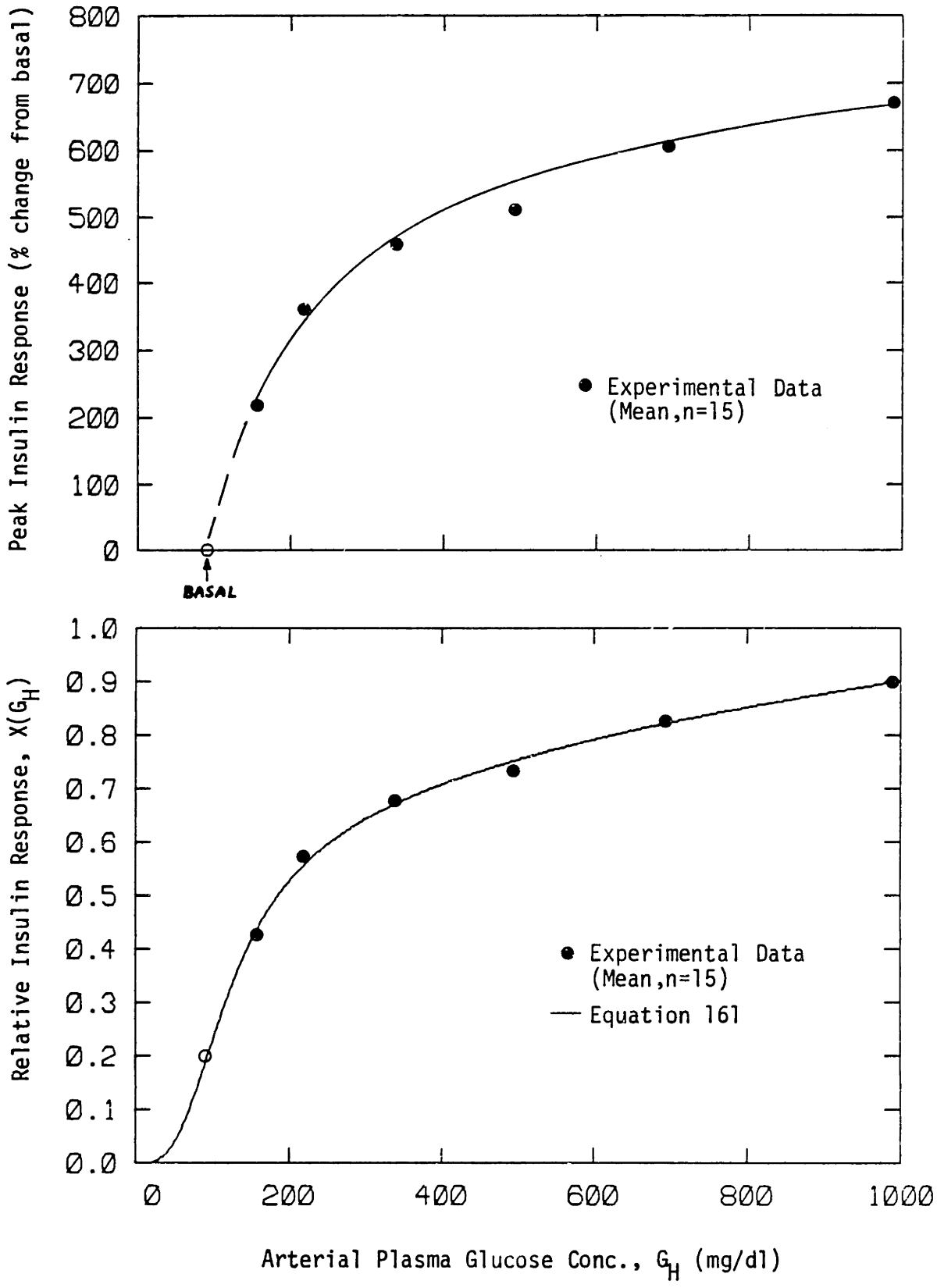

Fig. 51 Peak and relative insulin response curves for humans derived from variable-dose IVGTT studies.

readjustment of the model parameters K, α, β, M_1, M_2, γ, and Q_0. In addition, since good human data for late phase insulin response to prolonged graded hyperglycemia was not available for quantification of the late insulin response function $P_\infty(G_H)$, it was assumed (on the basis of Equation 144)

$$P_\infty(G_H) = Y(G_H) = [X(G_H)]^\delta \tag{152}$$

where parameter δ was also allowed to vary during parameter adjustment. Having established the nonlinear glucose dose-response input function $X(G_H)$, model simulations of a standard 0.5 g/kg body weight IVGTT were run and the above parameter values were varied so as to minimize the difference between model precdictions and experimental data (N = 110 normal adult males) for the time course of plasma insulin concentrations over a period of 180 min following glucose infusion. The IMSL library computer subroutine ZXSSQ was employed to generate a least squares fit of the nonlinear insulin model output to the experimental data. Until a pancreatic insulin release model was developed, IVGTT simulations used for adjusting liver metabolism in the glucose model were performed by arbitrarily fixing the rate of pancreatic insulin release as a function of time, $r_{PIR}(t)$, such that the plasma insulin time course in the insulin model matched experimental data (see Figure 30). In this manner, all insulin model concentrations were maintained at their proper levels while the glucose physiology was established. Once the glucose model was properly adjusted resulting in matching of the glycemic data during IVGTT simulation, the proper arterial glucose concentration as a function of time, $G_H(t)$, was in turn used as a fixed input during adjustment of the model pancreas parameters.

The resulting parameter set is listed in Table 26. As will be shown later in the results section, these parameter values yielded an excellent

TABLE 26. Parameter values for the insulin release model of Landahl and Grodsky (1982); comparison between rat values and those obtained for humans by parameter adjustment.

Model Parameters	Rat Model	Human Model
$K(min^{-1})$	0.035	0.00794
$\alpha(min^{-1})$	0.05	0.0482
$\beta(min^{-1})$	0.6	0.931
$M_1(min^{-1})$	0.27	0.00747
$M_2(min^{-1})$	0.9	0.0958
γ	0.45 µg/min	0.575 U/min
Q_o	1.2 µg	6.33 U
δ	(2)[a]	1.11

[a]Not varied during rat model parameter adjustment (fixed on basis of experimental data)

fit of the 0.5 g/kg body weight IVGTT plasma insulin data; a standard F test analysis of variance gave $P<0.01$ for a nonsignificant correlation. Furthermore, even though it was established on the basis of a single IVGTT study, the pancreatic insulin release model gave good predictions of plasma insulin responses to a wide variety of glycemic patterns without any further readjustment.

The parameter values for the human model were interesting in several respects. The reference quantity of insulin in the labile compartment Q_0 assumed a value of 6.3 U or roughly 2.5% of the total insulin content of the human pancreas. This was a reasonable result on a theoretical basis, since the fraction of labile insulin in the rat model was about 2% of total pancreatic insulin. In the rat model, the relationship between early and late insulin response was given by $\delta=2$ in Equation 152. Initial attempts to fix δ at this value for the human model resulted in failure to attain a reasonable fit of the IVGTT data. In retrospect, the value of δ was an artifact of the scaling of the "relative" insulin response curve of Figure 51; the resulting value of $\delta\approx1$ for the human model is significant only with respect to the scaling of the function $X(G_H)$ which was necessarily arbitrary since data below basal glucose concentrations was not available for its absolute determination. Although the parameter set listed in Table 26 appeared to be unique with respect to fitting of the IVGTT data, there was a reasonably high degree of parameter interaction and no formal attempt was pursued to determine if a global minimum in the least squares parameter space was truly realized.

The approach employed in the present study was conceptually similar to that used by Licko and Silvers (1975). Licko and Silvers used a threshold distribution model of pancreatic insulin release similar to that postulated

by Grodsky (1972) to analyze human IVGTT data. The insulin release model was coupled to a single-compartment plasma insulin distribution and metabolism model, and parameters of the insulin release model were adjusted by regression analysis to fit the observed time course of plasma insulin response following IVGTT administration in normal subjects. Licko and Silvers reported that parameter adjustment of the threshold distribution insulin release model could account not only for mean response of the 26 subjects studied, but also for the variety of observed individual response patterns (through adjustment of a particular parameter subset). Since earlier threshold distribution insulin release models cannot accurately account for insulin response over the wide range of glucose stimuli that can be predicted by the recent mixed model of pancreatic insulin release of Landahl and Grodsky (O'Connor et al., 1980), the general predictive capacity of Licko and Silvers' human insulin release model would be less certain than that of the insulin release model derived in the present study. A final factor which may be of importance in the modeling of insulin release involves the recent discovery that basal plasma insulin concentrations oscillate in monkeys (Goodner et al., 1977) and in man (Lang et al., 1982) with a periodicity of 14 min. Such oscillations have been found to exert a greater hypoglycemia effect than maintenance of similar constant mean plasma insulin levels (Matthews et al., 1983). Since receptors become less sensitive to hormonal stimuli when exposed to high steady concentratons, it has been suggested (Matthews et al., 1983) that oscillatory hormonal stimuli could help to maintain receptor integrity. The regulatory factors producing the oscillations in pancreatic insulin release have not been identified. One possibility is local islet regulation by autonomic nervous control. Alternately, a paracrine control system involving complex

relationships between alpha, beta, and delta cell hormonal interactions could be involved, since basal plasma glucagon concentrations also oscillate with the same periodicity as insulin levels but with a phase lag of 2 min (Lang et al., 1982). The possible role of basal somatostatin has not been investigated. Since neither the exact oscillatory nature of insulin release in man nor its physiologic significance have yet been determined, no attempt was made to introduce oscillatory behavior into the present model of pancreatic insulin release.

6) Comparison of Pancreatic Insulin Release Models

Because insulin release data is not available for the perfused human pancreas, there is no basis for direct comparison of model predictions with experimental data for known or controllable glucose stimuli. In vivo data relating arterial glucose concentration to plasma insulin response requires some interpretation. Since portal vein measurements are not attainable, insulin released from the pancreas must pass through the liver, a major site of insulin clearance, prior to systemic detection. Furthermore, hepatic venous effluent mixes with venous blood from other organ and tissue regions in passing through the cardiopulmonary system. The relationship between pancreatic insulin release and observable quantities such as arterial or peripheral venous plasma insulin is thus rather complicated, involving both dynamics of circulatory distribution and tissue clearances.

As a result of the complexities involved in interpreting the plasma insulin appearance data, models of insulin distribution and metabolism are generally employed to determine the pancreatic insulin release dynamics upon which the parameters of the insulin release model are then based. From a quanitative standpoint, insulin release models are thus no stronger

than the insulin distribution and metabolism models with which they were coupled during parameter adjustment. In the present study, effort was taken to formulate and independently quantify all aspects of the insulin model external to the pancreas prior to parameter adjustment of the insulin release equations. The importance of such independent quantification of internal model processes cannot be overstated. For example, of the recent physiologic models only in that of Cramp and Carson (1981) was insulin removal from plasma assumed to be a nonlinear process; it is interesting, but not surprising, that this was also the only model in which pancreatic insulin release was assumed linear. The mathematical ease with which nonunique internal components of a model can be coupled to produce an observable nonlinear output relationship is the major concern in development of complex physiologic system representations.

Attempting to compare the different insulin release models on a common basis was difficult because of differences in the operational and structural characteristics of the respective models. The best data base upon which to elucidate some of the basic characteristics of pancreatic insulin response to glucose is provided by the rat pancreas perfusion studies of Grodsky et al. One approach to comparing insulin release model would be to fit the parameters of all of the models to the rat data and to determine how the model fits compared with experimental data. However, there are a number of problems which arise in attempting to compare recent human insulin release models on this basis: 1) the model of Cobelli et al. (1980) has no definable steady state for an initial glucose concentration of zero, and the relationship between the nonlinear dose-response function for this model and its derivation from experimental data is unclear; 2) the model of Guyton et al. (1978) has 6 nonlinear input functions in addition to a

number of parameter values that could not be determined a priori from the available rat data; and 3) the model of Cramp and Carson (1981) has no dose-response saturation due to its linearized formulation, and thus selection of a single glucose level at which to quantify the absolute magnitude of insulin response would be rather arbitrary. In this section, recent models of human pancreatic insulin release are instead compared by examining their dynamic response characteristics to patterns of glucose stimulation analagous to those employed in the rat pancreas perfusion studies in the literature. This approach allows a direct qualitative comparison between the general response characteristics of the human insulin release models together with an indication of the desired response behavior as exhibited by the experimental response data of the rat pancreas. Comparison on this basis provides a meaningful assessment of the human models' relative capacities to predict successfully observed characteristics of insulin response over a wide range of glucose stimuli.

The human insulin release models were treated as the isolated perfused pancreas for these simulations. Since different models used different basal glucose steady state set points and respective insulin release rate outputs, the first step was to define a common basis for comparing model responses. Although the baseline or initial glucose stimulation level in the rat studies was 0 mg/dl, the model of Cobelli et al. (1980) had no definable steady state at this glucose concentration. For the human perfusion simulations, a baseline glucose input of 100 mg/dl was selected, as this represents a typical basal arterial plasma glucose level. All of the insulin release models had a steady state secretion rate for a glucose input of 100 mg/dl, but these values varied from model to model (see Table 27). Insulin release rates were thus normalized with respect to values at

TABLE 27. Comparison of steady state insulin model release rates for a glucose input of 100 mg/dl.

Model	Insulin release rate (mU/min)
Guyton et al., 1978	25.8
Cobelli et al., 1980	21.2[a]
Cramp and Carson, 1981	14.0
Landahl and Grodsky, Adapted	24.5

[a]70 kg body weight, G^B = 91.5 mg/dl in Equations 3 and 4

a glucose input of 100 mg/dl, i.e. insulin release rates were expressed by

$$\text{Normalized Insulin Release Rate} = \frac{r_{PIR}(G)}{r_{PIR}(G=100)} \tag{153}$$

for model comparisons.

Experimental results and model predictions for insulin response to multiple glucose step changes are presented in Figure 52. General response characteristics are demonstrated by the rat pancreas perfusion data in the upper left plot. Simulated response of the rat pancreas using the model of Landahl and Grodsky (1982) is included for comparison in the lower left plot. Model predictions for human pancreatic response to a similar pattern of glucose stimulation are shown in the figures to the right. For the initial step increase in glucose, all of the models yielded a biphasic response in insulin release, although the characteristic gradual increase in the rate of second phase release was not predicted by the model of Cramp and Carson. As shown by the rat data, repetition of the step increase in glucose following a short interim period elicited a greater insulin response. Similar potentiation of insulin release on repeated stimulation by glucose has been observed in man (Cerasi et al., 1974). The models of Landahl and Grodsky and Cobelli et al. predicted this potentiation effect of glucose exposure, whereas the model of Guyton et al. gave diminished response and that of Cramp and Carson yielded identical response. In comparing the human models there is roughly an order of magnitude difference in the predicted range of relative insulin responses. This cannot be explained by the differences in respective release rates for a glucose input of 100 mg/dl. The low response predicted by Cobelli et al. can be primarily attributed to rapid saturation of the glucose dose-response curve used in this model; a step increase in glucose concentration as small as

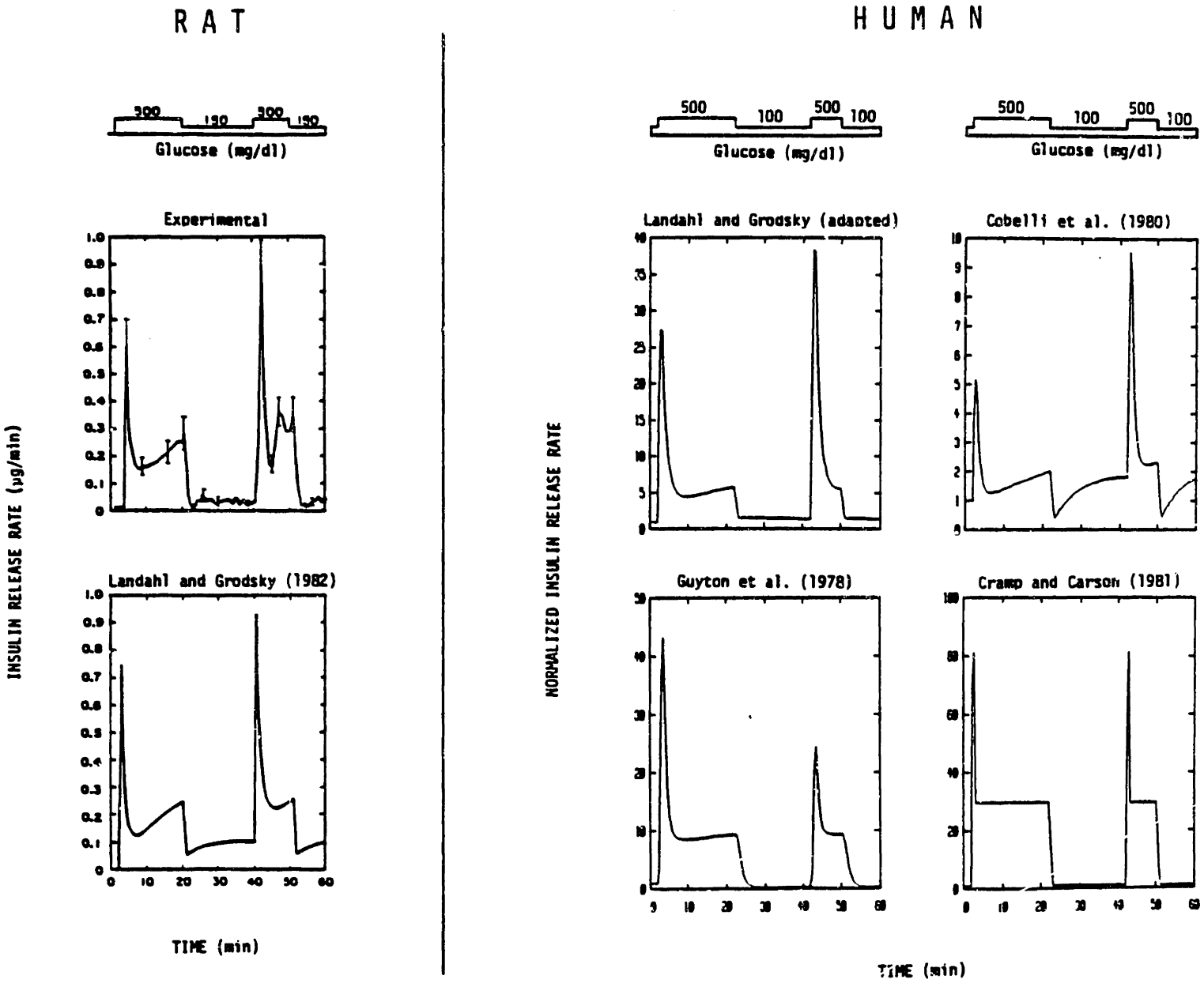

Fig. 52 Experimental data (rat) and model predictions (rat and human) for insulin response of the perfused pancreas to multiple glucose step changes.

from 100 mg/dl to 120 mg/dl essentially elicits maximal initial insulin response. The linear release model of Cramp and Carson, on the other hand, does not incorporate any dose-response saturation, and thus predicts much greater relative insulin response at high glucose concentrations.

Insulin response to a 50 mg/dl staircase glucose stimualtion pattern is shown in Figure 53. For the rat, each successive step increase in glucose concentration elicited a rapid spike response (above the threshold glucose level of 50 mg/dl). Staircase glucose stimulations of insulin release inman have induced similar early phase insulin release characteristics (Karam et al., 1974). Depletion of the labile insulin compartment by the initial glucose step in the model of Cobelli et al. resulted in the appearance of only one spike response. Both the models of Guyton et al. and Landahl and Grodsky predicted successive response spikes of decreasing magnitude. This is quite reasonable considering the glucose range being tested. For both the rat and man, the most sensitive region of the glucose dose-response curve lies between 100 and 150 mg/dl, and thus the step increase in glucose from 100 to 150 mg/dl should be expected to cause the maximal response in both cases, with decreasing release for glucose steps to either side of this range. Noting that the first step increase in the human simulations corrsponds to the maximal step response in the rat studies, the step responses for human release should decrease with each successive glucose step. This is contrary to the linear response predictions of Cramp and Carson's model which will always increase with glucose concentration.

Insulin response to a slow glucose ramp of about 5 mg/dl-min is presented in Figure 54. Again, due to differences in the glucose ranges covered and the relative shapes of dose-response curves, comparison between

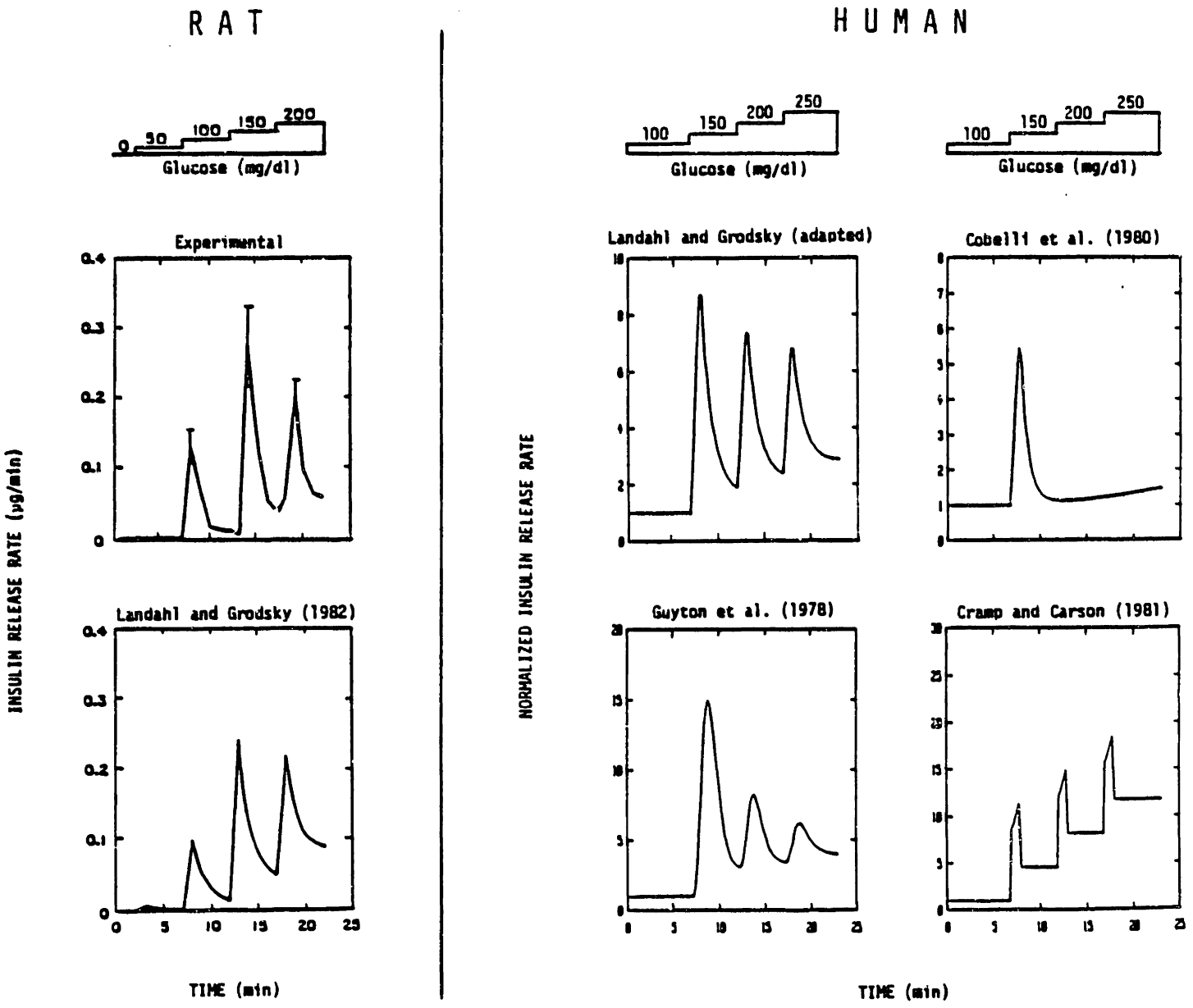

Fig. 53 Experimental data (rat) and model predictions (rat and human) for insulin response of the perfused pancreas to a 50 mg/dl glucose staircase stimulation.

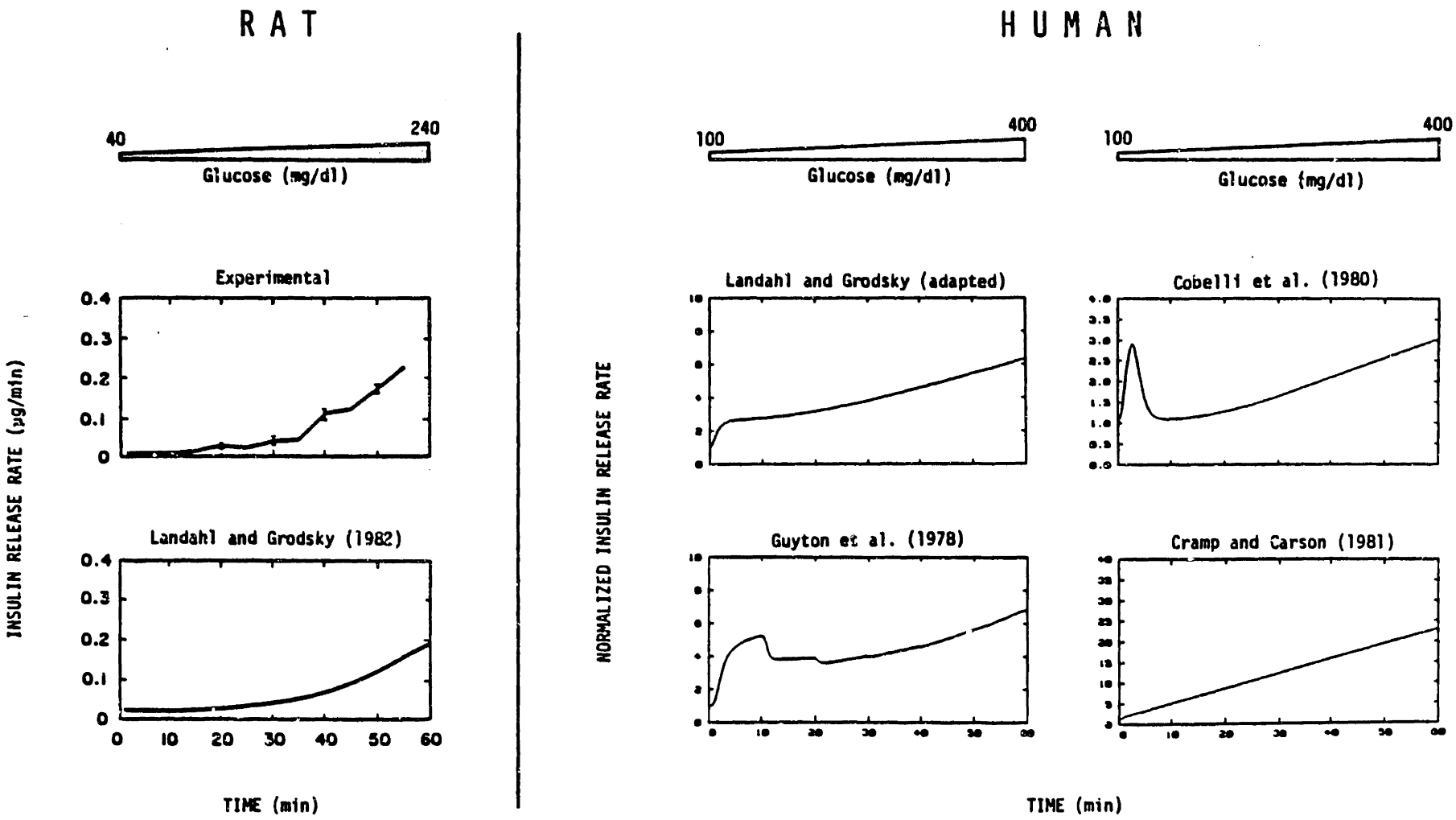

Fig. 54 Experimental data (rat) and model predictions (rat and human) for insulin response of the perfused pancreas to a slow ramp glucose stimulation of about (5 mg/dl)/min.

the rat data and human response predictions is difficult. Of interest is the comparative sensitivities of the human models for triggering of first phase insulin release. Whereas the small 5 mg/dl·min increase in glucose concentration elicited a distinct spike response similar to those caused by a step change in glucose concentration from the model of Cobelli et al., the contributon of first phase release was practically negligible in the response predicted by the model of Cramp and Carson. The model of Landahl and Grodsky yielded a subtle but noticeable initial first phase contribution, while that of the model of Guyton et al. was less subtle and displayed rather unstable characteristics. Since the glucose ramp was initiated at a glucose level of 100 mg/dl in the human simulation and this is a region of maximum dose-response sensitivity, it would seem reasonable that some degree of first phase release could be triggered. The shape of the rat response data over this glucose region, however, would suggest that such a contribution would most likely not be dominant. The response predicted by the model of Landahl and Grodsky would thus appear to be the most realistic.

Insulin response to a faster glucose ramp of about 50 mg/dl·min is shown in Figure 55. Here the rate of increase in glucose concentration was clearly sufficient to induce first phase response characteristics with peak release occurring prior to attainment of the maximum glucose level. This behavior was predicted with varying degrees of success by all of the human model except that of Cramp and Carson for which the maximum release rate coincided with termination of the glucose ramp at the maximum plateau level. The peak rsponse predicted by the model of Cobelli et al. occurred within 1 min of initiating the glucose ramp and was identical to the maximal response elicited by an instantaneaous glucose step increase to 500

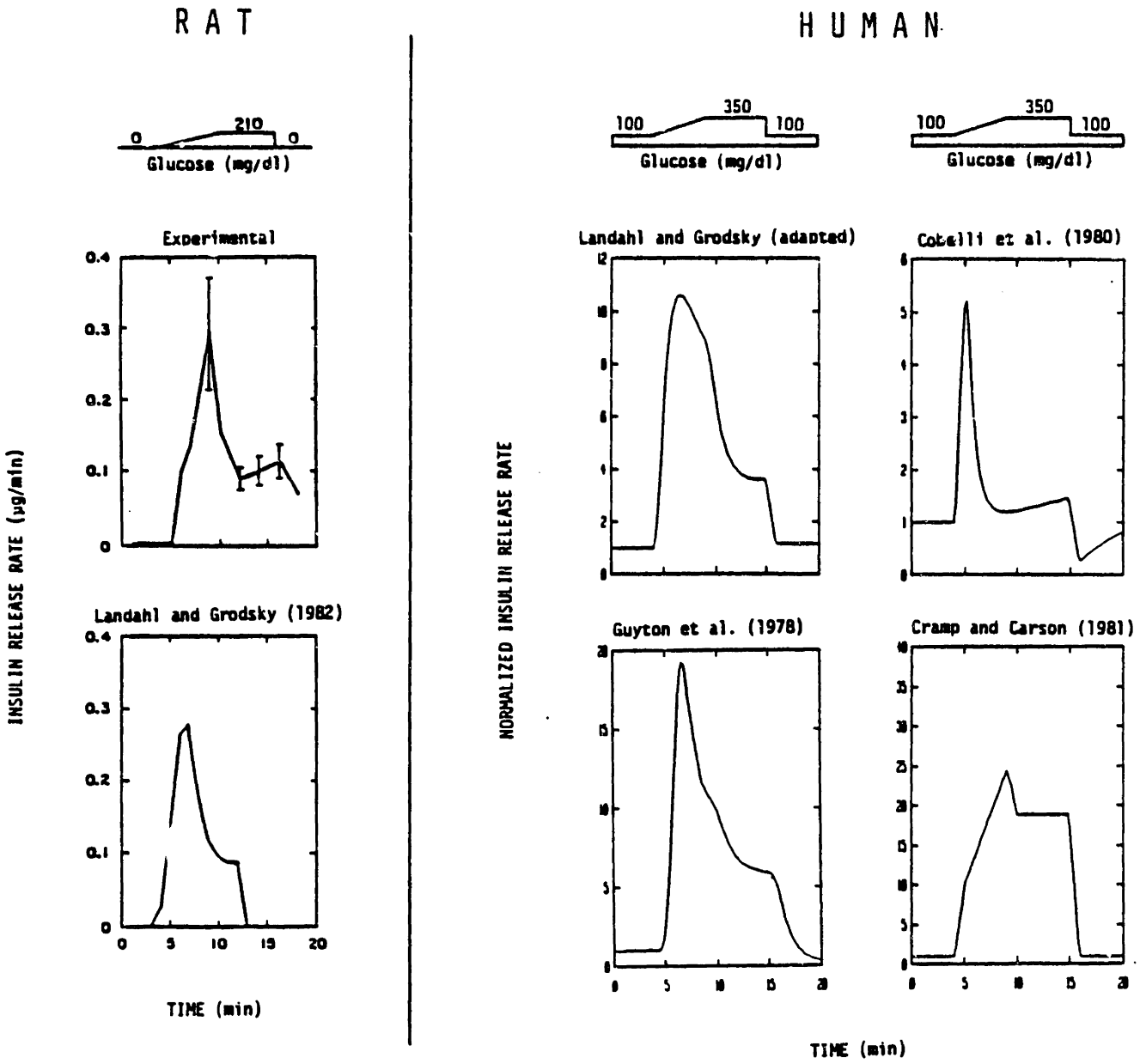

Fig. 55 Experimental data (rat) and model predictions (rat and human) for insulin response of the perfused pancreas to a fast ramp glucose stimulation of about (50 mg/dl)/min.

mg/dl (refer to Figure 52). The peak response rates predicted by the models of Landahl and Grodsky and Guyton et al. were delayed relative to those elicited by an instantaneous glucose step increase, a characteristic supported by the rat data.

In general, the pancreatic insulin release model of Landahl and Grodsky was the most successful in predicting the characteristics of insulin response, its positive attributes not having been affected by human parameter readjustment. The model of Cobelli et al. appeared overly reactive, giving essentially a similar maximal biphasic insulin response to all glucose stimuli. In addition, this model lacked the capacity to produce rapid successive first phase spike responses to a staircase glucose stimulation. The model of Guyton et al. did not demonstrate expected potentiation characteristics and was somewhat unstable with respect to first phase insulin release during a gradual rise in glucose concentration. Finally, the simplistic linear model of Cramp and Carson did not predict any of the more subtle features of pancreatic insulin release and displayed unrealistic trends in relative response magnitudes due to omission of a sigmoidal dose-response characteristic.

O) Distribution of Glucagon in the Body

The total distribution volume for glucagon in the human body may be assumed to equal that for insulin. Thus, summing the vascular and interstitial fluid volumes of the insulin model gives a glucagon distribution volume of 11.31 l.

P) Heterogeneity of Plasma Glucagon

Glucagon is a single polypeptide of 29 amino acids with a molecular weight of 3,485. Measurements of plasma glucagon by radioimmunoassay was

pioneered in the late 1950's (Unger et al., 1961). It was later discovered, however, that most of these antisera were not specific to pancreatic glucagon and cross-reacted with a protein called gut glucagon-like immunoreactivity (GLI) (Moody, 1972). It was not until the late 1960's that a specific antiserum for pancreatic glucagon was discovered (Eisentraut et al. 1968). Since plasma GLI may comprise more than 90% of the total plasma "glucagon" measured with the nonspecific antiseria (Unger et al., 1970), the quantitative validity of early studies with respect to measured values of plasma glucagon in man is questionable.

Subsequent to development of specific radioimmunoassay techniques, it has become evident that plasma immunoreactive glucagon (IRG) exists in a number of different forms in both normal subjects and patients with a variety of disorders (Jaspan and Rubenstein, 1977). Circulating IRG consists of as least four fractions: 1) < 2,000 daltons, 2) 3,500 daltons, 3) 9,000 daltons, and 4) > 40,000 daltons. The biologic significance of fractions other than the 3,500-dalton moiety (true glucagon) has not been established. After an overnight fast, the basal IRG level of a normal individual is about 75 pg/ml, of which only about 25 pg/ml is true glucagon (Unger and Orci, 1976).

Unfortunately, the glucagon model must be formulated from reported observations of IRG levels since distiction between the component fractions seldom appears in the literature. Thus the "glucagon" model predicts IRG levels, which in turn are used for correlating physiologic response in the glucose model. Thus, the distinction between biologically active glucagon and total measured IRG response is also lost in the model formulation. For example, elevation of glucose and insulin levels following a 100 g oral glucose load results in almost complete supression of true glucagon levels

in the circulation (Kuku et al., 1976); measured IRG concentrations seldom decline below about 50 percent of the fasting level, however, because the > 40,000-dalton moiety remains essentially constant under these conditions. The glucagon model predicts this change in IRG concentration by assuming a 50 percent reduction in pancreatic "glucagon" release. In the future, it may be possible to develop a model which directly predicts circulating levels of active glucagon, but such a formulation will require additional research to distinguish the relative fractions of IRG and their significance under various physiologic conditions.

Q) Metabolic Clearance of Glucagon

Plasma IRG is primarily cleared by the liver, which extracts only the 3,500-dalton component, and the kidney, which metabolizes both the 3,500-dalton fraction (by glomerular filtration and peritubular uptake) and the 9,000-dalton component (by peritubular uptake) (Jaspan and Rubenstein, 1977). Fisher et al. (1976) have studied the whole-body metabolic clearance rate (r_{MIC}) of glucagon by continuous infusion of crystalline glucagon in postabsorptive subjects; over the plasma IRG concentration range studied (200-600 pg/ml), glucagon removal was a linear function of plasma concentration with a mean calculated metabolic clearance rate of 13.5 ± 0.6 ml/kg·min based on results of 32 studies. Similar results have been reported by Alford et al. (1976) for studies in 9 normal subjects. Therefore, the metabolic clearance rate r_{MIC} for an average 70 kg man is about 0.91 l/min, and the total rate of plasma glucagon clearance from the body r_{PIC} was expressed

$$r_{PIC} = r_{MIC}\, I \tag{154}$$

R) Pancreatic Glucagon Release

Glucagon is secreted by the α_2 cells of the islets of Langerhans of the pancreas. Secretion of glucagon is regulated by a number of factors, including substrate and hormonal levels, and neural stimuli (Foa, 1972; Unger, 1976; Gerich, 1976a). For situations of interest here, the major factors influencing glucagon secretion would be glucose and insulin concentrations in arterial blood (Gerich, 1976). Amino acids (Rocha et al., 1972; Ohneda et al., 1968), particularly arginine and alanine, stimulate glucagon release. Following ingestion of a mixed meal, amino acids derived from the protein probably constitute an important stimulus for glucagon secretion (Gerich, 1976); in this situation, glucagon release is believed to prevent hypoglycemia secondary to aminogenic insulin secretion (Unger et al., 1969). Conditions of stress, such as trauma or infection, are associated with hyperglucagonemia (Unger, 1971; Bloom, 1973); in such cases, central nervous system response and increased secretion of adrenomedullary catecholamines play a key role.

Glucose and insulin are inhibitors of pancreatic glucagon release. Of primary physiologic significance is the glucagon-stimulating effect of hypoglycemia which signals the liver to increase glucose output. The effects of glucose and insulin on pancreatic IRG secretion were modeled in terms of basal multiplying factors,

$$r_{PIR} = M^{I}_{PIR}\, M^{G}_{PIR}\, r^{B}_{PIR} \tag{155}$$

Under quasi-steady conditions, the plasma IRG level is constant, and the rate of glucagon release equals its rate of clearance (Equation 24),

$$r_{PIR} = r_{PIR} = r_{MIC}\, I \tag{156}$$

Thus, for the basal state,

$$r^{B}_{PIR} = r_{MIC}\, I^{B} \tag{157}$$

and the basal rate of release can be determined directly from the basal IRG concentration. In addition, since the rate of glucagon clearance is proportional to the plasma IRG concentration,

$$r^{N}_{PIR} = \frac{r_{PIR}}{r^{B}_{PIR}} = \frac{I}{I^{B}} = I^{N} \tag{158}$$

Therefore, for any change from the basal to a quasi-steady state, the normalized change in plasma IRG concentration directly reflects the normalized change in pancreatic IRG release.

Presented in Table 28 is pancreatic IRG release rate data correlated form results of studies reported in the literature. The data were compiled from various studies of normal subjects in which plasma IRG levels were reported in response to 1) insulin-induced hypoglycemia (Gerich et al., 1974c; Sacca et al., 1979), 2) euglycemic hyperinsulinemia (Raskin et al., 1975), and 3) hyperglycemia caused by glucose infusions alone (Unger et al., 1970) or combined glucose-insulin infusions (Raskin et al., 1975). Also included are data of Palmer and Ensinck (1975) for glucagon response to ethanol-induced hypoglycemia in normal subjects; since ethanol inhibits hepatic gluconeogenesis, ethanol consumption results in combined hypoglycemia and hypoinsulinemia. In the table, normalized rates of pancreatic glucagon release were computed directly from reported plasma IRG concentrations (see Equation 158). It was desirable for modeling to correlate data in terms of arterial glucose and insulin levels since alpha-cell response results from sensed changes in the arterial plasma concentrations of blood perfusing the pancreatic islets. From the steady state peripheral

TABLE 28. Correlation of literature data relating pancreatic glucagon release to arterial glucose and insulin levels.

Reference	Subjects	Plasma IRG Conc., r (pg/ml)		Normalized Pancreatic Glucagon Release Rate,†	Venous Plasma Insulin Conc. (mU/l)		Normalized Arterial Plasma Insulin Conc.,††	Venous Plasma Glucose Conc., (mg/dl)		Normalized Arterial Plasma Glucose Conc., †††
		Basal	Steady	r^N_{PrR}	Basal	Steady	I^N_L	Basal	Steady	G^N_L
Unger et al., 1970	8	100	57	0.57	8	46	5.8	90	250	2.9
Gerich et al., 1974	15	150	420[a]	2.8	-	-	(>5)[b]	85	35[a]	0.45
	3	160	75	0.47	-	-	(~5)[b]	88	175	2.1
Raskin et al., 1975	10	75	52	0.67	8	40	5.0	75	75	1.1
	5	73	44	0.60	8	45	5.6	80	150	1.9
Palmer & Ensinck, 1975	6	57	68[c]	1.2	10	5[c]	0.5	90	80[c]	0.91
			100[d]	1.8		5[d]	0.5		71[d]	0.79
			260[e]	4.6		2[e]	0.2		55[e]	0.61
Sacca et al., 1979	6	140	155	1.1	11	26	2.4	90	68	0.72
	5	100	220	2.2	8	43	5.4	87	55	0.63

Estimated from: †Equation 168; ††Equation 171; †††Equation 176

[a]Mean Quasi-steady value: t = 30-60 min

[b]Assumed (data not reported)

Quasi-steady values: $^c t$ = 44h; $^d t$ = 56h; $^e t$ = 60h

compartment insulin mass balance (see Equation 107),

$$Q_P^I (I_H - I_{PV}) = F_{PIC}\, Q_P^I\, I_H \; (=r_{PIC}) \tag{159}$$

Solving for arterial insulin concentration gives

$$I_H = \left(\frac{1}{1-F_{PIC}}\right) I_{PV} \tag{160}$$

It thus follows

$$I_H^N = \frac{I_H}{I_H^B} = \frac{\left(\frac{1}{1-F_{PIC}}\right) I_{PV}}{\left(\frac{1}{1-F_{PIC}}\right) I_{PV}^B} = \frac{I_{PV}}{I_{PV}^B} = I_{PV}^N \tag{161}$$

and normalized arterial insulin concentrations were therefore calculated directly from reported peripheral venous insulin concentrations in Table 28. The peripheral compartment glucose mass balance equations (15-16) at steady state give

$$0 = Q_P^G (G_H - G_{PV}) - \frac{V_{PI}}{T_P^G} (G_{PV} - G_{PI}) \tag{162}$$

$$0 = \frac{V_{PI}}{T_P^G} (G_{PV} - G_{PI}) - r_{PGU} \tag{163}$$

from which it follows

$$r_{PGU} = Q_P^G (G_H - G_{PV}) \tag{164}$$

Solving for arterial glucose concentration yields

$$G_H = G_{PV} + \frac{r_{PGU}}{Q_P^G} \tag{165}$$

and thus normalized arterial glucose concentration is given by

$$G_H^N = \frac{G_H}{G_H^B} = \frac{G_{PV} + \frac{r_{PGU}}{Q_P^G}}{G_{PV}^B + \frac{r_{PGU}^B}{Q_P^G}} \tag{166}$$

Normalized arterial glucose concentrations in Table 28 were calculated from reported peripheral venous values using this expression to correct for the effects of peripheral glucose uptake. In these computations, rates of peripheral glucose uptake at the prevailing glucose and insulin levels of each study were estimated using the model functions for this metabolic process (Equations 50 and 51).

Presented in Figure 56 is a plot of normalized pancreatic glucagon release rate as a function of normalized arterial glucose concentration. Data points in the figure represent values correlated in Table 28 from studies in the literature. The glucose and insulin multiplier functions of Equation 155 were assumed to have the hyperbolic tangent form of Equation 27, and parameters were adjusted to obtain a least squares fit of the multiplier functions to the experimental data (IMSL library computer subroutine ZXSSQ). Results of the parameter adjustment yielded

$$M_{PIR}^G = 2.93 - 2.10 \tanh[4.18\ (G_H^N - 0.61)] \tag{167}$$

$$M_{PIR}^I = 1.31 - 0.61 \tanh[1.06\ (I_H^N - 0.47)] \tag{168}$$

for the effects of arterial glucose and insulin levels on pancreatic glucagon release rate, respectively. The glucose multiplier function M_{PIR}^G is shown by the curve in Figure 56. The isolated effects of arterial insulin on pancreatic glucagon release rates are shown in Figure 57. Here, using the glucose multiplier function of Equation 167, values of the insulin

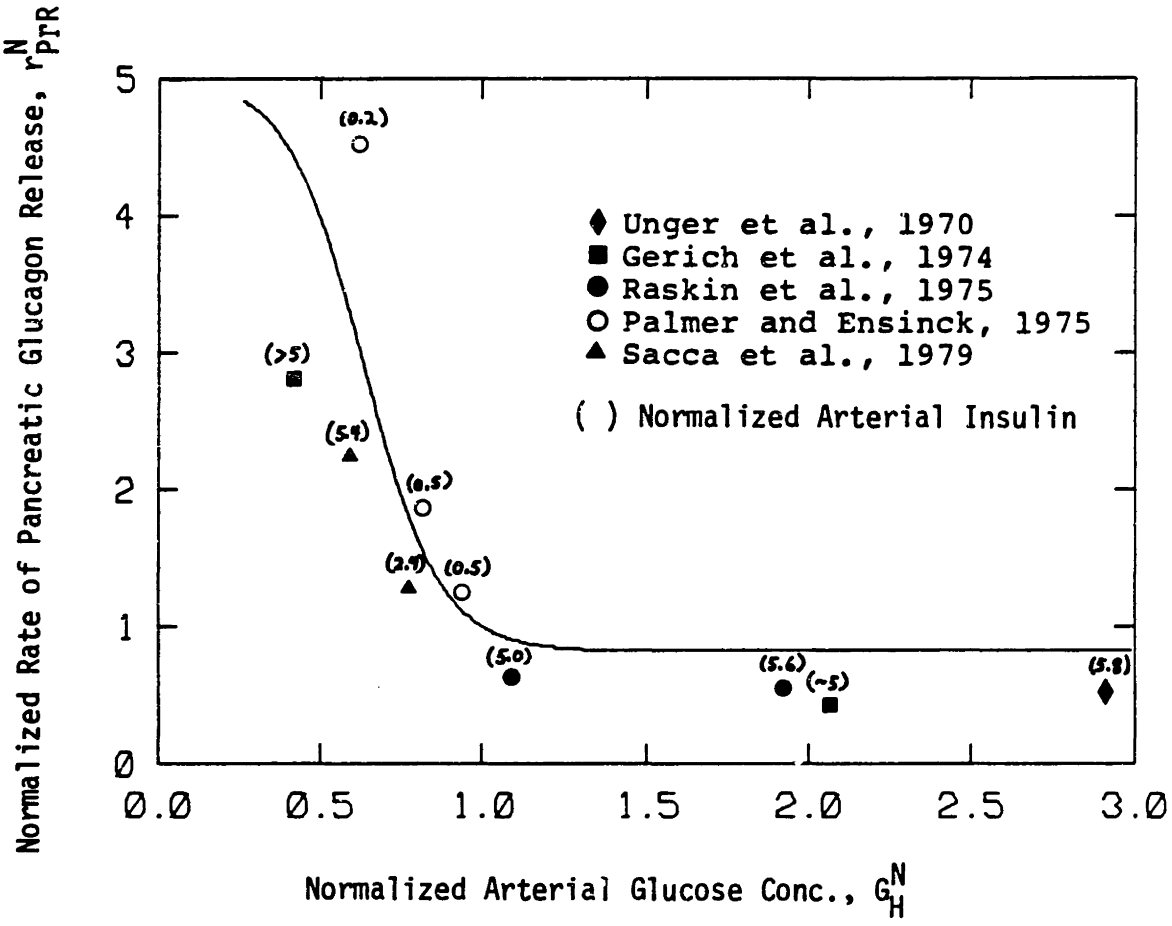

Fig. 56 Plot of normalized rate of pancreatic glucagon release as a function of normalized arterial glucose concentration. The curve indicates the model function for the effect of arterial glucose concentration on pancreatic glucagon release (Equation 167).

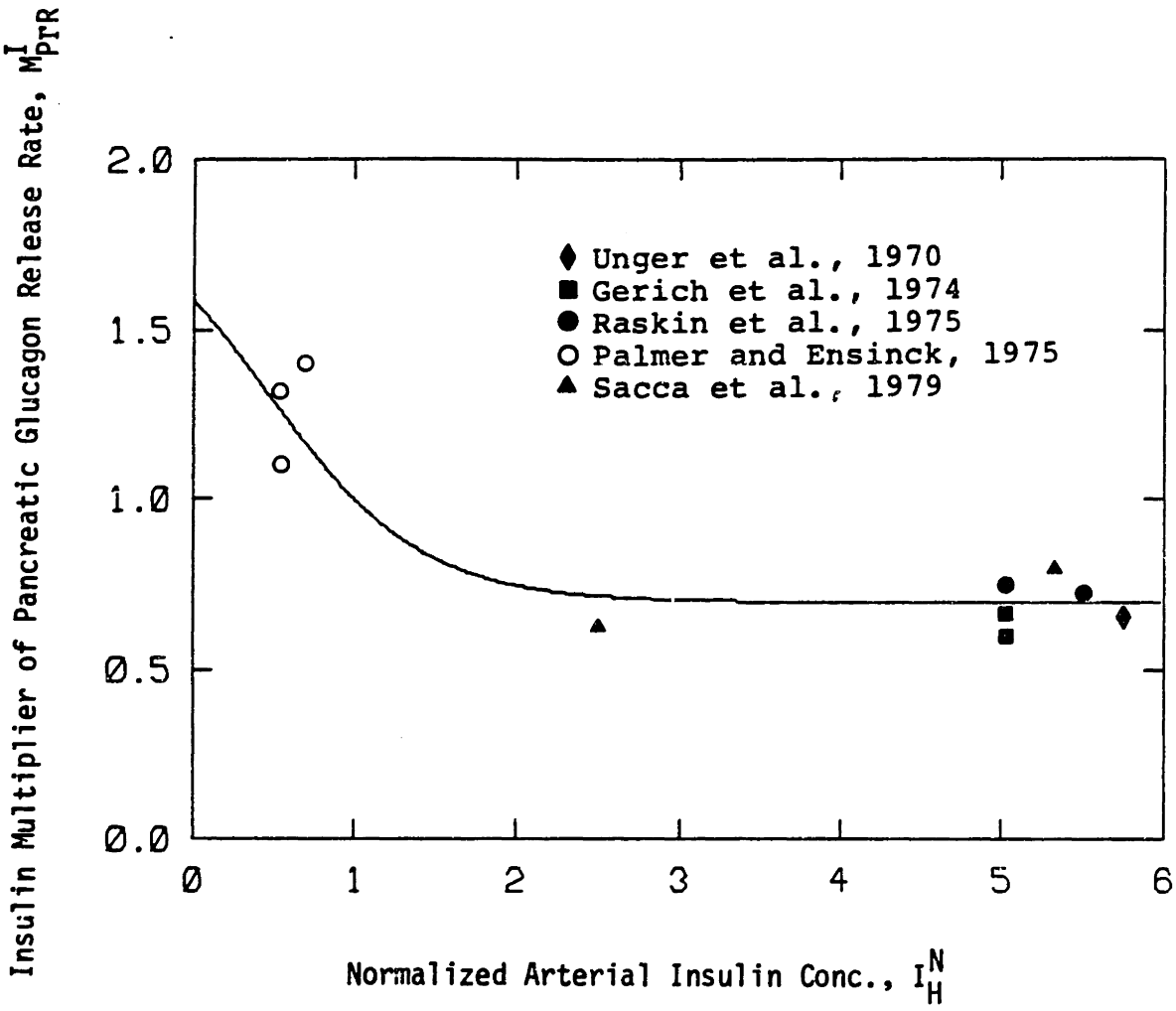

Fig. 57 Plot of insulin multiplier of pancreatic glucagon release rate as a function of normalized arterial insulin concentration. The curve represents the model function for the effect of arterial insulin on pancreatic glucagon release rate (Equation 168).

multiplier for each of the data points (Table 28 and Figure 56) were computed from Equation 155

$$M^{I}_{PrR} = \frac{r^{N}_{PrR}}{M^{G}_{PrR}} \tag{169}$$

and these values were plotted versus normalized arterial insulin concentration. The curve in Figure 57 indicates the insulin multiplier function of Equation 168. As shown in Figure 58, the model multiplier functions for the effects of arterial glucose and insulin concentration yielded good predictions for the rate of pancreatic glucagon release over the range of available data.

S) Summary of Model Equations, Parameter Values, and Mathematical Nomenclature

In this section, a complete summary of the mathematical model is provided, including the differential mass balance equations, the metabolic source and sink function equations, all parameter values in their proper units, and a reference summary of the mathematical nomenclature employed for defining the variables in the normal model.

Glucose Model

Mass Balances:

$$\text{BRAIN:} \quad V^{G}_{BV}\frac{dG_{BV}}{dt} = Q^{G}_{B}(G_H - G_{BV}) - \frac{V_{BI}}{T_B}(G_{BV} - G_{BI})$$

$$V_{BI}\frac{dG_{BI}}{dt} = \frac{V_{BI}}{T_B}(G_{BV} - G_{BI}) - r_{BGU}$$

$$\text{HEART AND LUNGS:} \quad V^{G}_{H}\frac{dG_H}{dt} = Q^{G}_{B}G_{BV} + Q^{G}_{L}G_{L} + Q^{G}_{K}G_{K} + Q^{G}_{P}G_{PV} - Q^{G}_{H}G_{H} - r_{RBCU}$$

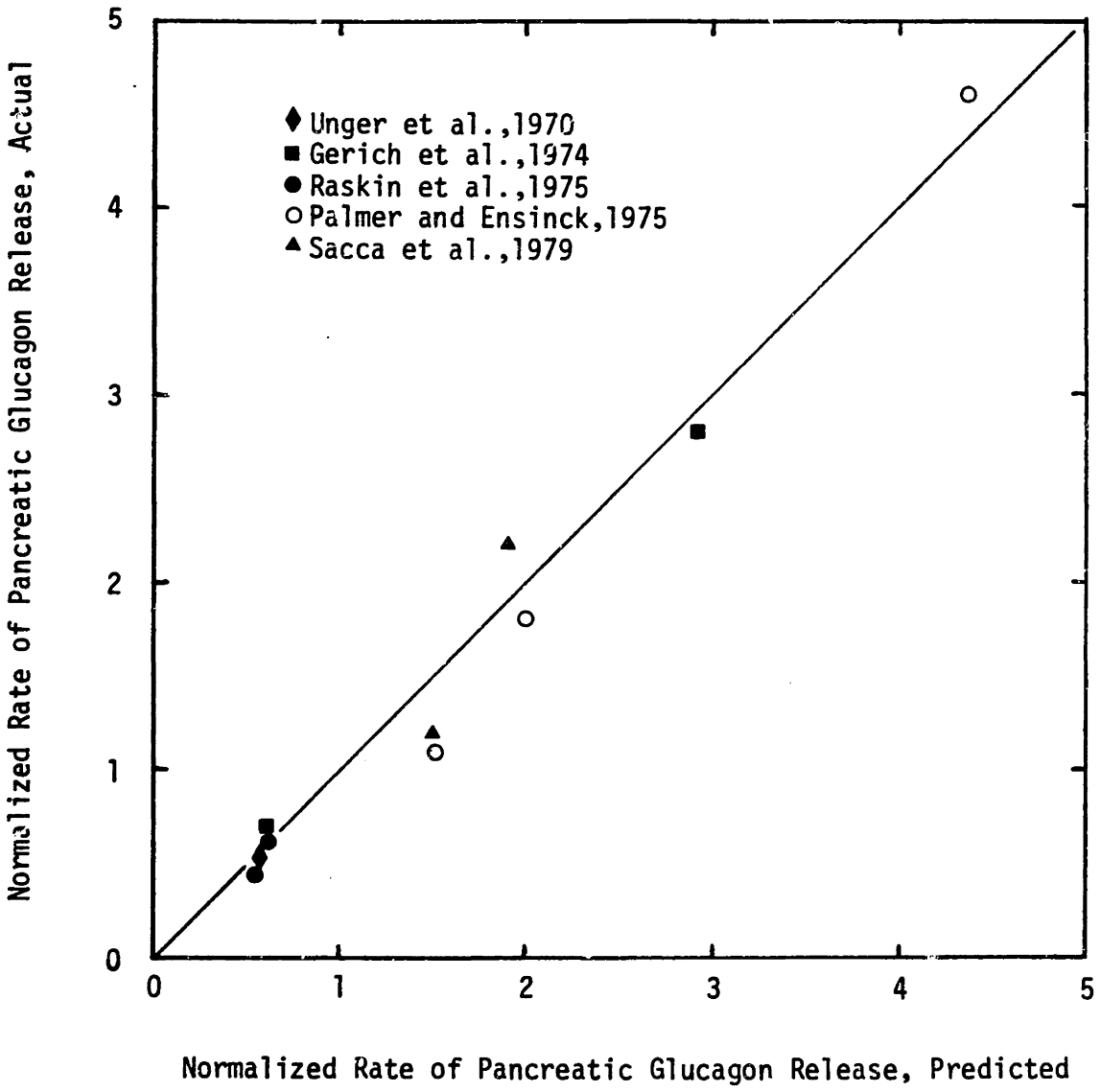

Fig. 58 Plot of actual versus predicted values for normalized rate of pancreatic glucagon release.

$$\text{GUT:} \quad V_G^G \frac{dG_G}{dt} = Q_G^G(G_H - G_G) - r_{GGU}$$

$$\text{LIVER:} \quad V_L^G \frac{dG_L}{dt} = Q_A^G G_H + Q_G^G G_G - Q_L^G G_L + r_{HGP} - r_{HGU}$$

$$\text{KIDNEY:} \quad V_K^G \frac{dG_K}{dt} = Q_K^G (G_H - G_K) - r_{KGE}$$

$$\text{PERIPHERY:} \quad V_{PV}^G \frac{dG_{PV}}{dt} = Q_P^G (G_H - G_{PV}) - \frac{V_{PI}}{T_P^G} (G_{PV} - G_{PI})$$

$$V_{PI} \frac{dG_{PI}}{dt} = \frac{V_{PI}}{T_P^G} (G_{PV} - G_{PI}) - r_{PGU}$$

Metabolic Sources and Sinks:

r_{BGU} = 70 mg/min (constant)

r_{RBCU} = 10 mg/min (constant)

r_{GGU} = 20 mg/min (constant)

$$r_{PGU} = M_{PGU}^I M_{PGU}^G r_{PGU}^B$$

$$r_{PGU}^B = 35 \text{ mg/min}$$

$$M_{PGU}^I = 7.03 + 6.52 \tanh[0.338(I_{PI}^N - 5.82)]$$

$$M_{PGU}^G = G_{PI}^N$$

$$r_{HGP} = M_{HGP}^I M_{HGP}^r M_{HGP}^G r_{HGP}^B$$

$$r_{HGP}^B = 155 \text{ mg/min}$$

$$\frac{d}{dt}[M_{HGP}^I] = \frac{1}{\tau_I}[M_{HGP}^{I\infty} - M_{HGP}^I]$$

$$\tau_I = 25 \text{ min}$$

$$M^{I\infty}_{HGP} = 1.21 - 1.14 \tanh[1.66(I^N_L - 0.89)]$$

$$M^{\Gamma}_{HGP} = M^{\Gamma o}_{HGP} - f_2$$

$$M^{\Gamma o}_{HGP} = 2.7 \tanh[0.39\ \Gamma^N]$$

$$\frac{d}{dt}[f_2] = \frac{1}{\tau_\Gamma}\left[\left(\frac{M^{\Gamma o}_{HGP} - 1}{2}\right) - f_2\right]$$

$$\tau_\Gamma = 65 \text{ min}$$

$$M^{G}_{HGP} = 1.42 - 1.41 \tanh[0.62(G^N_L - 0.497)]$$

$$r_{HGU} = M^{I}_{HGU} M^{G}_{HGU} r^{B}_{HGU}$$

$$r^{B}_{HGU} = 20 \text{ mg/min}$$

$$\frac{d}{dt}[M^{I}_{HGU}] = \frac{1}{\tau_I}\left[M^{I\infty}_{HGU} - M^{I}_{HGU}\right]$$

$$M^{I\infty}_{HGU} = 2.0 \tanh[0.55\ I^N_L]$$

$$M^{G}_{HGU} = 5.66 + 5.66 \tanh[2.44(G^N_L - 1.48)]$$

$$r_{KGE}(\text{mg/min}) = \begin{cases} 71 + 71 \tanh[0.11(G_K - 460)] & 0 < G_K < 460 \text{ mg/min} \\ -330 + 0.872\ G_K & G_K > 460 \text{ mg/min} \end{cases}$$

Parameter values:

$V^G_{BV} = 3.5$ dl	$Q^G_B = 5.9$ dl/min	$T_B = 2.1$ min
$V_{BI} = 4.5$ dl	$Q^G_H = 43.7$ dl/min	$T^G_P = 5.0$ min
$V^G_H = 13.8$ dl	$Q^G_A = 2.5$ dl/min	
$V^G_L = 25.1$ dl	$Q^G_L = 12.6$ dl/min	
$V^G_G = 11.2$ dl	$Q^G_G = 10.1$ dl/min	

$V_K^{\wedge}$ = 6.6 dl Q_K^G = 10.1 dl/min

V_{PV}^G = 10.4 dl Q_P^G = 15.1 dl/min

V_{PI} = 67.4 dl

NOMENCLATURE

Variables:

G = glucose concentration (mg/dl)

Q = vascular blood water flow rate (dl/min)

r = metabolic source or sink rate (mg/min)

M = multiplier of basal metabolic rate (dimensionless)

T = transcapillary diffusion time constant (min)

V = volume (dl)

τ = time constant (min)

t = time (min)

First Subscript: Physiologic Compartment

B = brain

G = gut

H = heart and lungs

L = liver

P = periphery

(A = hepatic artery)

Second Subscript: Physiologic Subcompartment (if required)

I = interstitial fluid space

V = vascular blood water space

Metabolic Rate Subscripts:

BGU = brain glucose uptake

GGU = gut glucose utilization

HGP = hepatic glucose production

HGU = hepatic glucose uptake

KGE = kidney glucose excretion

PGU = peripheral glucose uptake

RBCU = red blood cell glucose uptake

First Superscript

G = glucose model

I = insulin

Γ = glucagon

B = basal value

N = normalized value (divided by basal value)

Second Superscript

0 = initial value (normalized value as $t \to 0^+$)

∞ = asymptotic or final steady state value (normalized)

Insulin Model

Mass Balances:

$$\text{BRAIN:} \quad V_B^I \frac{dI_B}{dt} = Q_B^I(I_H - I_B)$$

$$\text{HEART AND LUNGS:} \quad V_H^I \frac{dI_H}{dt} = Q_B^I I_B + Q_L^I I_L + Q_K^I I_K + Q_P^I I_{PV} - Q_H^I I_H$$

$$\text{GUT:} \quad V_G^I \frac{dI_G}{dt} = Q_G^I(I_H - I_G)$$

$$\text{LIVER:} \quad V_L^I \frac{dI_L}{dt} = Q_A^I I_H + Q_G^I I_G - Q_L^I I_L + r_{PIR} - r_{LIC}$$

$$\text{KIDNEY:} \quad V_K^I \frac{dI_K}{dt} = Q_K^I (I_H - I_K) - r_{KIC}$$

PERIPHERY:
$$V_{PV}^{I}\frac{dI_{PV}}{dt} = Q_{P}^{I}(I_{H} - I_{PV}) - \frac{V_{PI}}{T_{P}^{I}}(I_{PV} - I_{PI})$$

$$V_{PI}\frac{dI_{PI}}{dt} = \frac{V_{PI}}{T_{P}^{I}}(I_{PV} - I_{PI}) - r_{PIC}$$

Metabolic Sources & Sinks:

$$r_{LIC} = F_{LIC}[Q_{A}^{I}I_{H} + Q_{G}^{I}I_{G} + r_{PIR}]$$

$$F_{LIC} = 0.40$$

$$r_{KIC} = F_{KIC}[Q_{K}^{I}I_{K}]$$

$$F_{KIC} = 0.30$$

$$r_{PIC} = \frac{I_{PI}}{[(\frac{1-F_{PIC}}{F_{PIC}})(\frac{1}{Q_{P}^{I}}) - (\frac{T_{P}^{I}}{V_{PI}})]}$$

$$F_{PIC} = 0.15$$

$$r_{PIR} = \frac{S(G_{H})}{S(G_{H}^{B})}r_{PIR}^{B} \qquad \text{[pancreatic insulin release model]}$$

$$\frac{dP}{dt} = \alpha[P_{\infty} - P]$$

$$\frac{dI}{dt} = \beta[X - I]$$

$$\frac{dQ}{dt} = K(Q - Q_{0}) + \gamma P - S$$

$$S = [M_{1}Y + M_{2}(X-I)^{0^{+}}]Q$$

$$X = \frac{(G_{H})^{3.27}}{(132)^{3.27} + 5.93(G_{H})^{3.02}}$$

$$P_{\infty} = Y = (X)^{1.11}$$

P = potentiator (dimensionless)

I = inhibitor (dimensionless)

Q = labile insulin (U)

S = secretion rate (U/min)

X, Y, P_∞ = intermediate variables (dimensionless)

Constants: $= 0.0482\ min^{-1}$ $M_2 = 0.0958\ min^{-1}$

$= 0.931\ min^{-1}$ $= 0.575$ U/min

$K = 0.00794\ min^{-1}$ $Q_0 = 6.33$ U

$M_1 = 0.00747\ min^{-1}$

Parameter values:

V_B^I	= 0.26 l	Q_B^I	= 0.45 l/min	T_P^I	= 20 min
V_H^I	= 0.99 l	Q_H^I	= 3.12 l/min		
V_G^I	= 0.94 l	Q_A^I	= 0.18 l/min		
V_L^I	= 1.14 l	Q_K^I	= 0.72 l/min		
V_K^I	= 0.51 l	Q_P^I	= 1.05 l/min		
V_{PV}^I	= 0.74 l	Q_G^I	= 0.72 l/min		
V_{PI}	= 6.74 l	Q_L^I	= 0.90 l/min		

NOMENCLATURE

Variables:

I = insulin concentration (mU/dl)

Q = vascular plasma flow rate (l/min)

r = metabolic source or sink rate (mU/min)

F = fractional clearance (dimensionless)

T = transcapillary diffusion time constant (min)

V = volume (l)

t = time (min)

First Subscript: Physiologic Compartment

B = brain

G = gut

H = heart and lungs

L = liver

P = periphery

(A = hepatic artery)

Second Subscript: Physiologic Subcompartment (if required)

I = interstitial fluid space

V = vascular plasma space

Metabolic Rate Subscripts:

KIC = kidney insulin clearance

LIC = liver insulin clearance

PIC = peripheral insulin clearance

PIR = pancreatic insulin release

First Superscript

I = insulin model

B = basal value

Glucagon Model

Mass Balance: $V^{\Gamma} \frac{d\Gamma}{dt} = r_{P\Gamma R} - r_{P\Gamma C}$

Metabolic Sources & Sinks:

$$r_{P\Gamma C} = r_{M\Gamma C}{}^{\Gamma}$$

$$r_{M\Gamma C} = 9.10 \text{ ml/min}$$

$$r_{P\Gamma R} = M^{G}_{P\Gamma R} M^{I}_{P\Gamma R} r^{B}_{P\Gamma R}$$

$$M^{G}_{P\Gamma R} = 2.93 - 2.10 \tanh[4.18(G^{N}_{H} - 0.61)]$$

$$M^{I}_{P\Gamma R} = 1.31 - 0.61 \tanh[1.06(I^{N}_{H} - 0.47)]$$

Parameter values: $V^{\Gamma} = 11310$ ml

NOMENCLATURE

Variables:

Γ = glucagon concentration (pg/ml)

V = glucagon distribution volume (ml)

r = metabolic source or sink rate (pg/min)

M = multiplier of basal metabolic rate (dimensionless)

t = time (min)

Metabolic Rate Subscripts:

$P\Gamma C$ = plasma glucagon clearance

$M\Gamma C$ = metabolic glucagon clearance

$P\Gamma R$ = pancreatic glucagon release

First Superscript

G = glucose

I = insulin

Γ = glucagon

B = basal value

N = normalized value (divided by basal value)

III. LITERATURE MODELS OF GLUCOSE METABOLISM

A) Review of Literature Models of Glucose Metabolism

Early mathematical models of glucose metabolism used a linearized two-compartment formulation as originally postulated by Bolie (1960). The model of Ackerman et al. (1965)(Gatewood et al., 1968), shown in Figure 59, provides an example of this approach. Here, glucose in the blood was represented by one compartment (labeled G) and insulin in the blood by a second compartment (labeled H). Glucose was assumed to enter the blood from the intestines at a rate J(t) following an oral dose (model input). In response to this stimulation, glucose and insulin were known to appear and disappear from the blood as a result of various metabolic processes in the body (identified by solid arrows in the figure). In order to minimize mathematical complexity, these metabolic sources and sinks were assumed to add or remove glucose and insulin at rates proportional to the levels of glucose and insulin in the blood compartments. Concentrations of glucose (G) and insulin (I) in the blood were determined by writing mass balances for the blood compartments, given by

$$V_B \frac{dG}{dt} = - m_1(G-G_{basal}) - m_2 (I-I_{basal}) + J(t) \qquad (170)$$

$$V_B \frac{dI}{dt} = - m_3(I-I_{basal}) + m_4 (G-G_{basal}) \qquad (171)$$

where V_B is the volume of the blood compartments, and coefficients m_i are the rate constants for the respective metabolic sources and sinks defined in Figure 59. In order to estimate values for the rate constants, Ackerman et al. assumed a functional representation for the gut glucose input rate J(t) and matched predictions from Equations 170 and 171 with experimental data for the time courses of glucose and insulin during oral glucose

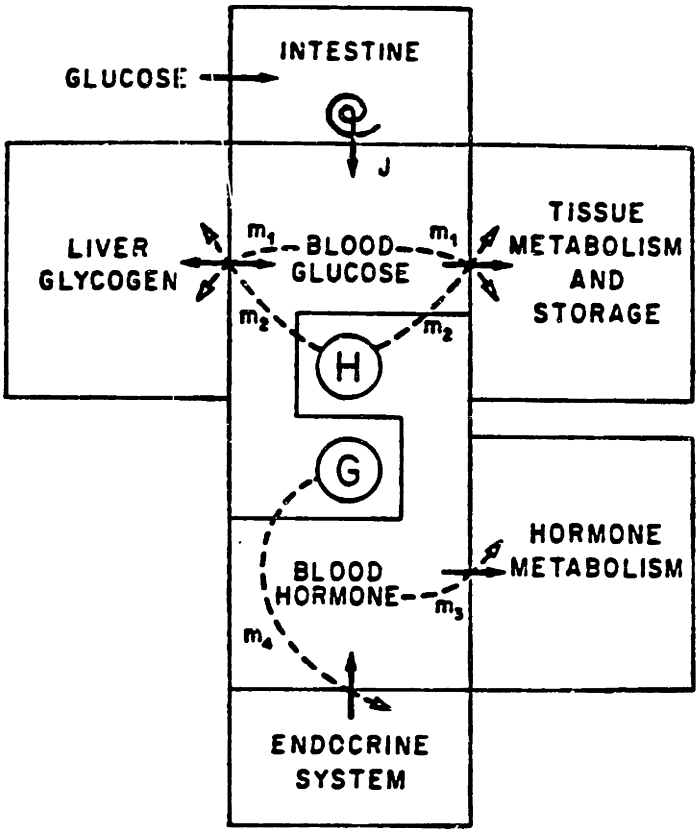

Fig. 59 Linearized two-compartment glucose metabolism model of Ackerman et al. (1965).

tolerance tests. Similar methods were later employed by Segre et al. (1973) to estimate a set of linearized rate constants for predicting blood glucose and insulin concentrations during intravenous glucose tolerance tests. As acknowledged by the authors, these second-order mathematical models were extremely simplified representations of the glucose regulatory system, particularly with respect to linearization of the metabolic rate functions; for example, use of linearization required omission of urinary removal of glucose, because this metabolic process was known to occur only above a threshold level of blood glucose concentration. In addition, the method of using a single input to establish the response characteristics of a model may or may not yield a representation which is adequate in providing a general description of response over a wider spectrum of inputs.

The model of Charette et al. (1967) was one of the first to incorporate nonlinear representations and multihormonal control in describing the glucose metabolic system (for a comprehensive review of earlier models, see Charette et al., 1969). A schematic representation of this model in control system block diagram form (Laplace space) is shown in Figure 60. The mathematical equations for this system were given by

$$\frac{d}{dt}[C] = -K_{19}C + K_{18}[F+f_{LO}(C,X_2)-f_{LU}(C,X_1,Y_3)-f_R(C)-f_U(C,X_2)-GU] \quad (172)$$

$$\frac{d}{dt}[X_1] = -K_8X_1 + K_7[I+f_1(C)] \quad (173)$$

$$\frac{d}{dt}[X_2] = -K_{11}X_2 + K_{10}[G+f_2(C)] \quad (175)$$

where:

C = Plasma Glucose Concentration
X_1 = Plasma Insulin Concentration
X_2 = Plasma Glucagon Concentration
Y_3 = Liver Glycogen Content
F = Intravenous Glucose Input Rate

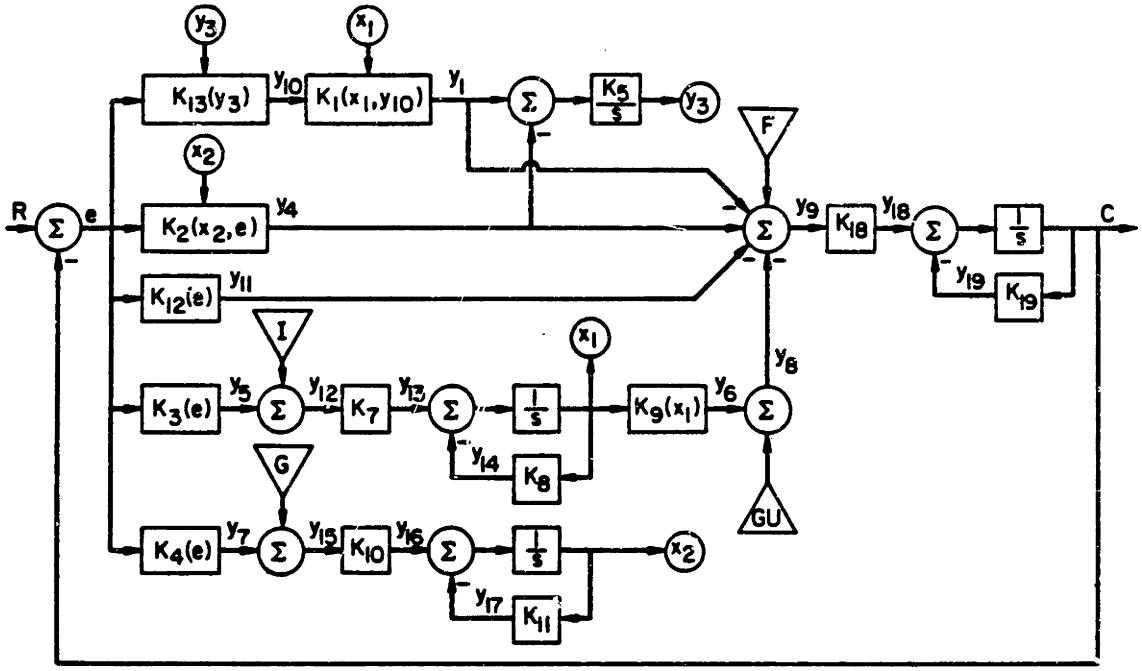

Fig. 60 Glucose metabolism model of Charette et al. (1967) shown in control system block diagram form (Laplace space). (From Charette et al., 1969)

GU = CNS Glucose Utilization Rate

I = Intravenous Insulin Input Rate

G = Intravenous Glucagon Input Rate

$f_{LO}(C,X_2)$ = Liver Glucose Output Rate

$f_{LU}(C,X_1,Y_3)$ = Liver Glucose Uptake Rate

$f_R(C)$ = Renal Excretion Rate

$f_U(C,X_1)$ = Insulin-Dependent Peripheral Tissue Glucose Uptake Rate

$f_1(C)$ = Insulin Secretion Rate

$f_2(C)$ = Glucagon Secretion Rate

K_{18},K_7,K_{10} = Circulation Volumes

K_{19},K_8,K_{11} = Inverse Degradation time Constants

In this model, single compartment representations were included for plasma glucose, insulin, and glucagon, respectively, with an additional equation used to monitor liver glycogen content. Hormonal secretion rates f_i were expressed in terms hyperbolic tangent functions of the plasma glucose concentration, and glucose metabolic rates f were given by nonlinear functions of the plasma glucose and hormone levels. The system was defined to represent a normal, 70 kg unstressed adult. Model parameters were obtained from intrepretation of the literature, and refined by simulating glucose and insulin infusion experiments.

The glucose homeostatis model of Foster et al. (1973) (Foster, 1970) is shown in Figure 61. In this model, glucose metabolism was formulated in terms of three compartments, representing blood glucose, liver glycogen, and muscle glycogen. In addition, single compartment representations were included for plasma insulin, glucagon, and free fatty acids. The nonlinear metabolic processes causing addition or removal of substances from their respective compartments are identified in the figure. The mass balance equations for this model were given by

$$\frac{d}{dt}[GG] = INJ-U-NSU-RBCU+GLUNEO+GLYO-GLYS-ATU-MU+LULAC \qquad (175)$$

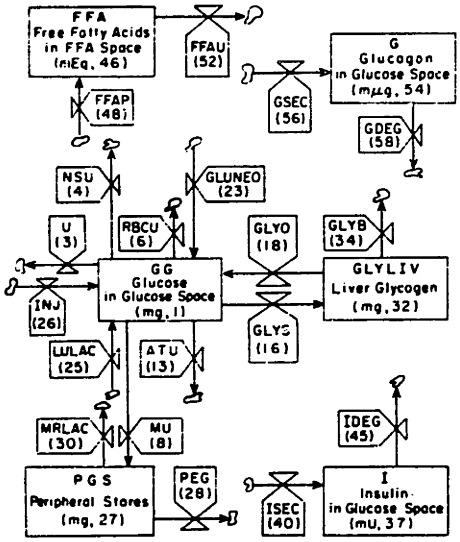

Fig. 1 Symbols: The rectangles represent levels (i.e., amounts-units are in mass, viz., mg, mEq., etc). The decantor-shaped figures represent rates (i.e., mg/min, etc.). The small irregular shapes represent compartments. (The numbers are computer programming designations and can be disregarded.)

The basic features and components of the model for glucose homeostasis are shown with a provision for intravenous perturbations with glucose (INJ). The glucose in the glucose space (GG) can exit or enter via multiple pathways including urine loss (U), nervous system uptake (NSU), red blood cell uptake (RBCU), gluconeogenesis (GLUNEO), adipose tissue utilization (ATU), or muscle uptake (MU). Peripheral glucose storage (PGS) is primarily muscle. Muscle release of lactate (MRLAC) and liver uptake of lactate (LULAC) are shown. In addition, provision is made for muscle utilization of glucose for energy (PEG).

The hepatic glucose uptake rate (GLYS), hepatic glucose release rate (GLYO) and glycogen breakdown rate (GLYB) regulate the hepatic glycogen stores (GLYLIV).

The amount of insulin in the glucose space (I) is regulated by the insulin secretion rate (ISEC) and insulin degradation rate (IDEC). Similarly, the amount of glucagon in the glucose space (G) is regulated by both the glucagon secretion rate (GSEC) and the glucagon degradation rate (GDEG).

The free fatty acids in the free fatty acid space (FFA) are regulated by both the free fatty acid production rate (FFAP) and the free fatty acid utilization rate (FFAU) (from reference [18]).

Fig. 61 Physiologic model of glucose metabolism as formulated by Foster et al. (1973).

$$\frac{d}{dt}[GLYLIV] = GLYS-GLYB \quad (176)$$

$$\frac{d}{dt}[PGS] = MU-PEG-MRLAC \quad (177)$$

$$\frac{d}{dt}[FFA] = FFAP-FFAU \quad (178)$$

$$\frac{d}{dt}[G] = GSEC-GDEG \quad (179)$$

$$\frac{d}{dt}[I] = ISEC-IDEG \quad (180)$$

where:
GG = Glucose in Glucose Space
GLYLIV = Liver Glycogen
PGS = Peripheral Tissue Glucose Stores
FFA = Free Fatty Acids in FFA Space
G = Glucagon in Glucagon Space
I = Insulin in Insulin Space
INJ = Intravenous Glucose Infusion Rate
U = Urinary Glucose Loss Rate
NSU = Nervous System Glucose Uptake Rate
RBCU = RBC Glucose Uptake Rate
GLUNEO = Rate of Glucose Production by Liver Gluconeogenesis
GLYS = Rate of Glucose Conversion to Liver Glycogen
GLYO = Rate of Glucose Production from Liver Glycogen Breakdown
ATU = Adipose Tissue Glucose Uptake Rate
MU = Muscle Glucose Uptake Rate
LULAC = Rate of Liver Lactate Uptake
PEG = Rate of Muscle Glucose Utilization for Energy
MRLAC = Muscle Lactate Release Rate
FFAP = FFA Production Rate
FFAU = FFA Utilization Rate
GSEC = Glucagon Secretion Rate
GDEG = Glucagon Degradation Rate
ISEC = Insulin Secretion Rate
IDEG = Insulin Degradation Rate

Particular attention was focused on developing a representation of

pancreatic insulin secretion rate (ISEC) as related to the dynamics of blood glucose following rapid glucose infusion. By assuming that the rate of pancreatic insulin release was a function not only of the glucose concentration but also of the rate of change of the glucose concentration with time, the model was quite successful in predicting the qualitative features of the plasma insulin dynamics following rapid glucose infusion.

Cerasi et al. (1974) developed a mathematical model for the purpose of analyzing the interplay of glucose and insulin during glucose infusions. The model used a single compartment to represent glucose dynamics during hyperglycemia and included nonlinear glucose removal by tissues, endogenous glucose appearance during hypoglycemia, and glucose excretion through urine. Insulin dynamics were modeled in terms of a three-compartment representation. This formulation was originally derived by Silvers et al. (1969) to describe the rate of plasma insulin-I^{131} disappearance in man, and assumed that insulin was distributed in plasma, interstitial fluids, and a third, hypothetical compartment. The glucose metabolism model, shown in schematic block diagram form in Figure 62, was described by

$$V_g \frac{dg}{dt} = G_{in} - r_{KGE}(g)+r_{GIH}(g)-r_{PGU}(i_L,g) \tag{181}$$

$$\frac{di_p}{dt} = -(\frac{1}{\tau_{ip}})i_p-r_i(i_p-i_L)+C_1 r_{PIR}(g) \tag{182}$$

$$\frac{di_L}{dt} = r_i \varepsilon_i(i_p-i_L)-r_{iL}\ (i_L-i_3) \tag{183}$$

$$\frac{di_3}{dt} = r_{iL}\varepsilon_{iL}(i_L-i_3)-(\frac{1}{\tau_{i3}})i_3 \tag{184}$$

where: g = Glucose Concentration Above Fasting Level

i_p = Plasma Insulin Concentration Above Fasting Level

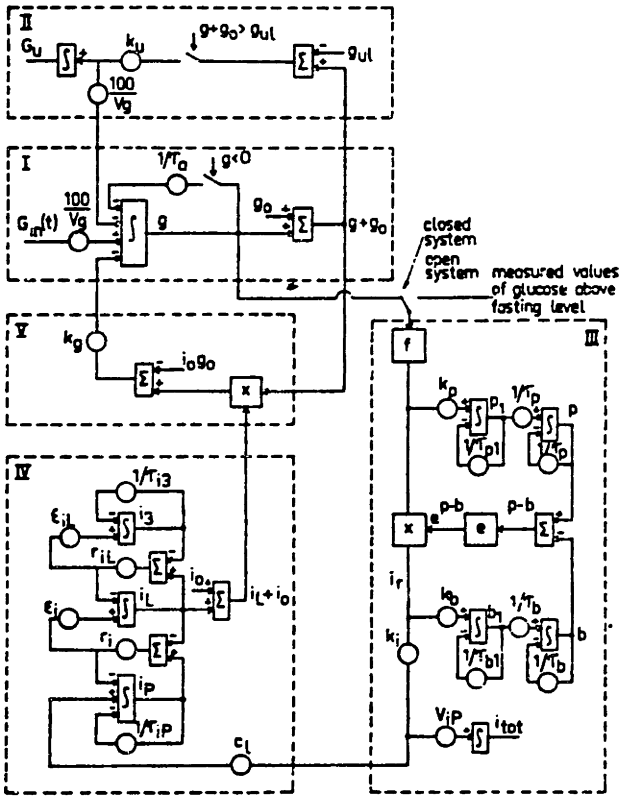

Fig. 62 Schematic control system diagram (Laplace space) of the glucose metabolism model of Cerasi et al. (1974).

i_L = Interstitial Fluid Insulin Concentration Above Fasting Level

i_3 = Insulin Concentration Above Fasting Level in Hypothetical Compartment

V_g = Glucose Distribution Volume

G_{in} = Intravenous Glucose Infusion Rate

r_{KGE} = Kidney Glucose Excretion Rate

r_{GIH} = Rate of Glucose Input during Hypoglycemia

r_{PGU} = Peripheral Tissue Glucose Uptake Rate

r_{PIR} = Pancreatic Insulin Release Rate above Basal

τ_{ip}, τ_{i3}, = Insulin Degradation Time Constants

r_i, r_{iL} = Insulin Transfer Rate Constants

$\varepsilon_i, \varepsilon_{iL}$ = Dimensionless Distribution Parameters

C_1 = Fraction of Insulin Passing Through Liver Without Being Degraded

Cerasi et al. combined modeling studies and experimental studies primarily to elucidate the factors governing glucose stimulation of insulan release rate from the pancreas (r_{PIR}). Based on the experimental observation that repeated glucose stimuli induced different insulin responses depending on the time-intervals of the infusion and recovery periods, time variance was introduced into the model functions for insulin secretion. The resulting formulation employed a series of 5 equations (4 differential equations) to relate the rate of insulin release to the blood glucose concentration. This submodel of pancreatic insulin release (see review in pancreatic insulin release section) incorporated hypothetical potentiators and inhibitors of insulin release that varied with time as a result of hyperglycemia, this providing an empirical formulation to account for the observed variances in insulin response to repeated glucose stimulation.

Insel et al. (1975) used insulin and glucose models to analyze insulin mediated glucose disposal during euglycemic hyperinsulinemia (glucose clamp

technique) in normal subjects. Three-compartment glucose and insulin models were employed as illustrated in Figure 63. The glucose model included a central blood water compartment (6) in rapid equilibrium with a smaller compartment (9) and in slow equilibrium with a larger compartment (7). Metabolic glucose sinks included constant central nervous system glucose removal from the blood and insulin-dependent glucose removal from the rapidly equilibrating compartment. Glucose inputs included endogenous (liver) glucose production and the intravenous glucose required to maintain euglycemia following elevation of plasma insulin levels. The insulin model was that originally developed by Sherwin et al. (1974) based on studies of insulin kinetics in man: plasma insulin (compartment 1) was assumed in rapid equilibrium with a small compartment (2) and in slow equilibration with a larger compartment (3). Insulin was removed from the plasma by a linear first-order process, and endogenous (pancreatic) insulin release was assumed to remain constant at its basal value during euglycemic clamping. Intravenous insulin was also included as a plasma insulin input. During the euglycemic clamp experiments, [^{14}C]-glucose turnover was used to measure the rate of endogenous glucose production. Thus, the total rate of glucose disposal could be calculated from the difference between the glucose infusion input required to maintain normal glycemia and the endogenous glucose production rate. By comparing model simulations with experimental data, Insel et al. observed that following elevation of plasma insulin levels, the increase in glucose disposal correlated well with insulin concentration in the slowly equilibrating insulin model compartment. It was thus proposed that the change in glucose disposal per unit change in the slowly equilibrating insulin compartment could provide a clinical index of patient insulin sensitivity.

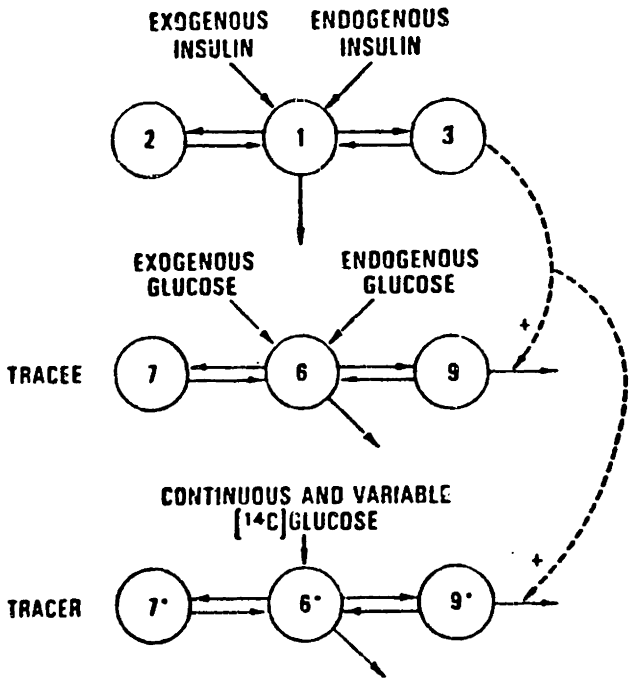

Fig. 63 Combined glucose and insulin models employed by Insel et al. (1975) to analyze euglycemic insulin clamp data. The dashed lines indicate the observed result that insulin-dependent glucose utilization correlated well with concentration of insulin in the slowly equilibrating insulin model compartment.

Over the last decade, accumulation of experimental data has provided greater insight into the mechanisms of glucose regulation. This has spawned a new generation of mathematical models. Recent models include that of Cramp and Carson (1981) which is shown in Figure 64. The role of the liver in glucose metabolism was emphasized by inclusion of compartments for hepatic glucose 6-phosphate and hepatic glycogen in addition to plasma and portal glucose compartments. Portal and plasma compartments were provided for insulin and glucagon, and a single compartment for plasma adrenalin. Metabolic processes causing addition or removal of substances from their respective compartments are identified in the figure. In this model, the pancreatic insulin release rate was assumed to be proportional to both the portal glucose level and its rate of change with respect to time. Nonlinear representations were employed to model the rate of peripheral tissue uptake of plasma glucose and the enzymatic reactions involved in liver metabolism. Mass balance formulations for each compartment resulted in a set of 9 nonlinear ordinary differential equations. Plasma and hormonal distribution volumes were selected to represent a 70 kg subject with a liver mass of 1.5 kg. The mass balance equations for this model, as published, were difficult to interpret because numerical values were inserted directly into the formulations without any term-by-term identification of the contributing processes. Furthermore, the compartment volumes were apparently abstractions, since both "plasma" and "portal" distribution volumes were assigned equal values of 3.2 l. Finally, the model's initial conditions were cited in units that were not in agreement with the units specified in the equations. Unfortunately, communication with the authors failed to clarify these issues.

The model of Cobelli et al. (1982) is presented in Figure 65. Glucose

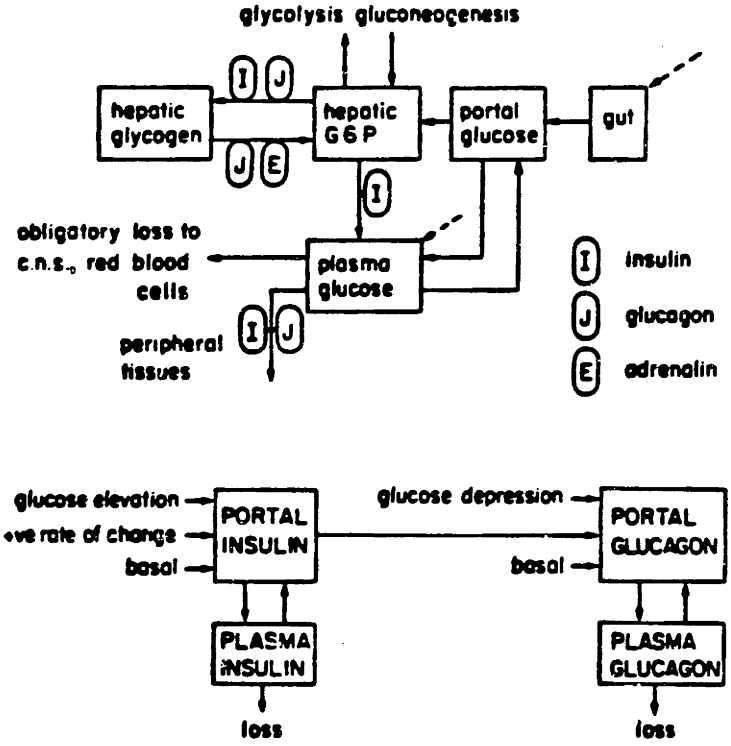

Fig. 64 Schematic representation of glucose model developed by Cramp and Carson (1981).

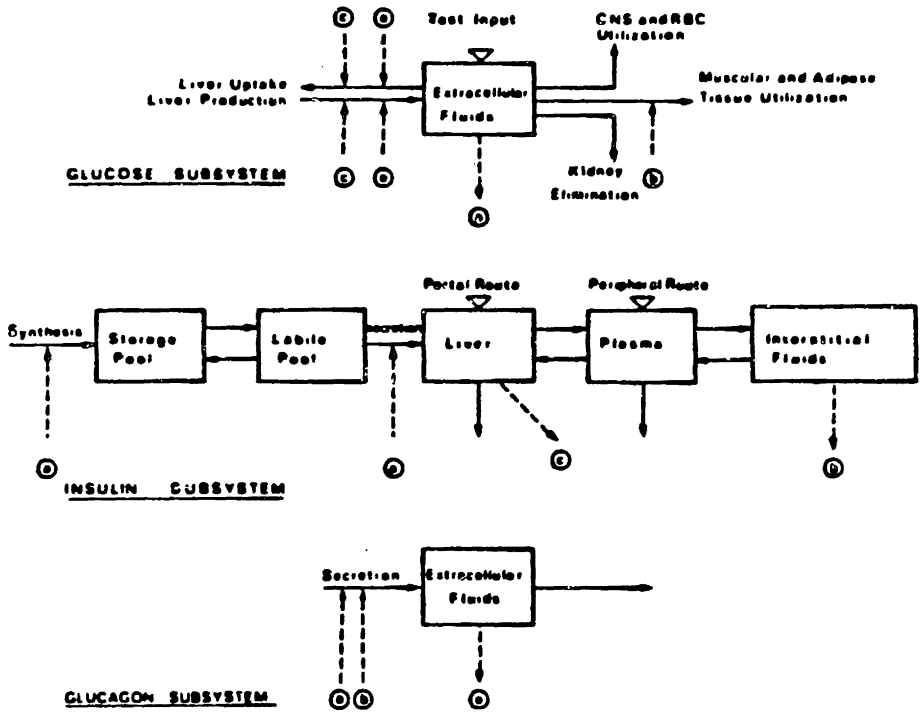

Fig. 65 Model of glucose metabolism formulated by Cobelli et al. (1982). (Figure from Cobelli et al., 1983)

was described by a single compartment representing extracellular fluids. The metabolic processes associated with glucose metabolism included renal excretion, liver glucose uptake and production, glucose utilization by muscle and adipose tissues, and insulin independent glucose utilization by the central nervous system and red blood cells. Insulin distribution was formulated on the basis of the three-compartment model originally developed by Sherwin et al. (1974); based on the analysis of studies of insulin kinetics in man, plasma insulin was assumed to equilibrate with two extravascular compartments: a large compartment associated with interstitial fluids (slow equilibration), and a small compartment assumed to be liver (rapid equilibration). Insulin secretion was formulated in terms of a two-compartment model (Cobelli et al., 1980) in which insulin synthesis and secretion rates were nonlinearly controlled by glucose. Glucagon was described using a single compartment. The model formulation resulted in a set of nonlinear ordinary differential equations, given by

$$\frac{d}{dt}[x_1] = F_1(x_1,u_{12},u_2) - F_2(x_1,u_{12}) - F_3(x_1) - F_4(x_1,u_{13}) - F_5 + I_x \quad (185)$$

$$\frac{d}{dt}[u_{11}] = -(m_{01} + m_{21} + m_{31})\, u_{11} + m_{12}u_{12} + m_{13}u_{13} + I_u \quad (186)$$

$$\frac{d}{dt}[u_{12}] = -(m_{02} + m_{12})\, u_{12} + m_{21}u_{11} + F_6(x_1) \quad (187)$$

$$\frac{d}{dt}[u_{13}] = -m_{13}u_{13} - m_{31}u_{11} \quad (188)$$

$$\frac{d}{dt}[u_2] = -h_{02}u_2 + F_7(x_1, u_{13}) \quad (189)$$

where:

x_1 = Quantity of Glucose in Plasma and Extracellular Fluids
u_{11} = Quantity of Insulin in Plasma
u_{12} = Quantity of Insulin in Liver
u_{13} = Quantity of Insulin in Extracellular Fluids
u_2 = Quantity of Glucagon in Plasma and Extracellular Fluids

$F_1(x_{11},u_{12},u_2)$ = Liver Glucose Production Rate

$F_2(x_1,u_{12})$ = Liver Glucose Uptake Rate

$F_3(x_1)$ = Renal Glucose Excretion Rate

$F_4(x_1,u_{13})$ = Peripheral Insulin-Dependent Glucose Uptake Rate

F_5 = Peripheral Insulin-Independent Glucose Utilization Rate

I_x = Intravenous Glucose Infusion Rate

m_{ij} = Insulin Transfer Rate Constants

h_{02} = Inverse Time Constant for Glucagon Degradation

$F_7(x_1,u_{13})$ = Glucagon Secretion Rate

$F_6(x_1)$ = Insulin Secretion Rate

and where the rate of pancreatic insulin secretion $F_6(x_1)$ was calculated from the two-compartment insulin release model previously reviewed in the pancreatic insulin release section of the text. Distribution volumes of the various compartments were assumed to constitute a fixed percentage of body weight and metabolic rates were formulated on a per kg basis. The nonlinear metabolic functions F_i were formulated in terms of multiplicative hyperbolic tangent functions.

Tiran et al. (1975) have employed compartmentalization techniques similar to those originally developed for simulating drug distribution. As shown in Figure 66, the body was divided according to the main organs and tissues involved in glucose dynamics, and the resulting compartments were interconnected according to their relative locations in the circulatory system. Mass balance formulations with respect to this approach were explained in detail earlier in the text. Physiologic parameters (distribution volumes and blood flow rates) were selected to represent a 70 kg man. This model was employed to simulate the initial dynamics of glucose distribution following rapid intravenous glucose infusions. For these preliminary studies, the glucose model was not coupled with an insulin representation and mediation of glucose metabolism was not included in the

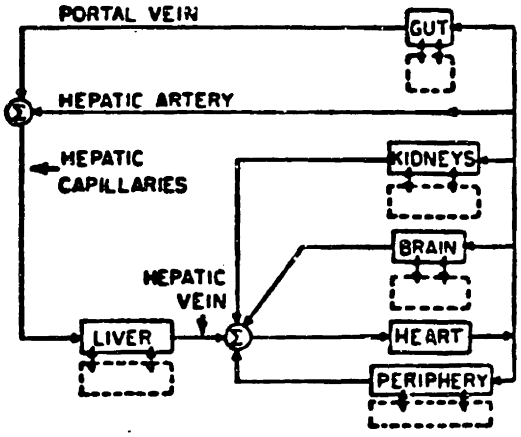

Fig. 66 Schematic diagram of physiologic compartmentalization employed by Tiran et al. (1975).

formulation. Since publication of these initial studies with the human model, Tiran et al. have directed their efforts toward mathematical modeling of glucose and insulin dynamics in the dog. Here, the basic compartmentalization illustrated in Figure 66 was retained, and physiologic parameters typical of a 12 kg dog were selected. A model of insulin dynamics (Tiran et al., 1979) was developed first. In this model, the kidney and liver removed insulin in direct proportion to its rate of delivery (in the blood), while peripheral tissue insulin removal was represented in a nonlinear fashion. No formulation for pancreatic insulin release was included. The insulin model was later coupled with a glucose model (Tiran et al., 1980). The glucose model included constant glucose utilization by brain, gut, and red blood cells, kidney glucose excretion, and nonlinear glucose and insulin mediated glucose utilization by liver and periperhal tissues. The combined model was used to simulate experimental results obtained during glucose and insulin infusions in pancreatectomized dogs, and has subsequently been modified (Tiran et al., 1981) to include separate compartmentalization of red blood cells within each vascular space. This improved model performance by taking into account the limited permeability of dog erythrocytes to glucose. The complete glucose-insulin model formulation of Tiran et al. (1981) resulted in a total of about 40 compartments and is shown in block diagram form in Figure 67.

Guyton et al. (1978) (Guyton, 1973) have used the tissue and organ compartmentalization approach to model glucose metabolism in man. A schematic representation of the model is shown in Figure 68. Physiologic parameters were selected to represent a 70 kg adult man. In the glucose model, glucose utilization by red blood cells, brain, and central organ compartment tissues (gut and heart muscle) were constant. Loss of glucose through

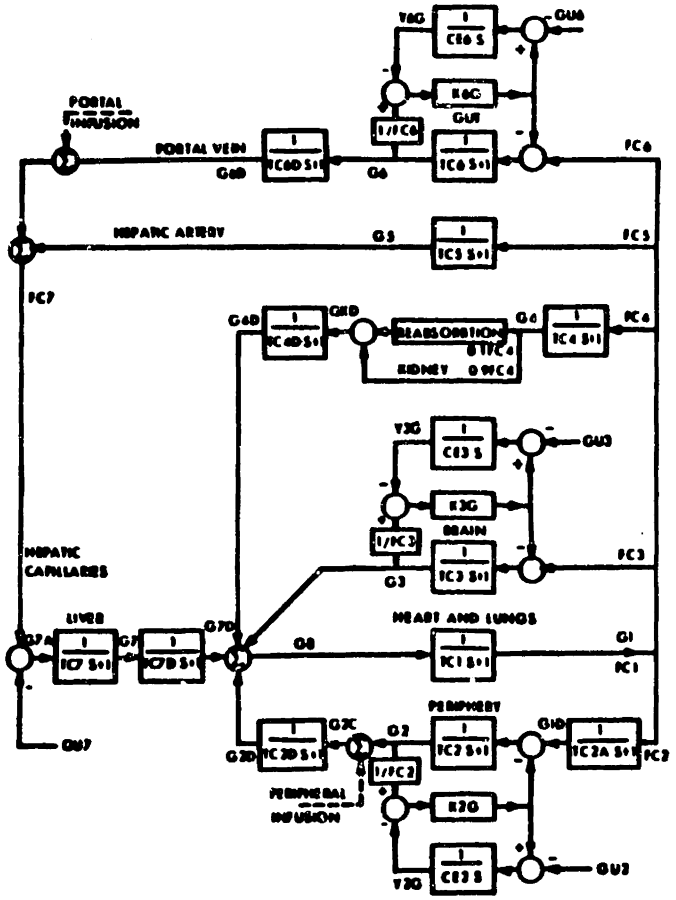

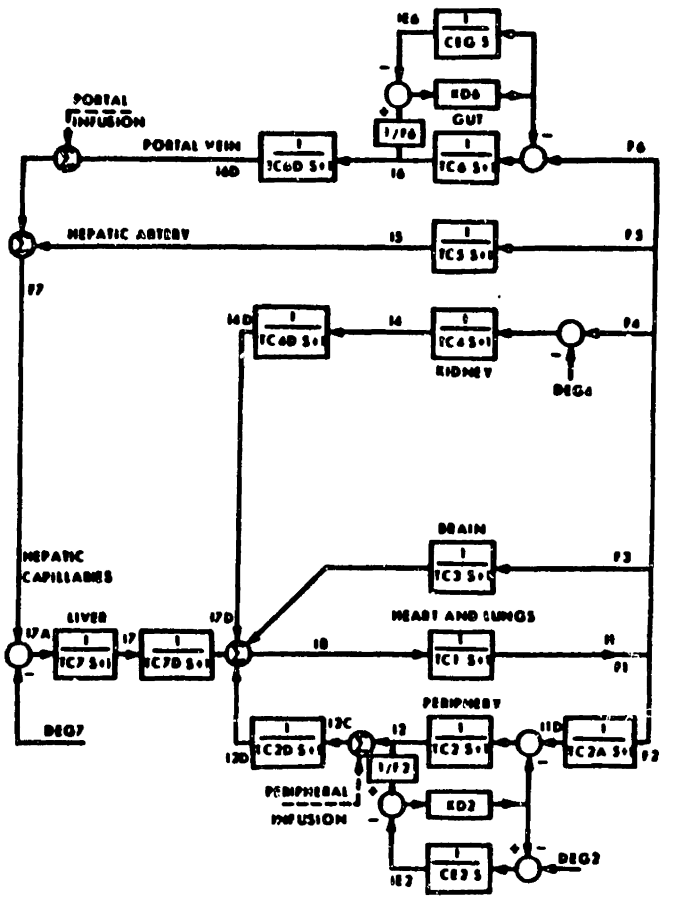

System block diagram of the circulation paths, organs, and tissues for A, the glucose model, and B, the insulin model: $GI(GID), \ldots, G8$ = plasma glucose concentrations (mg/dl), $II(IID), \ldots, I8$ = insulin concentrations (μU/ml), $FC1, \ldots, FC7$ = blood flows (ml/min), $F1, \ldots, F7$ = plasma flows (ml/min), $K2G, \ldots, K6G$ = transcapillary diffusion constants for glucose (ml/min), $KD2, \ldots, KD6$ = transcapillary diffusion constants for insulin (ml/min), $CE2, \ldots, CE6$ = extracellular (interstitial) volumes (ml), $TC1, \ldots, TC7$ = small vessel volume-associated time constants (min), $TC2D(TC2A), \ldots, TC7D$ = venous (or arterial) volume-associated time constants (min). $GU2, \ldots, GU7$ = glucose uptake rates (mg/min), $DEG2, \ldots, DEG7$ = insulin degradation rates (mU/min), S = Laplace operator (min^{-1}).

Fig. 67 System block representation of models develped by Tiran et al. for simulation of glucose and insulin dynamics in the dog. (from Tiran et al., 1981)

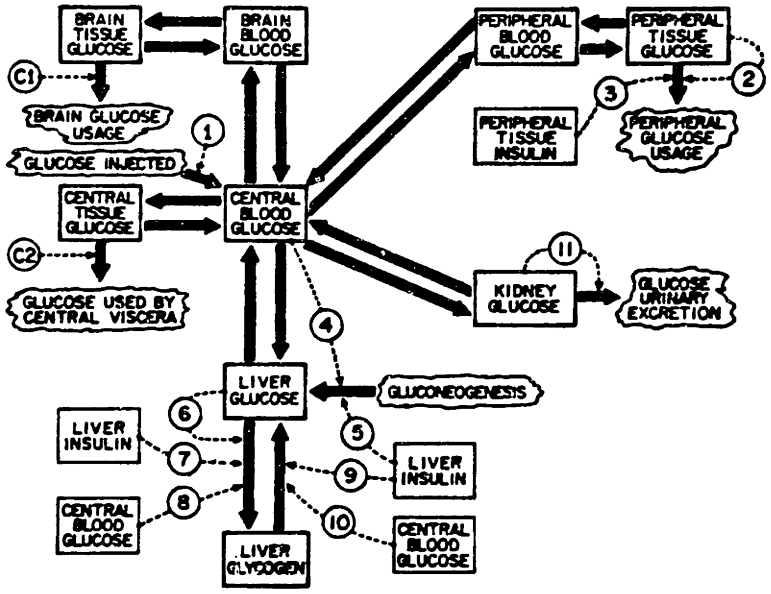

Design of glucose circulation. *Levels* are represented by boxes and *rates* by solid arrows. Cloud-like figures represent entrance and exit junctures for glucose. The functional relationships that govern rates of glucose flux are represented by numbered circles and broken lines. The boxes represent levels that affect glucose dynamics.

Fig. 68 Schematic representation of the glucose metabolism model of Guyton et al. (1978).

urinary excretion resulted if a threshold glucose concentration was exceeded in the kidneys. A nonlinear representation of peripheral tissue glucose uptake included glucose and insulin mediation. Hepatic glucose exchange was modeled in terms of the separate metabolic pathways contributing to liver glucose production (glycogen breakdown and gluconeogenesis) and liver glucose removal (glycogen synthesis). Glucose removal by hepatic glycolysis was not considered. A liver glycogen compartment was included in the formulation, and metabolic rates were given as nonlinear functions of glucose, insulin, and liver glycogen levels. Insulin mediation of glucose metabolism was assumed to occur via a 3-min time delay in all physiologic rate representations. In the insulin model, insulin was removed as a linear function of its rate of presentation to liver, kidney, and peripheral tissues. The model incorporated a heterogeneous fast pool theory of pancreatic insulin release (reviewed in pancreatic insulin release section of text). This formulation for insulin release was structured to account for observed patterns of plasma insulin appearance following various glucose infusions and related the rate of pancreatic insulin secretion to arterial glucose concentration through a rather complex set of 11 nonlinear ordinary differential equations. The complete model of glucose and insulin dynamics yielded a system of 32 simultaneous nonlinear ordinary differential equations. The model was subsequently modified by Hillman (1977) to incorporate physiology unique to the simulation of oral glucose challenges, including gut hormone augmentation of pancreatic insulin release and modeling of a 100g OGTT gut glucose absorption function. Although the original formulation of Guyton's model was programmed in a computer language called DYNAMO (a forward-difference numerical integrating package), the mathematical equivalent of the model

was later implemented in FORTRAN by Sorensen et al. (1982) for integration using a fourth-order Runge Kutta method. The restructured model of Guyton et al. (including the modifications of Hillman) was presented by Sorensen et al. in a more traditional organ and tissue compartmentalization format as shown in the schematic diagram in Figure 69. The mathematical equations of the model are documented in Appendix B of the text.

Bergman et al. (1981) have used mathematical modeling of glucose and insulin dynamics to develop clinical indices of value in characterizing individual response. The objective here was not to develop generalized physiologic models yielding predictions of mean normal response over a wide variety of inputs, but rather to generate minimal mathematical models capable of explaining variations in individual response to a single input, the IVGTT. The general minimal modeling approach employed by Bergman et al. is shown in Figure 70. Following intravenous glucose infusion, the time courses of plasma glucose G(t) and insulin I(t) were determined experimentally. The parts of the system above and below the dashed line in the figure were then considered separately: 1) beta cell sensitivity to glucose (Toffolo et al., 1980) was modeled using G(t) as the input and testing various black box mathematical formulations that, by parameter variation, could predict I(t); and 2) insulin sensitivity of glucose utilization (Bergman et al., 1979) was modeled using I(t) as the input and testing black box mathematical formulations that could predict G(t) by parameter adjustment. The black box mathematical formulations were tested in order of increasing complexity until all observed individual variations could be accounted for by simple adjustment of parameters within a single minimal model. Thus, by comparing parameter values of the individual against those of a population, quantitative indices of beta cell sen-

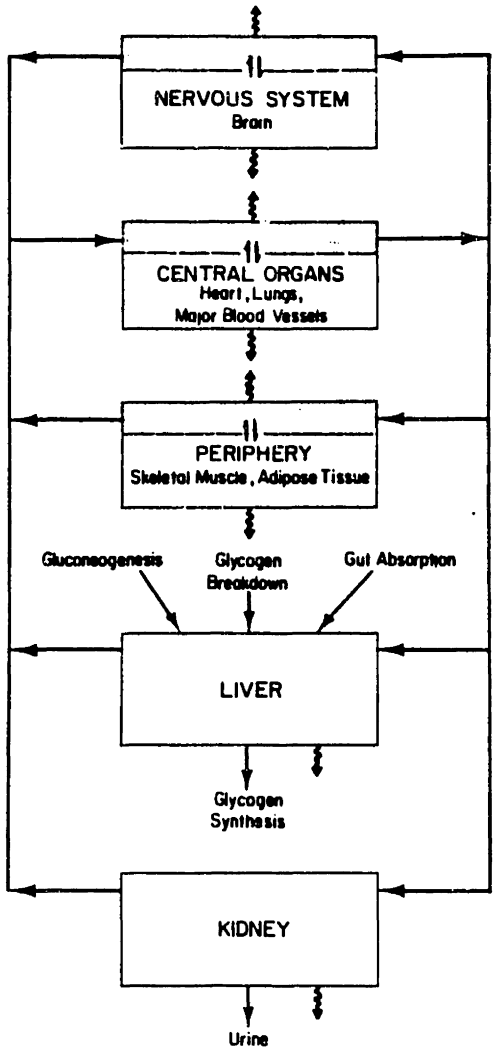

Schematic representation of the glucose model.

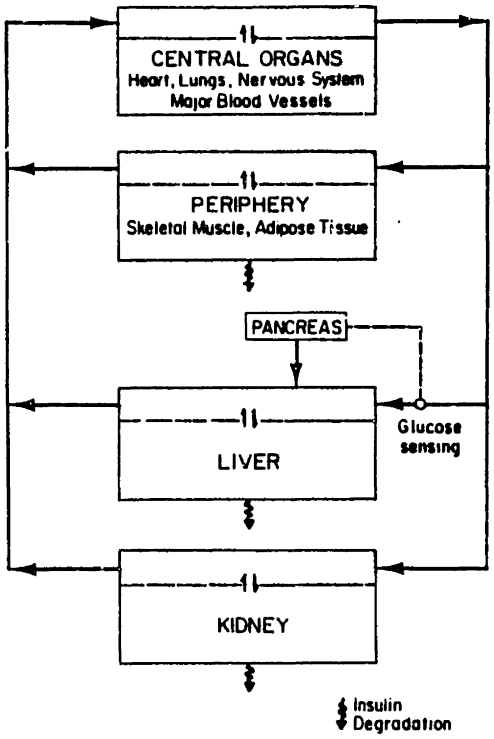

Schematic representation of the insulin model.

Fig. 69 Glucose homeostasis model of Guyton et al. (1978) as presented by Sorensen et al. (1982).

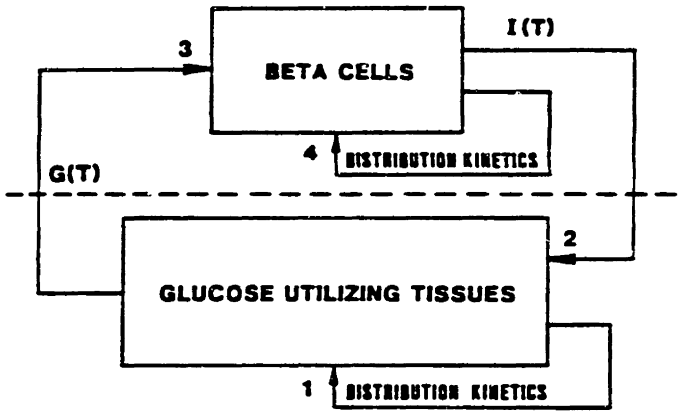

Fig. 70 Minimal modeling approach employed by Bergman et al. (1981).

sitivity to glucose and of glucose utilization insulin sensitivity were defined.

B) Comparison of Models of Glucose Metabolism

Because of the wide range of variation in form and detail, direct comparison of the various models of glucose metabolism is virtually impossible. (This may account for the fact that there have been no attempts to do so in the recent literature.) It is important, however, to discuss distinguishing features of these models and to attempt to assess the probability that respective model structures would lead to sound mathematical representations of the glucose regulatory system.

The linearized two-compartment formulations utilized in the early models of Bolie (1961), Ackerman et al. (1965), Gatewood et al. (1968), and Segre et al. (1973) were clearly oversimplifications of the glucose regulatory system, both with respect to the degree of body compartmentalization and linearization of the metabolic sources and sinks. In particular, use of a single plasma insulin compartment to model the regulatory effects of insulin on glucose metabolism cannot be appropriate, since the insulin-dependence of glucose disposal correlates with insulin levels in a compartment in slow equilibrium with plasma (Sherwin et al. 1974; Insel et al., 1975), or alternatively via a time lag in the hormonal action. Because parameters in the above models were established by fitting experimental data of a single glucose input (either an IVGTT or an OGTT), however, it was necessary to use extremely simplified models to avoid complete arbitrariness in the resulting parameter sets.

Charette et al. (1967) and Foster (1970) retained simple compartmentalization formats but included nonlinear metabolism in their models. With

the introduction of nonlinear functions, concern arose (and justifiably so) as to the uniqueness and correctness of metabolic formulations derived through parameter adjustment techniques. Both Charette et al. and Foster consulted the literature to formulate, at least in a qualitative sense, the metabolic source and sink characteristics. Model simulations were then employed to test and refine the models. The model of Foster et al. (1973) included metabolic scrutiny on a rather detailed level, far in excess of available information for direct quantification; the model, however, was reasonably succcessful in predicting the qualitative features of insulin and glucose response to intravenous glucose. Inclusion of amino acid and FFA acid compartments also suggested that variation in the plasma levels of these entities exerts little regulatory influence on glucose and insulin dynamics following intravenous glucose. In addition, the success of Foster et al. in qualitatively predicting insulin repsonse using a simple insulin release model based on glucose level and its rate of change with respect to time was notable.

Cerasi et al. (1974) and Insel et al. (1975) adopted similar three-compartment insulin formulations from the literature for their modeling efforts. This provided an improvement over earlier one-compartment insulin models as previously discussed. Cerasi et al. (1974) primarily employed modeling to study glucose-insulin interactions following intravenous glucose and to formulate an insulin release model, while Insel et al. (1975) were primarily concerned with analyzing euglycemic insulin clamp data. To this end, the metabolic processes causing addition and removal of glucose were cast into somewhat abstract terms in these models; for example, insulin-dependent glucose disposal was not partitioned between muscle and liver in these formulations. These models served their respective pur-

poses, but were not intended to be good physiologic representations of widespread applicability.

Improved understanding of glucose metabolism and its regulation has led to the recent development of several explanatory physiologic model formulations, including the model presented herein. A general comparison of the relative mathematical complexities of these models is provided in Table 29. Differences in the number of differential equations primarily reflect the degree of body compartmentalization employed, with the tissue and organ compartmentalization models of Guyton et al. (1978), Tiran et al. (1981), and the present model utilizing significantly larger differential equation sets than the lumped compartmental models of Cramp and Carson (1976) and Cobelli et al. (1982). Interestingly enough, a similar number of parameters entered into each of the model formulations with the exception of the model of Guyton et al. (1978) which employed a higher parameter count as a result of the relatively complex pancreatic insulin release formulation used therein. The number of nonlinear functional relationships utilized for modeling metabolic sources and sinks ranged from a high value of 16 for the model of Guyton et al. (1978), because of its complicated insulin release formulation, to a low value of 6 for the canine model of Tiran et al. (1981), due to exclusion of glucose counterregulation and insulin release considerations in this model.

In assessing the model of Cramp and Carson (1981), a number of issues were of concern from a physiologic standpoint. For a 70 kg subject, the total distribution volume for glucose, as well as for the hormones insulin, glucagon, and adrenalin, was 3.2 l; since this value roughly corresponds to total blood plasma volume, consideration of interstitial fluid distribution was clearly omitted from the model formulation. Furthermore, the vascular

TABLE 29. Summary comparison of the relative mathematical complexities of recent physiologic models of glucose metabolism.

MODELS	MATHEMATICAL COMPLEXITY		
	Differential Equations	Parameters	Nonlinear Input Functions
Guyton et al. 1978	32	70	16
Cramp and Carson 1976, 1981	9	48	11
†Tiran et al. 1979, 1980, 1981	40	50	6
Cobelli et al. 1982	7	54	13
New Model	22	42	11

†Canine Model

distribution volume for glucose should be significantly larger than for hormones because of glucose penetration into red blood cells. In addition, use of a lumped compartmentalization approach for insulin required insulin-dependent peripheral tissue glucose uptake to be modeled as an instantaneous function of plasma insulin concentration; this conflicts with the observation (Sherwin et al., 1974; Insel et al., 1975) that glucose uptake is mediated by an insulin compartment in slow equilibrium with plasma during euglycemic insulin clamps. Cramp and Carson emphasized underlying biochemistry by modeling metabolic sources and sinks for glucose in terms of enzyme kinetic expressions. Mathematically, such expressions yield nonlinear sigmoidal response curves similar to those resulting from hyperbolic tangent functions. An interesting aspect of the model was the representation of liver glucose metabolism in terms of the major contributing biochemical pathways (glycolysis, gluconeogenesis, hepatic glycogen synthesis and breakdown) and the inclusion of hepatic glucose 6-phosphate and hepatic glycogen compartments (see Figure 64). Whether scrutiny of liver metabolism to such a high degree can be justified from a quantitative standpoint, however, is questionable; no evidence was presented to verify the accuracy with which the model liver formulation could predict measurable in vivo response, such as net hepatic glucose production and uptake. Although the model was used to simulate intravenous glucose tolerance tests, no provision for kidney glucose excretion was included in the formulation. Pancreatic insulin release was modeled in terms of an extremely simplified linearized formulation (as previously discussed in the section on pancreatic insulin release models), and although gut hormone intervention significantly augments pancratic insulin response to oral glucose, Cramp and Carson employed the same insulin release model for simu-

lating both intravenous and oral glucose challenges. Finally, inclusion of adrenalin (epinephrine) may not have been necessary, as changes in plasma epinephrine levels under normal unstressed conditions probably do not cause quantitative alterations in glucose regulation (Gerich et al., 1981). The model of Cramp and Carson was successful, at least in a qualitative sense, in predicting normal response to intravenous glucose, insulin and glucagon. The model was further employed to study the effects of altering enzyme activity on overall plasma glucose response.

Although the canine model of Tiran et al. (1981) cannot be used ror prediction of human response, it certainly deserves mention. This tissue and organ compartmentalization model was well conceived and maintained a high degree of physiologic correspondence. The same basic compartmental design was employed in this model as was used in the formulation of the present human model, except for inclusion of limited glucose permeability of red blood cells (the canine RBC is less permeable than the human RBC) and introduction of separate vessel volumes to represent blood in the large arteries and veins. Since the longest time constant for any of the vessel volume compartments was only 0.37 min, their inclusion offered refinement in the rapid dynamics of blood pool mixing over small time scales; thus, lumping of these volumes into the organ and tissue vascular volumes would have most likely introduced minimal error for situations of interest. To date, the canine model has been used to analyze glucose and insulin infusion experiments in pancreatectomized dogs, and thus pancreatic insulin release and glucagon counterregulation have not been considered in the model formulation. Tiran, et al. did not distinguish between liver glucose uptake and production, but rather modeled liver glucose metabolism in terms of net hepatic glucose release rate (or net hepatic glucose balance) which

could assume positive or negative values. Because sufficient data was not available to define the net hepatic glucose release and peripheral glucose uptake functions, the authors stated that "the details (but not the character)" of these relationships constituted the major assumptions in the model. Because of the care employed in its formulation, however, the model yielded reasonably good agreement between simulated model predictions and experimentally observed data following glucose and insulin infusions in the dog.

Cobelli et al. (1982) used a lumped compartmental representation and relied heavily on adaptive fitting techniques to match model predictions to experimental data in a variety of simulation studies. Although utilization of a single glucose distribution space was an obvious simplification, this approach may have been reasonable since glucose equilibrates fairly rapidly between vascular and extravascular interstitial fluids in the body; information is lost, however, with respect to local variations in glucose concentrations, such as differences in arterial, venous and portal concentrations during an OGTT. The three-compartment insulin distribution model was originally derived by Sherwin et al. (1974); this was the minimal linearized model that, through adjustment of its 10 parameters, yielded good predictions of plasma insulin concentrations following insulin injection and euglycemic insulin clamping (high and low doses) in normal subjects. The compartments of this black box mathematical model were later assigned a somewhat abstract physiologic interpretation based on their respective volumes and relative equilibration times with plasma insulin, i.e. the small rapidly equilibrating compartment was assumed to represent liver and the large slowly equilibrating compartment was assumed to represent peripheral interstitial fluids. The general applicability of this

insulin distribution and metabolism model should be questioned because of 1) the limited variety of data upon which it was derived, and 2) the nonuniqueness of the three-compartment model in fitting the data. Indeed, Sherwin et al. demonstrated that an alternative three-compartment model explained the data equally well, a model for which no degradation was assoicated with the "liver" compartment! The pancreatic insulin release model employed by Cobelli et al. was extrapolated from perfused canine pancreas studies and was reviewed earlier in the pancreatic insulin release section of the text. A simple one-compartment model for glucagon was included to account for counterregulation during hypoglycemia. It was curious that the effect of insulin on pancreatic glucagon release was expressed as a function of "interstitial" insulin concentration (slow equilibration with plasma) since arterial insulin would be expected to exchange rapidly with pancreatic islet cells. Cobelli et al. (1982) were extremely conscious of the fact that use of parameter fitting to establish the nonlinear metabolic source and sink functions in the model could lead to nonunique, incorrect partitioning of glucose disposal among the organs and tissues. A wide variety of simulation studies (glucose and insulin infusions) were thus employed to establish a single set of model parameters that yielded reasonably good agreement between model predictions and experimental observations. In recently attempting to validate the model's performance with respect to predicting OGTT data, however, Cobelli and Mari (1983) had to alter significantly virtually all of the internal model parameters, including changing the functional forms of the liver glucose production and uptake functions to increase the number of adjustable parameters. Considering that the newest revised model uses 20 parameters to adjust the nonlinear metabolism associated with liver and peripheral

tissue handling of glucose, the uniqueness and physiologic correctness of this model remain an issue of concern.

Guyton et al. (1978) used a tissue and organ compartmentalization similar to the model presented in the text except for the following differences: 1) the gut tissues were lumped into the central organs compartment in the glucose model; 2) both brain and gut tissues were lumped into the central organs compartment in the insulin model; and 3) a small but non zero transcapillary diffusion time was included for plasma insulin exchange with liver and kidney interstitial fluid spaces. In addition, glucagon counterregulation was not explicitly included in the model; however, a nonlinear effect of low arterial glucose concentration was used to potentiate liver glucose production during hypoglycemia. Guyton et al. used the heterongeneous fast pool model of pancreatic insulin release (see section on pancreatic insulin release); this hypercomplex insulin secretion model added greatly to the overall mathematical complexity of the glucose metabolism model. Liver glucose metabolism was modeled in terms of biochemical pathways, except the pathway of glycolysis, a major route of hepatic glucose processing, was neglected. The metabolic processes for the liver were quantified from reviewing data in the literature; the available data, however, was insufficient to provide a firm basis for determining such fine detail. The resulting liver formulation does not accurately predict hepatic response on the whole organ level. For example, liver glucose output from gluconeogenesis in the model was assumed never to fall below about 50% of the basal glucose production rate because this process is limited by substrate availability (flux of gluconeogenic presursors to the liver). This is inconsistent with in vivo measurements indicating complete suppression of hepatic glucose production in response to modest increases

in plasma insulin levels, even if gluconeogenic presursors are available to the liver. Furthermore, recent studies (Shakima and Ui, 1978) have suggested that glucose loading can divert hepatic glucose 6-phosphate produced from gluconeogenesis to glycogen storage. Once the model functions for liver glucose metabolism had been established, insulin-dependent peripheral glucose uptake was quantified by simulating variable-dose IVGTT experiments and fitting model predictions to experimental data for blood glucose responses. Thus, peripheral glucose metabolism was simply adjusted to compensate for errors in the liver glucose metabolic formulations such that the model acurately predicted glucose response to intravenous challenges. The ease with which such arbitrary balances in liver and muscle metabolism can be used to predict glucose profiles during IVGTT's was clearly demonstrated in the text.

Of the tissue and organ compartmentalization models of glucose metabolism, the new model presented herein used the least number of differential equations, primarily because of its simplified pancreatic insulin release formulation. At first it might seem that tissue and organ compartmentalization, although yielding a high degree of physiologic correspondence, introduced a large number of parameters into the formulation, and thus was disadvantageous relative to simpler lumped compartmental formulations. Due to the high level of physiologic correspondence, however, the parameters so introduced, such as tissue volumes and blood flow rates, could be directly established from available data in the literature. For example, external to the model pancreas formulation, not a single parameter in the model of insulin distribution and metabolism needed to be established by parameter fitting. Likewise, the entire glucose distribution model (neglecting the metabolic sources and sinks) required fitting of only a single parameter,

the peripheral transcapillary diffusion time constant. The simpler three-compartment insulin distribution model employed by Cobelli et al. (1981), however, was basically established by a 10-parameter fitting of experimental data. Over the course of developing and using the present model, a great advantage of organ and tissue compartmentalization resulted from the ability to distinguish between arterial and venous concentrations in the model; this meant that any measured quantity in the literature directly corresponded to a quantity in the model, thus facilitating model development and testing. With respect to modeling of the nonlinear metabolic source and sink relationships, it was immediately acknowledge that confidence in the physiologic correctness of the model would reside in direct quantification of the component metabolic processes. To this end, a great deal of painstaking work was directed toward collecting, interpreting, and correlating experimental data from the literature. Sufficient local organ response data was available to quantify kidney glucose excretion, peripheral glucose uptake, hepatic glucose production, tissue and organ insulin clearances, and pancreatic glucagon secretion. The only model functions that required fitting of IVGTT plasma response data for quantification were hepatic glucose uptake, because the human liver data was too inconsistent and scattered, and pancreatic insulin release, because plasma insulin appearance was the only accessible indicator of pancreatic activity in humans. Since single sink and source functions required fitting in the glucose and insulin models, respectively, these functions were adequately determined by parameter adjustment during a standard IVGTT simulation. The major pitfalls of parameter fitting were thus avoided: 1) the problem of nonunique interpretations when multiple nonlinear functions are fit simultaneously, and 2) the need to use adaptive fitting to iterati-

vely tune the model over a wide spectrum of simulation studies. It should be mentioned that the resulting hepatic glucose uptake function agreed well with oral uptake data in humans, while the pancreatic insulin release model, having been adapted from a well tested animal model, displayed good physiologic behavior. Finally, liver glucose metabolism in the present model was scrutinized only on the level of whole organ production and uptake, since these quantities are independently measureable in humans. It would appear that some modelers have attempted to incorporate biochemical detail at the expense of accurately quantifying whole organ response; an interesting exercise would be to use the more accurate production and uptake liver model as an overall constraint in further studying the relative partitioning of glucose movement through the underlying biochemical pathways. A unique feature of the present model was incorporation of time dependence into the hormonal regulation of liver glucose metabolism on the basis of direct interpretation of experimental data in the literature. The time dependence of liver hormonal action further supports the notion that plasma insulin levels have an indirect, or delayed effect on glucose metabolism.

A PHYSIOLOGIC MODEL OF GLUCOSE METABOLISM IN MAN AND ITS USE TO DESIGN AND ASSESS IMPROVED INSULIN THERAPIES FOR DIABETES

VOL. 2

by

JOHN THOMAS SORENSEN

B.S., University of California, Berkeley

(1978)

SUBMITTED TO THE DEPARTMENT OF
CHEMICAL ENGINEERING IN PARTIAL
FULFILLMENT OF THE
REQUIREMENTS FOR THE
DEGREE OF

DOCTOR OF SCIENCE

at the

MASSACHUSETTS INSTITUTE OF TECHNOLOGY

April 1985

Signature of Author ..... John Thomas Sorensen .....
Department of Chemical Engineering
April 18, 1985

Certified by ..... Clark K. Colton .....
Clark K. Colton
Thesis Supervisor

Accepted by ..... William M. Deen .....
William M. Deen
Chairman, Department Graduate Committee

IV. SIMULATION STUDIES FOR ASSESSING PERFORMANCE OF NORMAL MODEL

A) Computer Formulation and Model Initialization

Final formulation of the glucose metabolism model resulted in a system of 22 simultaneous nonlinear ordinary differential equations: 11 associated with the glucose model (of which 3 were for time dependent liver metabolism), 10 with the insulin model (of which 3 were for the model pancreas), and 1 with the glucagon model. The model of glucose metabolism was programmed on a Digital Equipment Corporation VAX11/780 computer system at the MIT Joint Computer Facility. A printout of the computer source code (Fortan 77) is included in Appendix A. Numerical solutions were generated using a fourth-order Runge-Kutta integration provided by a library routine DYSYS (DYnamic SYstem Simulator) on the Joint Computer Facility system. A time step of 0.1 min was used for all model simulations.

The initial condition for the model was defined as the basal postabsorptive state. For model initialization, the metabolic sources and sinks in the glucose model must assume their basal values by definition, and all multipliers of the basal metabolic rates are identically unity. This decouples the glucose model from the insulin and glucagon models. Setting the time derivatives of the glucose model mass balance equations (9-16) equal to zero (steady state) results in a set of 8 simultaneous linear algebraic equations in 8 unknowns. The eight glucose concentrations cannot be uniquely determined from this set of algebraic equations, however, because the coefficient matrix for this system is rank 1 (i.e. one of the equations is not linearly independent, as summing the equations yields cancellation to zero). Thus, the single degree of freedom was eliminated by specifying any one of the initial basal glucose concentrations in the glu-

cose model, and this uniquely determined the remaining 7 glucose concentrations. Equating the time derivative of the pancreatic insulin release model equations (137-139) to zero yields a set of three simultaneous algebraic equations that can be solved uniquely for the initial values of P,I, and Q once the initial arterial glucose concentration has been determined. Setting the time derivatives in the insulin model mass balance equations (17-23) to zero yields a set of 7 algebraic equations. This set of simultaneous algebraic equations is linear because: 1) the rates of liver, kidney, and peripheral insulin clearance are linear functions of insulin concentrations, and 2) as discussed in the text, initialization of the pancreatic insulin release model does not determine the basal rate of pancreatic insulin release (it is essentially an unknown, thus decoupling the insulin model from the glucose model). The insulin model algebraic equation set has a coefficient matrix of rank 0 and forms a system of 7 equations in 8 unknowns (the seven initial insulin concentrations and the basal pancreatic insulin release rate). Thus, specification of any one of the initial insulin model concentrations or the basal pancreatic insulin release rate allows unique initialization of the insulin model.

Since equating the time derivative in the glucagon model mass balance equation (24) yields a single algebraic equation in one unknown, one method of initializing the glucagon model would have been to specify directly the initial basal glucagon concentration. An alternative approach was employed for glucagon model initialization, however, for two reasons: 1) plasma glucagon levels are seldom reported for studies in the literature, and 2) when reported, basal plasma glucagon concentrations vary over a wide range (typically 50-150 pg/ml) due primarily to variations in the specificity of

the assays employed by different investigators. Because of these reasons, and for convenience, the need for specifying an initial condition for the glucagon model mass balance equation was circumvented. Since the glucagon model uses a one-compartment formulation, initialization requirements could be eliminated by simply normalizing the glucagon mass balance equation such that the dynamic variable was transformed from $\Gamma(t)$ to $\Gamma^N(t)$. This was accomplished as follows. The glucagon model mass balance equation (24) was divided through by the basal plasma glucagon concentration Γ^B, yielding

$$V^\Gamma \frac{d\Gamma^N}{dt} = \frac{1}{\Gamma^B}(r_{P\Gamma R} - r_{P\Gamma C}) \tag{190}$$

Using Equations 154 and 155 to expand the metabolic rate terms gives

$$V^\Gamma \frac{d\Gamma^N}{dt} = M^I_{P\Gamma R} M^G_{P\Gamma R}\left(\frac{r_{P\Gamma R}}{\Gamma^B}\right) - r_{M\Gamma C}\Gamma^N \tag{191}$$

But, under steady basal conditions (from Equation 157),

$$r^B_{P\Gamma R} = r_{M\Gamma C}\Gamma^B \tag{192}$$

Substituting Equation 192 into Equation 191 and simplifying yields

$$V^\Gamma \frac{d\Gamma^N}{dt} = \Gamma^N (M^I_{P\Gamma R} M^G_{P\Gamma R} - r_{M\Gamma C}) \tag{193}$$

for which the basal state initial condition is always given by

$$\Gamma^N = 1 \tag{194}$$

by definition. Use of Equation 193 as an alternative (but equivalent) representation of the glucagon model mass balance equation in the computer formulation thus eliminated the requirement for specifying a basal plasma glucagon value for each simulation. For those simulations in which the

time course of plasma glucagon concentration was desired for comparison with reported data, the plasma glucagon concentration was simply determined from Equation 193 and specification of the basal glucagon concentration value Γ^B according to the relationship

$$\Gamma = \Gamma^N \Gamma^B \tag{195}$$

To summarize, model initialization required specification of a single glucose concentration and a single insulin concentration (or the basal pancreatic insulin release rate), with specification of the basal plasma glucagon concentration being optional. The computer program was designed to calculate the model initial condition values from the two required input specifications on the first integration call. For most simulations, basal state arterial or peripheral venous glucose and insulin concentration values were used to initialize the model, as these were most commonly reported for experimental studies in the literature. A summary of the model initialization calculations starting from specification of peripheral venous or arterial glucose and insulin concentrations is presented in Table 31. Also included in the table is a listing of the variables for which the basal state values must be stored for reference during subsequent computations. For simulation of studies for which no basal values were reported for one or both of the required initialization specifications, the following values were assumed for default purposes: 1) peripheral blood glucose concentration equaled 75 mg/dl corresponding to G_{pv} = 89 mg/dl; and 2) peripheral venous plasma insulin concentration equaled 13 mU/l corresponding to I_{pv} = 13 mU/l. The above represent mean basal state values measured in 256 normal adult males as compiled from the Joslin Research Laboratory data base.

Table 31. Summary of model initialization calculations corresponding to specification of peripheral venous (or arterial) glucose and insulin concentrations.

Glucose Model

Mass Balances:

G_{PV} = [input peripheral venous glucose conc.]

G_H = [input arterial glucose conc.]

$$G_H = G_{PV} + \frac{r^B_{PGU}}{Q^G_P}$$

or

$$G_{PV} = G_H - \frac{r^B_{PGU}}{Q^G_P}$$

$$G_K = G_H$$

$$G_{BV} = G_H - \frac{r_{BGU}}{Q^G_B}$$

$$G_G = G_H - \frac{r_{GGU}}{Q^G_G}$$

$$G_L = \frac{1}{Q^G_L}(Q^G_A G_H + Q^G_G G_G + r^B_{HGP} - r^B_{HGU})$$

$$G_{BI} = G_{BV} - \frac{r_{BGU} T_B}{V_{BI}}$$

$$G_{PI} = G_{PV} - \frac{r_{BGU} T^G_P}{V_{PI}}$$

Metabolism:

$$M^I_{HGP} = 1$$

$$M^I_{HGU} = 1$$

$$f_2 = 0$$

Table 31. Summary of model initialization calculations corresponding to (cont.) specification of peripheral venous (or arterial) glucose and insulin concentrations.

Insulin Model

Mass Balances:

I_{PV} = [input peripheral venous insulin conc.]

I_H = [input arterial insulin conc.]

or

$$I_H = \frac{I_{PV}}{(1-F_{PIC})}$$

$$I_{PV} = I_H(1-F_{PIC})$$

$$I_K = I_H\,(1-F_{KIC})$$

$$I_B = I_H$$

$$I_G = I_H$$

$$I_{PI} = I_{PV} - \left[\frac{Q_P^I T_P^I}{V_{PI}}(I_H - I_{PV})\right]$$

$$I_L = \frac{1}{Q_L^I}(Q_H^I I_H - Q_B^I I_B - Q_K^I I_K - Q_P^I I_{PV})$$

$$r_{PIR}^B = \left(\frac{Q_L^I}{1-F_{LIC}}\right)I_L - Q_G^I I_G - Q_A^I I_H)$$

Model Pancreas:

$$X = \frac{(G_H)^{3.27}}{(132)^{3.27} + 5.93(G_H)^{3.02}}$$

$$P_\infty = X^{1.11}$$

$$Y = X^{1.11}$$

$$P = P_\infty$$

$$I = X$$

$$Q = \frac{HQ_0 + \gamma P_\infty}{H + M_1 Y}$$

Table 31. (cont.) Summary of model initialization calculations corresponding to specification of peripheral venous (or arterial) glucose and insulin concentrations.

Glucagon Model

Mass Balance:

$r^N = 1$

r = [input plasma glucagon conc.] (optional, see text)

Stored Values

The following basal values are stored for reference and are required for subsequent computations:

$$G_{PI}^B,\ G_L^B,\ G_H^B,\ I_{PI}^B,\ I_L^B,\ I_H^B,\ r_{PIR}^B, S(G_H^B) = M_1 YQ$$

B) Simulation Studies

A number of clinical experiments were simulated and model predictions compared with experimental results to assess model performance. A listing of these clinical simulations is provided in Table 30. As indicated in the table, these experimental situations encompassed a wide variety of response behavior, not only with respect to relative glycemia and hormonal levels, but also with respect to relative temporal dynamics. With the exception of the standard 0.5 g/kg IVGTT study, which was employed for parameter determinations, the model simulations were run without any interactive modification of the mathematical model and thus demonstrated the general predictive capacity of the physiologic model formulation.

Before reviewing the simulation studies, a few aspects of general methodology should be clarified. For all simulations, the initial condition was defined as the basal postabsorptive steady state, and the mathematical model was initialized as previously discussed using actual reported basal arterial or venous concentrations (whenever available). Since experimental infusions are introduced intravenously, the infusate is rapidly transported via the venous circulation to the cardiopulmonary pool where it is rapidly mixed and distributed to the body via the arterial circulation. Thus, for simulations, glucose and insulin infusions were input as source terms in the heart and lung compartments mass balance equations of the glucose (Equation 11) and insulin (Equation 18) models, respectively:

Intravenous Glucose Infusion: (modification of Equation 11)

$$V_H^G \frac{dG_H}{dt} = Q_B^G G_{BV} + Q_L^G G_L + Q_K^G G_K + Q_P^G G_{PV} - Q_H^G G_H - r_{RBCU} + r_{IVG} \qquad (11a)$$

TABLE 30. Listing of simulation studies employed for testing model performance.

Clinical Experiment	LEVELS RELATIVE TO BASAL			Dynamics	Used for Parameter Determination
	Glucose	Insulin	Glucagon		
Standard 0.5 g/kg IVGTT	+	+	0	rapid	yes
Variable Dose IVGTT	+	+	0	rapid	no
0.04 U/kg IVITT	-	+	+	rapid	no
0.25 mU/min/kg Insulin Infusion	-	+	+	slow	no
0.40 mU/min/kg Insulin Infusion	-	+	+	slow	no
Euglycemic Insulin Claim	0	+	-	combined	no
Deactivation of Insulin Action	0	+	-	combined	no
Hyperglycemic Clamp	+	+	-	combined	no
Standard 100 g OGTT	+	+	0	slow	no

where: r_{IVG} = intravenous glucose infusion rate (mg/min)

Intravenous Insulin Infusion: (modification of Equation 18)

$$V_H^I \frac{dI_H}{dt} = Q_B^I I_B + Q_L^I I_L + Q_K^I I_K + Q_P^I I_{PV} - Q_H^I I_H + r_{IVI} \quad (18a)$$

where: r_{IVI} = intravenous insulin infusion rate (mU/min)

Because peripheral venous infusions enter blood which has already perfused tissue capillary beds, such infusions should not be input as source terms in the peripheral compartment blood space; this has been a point of confusion in a number of past modeling studies. For simulating the 100g oral glucose test, the rate of gut glucose absorption was introduced as a source term in the gut compartment mass balance equation of the glucose model (Equation 12):

Oral Glucose Challenge: (modification of Equation 12)

$$V_G^G \frac{dG_G}{dt} = Q_G^G (G_H - G_G) - r_{GGU} + r_{OGA} \quad (12a)$$

where: r_{OGA} = gut oral glucose absorption rate (mg/min)

1) Standard 0.5 g/kg IVGTT

Plotted in Figure 71 are simulated normal response curves for a standard 0.5 g/kg 3-min IVGTT. Also plotted for comparison are the mean experimental results for 110 normal adult males whose body weights averaged near ideal for their ages and heights. This clinical data base was collected at the Joslin Research Laboratory in Boston. The basal state initial conditions were as follows: 1) peripheral venous blood glucose concentration equaled 75 mg/dl (corresponding to G_{PV}^B= 89 mg/dl); peripheral

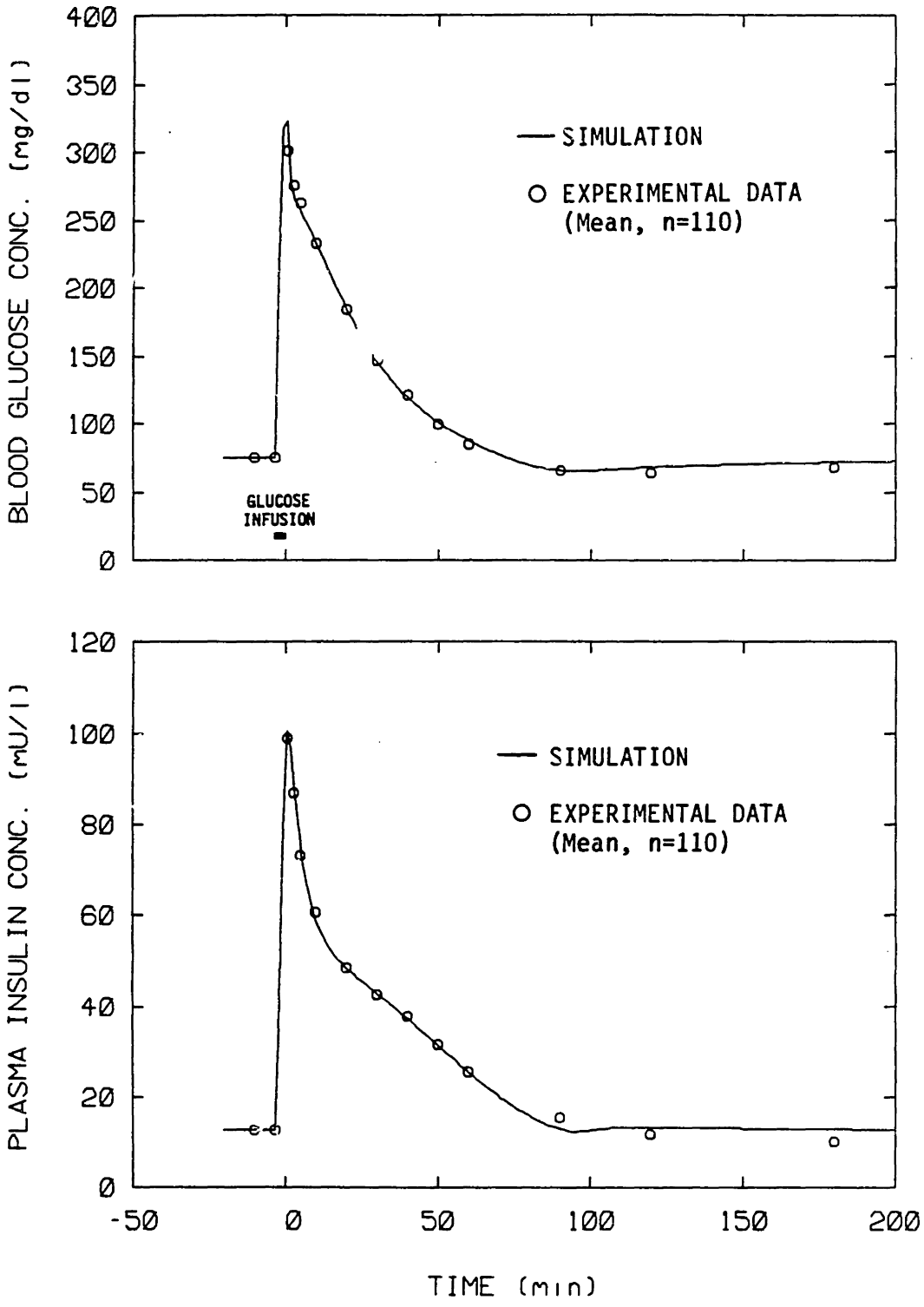

Fig. 71 Comparison between model predictions and experimental data for a standard 0.5 g/kg IVGTT. (Data provided by the Joslin Research Laboratory)

venous insulin concentration equaled 12.8 mU/l (I^{B}_{PV}= 12.8 mU/l).

As indicated in Figure 71, the final model formulation was extremely accurate in predicting glucose and insulin response to the standard IVGTT. This was not particularly surprising, however, since, as discussed in the text, liver glucose metabolism was adjusted to minimize differences between model predictions and experimental data for glucose response, and insulin release parameters were adjusted to minimize the difference between model predictions and experimental data for insulin response. Furthermore, the glucose peripheral transcapillary diffusion time constant was established from the initial postinfusion glucose data. Nonetheless, the model's capacity to predict some of the more subtle response dynamics was noteworthy.

Use of the model of Guyton et al. (1978) to predict glucose and insulin responses to the standard 0.5 g/kg 3-min IVGTT is illustrated in Figure 72; here, the Joslin Research Laboratory clinical data has again been included for comparison. Although Guyton (1973) used IVGTT data to adjust peripheral glucose metabolism and insulin release functions in the model, he employed trial and error instead of more sophisticated mathematical methods for fitting model predictions to experimental data. This, coupled with other less accurate physiologic representations in the model, resulted in reasonable but not extremely accurate model predictions of IVGTT response. In particular, the model tended to return to steady state too rapidly, indicating problems associated with the counterregulatory modeling and its time dependence.

2) Variable-Dose IVGTT

A comparison between model predictions and clinical data is presented in Figure 73 for normal responses to 3-min IVGTT's in which the glucose

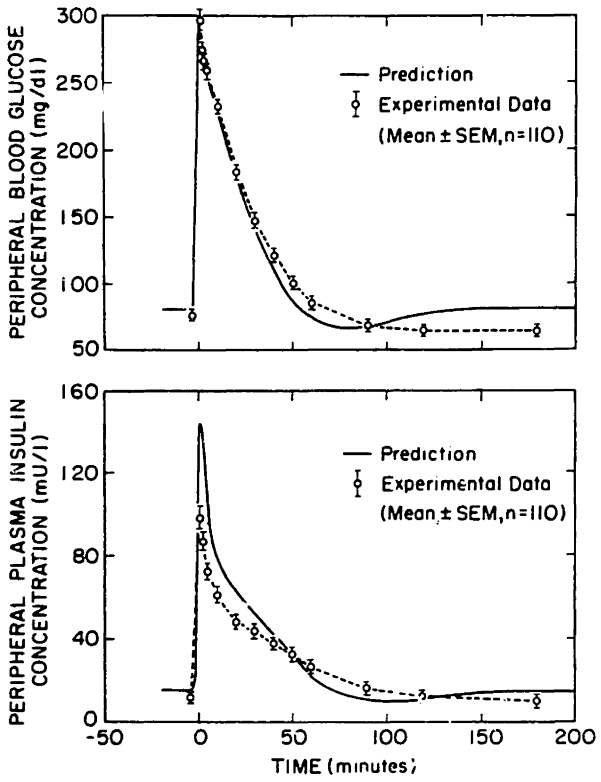

Fig. 72 Simulation study of a standard 0.5 g/kg IVGTT using the mathematical model of Guyton et al. (1978) to predict glucose and insulin responses. (Figure from Sorensen et al., 1982)

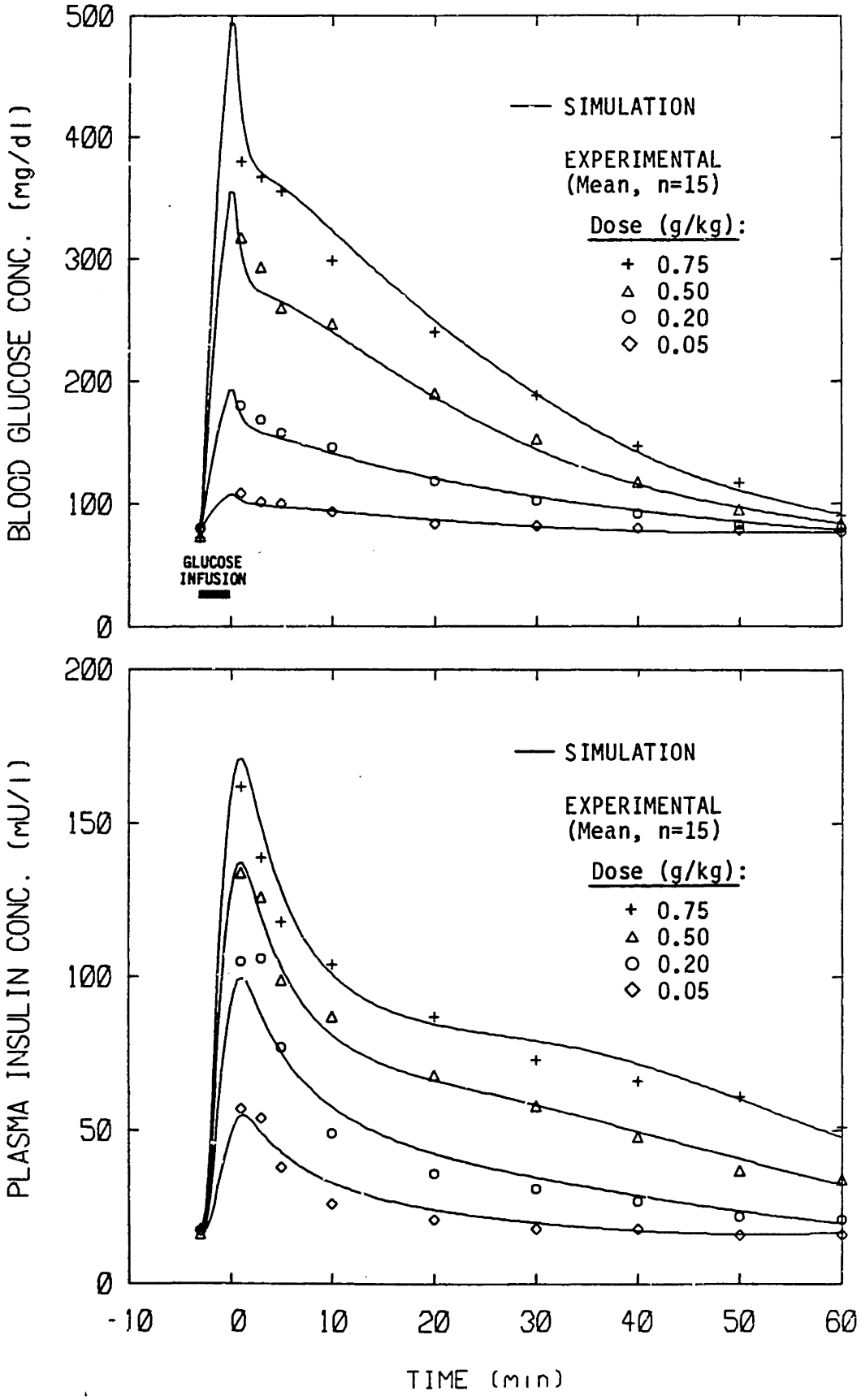

Fig. 73 Comparison between model predictions and clinical data for variable-dose IVGTT studies. (Data from Joslin Research Laboratory)

dose was varied between 0.05 and 0.75 g/kg body weight. Clinical data in the figure represent mean responses of 15 normal subjects measured at the Joslin Research Laboratory. The initial basal state conditions for these studies are tabulated in Table 32.

Variation of the glucose dose over an order of magnitude resulted in glucose and insulin responses covering a broad concentration range. As demonstrated in Figure 73, the model predictions were in good agreement with the clinical data over the entire range of investigation.

In working with the model it became apparent that insulin responses predicted by the insulin model were quite sensitive to the basal plasma insulin concentration level. This was because referencing pancreatic insulin release as a multiplicative function of the basal release rate resulted in a highly leveraged insulin release model, as circulating insulin levels can normally increase by a factor of 10-20 times basal. The impact of such a leveraging effect can be seen by comparing the 0.5 g/kg dose levels of Figures 71 and 73. Although the glucose infusions caused similar glycemic responses in both of the experimental groups, the insulin response of the group in Figure 71 was significantly lower relative to the insulin response of the group in Figure 73; for example, the peak plasma insulin concentration in Figure 71 was about 100 mU/l, whereas the peak value in Figure 73 was roughly 135 mU/l. The model accurately predicted the different insulin responses of both groups, however, because the mean basal venous plasma insulin concentration of the former group (13 mU/l) was also significantly less than that of the latter group (17 mU/l). In studying the relationship between fasting insulin levels and insulin response to glucose, Bagdade et al. (1967) first postulated a significant correlation between basal insulin and insulin response. The fact that insulin response

TABLE 32. Basal state initial conditions for variable-dose IVGTT studies.

Dose (g/kg)	Glucose Conc.(mg/dl)		Peripheral Venous Plasma Insulin Conc., I_{PV} (mU/l)
	Peripheral Venous Blood	Corresponding Model, Input G_{PV}	
0.05	76	90	18
0.2	77	92	19
0.5	76	90	17
0.75	72	86	21

was well represented by multiplicative rather than additive (or incremental) response behavior may explain to some extent the high degree of variability and scatter characteristic of insulin response data.

3) 0.04 U/kg Intravenous Insulin Tolerance Test (IVITT)

Plotted in Figure 74 are simulated results for normal response to a 0.04 U/kg 3-min IVITT. Included for comparison are experimental data reported by Gerich et al. (1980) for mean responses measured in 15 normal subjects. Initial basal conditions for this study were as follows: 1) venous plasma glucose concentration equaled 91 mg/dl (corresponding to G_{pv} = 98 mg/dl); 2) venous plasma insulin concentration was not reported, so a default value of 13 mU/l was assumed, (I_{pv} = 13 mU/l); 3) plasma glucagon concentration equaled 120 pg/ml (r = 120 pg/ml).

The IVITT insulin infusion causes an acute transient elevation of plasma insulin concentration, as shown in the center panel of Figure 74. Elevated insulin levels in turn cause suppression of hepatic glucose production and increase peripheral tissue glucose uptake, leading to a rapid decrease in glucose concentration. As insulin levels return to normal, glucose counter-regulation in response to hypoglycemia rapidly enhances liver glucose production rate causing glucose levels quickly to rebound back to normal. As demonstrated in Figure 74, the model was quite successful in predicting the transient hypoglycemia of the IVITT, and, as shown in the lower panel of the figure, the simple one-compartment glucagon model yielded reasonably good predictions of the plasma glucagon counter-regulatory response. The IVITT provided a good test of the model's counterregulatory functions, particularly with respect to hepatic glucose production, since the rapid interplay between the dynamic effects of insu-

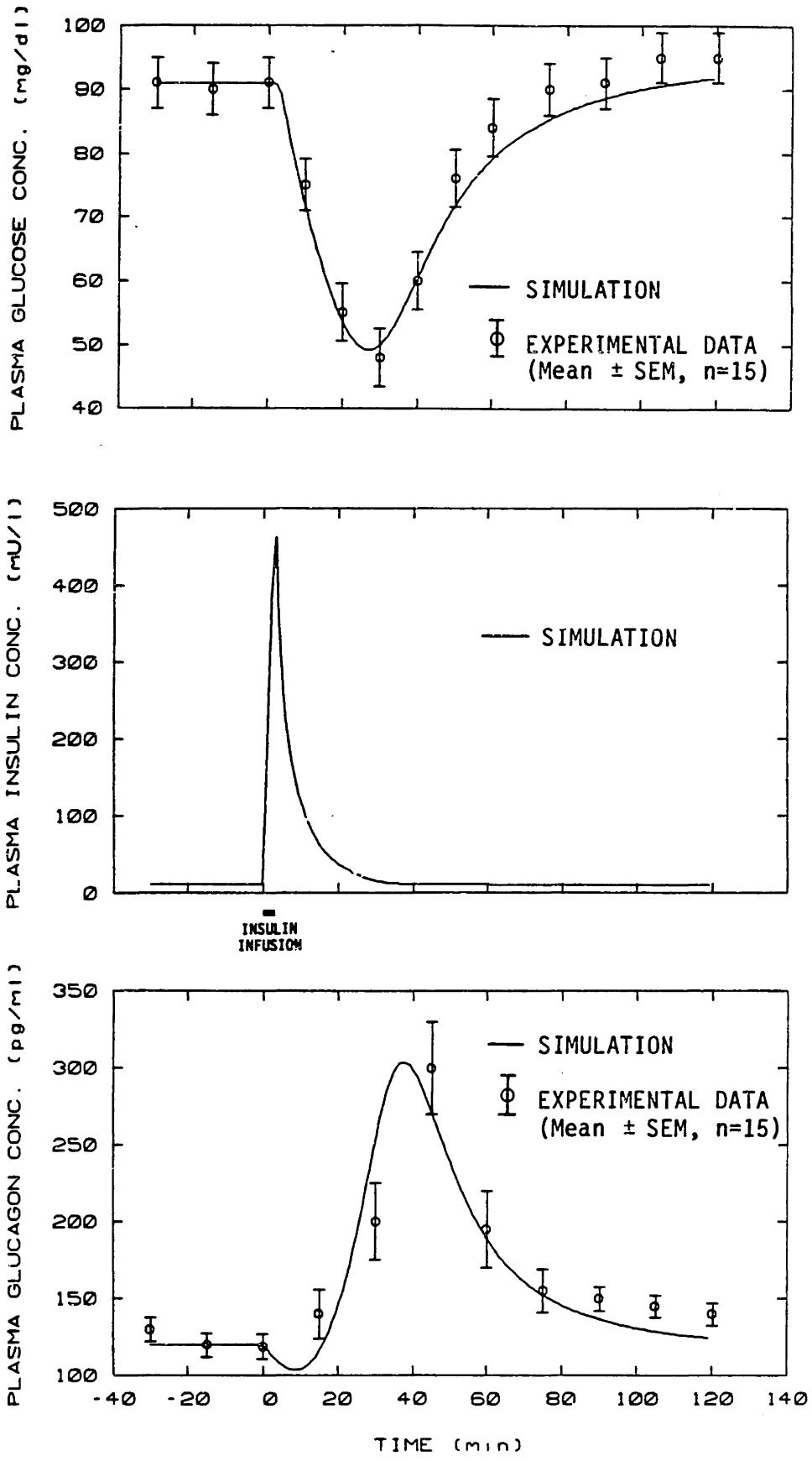

Fig. 74 Comparison between model predictions and experimental data for response to a 0.04 U/kg 3-min IVITT. (Data from Gerich et al., 1980)

lin, glucose, and glucagon on the hepatic glucose production rate would be primarily responsibile for determining the transient hypoglycemic response characteristics.

4) Continuous Intravenous Insulin Infusions

Shown in Figure 75 is a comparison between model predictions and experimental data for response to a 0.25 mU/kg/min continuous intravenous insulin infusion. Experimental data in the figure represent mean values reported by Sacca et al. (1979) for 5 normal subjects. The initial basal state conditions for this study were: 1) venous plasma glucose concentration equaled 90 mg/dl (corresponding to G_{pv} = 97 mg/dl); 2) venous plasma insulin concentration equaled 11 mU/l (I_{pv} = 11 mU/l).

The continuous insulin infusion experiment differs from the IVITT because of the sustained rather than transient elevation of plasma insulin levels. The continous insulin infusion thus results in attainment of a hypoglycemic steady state, the plasma glucose level of which is determined by the balance between insulin's action in lowering glucose levels and hypoglycemic counterregulation of this action. As shown in Figure 74, model predictions agreed well with experimental data for the time course of plasma glucose concentration during the prolonged continuous insulin infusion experiment, both with respect to the final hypoglycemic steady state level and the dynamics of the transition to this state.

Presented in Figure 76 is a comparison between model predictions and clinical data for response to a continous insulin infusion at a higher dose level of 0.4 mU/kg/min. Experimental data in the figure are mean values reported by Sacca et al. (1979) for 6 normal subjects. The initial basal state for this study was defined by the following: 1) venous plasma glucose

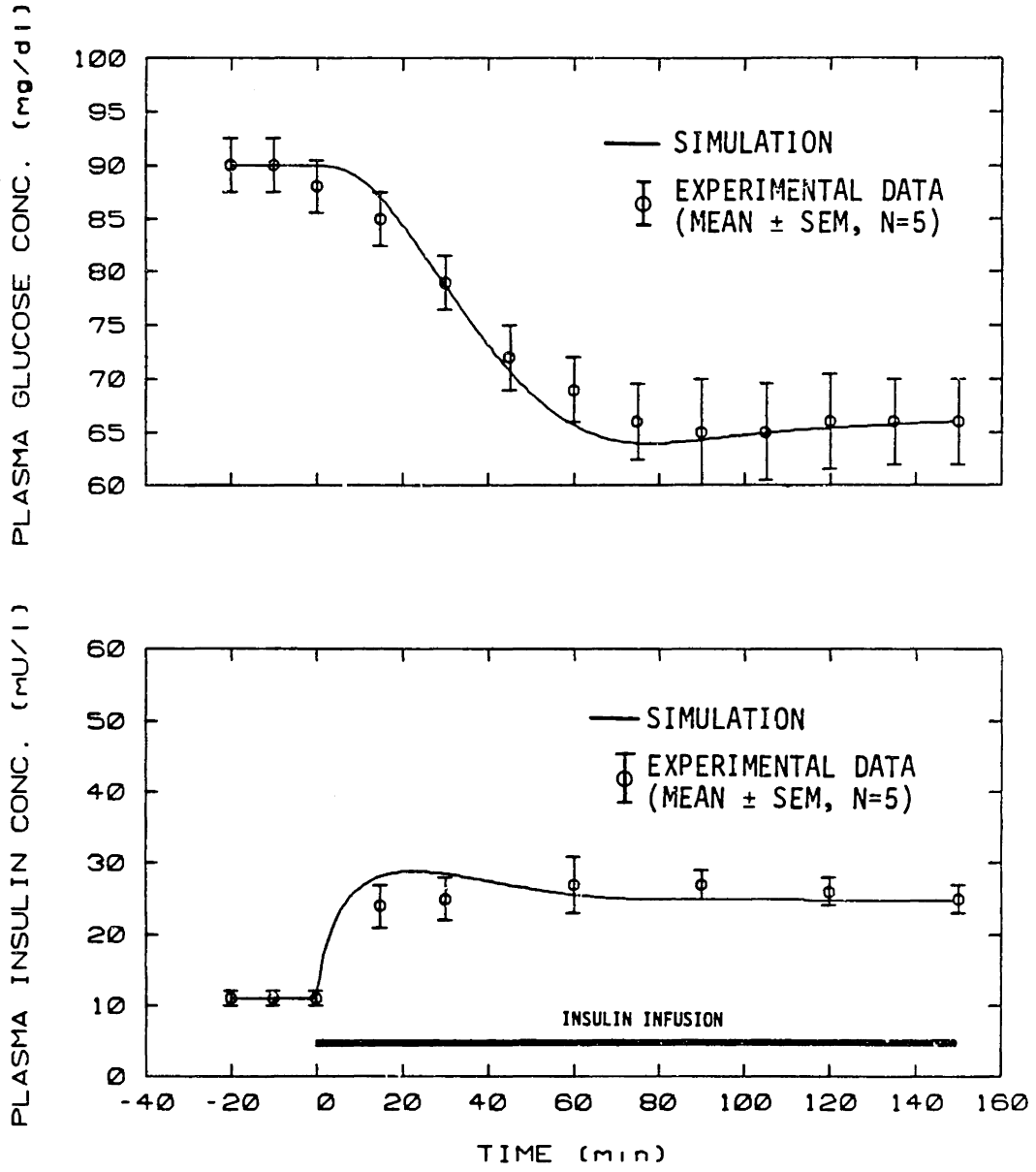

Fig. 75 Comparison of model predictions and clinical data for response to a continuous 0.25 mU/kg/min intravenous insulin infusion. (Data from Sacca et al., 1979)

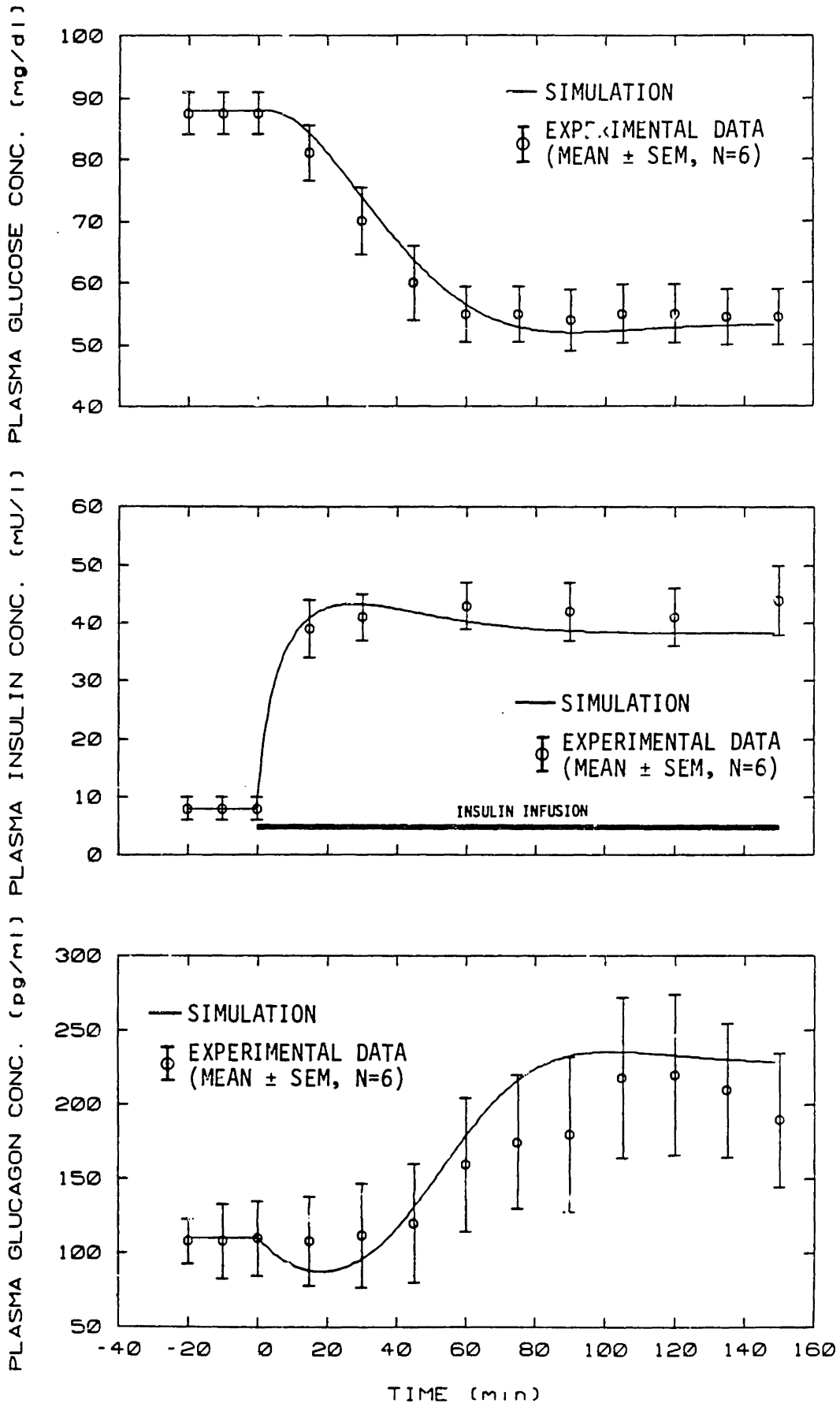

Fig. 76 Comparison between model predictions and clinical data for response to a continuous 0.4 mU/kg/min intravenous insulin infusion. (Data from Sacca et al., 1979)

concentration equaled 88 mg/dl (corresponding to G_{pv} = 95 mg/dl); 2) venous plasma insulin concentration equaled 8 mU/l (I_{pv} = 8 mU/l); and 3) plasma glucagon concentration equaled 110 pg/ml (Γ=110 pg/ml). The higher insulin dosage resulted in a more pronounced drop in glycemic levels, and again good agreement was obtained between model predictions and experimental data.

A comparison of model predictions for the 0.4 mU/kg/min continuous insulin infusion experiment is presented in Figure 77. Here, predictions of the present model and the experimental data of Figure 76 have been compared with 1) predictions reported for the model of Cobelli et al. (1982), and 2) predictions obtained from simulations using the model of Guyton et al. (1978). As shown in the upper panel of the figure, the present model was the only one to predict correctly the time course of plasma glucose concentration; whereas Guyton's model underestimated the hypoglycemic impact and attained a premature steady state behavior, Cobelli's model failed to predict a hypoglycemic steady state with glucose concentration continuing to decline at termination of the study. Elevation in plasma insulin concentration resulting from the insulin infusion was predicted reasonably well by Guyton's model as shown in the center panel of Figure 77. Cobelli et al. (1982) did not report insulin response predictions for this study. Although there was considerable scatter in the plasma glucagon response data (lower panel of Figure 77), the simple one-compartment glucagon model formulation of the present model yielded a somewhat more accurate prediction of plasma glucagon response than did that of Cobelli's model. Guyton's model did not include glucagon in the formulation.

5) Euglycemic Insulin Clamp

In the euglycemic clamp technique, arterial plasma insulin is acutely

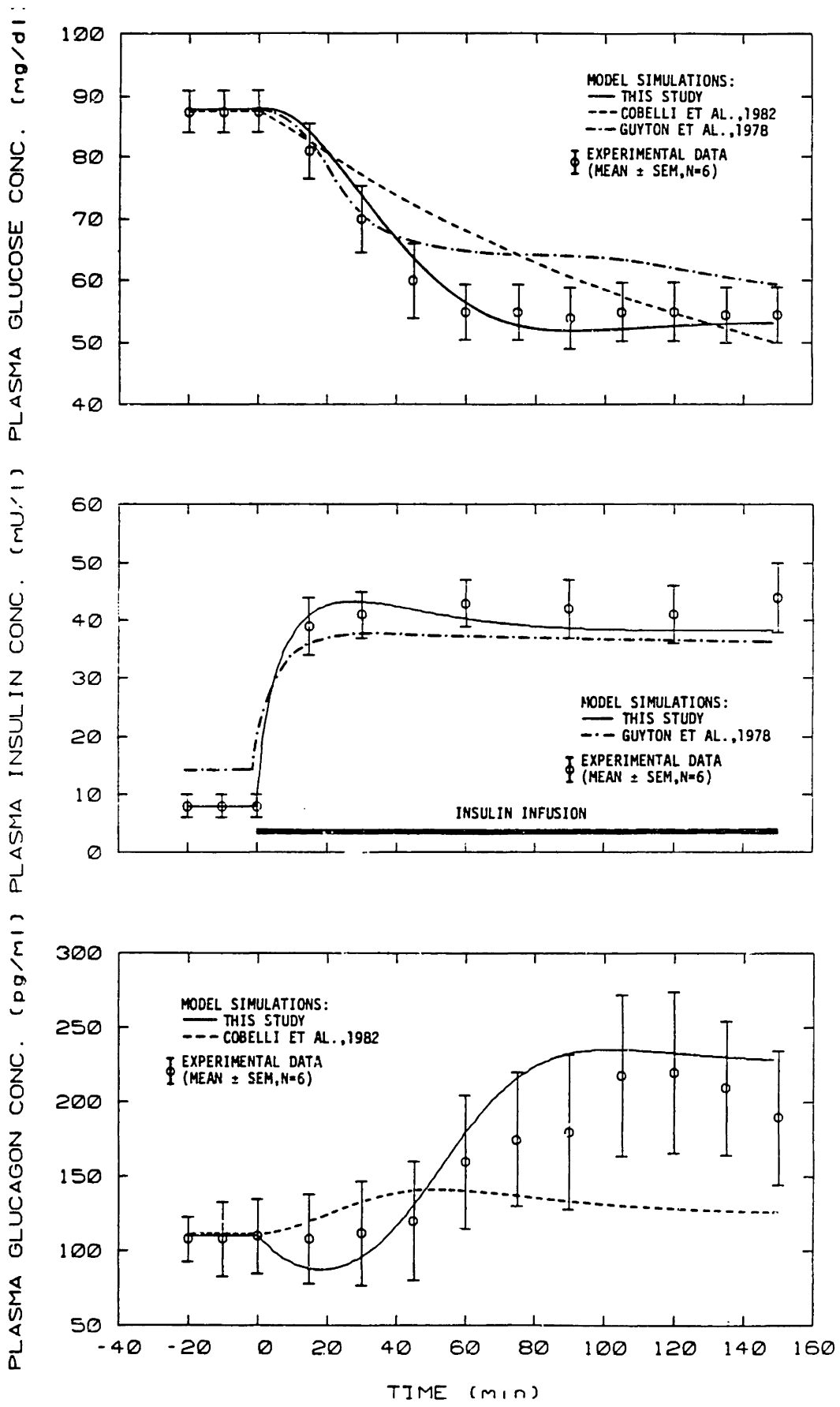

Fig. 77 Comparison of model predictions for 0.4 mU/kg/min continuous intravenous insulin infusion experiment of Sacca et al. (1979).

raised by intravenous infusion of a preset empirical insulin dose while arterial plasma glucose concentration is maintained at basal level by periodic adjustment of an intravenous glucose infusion rate. The insulin dose schedule and glucose infusion algorithm have been described in detail in DeFronzo et al. (1979). The insulin dose schedule for a 70 kg subject is given in Table 33. As indicated in the table, the insulin infusion consists of an initial 10-min priming dose followed by a continuous steady infusion rate. Arterial plasma glucose concentrations are measured at 5-min intervals (starting at t=10 min), and these measured values are used to adjust a glucose infusion according to the following algorithm (70 kg subject):

$$r = 0 \qquad 0 \leq t < 4 \text{ min} \tag{196}$$

$$r = 140 \qquad 4 \leq t < 10 \text{ min} \tag{197}$$

$$r_1 = \gamma (G_b - G_i) + SM_i \qquad i\Delta t \leq t < (i+1)\Delta t;\ i=2,3,\ldots;\ \Delta t = 5 \text{ min} \tag{198}$$

$$SM_i = SM_{i-2} \times FM_{i-1} \times FM_i \tag{199}$$

$$FM_i = \frac{G_b}{G_i} \tag{200}$$

where: r = glucose infusion rate (mg/min)

G_i = arterial plasma glucose concentration at $t = i\Delta t$ (mg/dl)

G_b = basal arterial plasma glucose concentration (mg/dl)

SM = metabolic infusion component (mg/min)

FM = correction factor (dimensionless)

γ = empirical constant = 8.87 dl/min

with initial conditions:

$SM_0 = 280$ mg/min

$SM_1 = 280$ mg/min

$FM_1 = 1.0$

TABLE 33. Preset empirical insulin dose schecule calculated to raise plasma insulin concentration 100 uU/ml during the euglycemic clamp in a 70 kg subject.

Time (min)	Insulin Infusion Rate (mU/min)
0-1	221
1-2	197
2-3	175
3-4	156
4-5	139
5-6	124
6-7	110
7-8	98
8-9	87
9-10	78
10-120	69

Model simulation of a euglycemic insulin clamp experiment is presented in Figure 78. Included for comparison in the figure are mean experimental values measured in 11 normal subjects during the euglycemic insulin clamp studies of DeFronzo et al. (1979). The basal state initial conditions for this study were: 1) arterial plasma glucose concentration equaled 92 mg/dl (corresponding to G_H = 99 mg/dl); 2) arterial plasma insulin concentration equaled 14 mU/l (I_H = 14 mU/l).

As shown in the lower panel of Figure 78, model predictions agreed well with experimental data for the arterial plasma insulin response to the empirical primed-continuous insulin infusion, both with respect to the rapid initial distribution dynamics in response to the priming dose and the steady state plasma insulin level achieved by the continuous infusion. As indicated in the upper panel of the figure, the glucose infusion algorithm varied the glucose infusion rate such that the simulated arterial plasma glucose concentration remained essentially constant at its initial basal value (92 mg/dl). From a physiologic standpoint, the euglycemic insulin clamp experiment is particularly interesting because it provides an assessment of the insulin sensitivity of the body's glucose disposal processes independent of changes in glycemia. Assuming hepatic glucose production is essentially suppressed completely by the elevated insulin levels, the rate of glucose infusion required to maintain euglycemia must just balance the total rate of tissue glucose disposal in the body. The glucose infusion rate thus provides an index of insulin sensitivity. As shown in the upper panel of Figure 78, the glucose infusion rate required to maintain euglycemia for the model gradually increased to a steady value of approximately 5.5 mg/kg·min. For the group of subjects studied by Defronzo et al. (1979), the glucose infusion rate followed essentially the

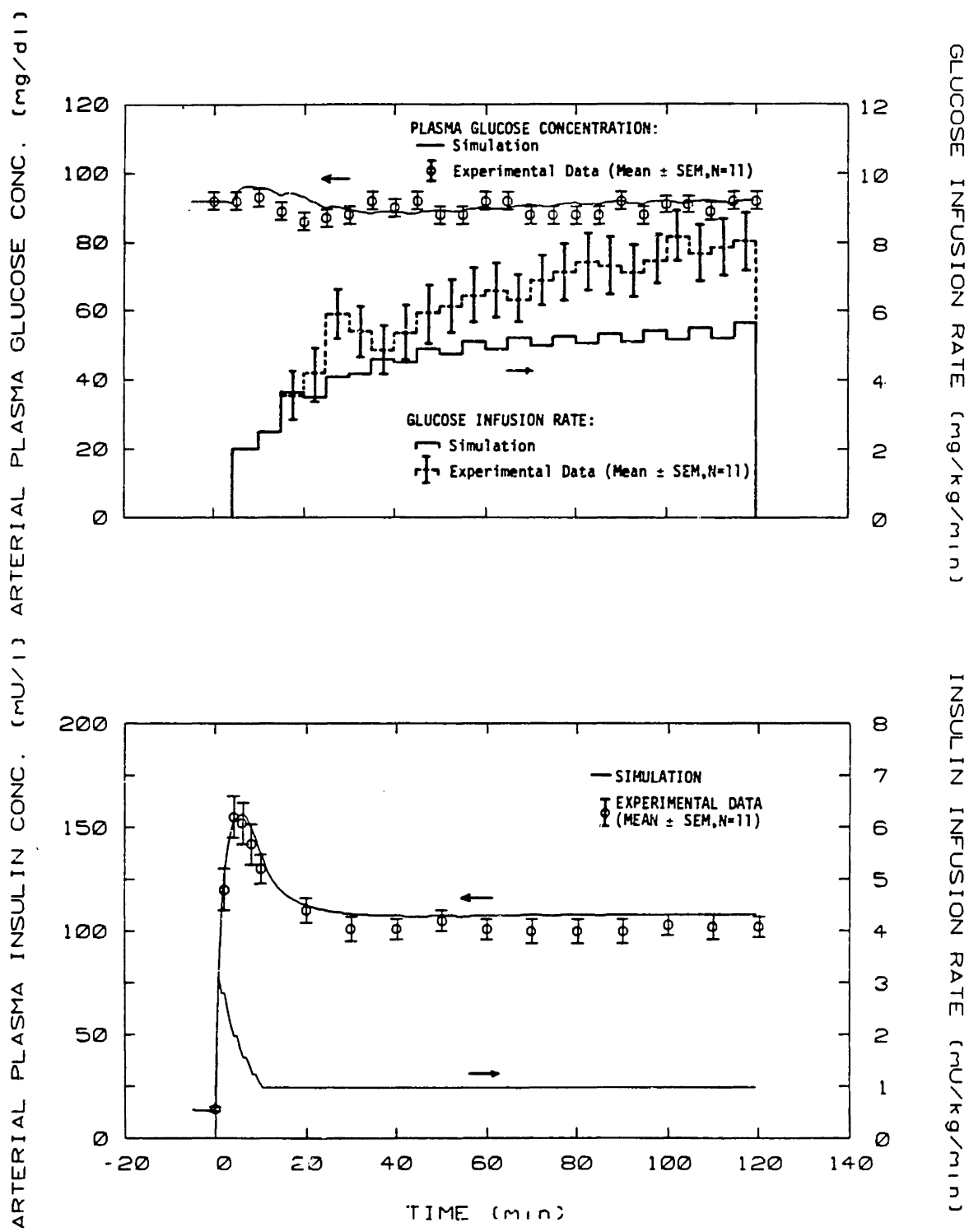

Fig. 78 Comparison between model predictions and clinical data for a 100 mU/l euglycemic insulin clamp. (Data from DeFronzo et al., 1979)

same time course but rose to a somewhat higher final value of about 8 ± 0.75 mg/kg·min by 120 min. This could suggest that the insulin-sensitivity of glucose disposal is greater than its quantification in the glucose model; however, as will be shown in the next simulation study, the model accurately predicted the 120 min glucose infusion rate reported during euglycemic clamps for the group of 8 subjects studied by Gray et al. (1982).

6) Deactivation of Insulin Action

Model simulation of a study designed by Gray et al. (1982) to examine the deactivation of insulin action in man is presented in Figure 79. Following a 120-min euglycemic insulin clamp, insulin infusion was abruptly discontinued (t = 0) while arterial glucose concentration remained clamped at euglycemic through use of a variable-rate glucose infusion. The euglycemic insulin clamp (initiated at t = -120 min) employed the same insulin infusion pattern and glucose infusion algorithm as described in the previous section (Table 33 and Equations 196-200). Experimental data included in Figure 79 are mean responses of 8 normal subjects reported by Gray et al. (1982). The initial basal state conditions (t = -120 min) for the study were as follows: 1) arterial plasma glucose concentration equaled 91 mg/dl (corresponding to G_H = 98 mg/dl); 2) arterial plasma insulin concentration equaled 12 mU/l (I_H = 12 mU/l).

As shown in the upper panel of Figure 79, termination of the insulin infusion caused an acute decrease in arterial plasma insulin concentration. Of interest here was the observation that the simulated plasma insulin response did not drop significantly below experimental values during the initial rapid decline, a result that would have been expected had there

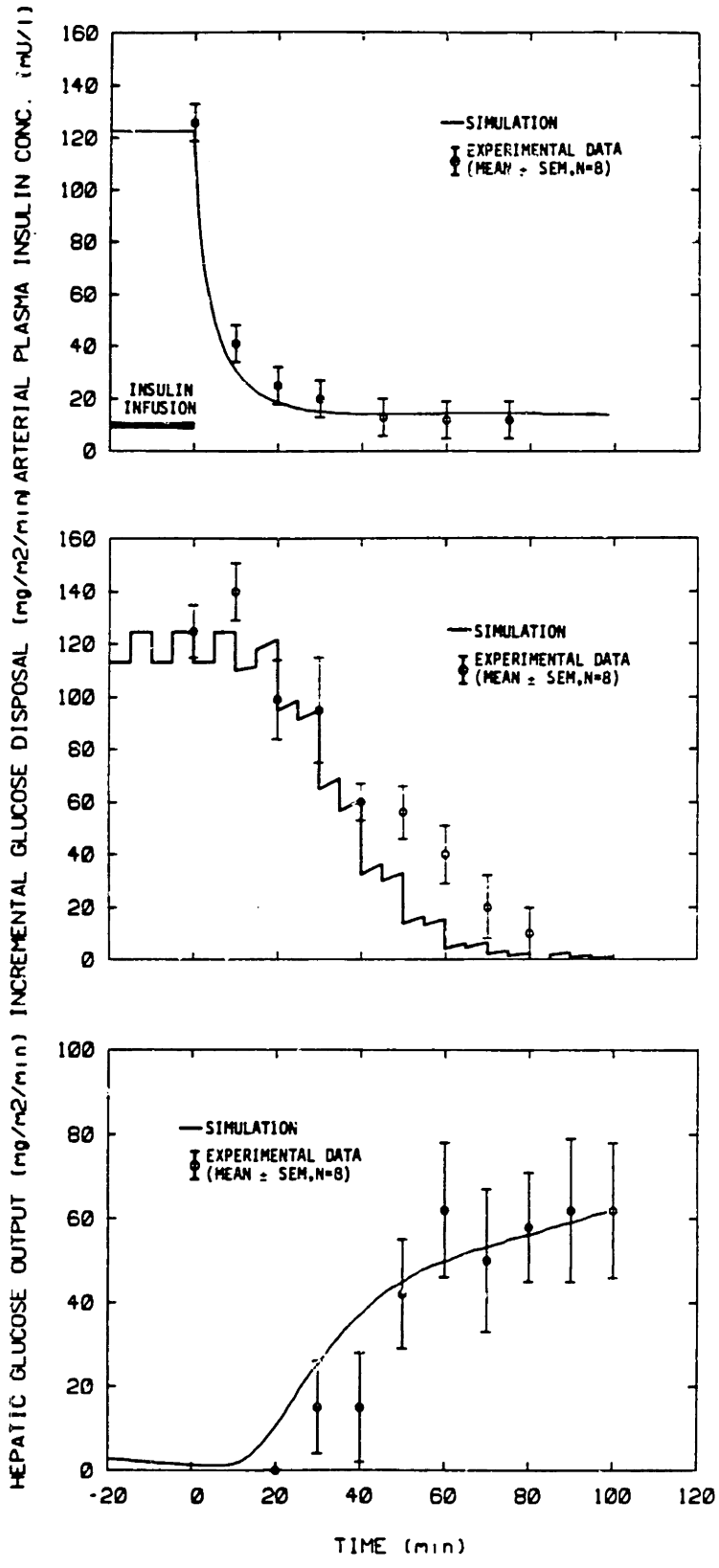

Fig. 79 Model simulation of studies to examine the deactivation of insulin action in man. (Data from Gray et al., 1982)

been a significant release of reversibly bound insulin in the body. In the center panel of the figure, the total rate of body glucose disposal was expressed in terms of incremental glucose disposal, defined as

$$\begin{aligned}\text{Incremental glucose disposal rate} = &(\text{glucose infusion rate}) \\ &+ (\text{hepatic glucose production rate}) \\ &- (\text{basal hepatic glucose production rate})\end{aligned} \tag{201}$$

where the glucose infusion rate was that required to maintain euglycemic levels. A body surface area of 1.73 m^2 was assumed for an ideal weight 70 kg man in order to convert model results to units used by Gray et al. Data in the center panel of Figure 79 indicate the decline in the total body glucose disposal rate as insulin levels returned to normal following termination of the 120-min euglycemic insulin clamp. As mentioned previously, in this study the glucose infusion rate required to maintain euglycemia at termination of the euglycemic insulin clamp was accurately predicted by the model ($\sim$ 5 mg/kg·min), but this was significantly lower than the infusion rate reported by DeFronzo et al. (1979) ($\sim$ 8 mg/kg·min). In the lower panel of Figure 79 is a comparison between simulated and experimentally measured rates of hepatic glucose production. By comparing the top and bottom panels in the figure it can be seen that there was a significant delay associated with hepatic recovery from insulin exposure. The model was quite successful in predicting this interesting result, a consequence of incorporating time dependence into the formulation of hormonal regulation of hepatic processes in the model.

7) Hyperglycemic Clamp

In the hyperglycemic clamp method, arterial plasma glucose concentration is acutely raised by intravenous infusion of a preset empirical glucose priming dose, and is maintained at the hyperglycemic level through

the duration of the study by use of a periodically adjusted glucose infusion. The glucose priming dose and infusion algorithm were described in detail in DeFronzo et al. (1979). Arterial plasma glucose concentrations are measured at 5-min intervals (starting at t = 10 min), and these measured values are employed to maintain the desired hyperglycemic arterial plasma glucose concentration. The following equations describe the glucose infusion for a +125 mg/dl hyperglycemic clamp (70 kg subject):

Priming Dose:

$$\begin{aligned} r &= 3059 \quad 0 \leq t < 1 \text{ min} \\ r &= 2470 \quad 1 \leq t < 2 \text{ min} \\ r &= 2000 \quad 2 \leq t < 3 \text{ min} \\ r &= 1588 \quad 3 \leq t < 4 \text{ min} \\ r &= 1353 \quad 4 \leq t < 5 \text{ min} \\ r &= 1118 \quad 5 \leq t < 6 \text{ min} \\ r &= 941 \quad 6 \leq t < 7 \text{ min} \\ r &= 765 \quad 7 \leq t < 8 \text{ min} \\ r &= 706 \quad 8 \leq t < 9 \text{ min} \\ r &= 647 \quad 9 \leq t < 10 \text{ min} \end{aligned} \tag{202}$$

Algorithm:

$$r_i = \alpha(G_d - G_i) + SM_i \qquad i\Delta t \leq t < (i+1)\Delta t;\ i=2,3,\ \ldots \quad \Delta t = 5 \text{ min} \tag{203}$$

$$SM_i = SM_{i-2} \times FM_{i-1} \times FM_i \tag{204}$$

$$FM_i = \frac{(G_d - G_b)}{(G_i - G_b)} \tag{205}$$

where:

r = glucose infusion rate (mg/min)

G_i = arterial plasma glucose concentration at $t = i\Delta t$ (mg/dl)

G_b = basal arterial plasma glucose concentration (mg/dl)

G_d = desired arterial plasma glucose concentration (mg/dl)
$= G_b + 125$ mg/dl

SM = metabolic infusion component (mg/min)
FM = correction factor (dimensionless)
α = empirical constant = 8.87 dl/min

with intial conditions:

SM_0 = 412 mg/min
SM_1 = 412 mg/min
FM_1 = 1.0

Model simulation of a +125 mg/dl hyperglycemic clamp experiment is presented in Figure 80. Included in the figure for comparison are mean experimental values measured in 11 normal subjects during the hyperglycemic clamp studies of DeFronzo et al. (1979). The basal state initial conditions for this study were as follows: 1) arterial plasma glucose concentration equaled 92 mg/dl (corresponding to G_H = 99 mg/dl); 2) arterial plasma insulin concentration equaled 14 mU/l (I_H = 14 mU/l).

As shown in the upper panel of Figure 80, the initial glucose priming dose caused an acute elevation in the simulated arterial plasma glucose concentration of about 125 mg/dl, and the infusion algorithm varied the subsequent glucose infusion rate such that this level of hyperglycemia was maintained. The hyperglycemic clamp method is particularly interesting because plasma insulin response reflects in vivo pancreatic insulin response to essentially a step change in arterial glucose concentration. As indicated in the lower panel of Figure 80, model predictions agreed reasonably well with arterial plasma insulin concentration data over roughly the first hour of hyperglycemia, reflecting the biphasic nature of pancreatic insulin response to a step increase in glucose concentration. Between 60-120 min, however, the predicted insulin response began to noticeably lag below the experimental response data. Recalling that no provi-

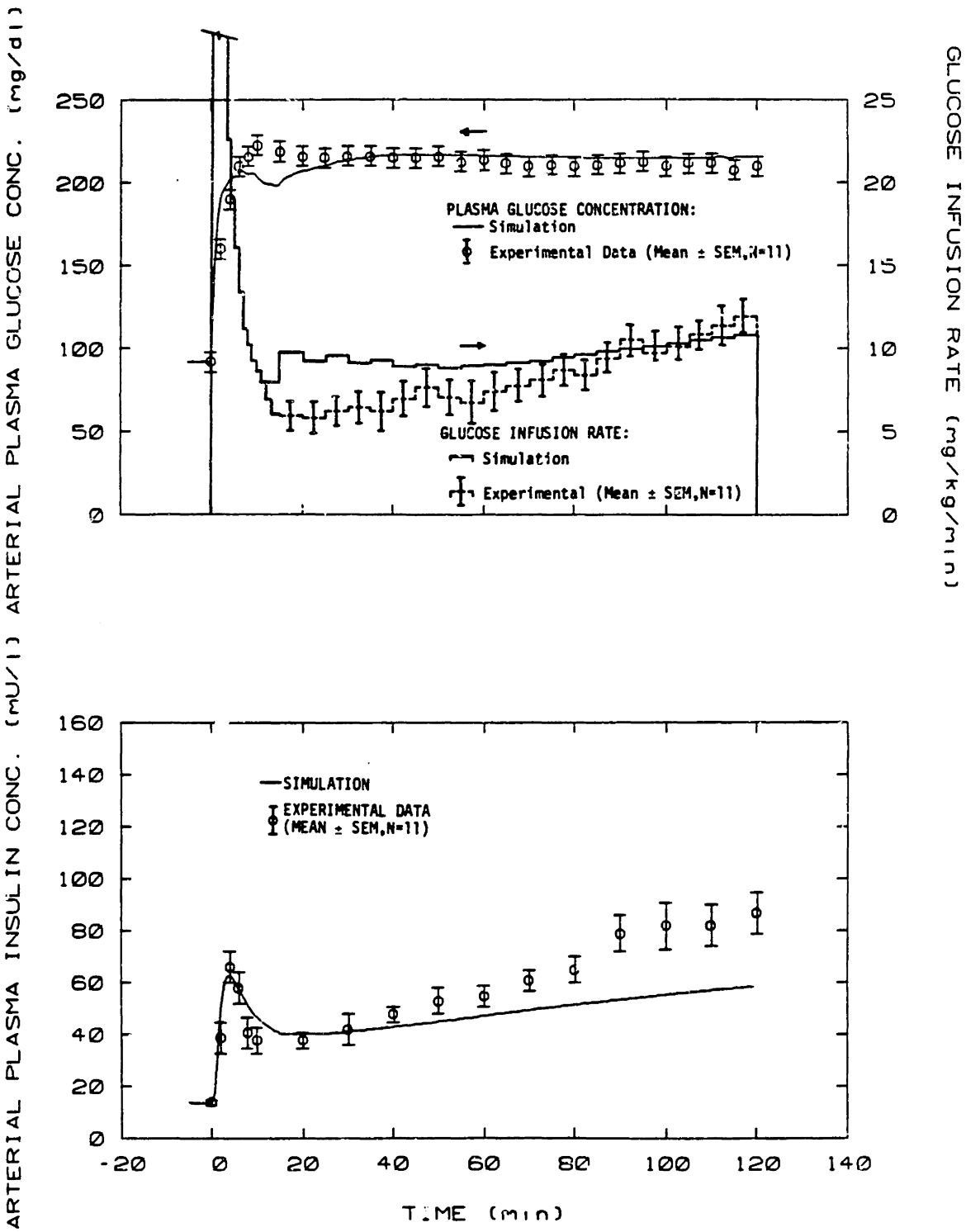

Fig. 80 Comparison between model predictions and experimental data for a +125 mg/dl hyperglycemic clamp. (Data from DeFronzo et al., 1979)

sion for insulin synthesis was included in the pancreatic insulin release model, this behavior could have been anticipated. Experimental studies have shown that newly synthesized insulin begins to appear in secreted insulin about 1-2 hours following glucose stimulation of the beta cell (Gold et al., 1982), with maximal contribution of newly synthesized insulin occuring within about 2.5 - 3.5 hours of stimulation (Howell and Taylor, 1967). A pancreatic insulin release model intended to yield accurate predictions over long time scales of prolonged hyperglycemia would thus require consideration of the insulin synthesis process and its delayed augmentation of insulin secretion.

8) Standard 100g Oral Glucose Tolerance Test (OGTT)

In attempting to simulate an oral glucose challenge there were two important issues to consider that had not been encountered in the studies presented thus far. First, since gut hormone intervention quantitatively enhances pancreatic insulin response to oral glucose (Perley and Kipnis, 1967; Elrick et al., 1964; McIntyre et al., 1965), the model pancreas could not be expected to yield good predictions of insulin response to glycemia resulting from an oral challenge. Second, since portal glucose concentration measurements are not attainable in human studies, the rate of gut absorption of a 100 g oral glucose load has never been directly quantified, and thus the model input for simulating a 100 g OGTT could not be defined a priori. With these considerations in mind, the objectives of the OGTT simulation studies were as follows: 1) to use the physiologic model together with experimental plasma glucose and insulin response data to predict the time course of gut glucose absorption, and 2) to use the model to examine the underlying metabolic processes which contribute to the observed

glucose tolerance, in particular the partitioning of glucose disposal among the tissues.

The data base employed for the OGTT simulation studies was obtained from the Joslin Research Laboratory and consisted of venous blood glucose and plasma insulin measurements correlated from 100 g OGTT's administered to a population of 145 normal adult males whose body weights averaged near ideal for their ages and heights. Mean basal state data for this group were as follows: 1) peri-pheral venous blood glucose concentration equaled 75 mg/dl (corresponding to G_{pv} = 89 mg/dl); 2) peripheral venous plasma insulin concentration equaled 13 mU/l (I_{pv} = 13 mU/l).

Since the model pancreas could not be used for predicting insulin response, the first task was to determine the time course of pancreatic insulin release. This was accomplished by bypassing the pancreatic insulin release model (which decoupled the insulin model from the glucose model) and iteratively adjusting the rate of pancreatic insulin input into the insulin model until the predicted plasma insulin time course matched the experimental data. The final pancreatic insulin release rate input function, derived by trial and error, is shown in the lower right plot in Figure 81. Use of this insulin input function yielded excellent correspondence between model predictions and experimental data for the time course of plasma insulin concentration, as demonstrated in the lower left plot of the figure.

Having established a pancreatic insulin input capable of generating proper dynamic response in the insulin model, the glucose model (through its metabolic processes) was again recoupled with the insulin and glucagon models. Next, a test input function for the rate of gut oral glucose absorption was inserted and adjusted so as to match model predicitons with

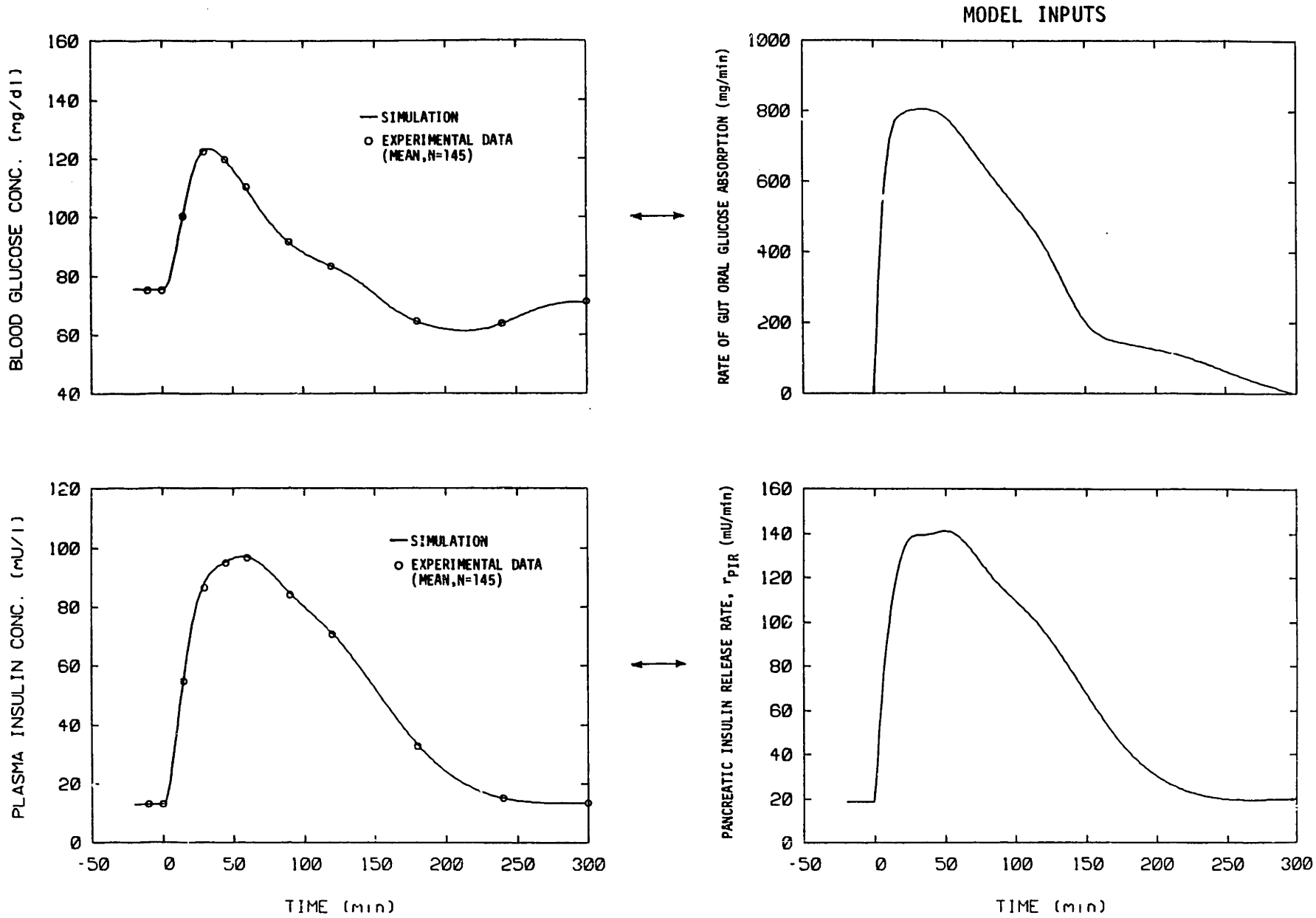

Fig. 81 Summary of the 100g OGTT simulation studies, showing the model inputs (right plots) and the corresponding agreement between model predictions and experimental data attained by their use. (Data from the Joslin Research Laboratory, Boston)

experimental data for the time course of peripheral blood glucose response. The method employed for iterating trial gut glucose absorption input functions was as follows: 1) values for the rate of absorption were specified at 25-min intervals over the 300-min duration of the study; 2) a smooth gut absorption rate curve was generated from the discrete time values by cubic spline interpolation; 3) the smoothed continuous gut absorption curve was input to the glucose model for OGTT simulation. This technique proved quite successful for providing a means of rapidly and easily adjusting and testing the trial input functions.

Seven trial and error iterations were required to obtain the input gut glucose absorption rate function shown in the upper right plot in Figure 81. Use of this input function resulted in matching model predictions and experimental data for the time course of blood glucose concentration response, as demonstrated in the upper left plot of the figure.

In order to assess the physiologic significance of the resulting glucose absorption curve, the area under the curve was first calculated to determine the total dose. The value obtained was 100.3 g! This was an amazing result; based on the time courses of glucose and insulin over the 300-min postprandial period, the model predicted tolerance of exactly the correct quantity of exogenous glucose. Although the extremely small magnitude of the error (0.3%) must be attributed in part to some good fortune, the implications of the result in a more general sense clearly suggest extreme accuracy of the model in predicting glucose disposal within these plysiologic ranges of glucose and insulin concentration.

With respect to the temporal patterning of the resulting gut glucose absorption curve, the glucose absorption rate initially rose rapidly to a maximum of about 800 mg/min which was sustained for roughly 40 min. Such

an initial rapid plateauing response is characteristic of intestinal absorption behavior and has been demonstrated in animal studies from portal glucose measurements following oral loading (Waddel and Sussman, 1967). Intestinal absorption of glucose occurs via active transport of glucose across the intestinal mucosa, a process that may be rate-limited by intra-lumenal diffusion and/or carrier availability (Wilson, 1962; Csaky, 1975). The inital plateauing in the glucose absorption rate most likely corresponds to effective saturation of the intestinal absorption mechanism upon initiation of gastric emptying of a large glucose load (Langerlof et al., 1976). The maximal absorption rate of 800 mg/min agrees well with the value estimated by Hillman (1977) based on his review of available data from intestinal perfusion studies. Following the maximum absorption response, the gut absorption curve of Figure 81 indicated a slow decline in the absorption rate back to the baseline. The temporal behavior of the decline in the glucose absorption rate appeared to follow a general first order exponential decay, but with superimposed secondary increases in the rate of absorption centered at about 120 and 200 min (see Figure 81). Such secondary absorptive increases have been commonly observed in experimental studies and presumably reflect multiple gastric injections of glucose into the duodenum (Bergman et al., 1982). Multiple gastric emptying, as evidenced by secondary increases in the rate of splanchnic glucose release, has been demonstrated by direct hepatic venous catheterization measurements (Felig et al., 1975) and double tracer turnover analysis (Pilo et al., 1981; Radzuik, 1981) in humans following 100g oral glucose ingestion. Finally, with respect to the total duration required for complete absorption of the glucose load, it was originally believed that gut glucose absorption was completed within about 180 min following 100g oral glucose

administration. This was because measured blood glucose levels return to (cross) basal by 180 min, as shown by the blood glucose response curve in Figure 81. However, recent tracer experiments (Radziuk et al., 1978; Pilo et al, 1981) as well as studies using indirect calorimetry (Jacot et al., 1982) have indicated that complete absorption of such large glucose loads takes considerably longer than 2-3 hours. The 300-min absorption time predicted in the present study is in good agreement with such recent findings. Noting that plasma insulin concentration remains elevated at about 3 times basal level at 180 min (see Figure 81), and that such insulin levels are sufficient to suppress endogeneous hepatic glucose production, the return of blood glucose levels to basal at 180 min would correspond to the situation in which the rate of intestinal glucose absorsption just balances the suppression in hepatic glucose production rate from normal. Whereas recent tracer experiments can distinguish between endogenous and oral glucose output from the splanchnic organs, traditional hepatic venous catheterization measurements would simply suggest the splanchnic glucose output had returned to normal by 180 min, thus providing a false indication that gut glucose absorption was completed.

Predicted rates of glucose metabolism during the 100g OGTT are presented in Figure 82. As shown in the figure, hepatic glucose production was rapidly suppressed and remained so for about 200 min following glucose administration, gradually returning to its basal rate by 300 min. Peripheral and hepatic glucose uptake rates, on the other hand, rapidly increased to dispose of the incoming oral glucose load. In order to examine partitioning of the glucose load among the various metabolic disposal routes, the curves in Figure 82 were integrated and the results were used to compile the 180 min 100g OGTT glucose balance sheet presented in Table

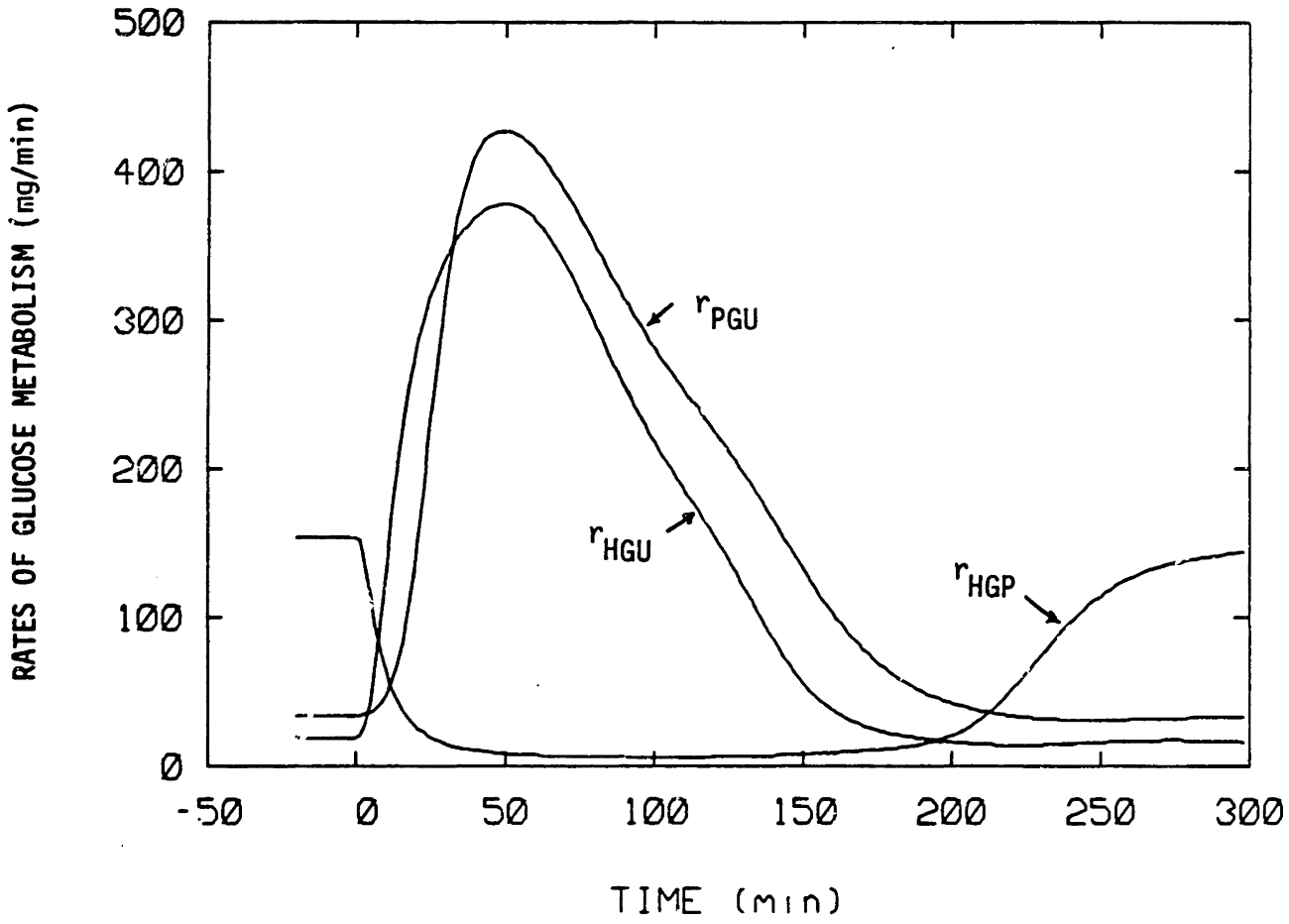

Fig. 82 Model predictions for the rates of peripheral glucose uptake (r_{PGU}), hepatic glucose uptake (r_{HGU}), and hepatic glucose production (r_{HGP}) during the 100g OGTT.

34. Only 7% of the glucose load remained unabsorbed after 180 min. Since endogenous liver glucose production was almost completely suppressed, tissue uptake accounted for nearly balancing the quantity of exogenous glucose load introduced over this period. Although obligatory utilization of glucose by the insulin insensitive tissues (primarily brain) accounted for disposal of 19 g of glucose, muscle and liver played relatively equal roles in disposing of the remaining 77 g of glucose. The results presented in Table 34 are in excellent agreement with direct experimental measurements reported in the literature. First, Jackson et al. (1973) measured the time course of forearm glucose uptake during the 180-min period following 100 g oral glucose administration in 25 normal subjects; by integrating the forearm glucose uptake curves over the duration of the experiment and extrapolating the results to total muscle mass, the quantity of peripheral glucose uptake may be estimated to total 41 g, a value in excellent agreement with model predictions. Second, including consideration of the quantity of unabsorbed glucose remaining in the gut, hepatic glucose uptake, and the insulin-insensitive gut tissue utilization of glucose, the total predicted quantity of glucose remaining in the splanchnic bed at 180 min was 48 g. Correcting this value to account for endogenous liver glucose production, the model predicted an apparent total 180-min splanchnic glucose retention of 45 g, or 45% of the total glucose load. Although experimental estimates of splanchnic glucose retention vary over a large range (30-60%) (see Table 21), the model prediction of 45% represents a good average of the available human data.

Although several other investigators have used models of glucose metabolism to simulate the OGTT, these studies have differed from the methods of input-output inversion employed in the present modeling study. Hillman

TABLE 34. 100g OGTT balance sheet (180 min).

Unabsorbed after 180 min	7
Insulin-Independent Tissue Uptake	
Brain	13
RBC	2
Gut	4
Insulin-Dependent Tissue Uptake	
Muscle	40
Liver	37
Urinary Loss	0
Remaining in Glucose Space at 180 min	~0
TOTAL	103
-Endogenous Glucose Production	
Liver	-3
TOTAL	100g

(1977) modified the physiologic model developed by Guyton (1973) for simulation of the 100 g OGTT. Hillman modified the heterogeneous fast pool pancreatic insulin release model of Guyton so as to potentiate insulin response to oral glucose, and assumed a gut glucose absorption rate input function derived primarily on the basis of theoretical considerations and a review of available gut absorption data in the literature (see Appendix B). The resulting model predictions for glucose and insulin response during a 100 g OGTT are compared with experimental data in Figure 83. As indicated in the figure, Hillman's approach was only modestly successful in yielding response predictions. Cramp and Carson (1981) presented model simulations of a 50 g OGTT. In these studies, gut glucose absorption was assumed to rise instantaneously to a maximum rate that remained constant for 30 min, followed by an exponential decay back to zero over a period of about 20 min. No modification in the pancreatic insulin release formulation was provided to account for agumented insulin response to oral glucose. The resulting model predictions for the time courses of glucose and insulin response to the 50 g OGTT agreed, at least in a qualitative sense, with the general temporal response patterns observed experimentally in humans. Finally, Cobelli and Mari (1983) used the basic model presented by Cobelli et al. (1982) to simulate the 100 g OGTT. Since a single compartment glucose model was used, a prespecified fraction of the oral glucose load (8%) was assumed to be removed by the liver on initial passage, and the oral glucose input became the rate of splanchnic glucose release to the systemic pool. Parameters in the model were then adjusted such that the desired level of partitioning of the glucose load among the various tissues was realized while matching the time course of plasma glucose concentration with experimental data. Since the single "plasma glucose concentration" in

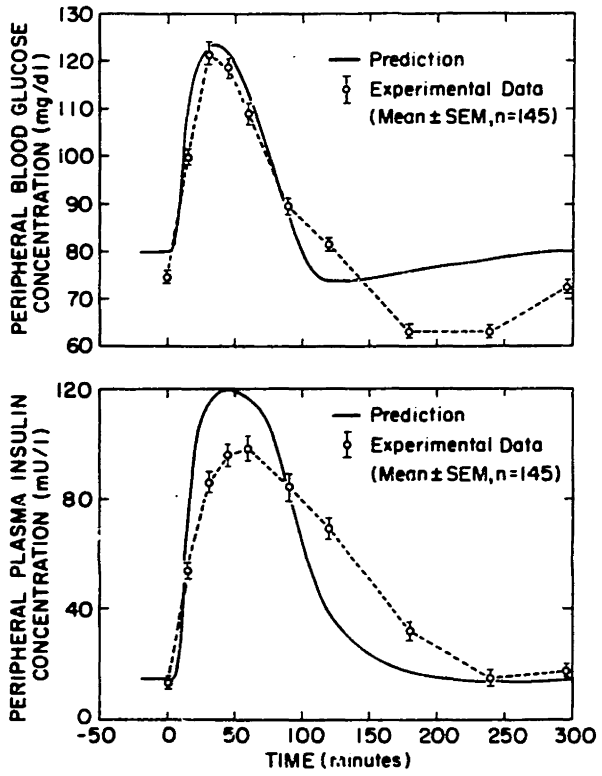

Fig. 83 Comparison between experimental data and model predictions for glucose and insulin response during a standard 100g OGTT. Model predictions were generated using Hillman's modified version of the glucose metabolism model of Guyton. (Data from Joslin Research Laboratory; figure from Sorensen et al., 1982)

the one-compartment glucose model could not directly account for differences between splanchnic glucose levels (that affect liver glucose uptake) and systemic glucose levels (that influence peripheral tissue glucose uptake) during oral glucose loading, the physiologic correctness of the resulting metabolic functions adjusted on the basis of this OGTT study should be viewed with some skepticism.

C) Conclusion

Using a single set of model parameters, model predictions agreed well with clinical data over the wide range of physiologic conditions encompassed by the simulation studies. The model's unique design offered a higher degree of physiologic correspondence and demonstrated predictive capacity and accuracy superior to prior models. The physiologic model of glucose metabolism in normal man thus provided a firm foundation for subsequent development of diabetic models for assessing efficacies of new diabetic therapies.

V. MODELING OF GLUCOSE METABOLISM IN TYPE I (INSULIN-DEPENDENT) DIABETES MELLITUS

A) Diabetes Mellitus: A General Overview

1) Aberrent Homeostasis and the Overt Symptoms of Diabetes

In general, diabetes mellitus is caused by an insufficiency of insulin relative to the requirements of the tissues for this hormone. As implied by this definition, the diabetic state can result from abnormalties associated with both availability of insulin to the tissues and tissue sensitivity to the available insulin. In either case, one of the major manifestations of diabetes mellitus is an excessively high level of glucose in the circulation.

Diabetic homeostasis has been described as a "super-fasted" state (Cahill and Soeldner, 1969) because the normal modes of fuel mobilization characteristic of the fasting state are accelerated in the diabetic state, in spite of the excessive circulating fuel levels which result. Illustrated in Figure 84 is typical basal glucose metabolism in the fasting diabetic. Breakdown and release of muscle protein supplies excessive quantities of circulating amino acids for liver gluconeogenesis, but much of the glucose thus produced is in excess of the fuel requirements of the glucose-consuming tissues. This additional glucose, generated at the expense of muscle protein, begins to spill into the urine when the blood glucose concentration exceeds the renal threshold. Because of the osmotic effect of glucose in the kidney tubules to prevent tubular reabsorption of fluid, loss of glucose in the urine causes diuresis. Consequently two classic symptoms of diabetes are polyuria (excessive urination) and polydipsia (excessive thirst).

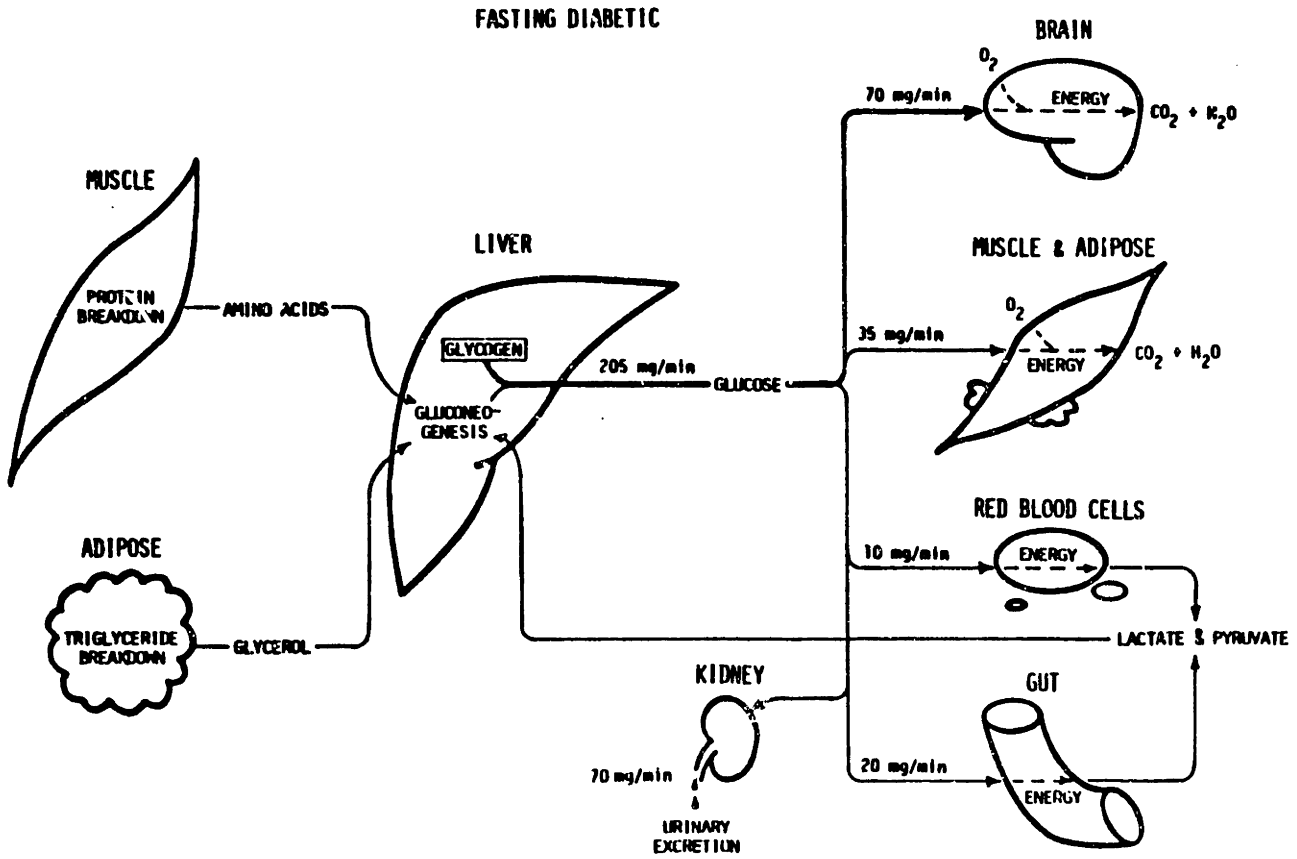

Fig. 84 Typical basal glucose metabolism in the fasting diabetic.

In a similar manner, breakdown of triglycerides in adipose tissue supplies circulating fatty acids. Fatty acids are converted to ketone bodies (β-hydroxybutyrate and acetoacetate) by the liver. Hepatic ketogenesis is normally the primary source of energy production for liver tissues during fasting, as the β-oxidation of fatty acids produces high energy phosphate bonds. In the diabetic state, however, ketogenesis increases, and the rate of hepatic ketone body production exceeds the rate of their uptake and utilization for energy by peripheral tissues. As a result, the circulating concentration of keto acids in the blood may rise from a normal value of about 1 mEq/l to as high as 30 mEq/l. Keto acids have a low threshold for excretion by the kidneys, and thus begin to spill into the urine. Both hyperketonemia and ketonuria contribute to acidosis in diabetics. Both β-hydroxybutyrate and acetoacetate are moderately strong acids, and thus increases in their circulating concentrations contribute directly to acidososis. Even more important in the case of acidosis is the indirect effect of sodium loss which accompanies ketonuria. Since keto acids are fairly strong, only a small portion are excreted in acidic form, but most combine with sodium derived from extracellular fluid. Thus, sodium ion concentration in extracellular fluid decreases, and this depletion of alkali buffering reserve further exacerbates the acidosis already present from excessive keto acid levels. The combined effects of hyperketonemia and ketonuria, called ketosis, thus lead to acidosis, or ketoacidosis. Ketoacidosis is a very serious complication of acute and marked insulin deficiency may be fatal if left untreated.

2) Classification, Diagnosis, and Etiologies of Glucose Intolerance

In 1979, the National Diabetes Data Group of the NIH published the

results of an international workgroup which was convened for the purpose of developing standardized criteria for classification and diagnosis of various modes of glucose intolerance, including diabetes mellitus (National Diabetes Data Group, 1979). Because of the subsequent wide acceptance of their recommendations, a brief review of the terminology and classification system is presented in the section, along with supplementary discussion regarding etiologic factors.

In order to provide for standardized clinical classifications, the heterogeneity of glucose intolerance was partitioned into three basic categories: 1) diabetes mellitus (DM), 2) impaired glucose tolerance (IGT), and 3) gestational diabetes (GDM). In addition, heterogeneity within the diabetic syndrome was further partitioned into two basic DM subclasses: 1) Type I, or insulin-dependent diabetes mellitus (IDDM), and 2) Type II, or noninsulin-dependent diabetes mellitus (NIDDM).

The Type I diabetic is ketosis-prone and requires exogeneous insulin to sustain life. This subclass of diabetes classically occurs in juveniles with abrupt onset of symptoms; it has been found, however, that the former term for this disease, juvenile-onset diabetes, is inappropriate in that it can be recognized and become symptomatic for the first time at any age. IDDM appears to be heterogenous with respect to genetic and environmental factors which precipitate the disease. In the majority of patients, genetic determinants associated with histocompatibility antigens are thought to be important. More specifically, studies have indicated a twofold to fourfold increased risk of developing IDDM in individuals possessing certain human leukocyte antigen (HLA) types on chromosome 6 (Ganda and Soeldner, 1977). These HLA types appear to create a susceptibility for a gene-virus interaction to trigger an islet-cell autoimmune reaction, destroying the beta

cell insulin function. On the contrary, there is no statistically significant difference in risk of developing NIDDM between "control" populations and individuals possessing these same HLA types.

The Type II noninsulin-dependent diabetic is not ketosis-prone and is not dependent on insulin for the prevention of ketonuria; ketosis may develop under certain circumstances, however, such as severe stress resulting from infection or trauma. Patients with NIDDM are generally treated by control of diet and oral agents, with occasional insulin utilization for correction of persistent fasting hyperglycemia. In a majority of cases, onset of NIDDM is after the age of 40, and NIDDM was formerly termed maturity-onset diabetes for this reason; as before, use of this terminology was inappropriate since onset can occur at any age. The symptoms of NIDDM are extremely heterogeneous in nature. Plasma insulin levels may range from mild hypoinsulinemia, to normal, to above normal in cases associated with insulin resistance. Patients often show very slow progression of onset, and fasting hyperglycemia is not associated with many cases. It must be noted, however, that the typical chronic complications associated with diabetes, such as neuropathy and retinopathy, also occur in NIDDM patients. The cateogry NIDDM has been divided into two subclasses, according to whether or not obesity is present. Obesity is associated with etiologic factors such as insulin resistance resulting from tissue insulin receptor malfunction (Beck-Nielson, 1978; Kolterman et al., 1980), often leading to plasma insulin levels which are elevated relative to normal. NIDDM appears to have a stronger genetic basis than does IDDM, as evidenced by more frequent familial pattern of occurrence. The heterogeneous nature of this genetic predisposition suggests an interplay between genetic background and environmental modulation for expression of the genome (Ganda

and Soeldner, 1977).

Individuals with plasma glucose concentrations which are intermediate between those considered normal and those considered diabetic are assigned to the classification Impaired Glucose Tolerance (IGT). For psychological reasons, previous terms such as chemical diabetes, latent diabetes, and asymptomatic diabetes were abandoned. While individuals in this class are not considered diabetic, they run a higher risk than the normal population of developing diabetes. IGT is an intermediate stage in the natural development of NIDDM for some patients, whereas some individuals will spontaneously return to normal glucose tolerance.

The classification Gestational Diabetes Mellitus (GDM) is reserved for women who exhibit glucose intolerance for the first time during pregnancy. GDM develops in approximately 1-2% of all pregnancies; deterioration in glucose tolerance normally occurs during the third trimester of pregnancy and is thought to result from complex metabolic and hormonal changes which are not well understood at present (O'Sullivan, 1970). Associated with GDM are increased perinatal morbidity and mortality (O'Sullivan et al., 1971), and a higher risk of developing overt diabetes within 5-10 yrs after parturition (O'Sullivan and Mahan, 1964). Following termination of pregnancy, the woman is reclassified into an approprate category of glucose intolerance based on her postpartum plasma glucose levels.

In addition to the clinical classifications outlined above, two statistical risk classes of glucose intolerance have been established. The category Previous Abnormality of Glucose Tolerance (PrevAGT) is restricted to persons who now have normal glucose tolerance but who have previously demonstrated impaired glucose intolerance or diabetic hyperglycemia. For example, obese diabetics whose glucose tolerance returns to normal after

loss of weight, and gestational diabetics whose glucose tolerance returns to normal following parturition would be included under the classification PrevAGT. The second statistical risk classification is Potential Abnormality of Glucose Tolerance (PotAGT). This class would include persons who have never exhibited glucose intolerance, but who are at a substantially increased risk of developing diabetes mellitus. Individuals at increased risk for development of IDDM include: 1) persons with islet-cell antibodies, 2) monozygotic twins of IDDM diabetics, 3) siblings of IDDM diabetics, and 4) offspring of IDDM diabetics. Persons who are at increased risk for development of NIDDM included: 1) monozygotic twins of NIDDM diabetics, 2) first-degree relatives of NIDDM diabetics (e.g. sibling, parent, or offspring), and 3) members of ethnic or racial groups among which high prevalence of diabetes has been observed. Although the above are listed in decreasing order of apparent risk, the actual risk associated with any of these circumstances is not well established as yet.

With respect to classification of subjects, the National Diabetes Data Group (1979) recommended the following criteria for the diagnosis of diabetes mellitus in nonpregnant adults. First, unequivocal hyperglycemia in the presence of classic diabetic symptoms such as polyuria, polydipsia, ketonuria, and rapid weight loss is considered diagnostic of diabetes. Otherwise, diagnosis is based on measurement of plasma glucose concentration. A fasting venous plasma glucose concentration in excess of 140 mg/dl (normal value defind as <115 mg/dl) on more than one occasion constitutes diagnosis. Under such circumstances, administration of an OGTT is not required, because virtually all persons with a fasting venous plasma glucose concentration in excess of 140 mg/dl would exceed the OGTT criteria. Finally, diagnosis based on a 75 g OGTT requires sustained elevation of

plasma glucose concentration on more than one occasion; elevated glucose concentration is defined as venous plasma glucose concentration in excess of 200 mg/dl (normal value defined as <140 mg/dl) for the 2-h sample and in excess of 200 mg/dl (normal value defined as <200 mg/dl) for an additional sample taken between dose administration and 2-h. Subjects whose glucose values are above those defined as normal but below those considered diagnostic of diabetes are generally classified as IGT patients. Specialized criteria for the diagnosis and classification of glucose intolerance in children and pregnant adults were also recommended by the National Diabetes Data Group (1979); details of these criteria can be obtained by the interested reader from the original report.

B) Abnormal Physiology in Diabetes Mellitus and Its Reversibility

The ultimate objective of medical research is to prevent disease, or, in the absence of absolute prevention, to develop effective cures. Unfortunately, the development of β-cell defects and their causes are not well understood, and thus it is unlikely that prevention or absolute cure of diabetes will be realized in the foreseeable future. A great deal of effort is therefore being directed toward treatment of the disease, and in particular toward developing improved insulin therapies in the hopes of preventing the chronic complications associated with diabetes. Within this context, a physiologic model of glucose metabolism provides a powerful tool for developing and assessing the effectiveness of insulin therapies.

Using the model of glucose metabolism in normal, nondiabetic subjects as a starting point, development of diabetic model(s) entails the identification, characterization, and modeling or remodeling of the metabolic processes that deviate or cause deviation from normal behavior. Such

abnormal physiology can be divided into two categories, primary and secondary. The primary, or causal abnormal physiology of diabetes is deranged pancreatic insulin response to glycemia. Other aberrant physiology, generally considered secondary to the development of diabetes, includes insulin resistance and reduced counterregulatory response to hypoglycemia. The distinguishing feature of the secondary physiologic abnormalities is the possibility of their avoidance and/or reversibility as a result of improved glycemic control and insulin delivery.

In this section, the abnormal physiology associated with glucose metabolism in diabetics will be discussed, together with evidence concerning its reversibility. Since the present objective of diabetic modeling is to develop a tool for assessing the efficacies of insulin therapies, emphasis will be placed on abnormal physiology related to insulin-dependent, or Type I diabetes mellitus.

1) Pancreatic Insulin Response to Glycemia

Deranged insulin response to glycemia is characteristic of diabetes mellitus. Presented in Figure 85 are data correlated by Reaven and Miller (1968) showing the relationships between glucose and insulin responses to oral glucose for subjects with varying degrees of glucose intolerance. As demonstrated in the upper plot, increased severity of glucose intolerance was clearly associated with a systematic increase in plasma glucose concentration. As evidenced in the lower plot, however, plasma insulin responses exhibited a rather complex behavior. For subjects with impaired glucose tolerance, insulin levels were substantially higher than normal; in a more absolute sense, however, relative to the elevated glycemia accompanying the impaired glucose tolerance, insulin response was probably

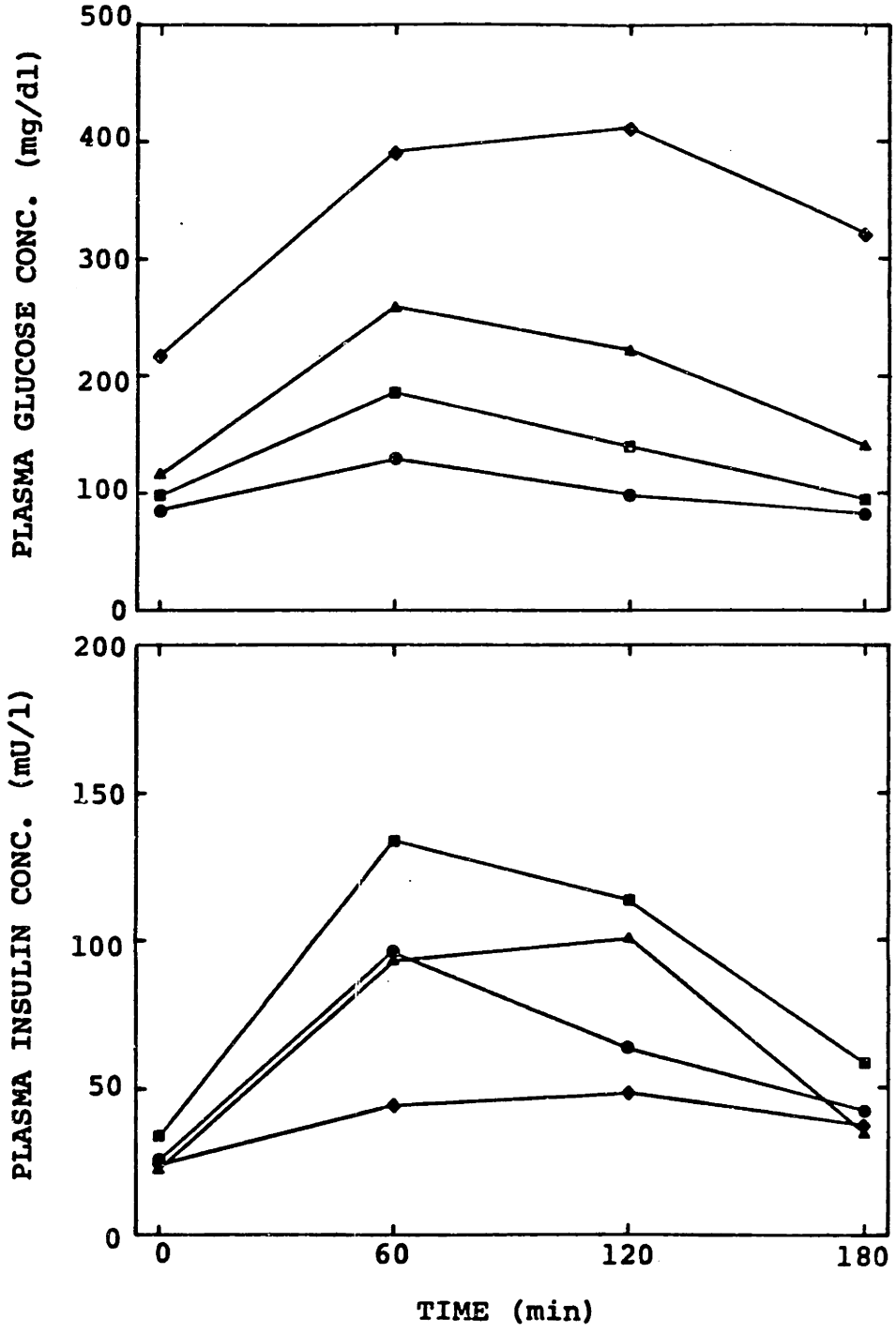

Fig. 85 Plasma glucose and insulin responses during an OGTT characteristic of various degrees of glucose intolerance. (Data from Reaven and Miller, 1968)

somewhat diminshed from normal. Although more severe diabetes was characterized by a greatly attenuated insulin response, mild diabetic glucose intolerance was associated with an intermediate impairment of insulin response (relative to glycemia) together with a deranged temporal patterning suggestive of delayed pancreatic responsiveness. Similar glucose-insulin relationships following OGTT administration have been reported by Seltzer et al. (1967) and appear to be characteristic of the various degrees of glucose intolerance.

NIDDM patients display a great diversity of insulin responses to glucose (Reaven, 1984). In response to an OGTT, insulin levels seem to increase with progressive degrees of hyperglycemia up to a certain point, but patients with the most severe NIDDM have the lowest insulin levels (Reaven and Miller, 1979). Brunzell et al. (1976) have demonstrated that the acute insulin response during the first few minutes after an intravenous glucose challenge is abolished in NIDDM patients with fasting plasma glucose levels in excess of 115 mg/dl. It is interesting, however, that patients with NIDDM who have lost the acute insulin response to intravenous glucose show relatively normal acute insulin response to other intravenous secretagogues, such as isoproterenol (Robertson and Porte, 1973) and arginine (Palmer et al., 1976), suggesting a primary defect in NIDDM is loss of acute β-cell responsiveness to glucose. Although NIDDM patients with severe fasting hyperglycemia show absolute hypoinsulinemia in response to an OGTT, Lui et al. (1983) have demonstrated that the day-long circulating insulin levels are within normal limits in these severely hyperglycemic NIDDM patients. It is obvious from the above that the β-cell defects in NIDDM are complex and result in a wide spectrum of insulin responses.

In Type I diabetes mellitus, the prediabetic period prior to onset of

clinically overt diabetes is characterized by appearance of islet cell antibodies and activated T-lymphocytes together with a progressive loss of acute early-phase insulin response to intravenous glucose (Srikanta et al., 1983a; 1983b; 1984). IDDM usually results in an abrupt onset of overt symptoms. Prior to diagnosis, insulin insufficiency can contribute to catabolism of the β-cell and can thus cause an acute functional disturbance of those cells not having been morphologically destroyed (Menzel et al., 1981). Initial insulin therapy often triggers a temporary remission with increased capacity for endogenous insulin reponse (Park et al., 1974) resulting from reversal of the functional disturbance of the intact β-cells (Menzel et al., 1981). Independent of this, however, the irreversible process of morphological destruction of the β-cell progresses with duration of diabetes. Although the interpretation of such data is somewhat controversial (Polonsky and Rubenstein, 1984), several investigators (Block et al., 1972; Yue et al., 1978; Menzel et al., 1981) using circulating C-peptide immunoassay have shown that residual insulin secretion (RIS) is quantitatively insignificant for the majority of IDDM patients and is particularly difficult to observe in unstable patients or in diabetics for whom the duration of the overt disease has exceeded several years. Thus, in contrast to NIDDM, IDDM is generally characterized by abrupt onset of symptoms and nearly complete failure of β-cell function.

2) Insulin Resistance

Insulin resistance is a common feature of diabetes mellitus. There are two basic causes of insulin resistance. The first involves tissue resistance to the action of insulin in regulating glucose metabolism. The second is associated with the presence of circulating insulin antibodies in

insulin-treated diabetics which result from the immunogenicity of conventional exogenous insulins.

a) Tissue Resistance to the Action of Insulin

As was evidenced by the plasma glucose and insulin OGTT response curves of Figure 85, certain types of impaired glucose tolerance are characterized by hyperglycemia in the presence of insulin levels that are higher than normal. Such behavior is associated with tissue resistance to insulin as excessive insulinemia fails to stimulate normal glucose disposal and tolerance.

The euglycemic insulin clamp technique (DeFronzo et al., 1979) has provided a means for assessing dose-response characteristics for the effects of insulin on glucose disposal (Rizza et al., 1981). In the euglycemic insulin clamp technique, plasma insulin is acutely elevated to a predetermined constant level by a primed-continuous infusion of exogenous insulin, while plasma glucose is maintained constant at a euglycemic level by means of a variable infusion of exogenous glucose. The glucose infusion rate required to maintain euglycemia equals the sum of the decrement in endogenous glucose production rate and the increment in tissue glucose uptake rate and thus serves as an index of the overall effect of insulin on total-body glucose metabolism. Dose-response curves are generated by repeating the euglycemic insulin clamp at various plasma insulin levels and plotting steady state glucose infusion rate as a function of steady state plasma insulin concentration. Such a dose-response relationship for normal man (Rizza et al., 1981) is illustrated in the upper plot of Figure 86. By combining the euglycemic insulin clamp technique with simultaneous isotope turnover measurement of endogenous glucose production, the separate effects

of insulin level on endogenous glucose production and tissue glucose uptake can be distinguished (DeFronzo et al., 1978) as shown for normals (Rizza et al., 1981) in the lower panel of Figure 86.

Insulin resistance results in a shift from normal of the sigmoidal dose-response curves for insulin stimulation of glucose metabolism. Since insulin exerts its biologic action through binding to specific cell membrane receptors (for review see Kahn, 1979), the effects of receptor versus postreceptor defects on shifting of in vivo insulin stimulation of glucose metabolism can be predicted (Kahn, 1978; Olefsky, 1981) as shown in Figure 87. The first type of insulin resistance, as defined by theoretical insulin dose-response curves, is the pure receptor defect, termed decreased sensitivity. The pure receptor defect is caused by a reduction in the number of insulin receptors at the target tissue cell membrane. Since the biologic acitivity of insulin is dictated by the quantity of receptor-bound insulin, and this is generally an equilibrium-limited association, a reduction in the number of receptors requires higher insulin concentrations to affect the same quantity of bound insulin. Because of the great excess in the number of receptors normally available for binding at high insulin concentrations, the maximal biologic response can be realized even in the presence of a reduction in total receptors available for binding at a given insulin concentration. The pure receptor defect is thus characterized by a rightward shift in the insulin dose-response curve without change in the maximal response (see Figure 87). The second type of insulin resistance in the pure postreceptor defect, termed decreased responsiveness. The pure postreceptor defect is caused by a lack of proper intracellular metabolic response to a given level of receptor-bound insulin. Such impaired response could arise from abnormal intracellular enzyme levels. The pure

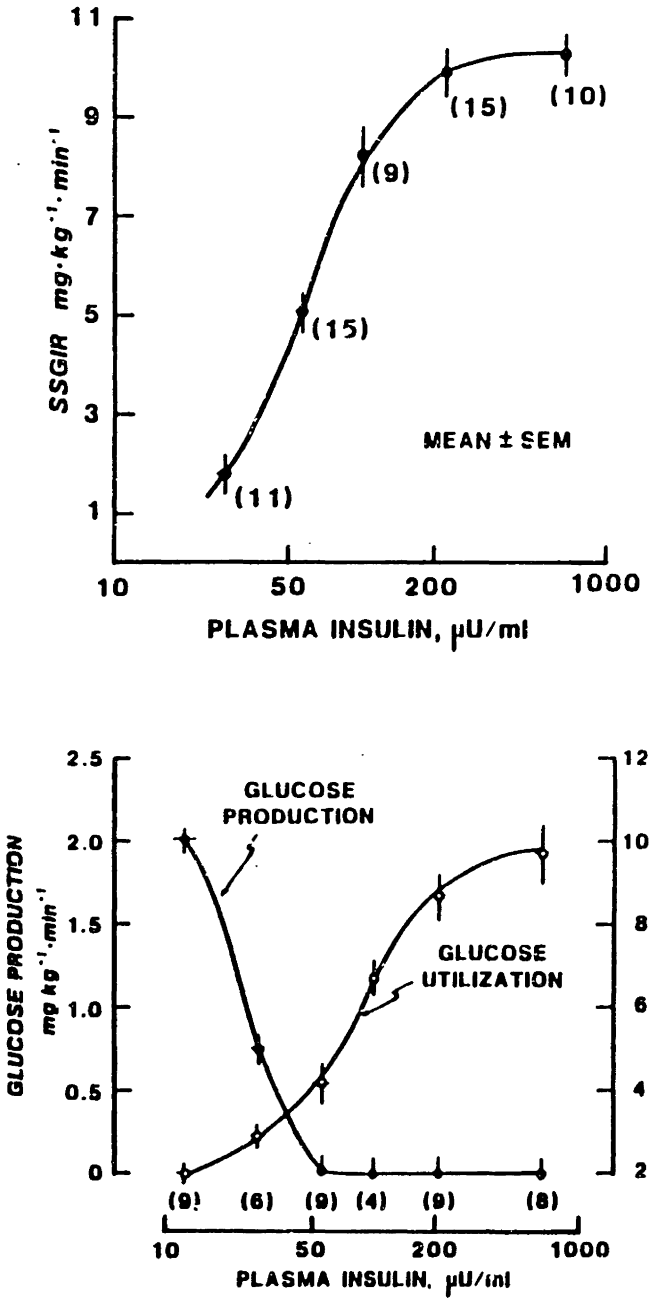

Fig. 86 Insulin dose-response curve for whole-body glucose metabolism in normal man is shown in the upper plot; here, the steady state glucose infusion rate (SSGIR) required to maintain euglycemia is plotted versus the steady state plasma insulin levels achieved by graded insulin clamping. The separate insulin dose-response curves for hepatic glucose production and tissue glucose utilization in normal subjects are shown in the lower plot. Numbers of subjects are indicated in parentheses. (From Rizza et al., 1981)

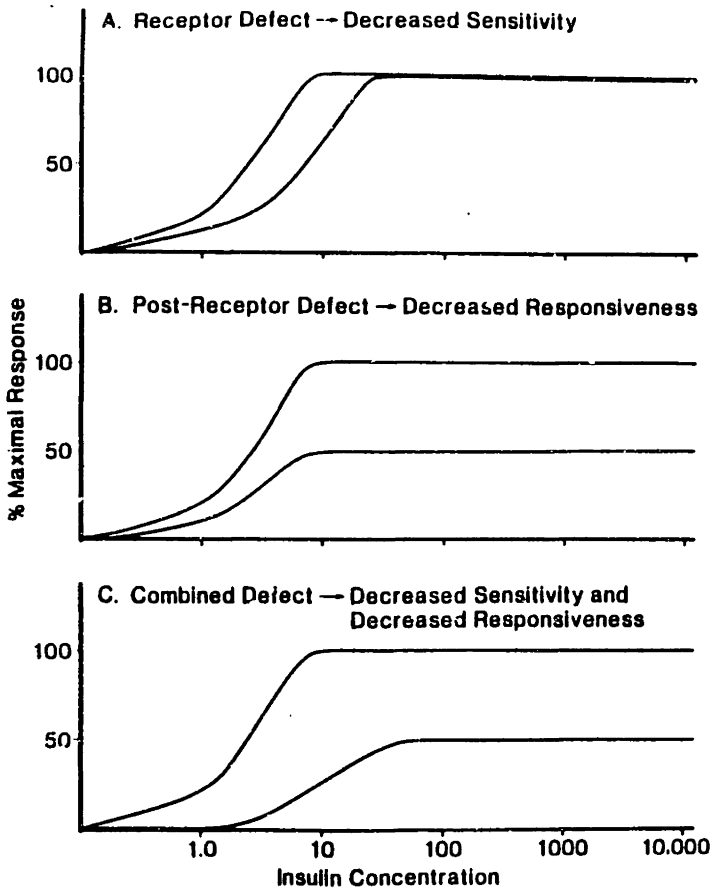

Fig. 87 Theoretical shifts in the dose-response curves for the biological action of insulin resulting from a pure receptor defect (A), a pure postreceptor defect (B), and a combined receptor and postreceptor defect (C). (From Olefsky, 1981)

postreceptor defect in characterized by a proportionate reduction in response at all insulin levels and an impairment of maximal response (see Figure 87). Finally, a coexistence of receptor and postreceptor defects would be represented by a rightward shift in the dose-response curve together with a decrease in maximal response.

Because hyperglycemia in the presence of hyperinsulinemia is often observed in NIDDM patients, insulin resistance in NIDDM has been extensively studied (Ginsberg and Rayfield, 1981; Scarlett et al., 1982; Mandarino and Gerich, 1984; Andrews et al., 1984) in an effort to elucidate the complex interplay between the defects in insulin secretion and insulin action which manifest the disease (Reaven, 1984; Skyler, 1984). Use of the euglycemic insulin clamp method to generate in vivo insulin dose-response curves in NIDDM subjects (Scarlett et al., 1982; Mandarino and Gerich, 1984) has demonstrated a decrease in insulin sensitivity suggestive of a postreceptor defect, as shown by the data of Mandarino and Gerich (1984) in Figure 88. As previously discussed, insulin action can be attributed both to suppression of endogenous glucose production and to stimulation of tissue (muscle and liver) glucose uptake. By use of [3-^{3}H] glucose infusions and isotope turnover analysis, Ginsberg and Rayfield (1981) and Mandarino and Gerich (1984) have directly shown that the overall insulin resistance in NIDDM is a result of both decreased insulin suppression of hepatic glucose production and decreased insulin stimulation of tissue glucose uptake.

An important aspect of insulin resistance concerns its reversibility. Reaven et al.(1977) have shown that insulin insensitivity develops in normal dogs made diabetic with alloxan, but that this acquired insulin resistance is reversed by treatment with exogenous insulin. Thus, it is

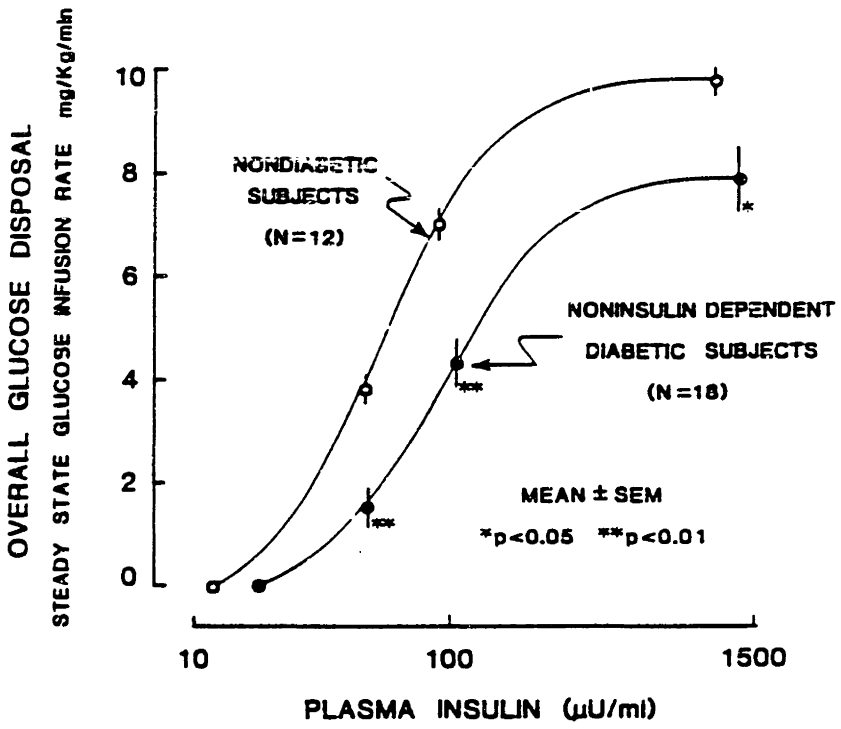

Fig. 88 Dose-response curves for insulin-stimulated glucose metabolism in patients with NIDDM and in age- and weight-matched nondiabetics. (From Mandarino and Gerich, 1984)

possible that the insulin resistance observed in NIDDM is secondary to abnormal insulinemia. This possibility has been studied in insulin-deficient NIDDM by use of insulin administration or oral hypoglycemic agents to correct for insulin deficiency and improve glycemic regulation. Hidaka et al.(1982) reported little improvement in in vivo insulin action following 7 days of insulin treatment (4 subcutaneous injections of regular insulin per day) in obese NIDDM subjects. Scarlett et al. (1982), however, indicated that 14 days of insulin treatment (2 injections of regular and NPH purified pork insulin per day) essentially reversed the insulin resistance in patients with NIDDM. Ginsberg and Rayfield (1981) found improvement in insulin responsiveness attributable to both hepatic and tissue contributions following 1-8 weeks of insulin therapy (single injection of intermediate-acting insulin per day) in some of the NIDDM patients studied, but results varied greatly over the group of NIDDM patients as a whole, suggesting that the underlying causes of insulin resistance may be heterogeneous with some defects being unresponsive to insulin replacement. In a recent study, Andrews et al. (1984) reported that 1 month of insulin treatment (3 subcutaneous injections of monocomponent insulin per day) caused improvement in insulin action in a group of 13 NIDDM patients and that insulin sensitivity no longer deviated significantly from a weight- and age-matched group of normals, although this improvement varied considerably from patient to patient. In addition, the observed improvement in insulin action persisted for at least 2 weeks after cessation of insulin therapy. Finally, Mandarino and Gerich (1984) showed that prolonged (~4 mo) administration of an oral hypoglycemic agent (tolazamide) resulted in decreasing insulin resistance in a group of 18 NIDDM patients, and this decrease in insulin resistance was attributable to correction of post-

receptor disorders associated with both the suppression of hepatic glucose production and the stimulation of tissue glucose uptake. Similar results have been reported by Kolterman and Olefsky (1984) for NIDDM subjects as a result of prolonged (3-18 mo) treatment with the oral hypoglycemic agent glyburide. Since oral hypoglycemic agents, in addition to stimulating β-cell insulin secretion, can act directly on the level of cell metabolism and its regulation by hormones (Levine, 1984), the reversal of insulin resistance noted in the above studies could have in part resulted from factors other than enhancement of insulinemia. Nonetheless, although the results to date are somewhat mixed, increasing evidence supports the notion that the insulin resistance associated with insulin-deficient NIDDM can be reversed with proper insulin replacement.

Although insulin resistance has been a well-recognized feature of NIDDM, only recently has insulin resistance also been recognized as a prominent feature of Type I IDDM. DeFronzo et al. (1982) used insulin clamp methods to study insulin resistance in IDDM subjects. When euglycemic levels of plasma glucose were maintained while plasma insulin concentration was elevated to comparable levels (~ 100 mU/ml) in both a group of Type I diabetics (n = 8) and a group of nondiabetic controls (n = 36), insulin-mediated glucose metabolism rose to 3.39 ± 0.30 mg/kg·min in the diabetic group versus 7.03 ± 0.22 mg/kg·min in the control group; thus, response to insulin was only 48% of normal in the diabetics. When the insuin clamp experiment was repeated at hyperglycemic plasma glucose levels (~ 170 mg/dl), insulin-mediated glucose metabolism was 4.77 ± 0.18 mg/kg·min in the diabetic group (n = 11) versus 12.14 ± 0.96 mg/kg·min in the control group (n = 5); in this case, insulin response was only 39% of normal in the diabetics.

Revers et al. (1984) and Pernet et al. (1984) have employed euglycemic insulin clamp methods to construct dose-response curves for insulin stimulation of glucose metabolism in Type I diabetics. Revers et al. (1984) studied the insulin dose-response relationship in 5 well controlled Type I diabetics (6 weeks of intensive conventional injection therapy, home glucose monitoring 2-4 times daily and frequent adjustments in insulin dosage; glycosylated hemoglobin of 7.2 ± 0.2%), 5 poorly controlled Type I diabetics (conventional injection therapy, urinary glucose measured daily and relatively fixed insulin dosage; glycosylated hemoglobin of 11.7 ± 0.6%), and 21 age-matched normal subjects (glycosylated hemoglobin range of 5.5 - 7.0%); the dose-response curves for these three groups are shown in Figure 89. Insulin-stimulated glucose disposal in the well controlled diabetic subjects was comparable to that in the normal subjects, with similar half-maximally effective insulin levels and virtually identical maximal rates of glucose disposal. In contrast, the dose-response curve for insulin stimulation of glucose disposal in the poorly controlled diabetic subjects was significantly right-shifted with a marked reduction in the maximal glucose disposal rate. Thus, the insulin resistance observed in the poorly controlled Type I diabetics was significantly right-shifted with a marked reduction in the maximal glucose disposal rate. Thus, the insulin resistance observed in the poorly controlled Type I diabetics was characteristic of a combined receptor (decreased sensitivity) and postreceptor (decreased responsiveness) defect (see Figure 87).

Pernet et al. (1984) used sequential graded euglycemic insulin clamps to study the insulin dose-response curve for glucose metabolism in 6 Type I diabetics (conventional insulin injection therapy; glycosylated hemoglobin of 9.8 ± 0.5%) and 8 normal controls (glycosylated hemoglobin of 6.6 ±

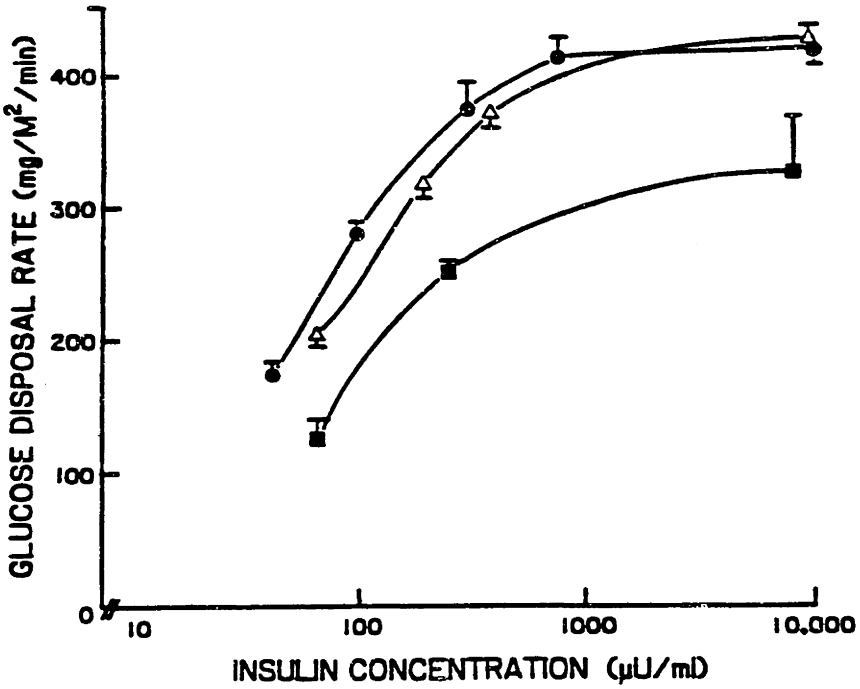

Experimental Data (Mean ± SEM):

- ● Normal Subjects (n=21)
- △ Well Controlled Diabetic Subjects (n=5)
- ■ Poorly Controlled Diabetic Subjects (n=5)

Fig. 89 Comparison of dose-response curves for insulin stimulation of glucose metabolism in normal subjects, well controlled Type I diabetics, and poorly controlled Type I diabetics. Glucose disposal rate was based on the steady state glucose infusion rate required to maintain euglycemia during graded insulin clamping. (From Revers et al., 1984)

0.2%); the reported dose-response data from this study is plotted in Figure 90. As shown in the figure, the dose-response curve for insulin-stimulated glucose metabolism was significantly right-shifted for the diabetic group, but the maximal stimulation at high insulin levels was comparable to that in the normal subjects. The insulin resistance observed in this group of Type I diabetics was thus characteristic of a receptor (decreased sensitivity) type of defect. It should be mentioned that the glycosylated hemoglobin levels in the IDDM subjects studied by Pernet et al. were intermediate between the levels distinguishing the poorly and well controlled IDDM subjects in the study of Revers et al. Thus, comparison of the dose-response curves in Figures 89 and 90 could suggest that the postreceptor defect is a consequence of a more poorly controlled diabetic state than is the receptor defect.

With respect to the underlying causes of the insulin resistance observed in Type I diabetics, dose-response curves distinguishing between suppression of hepatic glucose production and tissue glucose uptake have not been reported to date. Although normal inhibition (essential suppression) of hepatic glucose production has been demonstrated in Type I diabetics at high physiologic insulin levels ($>$ 100 mU/ml) (DeFronzo et al., 1982; Proietto et al., 1983; Revers et al., 1984), studies at low physiologic insulin levels have not been performed, and thus the possibility of a receptor defect (or decreased sensitivity) cannot be excluded. Since hepatic glucose production was essentially suppressed at the high physiologic insulin levels employed in the studies of DeFronzo et al. (1982) and Revers et al. (1984), the observed insulin resistance must be attributed to a defect in tissue glucose uptake.

Since insulin-sensitive glucose uptake occurs in muscle and liver,

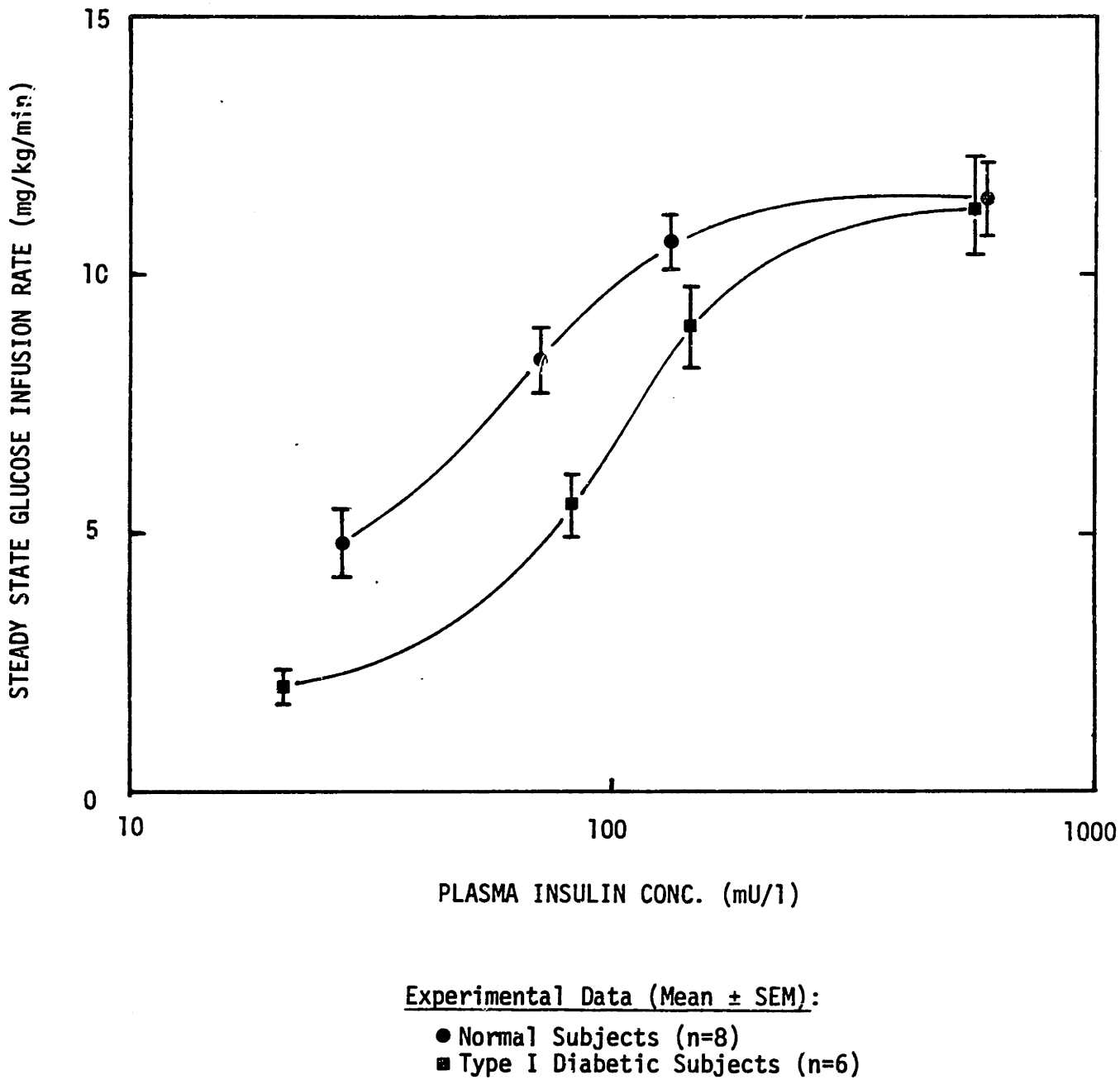

Fig. 90 Dose-response curves for insulin stimulation of glucose metabolism in normal subjects and in Type I diabetics. (Data from Pernet et al., 1984)

there are two underlying modes that could contribute to the observed insulin resistance in tissue glucose uptake in the Type I diabetic. In a recent study at the Joslin Research Laboratory, Meistas et al. (1984) provided the first direct measure of insulin resistance across forearm in IDDM subjects. A group of 6 IDDM subjects receiving conventional insulin therapy (CIT) were studied initially on CIT and again after 5 days of intensive closed-loop insulin therapy on the artificial beta cell (ABC). A group of 5 age- and weight-matched normal controls was also studied. The euglycemic insulin clamp technique was combined with forearm glucose uptake measurements such that both whole-body glucose metabolism rate and forearm glucose uptake rate could be simultaneously determined under comparable conditions of euglycemic hyperinsulinemia in both the IDDM and normal subjects. Results of the study are summarized in Table 35. The rate of insulin-stimulated glucose metabolism (glucose infusion rate) was markedly reduced in the IDDM subjects (~ 48% of normal) and was not significantly improved by 5 days of ABC therapy. Similarly, there was significant resistance to insulin-stimulated glucose uptake by forearm in the IDDM subjects (~ 39% of normal) that was also not significantly improved by the intensive insulin therapy.

Although the above forearm data provides direct confirmation of muscle insulin resistance in the Type I diabetic, it is interesting to extrapolate the forearm values to whole-body muscle uptake to examine whether the muscle insulin resistance entirely accounted for the observed whole-body resistance to insulin stimulation of glucose metabolism. The mean rate of forearm glucose uptake in the IDDM (CIT and ABC) studies was 0.21 mg/100 ml forearm/min, or 0.33 mg/100 ml forearm/min less than that measured in the normal subjects. Extrapolating this decrement in forearm glucose uptake to

Table 35. Steady state data (mean ± SEM) of Meistas et al. (1984) for combined euglycemic insulin clamp and forearm glucose uptake studies in IDDM and normal subjects.

SUBJECTS	PLASMA GLUCOSE CONC. (mg/dl)	PLASMA INSULIN CONC. (mU/l)	GLUCOSE INFUSION RATE (mg/kg/min)	RATE OF FOREARM GLUCOSE UPTAKE (mg/100ml forearm/min)
IDDM (n=6)				
CIT	84 ± 4	78 ± 2	3.26 ± 0.77	0.18 ± 0.07
ABC	90 ± 4	76 ± 4	3.90 ± 1.01	0.24 ± 0.10
Normal (n=5)	69 ± 2	82 ± 3	7.49 ± 1.01	0.54 ± 0.22

a whole-body muscle value (extrapolation of forearm data was detailed in a previous section, Basal Metabolism of Peripheral Tissues) yields a total muscle resistance of 155 mg/min in a 70 kg man, or 2.21 mg/kg (body weight)/min. From the glucose infusion data of Table 35, however, the total observed mean insulin resistance in the IDDM subjects (CIT and ABC) was 3.91 mg/kg/min relative to normal. Thus, decreased muscle glucose uptake could only account for roughly 60% of the observed insulin resistance. Assuming that hepatic glucose production was essentially supressed at the insulin levels of this study, the above evidence would suggest a defect in liver insulin sensitivity which, together with muscle insulin resistance, is not significantly improved by 5 days of intensive ABC insulin therapy.

One explanation for decreased muscle response to insulin stimulation of glucose uptake is the possibility that the muscle glycogen storage capacity in diabetics is relatively saturated most of the time (Aoki, 1984). As discussed in a previous section, the major route of glucose disposal in muscle tissue is conversion to muscle glycogen. Normal subjects exhibit a large capacity to store glucose as muscle glycogen, and the muscle glycogen in turn is depleted for use as an energy source for muscle tissue during exercise. The peripheral hyperinsulinemia associated with peripheral insulin therapies together with high circulating glucose levels in diabetics could result in enhanced muscle glycogen formation causing effective saturation of muscle glycogen storage capacity. In such a case, muscle response to insulin-stimulated glucose uptake would be inhibited leading to an observed resistance to the action of insulin. Unfortunately, muscle glycogen content has not been assessed in any of the insulin resistance studies to appear in the literature to date and thus may constitute an

important uncontrolled variable lending difficulty to the interpretation of these studies.

Increasing evidence suggests that the insulin resistance observed in poorly controlled Type I diabetics is reversible. Mayfield et al. (1983) reported a significant decrease in the insulin dose needed to maintain blood glucose control during the first 5-10 days of placing poorly controlled IDDM subjects on continuous subcutaneous insulin infusion pump therapy. Furthermore, there was a correlation between the initial glycosylated hemoglobin levels (HbA_{1c} levels correlate inversely with glycemic control) in patients and the subsequent decrease in insulin dosage required to maintain glycemic control; the insulin dose decreased 31.3 ± 4.1% in patients with initial $HbA_{1c} > 11\%$, whereas in patients with initial $HbA_{1c} < 11\%$ the insulin dose decreased only 8.6 ± 4.9%. Thus, patients most poorly controlled by conventional therapy demonstrated the greatest apparent reversal of insulin resistance.

Foss et al. (1982) recently reported that glucose processing (oxidation and storage) in Type I diabetic patients was gradually restored by 48-72 h of intensive ABC insulin therapy. In particular, a progressive rise in carbohydrate oxidation rates in response to the ingestion of a mixed meal was induced over the duration of the study. Since CO_2 production across forearm does not significantly increase above basal during an OGTT (Aoki, 1983a), the increase in carbohydrate storage was attributed to restoration of hepatic glucose processing capacity. In a subsequent study, Aoki et al. (1983b) measured forearm glucose uptaking during an OGTT in Type I diabetics on CIT and after 72 h of ABC insulin treatment; the total quantity of glucose taken up by muscle did not significantly change as a result of the ABC insulin therapy and further enforced the notion that the

restoration of glucose processing induced by 72 h of ABC treatment was the result of improvement of a hepatic defect. At first, the above results might appear inconsistent with interpretation of the forearm insulin clamp studies of Meistas et al. reviewed earlier. It must be noted that Foss et al. and Aoki et al. were concerned only with normalization of the quantities of glucose processed by muscle and liver, respectively, following OGTT administration, and not with the insulinemia required to affect these results; after 72 h of ABC therapy, even though the total glucose processing capacity had been restored to normal, the circulating plasma insulin levels required to realize this improvement were still two-to-threefold higher than those observed in normal subjects during the OGTT. In contrast, Meistas et al. (1984) demonstrated that the rate of insulin-stimulated glucose metabolism in both muscle and liver remained significantly impaired in Type I diabetics after 72 h of ABC insulin therapy in comparison to that observed in normals when each group was tested at comparable levels of euglycemic hyperinsulinemia. Thus, insulin resistance was in evidence following 72 h of ABC in all of the above studies, but apparently the intensive closed-loop insulin delivery affected a partial improvement in a hepatic glucose processing postreceptor defect such that the elevated insulinemia evoked by ABC therapy was successful in normalizing the quantity of glucose processed during the OGTT.

Beck-Nielson et al. (1984) recently studied insulin resistance in a group of IDDM subjects changed from conventional injection therapy to continuous subcutaneous insulin infusion (CSII) treatment with a portable pump. During eugylcemic insulin clamping (plasma insulin concentration of about 80 mU/l), insulin stimulation of glucose metabolism was 4.3 ± 2.0 mg/kg/min in a group of 11 IDDM subjects treated conventionally (diet and

injection therapy, duration of diabetes 10.7 ± 5.6 yr; HbA_{1c} of 8.9 ± 1.9%) compared with 11.5 ± 4.0 mg/kg/min in a group of 10 normal controls. The IDDM group was then placed on CSII pump treatment for 6 mo and the measurements repeated; the CSII therapy resulted in improved glycemic control (HbA_{1c} decreased to 7.4 ± 1.2%) and insulin-stimulated glucose metabolism increased about 80% to 7.5 ± 3.5 mg/kg/min during insulin clamping. Thus, 6 mo of CSII insulin treatment affected a significant reversal of the tissue insulin resistance observed in the conventionally treated IDDMs.

The strongest evidence to date for the reversibility of insulin resistance in Type I diabetics was provided by the studies of Revers et al. (1984). As was previously shown in Figure 89, the dose-response curve for insulin stimulation of glucose metabolism for the group of well controlled IDDM subjects was virtually identical to that in the normal controls, whereas significant insulin resistance was evidenced in the group of poorly controlled IDDM subjects. To assess the effect of diabetic control on insulin resistance, Revers et al. studied one Type I diabetic at a time of poor control and then 6 weeks after good control was established with careful glucose monitoring and intensive multiple daily insulin injection therapy. As illustrated in Figure 91, 6 weeks of intensive insulin therapy and good glycemic control resulted in significant reversal of insulin resistance and normalization of maximal insulin-stimulated glucose metabolism in this patient. The duration of the above experiments suggests that a substantial period of good control may be required for normalization of all of the varous modes of insulin resistance in the Type I diabetic.

To summarize, insulin resistance is a prominent feature of both NIDDM and IDDM, and is associated with defects in both hepatic and peripheral glucose processing. Evidence strongly suggests, however, that the insulin

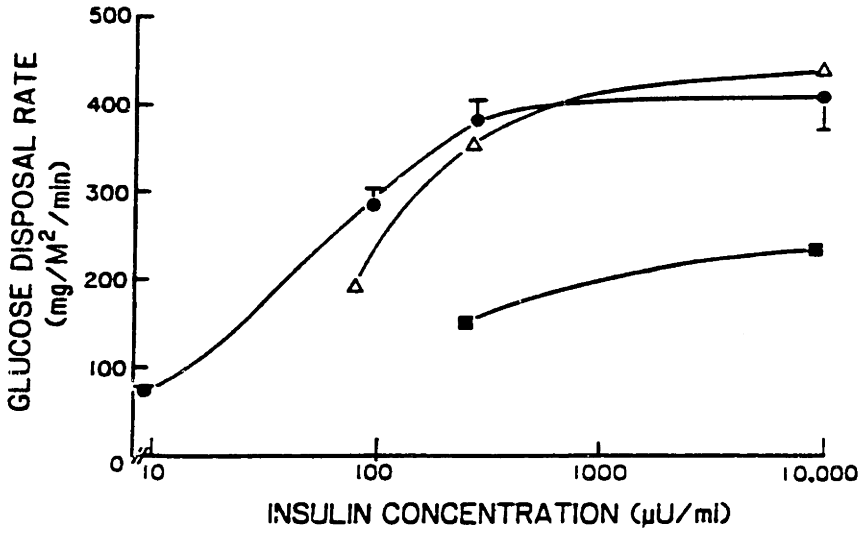

Experimental Data:

- ● Normal Subjects (mean ± SEM, n=21)
- ■ Type I Diabetic subject before insulin therapy
- △ Type I Diabetic subject after 6 weeks of intensive insulin management

Fig. 91 Reversal of insulin resistance in a poorly controlled Type I diabetic subject after 6 weeks of intensive (conventional) insulin management. (From Revers et al., 1984)

resistance observed in insulin-deficient NIDDM and poorly controlled IDDM is reversible with improved glycemic control and insulin management. The time required and the degree of glycemic control and insulin management necessary to affect normalization of insulin resistance are not as yet well understood and will require further study.

b) Insulin Binding to Circulating Anti-Insulin Antibodies

Conventional insulins used for the treatment of diabetes are immunogenic and cause the development of circulating antibodies to insulin as orignally shown in the early studies of Berson et al. (1956). Insulin antibodies bind plasma free insulin, and antibody-bound insulin is biologically inactive (Antoniades and Simon, 1972; De Pirro et al. 1980).

The capacity of antibodies to bind free insulin in diabetic patients can be estimated from in vitro binding studies. Berson and Yalow (1959) analyzed insulin antibody binding in plasma samples drawn from two groups of insulin-treated diabetics, an insulin-resistant group of 5 subjects categorized as such due to their extremely high daily insulin dosage requirements (230 ± 70 U/day), and a nonresistant group of 5 subjects whose insulin requirements were more typical (18 ± 4 U/day). Equilibrium cross-competition binding between labeled and cold insulin was repeated at various free insulin concentrations, and the resulting quantities of bound and free insulin were determined. The experimental equilibrium binding data was analyzed using the classical Scatchard plot; values for the ratio of bound to free insulin concentration (B/F) were plotted against the concentration of bound insulin (B). The characteristic nonlinear shape of the resulting Scatchard plots were ascribed to the presence of two distinct classes of antibody binding sites (see De Meyts and Roth, 1975), a high

affinity site of low capacity, and a low affinity site of high capacity. For each class of sites, a chemical reaction equations may be written,

$$F + E_1 \underset{k_1^-}{\overset{k_1^+}{\rightleftarrows}} B_1 \tag{206}$$

$$F + E_2 \underset{k_2^-}{\overset{k_2^+}{\rightleftarrows}} B_2 \tag{207}$$

where F = concentration of free insulin (U/l)

E_i = concentration of empty binding sites (U/l)

B_i = concentration of antibody-bound insulin (U/l)

k_i^+ = rate constant for insulin antibody association $(l/U \cdot min)^{-1}$

k_i^- = rate constant for insulin antibody dissociation $(min)^{-1}$

From classical chemical kinetics, the opposing first and second order reactions of Equations 206 and 207 may be expressed

$$\frac{dB_1}{dt} = k_1^+ FE_1 - k_1^- B_1 \tag{208}$$

$$\frac{dB_2}{dt} = k_2^+ FE_2 - k_2^- B_2 \tag{209}$$

Under equilibrium conditions, it follows that

$$0 = k_1^+ FE_1 - k_1^- B_1 \tag{210}$$

$$0 = k_2^+ FE_2 - k_2^- B_2 \tag{211}$$

and thus an equilibrium constant may be defined for each class of binding site,

$$K_1 = \frac{k_1^+}{k_1^-} = \frac{B_1}{FE_1} \tag{212}$$

$$K_2 = \frac{k_2^+}{k_2^-} = \frac{B_2}{FE_2} \tag{213}$$

Letting B_i^o denote the total concentration of binding sites of a particular type, for a constant antibody level

$$B_1^o = B_1 + E_1 \tag{214}$$

$$B_2^o = B_2 + E_2 \tag{215}$$

Substituting Equations 214 and 215 into Equations 212 and 213 to eliminate E_1 and E_2 respectively, the ratios of bound to free insulin for each class of sites may be expressed

$$\frac{B_1}{F} = K_1(B_1^o - B_1) \tag{216}$$

$$\frac{B_2}{F} = K_2(B_2^o - B_2) \tag{217}$$

Since the total concentration of antibody-bound insulin B is simply given by

$$B = B_1 + B_2 \tag{218}$$

it thus follows from Equations 216 and 217 that

$$\frac{B}{F} = K_1(B_1^o - B_1) + K_2(B_2^o - B_2) \tag{219}$$

From nonlinear experimental Scatachard plots of B/F versus B, Berson

and Yalow used curve-fitting methods to determine values of the equlibrium constants K_1 and K_2 and the maximum capacities of sites B_1 and B_2 for the plasma samples of each individual studied. In addition, transient state dissociation experiments were performed for the determination of the rate constants k_1 and k_2. Mean parameter values for the insulin resistant and nonresistant groups are summarized in Table 36.

The parameter values listed in Table 36 together with Equations 218 and 219 were used to generate representative Scatchard equilibrium binding plots for the insulin-resistant and nonresistant diabetic groups, respectively, as presented in the upper panels of Figure 92. Although Scatchard plots are particularly useful for analyzing equlibrium binding data, the quantitative implications of insulin antibody binding are more readily interpreted from plots relating bound insulin concentration and free insulin concentration. Solving Equations 216 and 217 for bound insulin, respectively, yields

$$B_1 = \frac{K_1}{(\frac{1}{F} + K_1)} B_1^o \tag{220}$$

$$B_2 = \frac{K_2}{(\frac{1}{F} + K_2)} B_2^o \tag{221}$$

and successive substitution of these expressions into Equation 222 gives

$$B = \frac{K_1}{(\frac{1}{F} + K_1)} B_1^o + \frac{K_2}{(\frac{1}{F} + K_2)} B_2^o \tag{222}$$

Substitution of the parameter values of Table 36 into Equation 222 pro-

Table 36. Insulin antibody binding parameters. Mean ± SEM values were calculated from the individual plasma sample values reported by Berson and Yalow (1959) for a group of 10 insulin-treated diabetics, with binding capacities segregated between the subgroups of nonresistant (n=5) and insulin-resistant (n=5) subjects.

High-Affinity Site:	K_1 = 10.3 ± 4.0 l/U	
	k_1^- = 0.0030 ± 0.0010 min^{-1}	
	k_1^+ = 0.025 ± 0.014 l/U·min (calculated)	
	B_1^o = 0.46 ± 0.21 U/l	nonresistant subgroup
	B_1^o = 14.5 ± 4.2 U/l	resistant subgroup
Low-Affinity Site:	K_2 = 0.307 ± 0.096 l/U	
	k_2^- = 0.11 ± 0.03 min^{-1}	
	k_2^+ = 0.029 ± 0.007 l/U·min (calculated)	
	B_2^o = 7.6 ± 3.2 U/l	nonresistant subgroup
	B_2^o = 83. ± 18 U/l	resistant subgroup
Total Binding Capacity:		
	$B_1^o + B_2^o$ = 8.1 ± 3.4 U/l	nonresistant subgroup
	$B_1^o + B_2^o$ = 98 ± 22 U/l	resistant subgroup

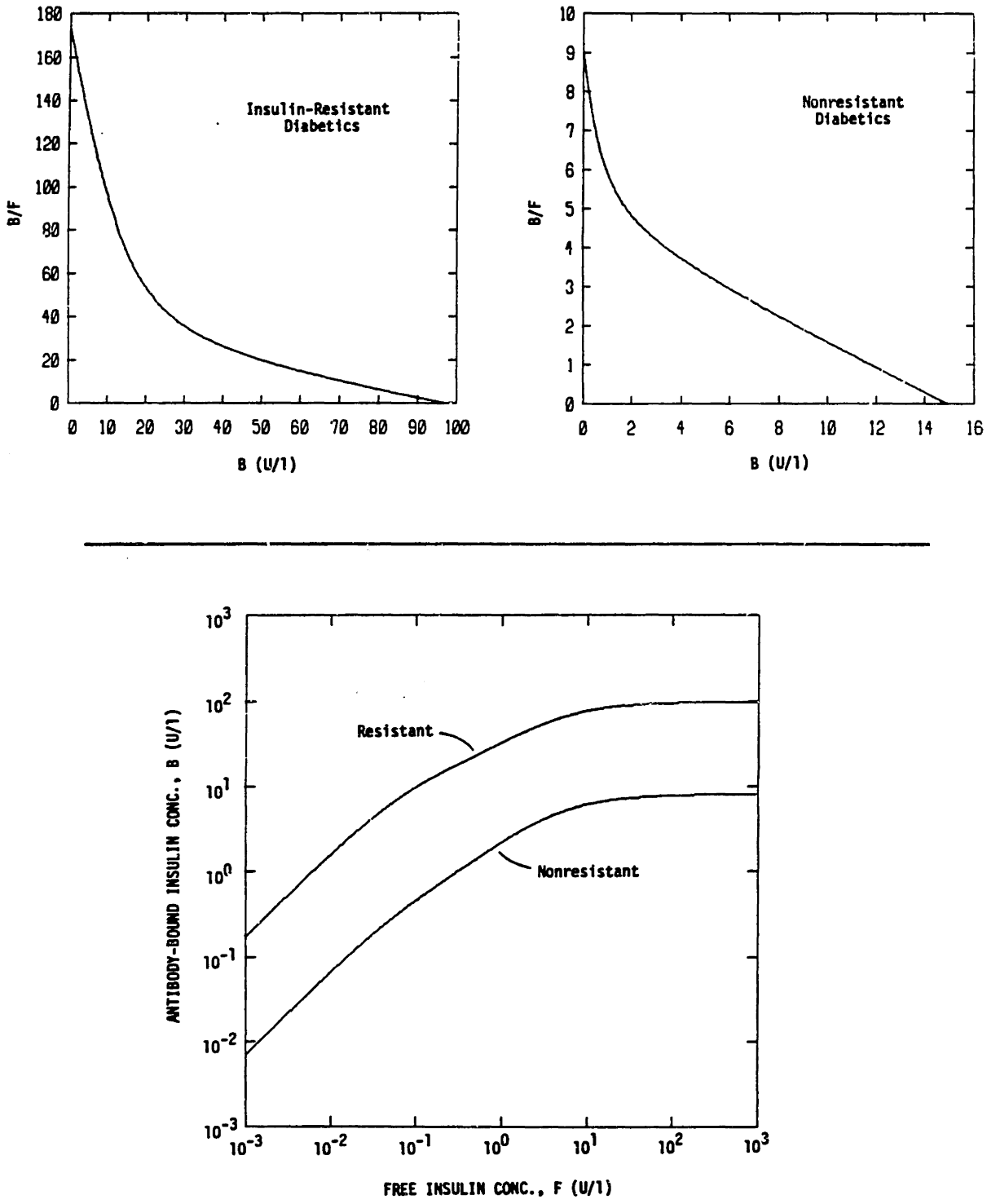

Fig. 92 Scatchard binding curves (upper panel) and plot of antibody-bound versus free insulin concentrations (lower panel) for insulin-resistant and nonresistant diabetics. Plots were generated from the binding parameters of Table 36 obtained from the studies of Berson and Yalow (1959).

vided the means for generating plots of B versus F, and the resulting curves are presented in the lower panel of Figure 92. Additional plots showing the fractions of free and bound insulin as functions of free insulin concentration are included in Figure 93.

As indicated in Table 36 and the lower plot of Figure 92, the maximum capacity to bind insulin, or the total concentration of antibody-binding sites, was 8.1 and 98 U/l in the nonresistant and and resistant groups, respectively. Although the maximum binding capacities were quite large, saturation of binding sites at these high values was realized at supraphysiologic plasma free insulin concentrations (>10,000 mU/l). Of more practical interest is the quantity of bound insulin expected over physiologic ranges of plasma free insulin concentration (~10-100 mU/l). It can be interpolated from the lower plot in Figure 92 that increasing plasma free insulin concentration from 10 to 100 mU/l would elevate the antibody-bound insulin concentration from about 70 to 420 mU/l in the more typical nonresistant diabetic, or result in the equilibrium binding of 350 mU/l of insulin; the same case in the resistant diabetic would elevate the antibody-bound insulin concentration from about 1,500 to 10,000 mU/l, or result in the equilibrium binding of 8,500 mU/l of insulin. Since the plasma volume in a 70 kg subject is about 3.36 l, the total increase in bound insulin would be roughly 1.2 U in the nonresistant and 29 U in the resistant cases, respectively. It is thus apparent that a sizeable quantity of insulin may be antibody-bound over physiologic changes in plasma free insulin concentrations in the insulin-treated diabetic. Furthermore, it is apparent from the lower plot of Figure 93 that the majority of circulating inslin would be antibody-bound at physiologic free insulin levels; over the free insulin concentration range of 10-100 mU/l, the mean fraction

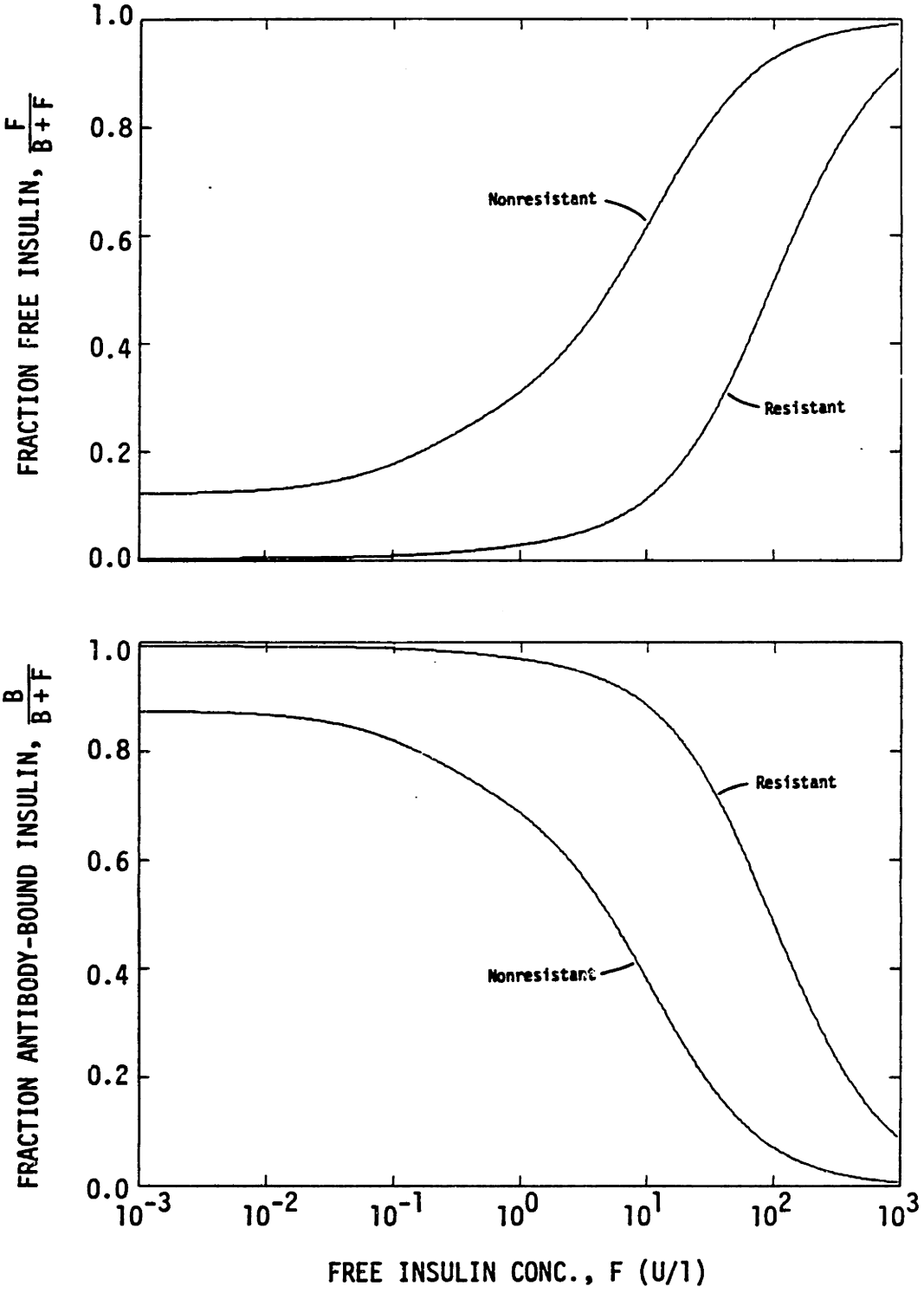

Fig. 93 Fractions of free and bound insulin as functions of free insulin concentration for insulin-resistant and nonresistant diabetics. Plots were generated from the binding parameters of Table 36 obtained from the studies of Berson and Yalow (1959).

of bound insulin would be about 0.85 in the nonresistant diabetic and roughly 0.98 in the insulin-resistant diabetic.

Although the presence of insulin-binding antibodies would not alter the incremental insulin infusion rate required to affect a given change in plasma free insulin concentration from one steady state level to another (Scott et al., 1978), their presence would be expected to change the kinetics of the transition between steady states due to interaction of free insulin through association with or dissociation from the antibody-bound insulin pool. Berson and Yalow (1959) studied the kinetics of the reversible binding of insulin to insulin antibodies. For each type of binding site, dissociation of insulin was first order in concentration of antibody-bound insulin, and association of insulin was first order with respect to both free insulin concentration and concentration of empty antibody-binding sites (see Equations 208 and 209). From the kinetic studies of Berson and Yalow (1959) and the resulting values of the antibody-binding rate constants compiled in Table 36, it can be inferred that the time scales for reversible insulin antibody binding are on the order of minutes with respect to the low-affinity, high-capacity sites and on the order of hours with respect to the high-affinity, low-capacity sites.

Considering the size of the antibody binding pool and the time scales for reversible binding, it is not surprising that sluggish response of free insulin concentrations to therapy has been noted in patients with anti-insulin antibodies (Munkgaard Rasmussen et al., 1975). Such skewing of plasma free insulin response to insulin infusions in diabetics with insulin antibodies has recently been reported by clinical investigators. In studies of glucose counterregulation in IDDM subjects, Bolli et al. (1983) used a continuous 60-min insulin infusion of 28 $mU/m^2/min$ to induce

hypoglycemia in 6 IDDM patients with no detectable insulin antibodies, 5 IDDM subjects with insulin antibodies, and a group of 10 nondiabetic controls. Plasma insulin response of the diabetics without insulin antibodies did not differ significantly from normal response as a result of the insulin infusion. In contrast, the diabetics with antibodies exhibited a significantly delayed response as shown in the upper plot in Figure 94. Whereas the incremental increase in plasma free insulin levels affected by the continuous insulin infusion was comparable in the diabetics independent of the presence of insulin antibodies, both the plasma insulin increase during the infusion and subsequent decrease following termination of the infusion was much slower as a result of the presence of insulin antibodies, suggesting the association of insulin with antibodies as plasma insulin increased and its subsequent dissociation from antibodies as plasma insulin decreased. Similarly, in using euglycemic insulin clamps to generate dose-response curves to characterize insulin resistance in Type I diabetics and normal subjects, Revers et al. (1984) reported that whereas steady state insulin levels were achieved within 25 min in normal subjects, 90 min was required to achieve steady state insulin levels in the diabetic subjects.

The importance of insulin antibody binding in the management of IDDM patients has been highly controversial. As suggested by the above discussion, since binding of insulin to antibodies is reversible and equilibration occurs over time scales of minutes to hours, the capacity to bind insulin manifests sluggish response kinetics. Since insulin disappearance is slowed by the presence of antibodies, and insulin dissociation is not subject to glycemic feedback control, the presence of antibodies could increase the likelihood of hypoglyemic episodes in diabetics (Harwood, 1960; Ichihara et al., 1977; Bolli et al., 1983). Although Dixon et al.

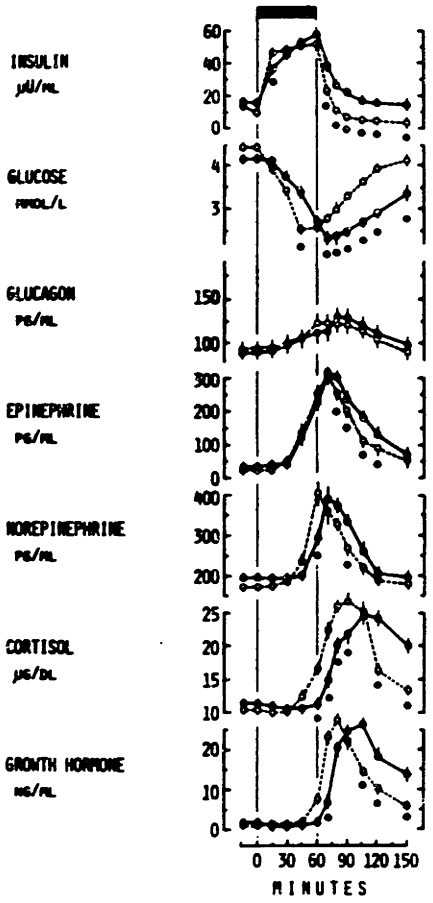

Fig. 94 Plasma insulin, glucose, and counterregulatory hormone responses to a continuous 28 mU/m^2/min insulin infusion in 6 diabetics without insulin antibodies (open circles) and in 5 diabetics with insulin antibodies (solid circles). (From Bolli et al.,1983)

(1975) have proposed that insulin antibodies may exert a favorable effect on metabolic control of diabetics because of the reversible buffering capacity of the antibody-bound insulin pool, other investigators (Shima et al., 1977; Yue et al., 1978; Asplin et al., 1978; Gonen et al., 1979) have reported no apparent relationship between antibody levels and the stability and metabolic control of diabetics. Furthermore, antibody binding would inhibit rapid insulin response to hyperglycemia, and such rapid response may be required for improved insulin therapies to affect tight glycemic regulation (Sorensen et al., 1982). With respect to the effects of insulin antibodies on insulin dosage requirements, early studies (Berson and Yalow, 1959; Berson and Yalow, 1970) indicated a correlation between insulin resistance and high antibody titers in diabetics. It is likely that the insulin resistance in these patients was not due to the presence of circulating insulin antibodies, but rather that the high daily insulin requirements of these (tissue) insulin-resistant diabetics caused their development. Since insulin antibody binding is reversible, the presence of antibodies should not alter the dosage requirements of diabetics, and more recent studies (Asplin et al., 1978; Kumar, 1979; Kurtz and Nabarro, 1980) have cast doubt on any quantitative relationship between insulin requirements and circulating insulin antibodies in Type I diabetic patients.

The immunogenicity of conventional insulins has been attributed to the presence of impurities and the species of origin. Fineberg et al. (1983) have recently studied the immunogenicity of purified pork insulins with and without trace contamination of beef insulin relative to mixed pork-beef insulins of lower purity. A group of 137 patients who had not previously been treated with insulin were divided into groups according to the type of insulin being administered, and serial assessment of antibody development

was monitored over the first year of treatment. Results of the study are shown in Figure 95. As indicated, significantly less antibody development was observed in the patients receiving the purified pork insulins relative to those receiving the less pure mixture of beef-pork insulin. In addition, even trace amounts of bovine insulin, which is more immunogenic than porcine insulin, enhanced antibody development in comparison with uncontaminated porcine insulin. With the increasing availability of highly purified insulins, several studies (Andreani, 1973; Bruni et al., 1973; Schlichtkrull et al., 1974) have demonstrated a decrease of antibody titers in patients who changed from conventional to purified insulins, and it has been suggested (Mustaffa et al., 1977) that all diabetics receiving insulin for the first time, whenever possible, should be treated with a highly purified insulin.

In summary, the immunogenicity of conventional insulins causes the development of circulating antibodies that bind insulin. Antibody levels vary greatly from patient to patient as evidenced by wide ranges in plasma binding capacities. Since insulin antibody binding is reversible, the presence of circulating antibodies causes sluggish insulin response kinetics but does not alter dosage requirements. Evidence suggests that the new purified insulins are significantly less immunogenic than conventional insulins of the past. Recent progress in purification methods together with the imminent availability of human insulin through recombinant DNA technologies offers the promise of insulins that will be essentially nonimmunogenic.

3) Impaired Counterregulation of Hypoglycemia

Patients with IDDM commonly exhibit blunted or absent glucagon respon-

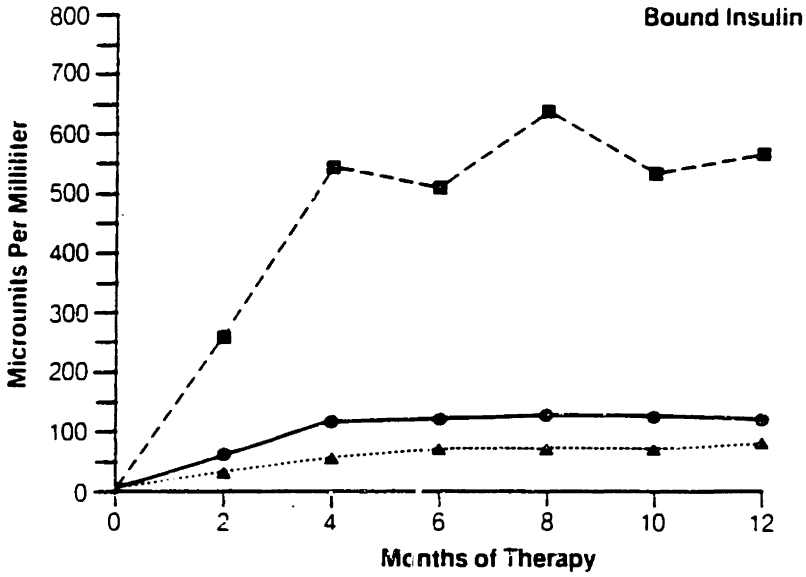

Fig. 95 Development of insulin antibodies over the first year of treatment with purified pork insulin (triangles), purified pork insulin with traces of beef insulin (circles), and less purified mixture of beef-pork insulin (squares) in respective groups of previously untreated diabetic subjects. (From Fineberg et al., 1983)

ses to hypoglycemia (Gerich et al., 1973; Benson et al., 1977; Maher et al., 1977; Kleinbaum and Shamoon, 1983), the severity of which largely segregates with the presence of autonomic nueropathy (Hilstead et al., 1981). Although glucagon provides the primary stimulus for normal glucose recovery from hypoglycemia, epinephrine compensates largely for deficient glucagon response in IDDM subjects (Cryer and Gerich, 1983).

As previously discussed, release of antibody-bound insulin can prolong the duration of recovery from hyperinsulinemia and promote hypoglycemia in diabetics. This situation is further complicated by abnormal glucagon counterregulatory response. Bolli et al. (1983) recently studied the abnormal glucose counterregulation in IDDM. Three groups of diabetic patients were studied: Group A - 5 diabetic patients, duration of diabetes less than one month; Group B - 11 diabetic patients, duration of diabetes 1-5 years; Group C - 5 diabetic patients, duration of diabetes 14-31 years and presence of autonomic neuropathy. A group of 10 age- and weight-matched nondiabetics was also studied for comparison. Resulting plasma free insulin, glucose, and counterregulatory hormone responses to insulin-induced hypoglycemia (28 $mU/m^2 \cdot min$ infusion for 60 min) are presented in Figure 96. In patients with recent-onset diabetes (Group A), insulin, glucose, and glucagon response did not differ from the nondiabetics. In patients with diabetes of longer duration, insulin response was more sluggish due to the presence of insulin antibodies, glucagon response was significantly diminished, and glycemic recovery from hypoglycemia was prolonged, and these effects became more pronounced with duration of diabetes (compare Groups B and C). When glucagon was subsequently infused during hypoglycemia in diabetics with impaired glucagon responses in order to simulate normal glucagon responses, glucose recovery was normalized in

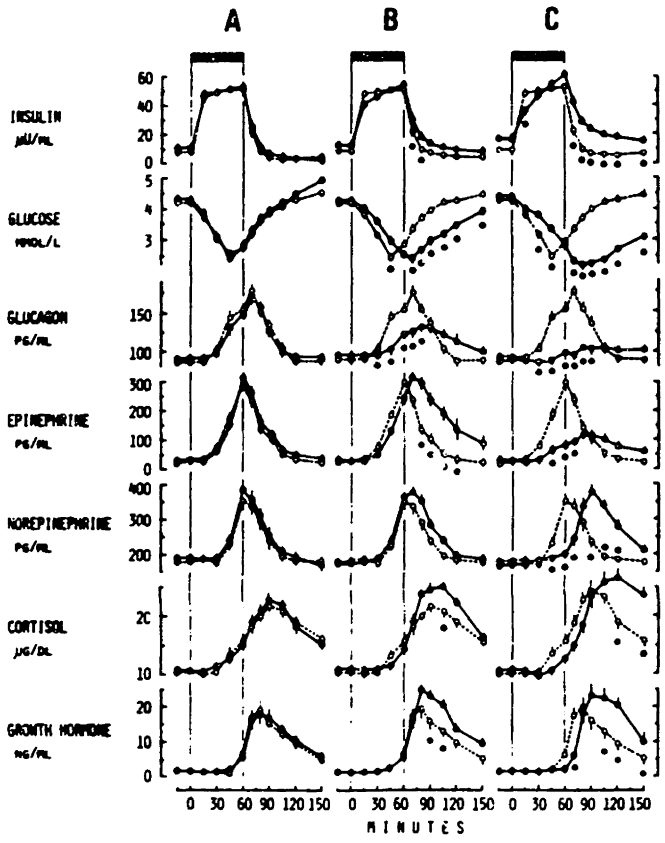

Fig. 96 Plasma insulin, glucose, and counterregulatory hormone responses to insulin-induced hypoglycemia (28 $mU/m^2/min$ infusion for 60 min) in three groups of diabetic patients (solid circles) versus nondiabetic controls (open circles). (From Bolli et al., 1983)

patients without significant antibody levels; thus, the impaired α-cell secretion was the predominant mechanism for the delayed glucose recovery in these patients.

Since impaired glucagon response is associated with duration of diabetes, and in particular with the chronic complication of autonomic neuropathy, the question arises whether good glycemic control and intensive insulin management could normalized α-cell function. Kawamori et al. (1980) have reported that pancreatic glucagon response to intravenous arginine is perfectly normalized in insulin-deficient NIDDM and IDDM subjects during intensive ABC insulin delivery. Bolli et al. (1984a) observed that counterregulatory response remained normal in 5 IDDM patients over the first year of insulin injection therapy with intensive management and good glycemic control (H_bA_1 of 7.9 ± 0.2%); in contrast, however, 9 months of improved glycemic control (intensive injection therapy) instituted in 7 IDDM patients of long duration (9 ± 0.5 yr) and initially poor glycemic control (glycosylated hemoblobin of 12.4 ± 0.2%) failed to improve glucose counterregulation in the presence of improved glycemic control (glycosolated hemoglobin of 7.9 ± 0.02%). Since NIDDM subjects (Boden et al., 1983), and newly-diagnosed IDDM subjects have normal glucagon response, and this normalization appears maintainable with good insulin management, new diabetics may experience reduced risk of hypoglycemic complications in the future. Because α-cell response to arginine can be normalized in the presence of adequate insulin in IDDM subjects, it would appear that inadequate counterregulatory response results from a reduced sensitivity specific to glucose in IDDM of long duration. Initial evidence concerning reversal of this α-cell defect in diabetics of long duration is not promising, particularly if autonomic neuropathy is evident, but further

study will be required. Nonetheless, standardized tests for adequate glucose counterregulation in Type I diabetics have been recently developed (Bolli et al., 1984b) and can be used to predict accurately and safely those patients who are at risk of developing severe hypoglycemia during intensive insulin therapy.

C) Formulation of the β-Cell Deficient, Metabolically-Normalized Type I Diabetic Model, and the Rationale for Its Use to Design and Assess Improved Insulin Therapies

Using the model of glucose metabolism in normal, nondiabetic man as a starting point, the first consideration in diabetic modeling concerning fixing the concentration scales used to calculate normal metabolic source and sink rates. In the nondiabetic model, metabolic rates were formulated in terms of local organ glucose and insulin concentrations that were normalized with respect to basal values. Upon model initialization, all metabolic rates were assumed to occur at their respective fixed basal rates by definition, while the corresponding basal organ glucose and insulin concentrations were allowed to float over a narrow range such that model initialization conditions could be matched to specified basal experimental conditions. Those initial basal state glucose and insulin concentrations requried for calculation of metabolic rates were stored for subsequent reference (see Table 31), as they in turn defined the basis for the normalized concentration scales used in the metabolic rate formulations.

Before starting to model the insulin-treated diabetic, it was desirable to fix the basal glucose and insulin concentrations used to calculate normal metabolic response. This was simply accomplished by adopting a reference set of organ concentrations deemed representative of the basal postabsorptive state in normals. These values were obtained by

running the normal model initialization routine with the following specified basal state initial conditions derived from measurements accumulated at the Joslin Research Laboratory for 267 normal adult males: 1) mean peripheral venous blood glucose concentration equaled 75.3 mg/dl (corresponding to G_{pv} = 89.6 mg/dl); 2) mean peripheral venous plasma insulin concentration equaled 12.9 mU/l (I_{pv} = 12.9 mU/l). The resulting set of reference basal organ glucose and insulin concentrations is listed in Table 37. These reference values were used as the basis for fixing the concentration scales defining normal metabolic response to local organ solute concentrations in all subsequent diabetic modeling.

Probably the most obvious aspect of diabetic modeling concerns alteration of normal pancreatic insulin response to glycemia. Since the purpose of diabetic modeling was to provide a basis for insulin therapy assessment, modeling efforts were focused on a physiologic representation of IDDM. The irreversible loss of β-cell function typical of Type I diabetes was simply evoked by removing the model pancreas from the normal model of glucose metabolism, or more specifically, the rate of pancreatic insulin release (r_{PIR}) as a metabolic source for insulin in the liver insulin mass balance formulation (Equation 20) was set equal to zero.

Although present modeling will be restricted to IDDM, NIDDM subjects experience the same chronic diabetic complications as IDDM subjects, and evidence suggests that insulin administration may be beneficial in improving the regulation of glycemia in NIDDM. Development of a physiologic model for assessing insulin therapies in the Type II diabetic would be very difficult due to the diverse range of abnormal pancreatic insulin responses which characterize NIDDM. A possible approach to modeling pancreatic insulin release in the Type II diabetic would be to use para-

Table 37. Reference normal basal state glucose and insuin concentrations used to fix the concentration scales defining normal metabolic source and sink rates.

REFERENCE NORMAL BASAL CONCENTRATIONS	USED FOR CALCULATION OF
G_L^B = 101 mg/dl	Hepatic Glucose Uptake, r_{HGU} Hepatic Glucose Production, r_{HGP}
G_{PI}^B = 86.8 mg/dl	Peripheral Glucose Uptake, r_{PGU}
G_H^B = 91.9 mg/dl	Pancreatic Glucagon Release, r_{PIR}
I_L^B = 21.4 mU/l	Hepatic Glucose Uptake, r_{HGU} Hepatic Glucose Production, r_{HGP}
I_{PI}^B = 5.30 mU/l	Peripheral Glucose Uptake, r_{PGU}
I_H^B = 15.2 mU/l	Pancreatic Glucagon Release, r_{PIR}

meter adjustment of the normal pancreas model so as to match the abnormal diabetic insulin response to a standard glucose input such as an IVGTT.

To this point, adaptation of the normal model to a representation of Type I diabetes included two major steps: 1) removing the model pancreas to represent C-peptide negative endogenous reponse to glycemic; and 2) fixing absolute concentration scales on the metabolic source and sink functions such that diabetic response to any particular combination of local glucose, insulin, and glucagon concentrations would be the same as normal response under similar conditions. The resulting diabetic model could thus be specifically termed a β-cell deficient, metabolically-normalized Type I diabetic model. This is a specialized representation, however, because as discussed previously, Type I diabetic patients commonly exhibit metabolic abnormalities secondary to β-cell dysfunction. An important issue must therefore be addressed: is a metabolically-normal model of Type I diabetes a valid basis upon which to design and assess improved insulin therapies?

It was apparent from a review of the literature that the abnormalities associated with IDDM metabolism could be quantitatively significant, but that these aberrant factors were not well characterized and could vary over an extremely wide range from individual to individual. Tissue response to insulin in IDDM subjects ranged from normal to observed responses characteristic of significant receptor and/or post-receptor defects, and evidence suggested the contribution of both muscle and liver defects to the overall observed insulin resistance. The presence of circulating insulin antibodies was reported to cause sluggish plasma insulin response kinetics in insulin-treated diabetics, and antibody-bound insulin could represent up to 98% of the circulating insulin. Blunted glucagon response to hypoglycemia was evidenced in IDDM subjects, and this abnormality was associated with

duration of diabetes and in particular with the presence of chronic autonomic neuropathy. From a modeling standpoint, one could thus envision a whole spectrum of Type I diabetic models encompassing varying degrees and combinations of metabolic abnormalities, ranging from an ideal metabolically-normal representation to that of an insulin-resistant, antibody-laden, glucagon-deficient Type I diabetic.

The present objective of diabetic modeling is to provide a basis for designing and assessing improved insulin therapies, and in particular for developing an insulin infusion algorithm for closed-loop insulin delivery based on blood glucose measurement. The widespread availability and competitive pricing of the new highly nonimmunogenic biosynthetic human insulins is imminent. These biosynthetic human insulins should prove even less immunogenic than the highly purified pork insulins available presently. No significant development of antibody levels would thus be anticipated in newly-diagnosed diabetics initially placed on these new nonimmunogenic insulins. With respect to the population of diabetics previously treated with conventional insulins, the insulin antibodies produced in response to the conventional insulins bind bovine, porcine, and human insulins without distinction (Goldman et al., 1979). But evidence to date has demonstrated that antibody titers decrease in diabetics changed from conventional to purified insulins, and thus abnormalities associated with the presence of insulin antibodies should be alleviated in those patients presently exhibiting high antibody titers on conventional insulins. Thus, abnormalities presently associated with the presence of insulin antibodies will soon be reduced to background phenomena of no quantitative significance in the insulin-treated diabetic and thus will not constitute an issue of importance in the development and application of new insulin delivery systems

(Soeldner, 1984). Therefore, for the purposes of algorithm design, the need for inclusion of antibody binding in a Type I diabetic model is not indicated.

The issue of tissue insulin resistance is more complicated. In the literature to date, the prominance of tissue insulin resistance has been loosely associated with lack of effective glycemic regulation in diabetic patients (as indicated by glycosylated hemoglobin levels), and normal insulin sensitivity represents an end state affiliated with "good" glycemic control. Since essential normalization of insulin sensitivity has been induced by 6 weeks of intensive CIT, i.e. home glucose monitoring 2-4 times daily and frequent adjustment of insulin dosage (see Figure 91), it seems reasonable to assume that end state normalization of tissue insulin sensitivity will be realized by the more precise glycemic regulation offered by closed-loop insulin management.

Unfortunately, insufficient experimental data exists to identify the precise mechanisms underlying tissue insulin resistance, or the factors which cause its apparent reversal during improved glycemic regulation. Most likely, chronic insulin deficiency would be associated with post-receptor defects related to the maintenance of proper intracellular enzyme levels, whereas chronic hyperinsulinemia would be associated with receptor down regulation. Since neglect of insulin resistance during design of an insulin infusion algorithm would result in a device that administers the minimal insulin dosage concommitant with glycemic normalization, such an algorithm would provide the best promise for the reversal and/or avoidance of insulin resistance in the Type I diabetic. Indeed, one could surmise than an algoirth designed to compensate for insulin resistance in seeking glycemic normalization would likely induce excessive hyperinsulinemia which

in turn would be detrimental to the reversal of insulin resistance.

Although pulsatile basal insulin delivery will not be encompassed in the present modeling studies, whether this will prove important in the maintenance of normal tissue insulin sensitivity in diabetics remains to be determined, however such action was clearly not mimiced during normalization of tissue insulin resistance induced through intensive CIT. Since basal pulsatile insulin delivery has a greater hypoglycemic effect than continuous insulin delivery (Mathews et al., 1983), pulsed basal insulin delivery could further reduce basal insulinemia, and thus might possibly affect a more rapid and complete normalization of tissue insulin resistance, particularly with respect to effects of receptor down regulation.

Finally, impaired glucagon response to hypoglycemia will not be incorporated into the Type I diabetic model during algorithm development for a number of reasons. First of all, the severity of impaired counterregulation normally observed in insulin-treated diabetics is largely attributable to prolonged hyperinsulinemia associated with release of antibody-bound insulin which serves to defeat glucagon effectiveness. As previously discussed, such problems related to insulin antibodies are anticipated to be of negligible importance in the near future. Furthermore, although the reversibility of impaired glucagon response by intensive CIT has not been demonstrated, it is possible that precise closed-loop insulin delivery may be able to affect such a normalization, particularly since normal glucagon response can be maintained in newly-diagnosed diabetics through careful CIT management, and thus impairment of glucagon response appears to be secondary to β-cell deficiency. Finally, since neglecting tissue insulin resistance will result in minimal closed-loop insluin dose

delivery, this will help lessen the likelihood of severe hypoglycemia and the need for acute counterregulatory capacity.

Because of the above reasons, a β-cell deficient, metabolically-normalized Type I diabetic model will be employed for the design and testing of an insulin infusion algorithm for closed-loop glycemic regulation. The strategy for diabetic modeling will thus be to neglect the abnormalities associated with diabetic physiology secondary to beta-cell dysfunction for the purposes of designing an insulin infusion algorithm. Once the closed-loop insulin delivery system has been designed, however, its effectiveness in regulating glycemia in the presence of such diabetic abnormalities will be studied. This will entail introducing representative metabolic abnormalities, including tissue insulin resistance, antibody binding, and impaired glucagon response to hypoglycemia into the Type I diabetic model and simulating the OGTT under closed-loop control. Results of these simulation studies will provide a basis for assessing performance of the resulting algorithm in the presence of diabetic metabolic abnormalities and may indicate possible compensatory algorithm modifications. In the next section, modeling and simulation of diabetic abnormalities will be explored using available data for diabetics administered the OGTT during ABC insulin delivery.

D) Simulation Studies with the Type I Diabetic Model

1) Model Initialization and the Postabsorptive Steady State in Diabetics

In a metabolic sense, the postabosorptive steady state in the insulin-treated diabetic is not internally defined, as it is manipualted by an external variable, namely the provision of exogeneous insulin. This is the primary reason that a reference set of normal basal state glucose and insu-

lin concentrations (Table 37) had to be adopted for computing metabolic rates during diabetic model simulations, as these values could not be defined upon model initializaiton as was the case for normal model simulations (see Table 31).

Initialization for Type I diabetic model simulations is outlined in Table 38. For diabetic modeling, the reference set of normal basal state concentrations (Table 37) was loaded and the pancreatic insulin release rate (r_{PIR}) was set to zero. The insulin model mass balance equations used in diabetic model simulations were the same as those used in normal nondiabetic simulations (Equations 17-23) except Equation 18a was substituted for Equation 18 to provide for intravenous insulin delivery (r_{IVI}). Equating the time derivatives to zero (steady state) in the modified set of insulin model mass balance equations yielded a set of 7 equations in 8 unknowns (7 insulin concentrations and r_{IVI}); thus, specification of the initial steady insuin delivery rate r_{IVI} allowed calculation of all initial insulin concentrations in the insulin model. Next, the glucose model mass balance equations (Equations 9-16) were employed to calculate the initial glucose concentrations. Equating the glucose model mass balance time derivatives to zero (steady state) resulted in a set of 8 equations in 8 unknowns (the respective glucose concentrations). In nondiabetic modeling, under basal conditions the rates of basal glucose metabolism were fixed with the sum of the metabolic sinks equaling the rate of hepatic glucose production; because the sources and sinks were fixed and cancelled from the set of equations, the glucose concentrations could not be uniquely determined, and thus a glucose concentration had to be specified for initialization (mathematically, because the fixed sources equaled the sinks, the resulting set of equations was not linearly independent but formed a rank 1

Table 38. Summary of initialization procedure for Type I diabetic model simulations

Reference set of normal basal state concentrations (Table 37) are loaded for subsequent computations of metabolic source and sink rates:

G_L^B = 101.0 mg/dl $\qquad$ I_L^B = 21.43 mU/l

G_{PI}^B = 86.81 mg/dl $\qquad$ I_{PI}^B = 5.304 mU/l

G_H^B = 91.89 mg/dl $\qquad$ I_H^B = 15.15 mU/l

Pancreatic insulin release rate is set to zero:

r_{PIR} = 0 mU/min (model pancreas removed)

Insulin Model

Mass Balances:

r_{IVI} = [input rate of peripheral venous insulin delivery] (See Eqn. 18a)

$$I_H = \frac{r_{IVI}}{Q_H^I - Q_L^I(1-F_{LIC}) - Q_K^I(1-F_{KIC}) - Q_P^I(1-F_{PIC}) - Q_B^I}$$

$$I_{PV} = I_H(1-F_{PIC})$$

$$I_K = I_H(1-F_{KIC})$$

$$I_L = I_H(1-F_{LIC})$$

$$I_B = I_H$$

$$I_G = I_H$$

$$I_{PI} = I - \frac{Q_P^I T_P^I}{V_{PI}}(I_H - I_{PV})$$

Table 38. (Continued)

Glucose Model

Mass Balance:

G_H = [Guess Arterial Glucose Conc.]

Initialize Glucagon Model:

Compute M^I_{PIR}, M^G_{PIR}

$$I^N = M^I_{PIR} M^G_{PIR}$$

$$G_{BV} = G_H - \frac{r_{BGU}}{Q^G_B}$$

$$G_G = G_H - \frac{r_{GGU}}{Q^G_G}$$

Compute M^I_{PGU}

$$G_{PV} = \frac{G_H}{\left(1 + \frac{V_{PI} M^I_{PGU} r^B_{PGU}}{Q^G_P V_{PI} G^B_{PI} + T^G_P Q^G_P M^I_{PGU} r^B_{PGU}}\right)}$$

G_K = [Guess Kidney Glucose Conc.]

Compute r_{KGE}

$$G_K = G_H - \frac{r_{KGE}}{Q^G_K}$$ [Check Kidney Glucose Conc.]

Table 38. (Continued)

G_L = [Guess Liver Glucose Conc.]

Compute r_{HGP}, r_{HGU}

$$G_L = \frac{1}{Q_L^G}\left(Q_A^G G_H + Q_G^G G_G + r_{HGP} - r_{HGU}\right)$$ [Check Liver Glucose Conc.]

$$G_H = \frac{1}{Q_H^G}\left(Q_B^G G_{BV} + Q_L^G G_L + Q_K^G G_K + Q_P^G G_{PV} - r_{RBCU}\right)$$ [Check Arterial Glucose Conc.]

$$G_{PI} = \frac{G_{PV}}{\left(1 + \frac{M_{PGU}^I \, r_{PGU}^B \, T_P^G}{V_{PI} G_{PI}^B}\right)}$$

$$G_{BI} = G_{BV} - \frac{T_B \, r_{BGU}}{V_{BI}}$$

Metabolism: (Initialize using values computed on last glucose model mass balance iteration)

M_{HGP}^I

M_{HGU}^I

$$f_2 = \frac{M_{HGP}^{Io} - 1}{2}$$

Glucagon Model

$r^N = M_{PIR}^I M_{PIR}^G$ (Computed during glucose model mass balance iteration)

matrix meaning there was a subset of 7 linearly independent equations). For diabetic modeling, since the concentration scales on the metabolic source and sink functions were specified a priori, the steady state metabolic rates now became functions of the initial glucose model concentrations. Thus, having computed all of the respective insulin concentrations, only one unique set of glucose concentrations would satisfy the steady state glucose model mass balance equations. The series of calculations required in solving for the initial glucose model concentrations is outlined in Table 38. As indicated, the process involved iterative solution due to the fact that some of the metabolic rates were nonlinear functions of local glucose concentration. Since the rate of pancreatic glucagon release was a function of arterial glucose concentration, and plasma glucagon concentration in turn affected hepatic glucose production rate, the glucagon model was initialized from steady state consideration of its normalized mass balance equation (193) during iteration of the glucose model concentrations.

In the absence of exogeneous glucose input (oral or intravenous loading), the steady state glucose and insulin levels are dependent on the rate of insulin delivery to the Type I diabetic. Presented in Figure 97 are the steady state peripheral venous plasma glucose and insulin concentrations resulting from various rates of continuous intravenous insulin infusion as predicted from the Type I diabetic model initialization procedures outlined above. It can be seen from Figure 97 that normalization of plasma glucose to a value of 90 mg/dl would require an insulin infusion rate of 20 mU/min with a resulting peripheral plasma insulin concentration of about 23 mU/l. These numbers are representative of those observed to maintain such fasting normoglycemia in patients on ABC therapy. It should

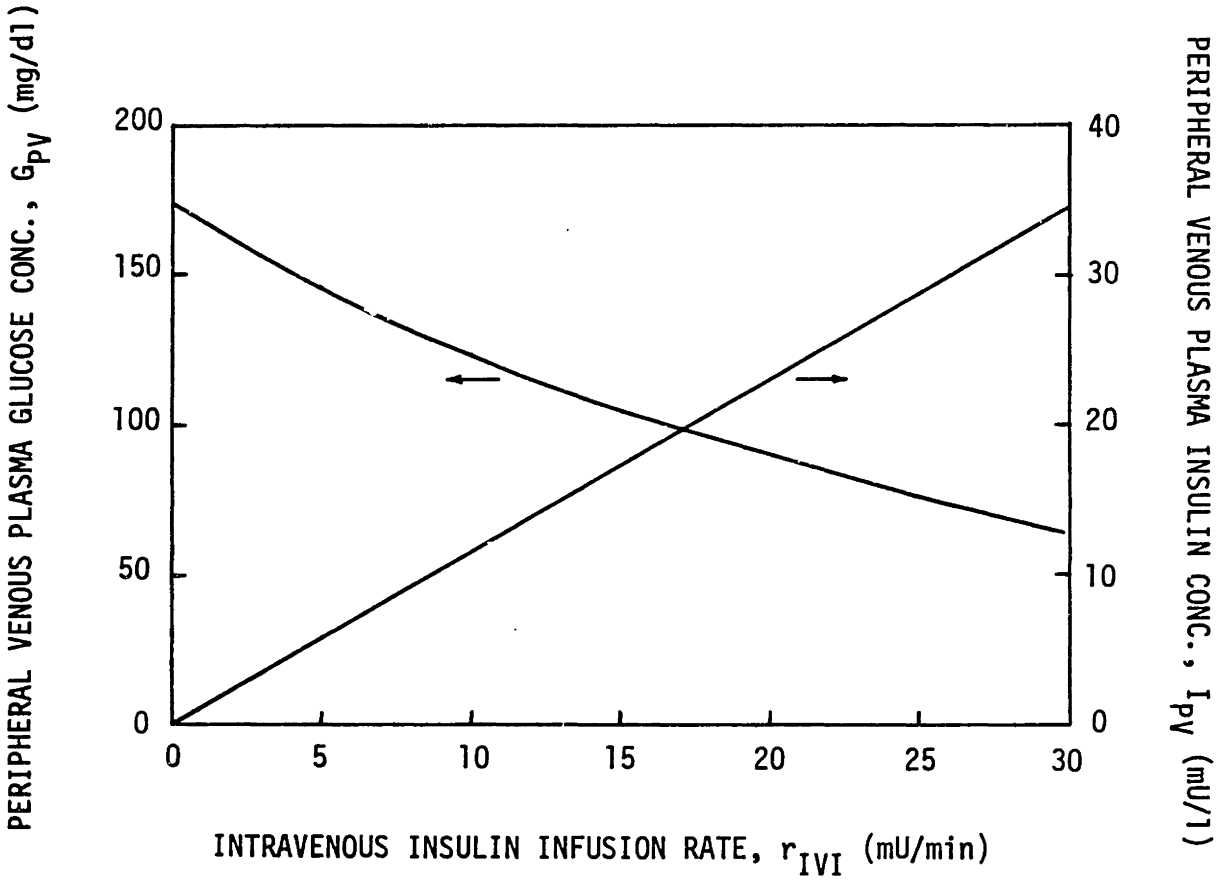

Fig. 97 Steady state plasma glucose and insulin concentrations resulting from various rates of continuous (peripheral) intravenous insulin infusion as predicted from initialization of the Type I diabetic model.

be noted that the steady state peripheral insulin level required to maintain fasting normoglycemia in the diabetic is roughly double that observed under basal state conditions in the nondiabetic. This is the consequence of peripheral routing of insulin delivery to the diabetic, as nonportal insulin input alters the relative steady state organ insulin levels compared with normal. In the normal subject, pancreatic insulin secretion into the portal vein results in a positive portal:peripheral insulin gradient. In contrast, peripheral insulin therapy causes a reversal in the normal portal:peripheral insulin gradient, and the fasting peripheral hyperinsulinemia required to maintain basal glycemia in the diabetic reflects the general level of insulinemia necessary to elevate sufficiently hepatic insulin such that excessive hepatic glucose production is avoided.

An interesting aspect of conventional insulin therapy arises from the above discussion. Since CIT provides for a relatively constant level of insulinemia over the course of a day, CIT results in peripheral hyperinsulinemia during fasting, and peripheral hypoinsulinemia during postprandial periods. Although peripheral closed-loop insulin delivery can provide for normalization of insulinemia during postprandial glucose excursions, such devices will still not circumvent baseline peripheral hyperinsulinemia. Whether such chronic elevation of tissue insulin levels will prove adverse to complete reversal of insulin resistance or possibly promote development of diabetic pathologies remains to be determined. A possible solution to the problem of basal peripheral hyperinsulinemia is intraportal insulin delivery to diabetics, but intraportal access would involve considerable additional risk to the patient. Another potential solution is the possibility that pulsatile baseline insulin deliveyr could lower the mean level of insulinemia required to maintain fasting nor-

moglycemia in the insulin-treated diabetic (Mathews et al., 1983) and thus could be incorporated into a closed-loop insulin delivery system.

2) Simulation Studies

Although the Type I diabetic model incorporating normal metabolism will be employed for the design and assessment of closed-loop insulin delivery systems, a number of preliminary Type I diabetic simulation studies were conducted and will be reviewed in this section. These diabetic model simulations were undertaken to demonstrate the model's capacity for predicting observed diabetic response and to illustrate methods of modifying the metabolically-normalized Type I diabetic model for simulating various diabetic metabolic abnormalities.

a) The OGTT on Conventional Therapy or Continuous Basal Insulin Delivery

The first simulation study using the Type I diabetic model (normal metabolism) was designed to explore the effectivness of constant basal insulin levels in regulating postprandial glycemia. For this study, a standard 100g OGTT was simulated by employing the rate of gut oral glucose absorption function previously derived from consideration of nondiabetic response profiles (see Figure 81) as an input to the gut compartment mass balance equation in the glucose model (Equation 12a). During the OGTT simulation, the rate of peripheral insulin delivery (r_{IVI} in Equation 18a) was fixed at a constant value; this would represent either a continuous rate of intravenous insulin absorption from a local injection site during CIT or the basal continuous insulin delivery rate provided by a simple open-loop insulin pump system.

Results of the simulation study are presented in Figure 98. So that the results could be directly compared with the nondiabetic response profi-

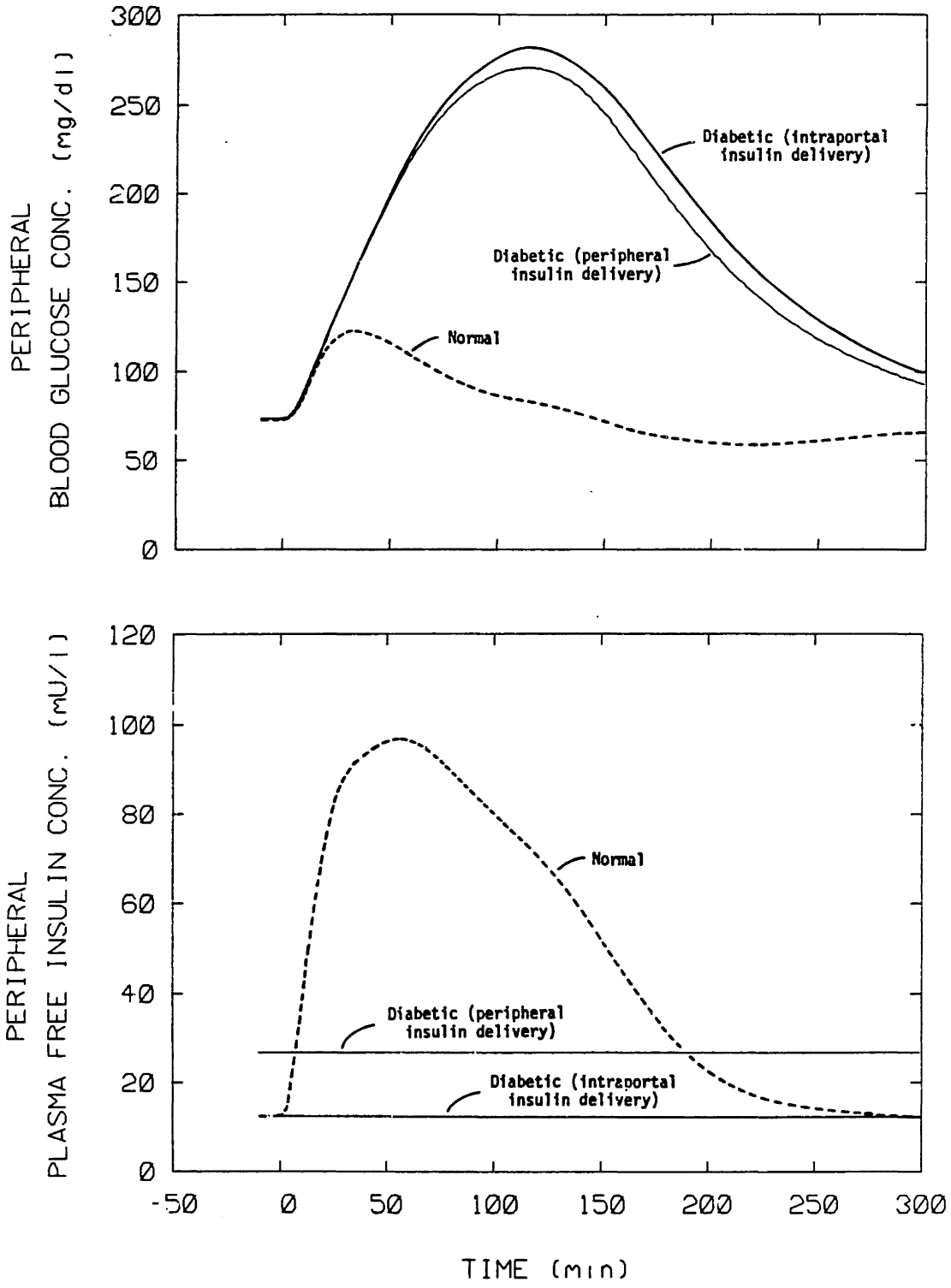

Fig. 98 Model predictions of Type I diabetic response to the standard 100g OGTT as a result of continuous peripheral (23 mU/min) or intraportal (19 mU/min) basal insulin delivery. Included for comparison are the normal peripheral venous glucose and insulin profiles from Figure 81.

les of Figure 81, the peripheral insulin delivery rate was selected from model initialization considerations such that the fasting diabetic glycemia matched that of the normal group used as the basis for the previous non-diabetic OGTT simulation studies (peripheral blood glucose concentration of 75 mg/dl); the resulting fixed insulin delivery rate was 23 mU/min and resulted in a peripheral plasma (free) insulin level of 27 mU/l in the diabetic.

As shown in Figure 98, the peripheral route of insulin delivery resulted in the normalization of fasting glycemia at the expense of basal peripheral hyperinsulinemia in the diabetic relative to that observed in normals. During the oral glucose challenge, however, circulating insulin levels generated from pancreatic insulin response in normal subjects greatly exceeded the insulinemia resulting from baseline insulin delivery to the diabetic. The lack of insulin response to glycemia lead to impaired glucose disposal and hyperglycemia in the diabetic as illustrated in the upper plot of Figure 98.

Since continuous peripheral basal insulin delivery would not unmask diabetic abnormalities associated with tissue insulin resistance or insulin antibody binding, the simulated ineffectiveness of this mode of therapy in providing for good postprandial glycemic regulation should be representative, and the duration and magnitude of the glycemic excursion shown in Figure 98 are comparable with glycemic behavior observed in Type I diabetics during OGTTs on CIT. In a sense, however, the simulation study reflected a best case of continuous peripheral insulin delivery, since perfect fasting normoglycemia and correspondingly high continuous insulin levels were considered. In most cases such an open-loop form of insulin delivery would not be tuned so precisely to alleviate the likelihood of

hypoglyemic episodes, and thus fasting hyperglycemia and lower average circulating insulin levels are more commonly observed in patients on conventional therapy. In such cases, hyperglycemic response to an OGTT is more severe owing primarily to the initial fasting hyperglycemic offset.

In order to assess the importance of the site of insulin delivery, an analogous OGTT simulation was run using a fixed continuous intraportal insulin infusion rate. For this simulation, the liver compartment mass balance equation in the insulin model (Equation 20) was modified to include a source term for intraportal insulin delivery

Intraportal Insulin Infusion: (modification of Equation 20)

$$I_L \frac{dV_L^I}{dt} = Q_A^I I_H + Q_G^I I_G - Q_L^I I_L + r_{PIR} - r_{LIC} + r_{IPI} \qquad (20a)$$

where: r_{IPI} = rate of intraportal insulin infusion (mU/min)

Specification of the initial intraportal insulin infusion rate allowed unique determination of the initial insulin concentrations in the insulin model, although the diabetic model initialization procedure outline in Table 38 had to be modified with resepct to the order in which the steady state insulin model mass balance equations were solved. The rate of intraportal insulin infusion was adjusted (by trial and error) until the fasting diabetic glycemia matched that of the normal group used as the basis for the previous OGTT simulations (peripheral blood glucose concentration of 75 mg/dl): the resulting fixed intraportal insulin delivery rate was 19 mU/min and resulted in a peripheral plasma (free) insulin level of 13 mU/l.

As shown in Figure 98, the intraportal, in contrast to the peripheral route of insulin delivery, did not require basal peripheral hyperin-

sulinemia for the normalization of fasting glycemia. During the oral glucose challenge, the magnitude of the glycemic excursion was similar whether insulin was delivered peripherally or intraportally, with lack of insulin reponse to glycemia resulting in elevated glucose levels relative to normal. Thus, with respect to continuous basal insulin delivery, the only apparent advantage to intraportal over peripheral delivery would be the elimination of fasting peripheral hyperinsulinemia. Furthermore, insulin response to glycemia is necessary for avoidance of postprandial hyperglycemia, independent of the route of insulin delivery.

b) The OGTT on Artificial Beta Cell Insulin Delivery

Available data for Type I diabetics on ABC therapy during the standard 100g OGTT provides a basis for studying the simulation of insulin resistance. In this section, insulin resistance due to tissue insensitivity and antibody binding will first be addressed separately, and then in combination.

i) Simulation of Tissue Insulin Resistance

Following 72 h of ABC therapy, Foss et al. (1982) administered 100 g OGTTs to 5 Type I diabetic subjects. The ABC is a closed-loop insulin delivery system; peripheral blood glucose concentration is meaured on a continuous basis and a variable intravenous insulin infusion is adjusted based on the glucose measurement as determined from an infusion algorithm. In order to study insulin resistance, the glucose and insulin models were first decoupled to allow isolation of contributing factors. For the study of tissue insulin resistance, the rate of intravenous insulin infusion (r_{IVI} in Equation 18a) was adjusted (by trial and error cubic spline fitting) such that the time course of peripheral plasma (free) insulin concentration

in the insulin model matched that reported in the Type I diabetics following OGTT administration as shown in the lower plot of Figure 99. Therefore, by matching the plasma free insulin levels, factors associated with the presence of insulin antibody binding were directly circumvented. Furthermore, by having properly fixed the insulin response levels in the insulin model, metabolism in the glucose model could then be studied independent of interactive changes in insulin concentrations in the insulin model.

For simulation of the 100 g OGTT, the gut glucose absorption rate function (Figure 81) was input to the gut compartment mass balance equation in the glucose model (Equation 12a) as described previously. As shown in the upper plot of Figure 99, use of normal metabolism in the glucose model lead to predicted glycemic response that was significantly lower than that actually observed in the diabetic subjects. Since the circulating insulin levels resulting from ABC insulin delivery were roughly three times higher than those normally observed in nondiabetics during the OGTT (see lower plot of Figure 99), it was not particularly surprising that normal insulin sensitivity in the metabolic functions of the glucose model caused excessive glucose disposal and hypoglycemia.

Since insulinemia had been fixed at the observed level, the above results suggested the presence of tissue resistance to the action of insuin in stimulating glucose disposal in the Type I diabetics, a conclusion supported by the data of Meistas et al. (1984) which directly demonstrated such resistance in Type I diabetics after 5 days of ABC therapy. Further simulation studies were thus undertaken to determine if introduction of tissue insulin resistance into the glucose model physiology could account for the observed diabetic glycemic response of Figure 99.

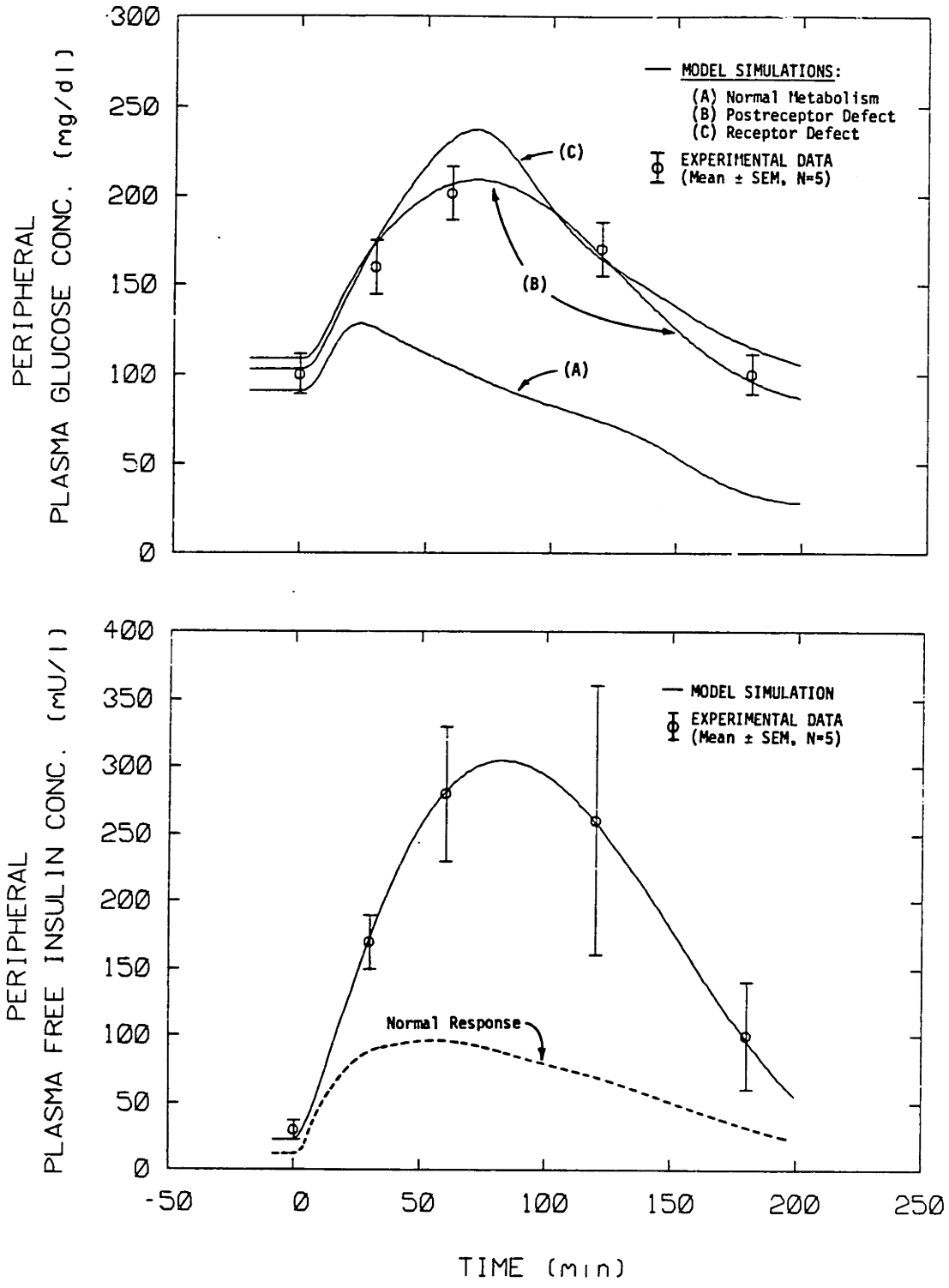

Fig. 99 Comparison between model predictions and experimental data for Type I diabetic response to the standard 100g OGTT during ABC insulin delivery. The insulin infusion rate was adjusted such that predicted insulinemia matched that observed experimentally (lower plot) while various modes of peripheral tissue insulin resistance were introduced into the glucose model. Resulting predicted glycemic responses corresponding to the tissue insulin resistance curves of Figure 100 are shown in the upper plot. (Data for 5 Type I diabetics from Fo[illegible] et al., 1982; normal OGTT response profile taken from Figure 81)

For simulating tissue insulin resistance, three possible glucose model functions could be considered: 1) the insulin multiplier of peripheral glucose uptake rate, M^{I}_{PGU} (Equation 51, Figure 13); 2) the insulin steady state insulin multiplier of hepatic glucose production rate, $M^{I\infty}_{HGP}$ (Equation 58, Figure 19); and 3) the steady state insulin multiplier of hepatic glucose uptake, $M^{I\infty}_{HGU}$ (Equation 95). To simplify matters, only the most dominant function, the insulin sensitivity of peripheral glucose uptake, was altered for simulating tissue insulin resistance. This strategy was adopted because, as previously shown during the development of the nondiabetic model, simultaneous adjustment of more than one metabolic function to fit model predictions with observed glycemic response is quite arbitrary, as the partitioning of effects between different sources and sinks can assume a multitude of symmetric compensatory balances.

Two types of peripheral tissue insulin resistance were considered, the pure receptor defect (a shift in the interstitial insulin concentration affecting half-maximal response) and the pure postreceptor defect (a proportional decrease in response at all interstitial insulin concentrations). Each of these respective shifts in the insulin multiplier of peripheral glucose uptake rate (M^{I}_{PGU}) could be realized by variation of a single function parameter. The general mathematical form for the function M^{I}_{PGU} was expressed by

$$M^{I}_{PGU} = E\ \{A + B\ \tanh[C(I^{N}_{PI} + D)]\} \qquad (223)$$

where, for normal metabolism (Equation 51),

$A = 7.03$

$B = 6.52$

$C = 0.338$

D = -5.82

E = 1

Thus, the pure postreceptor defect causing a proportionate decrease in response at all insulin levels was represented by varying parameter E in Equation 223, whereas the pure receptor defect causing a shift in the insulin concentration affecting half-maximal response was represented by varying parameter D. Having fixed the time course of the insulin model concentrations, OGTT simulations were repeated while varying the degree of each respective mode of insulin resistance until the best least-squares fit was attained between model predictions and experimental data for the time course of peripheral plasma glucose concentration. These one-dimensional least-squares fits were obtained by use of the IMSL library computer subroutine ZXSSQ. The resulting parameter values were E = 0.19 for the postreceptor shift and D = 24.9 for the receptor shift, respectively, in Equation 223.

The resulting shifts in peripheral tissue insulin sensitivity are presented in Figure 100, and their respective efficacies in providing for matching of model predictions and observed plasma glucose response are compared in the upper plot of Figure 99. As demonstrated in Figure 99, although the pure receptor defect shift in the insulin sensitivity of peripheral glucose uptake could generally account for the magnitude of the observed glycemic response, the pure postreceptor defect shift was most effective in accounting for both the magnitude and time course of the observed glycemic response with model predictions falling within the experimental error range at all times during the OGTT.

The magnitudes of the shifts in the insulin dose-response curves of Figure 100 were quite significant. Even though the insulin multiplier of

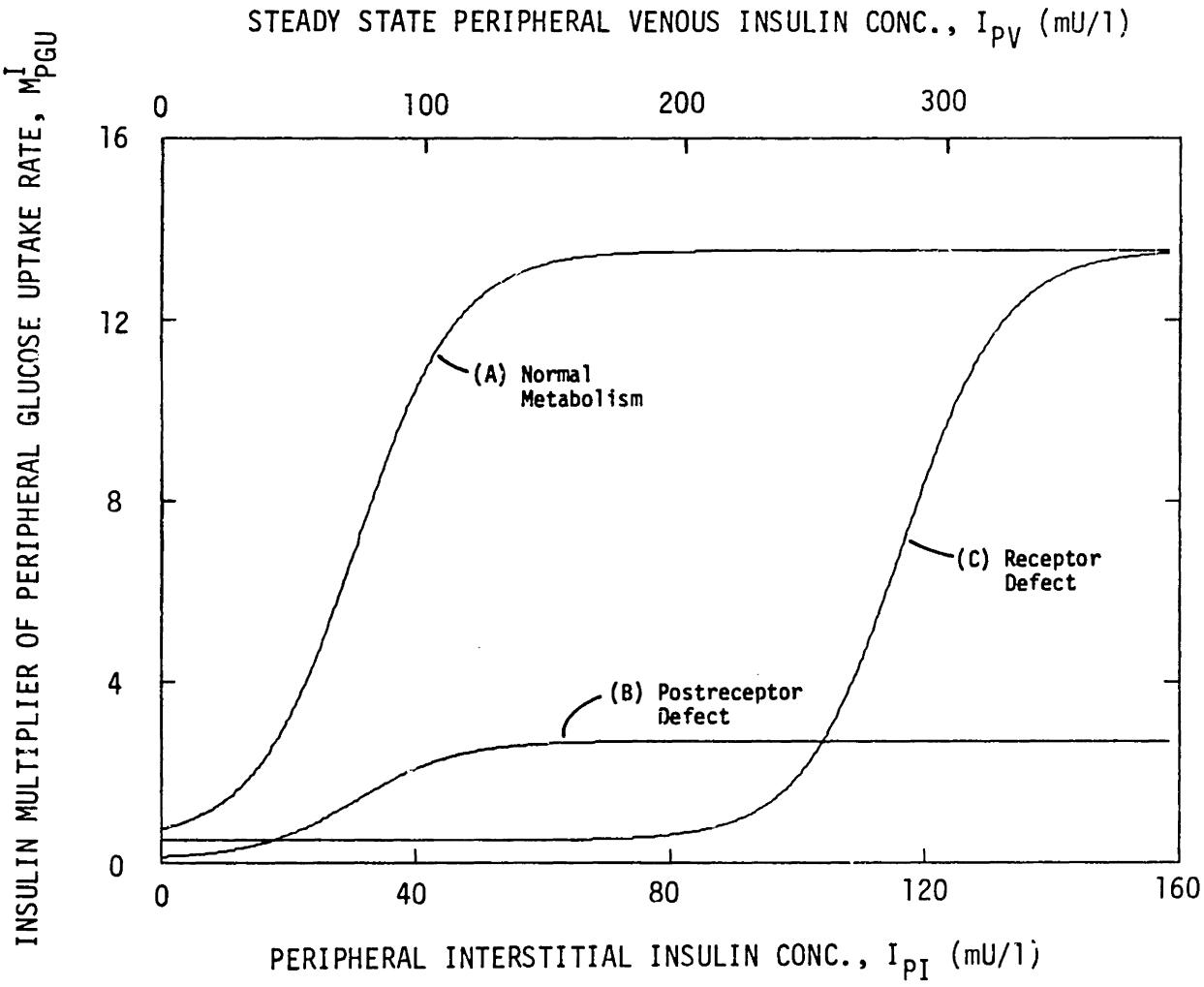

Fig. 100 Tissue insulin resistance curves resulting from pure receptor and postreceptor shifts in the effect of insulin on the rate of peripheral tissue glucose uptake in the glucose model. Magnitudes of the respective shifts were obtained by least-squares fitting of model predictions and experimental data for glycemic response of Type I diabetics during OGTTs (see Figure 99).

peripheral glucose uptake rate (M^{I}_{PGU}) was modeled as a function of peripheral interstitial insulin concentration (I_{PI}), an upper scale in the plot of Figure 100 was included to indicate the peripheral plasma insulin concentrations (I_{PV}) that would correspond to these interstitial insulin levels under steady state conditions. From the data of Meistas et al. (1984) previously presented in Table 35, insulin-stimulated forearm glucose uptake was only about 39% of normal at a steady-state peripheral plasma insulin concentration of approximately 80 mU/l in the group of 6 Type I diabetics studied. The postreceptor defect response curve in Figure 100 yielded an insulin-stimulated peripheral glucose uptake of roughly 20% of normal at all steady state peripheral plasma insulin concentrations including the value of interest here, 80 mU/l (I_{PV}= 80 mU/l). The apparent discrepancy between the above results can be attributed to two possible factors: 1) the data of Meistas et al. also indicated a defect in liver insulin sensitivity, thus having simply attributed all insulin resistance to peripheral tissue glucose uptake in the model simulation studies would lead to overestimation of its respective contribution to the total resistance; and 2) as indicated in the earlier review of tissue insulin resistance in Type I diabetics, the observed insulin dose-response curves appear to vary greatly from study to study.

An interesting aspect of ABC insulin delivery arises in analyzing the results of this simulation study of tissue insulin resistance. As was shown in Figure 99, ABC insulin delivery resulted in insulinemia roughly threefold higher than that observed during normal response to an OGTT challenge. But examining the dose-response curves in Figure 100, the post-receptor defect shift which could account for the observed OGTT glycemic response data saturated its maximal stimulation of glucose uptake at

corresponding plasma insulin levels significantly lower than those evoked by ABC therapy (the same saturation level observed in normals). It is thus quite possible that such excessive insulinemia (I_{PV} > ~150 mU/l) is unjustified because it can not provide effective compensation for this underyling mode of insulin resistance to the stimulation of glucose disposal. Furthermore, such high insulin levels could prove quite detrimental to the normalization of tissue insulin action, and thus the very character of present "intensive" ABC insulin therapy might defeat the goal of reversing tissue insulin resistance in Type I diabetics.

ii) Simulation of Insulin Antibody Binding

In order to study the effects of insulin antibody binding, the glucose and insulin models were again decoupled. As previously discussed, the rate of peripheral insulin delivered by the ABC is determined by an infusion algorithm based on measurement of peripheral blood glucose concentration. For the study of insulin antibody binding, a cubic spline fit of the time course of plasma glucose concentration was obtained from the data reported by Foss et al. (1982) for 5 Type I diabetics administered 100g OGTTs, as shown in the upper plot of Figure 101. This glucose profile (after conversion from plasma to blood glucose concentration) was input to the ABC infusion algorithm to determine the resulting rate of insulin delivery during the OGTT. The resulting insulin infusion rate is shown in Figure 102; although details of the mathematical form of the insulin infusion algorithm will be deferred to future discussion of closed-loop insulin delivery, the parameters of the ABC (Biostator) algorithm employed in generating the insulin delivery profile of Figure 102 are listed in its caption for reference. The insulin delivery rate shown in Figure 102 was

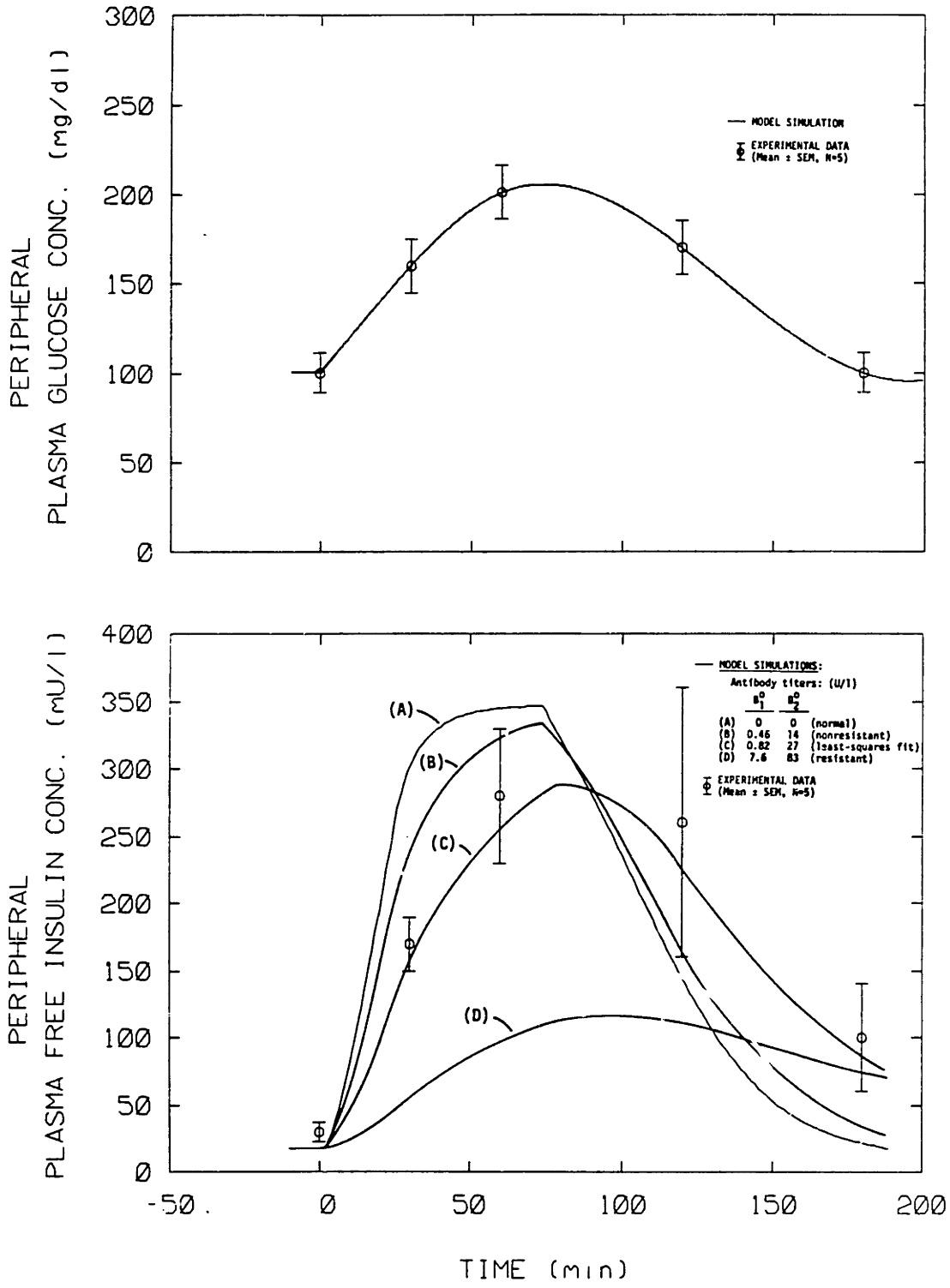

Fig. 101 Simulation studies of the effects of introducing insulin antibody binding on prediction of insulin response kinetics. A cubic spline fit of the experimental glucose response data (upper plot) was used to determine the rate of insulin delivered by the ABC as shown in Figure 102, while the antibody binding capacity was varied in the insulin model. (Data for 5 Type I diabetics from Foss et al., 1982)

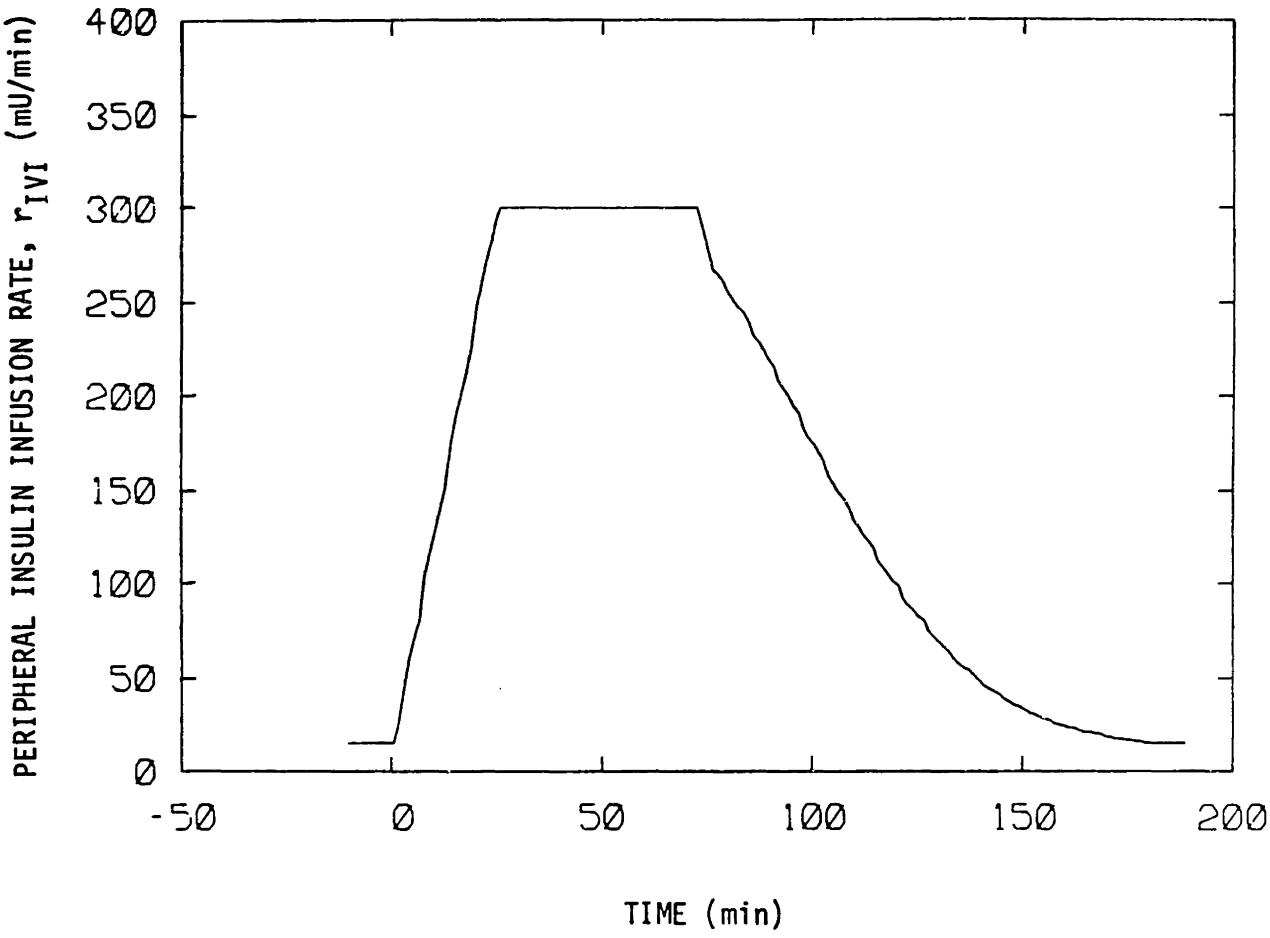

Fig. 102 Rate of peripheral insulin infusion resulting from input of the glycemic profile of Figure 103 into the ABC (Biostator) infusion algorithm. The following Biostator infusion algorithm parameters were employed: BI = 90 mg/dl, QI = 30 mg/dl, RI = 15 mU/min, FI = 300 mU/min, KR = 165, and KF = 45.

in turn used as the input to the insulin model (r_{IVI} in Equation 18a) for studying the effects of insulin antibody binding on the predictions of plasma insulin response. Thus, by having determined the proper closed-loop insulin infusion rate from a fit of the glycemic response data, factors associated with tissue insulin resistance in the glucose model were circumvented, since the insulin delivery in these simulations was not interactive with changes in predicted glycemic response (or with the glucose model at all).

As shown in the lower plot of Figure 101, use of the insulin model without including the effects of antibody binding (Curve A) resulted in a predicted plasma (free) insulin response that was less sluggish than that observed in the diabetic subjects. Therefore, additional simulation studies were undertaken to determine if the inclusion of insulin antibody binding in the insulin model could account for this discrepancy between predicted and observed insulin response kinetics.

Since plasma free insulin concentrations vary from organ to organ, an exacting approach to modeling of insulin antibody binding would be to develop a distributed binding model in which antibodies would flow and mix in the circulation and partially equilibrate bound insulin levels in response to local free insulin concentrations. Such a distributed binding model coupled with the existing insulin model would have been extremely complex. To explore the first order effects of antibody binding, a simplified lumped binding model was instead employed. For the lumped model, it was assumed that the plasma circulation time is reasonably small relative to characteristic antibody binding times; this was a reasonable assumption, since the longest local organ plasma space residence time (plasma volume divided by plasma flow rate) in the insulin model was 0.7 min (peripheral

compartment) whereas insulin antibody binding occurs over time scales of minutes to hours. Thus, for a lumped insulin antibody binding model, plasma free insulin was assumed to exchange with a single uniform antibody binding pool at a rate determined by the instantaneous mean mixed whole-body plasma free insulin level.

The insulin antibody binding model was formulated as follows. At each time step of numerical integration, a mean mixed whole-body plasma free insulin concentration was computed from the local plasma (free) insulin concentrations in the insulin model, given by

$$\bar{F} = \frac{\sum_i I_{iV} V_{iV}}{\sum_i V_{iV}} \tag{224}$$

where: $\bar{F}$ = mean plasma free insulin concentration (mU/l)

I_{iV} = plasma free insulin concentration in the ith insulin model compartment (mU/l)

V_{iV} = plasma equilibration volume of the ith insulin model compartment (l)

From Equations 208 and 209, the mean rates of insulin antibody binding to each class of binding site per unit volume of plasma would thus be

$$\frac{dB_1}{dt} = k_1^+ E_1 \bar{F} - k_1^- B_1 \tag{225}$$

$$\frac{dB_2}{dt} = k_2^+ E_2 \bar{F} - k_2^- B_2 \tag{226}$$

Using Equations 214 and 215 to eliminate E_1 and E_2 from Equations 225 and 226, respectively, yields

$$\frac{dB_1}{dt} = k_1^+ B_1^o \bar{F} - k_1^- B_1 - k_1^+ \bar{F} B_1 \quad (227)$$

$$\frac{dB_2}{dt} = k_2^+ B_2^o \bar{F} - k_2^- B_2 - k_2^+ \bar{F} B_2 \quad (228)$$

Thus, the total mean rate of free insulin binding to the antibody pool per unit volume of plasma was given by

$$r_{AIB} = \frac{dB}{dt} = \frac{dB_1}{dt} + \frac{dB_2}{dt} \quad (229)$$

where: r_{AIB} = mean rate of free insulin binding to antibodies [(mU/min)/l plasma]

Finally, a sink term was subtracted from each plasma space mass balance equation in the insulin model (Equations 17-22) to account for free insulin binding to the antibody pool, where each sink term was expressed

$$r_{AIB}^i = r_{AIB} V_{iV} \quad (230)$$

where: r_{AIB}^i = rate of free insulin binding to antibodies in the ith insulin model compartment (mU/min)

Because insulin antibody binding is reversible, the values of r_{AIB}^i could be positive or negative depending on whether free insulin was associating with or dissociating from the antibody pool, respectively.

For simulation studies incorporating the insulin antibody binding model modifications in the insulin model, the rate constants k_1^+, k_1^-, k_2^+ and k_2^- in Equations 227 and 228 were assigned the experimentally-determined values compiled in Table 36 from the studies of Berson and Yalow (1959). The capacity of the antibody binding pool, representing the in vivo antibody titer levels, was determined by specifying the values of

the binding capacity parameters B_1^o and B_2^o in Equations 227 and 228 (values listed in caption of Figure 101).

The effects of varying the insulin antibody binding capacities on the insulin model predictions of plasma insulin response to ABC insulin delivery during the OGTT are shown in the lower plot of Figure 101. As previously discussed, exclusion of insulin antibody binding (equivalent to letting $B_1^o = B_2^o = 0$) resulted in predicted plasma free insulin response kinetics that were faster than those observed in the experimental study (Curve A). Next, antibody binding capacities reported by Berson and Yalow (1959) for nonresistant (Curve B) and resistant (Curve C) groups of diabetics (see Table 36) were employed. Incorporation of insulin antibody binding into the insulin model resulted in slowing the predicted free insulin response kinetics, with the nonresistant and resistant response curves appearing to bracket the observed response behavior. Finally, the values of the binding capacities B_1^o and B_2^o were varied in order to obtain the best least-squares fit (library computer subroutine ZXSSQ) of model predictions with experimental data for the time course of peripheral plasma free insulin concentration response. The resulting binding capacities were intermediate between those reported for nonresistant and resistant diabetics (see caption of Figure 101), and the prediction of plasma free insulin response agreed well with the experimental data as shown by Curve C in the lower plot of Figure 101. In order to show the extent of insulin binding during this simulation, the mean levels of plasma free and total (bound plus free) insulin concentration are plotted as a function of time in Figure 103; as shown, the majority of circulating insulin was predicted to be in bound form as would be anticipated in the presence of significant antibody titers.

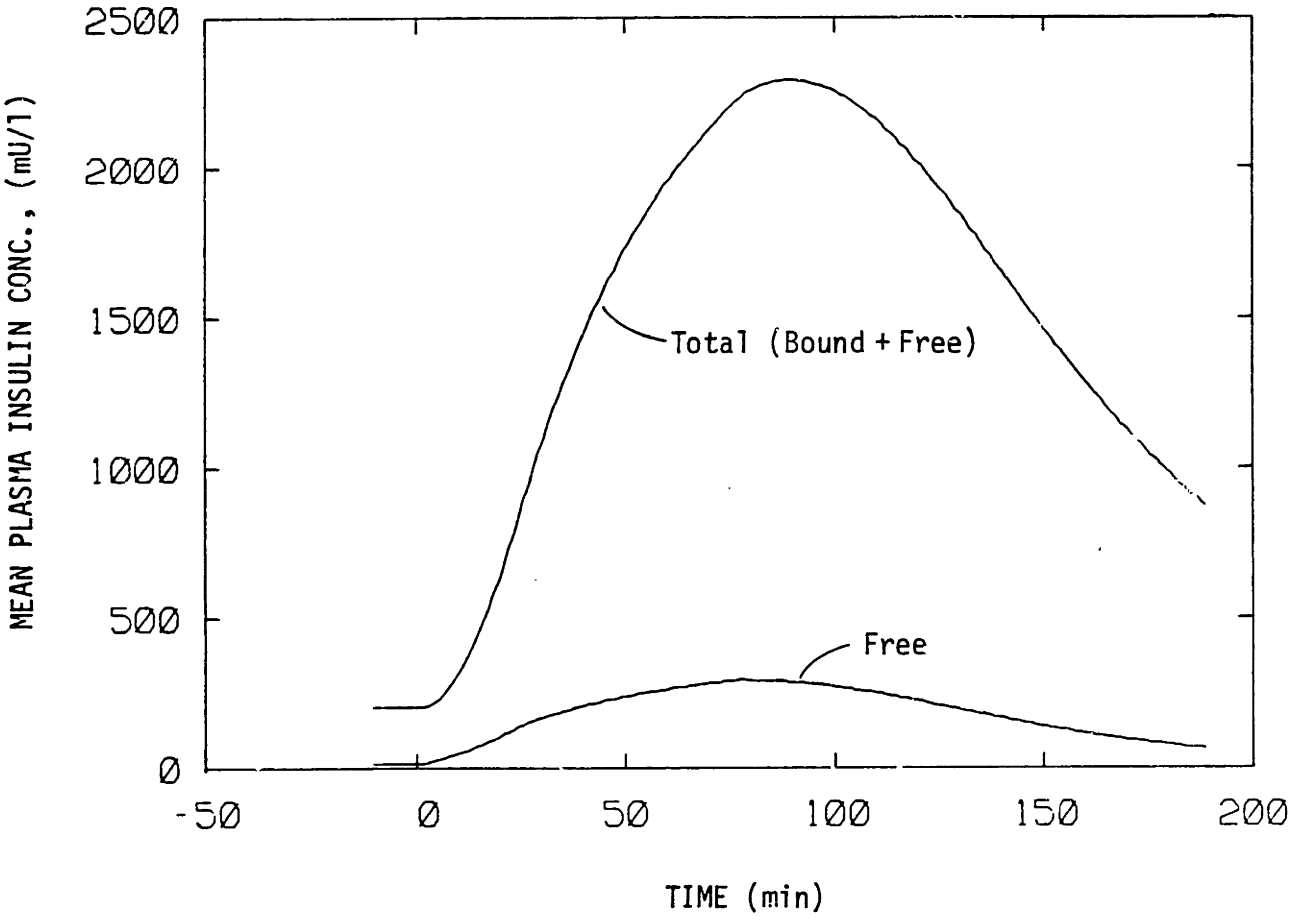

Fig. 103 Model predictions of the mean plasma insulin concentrations of free and total (bound + free) insulin during OGTT simulation of the Type I diabetic corresponding to Curve C in Figure 101.

iii) Combined Simulation of Tissue Insulin Resistance and Insulin Antibody Binding

Since the glucose and insulin models were essentially decoupled in the above simulations of tissue insulin resistance and insulin antibody binding, a final diabetic simulation study was conducted combining these effects with the glucose and insulin models coupled. For this simulation,the metabolically-normal Type I diabetic model was employed, except that tissue insulin resistance (the postreceptor defect of Figure 100, corresponding to Curve B in Figure 99) was introduced into the glucose model, and insulin antibody binding (antibody titers corresponding to response Curve C in Figure 101) was included in the insulin model. The 100g OGTT was again simulated, but the rate of insulin delivered by the ABC and used as the input to the insulin model was determined from interactive measurement of the peripheral blood glucose values generated by the glucose model.

Results of this simulation are presented in Figure 104. As shown in the figure, model predictions agreed well with the experimental data of Foss et al. (1982) when the diabetic abnormalities of tissue insulin resistance and insulin antibody binding were included in the Type I diabetic model.

For reasons previously stated, no diabetic metabolic abnormalities will be incorporated into the Type I diabetic model during design of a closed-loop insulin infusion algorithm. However, once this algorithm is designed, it will be very useful to assess its effectiveness if employed in a Type I patient who is not initially in a metabolically-normalized state. Since introduction of the above diabetic abnormalities into the Type I diabetic model was successful in predicting the data of Foss et al., the

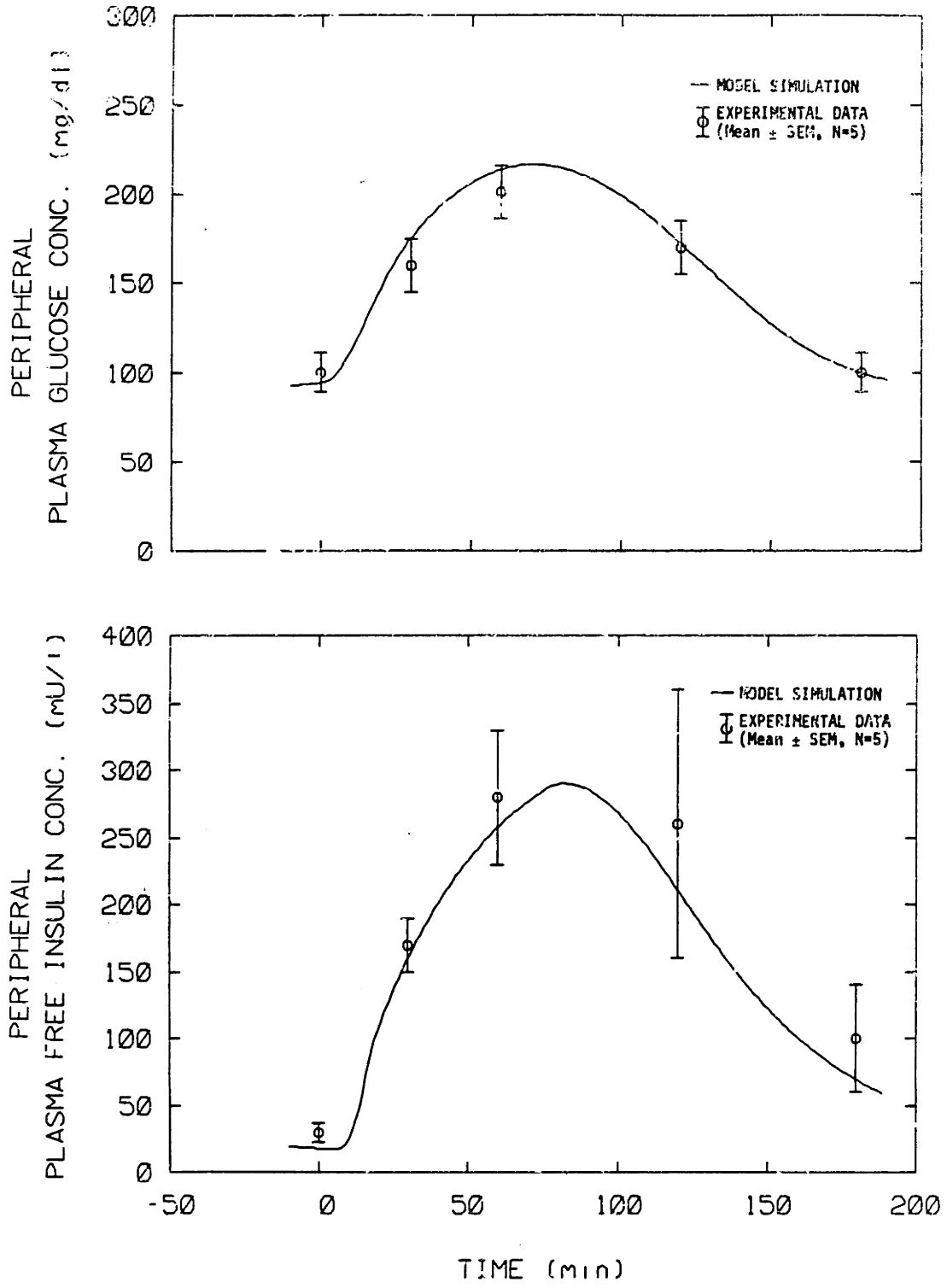

Fig. 104 Comparison of model predictions and experimental data for Type I diabetic response during the 100g OGTT with inclusion of combined peripheral tissue insulin resistance and insulin antibody binding effects in the otherwise metabolically-normal Type I diabetic model. (Data for 5 Type I diabetics from Foss et al., 1982)

potential interaction of these diabetic abnormalities with the newly-designed infusion algorithm can also be studied through model simulations. Thus, the above methods of modeling insulin resistance, together with the capability of representing blunted glucagon response to hypoglycemia by setting $M^{G}_{P\Gamma R}$ equal to unity in Equation 155 of the glucagon model, will will provide a valuable means for simulating diabetic abnormalities and testing algorithm performance in the metabolically "uncontrolled" Type I diabetic.

VI. DESIGN AND ASSESSMENT OF AN OPTIMAL GLUCOSE-CONTROLLED INSULIN DELIVERY SYSTEM

A) Optimal Control

1) Background

The present review is concerned with the algorithms for the computation of glucose-controlled insulin delivery that have evolved in conjunction with the development of various closed-loop systems.

Continuous in vivo determination of blood glucose concentration was made possible in the early 1960s through the invention and development of the double-lumen catheter (Weller et al., 1960) and the establishment of a continuous glucose analyzer for the laboratory, the Autoanalyzer (see Bannafe, 1977). Using these methodologies, Kadish (1963) pioneered clinical application of glucose-controlled insulin delivery; blood glucose was continuously monitored, and an insulin infusion system delivering 100 mU/min was actuated whenever the measured blood glucose concentration exceeded 150 mg/dl. Although this simple "on-off" control system failed to produce glycemic normalization, its realization was a notable achievement for its time.

Glucose-controlled insulin delivery has subsequently been advanced to a significantly higher state of sophistication by a number of groups of investigators, including Albisser et al. in Canada, Kraegen et al. in Australia, Clemens et al. in the United States (in close collaboration with medical researchers in Europe), and Shichiri et al. in Japan.

Albisser et al. (1974a) developed a bedside closed-loop insulin delivery system suitable for clinical applications. This system employed an algorithm for computer-controlled insulin delivery based on a hyperbolic

tangent functionality of blood glucose concentration (Albisser et al., 1974a; 1974b), given by

$$IR(k)= \frac{IR_{max}}{2}\{1-\tanh[S(G_p(k)-B)]\} \quad kT<t<(k+1)T;\ k=0,1,2,... \tag{231}$$

where $IR(k)$ = insulin infusion rate (mU/min)
$G_p(k)$ = projected blood glucose conc. (mg/dl)
T = sampling interval = 1 min

with parameters

IR_{max} = maximum insulin infusion rate (mU/min)
B = blood glucose conc. for half-maximal infusion rate (mg/dl)
S = sensitivity of infusion response to deviations in blood glucose conc. (dl/mg)

The hyperbolic tangent formulation was selected because it offered the theoretical advantage of closely resembling sigmoidal dose-response curves observed for steady state glucose stimulation of pancreatic insulin secretion (Grodsky, 1972). As indicated in Equation 231, the insulin infusion rate was based on a "projected" glucose concentration, expressed by

$$G_p(k)=G_m(k)+DF(k) \tag{232}$$

where $G_m(k)$ = measured blood glucose concentration (mg/dl)
$DF(k)$ = difference factor (mg/dl)

Thus, the present measured glucose concentration was modulated by a "difference factor," a rate-sensitive function defined by

$$DF(k)=K_1\left[\exp\left(\frac{\frac{dG_m(k)}{dt}}{K_2}\right)-1\right] \tag{233}$$

where K_1 = parameter (mg/dl)

K_2 = parameter (mg/dl·min)

and, for noise suppression, the derivative term was computed from an arithmetically weighted average of the rates of change over the previous 4 min of monitoring (Broekhuyse et al., 1981),

$$\frac{dG_m(k)}{dt} = \frac{1}{10} \sum_{i=1}^{4} i\left(\frac{G_m(k+i-4)-G_m(k+i-5)}{T}\right) \tag{234a}$$

$$= \frac{4G_m(k)-G_m(k-1)-G_m(k-2)-G_m(k-3)-G_m(k-4)}{10\ T} \tag{234b}$$

In effect, the difference factor introduced anticipatory derivative action into the infusion algorithm, and the resulting use of projected glucose values was found to improve glycemic regulation. Botz(1976) introduced an improved relationship for the difference factor, given by

$$DF(k)=K_1\left(\frac{dG_m(k)}{dt}\right)^3+ K_2\left(\frac{dG_m(k)}{dt}\right) \tag{235}$$

where K_1 = parameter ($dl^2 \cdot min^3/mg^2$)

K_2 = parameter (min)

Use of this difference factor formulation improved glycemic regulation (Botz, 1976) and it has subsequently been employed by Albisser and colleagues.

Kraegen et al.(1975,1977,1979) developed a bedside glucose-controlled insulin infusion system which has been applied to clinical research. The insulin infusion algorithm imcorporated into this device was that origi-

nally proposed by Albisser et al. (Equations 231-233), except the rate of change of glucose concentration was computed from a geometrically weighted average of the rates of change over the previous 4 min of monitoring (Kraegen et al., 1977),

$$\frac{dG_m(k)}{dt} = \frac{1}{15} \sum_{i=1}^{4} 2^{4-i} \left(\frac{G_m(k+1-i)-G_m(k-i)}{T}\right) \tag{236a}$$

$$= \frac{8G_m(k)-4G_m(k-1)-2G_m(k-2)-G_m(k-3)-G_m(k-4)}{15\ T} \tag{236b}$$

This relationship was used instead of the arithmetically weighted average employed by Albisser et al. (Equation 234) in order to achieve a better compromise between speed of response and immunity to artifactual noise.

To date, the only commercially available closed-loop insulin infusion device is the Biostator® Glucose Controlled Insulin Infusion System (GCIIS) developed by Miles Laboratories in close conjunction with medical researchers in Europe (Pfeiffer et al.,1974; Clemens and Chang,1976; Clemens et al.,1976). The Biostator GCIIS is a bedside unit which has been used extensively for clinical research applications. Clemens et al. developed a series of insulin infusion algorithms throughout the evolution of the Biostator GCIIS. The original algorithm utilized projected glucose values with a biquadratic control functionality (Clemens and Chang,1976; Clemens et al.,1977; Clemens and Meyers,1977), given by

$$IR(k) = \begin{cases} R\left(\frac{G_p(k)-B}{Q}\right)^4 & IR(k)<IR_{max} \\ IR_{max} & IR(k)\geq IR_{max} \end{cases} \qquad kT\leq t<(k+1)T;\ k=0,1,2... \tag{237}$$

where IR(k) = insulin infusion rate (mU/min)

$G_p(k)$ = projected blood glucose conc. (mg/dl)

T = sampling interval = 1 min

with parameters

IR_{max} = maximum insulin infusion rate (mU/min)

R = basal insulin infusion rate (mU/min)

B = basal blood glucose conc. (mg/dl)

Q = sensitivity of infusion response to deviations in blood glucose conc. (mg/dl)

The projected glucose concentration $G_p(k)$ was defined as in Equation 232, but the difference factor DF(k) was calculated according to

$$DF(k) = \begin{cases} \frac{KR}{10}\left(\frac{dG_m(k)}{dt}\right)^2 + K\left(\frac{dG_m(k)}{dt}\right) & \frac{dG_m(k)}{dt} > 0 \\ -\frac{KF}{10}\left(\frac{dG_m(k)}{dt}\right)^2 + K\left(\frac{dG_m(k)}{dt}\right) & \frac{dG_m(k)}{dt} < 0 \end{cases} \quad (238)$$

where KR = parameter for rising glucose conc. ($min^2 \cdot dl/min$)

KF = parameter for falling glucose conc. ($min^2 \cdot dl/min$)

K = fixed parameter = 6 min

and $dG_m(k)/dt$ was determined from Equation 234. Clemens et al used a biquadratic formulation for insulin infusion instead of the hyperbolic tangent functionalities of earlier algorithms because the control constants could be selected more directly in physiologically meaningful terms, such as basal glucose level and basal insulin infusion rate. In addition, use of Equation 238 for the calculation of the difference factor allowed for

altering the insulin infusion response depending on whether glucose was rising or falling.

Experience gained with the original Biostator GCIIS infusion algorithm led to the evolution of the presently employed control equations. The major change from the previous formulation was the introduction of explicit derivative control directly into the insulin infusion equation and the elimination of the use of projected glucose values. The present insulin infusion algorithm (Clemens,1979a; Clemens,1979b; Biostator GCIIS Operation Manual,©1980) is given by

$$IR(k) = \begin{cases} IR_1(k)+IR_2(k) & IR(k)<IR_{max} \\ IR_{max} & IR(k)\geq IR_{max} \end{cases} \qquad kT\leq t<(k+1)T;k=0,1,2... \qquad (239)$$

$$IR_1(k) = \begin{cases} R\left(\frac{\hat{G}(k)-B}{Q}+1\right)^2 & \frac{\hat{G}(k)-B}{Q}+1>0 \\ 0 & \frac{\hat{G}(k)-B}{Q}+1\leq 0 \end{cases} \qquad (240)$$

$$IR_2(k) = \begin{cases} \left(\frac{KR}{10}\right)\left(\frac{R}{100}\right)\left(\frac{d\hat{G}(k)}{dt}\right)\left(\hat{G}(k)-B\right) & \hat{G}(k)-B>0 \text{ and } \frac{d\hat{G}(k)}{dt}>0 \\ \left(\frac{KF}{10}\right)\left(\frac{R}{100}\right)\left(\frac{d\hat{G}(k)}{dt}\right)\left(\hat{G}(k)-B\right) & \hat{G}(k)-B>0 \text{ and } \frac{d\hat{G}(k)}{dt}\leq 0 \\ 0 & \hat{G}(k)-B\leq 0 \end{cases} \qquad (241)$$

where $IR(k)$ = insulin infusion rate (mU/min)

$\hat{G}(k)$ = estimated present blood glucose conc. (mg/dl)

T = sampling interval = 1 min

with parameters

IR_{max} = maximum insulin infusion rate (mU/min)

R = basal insulin infusion rate (mU/min)

B = basal blood glucose conc. (mg/dl)

Q = sensitivity of infusion response to deviations in blood glucose conc. (mg/dl)

KR = parameter for rising glucose conc. ($dl^2 \cdot min/mg^2$)

KF = parameter for falling glucose conc. ($dl^2 \cdot min/mg^2$)

For noise reduction, a linear regression fit over the previous five measured blood glucose concentration values (G_m) was utilized; the slope of the resulting regression line provided an estimate of the rate of change of glucose concentration,

$$\frac{d\hat{G}(k)}{dt} = \frac{2G_m(k)+G_m(k-1)-G_m(k-3)-2G_m(k-4)}{10\ T} \tag{242}$$

from which the present glucose concentration values was in turn estimated by

$$\hat{G}(k) = \frac{G_m(k)+G_m(k-1)+G_m(k-2)+G_m(k-3)+G_m(k-4)}{5} + 2\left(\frac{d\hat{G}(k)}{dt}\right) \tag{243}$$

The reported rationale for implementing derivative action more directly into the infusion algorithm was that the usage of projected glucose values was no longer needed to compensate for the Biostator's glucose measurement response time which, including the time required for blood transport from the patient, had been reduced from about 4 to 5 min in earlier units to less than 1.5 min in the more recent models (Clemens, 1979b). In general, derivative control action is primarily introduced into controller design to provide effective anticipatory action with respect to the inherent response

time of the process under regulation (in this case the time required for in vivo glycemic response of the diabetic patient to manipulation of the insulin infusion rate), although its secondary purpose may be to provide anticipatory compensation with respect to response time of the measurement signal. Since it is not clear that the implicit derivative action previously realized through the use of projected glucose values solely acted to affect measurement response time compensation, the contribution of reducing the Biostator CGIIS measurement response time to under 2 min in pursuing the achievement of good closed-loop glycemic regulation may have been overstated.

Shichiri et al. originally developed a glucose-controlled insulin delivery system (Kawamori et al., 1978; Goriya et al., 1979) that, in similarity to all other bedside-type units to date, used double-lumen catheter technology for withdrawal of a continuous stream of heparinized blood which in turn was fed to a glucose analyzer reporting measurements at 1 min intervals. More recently, Shichiri et al. (1983; 1984) reported on the development and initial testing of a wearable closed-loop insulin delivery system that utilized a needle-type glucose sensor inserted into the subcutaneous tissue. The insulin infusion algorithm employed in the above systems was given by

$$IR(k) = \begin{cases} K_p\hat{G}(k)+K_d\left(\frac{d\hat{G}(k)}{dt}\right)+K_c & IR(k)<IR_{max} \\ IR_{max} & IR(k)\geq IR_{max} \end{cases} \quad kT\leq t<(k+1)T;k=0,1,2... \quad (244)$$

where $IR(k)$ = insulin infusion rate (mU/min)

$\hat{G}(k)$ = estimated present blood glucose conc. (mg/dl)

T = sampling interval = 1 min

with parameters

IR_{max} = maximum insulin infusion rate (mU/min)

K_p = coefficient for proportional action (mU·dl/mg·min)

K_d = coefficient for derivative action (mU·dl/mg)

K_c = constant for basal insulin infusion rate (mU/min)

In order to compensate for time delays in the analysis of glucose concentration, the insulin infusion rate was calculated on the basis of estimated present glucose concentration values. For this purpose, a hyperbolic tangent curve was fit by least squares methods to the previous 10 min of measured glucose concentrations (G_m) and the estimated present glucose concentration was calculated by

$$\hat{G}(k) = G_m(k) + \left(\frac{\sum_{i=1}^{10} (G_m(k-i)-G_m(k))\tanh(iT\omega)}{\sum_{i=1}^{10} (\tanh(iT\omega))^2}\right)\tanh(m\omega) \qquad (245)$$

where m = glucose measurement delay (min)

ω = parameter (min^{-1})

and the rate of change of glucose concentration was in turn given by

$$\frac{d\hat{G}(k)}{dt} = \frac{\hat{G}(k)-\hat{G}(k-1)}{T} \qquad (246)$$

As indicated in Equation 244, the infusion algorithm derectly employed proportional (P) action based on glucose concentration plus derivative (D) action based on the rate of change of glucose concentration; Shichiri et al. selected a basic PD control structure because analysis of experimental

data in the perfused rat pancreas (Basabe et al., 1970) and with intravenous glucose infusions in normal man (Cerasi et al., 1974) suggested that the dynamics of natural pancreatic insulin secretion were based on both proportional and derivative responses to glycemia. Fischer et al. (1978;1980) arrived at a mathematically identical PD algorithm for insulin delivery through analysis of in vivo glucose-insulin relationships following oral and intravenous glucose tolerance tests in normal subjects.

The performance of a controller resides not only in the appropriateness of its mathematical structure in relation to the process being regulated, but also in adjustment of its parameters (tuning). For the various algorithm structures reviewed above, tuning parameter values have been attained through trial and error clinical experimentation until desired results were obtained. It is thus difficult to assess if such ad hoc tuning methods have resulted in full realization of a given algorithm's performance. For example, Christensen et al. (1981) performed repeated oral glucose tolerance tests (OGTTs) in diabetic subjects in order to "optimize" the tuning parameters of the Biostator GCIIS infusion algorithm (see Equations 239-241); results of the study indicated that a modified set of tuning parameters enabled normal glucose tolerance to be achieved while substantially reducing the amount of insulin delivered (by more than 50% in some patients) when compared to the amount of insulin delivered using the tuning parameters originally recommended by the manufacturer.

In this chapter, two important issues are addressed during formulation of an optimal controller for closed-loop glycemic regulation: 1) an appropriate mathematical structure for the optimal controller algorithm, and 2) tuning of the controller for optimal performance. Optimal controller design and tuning are derived through consideration of the dyna-

mics of the process being regulated, glucose metabolism in the insulin-dependent diabetic, via use of simulation studies.

Several groups have previously used simulation studies to approach problems concerned with closed-loop insulin delivery. Sorensen et al. (1982) and Cobelli and Ruggeri (1983) have both utilized models of glucose metabolism in diabetic man challenged with oral glucose to study peripheral versus the more physiologic portal routing of glucose-controlled insulin delivery. Broekhuyse et al. (1981) compared closed-loop insulin infusion algorithm responses by inputting the same blood glucose profiles to a number of the established mathematical algorithms and calculating the resulting insulin infusion rate output profiles. The effects of parameter tuning in changing or improving algorithm performance were not considered in any of the above studies.

To date, Swan (1982) has been the only investigator to apply optimal control analysis to the problem of closed-loop glycemic regulation in the diabetic. Swan used methods of variational calculus to determine the insulin delivery action that would minimize the time required to drive blood glucose concentration from an initial value to a desired steady state level. There were a several serious drawbacks to the analysis, however. First, the mathematical approach yielded an algorithm for insulin infusion rate as a linear combination of not only blood glucose level but also plasma insulin concentration as a function of time; thus, implementation of such a control principle would not be practical since monitoring of plasma insulin would be required. Second, the problem addressed was how to drive glucose level to some prescribed value in the absence of exogenous glucose input, either orally or intravenously introduced into the body; therefore, the solution did not determine the most effective way to minimize the

impact of glucose loading on changes in glycemia (the "regulator" problem), but rather provided an optimal method for changing glucose levels from one value to another in the absence of a glucose challenge (the "servo" problem). Finally, an extremely simplified linear two-compartment mathematical model was employed for prediction of in vivo glucose and insulin dynamics (see Ackerman et al., 1969). As acknowleged by Swan, a need existed for future application of optimal control analysis utilyzing a more realistic physiologic model of in vivo glucose metabolism. Such was the objective of the present study.

2) Optimal Controller Development

a) Basic Control Structure

Under basal steady state conditions, exogenous glucose input from the gut is zero, and blood glucose concentration in the insulin-dependent diabetic is maintained at a desirable basal level by means of basal insulin delivery. The basic problem was to develop an optimal controller for minimizing the impact of unknown rates of gut glucose input resulting from glucose ingestion on deviations in blood glucose concentration from its basal or setpoint level. Such would be considered a "regulator" problem in control terminology.

Internal Model Control (IMC) is a modern control methodology that allows for a very transparent and rational approach to optimal controller design (for review, see Garcia and Morari, 1982). IMC structure was employed for the basic closed-loop control configuration, as shown in Figure 105. Variables corresponding to the figure were defined as follows:

$y(t)$ = observed variable (mg/dl)
= deviation in glucose conc. $G(t)$ from its basal value G_b
= $G(t)-G_b$

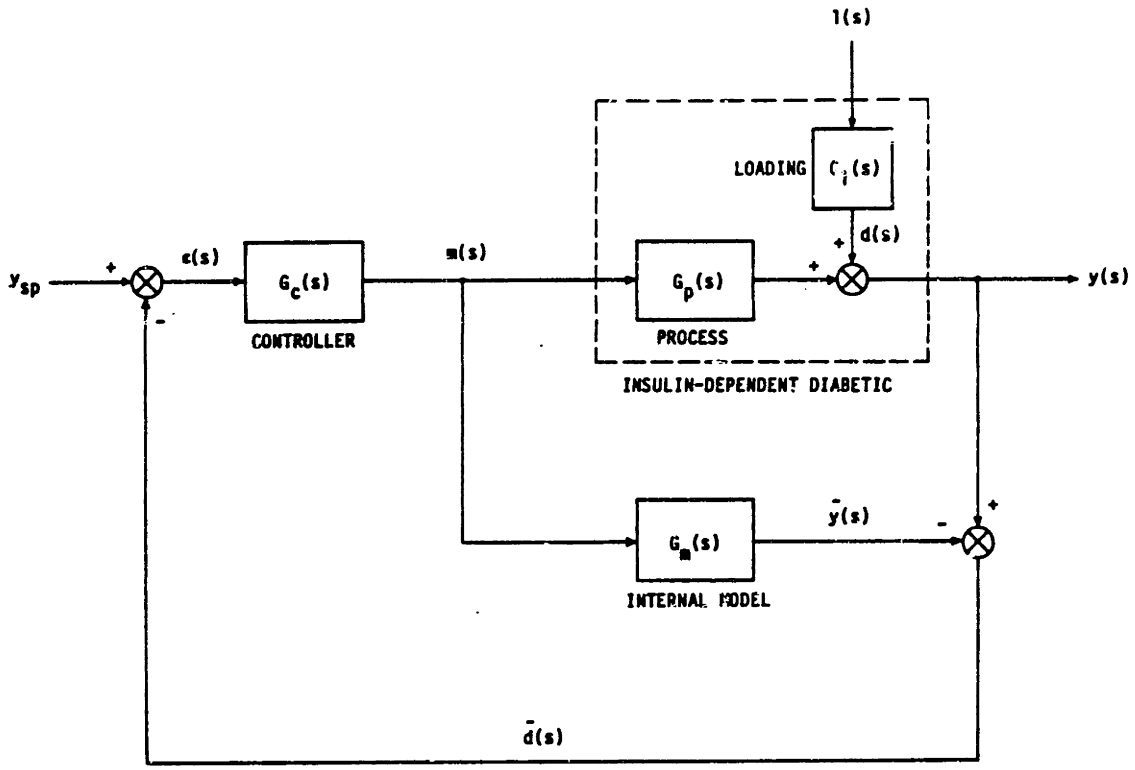

Fig. 105 Basic IMC structure for blood glucose regulation.

$m(t)$ = manipulated variable ($\mu U/kg \cdot min$)
= deviation in insulin infusion rate IR(t) from its basal rate IR_b
= $IR(t)-IR_b$

$l(t)$ = load (mg/min)
= rate of gut absorption of oral glucose

$d(t)$ = disturbance (mg/dl)
= contribution of gut glucose loading to $y(t)$

$\tilde{y}(t)$ = internal model prediction of $y(t)$ for $l(t)=d(t)=0$ (mg/dl)

y_{sp} = setpoint (mg/dl)
= desired value of $y(t)$
= 0 mg/dl

$\tilde{d}(t)$ = estimated disturbance (mg/dl)
= $y(t)-\tilde{y}(t)$

$\varepsilon(t)$ = error signal (mg/dl)
= $y_{sp}-\tilde{d}(t)$

Since control analysis is facilitated by use of time domain Laplace transformation (denoted by variable s), glucose concentration $y(t)$ and insulin infusion rate $m(t)$ were defined as deviation values such that all of the control variables in the loop assumed a value of zero at basal steady state. In the Laplace domain, the following transfer functions were defined (see Figure 105):

$G_m(s)$ = internal model transfer function
$= \frac{\tilde{y}(s)}{m(s)}$

$G_c(s)$ = controller transfer function
$= \frac{m(s)}{\varepsilon(s)}$

$G_p(s)$ = process transfer function
$= \frac{y(s)}{m(s)}$ for $l(s)=d(s)=0$

$G_l(t)$ = load transfer function

$$= \frac{d(s)}{l(s)}$$

As shown in Figure 105, IMC structure incorporates an internal model to compute $\tilde{y}(t)$, a prediction of what the observed variable y(t) would be as a result of changes in the manipulated variable m(t) under unloaded conditions. By subtracting $\tilde{y}(t)$ from the actual observation y(t), the resulting feedback signal $\tilde{d}(t)$ is an estimate of the disturbance d(t), the deviation in y(t) attributable to the presence of a load l(t). An error signal $\varepsilon(t)$ is taken as the difference between the setpoint y_{sp} and $\tilde{d}(t)$, and the controller changes the value of the manipulated variable m(t) on the basis of this error signal.

The dashed box in Figure 105 represents the insulin-dependent diabetic under closed-loop glycemic regulation, whose observed glycemia at any given time is determined by external changes in insulin infusion rate and the presence, if any, of oral glucose loading. For the purposes of designing and assessing an optimal controller in the present work, a physiologic model of the Type I (insulin-dependent) diabetic was employed to simulate in vivo glycemic response. The Type I diabetic model was obtained by removing endogenous pancreatic insulin release from the physiologic model of glucose metabolism and its regulation by insulin and glucagon as originally formulated for a normal 70 kg man. Since reversible diabetic abnormalities such as insulin resistance, insulin antibody binding, and impaired glucose counterregulation were not considered, the model was representative of a well-controlled, metabolically-normalized subject. Details of the formulation and verification of the physiologic models of glucose metabolism in nornal and Type I diabetic man are presented in Chapters II and V.

For interfacing of the Type I diabetic model with the control structure of Figure 105, observed glucose concentration was assumed to be that of peripheral venous blood, insulin infusion was routed intravenously, and the load corresponded to the rate of gut glucose absorption into the blood. For calculation of deviation variables, a basal peripheral venous blood glucose concentration G_b of 75 mg/dl was employed, as this represented the mean value of measurements accumulated from 267 ideal weight normal adults at the Joslin Research Laboratory, Boston; the basal insulin infusion rate IR_b to maintain the specified basal glycemia was 320 $\mu U/kg \cdot min$.

b) Process Characterization and the Internal Model

The internal model provides a simple input-output approximation of the process response to changes in the manipulated variable under unloaded conditions, or (see Figure 105)

$$G_m(s) \approx G_p(s) \tag{247}$$

The first step in designing the IMC control loop was to characterize the process transfer function $G_p(s)$ for use in the internal model.

The process transfer function relates in vivo glycemic response to changes in insulin infusion rate in the absence of glucose loading. In order to derive a suitable mathematical form for the process transfer function, open-loop "experiments" were performed with the diabetic model; step changes in the insulin infusion rate m(t) were input into the diabetic model and profiles for the time course of glycemic response y(t) were generated. A typical glycemic step-response profile is plotted in Figure 106. As commonly observed for many processes (Cohen and Coon, 1953), the step response curve had a sigmoidal shape that could be adequately approxi-

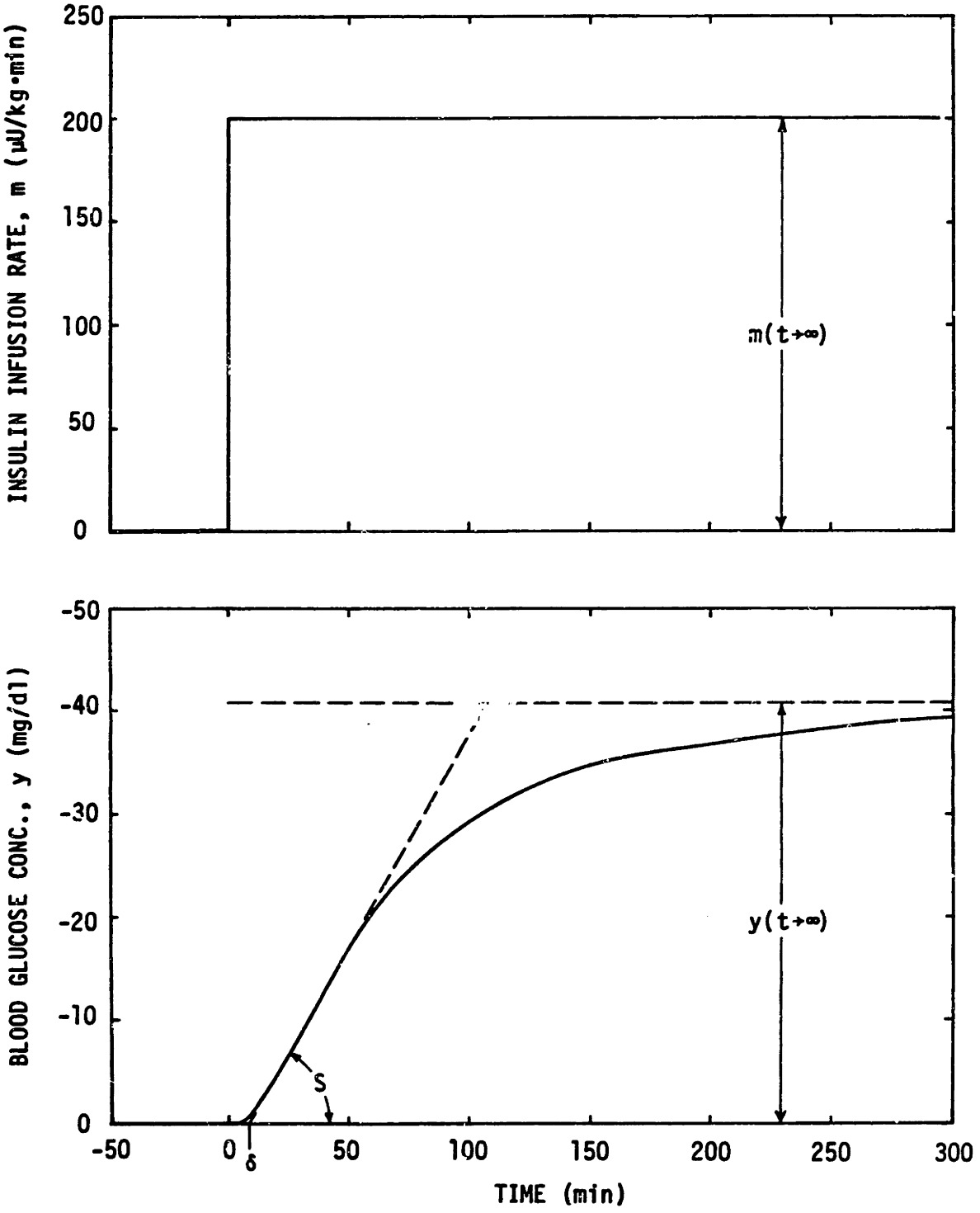

Fig. 106 Simulation of blood glucose concentration response to a step change in insulin infusion rate in the absence of glucose loading. Results were used to characterize the process of in vivo glycemic regulation.

mated by the response of a first-order system with dead time:

$$G(s) = \frac{Ke^{-\delta s}}{\tau s + 1} \tag{248}$$

where K = gain

τ = response time constant

δ = dead time

the parameters of which may be estimated from the sigmoidal step response curve according to (see Figure 106)

$$K = \frac{\text{steady state output}}{\text{steady state input}} = \frac{y(t \to \infty)}{m(t \to \infty)}$$

$$\tau = \frac{y(t \to \infty)}{S}, \text{ where } S \text{ is the slope of the inflection point tangent line}$$

δ = the abscissa intercept of the inflection point tangent line

Since in vivo regulation of glucose was known to be nonlinear with respect to insulinemia, step response curves were generated for insulin infusion step increases and decreases of varying magnitudes; resulting parameter values are summarized in Table 39. As would be anticipated, negative gain values were attained, indicating inverse steady state relationships between glucose concentration and insulin infusion rate, i.e. step increases in $m(t)$ yielded decreases in $y(t \to \infty)$, and vice versa. For large step inputs, the observed magnitutde of the response gain K_p decreased, presumably reflecting nonlinear saturation of insulin-stimulated glucose disposal at plasma insulin concentrations substantially removed from basal, whereas values of τ and δ remained relatively constant, implying similarity in the

Table 39. First-order response parameters for insulin infusion step changes of varying magnitudes as obtained by fitting of blood glucose concentration step response profiles as depicted in Figure 106.

$m(t \to \infty)$ ($\mu U/kg \cdot min$)	K $(mg/dl)(\mu U/kg \cdot min)^{-1}$	δ (min)	τ (min)
-200	-0.22	12	95
200	-0.21	10	92
400	-0.18	9.2	88
800	-0.09	7.9	75

response dynamics. For subsequent analysis, the linear model of Equation 248 was employed with the following fixed parameter values:

$$K_p = -0.21 \text{ (mg/dl)}(\mu\text{U/kg}\cdot\text{min})^{-1}$$

$$\tau_p = 90 \text{ min}$$

$$\delta_p = 10 \text{ min}$$

where the subscript p has been used to denote applicability to the process transfer function. These parameter values reflect linearization about the basal steady state (see Table 39), and this was assumed to be a valid first-order approximation over the operational ranges of interest.

The process transfer function thus established provided the internal model transfer function needed for IMC implementation:

$$G_m(s) = \frac{\tilde{y}(s)}{m(s)} = \frac{K_p e^{-\delta_p s}}{\tau_p s + 1} \tag{249}$$

Inversion of this expression from the Laplace domain yielded the equivalent internal model function relating $\tilde{y}(t)$ and m(t) in real time, given by

$$\tau_p \frac{d\tilde{y}(t)}{dt} + \tilde{y}(t) = K_p m(t-\delta_p) \tag{250}$$

3) Optimal Controller

Under the assumption that $G_m(s)=G_p(s)$ and that $G_p(s)$ is stable, it can be derived from optimal control theory that the sum of the squared errors is minimized for the regulator problem when the controller transfer function is given by the inverse of the process transfer function (Garcia and

Morari, 1982),

$$G_c(s) = \frac{1}{G_p(s)} \tag{251}$$

Because $G_c(s)$ must be stable, however, the following process transfer function factorization is introduced:

$$G_p(s) = G_-(s)G_+(s) \tag{252}$$

where $G_+(s)$ contains the time delays (their inversion would require a prediction) and the zeros outside the unit circle (their inversion would yield an unstable controller)(see Garcia and Morari, 1982). The optimal realizable controller is thus given by

$$G_c(s) = \frac{1}{G_-(s)} \tag{253}$$

For the process of glucose regulation in the diabetic, the process transfer function was given by

$$G_p(s) = \frac{K_p e^{-\delta_p s}}{\tau_p s + 1} \tag{254}$$

which upon factorization yielded

$$G_-(s) = \frac{K_p}{\tau_p s + 1} \tag{255}$$

$$G_+(s) = e^{-\delta_p s} \tag{256}$$

Here, $G_+(s)$ factored out the effect of the dead time δ_p in the glycemic

response to changes in the insulin infusion rate; inversion of $G_+(s)$ would have required the controller to have future knowledge (from time t to time $t+\delta_p$) of the time course of the insulin infusion rate. Although $G_+(s)$ contains the part of the process that limits achievable control quality, such limitations, inherently arising from the physical system under regulation, cannot be removed by any control system.

Finally, from Equations 253 and 255, the optimal controller was given by

$$G_c(s) = \frac{\tau_p s + 1}{K_p} \tag{257}$$

which upon inversion from the Laplace domain yielded

$$m(t) = \frac{\tau_p}{K_p} \frac{d\varepsilon(t)}{dt} + \frac{1}{K_p} \varepsilon(t) \tag{258}$$

Interestingly, by deriving the optimal controller via consideration of the inherent dynamics of in vivo glycemic regulation, the resulting optimal controller function incorporated proportional and derivative action with respect to the error signal $\varepsilon(t)$. The PD controller as given by Equation 258 is tuned for optimal performance within the IMC structure utilizing parameters directly provided by process characterization. Because the error signal fed to the IMC controller [$\varepsilon(t)=y_{sp}-d(t)$] differs from that employed in classical feedback control [in general, $\varepsilon(t)=y(t)-y_{sp}$], tuning of the PD controller in Equation 258 does not directly relate to selection of tuning parameters for a classical PD controller such as the one used by Shichiri et al. (see Equation 244).

For application of the optimal controller (Equation 258) to blood glu-

cose regulation, the following constraint was imposed:

$$m_{min} \leq m(t) \leq m_{max} \tag{259}$$

Regulation of in vivo glucose metabolism is a nonlinear process with respect to insulinemia; in particular, the incremental effectiveness of elevating peripheral insulin levels above about 100 μU/ml in stimulating increased glucose disposal rates diminishes rapidly (Mandarino and Gerich, 1984). Application of the linear controller of Equation 258 scheduling insulin delivery strictly on the basis of observed glycemia could thus induce circulating plasma insulin levels exceeding normally effective physiologic ranges, and the resulting exposure of the diabetic to such ineffective hyperinsulinemia could be detrimental to the maintenance of normal in vivo insulin responsiveness. In normal subjects, administation of a 100g OGTT (a rather large dose of oral glucose relative to normal mealtime intake) elicits a mean maximal venous plasma insulin concentration of about 100 μU/ml (Soeldner and Park, 1977); a value of m_{max} was thus imposed to constrain controller action such that peripheral venous insulin concentration would not exceed 100 μU/ml in the diabetic under closed-loop glycemic regulation. The maximum controller action m_{max} was assigned a value of 905 μU/kg•min, as this was the incremental infusion rate from basal predicted by use of the diabetic model to result in a venous plasma insulin concentration of 100 μU/ml. Since m(t) represents the deviation in insulin infusion rate IR(t) from its basal rate IR_b, the minimum controller action m_{min} was -320 μU/kg•min ($-IR_b$) such that IR(t) was limited to values greater than zero.

d) Summary of the Optimal IMC Equations

To summarize, process characterization and optimal control con-

siderations yielded the following relationships for implementing optimal IMC control of blood glucose concentration in the insulin-dependent diabetic:

Internal Model

$$\tau_p \frac{d\tilde{y}(t)}{dt} + \tilde{y}(t) = K_p m(t-\delta_p) \tag{260}$$

Optimal Controller

$$m(t) = \frac{\tau_p}{K_p} \frac{d\varepsilon(t)}{dt} + \frac{1}{K_p} \qquad m_{min} \leq m(t) \leq m_{max} \tag{261}$$

where $y(t)$ = deviation in blood glucose conc. $G(t)$ from its basal value G_b (mg/dl)
$= G(t) - G_b$
$\tilde{y}(t)$ = estimate of $y(t)$ in the absence of glucose loading (mg/dl)
$m(t)$ = deviation in insulin infusion rate $IR(t)$ from its basal rate IR_b (μU/kg·min)
$= IR(t) - IR_b$
$\varepsilon(t)$ = error signal $= y_{sp} - (y(t) - \tilde{y}(t))$

and y_{sp} = setpoint = 0 mg/dl
G_b = basal blood glucose conc. = 75 mg/dl
IR_b = basal insulin infusion rate = 320 μU/kg·min
m_{max} = maximum allowed value of $m(t)$ = 905 μU/kg·min
m_{min} = minimum allowed value of $m(t)$ = -320 μU/kg·min
K_p = process gain = -0.21 (mg/dl)(μU/kg·min)$^{-1}$
τ_p = process response time constant = 90 min
δ_p = process dead time = 10 min

The value of the maximal contraint imposed on Equation 261 was selected to limit peripheral venous plasma insulin concentration to 100 μU/ml.

C) Simulation Studies to Assess Optimal IMC Performance

Simulation studies using the Type I diabetic model were undertaken to assess optimal IMC performance in regulating glycemia during oral glucose loading. For computer simulations, the simultaneous first-order differential equations of the IMC internal model (Equation 260) and the diabetic model (see Chapter V) were solved numerically using fourth-order Runge-Kutta integration with a time step of 0.1 min.

Intestinal absorption of glucose occurs via active transport of glucose across the intestinal mucosa, a process that may be rate-limited by intralumenal diffusion and/or carrier availability (Wilson, 1962; Csaky, 1975). Initiation of gastric emptying of a large glucose load can lead to effective saturation of the intestinal absorption mechanism (Langerlof et al., 1976). The maximal rate of gut glucose absorption in man is about 800 mg/min, based on analysis of intestinal perfusion data (Hillman, 1977), interpretation of in vivo double tracer studies (Radziuk et al., 1978; Pilo et al., 1981), and simulation studies using physiologic models of glucose metabolism (Cobelli et al., 1983; see simulation of the 100g OGTT in Chapter IV). Thus, a viable closed-loop insulin delivery system must acceptably minimize blood glucose variations caused by gut glucose loading rates which may arbitrarily vary with time over a range of 0 to 800 mg/min.

Presented in Figure 107 are results of simulation studies to evaluate optimal controller regulation of gut glucose step loading. Simulations were performed for gut glucose load rate step inputs of 100, 400, and 800 mg/min (upper panel). The optimal controller action regulated glycemia within a narrow range (center panel), with blood glucose concentration peaking at a value of about 120 mg/dl in response to the maximal gut load rate of 800 mg/min. For gut load rates in excess of 400 mg/dl, a nonzero

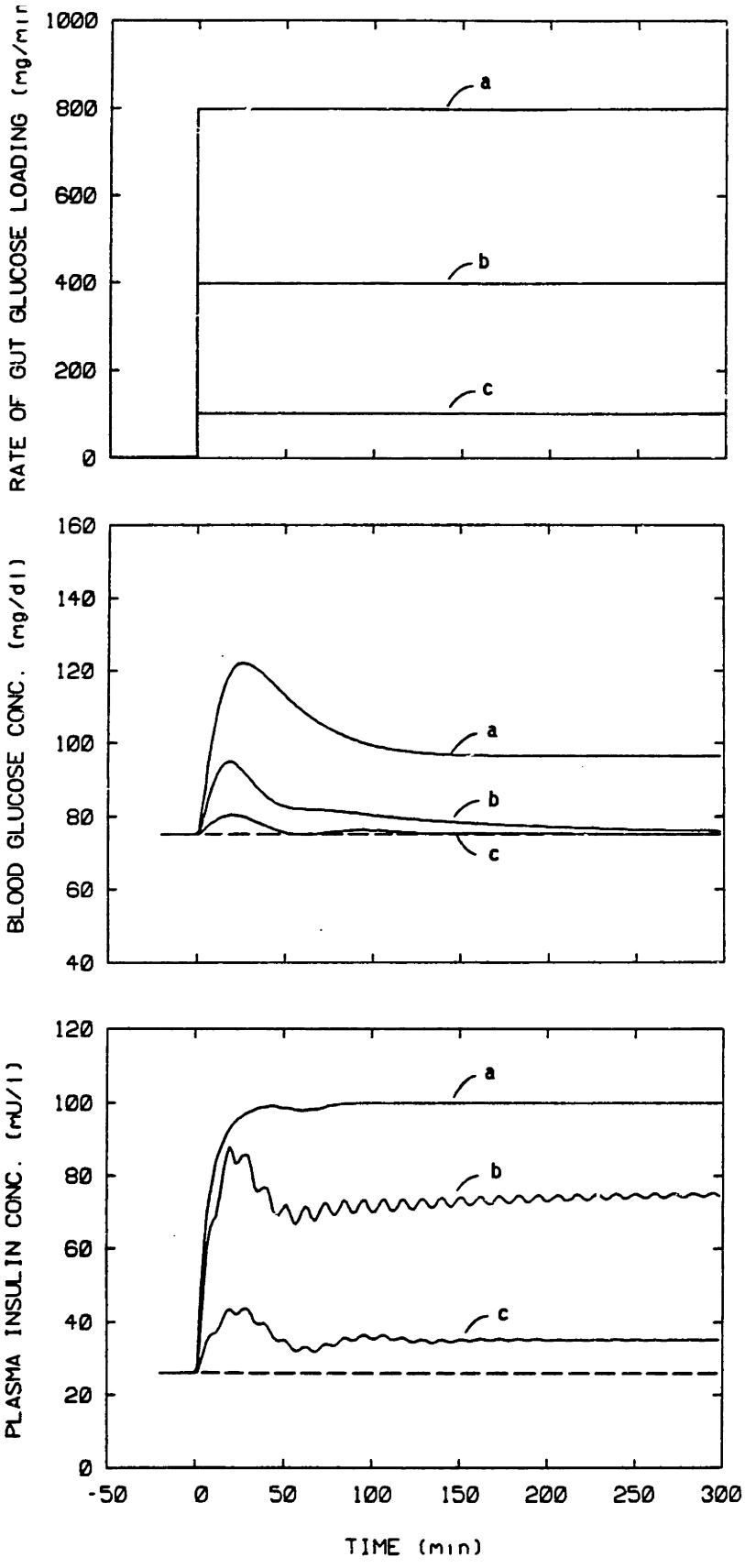

Fig. 107 Simulated blood glucose and plasma insulin responses to step inputs in gut glucose load rate resulting from optimal closed-loop insulin delivery.

steady state offset from basal glycemia resulted. The observed offset implied that use of a fixed gain, a linear approximation, did not precisely compensate for nonlinearities of actual in vivo glucose response under conditions most removed from basal. Although logic providing for on-line gain adjustment (nonlinear control) could have been introduced to eliminate the steady state glycemic offset, introducing the additional complexities of such an approach was deemed unjustified since maintenance of blood glucose concentration below 100 mg/dl would be quite acceptable under such extreme load conditions. Simulated plasma insulin response profiles resulting from optimal controller action are presented in the lower panel of Figure 107. The maximal step loading just saturated controller insulin delivery as evidenced by plateauing of the resulting plasma insulin concentratin response at a value of 100 μU/ml. It is interesting that, at lesser gut load rates, interaction of the process dead time and controller derivative action produced transient ascillations (period ~ 11 min) in plasma insulin level that damped with time. Regular oscillations have been observed in plasma insulin concentration profiles in normal man; these oscillations have a mean period of 13 min with a mean amplitude of 1.6 μU/ml under basal conditions (Lang et al., 1979) and persist with the same period but increased amplitude during intravenous glucose loading (Mathews et al., 1983). However, neither the physiologic importance of this phenomenon nor its driving force have as yet been fully elucidated (Verdin et al., 1984).

Although closed-loop insulin delivery is primarily directed toward minimizing hyperglycemic excursions following oral glucose ingestion, hypoglycemic excursions are potentially dangerous, and thus the regulatory characteristics of the controller must also avoid inducement of hypoglycemia. In order to assess optimal controller effectiveness in averting

serious hypoglycemia, a worst case scenario was simulated as shown in Figure 108. A continuous maximal rate of gut glucose loading was first imposed for a period of 150 min to elicit high levels of circulating insulin, then the glucose loading was acutely withdrawn. Upon termination of glucose loading, blood glucose concentration began to decrease rapidly. Controller action quickly modulated insulin delivery, however, such that the resulting maximum glycemic undershoot was only about 15 mg/dl below basal glucose concentration, thus maintaining absolute blood glucose levels above 60 mg/dl. Since hypoglycemic excursions to 60 mg/dl are commonly observed in normal subjects following oral glucose (Soeldner and Park, 1977), the above simulation study suggested that implementation of the optimal controller would not evoke hyperglycemia in excess of acceptable limits.

Having assessed controller performance with respect to the extremes of step loading, it was desirable to study how optimal closed-loop insulin delivery would control glycemia during a more physiologic temporal patterning of gut glucose loading. For this purpose, optimal controller regulation of the 100g OGTT was simulated (Figure 109). The gut glucose absorption rate profile employed for OGTT simulation (upper panel) was that originally derived from the study of glucose-insulin relationships observed in normals using the physiologic model of glucose metabolism in normal man (see simulation of the 100g OGTT in Chapter IV). In Figure 109, simulated blood glucose and plasma insulin profiles resulting from optimal controller action are compared with clinical data correlated from 100g OGTTs administered to a population of 145 ideal weight normal adult males at the Joslin Research Laboratory, Boston. Optimal closed-loop insulin delivery resulted in glycemic regulation comparable to that observed in normal man.

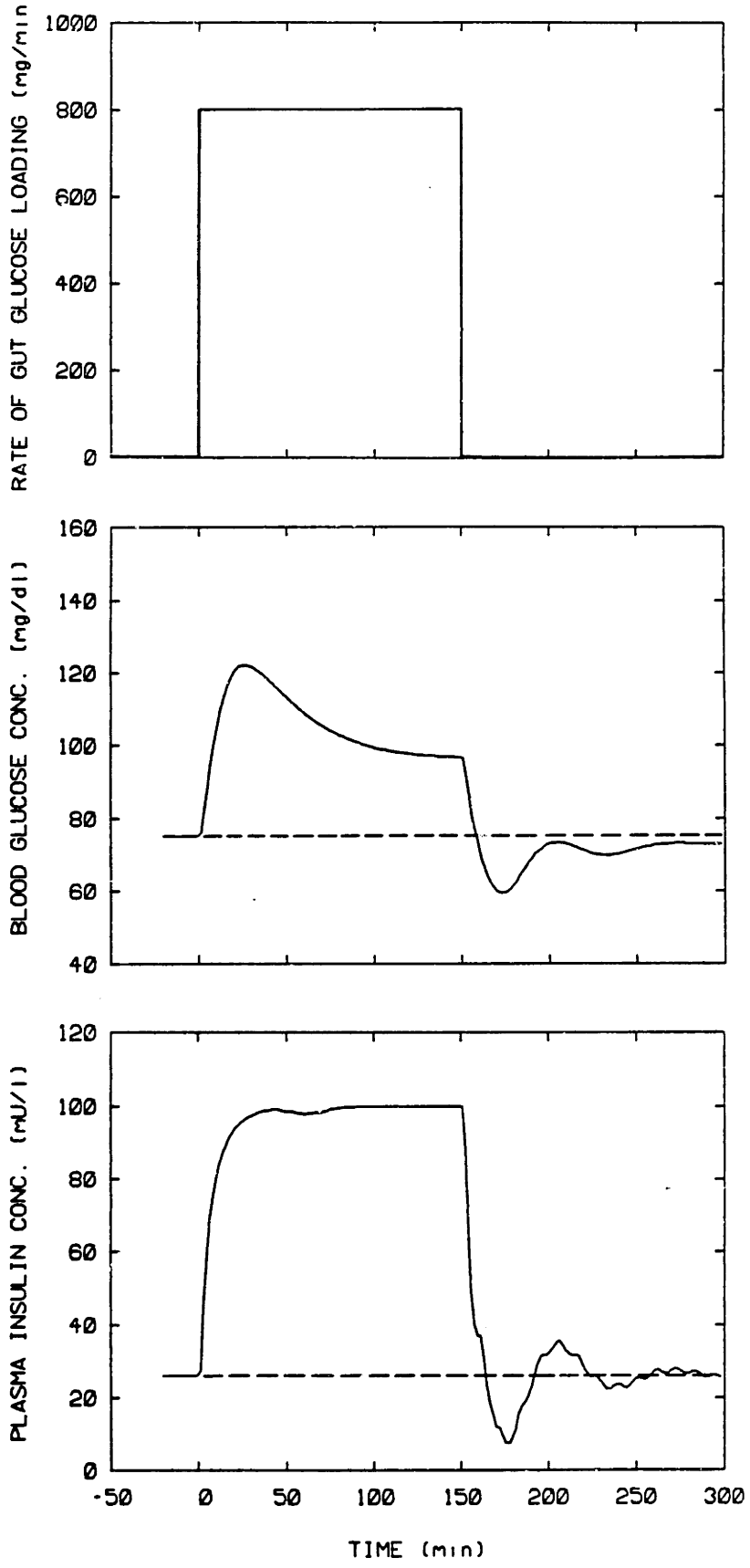

Fig. 108 Simulations to assess optimal controller performance in minimizing hypoglycemic excursions.

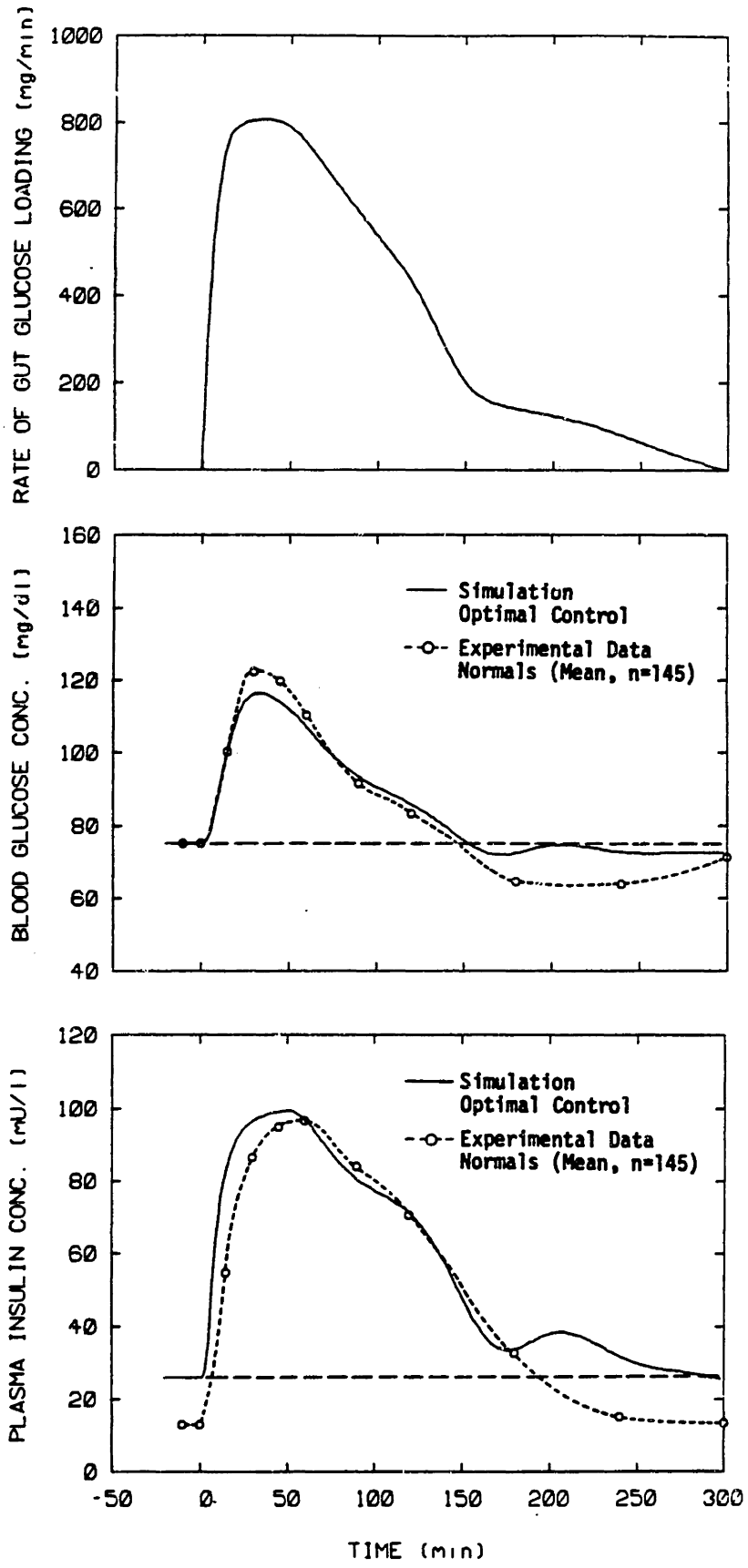

Fig. 109 Simulation study to assess optimal closed-loop control of the 100g OGTT. Blood glucose and plasma insulin response data in normal (nondiabetic) subjects has been included for comparison with respective simulated responses resulting from optimal controller action. (Experimental data from the Joslin Research Laboratory, Boston)

In addition, controller action generated a plasma insulin response that was quite similar to that normally resulting from endogenous pancreatic insulin release in the nondiabetic. (It should be noted that the offset between basal steady state insulin levels results because in normal man, the pancreas maintains basal glycemia by means of intraportal insulin release, whereas in the diabetic, basal glycemia is maintained by peripheral insulin delivery.) The similarity between optimal control and normal in vivo glycemic regulation was extremely interesting, interpretable in one of two ways: 1) assuming the normal pancreas represents a natural biological optimal controller, the physiologic model employed in the present study must have been a good representation of in vivo glucose metabolism, as its use for process characterization dictated optimal control behavior; or conversely, 2) assuming the physiological model was a good representation of in vivo glucose metabolism, the pancreas must have evolved as an optimal biological controller for the process of glucose metabolism.

4) Discussion

Through application of IMC methods, an optimal control scheme for blood glucose regulation was derived from consideration of characterizing the process of in vivo glycemic response to changes in insulin infusion rate. The resulting IMC structure offers mathematical simplicity, as its implementation only requires on-line integration of the linear first-order ordinary differential equation which constitutes the internal model (Equation 260) and calculation of insulin delivery rate from the PD controller (Equation 261). The effectiveness of optimal IMC was demonstated through simulation studies, and results suggested that optimal IMC is quite similar to the physiologic control provided by normal

pancreatic action in the nondiabetic.

In reviewing development of the algorithm of Albisser et al. (Equations 231-234) and the work of Clemens et al. leading to the control equations presently employed in the Biostator GCIIS (Equations 239-243), it became apparent that selection of the basic controller functionalities used in these control systems was loosely based on a combination of physiologic reasoning and experience gained from clinical trials. The insulin infusion algorithms that evolved as a result are rather complex, highly nonlinear formulations incorporating a number of tuning parameters for which values were attained by ad hoc means through clinical experimentation. The approach of Shichiri et al. was somewhat different and led to development of a PD controller (Equation 244) which resembles that obtained in the present study. Shichiri et al. derived the PD control functionality and based its tuning on analysis of glucose-insulin relationships observed during glucose loading in normal man. It is interesting that similar controller functions were attained by Shichiri et al. from studying the behavior of an assumed functional optimal controller, the pancreas, and from the present work applying optimal control analysis to the system being regulated, in vivo glucose metabolism.

Whether optimal performance has been attained from the controllers reported in the literature to date is unclear. Broekhuyse et al. (1981) input the same glucose profile to a number of established insulin infusion algorithms (including those of Albisser et al., Clemens et al., and the PD controller of Fischer et al.) and reported similarity between resulting insulin infusion responses despite the apparent diversity of the various algorithm functionalities. The optimal controller derived in this chapter thus may not provide for radical improvement in achievable blood glucose

regulation in the context of present applications, although its mathematical simplicity relative to most other algorithm formulations is certainly an attractive feature.

Emphasis must be placed, however, on the notion that existing applications of glucose-controlled insulin delivery (e.g the Biostator GCIIS) may reflect relatively ideal conditions compared with those which may be encountered in extending closed-loop insulin delivery to long-term implantable applications. In particular, glucose sensors used in present bedside systems provide minute-to-minute measurements, have response times on the order of one minute, and are quite accurate (if calibrated on a frequent basis). In contrast, implantable glucose sensors suitable for long-term in vivo applications will probably exhibit less ideal performance characteristics, thus requiring suitable control systems to function in the presence of less ideal glucose monitoring. Adaptation of the literature algorithms for use with less ideal sensors is not straightforward. In the best case, trial and error parameter readjustment may provide adequate compensation for some types of sensor nonidealities. It is quite possible, however, that the basic functional structures of these algorithms might be incompatible with certain types of sensor-induced feedback dynamics, in which case instabilities could develop and simple parameter readjustment would not prove satisfactory. In addition, since it is a good assumption that the normal pancreas can monitor blood glucose in a manner approaching ideality relative to man-made sensors, analysis of glusose-insulin relationships in normal man cannot be extended to provide insight into methods of coping with problems associated with control in the presence of nonideal glucose monitoring. IMC provides a straightforward approach to consideration of nonideal glucose measurement effects, however, and the power

of this approach will be demonstated in the next section as analysis is extended to explore optimal control in the presense of nonideal glucose sensing.

B) Effects of Measurement Characteristics on the Quality of Control

1) Background

Problems associated with development of a suitable glucose sensor have retarded progress towards a totally implantable glucose-controlled insulin delivery system. It is likely that the ultimate performance of implantable systems will be limited by the operational characteristics of the sensor component. We begin with a brief overview of glucose sensors, their measurement characteristics, and other problems related to in vivo glucose monitoring.

There are basically three types of glucose sensors under development, enzymatic, electrocatalytic, and affinity. The enzymatic glucose sensor is based on the oxidation of glucose by disolved oxygen in the presence of glucose oxidase:

$$\text{glucose} + O_2 + H_2O \xrightarrow{\text{glucose oxidase}} H_2O_2 + \text{gluconic acid} \qquad (262)$$

Glucose measurement is made by virtue of decreases in pO_2, increases in pH, or production of hydrogen peroxide. The electrocatalytic glucose sensor employs a platinum anode to catalyze the direct electrochemical oxidation of glucose:

$$\text{Anode:} \quad C_6H_{12}O_6 \xrightarrow{\text{platinum}} C_6H_{10}O_6 + 2H^+ + 2e^- \qquad (263)$$

$$\text{Cathode:} \quad \frac{1}{2}O_2 + H_2O + 2e^- \xrightarrow{\text{platinum}} 2OH^- \qquad (264)$$

Measurement of glucose is based on the potential difference and current flow between a working electrode and reference or counter electrodes. The affinity sensor is based on the competitive binding of glucose and fluoroscein-labeled dextran with specific receptor sites on immobilized concanavalin A. Measurement is made by optical detection of the unbound dextran label (Schultz et al., 1982).

At present, the enzymatic sensor is the most highly advanced and has been utilized in all of the bedside-type glucose-controlled insulin delivery systems to date. The most widely used and comercially successful enzymatic sensor has been the Clark-type glucose sensor (Clark, 1970) which employs polarographic detection of hydrogen peroxide oxidation catalyzed by a platinum electrode. This is the type of glucose sensor used in the Biostator GCIIS glucose sensing module (Santiago et al., 1979; Oberhardt et al., 1982). Other configurations of glucose oxidase sensors suitable for direct intravascular or subcutaneous applications are under development, including the needle-type sensor of Shichiri et al. (1983), the catheter-tip sensor of Clark and Duggan (1982), and the implantable oxygen electrode design of Kondo et al. (1982).

In general, the enzymatic glucose sensor offers good accuracy and rapid response characteristics. In reviewing a number of enzymatic sensors emplying various detection methods, Thevenot (1982) concluded that in vitro glucose determinatins seemed relatively easy to perform with an accuracy of 2-5% over glucose concentration ranges of physiologic interest. Guilbault (1982) compared in vitro response times of various enzymatic glucose sensors and reported values generally ranging between 1-10 min. It should be noted, however, that data such as the above reflect in vitro measurement characteristics, and thus may not be achievable under less

ideal in vivo conditions where, for example, local glucose availability (glucose is consumed by sensors), oxygen availabilty, or changes in pO_2 could effect sensor response. The major problem with the immobilized enzyme glucose sensor is that of long-term stability, as glucose oxidase is subject to mechanical, chemical, and enzymatic denaturation (Thevenot, 1982). Stability problems make enzymatic sensors susceptible to measurement drift. To date, long-term stability of enzymatic sensors has not been adequately studied in human fluids or tissues at 37° C. Experience with the Biostator GCIIS sensor, however, has indicated a limited sensor lifetime of up to 200 h and a need for frequent calibration (Oberhardt et al., 1982). Shichiri et al. (1983) reported that output current from their needle-type glucose sensor decreased 24% over 168 h of incubation in albumin-saline solution. Obviously, future improvements will be necessary before chronic implantation of enzymatic glucose sensors becomes feasible.

Electrocatalytic glucose sensors are being developed by a number of groups, including Lewandowinski et al. (1982), Richter et al. (1982), and Lerner et al. (1981; 1982). The electrochemical approach to glucose sensing offers a great advantage over enzymatic sensors with respect to the promise of long-term stability. In particular, the platinum electrode surface of the electrocatalytic sensor can be rejuvenated in situ by dedicating a portion of the elctrode potential cycling to surface oxidation to prevent surface poisoning, thus preserving catalytic activity (Richter et al., 1982; Lerner et al., 1982). The major problem with electrocatalytic sensors, however, is their susceptibility to interference in glucose measurement caused by co-reaction of physiologic agents, primarily amino acids and urea. For the sensor of Lerner et al. (1982), a physiologic change in amino acid concentration from 35 to 65 mg/dl caused a 25%

variation in glucose determination at 50 mg/dl of glucose, and 10% variation in glucose determination at glucose concentrations greater than about 125 mg/dl. Richter et al. (1982) reported an error of approximately 20% resulted from variation of urea concentration over a physiologic range. With respect to response time, the electrocatalytic sensor design of Richter et al. (1982) required about 17 min (20 cycles) to yield a steady state response following a step change in glucose concentration. To date, dynamic response data for other electrocatalytic sensors have not been reported in the literature.

The affinity sensor using optical glucose detection is being developed by Schultz et al. (1982). In vitro feasibility studies with a prototype design demonstrated reasonable glucose sensitivity over physiologic concentration ranges with a measurement response time on the order of 10 min. The affinity sensor offers a promising approach, but future work will be required to produce a viable implantable glucose sensor using this technology.

Independent of the approach employed for glucose sensing, certain other issues complicate in vivo glucose monitoring. Sensor placement in the subcutaneous or intraperitoneal environment may be advantageous over intravascular placement to avoid the hazards of intravascular thrombosis, and glucose concentration measurements at these possible sensor implant sites have suggested their feasibility (Wolfson et al., 1982). Relative to the vascular environment, however, absolute glucose concentrations are lower and dynamic response times are increased at these alternative monitoring sites. Shichiri et al. (1983) reported that glucose concentrations in subcutaneous tissues (forearm or abdomen) were 10% lower but highly correlated with blood glucose concentrations in the range of about 50-400

mg/dl. Furthermore, the mean rise time in output of the needle-type glucose sensor (intrinsic response time of 29 s) inserted into subcutaneous tissue was 5.1 min relative to changes in blood glucose concentration. Thus, extravascular sensing can add effective response time to glucose monitoring relative to that achievable by direct vascular access. Biocompatibility issues may also influence the quality of in vivo glucose monitoring, as so-called "protein fixation" (Shichiri et al., 1984) and fibroblast encapsulation could reduce sensitivity and increase response time of the implanted sensor. Shichiri et al. (1984) noted protein fixation on membranes of sensors kept in subcutaneous tissue for 72 h, and reported that 96 h of implantation prolonged the in situ sensor response time from 5.1 to 13.5 min relative to blood glucose concentration changes.

Although the quality of achievable in vivo glucose monitoring has yet to be determined by future research, it appears likely that glucose-controlled insulin delivery devices will have to rely on nonideal glucose measurements. To date, the only study to assess the effects of nonideal glucose measurement on closed-loop glycemic regulation was reported by Sorensen et al. (1982). Using a physiologic model of glucose metabolism developed by Guyton et al. (1978; Guyton, 1973) as adapted for oral glucose loading by Hillman (1977), simulations of OGTTs were repeated while glucose measurement dead time was varied from 1.5 to 30 min. An insulin infusion algorithm from the literature, the hyperbolic tangent infusion algorithm of Albisser et al.(see Equations 231-232,234) using projected glucose values as proposed by Botz (see Equation 235), was employed for calculation of insulin infusion rate. Results indicated that increased measurement dead time decreased the quality of glycemic regulation as initial delays in insulin response allowed greater hyperglycemic excursions. It should be

noted, however, that the issue of optimality was not addressed in the above study, neither with respect to the basic form of the infusion algorithm nor with respect to its tuning.

The purpose herein is to extend the previous discussion of optimal control in order to examine in a very broad sense the degree to which non-ideal glucose sensor characteristics limit the quality of achievable glycemic regulation.

2) Optimal IMC With Nonideal Process Observation

Analysis of optimal IMC implimentation is now extended to incorporate the possibility of nonideal process observation. As shown in Figure 110, a glucose sensor process transfer function $G_s(s)$ is inserted into the basic IMC structure to characterize the relationship between actual deviations in blood glucose concentration from basal $y(s)$ and that measured by the glucose sensor $y_m(s)$,

$$G_s(s) = \frac{y_m(s)}{y(s)} \tag{265}$$

Optimal control analysis parallels that presented earlier if a new "process" is defined as follows:

$$G_p^*(s) = G_p(s)G_s(s) \tag{266}$$

Here, the "process" $G_p^*(s)$ relates changes in insulin infusion rate $m(s)$ to measured glucose response $y_m(s)$ under unloaded conditions ($l(s)=d(s)=0$), and thus includes consideration not only of the actual process being regulated but also of the characteristics of the glucose sensor used to observe it.

Using variables as defined previously but employing a superscript *

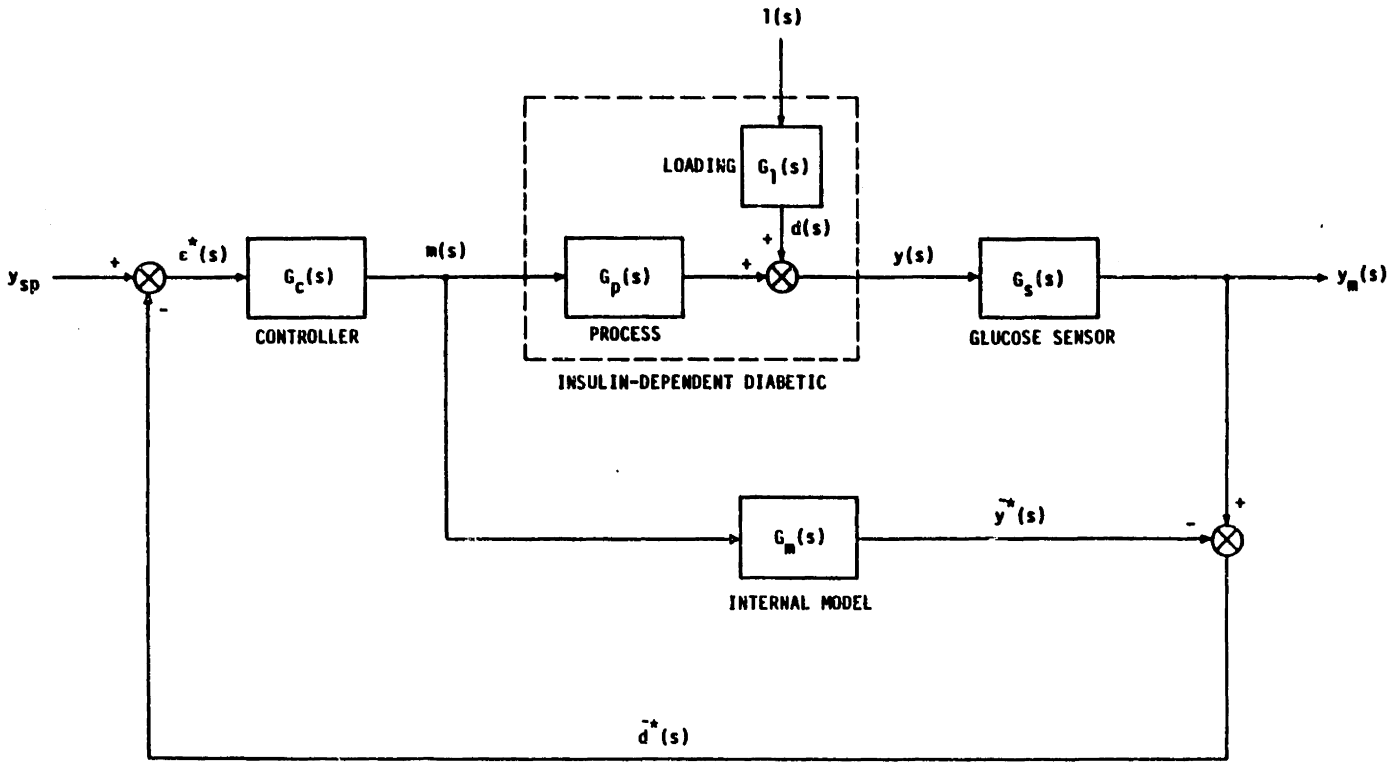

Fig. 110 Extension of basic IMC structure to include a glucose sensor measurement element. (Compare with Figure 105)

notation to imply reference to "process" $G_p^*(s)$ (compare Figures 105 and 110), the internal model transfer function becomes

$$G_m(s) = \frac{\tilde{y}^*(s)}{m(s)} \tag{267}$$

and, in analogy to previous optimal controller development, is approximated by

$$G_m(s) \approx G_p^*(s) \tag{268}$$

The optimal controller is given by

$$G_c(s) = \frac{1}{G_-^*(s)} = \frac{m(s)}{\varepsilon^*(s)} \tag{269}$$

where $G_-^*(s)$ results from the factorization

$$G_p^*(s) = G_-^*(s)G_+^*(s) \tag{270}$$

and represents the portion of $G_p^*(s)$ which upon inversion yields a stable, realizable controller.

The above approach accounts for stability and optimality of control in the presence of nonideal process observation. For the ideal glucose sensor,

$$G_s(s) = \frac{y_m(s)}{y(s)} = 1 \tag{271}$$

and the analysis reduces to the case of optimal control presented earlier.

3) Simulation Studies to Assess Effects of Nonideal Measurement on Optimal IMC Performance

Simulation studies were undertaken using the Type I (insulin-dependent) diabetic model under 100g OGTT loading to assess the effects of glucose sensor measurement characteristics on optimal IMC glycemic regulation. For these simulation studies, glucose measurement characteristics were defined by selection of the glucose sensor transfer function $G_s(s)$, and the internal model and controller transfer functions were appropriately modified to achieve stable, optimal control. The purpose here was to evaluate how the quality of optimal glycemic regulation degrades as closed-loop control is increasingly driven by the sensor response $G_s(s)$ rather than the real process response $G_p(s)$.

a) Sensor Dead Time

The glucose sensor transfer function corresponding to a system with measurement dead time is given by

$$G_s(s) = e^{-\delta_s s} \tag{272}$$

where δ_s = sensor dead time (min)

The internal model transfer function in this case becomes

$$G_m(s) = G_p^*(s) = G_p(s)G_s(s) \tag{273a}$$

$$= \left(\frac{K_p e^{-\delta_p s}}{\tau_p s + 1}\right)\left(e^{-\delta_s s}\right) \tag{273b}$$

$$= \left(\frac{K_p e^{-(\delta_p+\delta_s)s}}{\tau_p s + 1}\right) \tag{273c}$$

and thus the internal model incorporates the sum of the process and sensor dead times. Factorization of Equation 273c yields

$$G_-^*(s) = \frac{K_p}{\tau_p s + 1} \tag{274}$$

$$G_+^*(s) = e^{-(\delta_p+\delta_s)s} \tag{275}$$

from which the optimal controller is then given by

$$G_c(s) = \frac{1}{G_-^*(s)} = \frac{\tau_p s + 1}{K_p} \tag{276}$$

The resulting optimal controller is the same as that previously derived for the case of ideal process observation (Equation 257), since sensor dead time, like process dead time, only contributes to the noninvertible portion of the process factorization $G_+^*(s)$. Inverting the above equations from the Laplace domain to real time gives the following IMC relationships:

Glucose Sensor

$$y_m(t) = y(t-\delta_s) \tag{277}$$

Internal Model

$$\tau_p \frac{d\tilde{y}^*(t)}{dt} + \tilde{y}^*(t) = K_p m(t-\delta_p-\delta_s) \tag{278}$$

Optimal Controller

$$m(t) = \frac{\tau_p}{K_p} \frac{d\varepsilon^*(t)}{dt} + \frac{1}{K_p} \varepsilon^*(t) \qquad m_{min} \leq m(t) \leq m_{max} \tag{279}$$

Simulation studies were performed to assess the effects of glucose sensor dead time on the quality of achievable glycemic regulation as shown in Figure 111. The diabetic model was employed to simulate blood glucose and plasma insulin responses during the 100g OGTT while glucose sensor dead time δ_s was varied from 0 to 60 min in the optimal IMC equations. Results of the study showed that increasing the sensor dead time increased the delay in the initial response of insulin to rising blood glucose concentration causing larger and larger hyperglycemic excursions. Sensor dead time variation did not contribute to inducement of significant hypoglycemic excursions, however. As could be anticipated, for sensor dead time values much less than the process response time,

$$\delta_s << \tau_p \quad (= 90 \text{ min}) \tag{280}$$

or $$\delta_s \lesssim 9 \text{ min} \tag{281}$$

the impact of sensor dead time on degrading the quality of blood glucose control was quite minimal.

b) Sensor Response Time

A glucose sensor may not instantaneously respond to a step change in surrounding glucose concentration, but rather may require a finite time for its output to reflect fully a step input. With respect to sensor design, response time is associated with the time required for diffusion of glucose

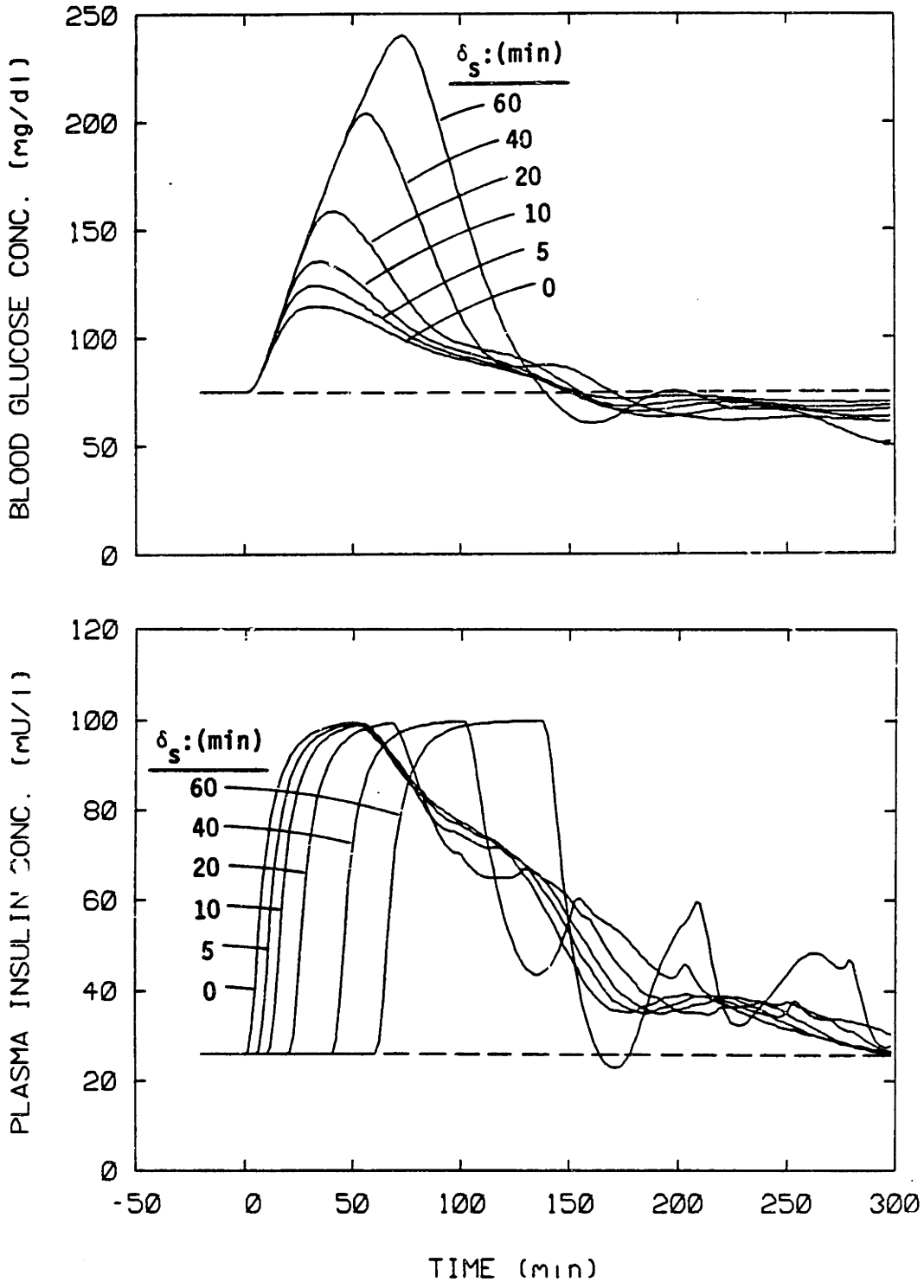

Fig. 111 Simulation studies to assess the effects of sensor dead time on achievable glycemic control during the 100g OGTT. The diabetic model was used to predict blood glucose and plasma insulin response profiles while sensor dead time δ_s was varied from 0-60 min.

across membranes coupled with intrinsic sensor measurement response kinetics. In addition, an apparent sensor response time can be induced by external factors, such as in vivo protein fixation to sensor membranes or tissue encapsulation of the sensor implant causing additional transport resistance. Furthermore, as previously discussed, subcutaneous sensing increases sensor response time relative to that obtained by direct vascular access.

In order to study the effects of glucose sensor response time on closed-loop glycemic control, a simple first-order response model was employed for the glucose sensor transfer function:

$$G_s(s) = \frac{1}{\tau_s s + 1} \tag{282}$$

where τ_s = sensor response time constant (min)

Output from such a sensor would reflect 63% of a step change input in one time constant τ_s. The internal model transfer function in this case becomes

$$G_m(s) = G_p^*(s) = G_p(s)G_s(s) \tag{283a}$$

$$= \left(\frac{K_p e^{-\delta_p s}}{\tau_p s + 1}\right)\left(\frac{1}{\tau_s s + 1}\right) \tag{283b}$$

$$= \left(\frac{K_p e^{-\delta_p s}}{(\tau_p s + 1)(\tau_s s + 1)}\right) \tag{283c}$$

Factorization of Equation 283c yields

$$G_-^*(s) = \frac{K_p}{(\tau_p s + 1)(\tau_s s + 1)} \tag{284}$$

$$G_+^*(s) = e^{-\delta_p s} \tag{285}$$

from which the resulting optimal controller is given by

$$G_c(s) = \frac{1}{G_-^*(s)} = \frac{(\tau_p s + 1)(\tau_s s + 1)}{K_p} \tag{286}$$

Inversion of the above expressions from the Laplace domain to real time yields the following IMC relationships:

Glucose Sensor

$$\tau_s \frac{dy_m(t)}{dt} + y_m(t) = y(t) \tag{287}$$

Internal Model

$$\tau_p \tau_s \frac{d^2\tilde{y}^*(t)}{dt^2} + (\tau_p + \tau_s)\frac{d\tilde{y}^*(t)}{dt} + \tilde{y}^*(t) = K_p m(t-\delta_p) \tag{288}$$

Optimal Controller

$$m(t) = \frac{\tau_p \tau_s}{K_p}\frac{d^2\varepsilon^*(t)}{dt^2} + \frac{(\tau_p+\tau_s)}{K_p}\frac{d\varepsilon^*(t)}{dt} + \frac{1}{K_p}\varepsilon^*(t) \quad m_{min} \leq m(t) \leq m_{max} \tag{289}$$

The above equations represent a rigorous treatment. Because the sensor response time transfer function $G_s(s)$ does not contribute to the noninvertible factorization $G_+^*(s)$ of the process transfer function $G_p^*(s)$, the optimal controller of Equation 289 provides complete mathematical compensation for the presence of sensor response time. Thus, use of the above

IMC relationships for sensors with finite response times τ_S yields blood glucose regulation identical to that obtained for the ideal case of instantaneous sensor response time (τ_S=0).

Although rigorous treatment can provide complete, ideal compensation for sensor response time, this introduces second-order derivative terms (dencted by dashed underlines) into the internal model (Equation 288) and controller (Equation 289). In practical applications, use of second-order derivative terms in the control loop equations may not be desirable due to problems associated with their accurate on-line calculation in real systems and because use of the second-order derivative terms makes control action particularly sensitive to sensor modeling inaccuracies such as inexact matching of true sensor response time and that assumed for the sensor in the control equations (note that τ_S multiplies τ_p in the second-order derivative terms of the above IMC control equations).

Since implementation of the second-order IMC sensor response compensation equations could present practical difficulties, studies were undertaken to examine the quality of suboptimal blood glucose regulation that would result with first-order response time compensation. Results of simulations to assess the effects of first-order sensor response time compensation on blood glucose regulation during the 100g OGTT are presented in Figure 112. Sensor response time τ_S was varied from 0-120 min in Equations 287-289 while the second-order derivative terms in the IMC internal model (Equation 288) and controller (Equatior 289) were neglected; it may be noted that the presence of sensor response time τ_S thus entailed use of an effective response time of $\tau_p+\tau_S$ in the resulting first-order control loop equations. Unlike the case of sensor dead time (see Figure 111) which caused a pure lag in initial insulin response, increased sensor response

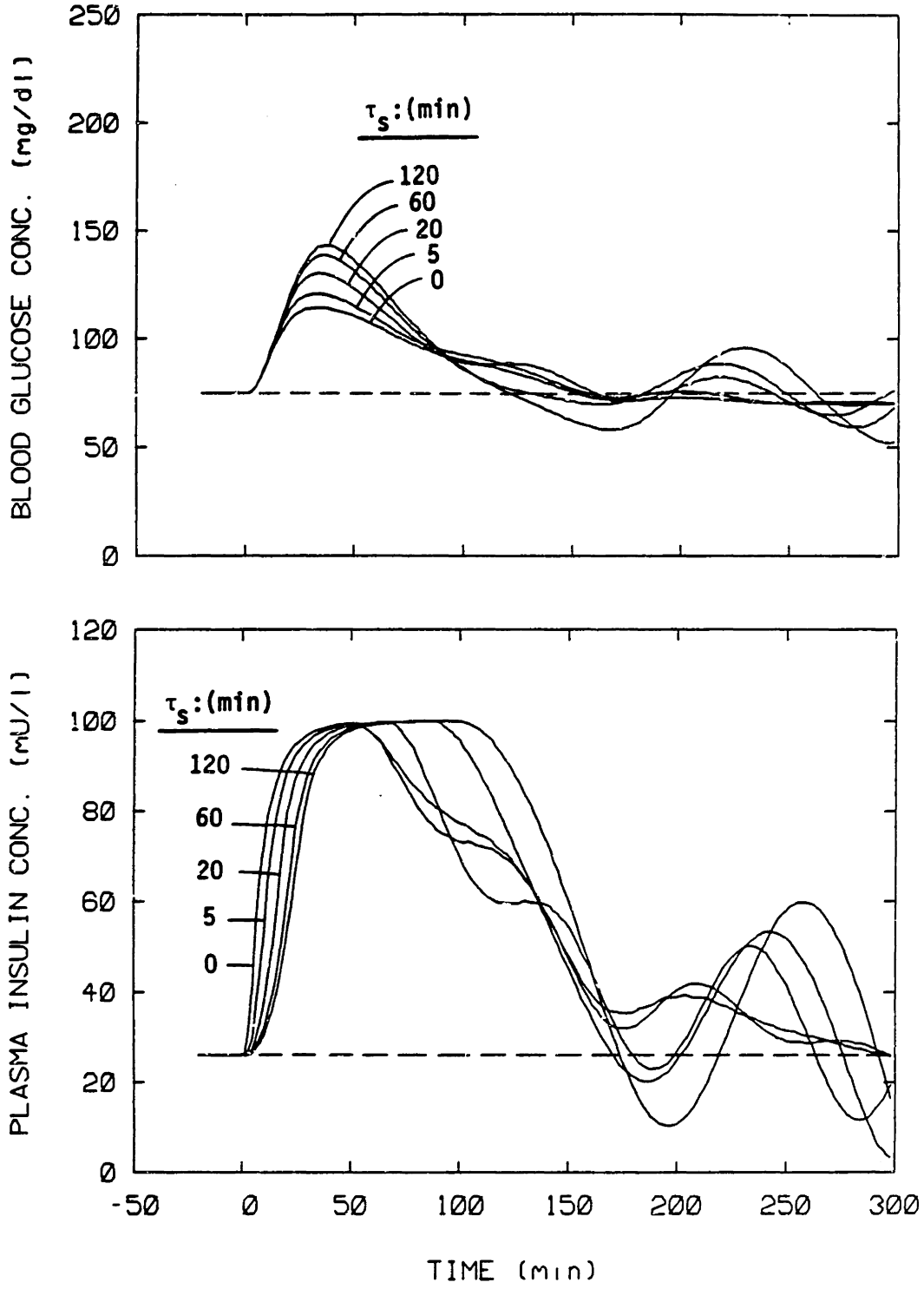

Fig. 112 Simulation studies to assess the effects of sensor response time on glycemic regulation of the 100g OGTT resulting from suboptimal (first-order) IMC control loop compensation. Sensor response time τ_S was varied from 0-120 min in the glucose sensor (Equation 287), and in the IMC internal model and controller (Equations 288 and 289, respectively; second-order derivative terms neglected).

time caused sluggish but immediate insulin response upon onset of rising glycemia; as a consequence, even sensor response times on the order of the process response time τ_p only resulted in modest hyperglycemia. As sensor response time τ_s approached the process response time τ_p, however, oscillations in blood glucose concentration reflecting second-order response interactions began to appear upon recovery to steady state. Such oscillations would not be desirable due to their observed penetration into hypoglycemic regimes. Finally, for sensor response times much less than the process response time, or

$$\tau_s \lesssim 9 \text{ min} \tag{290}$$

the effects of glucose sensor response time on achievable glycemic regulation were of minimal significance.

As discussed previously, increased sensor response time could result from factors such as tissue encapsulation of the sensor implant. Under such conditions, the actual change in measurement response might not be anticipated, in which case no modification of the control equations would be made. Thus, simulation studies were repeated where sensor response time τ_s was again varied from 0 to 120 min in the glucose sensor (Equation 287), but no compensatory modifications of the control equations was taken, i.e. the value of τ_s in the internal model (Equation 288) and controller (Equation 289) was set to zero for all sensor response time variations. Results of simulations to assess the effects of sensor response time on uncompensated closed-loop glycemic regulation during the 100g OGTT are shown in Figure 113. Comparison of Figures 112 and 113 clearly demonstrated the relative effectiveness of partial (first-order) compensation for glucose sensor response time in reducing the magnitudes of

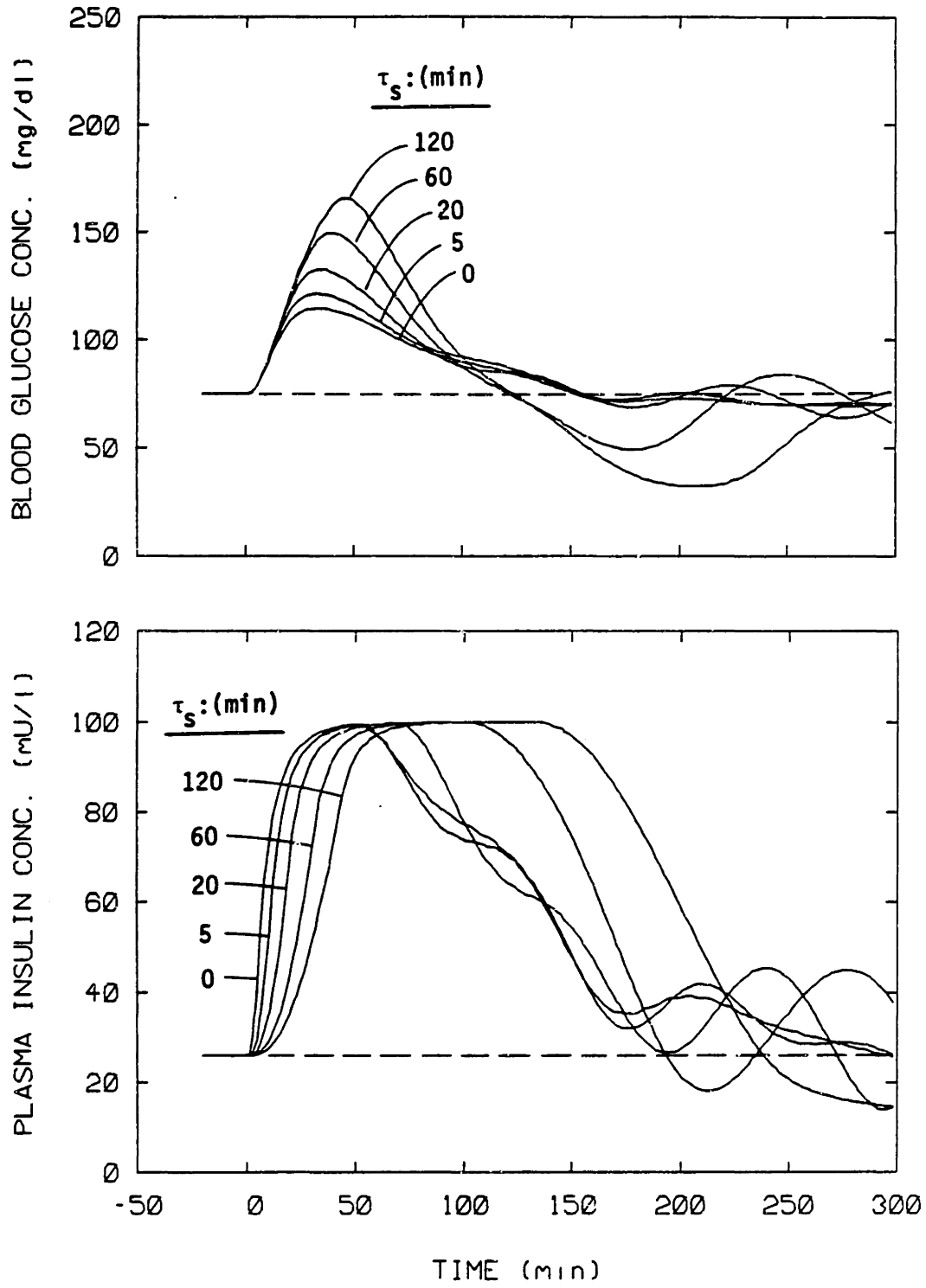

Fig. 113 Simulation studies to determine the effects of sensor response time on glycemic regulation during the 100g OGTT in the absense of control loop compensation. Here, the simulations of Figure 112 were repeated, except τ_s was set to zero in the internal model and controller (Equations 288 and 289, respectively) for all variations in glucose sensor response time.

resulting hyperglycemic and hypoglycemic excursions. Of particular importance were the dangerously large hypoglycemic oscillations caused by sensor response times approaching the process response time if no control loop compensation was adopted. Of course, for the conditions of Equation 290, lack of compensation was not important, and good glycemic regulation was maintained; this result could be anticipated from Equation 283c, because

$$G_p^*(s) \approx \frac{K_p e^{-\delta_p s}}{\tau_p s + 1} \qquad \tau_s \ll \tau_p \tag{291}$$

c) Systematic Sensor Measurement Error

A serious concern with development of a sensor suitable for long-term applications is the problem of systematic measurement error arising, for example, through error in the calibration curve or drift. To study measurement error effects, the following glucose sensor transfer function is defined:

$$G_s(s) = \gamma + (\gamma - 1)\frac{G_b}{y(s)} \tag{292}$$

where γ = measurement error parameter (dimensionsless)

G_b = basal blood glucose concentration (= 75 mg/dl)

Inversion of this expression from the Laplace domain to real time yields

Glucose Sensor

$$(y_m(t) + G_b) = \gamma\,(y(t) + G_b) \tag{293}$$

It can be seen from Equation 293 that the dimensionless parameter γ produces

a measurement error proportional to the absolute magnitude of the true blood glucose concentration. In general, the presence of systematic measurement error would not, from a control perspective, be detected. In this case, the internal model and optimal controller equations would remain as originally derived without consideration of nonideal process observation (Equations 260 and 261, respectively).

Simulation studies to assess the effects of systematic measurement error on blood glucose regulation during the 100g OGTT are presented in Figure 114. Here, the diabetic model was employed for prediction of blood glucose and plasma insulin response profiles while the magnitude of sensor measurement error was altered by varying the value of γ from 1.30 to 0.70 (±30% range in error). Variation in systematic measurement error resulted in proportional offset in the blood glucose response profiles, with the inconsistency in spacing between adjacent blood glucose profiles simply reflecting effects of system nonlinearities. Although decreases in measurement sensitivity ($\gamma<1.0$) induced roughly proportional increases in hyperglycemia, of concern were the more potentially hazardous effects of increased measurement sensitivity ($\gamma>1.0$) which caused hypoglycemic offset from normal. Although decreases in sensitivity might be more commonly anticipated, in reality such may not always be the case; indeed, enzymatic glucose sensors are prone to initial periods of increasing measurement sensitivity presumably attributable to establishment of diffusion channels within the enzyme matrix (Guilbault and Lubrano, 1973).

An interesting approach to dealing with sensor drift is suggested by the simulation results shown in Figure 114. At basal steady state, the controller drives the measured glucose concentration deviation $y_m(t)$ to its setpoint value of zero, thus generating basal offset in actual blood glu-

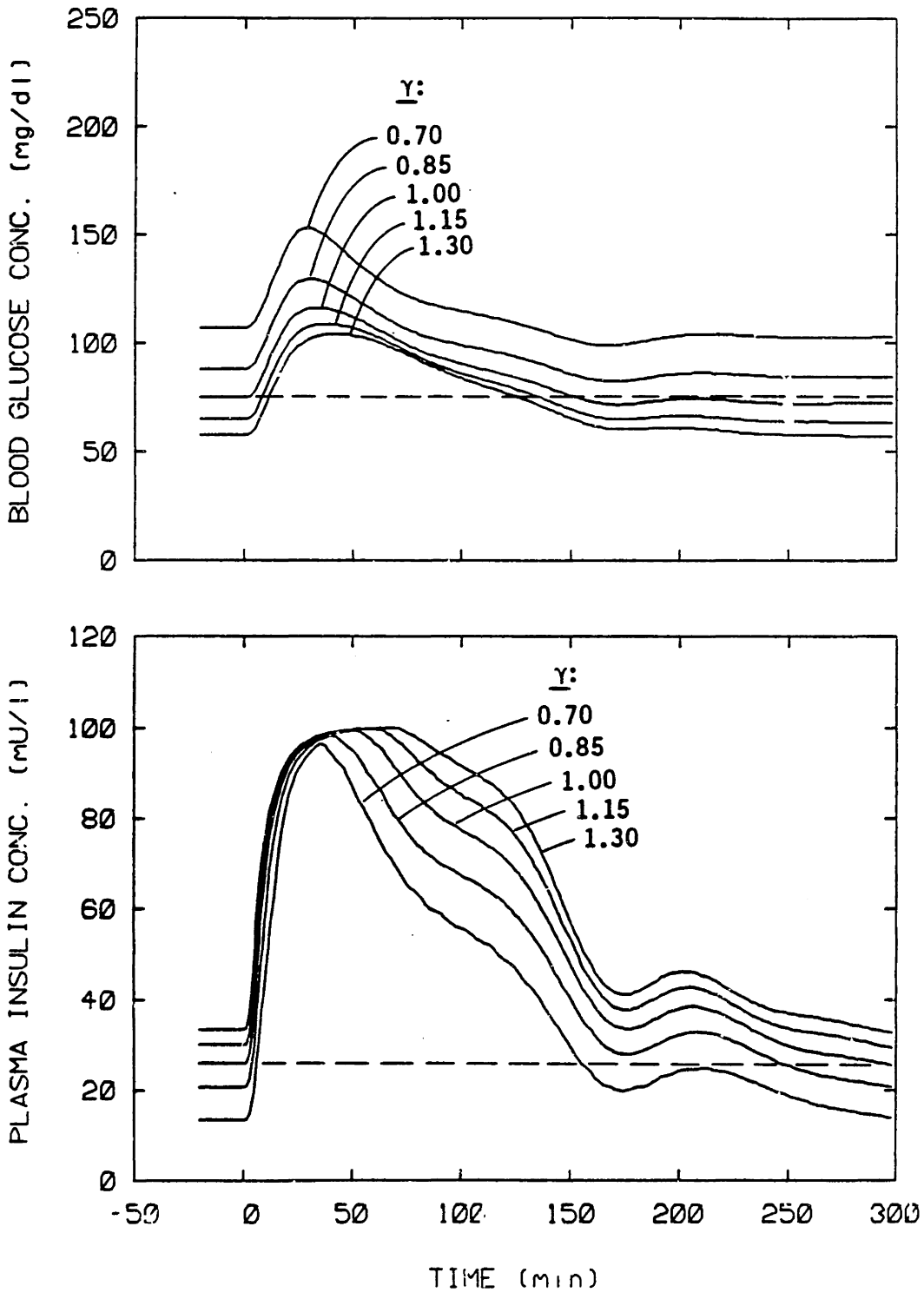

Fig. 114 Simulation studies to assess the effects of systematic sensor measurement error on glycemic control during the 100g OGTT. A measurement error of ±30% was introduced by variation of parameter γ from 1.30 to 0.70.

cose concentration in the presence of measurement drift. Under drift conditions, however, insulin concentration under basal conditions also changes as shown in the lower plot of Figure 114, thus reflecting changes in the actual steady state rate of insulin delivery. It might thus be possible to implement logic into the control system to warn of apparent measurement drift and to alert the patient of the need for sensor recalibration; such a warning would be issued when the system logic confronts the paradox of departure from normal basal baseline insulin infusion rate to produce "apparent" basal glycemia. Conceivably, an effective automatic recalibration procedure could be initiated based on logical interpretation of changes in m(t) from zero when $y_m(t)$ equals zero.

d) Sensor Sampling Interval and Digital Control

To this point, only continuous glucose measurement has been considered, and simulations of "continuous" time entailed use of numerical integration methods (fourth-order Runge-Kutta integration) based on a time step of 0.1 min (a time step deemed satisfactory for approximating continuous dynamics from previous experience with modeling of in vivo glucose regulation). Due to intrinsic sensor measurement characteristics and/or the possible need to conserve power expenditure of an implantable unit, however, it may be necessary or desirable to sample blood glucose concentration at specific times rather than on a continuous basis.

A glucose sensor providing discrete blood glucose concentration values is defined as follows:

$$y_m(kT) = y(kT) \qquad k = 0,1,2... \tag{294}$$

where T = sampling interval (min)

Discrete time IMC was analyzed by first considering the analogous continuous time system and then digitalizing the resulting control equations. The analogy between discrete and continuous system analysis holds if the effect of discrete sampling is considered equivalent to introducing an induced measurement dead time of T into a continuous system. Thus, the continuous system glucose sensor analogy to Equation 294 is given by the transfer function

$$G_s(s) = e^{-Ts} \tag{295}$$

Given this glucose sensor transfer function, optimal control analysis was identical to that previously described for the case of sensor dead time (compare the equivalence of the glucose sensor transfer functions of Equations 295 and 272 with dead times of T and δ_s, respectively). Thus, the resulting continuous time internal model is given by

$$\tau_p \frac{d\tilde{y}^*(t)}{dt} + \tilde{y}^*(t) = K_p m(t-\delta_p-T) \tag{296}$$

and the optimal controller by

$$m(t) = \frac{\tau_p}{K_p} \frac{d\varepsilon^*(t)}{dt} + \frac{1}{K_p} \varepsilon^*(t) \qquad m_{min} \leq m(t) \leq m_{max} \tag{297}$$

Digitalizing Equations 296 and 297 by using finite differences for approximating derivatives, the following set of relationships for discrete time IMC implimentation result:

Glucose Sensor

$$y_m(kT) = y(kT) \qquad k = C,1,2... \tag{298}$$

Internal Model

$$\tau_p \frac{\tilde{y}^*(kT)-\tilde{y}^*(kT-T)}{T} + \tilde{y}^*(kT) = K_p m(kT-\delta_p-T) \qquad k=0,1,2... \qquad (299a)$$

$$(\text{or}) \quad \tilde{y}^*(kT) = \frac{\tau_p \tilde{y}^*(kT-T) + TK_p m(kT-\delta_p-T)}{\tau_p + T} \qquad k = 0,1,2... \qquad (299b)$$

Optimal Controller

$$m(kT) = \frac{\tau_p}{K_p} \frac{\varepsilon^*(kT)-\varepsilon^*(kT-T)}{T} + \frac{1}{K_p}\varepsilon^*(kT) \qquad m_{min} \leq m(kT) \leq m_{max}; k=0,1,2... \qquad (300)$$

Finally, for coupling of discrete time control with the continuous process of in vivo glycemic regulation, the digital controller output m(kT) is converted to a continuous output m(t) via a zero-order hold:

$$m(t) = m(kT) \qquad kT \leq t < kT+T; \; k=0,1,2... \qquad (301)$$

Simulation studies to assess the effects of discrete sampling on glycemic regulation during the 100g OGTT are shown in Figure 115. The diabetic model was used to predict blood glucose and plasma insulin responses while the discrete glucose sampling interval T was varied from 0 to 60 min in the digitalized IMC equations. It should be noted that blood glucose responses for the case of sensor sampling would actually vary, particularly for large values of T, depending on alignment of sampling times relative to administration of the oral glucose challange at time t=0. The simulations in Figure 115 represented a worst case with respect to hyperglycemic excursions, because sampling was adjusted such that a glucose measurement was taken at time t=0 for all specified sampling intervals T. As shown in the lower panel of Figure 115, this approach maximized the delay in the initial insulin response to rising glucose concentration in all cases. The

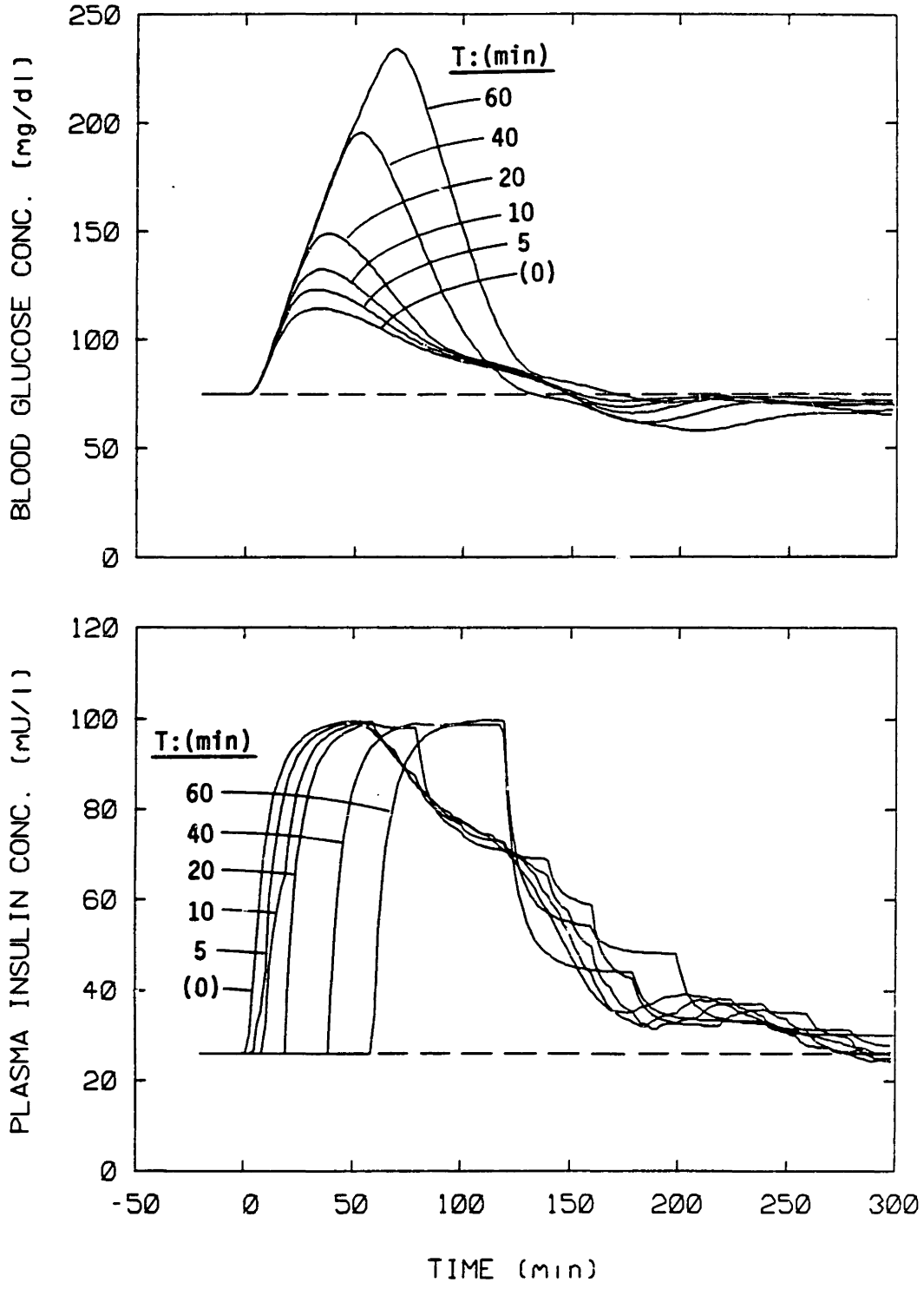

Fig. 115 Simulation studies to assess the effects of measurement sampling interval on discrete time glycemic control during the 100g OGTT. The interval T of discrete glucose sampling was varied from 5-60 min in the digital IMC Equations 298-300. Included for comparison are results for T→0, or the case of continuous measurement.

hyperglycemia resulting from discrete sampling interval values T was similar to, but modestly lower than that obtained for continuous time control with equivalent sensor dead time values δ_S (compare Figures 115 and 111). The reason for the slightly improved blood glucose regulation in the case of discrete sampling can be explained as follows. For equivalent values of T and δ_S, initial plasma insulin response to oral glucose is comparably delayed (compare lower plots in Figures 115 and 111). In the case of digital control, at time t=T, sampling of the present elevated glucose concentration immediately initiates a step increase in insulin infusion rate, whereas for the case of sensor dead time, at time $t=\delta_S$ the delayed initial rise in blood glucose concentration just begins to initiate increased insulin delivery. Thus, digital control results in a faster initial plasma insulin response than does the system with equivalent sensor dead time, and this provides for the observed improvement in hyperglycemic regulation. As shown in Figure 115, for values of the sampling interval T much less than the process response time τ_p, or

$$T \lesssim 9 \text{ min} \tag{302}$$

the resulting discrete time closed-loop glycemic control was comparable to that obtained for continuous time optimal control ($T \to 0$).

e) Coupling of Nonideal Sensor Characteristics

In this section, analysis is extended to consider coupling of the above sensor nonidealities. Generalized step responses for sensors operating in continuous time and discrete time modes respectively are depicted in Figure 116. The continuous time glucose sensor (center panel) is represented by coupling of dead time δ_S with a first-order response time

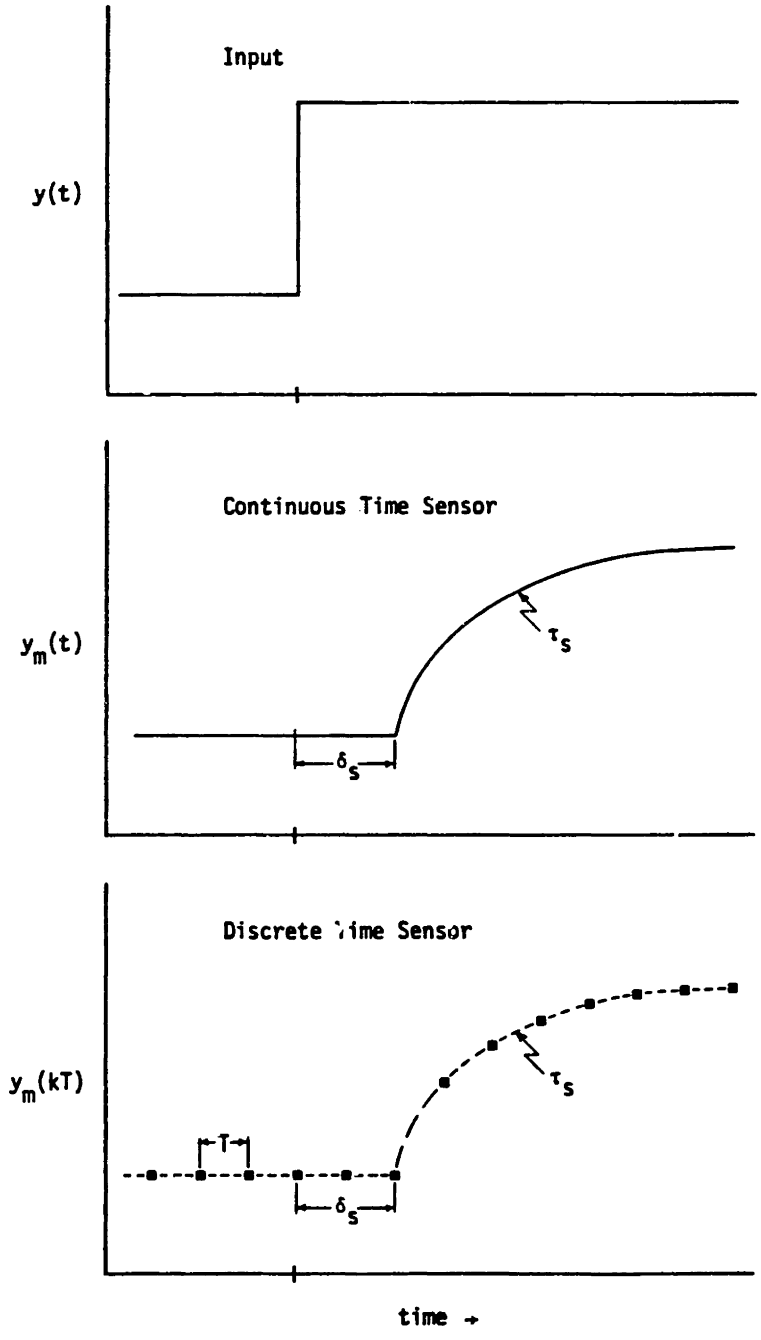

Fig. 116 Generalized sensor step responses depicting the coupling of dead time δ_s and first-order response time τ_s for a continuous time sensor (center panel), and extention to digital operation with superposition of sampling interval T for the discrete time sensor (lower panel).

τ_s. For the discrete time glucose sensor (lower panel), measurement output used for control purposes is sampled at time intervals T.

Extention of earlier analysis to consider coupling of sensor dead time δ_s and response time τ_s in continuous time is straightforward. In this case, the glucose sensor transfer function becomes

$$G_s(s) = \frac{e^{-\delta_s s}}{\tau_s s + 1} \tag{303}$$

The internal model is given by

$$G_m(s) = G_p^*(s) = G_p(s)G_s(s) \tag{304a}$$

$$= \left(\frac{K_p e^{-\delta_p s}}{\tau_p s + 1}\right)\left(\frac{e^{-\delta_s s}}{\tau_s s + 1}\right) \tag{304b}$$

$$= \frac{K_p e^{-(\delta_p+\delta_s)s}}{(\tau_p s + 1)(\tau_s s + 1)} \tag{304c}$$

Factorization of Equation 304c yields

$$G_-^*(s) = \frac{K_p}{(\tau_p s + 1)(\tau_s s + 1)} \tag{305}$$

$$G_+^*(s) = e^{-(\delta_p+\delta_s)s} \tag{306}$$

Because the presence of sensor dead time δ_s contributes only to $G_+^*(s)$, the optimal controller (given by the inverse of $G_-^*(s)$) is the same as that previously derived by consideration of sensor response time τ_s alone (Equation

286). Inverting the relevant expressions from the Laplace domain to real time gives the following IMC relationships:

Glucose Sensor

$$\tau_s \frac{dy_m(t)}{dt} + y_m(t) = y(t-\delta_s) \tag{307}$$

Internal Model

$$\tau_p \tau_s \frac{d^2\tilde{y}(t)}{dt^2} + (\tau_p+\tau_s) \frac{d\tilde{y}(t)}{dt} + \tilde{y}(t) = K_p m(t-\delta_p-\delta_s) \tag{308}$$

Optimal Controller

$$m(t) = \frac{\tau_p \tau_s}{K_p} \frac{d^2\varepsilon^*(t)}{dt^2} + \frac{(\tau_p+\tau_s)}{K_p} \frac{d\varepsilon^*(t)}{dt} + \frac{1}{K_p}\varepsilon^*(t) \qquad m_{min} \leq m(t) \leq m_{max} \tag{309}$$

Although the internal model (Equation 308) incorporates consideration of the presence of both dead time δ_s and response time τ_s in the glucose sensor measurement signal, the optimal controller (Equation 309) can provide compensation only for the presense of response time τ_s. If the second-order derivative terms in the above internal model and controller equations are retained, complete compensation for sensor response time τ_s is provided and the resulting quality of blood glucose regulation depends only on the sensor dead time δ_s; in this case, the quality of achievable control may be ascertained directly from results of the sensor dead time simulation studies presented in Figure 111.

As discussed previously, omission of the second-order derivative terms in the control loop equations may be desirable for practical applications. If partial (first-order) sensor response time compensation is employed in

the IMC equations, the quality of blood glucose control is affected not only by the sensor dead time δ_S, but also by the magnitude of the sensor response time τ_S. Simulation studies to assess the effects of such coupling of sensor dead time δ_S and sensor response time τ_S on blood glucose regulation during the 100g OGTT are shown in Figure 117. For these simulations, values of δ_S and τ_S were varied in Equations 307-309, but the second-order derivative terms (denoted by dashed underlines) were neglected in the IMC internal model (Equation 307) and controller (Equation 309). Within limits of the assumption that the process of in vivo glucose regulation is linear, it would be expected that coupling of sensor dead time and sensor response time would result in a superposition of the effects observed for each of these cases considered individually (see Figures 111 and 112, respectively). As shown in the lower plot of Figure 117, initial plasma insulin response to rising blood glucose concentration was delayed by a time period corresponding to δ_S (compare lower plot of Figure 111), and following this initial delay period, the initial dynamic insulin response was slowed due to the presence of sensor response time $_S$ (compare lower plot of Figure 112). The coupling of δ_S and τ_S in Figure 117 thus resulted in peak hyperglycemia reflecting the sum of the effects shown in the upper plots of Figures 111 and 112. With respect to recovery of blood glucose to its basal level, however, such superposition effects become difficult to anticipate due to the more complex dynamic interactions involved. As shown in the upper plot of Figure 117, for coupling of $\delta_S = \tau_S = 40$ min, which evoked combined sensor response time dynamics on the order of the process response time τ_p (=90 min), an unacceptable blood glucose nadir of 45 mg/dl resulted during the recovery period; this behavior is not predictable a priori by apparent superpositioning of the results presented in

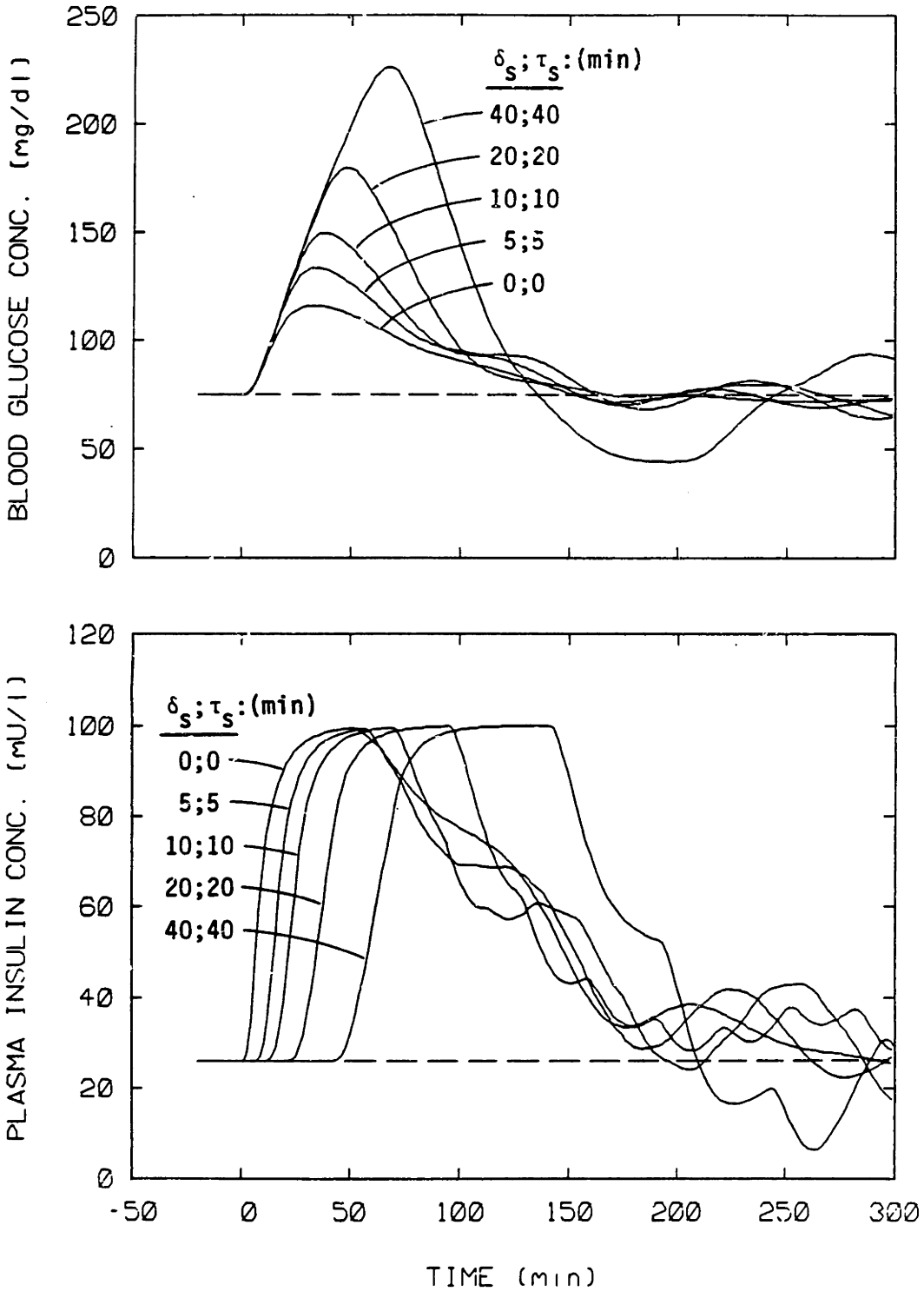

Fig. 117 Simulation studies to assess the effects of coupling sensor dead time and sensor response time on blood glucose regulation during the 100g OGTT. Values of δ_S and τ_S were varied from 0-40 min in Equations 307-309 (second-order derivative terms neglected).

Figures 111 and 112. For values of δ_s and τ_s of 20 min or less, however, coupling of these sensor characteristics led to acceptably small hypoglycemic excursions during blood glucose recovery to basal steady state. Finally, for coupling of sensor dead time and response time such that the induced measurement dynamics occur on time scales much less than the process response time τ_p, or

$$\delta_s + \tau_s \lesssim 9 \text{ min} \tag{310}$$

the resulting blood glucose control approaches that obtained for ideal glucose sensing.

Presented in Figure 118 is a comparison between true blood glucose concentration (equivalent to $y(t)+G_b$) and the blood glucose concentration sensor reading (equivalent to $y_m(t)+G_b$) for the case of $\delta_s=\tau_s=20$ min in Figure 117. Because of the sensor dead time δ_s, the initial rise in blood glucose concentration was first detected 20 min after its actual occurrence, resulting in a 20 min delay in the initial controller response (see lower panel of Figure 117). In addition to the pure measurement delay associated with δ_s, the sensor response time τ_s resulted in a sensor reading that was dynamically sluggish and attenuated in magnitude relative to the true blood glucose response.

For a glucose sensor with dead time δ_s and response time τ_s operating in a discrete time mode (see Figure 116), output from the senor as given by Equation 307 is sampled at time intervals T. The proper IMC equations for use in this case may be derived simply by digitalizing the above relationships for the generalized continuous time glucose sensor (Equations 307-309), recognizing that such digitalization adds an induced dead time T to the internal model (Equation 308). The following discrete time IMC

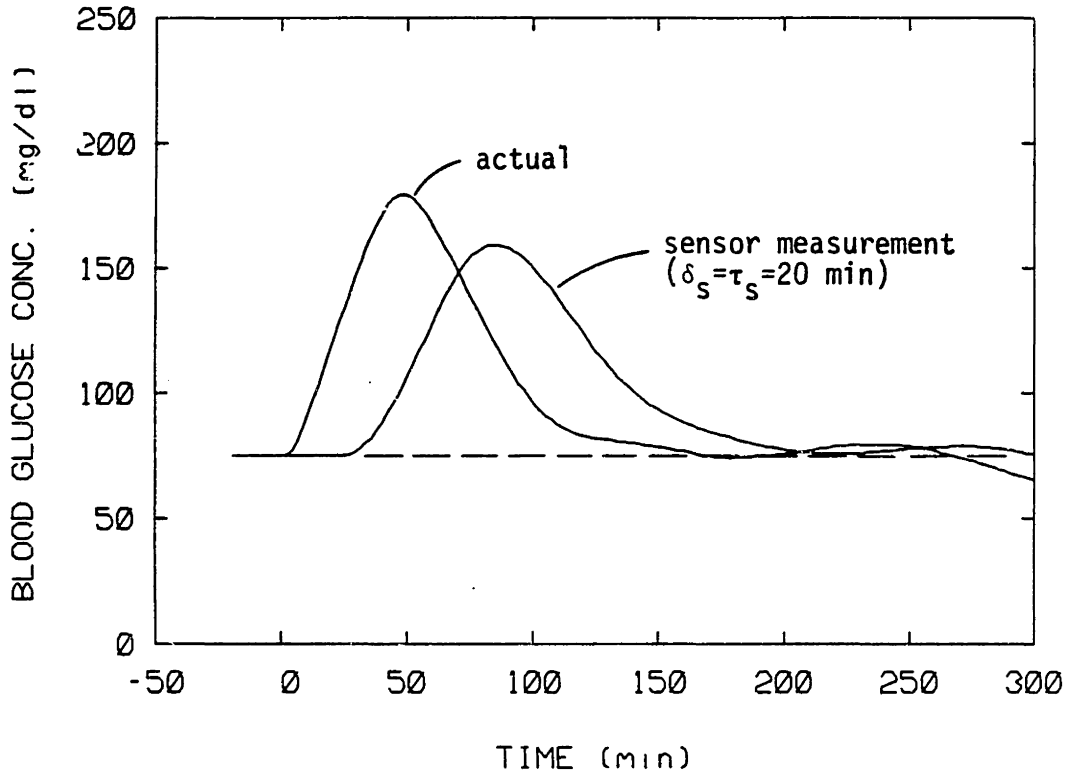

Fig. 118 Comparison between true blood glucose concentration and that measured by the glucose sensor for the case of $\delta_s = \tau_s = 20$ min in Figure 117.

relationships result:

Glucose Sensor

$$\tau_s \frac{dy_m(t)}{dt} + y_m(t) = y(t-\delta_s) \tag{311}$$

and $$y_m(kT) = y_m(t=kT) \qquad kT \leq t < kT+T;\ k=0,1,2... \tag{312}$$

Internal Model

$$\tau_p \tau_s \frac{\tilde{y}^*(kT)-2\tilde{y}^*(kT-T)+\tilde{y}^*(kT-2T)}{T^2} + (\tau_p+\tau_s)\frac{\tilde{y}^*(kT)-\tilde{y}^*(kT-T)}{T} + \tilde{y}^*(kT)$$

$$= K_p m(kT-\delta_p-\delta_s-T) \qquad k=0,1,2... \tag{313a}$$

$$(\text{or})\ \tilde{y}^*(kT) = \frac{K_p m(kT-\delta_p-\delta_s-T) + \frac{2\tilde{y}^*(kT-T)-\tilde{y}^*(kT-2T)}{T} + (\tau_p+\tau_s)\tilde{y}^*(kT-T)}{\frac{\tau_p\tau_s}{T} + (\tau_p+\tau_s) + 1} \tag{313b}$$

Optimal Controller

$$m(kT) = \frac{\tau_p\tau_s}{K_p}\frac{\varepsilon^*(kT)-2\varepsilon^*(kT-T)+\varepsilon^*(kT-2T)}{T^2} + \frac{(\tau_p+\tau_s)}{K_p}\frac{\varepsilon^*(kT)-\varepsilon^*(kT-T)}{T}$$

$$+ \frac{1}{K_p}\varepsilon^*(kT) \qquad k=0,1,2... \tag{314}$$

and the digital controller output m(kT) is converted to continuous time output m(t) by Equation 301.

The generalized discrete glucose sensor model introduces a dead time of δ_S+T and a response time of τ_S into the measurement signal, and the pre-

sence of these sensor characteristics is fully reflected in the IMC internal model formulation (Equation 313b). The optimal controller (Equation 314), however, provides compensation only for the presence of response time τ_S. For cases in which $\tau_S=0$, or if the second-order derivative terms (denoted by dashed underlines) in the above internal model and controller are retained to compensate fully for the presence of $\tau_S>0$, the quality of achievable blood glucose regulation depends only on the effective digital sensor dead time δ_S+T; the effects of coupling δ_S and T on blood glucose control can be approximately predicted simply by superimposing results presented for δ_S and T in Figures 111 and 115, respectively.

If, for practical applications, the second-order derivative terms are neglected in the digital IMC internal model (Equation 313b) and optimal controller (Equation 314), thus providing only partial or suboptimal (first-order) compensation for the presence of sensor response time $\tau_S>0$, the resulting blood glucose regulation is affected by coupling of τ_S with the sensor's effective dead time δ_S+T. For cases in which $\delta_S=0$, coupling of τ_S with induced dead time T would be closely approximated by the results presented in Figure 117 for the coupling of τ_S with dead time δ_S in the continuous time domain. Thus, only the effects of fully coupling δ_S and T in the presence of τ_S with first-order IMC compensation remains to be elucidated. Presented in Figure 119 are simulation studies to assess the effects of coupling sensor dead time δ_S, sensor response time τ_S, and digital control (sampling interval T) on blood glucose regulation during the 100g OGTT. Values of δ_S, τ_S, and T were vared in Equations 311-314, but the second-order derivative terms (denoted by dashed underlines) in the digital IMC internal model (Equation 313) and controller (Equation 314) were neglected. The results in Figure 119 may be viewed as reflecting the super-

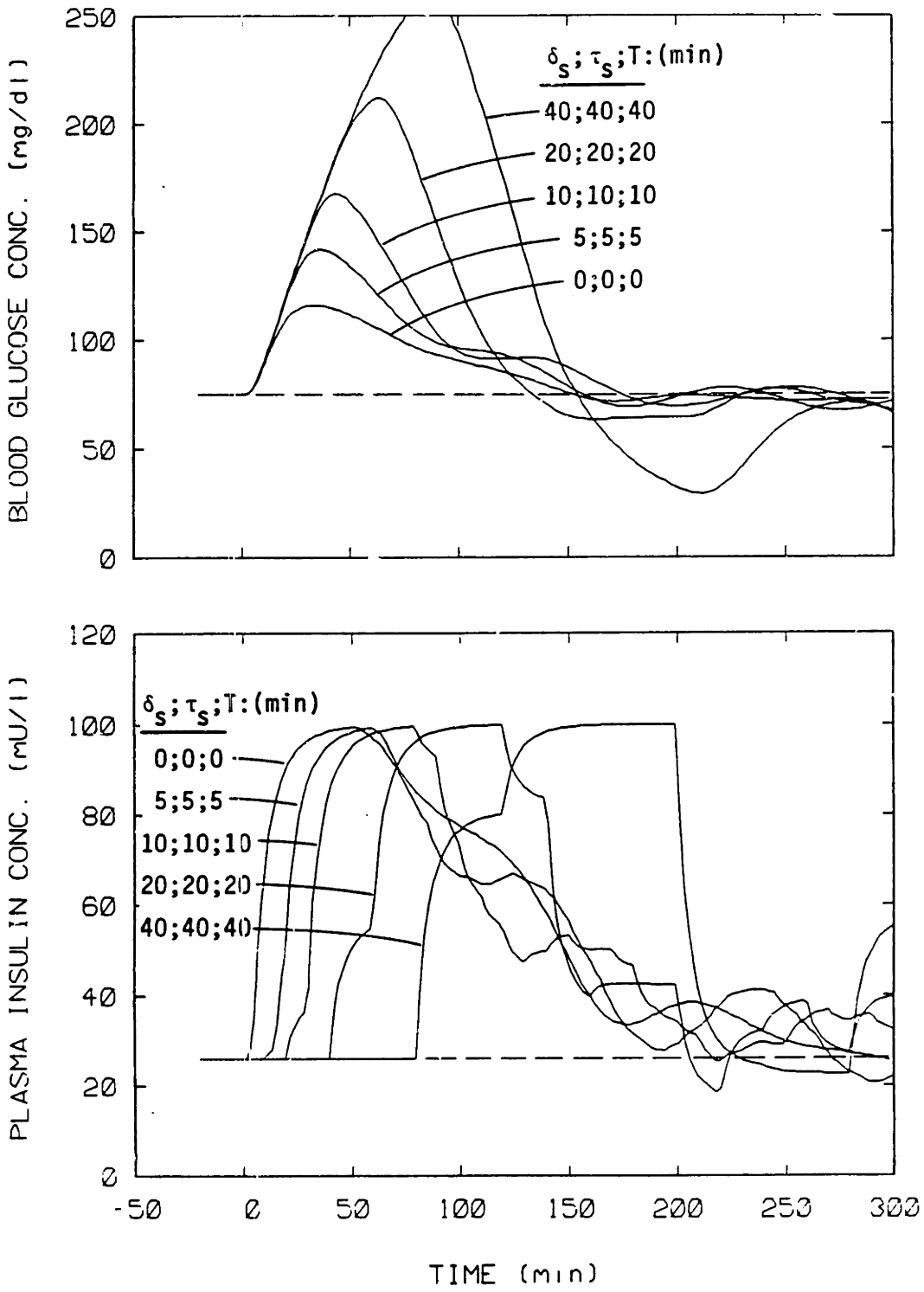

Fig. 119 Simulation studies to assess the effects of coupling sensor dead time, sensor response time, and digital IMC control on blood glucose regulation during the 100g OGTT. Values of δ_S, τ_S, and T were varied from 5-40 min in Equations 311-314 (second-order derivative terms neglected). Included for comparison are results for ideal continuous glucose measurment ($\delta_S = \tau_S = 0$; $T \to 0$).

position of digital sampling T on the results obtained in Figure 117 for coupling of δ_S and τ_S in continuous time. As shown in the lower plot of Figure 119, coupling of δ_S and T in the glucose sensor causes an initial lag in insulin response to rising blood glucose concentration corresponding to a total delay time of δ_S+T. Thus, the addition of sampling interval T to the coupling of δ_S and τ_S (as shown in Figure 117) further degrades the quality of achievable blood glucose regulation. The peak hyperglycemic excursions observed in the upper plots of Figure 119, however, are approximated nicely by superimposing the effects of digital sampling (as shown in the upper plot of Figure 115) on the effects of coupling δ_S and τ_S in continuous time (as shown in the upper plot of Figure 117); here, superposition refers to using the blood glucose response profile obtained for the ideal continuous sensor as the base case and superimposing the deviation effects caused by introduction of respective sensor nonidealities. With respect to inducement of hypoglycemia during recovery of blood glucose to its steady state basal level, the contribution of digital control per se led only to minor amplification of the magnitudes of the hypoglycemic excursions observed in Figure 117. Finally, for the coupling of δ_S, τ_S, and T, if the induced measurement dynamics correspond to time scales much less than the process response time τ_p, or

$$\delta_S + \tau_S + T \lesssim 9 \text{ min} \tag{315}$$

the quality of achievable blood glucose control approaches that obtainable with the ideal glucose sensor.

Presented in Figure 120 is a comparison between true blood glucose concentration and the digital blood glucose concentration sensor readings for the case of $\delta_S = \tau_S = T = 20$ min in Figure 119. With respect to sensor

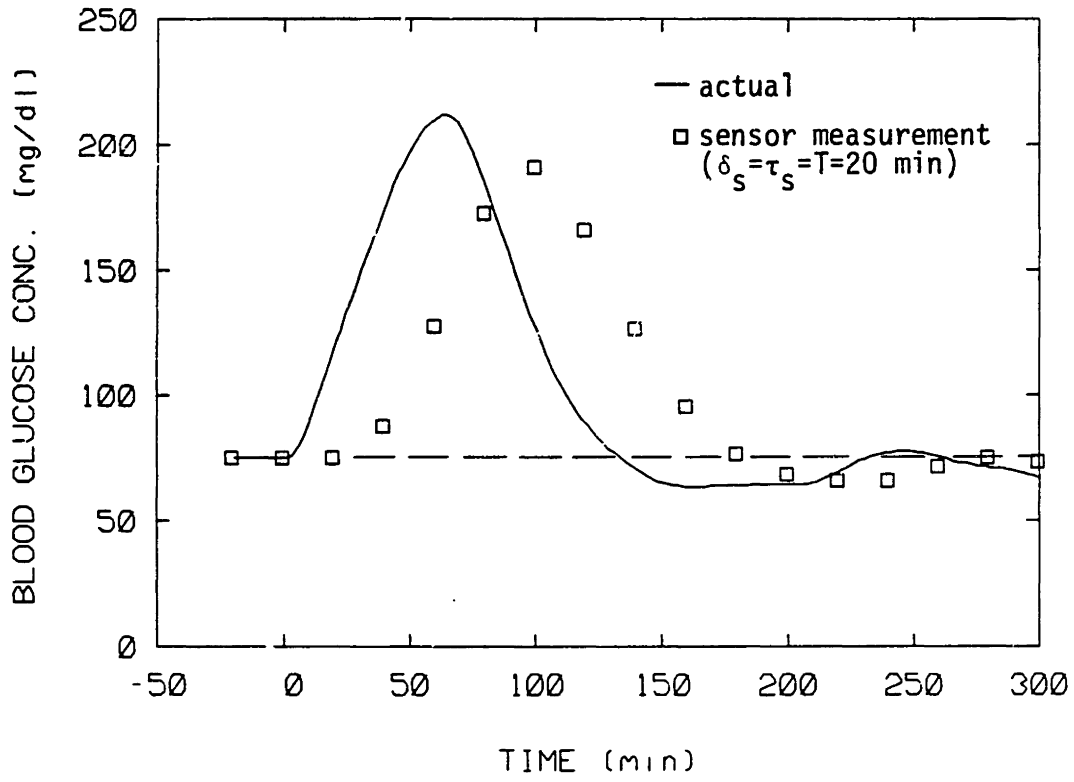

Fig. 120 Comparison between true blood glucose concentration and that measured by the glucose sensor for the case of $\delta_s = \tau_s = T = 20$ min in Figure 119.

response to initial rising blood glucose concentration, the sensor dead time δ_S caused sensor output at t=20 min to remain at basal concentration. Because of digital sampling, the first sensor reading to reflect a rise in blood glucose concentration occurred at t=40 min. Thus, controller response to initial rising blood glucose concentration resulted 40 min after its actual occurrance (see lower panel of Figure 119). This illustrates the notion that digital sampling per se induced a measurement dead time equal to the sampling interval T, as the sensor response delay was effectively δ_S+T=20+20=40 min in Figure 120. As suggested in Figure 120, the presence of sensor response time τ_S caused the digitalized sensor response to be dynamically sluggish and attenuated in magnitude relative to the true blood glucose response being monitored.

The effect of systematic sensor measurement error was not considered in the above analyses of sensor measurement characteristic couplings. Because the IMC structure is designed on the basis of variables for which values are defined in terms of deviations from basal steady state, the introduction of systematic sensor measurement error in the absence of control loop compensation simply offsets resulting blood glucose response profiles as was demonstrated earlier (see Figure 114). Thus, introduction of systematic sensor measurement error was not explicitly explored in the context of coupling sensor measurement characteristics, as its inclusion would simply lead to a predictable offsetting of the response behaviors generated in the above coupling studies.

f) Sensor Measurement Noise and Its Filtering

Measurement noise is an important consideration when implementing closed-loop control because superposition of noise on the measurement

signal is particularly detrimental to accurate calculation of derivatives in the control loop equations. It is therefore necessary to minimize interactions of noise signals by application of effective noise filtering.

In order to study measurement noise effects, a discrete time glucose sensor is defined as follows:

$$y_m(kT) = y(kT) + u(kT) \qquad k=0,1,2... \qquad (316)$$

where $u(kT)$ = zero-mean, random measurement deviates (mg/dl)

Here, a sensor with measurement noise is simulated by superposition of zero mean random deviates $u(kT)$ on the true sampled glucose concentration values $y(kT)$. The zero-mean random deviates $u(kT)$ are defined statistically by a gaussian distribution with a standard deviation (sd) given by

$$sd = \alpha \left(y(kT) + G_b\right) \qquad k=0,1,2... \qquad (317)$$

where α = measurement noise parameter (dimensionless)

G_b = basal setpoint blood glucose conc. (= 75mg/dl)

Thus, the standard deviation of the noise is assumed proportional to the (instantaneous) true blood glucose concentration, and the relative contribution of the noise component to the measurement signal is altered by varying the value of parameter α.

A measurement noise filter is inserted into the IMC structure as shown in Figure 121. The purpose of the filter is to provide a relatively noise-free measurement estimate $\hat{y}_m(kT)$ from the noise-contaminated measurement signal $y_m(kT)$. Although "filters" are commonly inserted into the $\tilde{d}(t)$ feedback loop of the IMC structure in the control literature (see Garcia and Morari, 1982), such filters provide a freedom to the designer to adjust

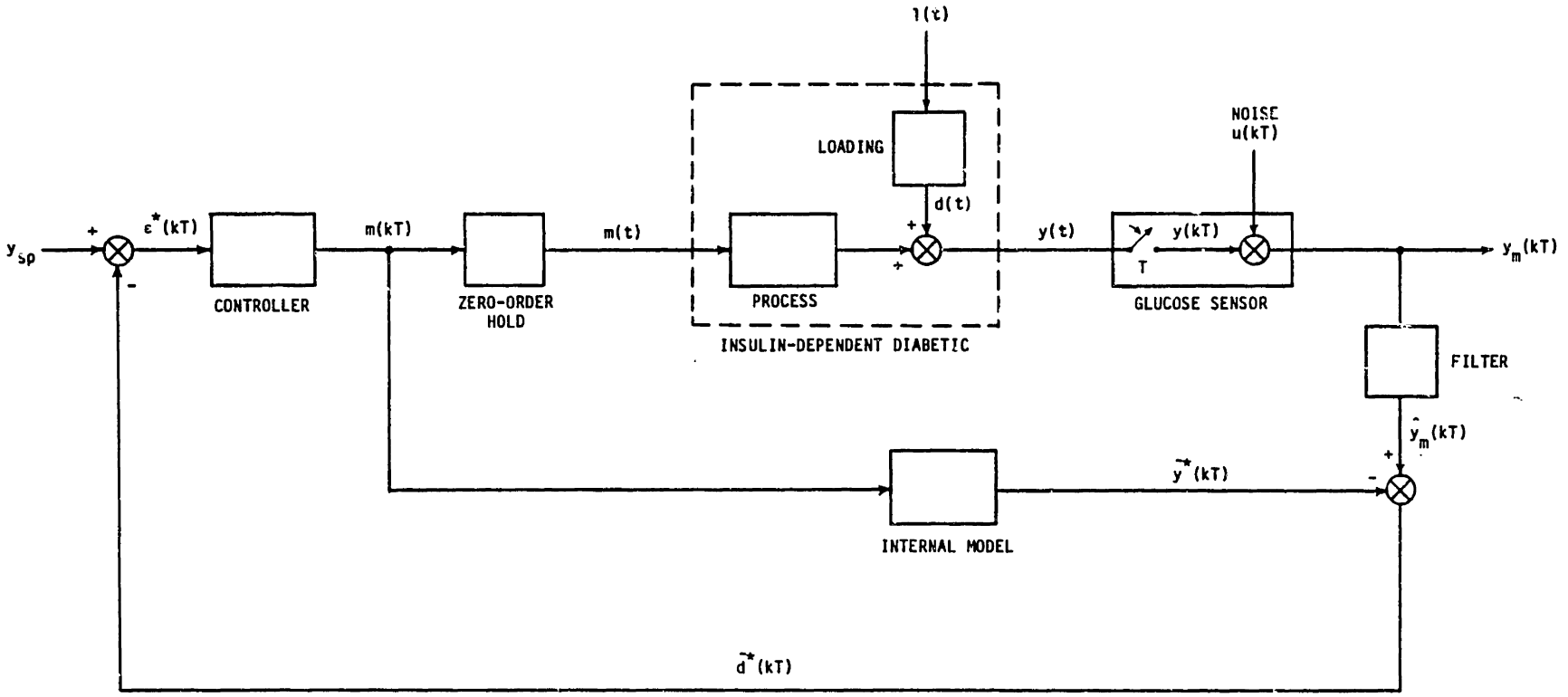

Fig. 121 Schematic depiction of discrete time IMC structure indicating insertion of a filter block for filtering measurement noise u(kT) introduced by the glucose sensor.

closed-loop response so as to achieve a desired behavior. The objective here, however, is simply to filter noise from the measurement signal without modifying the basic characteristics of optimal controller regulation of blood glucose.

For present purposes, a simple first-order response filter (single exponential smoothing)(see Koppel, 1968) is employed, which in discrete time form is given by

$$\tau_f \frac{\hat{y}_m(kT) - \hat{y}_m(kT-T)}{T} + \hat{y}_m(kT) = y_m(kT) \qquad k=0,1,2... \qquad (318a)$$

$$\text{or} \quad \hat{y}_m(kT) = \frac{\tau_f \hat{y}_m(kT-T) - T y_m(kT)}{\tau_f + T} \qquad k=0,1,2... \qquad (318b)$$

where τ_f = noise filter time constant (min)

Equation 318a can be recognized as the discrete time representation of a simple first-order response model with time constant τ_f. Thus, insertion of the filter into the IMC structure as shown in Figure 121 introduces a response time τ_f analogous to that introduced by previous consideration of a glucose sensor with response time τ_s. For noise filtering, however, the IMC internal model and controller are not modified to compensate for the presence of the filter in the measurement loop; the purpose for the filter is to provide an inverse for the noise component u(kT) in the measurement signal, and thus inclusion of IMC compensation for the filter would simply serve to reintroduce the noise component and counteract filter effectiveness. For the glucose sensor and noise filter described above, the following IMC relationships are employed:

Glucose Sensor

$$y_m(kT) = y(kT) + u(kT) \qquad k=0,1,2... \qquad (319)$$

Noise Filter

$$\hat{y}_m(kT) = \frac{\tau_f \hat{y}_m(kT-T) + T y_m(kT)}{\tau_f + T} \qquad k=0,1,2... \qquad (320)$$

Internal Model

$$\tilde{y}^*(kT) = \frac{\tau_p \tilde{y}^*(kT-T) + TK_p m(kT-\delta_p-T)}{\tau_p + T} \qquad k=0,1,2... \qquad (321)$$

Optimal Controller

$$m(kT) = \frac{\tau_p}{K_p} \frac{\varepsilon^*(kT)-\varepsilon^*(kT-T)}{T} + \frac{1}{K_p}\varepsilon^*(kT) \quad m_{min} \leq m(kT) \leq m_{min}; k=0,1,2... \qquad (322)$$

where the error signal is given by (see Figure 121)

$$\varepsilon^*(kT) = y_{sp} - (\hat{y}_m(kT) - \tilde{y}^*(kT)) \qquad k=0,1,2... \qquad (323)$$

and the digital controller output m(kT) is converted to continuous time output m(t) by Equation 301. Here, the internal model and controller (Equations 321 and 322) are the digital IMC control equations (Equations 299b and 300) previously derived for application to systems with discrete sampling interval T.

The quality of blood glucose regulation achieved by application of the above IMC equations is affected by the contribution of measurement noise u(kT) via parameter α, the discrete time sampling interval T, and the filter time constant τ_f. It should be noted that control generated by the

above approach does not represent optimality because optimal filtering with respect to the noise input u(kT) is not considered. Optimal filtering refers to application of filter designs, such as the Kalman filter, that provide for interactive gain adjustment such that the noise contribution is minimized as a function of time (for details, see Maybeck, 1982). Specification of the filter time constant τ_f in the present study, however, is equivalent to using a fixed filter gain. Application of optimal adaptive noise filtering to the problem of blood glucose control presents special difficulties due to the presence of the unmeasured rate of oral glucose loading that drives the system response. Because of this unmeasured input, extended-adaptive Kalman filtering methods of optimal estimation must be employed. Such methods are based on use of a stochastic (Markov) system model for prediction of the time-varying parameter to be estimated (Stephanopoulos and San, 1984), the system model being driven by a noise source for which the variance undergoes adaptive changes in response to observation noise (Jazwinski, 1970). The effectiveness of this estimation approach has been recently demonstrated for on-line control of bioreactors based on noise-contaminated data (Stephanopoulos and San, 1984; San and Stephanopoulos, 1984). The purpose of the present study, however, is to determine the effectiveness of a simple first-order response filter, and thus to determine the need, if any, for use of more sophisticated optimal filtering methods.

As stated previously, measurement noise primarily interacts with derivative controller action. For the case of blood glucose regulation, an important consideration with respect to measurement noise interaction is its possible inducement of baseline hypoglycemic drift. Under basal steady state conditions, derivative controller action is normally zero reflecting

a constant blood glucose level. The presence of artifactual measurement noise, however, can randomly drive the controller output about a mean (time-averaged) value independent of actual in vivo changes in blood glucose concentration. If measurement noise causes random insulin infusion rate deviations from basal with magnitudes exceeding the basal insulin infusion rate IR_b as shown in Figure 122, controller output is clipped because the insulin infusion rate IR(t) must be constrained such that its value is greater than zero. As a result of clipping the controller output, the time-averaged insulin infusion rate lies above the normal basal insulin infusion rate (the area represting $IR>IR_b$ (or $m>0$) becomes greater than the area representing $IR<IR_b$ (or $m<0$) with time in Figure 122). When the time-averaged insulin infusion rate exceeds the normal basal insulin infusion rate in the absence of glucose loading, hypoglycemia is induced. For example, in the worst case the insulin infusion rate would be randomly driven between zero and its maximum value of 1275 μU/kg•min (evoking both minimum and maximum constraint clipping), resulting in a time-averaged insulin infusion rate approaching 637 μU/kg•min; this value represents about twice the normal basal insulin infusion rate of 320 μU/kg•min and would cause a predicted time-averaged blood glucose concentration below 40 mg/dl. Thus, one objective of noise filtering is to avoid basal hypoglycemic drift. Of course the other objective is to minimize the adverse effects of noise interaction with controller regulation of blood glucose during oral glucose loading.

Simulation studies were undertaken to assess the effectiveness of first-order response noise filtering. For these studies, psuedo-random zero-mean gaussian deviates were generated using the IMSL library computer subroutine GNML. The standard deviation of these gaussian deviates was

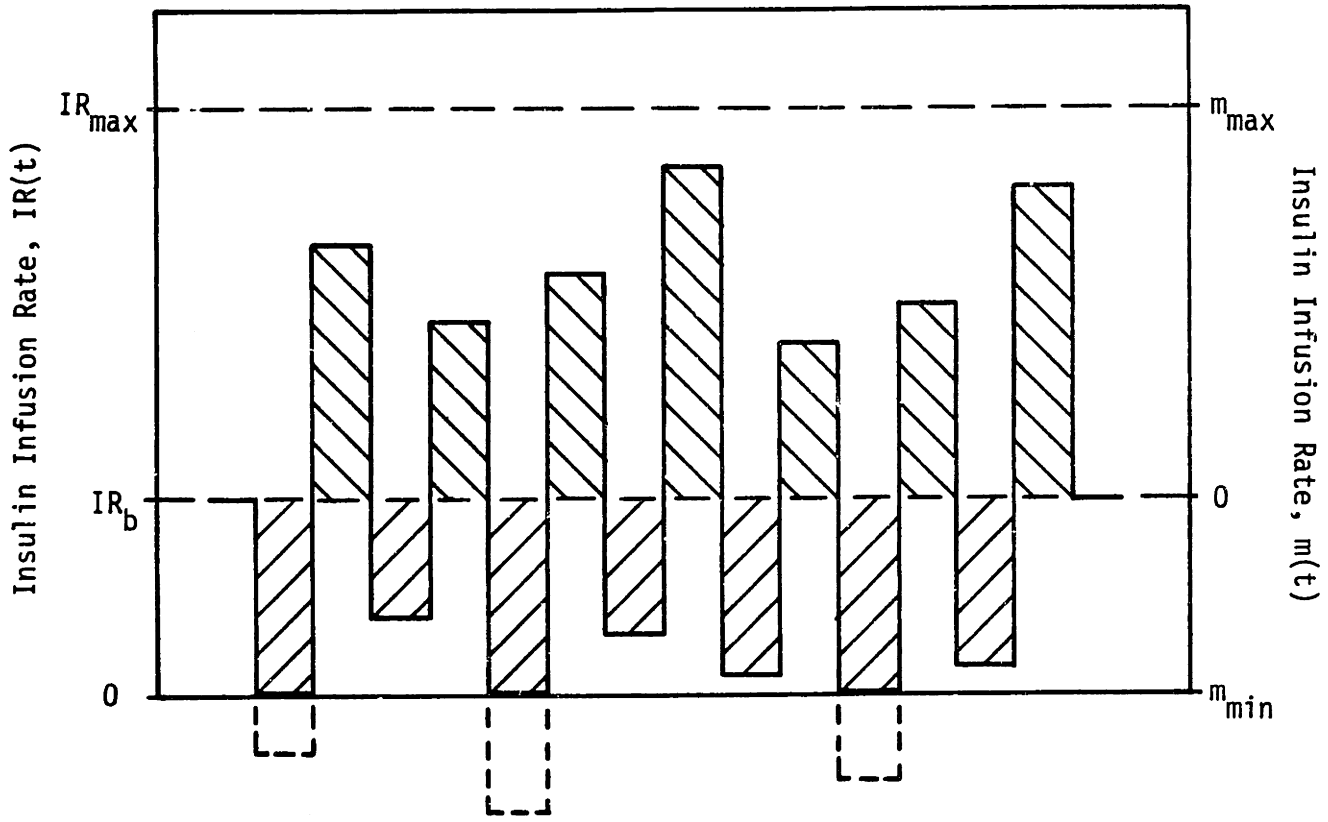

Fig. 122 Illustration depicting how basal state noise-driven deviations in insulin infusion rate can lead to clipping of controller output causing inducement of hypoglycemia.

varied via parameter α as defined by Equation 317, and the resulting zero-mean random gaussian deviates representing measurement noise u(kT) were superimposed on the discrete blood glucose concentration values according to Equation 316 to generate a simulated sensor measurement output $y_m(kT)$ contaminated with noise. The general approach taken was to examine tolerance of representative operating systems (T, τ_f fixed) to increases in the measurement noise (via increasing parameter α) as assessed with respect to resulting basal hypoglycemic drift and control of oral glucose loading during the 100g OGTT.

The effectiveness of the first-order response noise filter resides in the property that high frequency components of the input signal are attenuated to a greater extent than the low frequency components of the input signal upon passage of the signal through the filter. The resulting noise suppression for a fixed level of noise input thus increases as the ratio T/τ_f decreases. For a given sampling interval T, a design compromise must be reached between achievable noise suppression (favoring large values of τf) and avoidance of sluggish filter response in tracking of the input signal (favoring small values of τ_f). For practical applications of single exponential smoothing, a ratio $T/\tau_f=0.2$ represents a reasonable compromise (Koppel, 1968). Simulation studies were conducted to examine the noise tolerance of two representative system designs: 1) a discrete time IMC system with sampling interval T=1 min and a first-order response filter with time constant τ_f=5 min; and 2) a discrete time IMC system with sampling interval T=4 min and a first-order response filter with time constant τ_f=20 min. Filters with time constants τ_f>20 min were not considered on the basis of the simulation results presented in Figure 113 which demonstated that introducing sensor response time τ_s greater than about 20

min into the measurement signal (a case analogous to introducing filter response time τ_f into the measurement signal) leads to unacceptable blood glucose regulation in the absence of IMC control loop compensation.

Presented in Figures 123-126 are results of simulation studies to assess the noise tolerance characteristics of a digital IMC structure employing a sampling interval T=1 min coupled with a first-order response filter with time constant τ_f=5 min. The quality of IMC blood glucose regulation provided by Equations 319-322 was studied with respect to basal baseline drift (Figures 123 and 124) and during the 100g OGTT (Figures 125 and 126) as the magnitude of the measurement noise was varied (via parameter α) in Equation 317. As shown in the upper plot of Figure 123, introduction of 2.5% measurement noise (α=0.025) caused a small drift in basal blood glucose concentration from maintenance at the desired setpoint concentration of 75 mg/dl to a time-averaged concentration of about 73 mg/dl. Introduction of 5% measurement noise (α=0.05) further decreased the basal time-averaged blood glucose concentration to roughly 67 mg/dl. As indicated in the lower panel of Figure 123, the observed depression of basal glucose levels coincided with increased interaction of noise with controller insulin delivery as the measurement noise level was elevated. At the 5% measurement noise level, the filter's effectiveness was readily demonstrable, however, as its removal from the IMC structure resulted in rapid, unacceptable depression of basal blood glucose concentration caused by excessive noise-induced controller action. In the absense of measurement noise (α=0), the dead time T induced by digital control and the (uncompensated) measurement response time τ_f introduced by the filter only caused modest degradation in blood glucose control during the 100g OGTT from that obtainable under ideal conditions (see upper panel of Figure

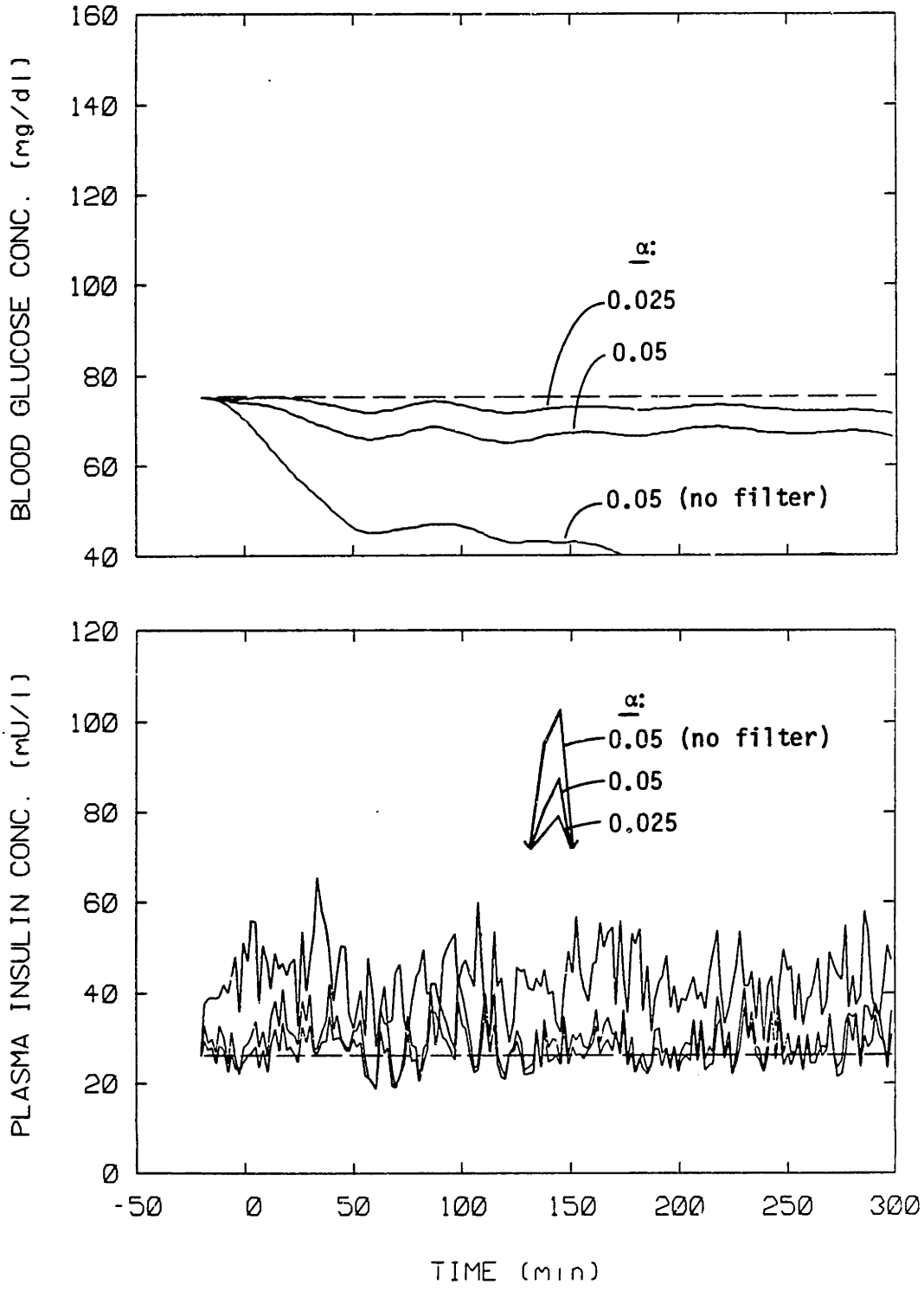

Fig. 123 Simulation studies to assess the basal state noise tolerance characteristics of digital IMC (Equations 319-322) with sampling interval T=1 min and first-order response filter with time constant τ_f=5 min. Gaussian measurement noise of 2.5-5% was introduced by variation of parameter α from 0.025-0.05 in Equation 317.

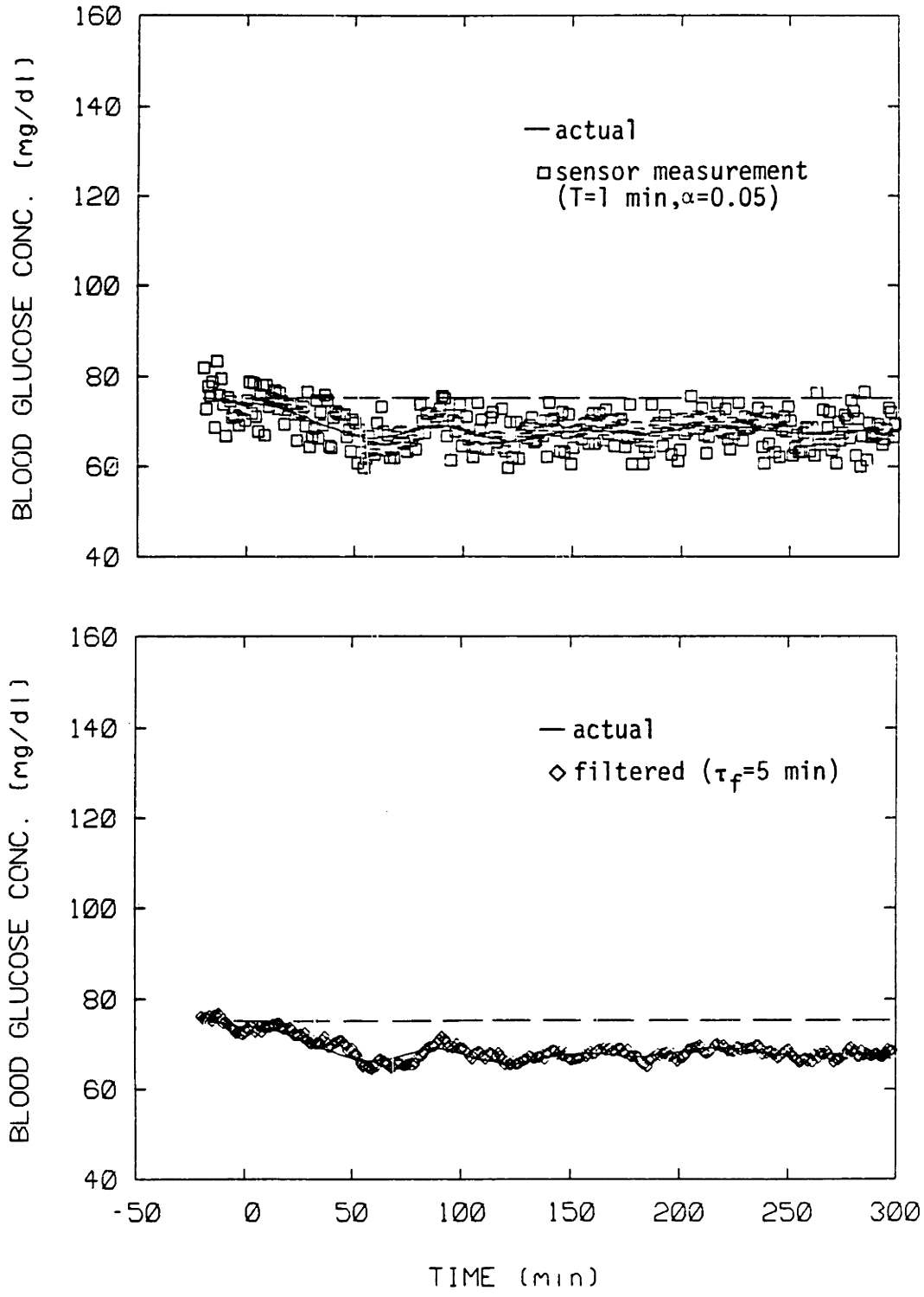

Fig. 124 In the upper panel, true blood glucose concentration is compared with its sensor measurement for the case of α=0.05 in Figure 123. In the lower panel, true blood glucose is compared with that obtained by filtering of the measured values with τ_f=5 min.

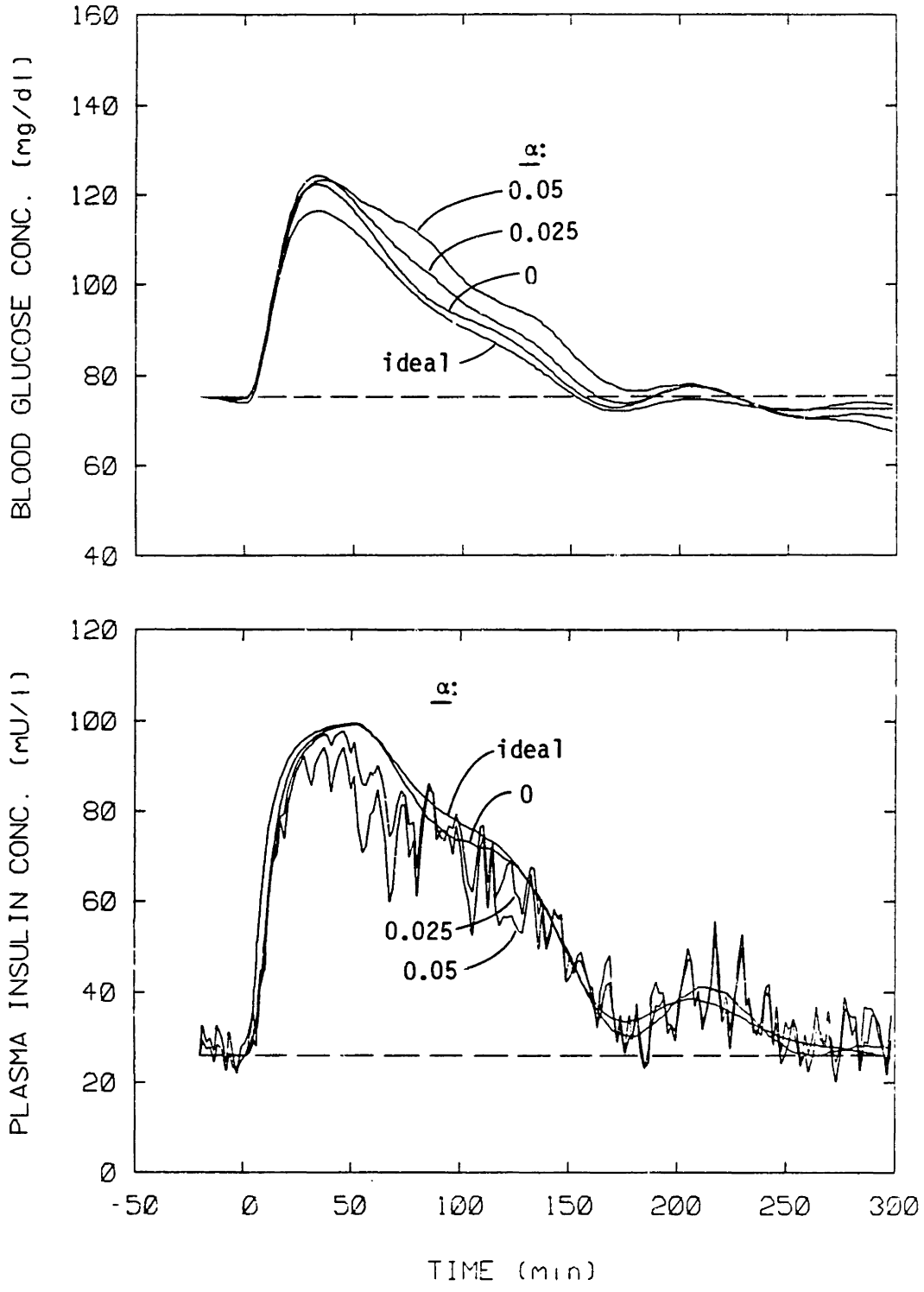

Fig. 125 Simulation studies to assess the noise tolerance characteristics of the digital IMC system of Figure 123 (T=1 min; τ_f=5 min) during the 100g OGTT. Measurement noise was varied from 0-5% by variation of parameter α in Equation 317. Included for comparison are results for the case of ideal continuous measurement (T→0; τ_f→0; α=0).

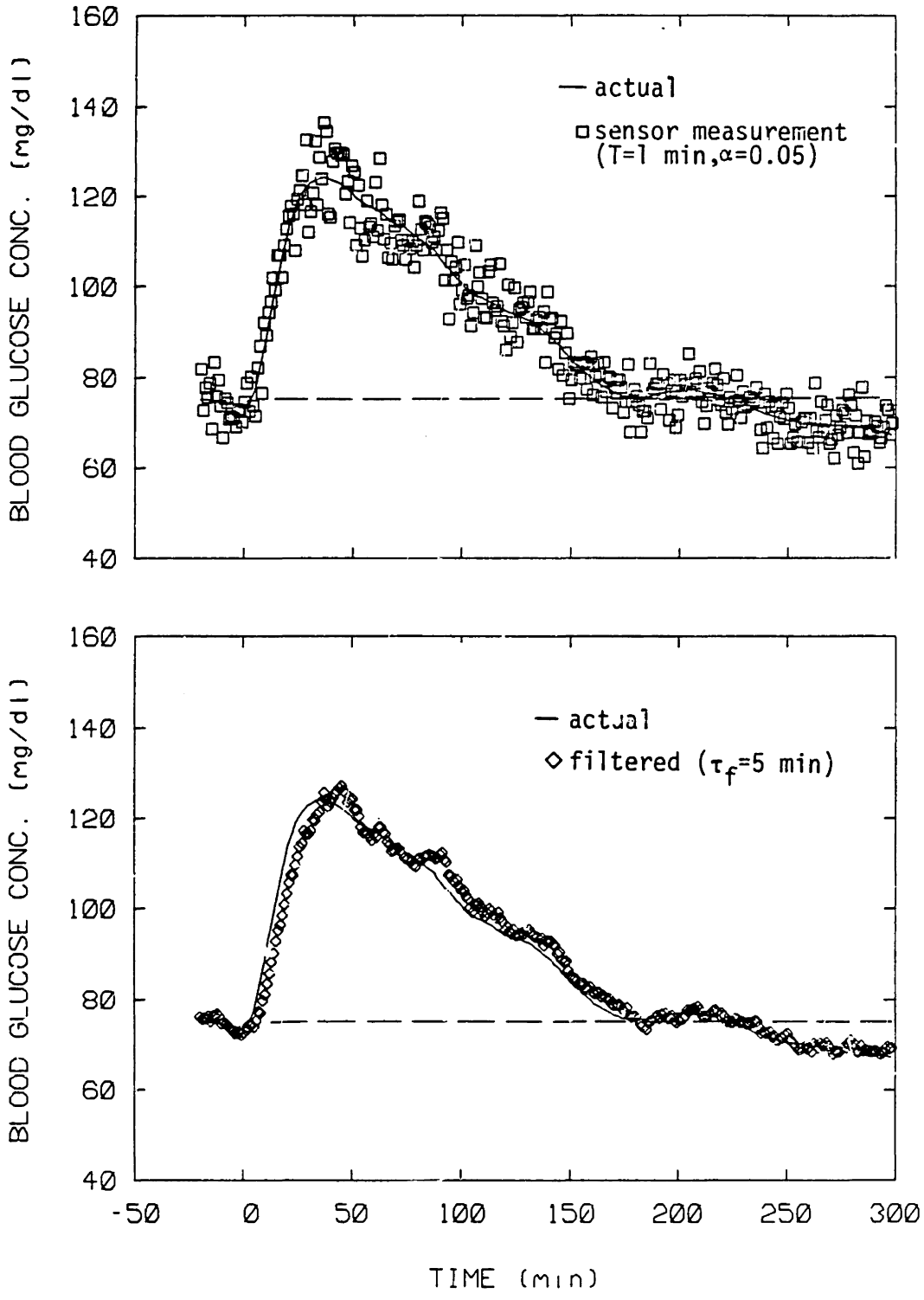

Fig. 126 In the upper panel, true blood glucose concentration is compared with its sensor measurement for the case of α=0.05 in Figure 125. In the lower panel, true blood glucose is compared with that obtained by filtering of the measured values with τ_f=5 min.

123). Presented in Figure 124 are comparisons between 1) true and measured (y_m+G_b) blood glucose concentration (upper panel), and 2) true and filtered ($\dot{y}_m+G_b$) blood glucose concentration (lower panel) for the case of 5% measurement noise (α=0.05) in Figure 123). The filter effectiveness is clearly demonstrated by noting the large scatter in the measured (upper panel) relative to the filtered (lower panel) values. (It should be noted to avoid misinterpretation of results that, for clarity, the blood glucose concentration scale employed in Figure 122 is expanded relative to that used for presentation of earlier sensor measurement interaction studies.) Introduction of measurement noise resulted in increased hyperglycemia during the OGTT (Figure 125) as noise interactions interfered with controller action in determining insulin delivery rate. During the period of blood glucose recovery to its steady state basal level, however, measurement noise did not induce hypoglycemic excursions in excess of those oberved in the baseline drift studies of Figure 123. To illustrate filter effectiveness, presented in Figure 126 are comparisons between 1) true and measured blood glucose concentration (upper panel), and 2) true and filtered blood glucose concentration (lower panel) for the case of 5% measurement noise (α=0.05) in Figure 125.

The above simulation studies were repeated to assess the performance characteristics of a digital IMC system utilizing a sampling interval of T=4 min coupled with a first-order response filter with time constant τ_f=20 min; results are presented for basal hypoglycemic drift and 100g OGTT loading studies in Figures 127-128 and 129-130, respectively. Under basal conditions (Figure 127), the uncompensated filter response time τ_f of 20 min induced oscillations (period ~120 min) in basal glucose concentration reflecting second-order control loop interactions. The mean time-averaged

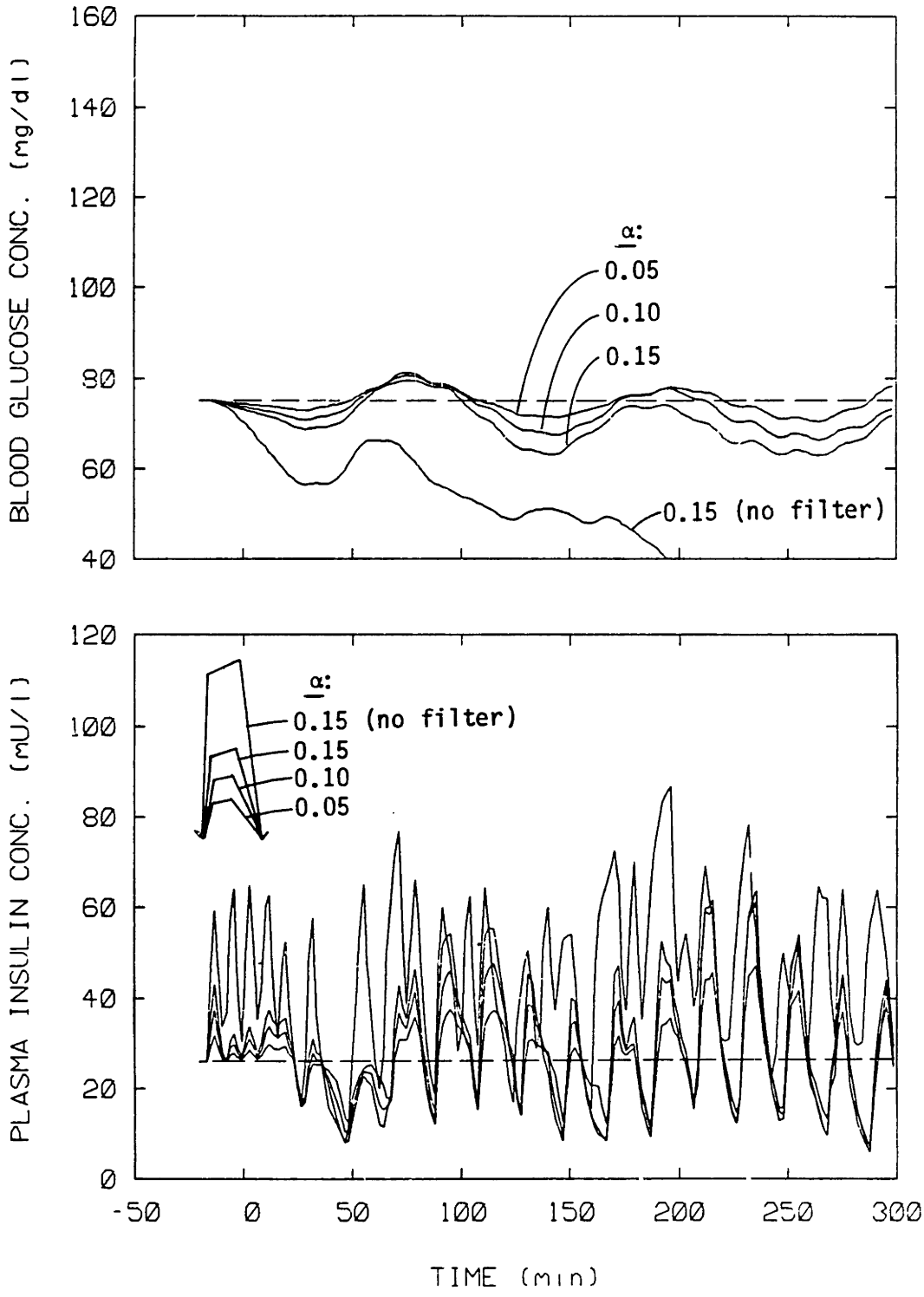

Fig. 127 Simulation studies to assess the basal state noise tolerance characteristics of digital IMC (Equations 319-322) with sampling interval T=4 min and a first-order response filter with time constant τ_f=20 min. Gaussian measurement noise of 5-15% was introduced by variation of parameter α from 0.05-0.15 in Equation 317.

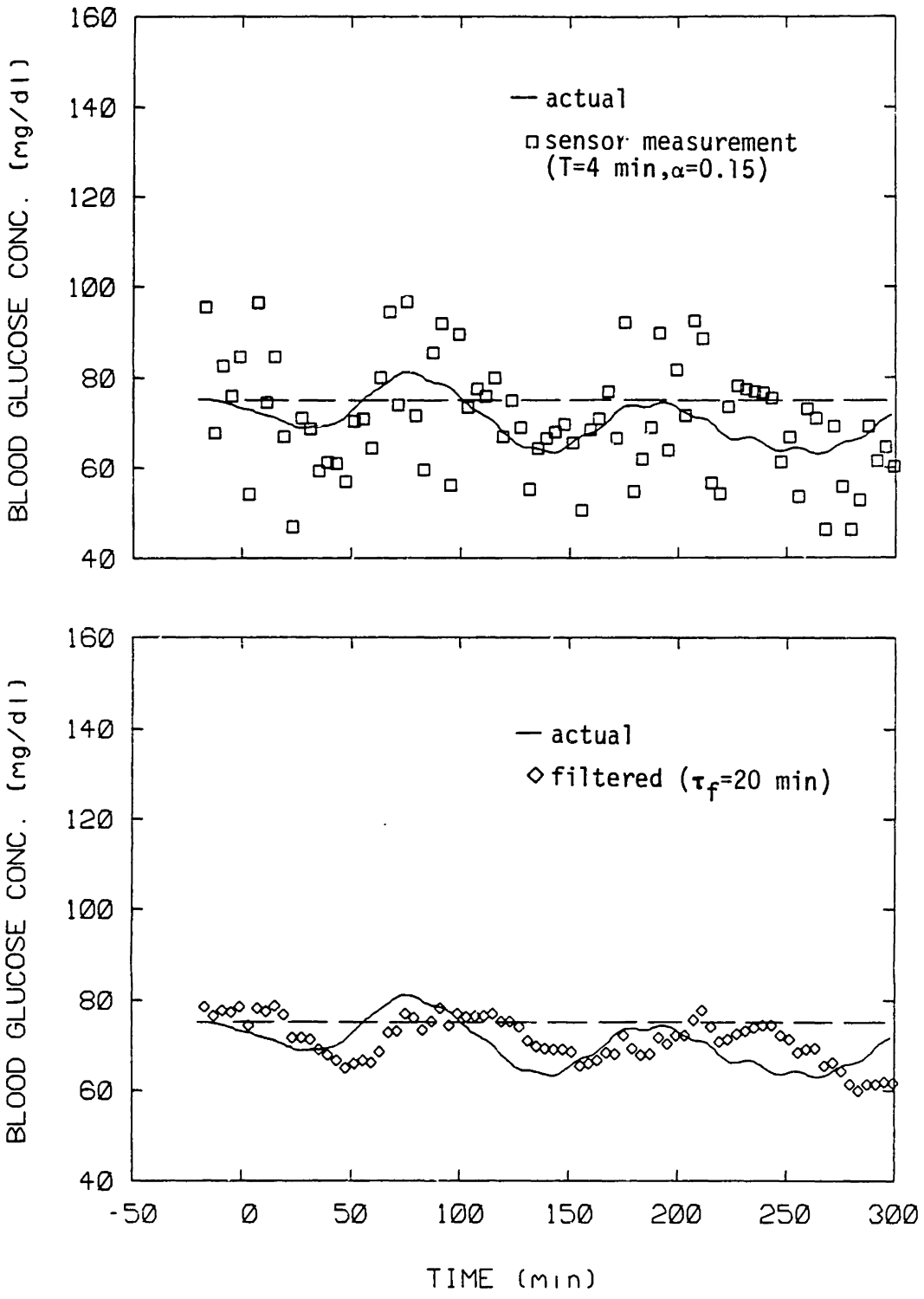

Fig. 128 In the upper panel, true blood glucose concentration is compared with its sensor measurement for the case of α=0.15 in Figure 127. In the lower panel, true blood glucose is compared with that obtained by filtering of the measured values with τ_f=20 min.

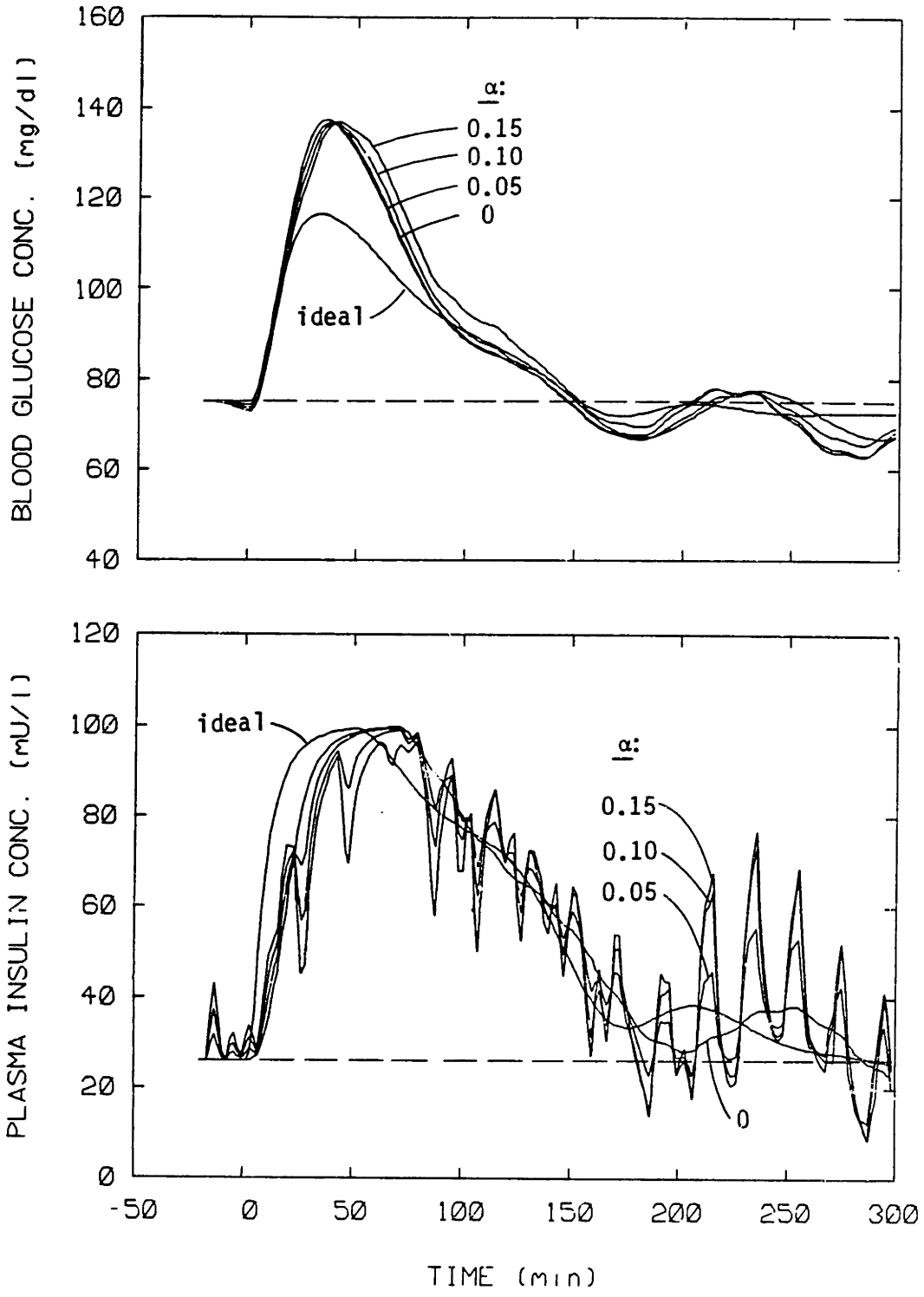

Fig. 129 Simulation studies to assess the noise tolerance characteristics of the digital IMC system of Figure 127 (T=4 min; τ_f=20 min) during the 100g OGTT. Measurement noise was varied from 0-15% via variation of parameter α in Equation 317. Included for comparison are results for the case of ideal continuous measurement (T→0; τ_f→0; α=0).

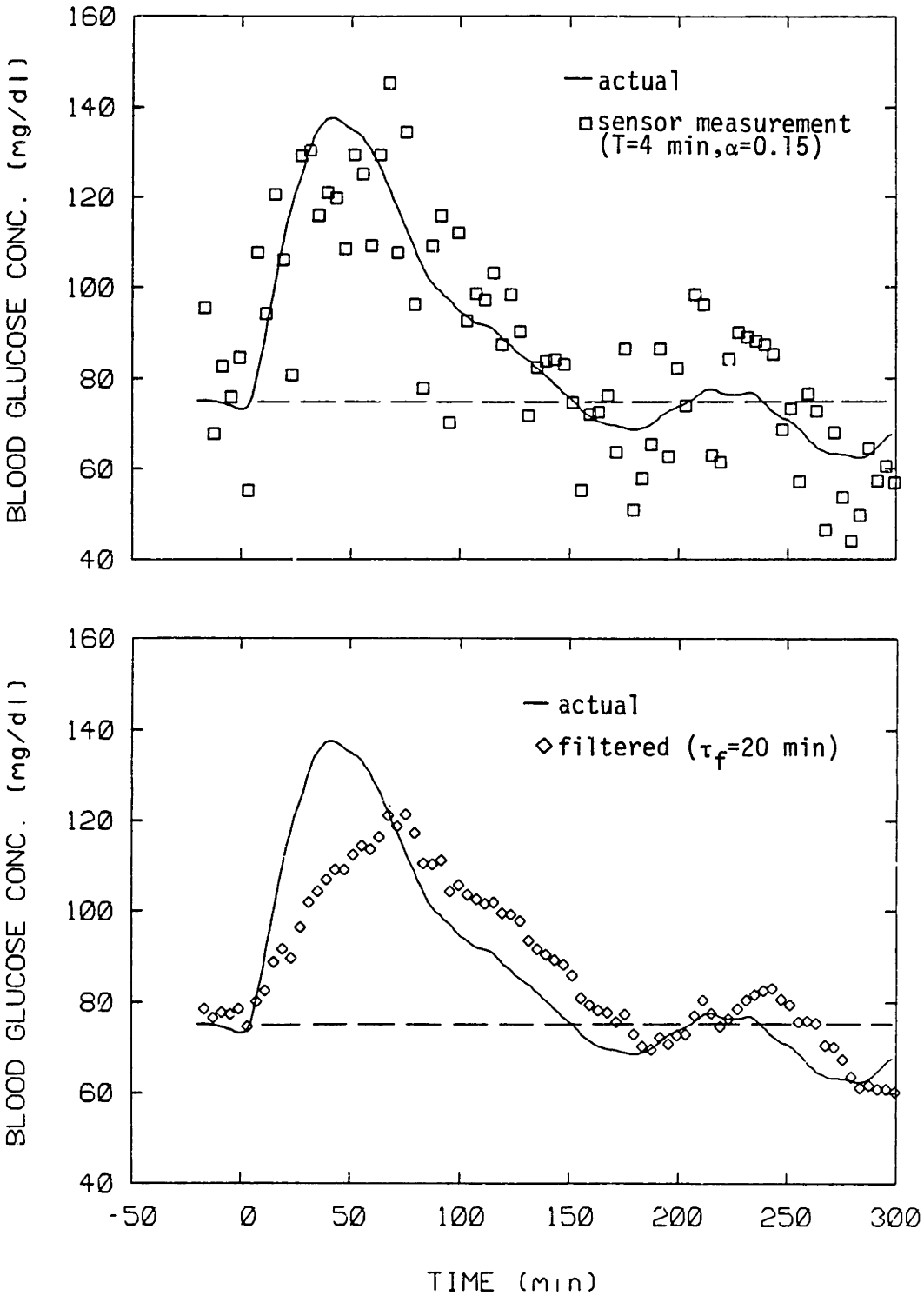

Fig. 130 In the upper panel, true blood glucose concentration is compared with its sensor measurement for the case of α=0.15 in Figure 129. In the lower panel, true blood glucose is compared with that obtained by filtering of the measured values with τ_f=20 min.

blood glucose concentration decreased with superposition of measurement noise; for measurement noise of 15% (α=0.15), however, baseline hypoglycemia below 60 mg/dl was not observed. In contrast, removal of the filter with 15% measurement noise caused rapid baseline drift to unacceptable hypoglycemic levels. To illustrate filter effectiveness, presented in Figure 126 are comparisons between 1) true and measured blood glucose concentration (upper panel), and 2) true and filtered blood glucose concentration (lower panel) for the case of 15% measurement noise (α=0.15) in Figure 125. As shown in Figure 129, the sampling interval T=4 min coupled with the uncompensated filter response time τ_f=20 min in the measurement signal caused a significant increase in peak hyperglycemia during the 100g OGTT relative to that obtainable under ideal conditions. The filter, however, provided for acceptable minimalization of further degradation in the quality of blood glucose regulation as the measurement noise content was increased to 15%. To demonstrate the filter effective, in Figure 130 measured (upper panel) and filtered (lower panel) blood glucose concentration values are compared with true blood glucose response for the case of 15% measurement noise (α=0.15) in Figure 129. It may be noted from the lower panel of Figure 130 that, although the filtered response was relatively noise free, passage of the blood glucose response signal through the filter resulted in a filter output signal that was dynamically sluggish and attenuated in magnitude relative to the true blood glucose response being monitored; this was attributable to the presence of response time τ_f=20 min in the digital filter.

Because filter effectiveness is primarily dictated by the ratio T/τ_f, it is interesting that the latter system (T=4 min; τ_f=20 min) tolerated roughly 15% noise , whereas the former system (T=1 min; τ_f=5 min) tolerated

only about 5% noise. The explanation for this behavior may be attributed to the notion that noise primarily interferes with derivative term calculations in the control loop equations; since first-order derivative term calculation errors are proportional to 1/T, passage of a given amount of noise-induced error through the filter results in less relative control loop interaction as the sampling interval T increases.

The above results suggest that simple first-order response noise filtering would provide acceptable performance under quite limited conditions. Because introduction of the filter and thus uncompensated response time τ_f into the measurement signal impacts on achievable blood glucose control, use of filter time constants τ_f>20 min would not be desirable. This restriction limits applications to systems employing sampling intervals T<4 min, such that T/τ_f<0.2. As shown in Figures 127 and 129, for a system with T=4 min and τ_f=20 min, 15% noise tolerance is achievable at the expense of basal hypoglycemic drift approaching 60 mg/dl and increased hyperglycemia during oral glucose loading. Although decreasing the filter time constant to τ_f=5 min improves blood glucose response characteristics as shown in Figures 123 and 125, this restricts the sampling interval T to 1 min or less and decreases acceptable noise tolerance to only about 5%. Furthermore, it must be noted that superposition of additional sensor measurement nonidealities (ζ_s, τ_s) was not considered in the above studies, and inclusion of these effects would cause additional degradation of observed blood glucose regulation when coupled with first-order response filter insertion into the IMC structure. It may thus be concluded that for real sensors producing measurement noise in excess of 5%, the potential benefits to be gained from designing more sophisticated optimal filtering schemes would be justified. For glucose

sensors with measurement characteristics approaching ideality ($T \leq 1$ min; $T+\delta_S+\tau_S \leq 9$ min), use of simple first-order response filtering is satisfactory for dealing with measurment noise of 5% or less.

4) Discussion

As illustrated in the first part of this chapter, IMC provides a simple and effective approach to closed-loop insulin delivery that results in optimal blood glucose regulation simliar to that observed in the nondiabetic. For initial treatment, however, ideal blood glucose measurment was assumed. Because glucose sensors suitable for long-term in vivo implantation will likely provide for nonideal glucose monitoring, IMC analysis was extended to explore blood glucose regulation in the presence of glucose sensor nonidealities.

IMC offers a very straightforward approach to consideration of glucose sensor measurement nonidealities. In general, the internal model directly incorporates all information with respect ot the measurement response dynamics resulting from the presence of the glucose sensor, and the optimal controller is taken as the inverse of that portion of the internal model transfer function which, upon factorization, leads to stable, realizable control.

Because introduction of blood glucose measurement dead time cannot be compensated by controller design modification, direct inclusion of sensor dead time δ_S (Figure 111) or indirect inducement of dead time T caused by digital control (Figure 115) significantly degrades achievable blood glucose control as effective measurement dead time approaches the process response time τ_p. Although optimal controller design is not affected by measurement signal dead time, inclusion of measurment dead time in the IMC

internal model is important because it provides for stable operation.

Unlike measurement dead time, the presence of sensor response time τ_S can be fully compensated by optimal controller design; thus, the effects of sensor response time can be cancelled out of the IMC loop signals and blood glucose control obtainable under ideal measurement conditions ($\tau_S \to 0$) results. Such IMC compensation, however, introduces second-order derivative terms into the internal model and controller equations. If, for practical reasons, only suboptimal first-order IMC response time compensation is employed, acceptable blood glucose control results as sensor response time approaches the process response time τ_p (see Figure 112). For cases in which unanticipated sensor response time arises from factors such as tissue encapsulation of the sensor implant, lack of IMC compensation leads to unacceptable blood glucose control for induced response times greater than about 20 min (see Figure 113).

The presence of systematic sensor measurement error causes an offset in blood glucose levels under IMC closed-loop regulation (Figure 114). An overestimate of glucose concentration causes hypoglycemic offset and is thus potentially hazardous. Concomitant with basal blood glucose offset induced by systematic measurement error, however, is altered basal insulin delivery rate; it may thus be possible to implement system logic to detect such conditions.

Coupling of sensor nonidealities (Figures 117 and 119) leads to superposition of the effects observed by consideration of nonidealities individually. Of particular note is the constraint of Equation 315 which indicates that blood glucose control approaches that attainable with an ideal sensor if the sum of the nonideal sensor measurement characteristic times ($\delta_S+\tau_S+T$) is much less than the process response time τ_p. It is

clear that present bedside systems such as the Biostator GCIIS operate within limits of ideal glucose observation. With respect to realizable glucose sensors for long-term in vivo implantation, however, the above constraint will be difficult to meet. For such systems, realization of good blood glucose control will necessitate use of effective control loop designs in order to minimize the impact of sensor nonidealities.

IMC of blood glucose in the presence of meausurement noise was briefly addressed. Results suggest that acceptable 5% noise tolerance may be obtained using simple first-order response noise filtering for systems with sensors providing otherwise ideal measurement characteristics (as defined by Equation 315). For sensors with measurment noise in excess of 5%, design of more sophisticated optimal filtering schemes would be potentially beneficial, as introduction of the first-order response filter into the IMC measurment signal, due to filter response time τ_f, degrades observed blood glucose regulation as the value of τ_f is increased.

Finally, it may be noted that the results obtained in studying the effects of sensor nonidealities on blood glucose regulation have rather widespread applicability with respect to problems associated with closed-loop insulin delivery in general. This is because the generalized glucose measurment models employed in the present work can be used to approximate consideration of parallel design problems. For example, relative to vascular glucose sensing, placement of a glucose sensor with a needle configuration in subcutaneous tissue leads to inducement of approximately a 5 min response time and roughly a 10% decrease in glucose concentration measurement (Shichiri et al., 1984); such effects of subcutaneous sensor placement may be readily analyzed in terms of results presented herein. Furthermore, in addition to closed-loop electromechanical systems, research

efforts are presently being directed toward therapies based on transplantation of insulin-secreting tissue. One of the most promising approaches to tissue transplantation therapy is the hybrid artificial or bioartificial pancreas (for review, see Reach, 1984). The hybrid artificial pancreas consists of intact pancreatic islets or individual beta-cells protected from tissue rejection by semipermeable membranes; the membrane pore size is selected such that glucose and insulin may freely pass through, but passage of larger entities such as gamma globulins and lymphocytes is blocked. The device is implanted as an arteriovenous shunt, and fluctuation of blood glucose levels stimulates insulin release via normal biological feedback response from the insulin-secreting tissue. Due to the presence of the protective membrane and the volume associated with the tissue chamber, diffusive and/or convective delays in glucose and insulin transport will degrade device performance, and consideration of such effects on device response is presently under investigation (Sparks et al., 1982; Weinless and Colton, 1983; Reach et al., 1984).

Insight into design requirements for provision of good blood glucose regulation by the hybrid artificial pancreas can be attained by drawing analogies between such biological feedback systems operating with tranport-induced dynamic nonidealities and the IMC system operating with measurement-induced dynamic nonidealities. The hybrid pancreas may be modeled in terms of transfer functions accounting for 1) the dynamics of glucose transport from the blood into the beta-cell chamber, and 2) the dynamics of insulin transport from the beta-cell chamber into the blood. Using first-order lag models to represent these transport dynamics, the following relationships are defined:

$$G_g(s) = \frac{y_c(s)}{y(s)} = \frac{e^{-\delta_g s}}{\tau_g s + 1} \tag{324}$$

$$G_i(s) = \frac{m(s)}{m_c(s)} = \frac{e^{-\delta_i s}}{\tau_i s + 1} \tag{325}$$

where $G_g(s)$ = tranfer function for glucose transport from the blood into the beta-cell chamber

$G_i(s)$ = transfer function for insulin transport from the beta-cell chamber into the blood

$y_c(s)$ = glucose concentration in the beta-cell chamber (mg/dl)

$y(s)$ = blood glucose concentration (mg/dl)

δ_g = glucose transport delay time (min)

τ_g = glucose transport response time constant (min)

$m(s)$ = rate of insulin release into the blood (μU/kg·min)

$m_c(s)$ = rate of insulin release from the beta-cells (μU/kg·min)

δ_i = insulin transport delay time (min)

τ_i = insulin transport response time constant (mU/kg·min)

For the hybrid artificial pancreas, a lumped process transfer function $G_p^*(s)$ may be defined in a manner similar to that used earlier for consideration of glucose sensor nonidealities, i.e.

$$G_p^*(s) = \frac{y_c(s)}{m_c(s)} = G_i(s)G_p(s)G_g(s) \tag{326a}$$

$$= \frac{e^{-\delta_i s}}{(\tau_i s + 1)} \frac{K_p e^{-\delta_p s}}{(\tau_p s + 1)} \frac{e^{-\delta_g s}}{(\tau_g s + 1)} \tag{326b}$$

where, as before, $G_p(s)$ represents the process transfer function for in vivo blood glucose response to changes in insulin delivery rate. Unlike the IMC structure which can be modified to compensate for deviations between $G_p^*(s)$ and $G_p(s)$, intrinsic beta-cell insulin response to glucose stimulation linking $y_c(t)$ and $m_c(t)$ in Equation 326a cannot be altered to compensate for the presence of transport-induced nonidealities in the biological feedback loop configuration. Thus, for the hybrid pancreas to provide blood glucose regulation approaching that observed in normal man, device design must minimize the deviations between $G_p^*(s)$ and $G_p(s)$ such that

$$G_p^*(s) \approx G_p(s) \tag{327}$$

This condition is approached if the total characteristic time associated with glucose and insulin transport dynamics in the device is much less than the process respose time τ_p, or

$$\delta_g + \tau_g + \delta_i + \tau_i \lesssim 9 \text{ min} \tag{328}$$

To summarize, because the biological controller (the beta-cell) is "tuned" for optimal performance in the absence of response constraints introduced by superposition of the hybrid pancreas configuration, the device design must introduce response nonidealities that, in combination, interfere with the feedback loop response dynamics on time scales much less than the response time τ_p for in vivo blood glucose response to changes in insulin delivery rate. The resulting constraint of Equation 328 imposes severe limitations on device transport delays; it may thus be importan to minimize such delays though careful design analysis if effective hybrid artificial pancreas systems are to be realized in the future.

C) Abnormalities of Diabetic Metabolism and Control

The Type I diabetic model employed for IMC design was obtained by removing endogenous pancreatic insulin reslease from the physiologic model of glucose metabolism originally formulated for normal man. This diabetic model represents the ideal case of a well-controlled, metabolically-normalized subject; the insulin-dependent diabetic for which all metabolism is normal (with the exception of pancreatic insulin release) may be termed a "controlled" Type I diabetic.

As discussed in Chapter V, however, abnormalities such as insulin resistance, insulin antibody binding, and impaired glucose counter-regulation are commonly observed in Type I diabetics. The extent to which these abnormalities appear to influence in vivo glucose regulation varies over a wide range from patient to patient. Although the pathophysiologies of these diabetes-related disorders are not well understood at present, increasing clinical evidence suggests that the prevalence of these abnormalities is inversely related to the quality of therapy provided. Furthermore, recent studies indicate reversibility of diabetic abnormalities upon provision of improved control. Because diabetic abnormalities are observed to a greater extent in poorly controlled subjects, the term "uncontrolled" Type I diabetic is often applied to the insulin-dependent diabetic displaying such metabolic disorders. In Chapter V, an uncontrolled Type I diabetic model was formulated by introducing tissue insulin resistance and insulin antibody binding into the controlled Type I diabetic model. The resulting model may be assumed representative of the uncontrolled Type I diabetic, as its use provided good predictions of 100g OGTT response data for typical IDDM subjects during Biostator GCIIS therapy (see Figure 104).

Since the IMC system was designed using the controlled Type I diabetic model, addition studies were performed to explore the effectiveness of this system if applied to diabetics not initially in a metabolically-normalized state. For these studies, the uncontrolled Type I diabetic model of Chapter V was further modified to include the presence of inhibited glucose counterregulatory capacity. Patients with diabetes of long duration treated by conventional injection therapies may not respond with any increase above basal in circulating glucagon levels during hypoglycemia (see Figure 93 from Bolli et al., 1983). Such impaired counterregulatory response was modeled by setting $M^{G}_{P_{IR}}$ equal to unity in Equation 155 such that glucagon response would be fixed at basal sensitivity independent of changes in arterial glucose concentration. For simulation studies coupling the uncontrolled Type I diabetic model with IMC insulin delivery, a steady state blood glucose concentration of 75 mg/dl required a basal insulin infusion rate IR_b of 390 $\mu U/kg \cdot min$. Due to the presence of insulin resistance in the uncontrolled Type I diabetic model, the value of IR_b here is greater than that used previously for simulations with the controlled Type I diabetic model (IR_b=320 $\mu U/kg \cdot min$).

For the IMC insulin delivery system derived earlier in this chapter (Equations 260 and 261), four design parameters influence performance. Three of these parameters, namely K_p, τ_p, and δ_p, resulted from characterization of in vivo blood glucose response to changes in insulin delivery rate. The fourth parameter, m_{max}, was imposed to limit plasma insulin levels resulting from maximal controller action. For the controlled Type I diabetic, m_{max} was assigned a value of 905 $\mu U/kg \cdot min$ such that the maximum insulin delivery rate to the patient IR_{max} equaled 1225 $\mu U/kg \cdot min$; this constraint limited plasma insulin concentration to 100 $\mu U/ml$ or less, the

range obseved in normal subjects following oral glucose loading.

Because the controlled Type I diabetic model was employed for IMC design and parameter selection, simulation studies were performed to explore the effectiveness of this system if used to regulate blood glucose in the Type I diabetic not initially in a metabolically-normalized state. Simulation studies to assess the effects of IMC parameter selection on blood glucose regulation in the uncontrolled Type I diabetic during the 100g OGTT are presented in Figure 131. Here, the IMC system was interfaced with the uncontrolled Type I diabetic model while parameters K_p, τ_p, δ_p, and m_{max} (via designation of IR_{max}) were varied in the IMC internal model (Equation 260) and controller (Equation 261). As shown in the upper panel of Figure 131, use of the IMC parameter set originally derived for the controlled Type I diabetic (denoted IMC1) resulted in peak hyperglycemia of 205 mg/dl, but IMC action did not induce hypoglycemia as blood glucose concentration remained modestly elevated 300 min after oral glucose administation. Included for comparison in Figure 131 are results presented earlier (see Figure 109) from application of parameter set IMC1 to the controlled Type I diabetic. As shown in the lower panel of Figure 131, initial plasma (free) insulin response to rising blood glucose concentration was much slower in the uncontrolled than in the controlled Type I diabetic using parameter set IMC1. Such sluggishness of plasma free insulin response to changes in insulin infusion rate result from the presence of circulating insulin antibodies in the uncontrolled diabetic.

Because application of parameter set IMC1 to the uncontrolled Type I diabetic resulted in significantly higher blood glucose than resulted by IMC1 application to the controlled Type I diabetic (see upper panel of Figure 131), further work was undertaken to determine if improved IMC blood

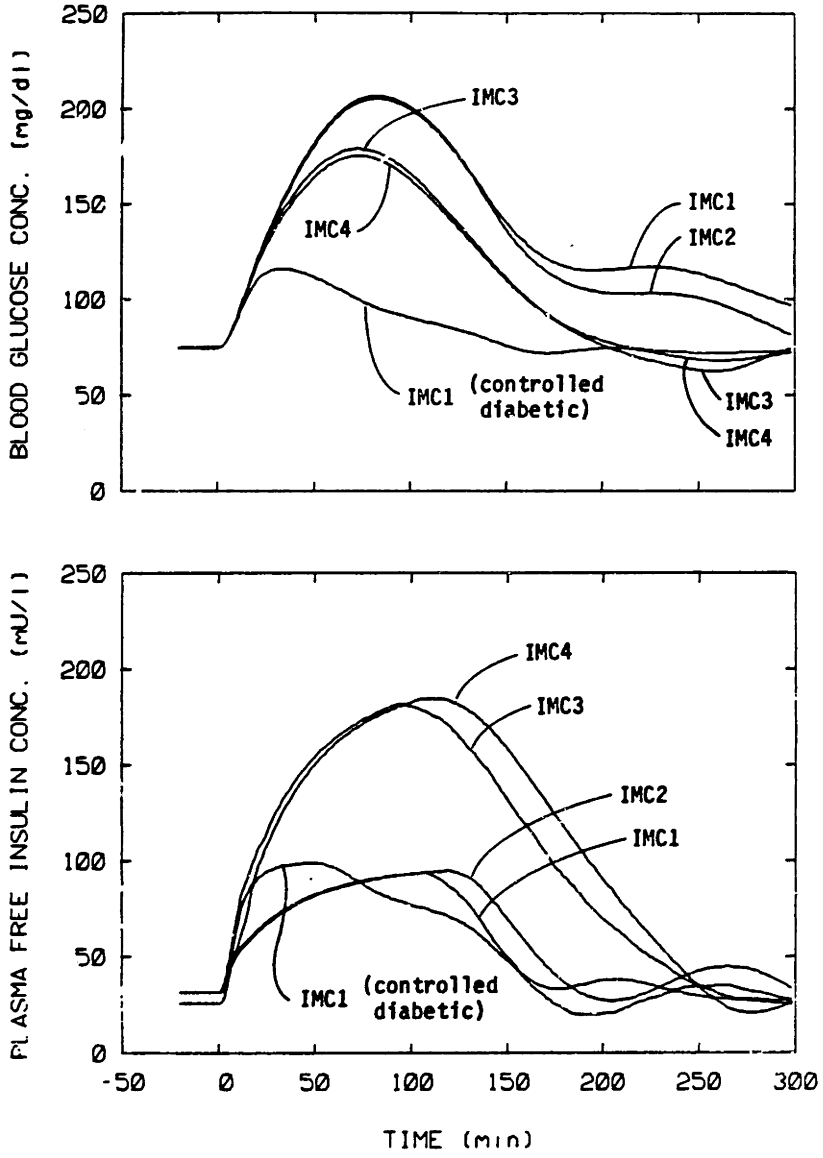

Designation	K_p (mg/dl)(kg·min/μU)	τ_p (min)	δ_p (min)	IP_{max} (μU/kg·min)
IMC1	-0.21	90	9	1225
IMC2	-0.19	150	22	1225
IMC3	-0.21	90	9	2450
IMC4	-0.19	150	22	2450

Fig. 131 Simulation studies to assess the effects of IMC parameter selection on blood glucose control in the uncontrolled Type I diabetic during the 100g OGTT. Parameter values for K_p, τ_p, δ_p, and m_{max} (via designation of IR_{max}) were varied in Equations 261 and 262 as defined in the figure legend. Included for comparison is application of parameter set IMC1 to regulation of the controlled Type I diabetic.

glucose control could be attained in the uncontrolled dabetic by changing the IMC parameter values. Since parameters K_p, τ_p, and δ_p are selected on the basis of characterization of in vivo blood glucose response to changes in insulin infusion rate, a logical approach to improvement of control was to recharacterize this process using the uncontrolled Type I diabetic model. For this purpose, an insulin infusion step change "experiment" identical to that previously described for characterizing response in the controlled diabetic (Figure 106) was repeated for the uncontrolled diabetic; the resulting blood glucose response curve yielded the following parameter values: K_p=-0.19 (mg/dl)(min•kg/μU), τ_p=150 min, and δ_p=22 min. Changes in parameter values from those obtained for the controlled diabetic are easily interpreted. For a step change in insulin delivery rate, the presence of insulin antibodies does not affect the resulting steady state plasma free insulin levels but does slow the dynamic transition between the steady states. Thus, insulin antibody binding has no effect on the process gain K_p, which solely reflects steady state response, but increases the process response time τ_p and dead time δ_p, which reflect dynamic response. In contrast, for a given plasma insulin concentration, the presence of tissue resistance to insulin action generally lowers the in vivo steady state tissue glucose utilization rate. Therefore, tissue insulin resistance decreases the magnitude of the process gain K_p, reflecting less incremental blood glucose response to incremental insulin infusion rate changes, but does not effect values of dynamic response time τ_p or dead time δ_p.

As shown in Figure 131, use of the above process characterization parameters in the IMC parameter set (denoted IMC2) only resulted in modest improvement in blood glucose regulation of the uncontrolled Type I diabetic

relative to that obtained by use of parameter set IMC1. In particular, maximum hyperglycemia was almost identical in both cases as the speed of initial plasma free insulin response was not significantly improved by use of parameter set IMC2. Parameter set IMC2, however, did result in lowering blood glucose at later times during the period of blood glucose recovery to steady state.

Finally, the effects of varying the maximum allowed insulin delivery rate IR_{max} was explored. Simulation studies were repeated using the process characterization parameter values (K_p, τ_p, δ_p) obtained for the controlled and uncontrolled diabetic cases, respectively, but the value of IR_{max} was increased twofold, from 1225 to 2450 $\mu U/kg \cdot min$. As shown in the upper plot of Figure 131, increasing the value of IR_{max} significantly reduced hyperglycemia during the 100g OGTT, but coupling higher IR_{max} with process characterization parameters (K_p, τ_p, δ_p) for the uncontrolled (IMC4) versus the controlled (IMC3) diabetic states resulted in very modest improvement in blood glucose regulation. As shown in the lower plot of Figure 131, increasing IR_{max} had two primary effects: 1) the speed of initial dynamic plasma free insulin response to rising blood glucose concentration became comparable to that attainable in the controlled diabetic, and 2) the plasma free insulin levels essentially increased twofold as a result of controller action during the 100g OGTT. In spite of higher plasma free insulin concentration levels over the duration of the 100g OGTT, however, blood glucose concentration peaked at 175 mg/dl, a value significantly higher that that achievable for the controlled Type I diabetic (see upper plot of Figure 131). Although not shown in Figure 131, use of even higher values of IR_{max} did not significantly reduce hyperglycemia, but the resulting increases in plasma insulin response levels became sufficient to

induce hypoglycemic excursions below 60 mg/dl for values of IR_{max}>3000 μU/kg•min.

Results of the simulation studies presented in Figure 131 r·ise a number of important issues. The controlled Type I diabetic represents the idealized end state. The real issue thus lies in how application of closed-loop insulin delivery can affect such a normalized metabolic state if applied to diabetics initially in an uncontrolled metabolic state. Insulin dosage may play a key role in the normalization process. The Type I diabetic on conventional therapy typically exhibits some degree of insulin resistance and, depending on the quantity and quality (primarily purity) of daily exogenous insulin administation, significant titers of circulating insulin antibodies. Insulin antibodies are the result of immunogenic response to exogenous insulins, and antibody titers decreas in patients changed from conventional to highly purified insulins. Use of purified insulins together with low insulin dosages would thus favor reduction in insulin antibody interactions. As shown in Figure 131, doubling the insulin levels in the uncontrolled Type I diabetic may not normalize blood glucose levels during oral glucose loading if tissue insulin resistance at high insulin levels is in evidence (post-receptor insulin resistance). Clinical studies (Revers et al., 1984) have demonstated that post-receptor insulin resistance in the poorly controlled Type I diabetic on conventional injection therapy can be essentially reversed by 6 wks of intensive injection therapy (i.e. home blood glucose monitoring 2-4 time daily and frequent insulin dosage adjustments). It is highly likely that the initial blood glucose control provided by parameter set IMC1 would be superior to control achieved by intensive injection therapy, and thus use of this parameter set would be expected to affect insulin resistance rever-

sal while gradually reducing hyperglycemia. Furthermore, restricting plasma free insulin levels to normal ranges (<100 μU/ml) during the normalization period could play an important role in preventing the development of receptor type insulin resistance which presumably results from insulin receptor down-regulation in response to prolonged exposure to high insulin levels. Because increasing IR_{max} to affect initial improvement in blood glucose regulation in the uncontrolled diabetic achieves such improvement at the expense of high insulin dosages, which could enhance development of insulin antibodies, and at the expense of concomitant inducement of abnormally high plasma insulin levels, which could induce receptor type insulin resistance, the modest benefits to be gained by increasing initial IMC insulin delivery capacity appear to be outweighed by the potential consequences of such action. Future clinical experimentation, however, may lead to better clarification of the factors affecting reversal of diabetic abnormalities and could thus possibly allow for optimization of IMC parameter variation to more rapidly affect such normalization.

Finally, the notion of adjusting the process characterization parameters (K_p, τ_p, δ_p) to reflect states of initial metabolic control can be extended to the concept of performing insulin infusion step change experiments on diabetic patients and using the resulting blood glucose response profiles to directly taylor the IMC parameters to the individual patient. Blood glucose response to step changes in insulin infusion rate is reported to be highly reproducible upon repetition in Type I diabetics (Bolli et al., 1984b), and such experiments would thus seem quite suitable for IMC parameter determination. As suggested by the results of Figure 131, although IMC performance improves with precise selection of the process characterization parameters, such improvement may not be very dramatic.

A desirable feature of control systems is to achieve specified response behavior which in turn is not extremely sensitive to the controller parameter values. Such systems displaying such behavior are referred to as robust in control terminology. Robustness is desirable because system performance is not sensitive to errors in model-derived control parameters when such parameters are applied to control of real processes. Thus, in the context of applying IMC to blood glucose regulation, a single representative parameter set may provide good control in spite of individual variations in actual blood glucose sensitivity to changes in insulin infusion delivery rate. Clinical experimentation will ultimately determine if this is indeed the case; should individualized parameter adjustment be deemed desirable, however, it should be feasible to determine parameter values from analysis of individual experimental step response profiles.

VII. REFERENCES

1) Ackerman,E.,Gatewood,L.C.,Rosevear,J.W.,and Molnar,G.D.(1965). Model studies of blood-glucose regulation. Bulletin of Math. Biophy. 27: 21-37.

2) Albisser,A.M.,Leibel,B.S.,Ewart,T.G.,Davidovac,Z.,Botz,C.K.,Zingg,W., and Gander,R.(1974a). Clinical control of diabetes by the artificial pancreas. Diabetes 23:397-404.

3) Albisser,A.M.,Leibel,B.S.,Ewart,T.G.,Davidovac,Z.,Botz,C.K.,and Zingg, W.(1974b). An artificial endocrine pancreas. Diabetes 23:389-96.

4) Alford,F.P.,Bloom,S.R.,and Nabarro,D.N.(1976). Glucagon metabolism in man. Studies on the metabolic clearance rate and the plasma acute disappearance time of glucagon in normal and diabetic subjects. J. Clin. Endocrinol. Metab. 42:830-38.

5) Allison,S.P.,Prowse,K.,and Chamberlain,M.J.(1967). Failure of insulin response to glucose load during operation and after myocardial infarction. Lancet I:478-81.

6) Altman,D.L.,and Dittmer,D.S.(1974). Biological Data Book, Volume III, Federation of American Societies for Experimental Biology, Bethesda.

7) Andres,R.,Cader,G.,and Zierler,K.L.(1956). The quantitatively minor role of carbohydrate in oxidative metabolism by skeletal muscle in intact man in the basal state. Measurements of oxygen and glucose uptake and carbon dioxide and lactate production in the forearm. J. Clin. Invest. 35:671-82.

8) Andres,R.,and Zierler,K.L.(1958). Stability of glucose uptake by human forearm despite increased arterial glucose concentration. (abstr.) Fed. Proc. 17:4.

9) Andrews,W.J.,Vasquez,B.,Nagulesparan,M.,Klimes,I.,Foley,J., Unger,R., and Reaven,G.M.(1984). Insulin therapy in obese, non-insulin-dependent diabete induces improvements in insulin action and secretion that are maintained for two weeks after insulin withdrawasl. Diabetes 33: 634-42.

10) Andriani,D.(1973). Some aspects of treatment with monocomponent (MC) and monospecies (MS) insulins. Excerpta Medica Int. Congr. Ser. 316: 68-75.

11) Antoniades,H.N.,and Simon,J.D.(1972). Neutralisation of the biologic activity of human serum bound insulin by potent insulin antiseria. Diabetes 21:930-34.

12) Anyan,W.R.,Jr.(1978). Adolescent Medicine in Primary Care, John Wiley & Sons Ltd., New York.

13) Aoki,T.T.(1982). Unpublished data, Joslin Research Laboratory, Boston.

14) Aoki,T.T.(1983a). Unpublished data, Joslin Research Laboratory, Boston.

15) Aoki,T.T.,Vlachokosta,F.V.,Foss,M.C.,and Meistas,M.T.(1983b). Evidence for restoration of hepatic glucose processing in Type I diabetes mellitus. J. Clin. Invest. 71:837-39.

16) Aoki,T.T.(1984). University of California, Davis, personal communication.

17) Asplin,C.M.,Hurtog,M.,and Geldie,D.J.(1978). The relationship between circulating free and bound insulin, insulin antibodies, insulin dosage and diabetic control in insulin treated diabetes. Acta Endocrinol. (Copenh.) 87:330-38.

18) Bagdade,J.D.,Bierman,E.L.,and Porte,D.,Jr.(1967). The significance of basal insulin levels in the evaluation of the insulin response to glucose in diabetic and nondiabetic subjects. J. Clin. Invest. 46(10): 1549-55.

19) Barrett,E.,Ferrannini,E.,Gusberg,R.,Felig,P.,and DeFronzo,R.(1980). Glucose metabolism by hepatic and extrahepatic tissues following oral and intravenous glucose. (abstr.) Clin. Res. 28:385A.

20) Basabe,J.,Lopetz,N.,Victoria,J.,and Wolff,F.(1970). Studies of insulin secretion in the perfused rat pancreas. Effect of diazoxide and A025. Diabetes 19:271-81.

21) Beck-Nielsen, H. (1978). The pathogenic role of an insulin-receptor defect in diabetes mellitus of the obese. Diabetes 27:1175-81.

22) Beck-Nielsen, H., Richelson, B., Hasling, C., Nielsen, O.H., Heding, L., and Sorensen, S.(1984). Improved in vivo insulin effect during continuous subcutaneous insulin infusion in patients with IDDM. Diabetes 33:832-37.

23) Beischer,W.,Schmid,M.,Kerner,W.,Keller,L.,and Pfeiffer,E.F.(1979). Feedback Inhibition of insulin in healthy and overweight subjects studied by use of an artificial endocrine pancreas. Horm. Metab. Res. (suppl.) 8:97-106.

24) Benson,J.W.,Jr.,Johnson,D.G.,Palmer,J.P.,Werner,P.L.,and Ensinck, J.W.(1977). Glucagon and catecholamine secretion during hypoglycemia in normal and diabetic man. J. Clin. Endocrin. Metab. 44:45^{9}-64.

25) Berger,S.,and Vongaraya,N.(1966). Insulin response to ingested protein in diabetes. Diabetes 15:303-6.

26) Bergman,R.N.,and Urquhart,J.(1971). The pilot gland approach to the study of insulin secretory dynamics. Rec. Prog. Hormonal Res. 26:583-605.

27) Bergman,R.N.,and Bucolo,R.J.(1973) Nonlinear metabolic dynamics of the pancreas and liver. J. Dyn. Syst. Meas. Control 95(3):296-300.

28) Bergman,R.N.,and Bucolo,R.J.(1974). Interaction of insulin and glucose in the control of hepatic glucose balance. Am. J. Physiol. 227(6): 1314-22.

29) Bergman,R.N.,Ider,Y.Z.,Bowden,C.R.,and Cobelli,C.(1979). Quantitative estimation of insulin sensitivity. Am. J. Physiol. 236(6):E667-77.

30) Bergman,R.N.,Bowden,C.R.,and Cobelli,C.(1981). The minimal model approach to quantification of factors controlling glucose disposal in man. In: Cobelli,C.,and Bergman,R.N.,(eds.), Carbohydrate Metabolism, pp269-96,John Wiley & Sons Ltd.,Chichester.

31) Bergman,R.N.,Beir,J.R.,and Hourigan,P.M.(1982). Intraportal glucose infusion matched to oral glucose absorption. Diabetes 31:27-35.

32) Bergstrom,J.,Hermansen,L.,Hultman,E.,and Saltin,B.(1967). Diet, muscle glycogen and physical performance. Acta. Physiol. Scand. 71:140-50.

33) Berson,S.A.,Yalow,R.S.,Bauman,A.,Rothchild,M.A.,and Newerly,K.(1956). Insulin-I131 metabolism in human subjects. Demonstation of insulin binding globulin in the circulation of insulin treated subjects. J. Clin. Invest. 35:170-90.

34) Berson,S.A.,and Yalow,R.S.(1959). Quantitative aspects of the reaction between insulin and insulin-binding antibody. J. Clin. Invest. 38: 1996-2016.

35) Berson,S.A.,and Yalow,R.S.(1970). Insulin antagonists and insulin resistance. In: Ellenberg,M.,and Rifkin,H.,(eds), Diabetes Mellitus: Theory and Practice, pp388-423, McGraw-Hill, New York.

36) Biostator® Glucose Controlled Insulin Infusion System, Operating Manual (1980). Miles Laboratories, Inc.

37) Bischoff,K.B.,and Brown,R.G.(1966). Drug distribution in mammals. Chem. Eng. Prog. Symp. Ser. 62:33-45.

38) Bishop,C.,and Surgenor,D.M.(1964). The Red Blood Cell, Academic Press, New York.

39) Bishop,J.S.(1970). Inability of insulin to activate liver glycogen transferase D phosphatase in the diabetic pancreotectomized dog. Biochim. Biophys. Acta 208:208-18.

40) Bjorntorp,P.Schersten,T.,and Gottfries,A.(1968). Effects of glucose infusions on adipose tissue lipogenesis in man. Acta. Med. Scand. 183:565-71.

41) Bjorntorp,P.,and Sjostrom,L.(1978). Carbohydrate storage in man: speculations and some quantitative considerations. Metabolism 27(12) suppl. 2:1853-65.

42) Block,M.B.,Mako,M.E.,Steiner,D.F.,and Rubenstein,A.H.(1972). Circulating C-peptide immunoreactivity: studies in normal and diabetic patients. Diabetes 21:1013-26.

43) Bloom,S.(1973). Glucagon, a stress hormone. Postgrad Med. J. 49 (suppl.):607-11.

44) Boden,G.,Soriano,M.,Heoldtke,R.D.,and Owen,O.E.(1983). Counter-regulatory hormone release and glucose recovery after hypoglycemia in non-insulin-dependent diabettic patients. Diabetes 32:1055-59.

45) Bolie,V.W.(1960). Coefficients of normal blood glucose regulation. J. Clin. Invest. 39(2):783-88.

46) Bolli,G.,De Feo,P.,Compagnucci,P.,Cartechini,M.G.,Angeletti,G., Santeusanio,F.,Brunetti,P.,and Gerich,J.E.(1983). Abnormal glucose counterregulation in insulin-dependent diabetes mellitus. Interaction of anti-insulin antibodies and impaired glucagon and epinephrine secretion. Diabetes 32:134-41.

47) Bolli,G.,De Feo,P.,De Cosmo,S.,Perriello,G.,Angeleti,G.,Ventura,M.R., Santeusanio,F.,Brunetti,P.,and Gerich,J.E.(1984a). Effects of long-term optimization and short-term deterioration of glycemic control on glucose counterregulation in type I diabetes mellitus. Diabetes 33: 394-400.

48) Bolli,G.B.,De Feo,P.,De Cosmo,S.,Perriello,G.,Ventura,M.M.,Massi Benedetti,M.,Santeusanio,F.,Gerich,J.E.,and Brunetti,P.(1984b). A reliable and reproducible test for adequate glucose counterregulation in type I diabetes mellitus. Diabetes 33:732-37.

49) Bomboy Jr.,J.D.,Lewis,S.B.,Sinclair-Smith,B.C.,Lacy,W.W.,and Liljenquist,J.E.(1977). Insulin-glucagon interaction in controlling splanchnic glucose production in normal man. J. Clin. Endocrinol. Metab. 44(3):474-80.

50) Bonaffe,M.(1977). General review of automated in vivo analysis. Horm. Metab. Res. (suppl.) 7: 2-9.

51) Botz,C.K.(1976). An improved control algorithm for an artificial β-cell. IEEE Trans. Biomed. Eng., vol. BME-23(3):252-55.

52) Brewer,G.J.,Eaton,J.W.,Weil,J.V.,and Grover,R.F.(1970). Studies of red cell glycolysis and interactions with carbon monoxide, smoking, and altitude. In: Brewer,G.J.,(ed.), Red Cell Metabolism and Function, pp95-114, Plenum Press, New York.

53) Britton,H.G.(1964). Permeability of the human red cell to labelled glucose. J. Physiol. 170:1-20.

54) Brod,J.(1973). The Kidney. Butterworth & Co. (Publishers) Ltd., London.

55) Broekheyse,H.M., Nelson,J.D.,Zinman,B.,and Albisser,A.M.(1981). Comparison of algorithms for the closed-loop control of blood glucose using the artificial beta cell. IEEE Trans. Biomed. Eng., vol. BME-28 (10):678-87.

56) Bruni,B.,D'Alberto,M.,Osenda,M.,Ricci,C.,and Turco,G.L.(1973). Clinical trial with monocomponent lente insulins. Diabetologia 9:492-98.

57) Brunzell,J.D.,Robertson,R.P.,Lerner,R.L.,Hazzard,W.R.,Ensinck,J.W., Bierman,E.L.,and Porte,D.,Jr.(1976). Relationships between fasting plasma glucose levels and insulin secretion during intravenous glucose tolerance tests. J. Clin. Endocrinol. Metab. 42:2-29.

58) Bucolo,R.J.,Bergman,R.N.,Marsh,D.J.,and Yates,F.E.(1974). Dynamics of glucose autoregulation in the isolated, blood-perfusedd canine liver. Am. J. Physiol. 227(1):209-17.

59) Butterfield,J.H.,Garratt,C.J.,and Whichelow,M.J.(1963). Peripheral hormone action: studies on the clearance and effect of [131-I] iodo-insulin in the peripheral tissues of normal, acromegalic, and diabetic subjects. Clin. Sci. 24:331-41.

60) Cahill,G.F.,Ashmore,J.,Earle,A.S.,and Zottu,S.(1958). Glucose penetration into liver. Am. J. Physiol. 192(3):491-6.

61) Cahill,G.F.,Jr.,Herrera,M.G.,Morgan,A.P.,Soeldner,J.S.,Steinke,J., Levy,P.L.,Reichard,G.A.,Jr.,and Kipnis,D.M.(1966). Hormone-fuel interrelationships during fasting. J. Clin. Invest. 45:1751-69.

62) Cahill,G.F.,and Owen,O.E.(1968). Some observations on carbohydrate metabolism in man. In: Dickens,F.,Randle,P.J.,and Whelan,W.J.,(eds.), Carbohydrate Metabolism and Its Disorders, pp497-522, Academic Press, New York.

63) Cahill,G.F.,and Soeldner,J.S.(1969). Glucose homeostasis: a brief review. In: Stear,E.B.,and Kadish,A.H.,(eds), Hormonal Control Systems, pp84-114, American Elsevier Publishing Co., Inc., New York.

64) Cahill,G.F.(1981). Gluconeogenesis in man. In: Veneziale,C.M.,(ed.), The Regulation of Carbohydrate Formation and Utilization in Mammals, pp.459-68, University Park Press, Baltimore.

65) Camus,F.,and Rasio,E.(1972). Peripheral glucose uptake in relation to physiological levels of plasma and lymph insulin. Europ. J. Clin. Invest. 2:188-94.

66) Carson,E.R.,and Finkelstein,L.(1973). Problems of identification in metabolic systems. In: Eykhoff,P.,(ed.), Proc. 3rd IFAC Symp. on Identification and System Parameter Estimation, Delft,Amsterdam, North-Holland, p195.

67) Carson,E.R.,and Cramp,D.G.(1976). A systems model of blood glucose control. Int. J. Bio-Medical Computing 7:21-34.

68) Carson,E.R.,Cobelli,C.,and Finkelstein,L.(1983). The Mathematical Modeling of Metabolic and Endocrine Systems, John Wiley & Sons Ltd., New York.

69) Cerasi,E.,Fick,G.,and Rudemo,M.(1974). A mathematical model for the glucose induced insulin release in man. Europ. J. Clin. Invest. 4: 267-78.

70) Chamberlain,M.J.,and Stimmer,L.(1967). The renal handling of insulin. J. Clin. Invest. 46(6):911-19.

71) Charrette,W.P.,Kadish,A.H.,and Sridhar,R.(1967). A nonlinear dynamic model of endocrine control of metabolic processes. 7th Int. Conf. on Med. and Biol. Eng., Stockholm, August 16.

72) Charrette,W.P.,Kadish,A.H.,and Sridhar,R.(1969). Modeling and control aspects of glucose homeostasis. In: Stear,E.B.,and Kadish,A.R., Hormonal Control Systems, Supplement 1, Mathematical Biosciences, pp115-49.

73) Cherrington,A.D.,Liljenquist,J.E.,Shulman,G.I.,Williams,P.E.,and Lacy,W.W.(1979). Importance of hypoglycemia-induced glucose production during isolated glucagon deficiency. Am. J. Physiol. 236(3):E263-71.

74) Cherrington,A.D.,Williams,P.E.,Shulman,G.I.,and Lacy,W.W.(1981). Differential time course of glucagon's effect on glycogenolysis and gluconeogenesis in the conscious dog. Diabetes 30:180-87.

75) Cherrington,A.D.,Diamond,M.P.,Green,D.R.,and Williams,P.E.(1982). Evidence for an intrahepatic contribution to the waning effect of glucagon on glucose production in the conscious dog. Diabetes 31:917-22.

76) Christiansen,J.S.,Svendsen,P.A.,Soegaard,U.,Frandsen,M.,Mathiesen,E., Winther,K.,and Deckert,T.(1981). An artificial betacell: assessment of the glucose analyzer, infusion system and optimization of constants for the algorithms. Scand. J. Clin. Lab. Invest. 41: 647-654.

77) Clark,L.C.,Jr.(1970). Membrane polarographic electrode system and method with electrochemical compensation. U.S. Patent No. 3,539,455, Novenber 10.

78) Clark,L.C.,Jr.,and Duggan,C.A.(1982). Implanted electroenzymatic glucose sensors. Diabetes Care 5(3):174-80.

79) Clauvel,M.,Schwartz,K.,and Terrier,E.(1965). Rev. Franc. Etudes Clin. et Biol. 10:753.

80) Clemens,A.H., and Chang,P.H.(1976). Development of an on-line blood glucose analyzer (RBGA) in a glucose controlled insulin infusion system (GCIIS). Diabetes 25:358.

81) Clemens,A.H.,Chang,P.H.,and Meyers,R.W.(1976). Le developpement d'un systeme automatique d'infusion d'insuline controle par la glycemic, son systeme de dosage de glucose et ses algorithmes de controle. Journes de Diabetologie, pp269-78, Fammarion Medicine-Sciences, Hotel-Dieu.

82) Clemens,A.H.,and Meyers,R.W.(1977). Blood glucose control apparatus, U.S. Patent No. 4,055,175, October 25.

83) Clemens,A.H.,Chang,P.H.,and Meyers,R.W.(1977). The development of Biostator®, a glucose controlled insulin infusion system (GCIIS). Horm. Metab. Res. (suppl.) 7:23-33.

84) Clemens,A.H.(1979a). Control algorithms for artificial beta cell. Horm. Metab. Res.(suppl.) 8:35-38.

85) Clemens,A.H.(1979b). Feedback control dynamics for glucose controlled insulin infusion system. Med. Progr. Technol. 6:91-98.

86) Cobelli,C.,Pacini,G.,and Salvan,A.(1980). On a simple model of insulin secretion. Med. & Biol. Eng. & Comput. 18:457-63.

87) Cobelli,C.,Federspil,G.,Pacini,G.,Salvan,A.,and Scandellari,C.(1982). An integrated mathematical model of the dynamics of blood glucose and its hormonal control. Mathematical Biosciences 58:27-60.

88) Cobelli,C.,and Ruggeri,A.(1983). Evaluation of portal/peripheral route and of algorithms for insulin delivery in the closed-loop control of glucose in diagetes - a modeling study. IEEE Trans. Vol. BME-30: 93-103.

89) Cobelli,C.,and Mari,A.(1983b). Validation of mathematical models of complex endocrine-metabolic systems. A case study on a model of glucose metabolism. Med. & Biol. Eng. & Comput. 21:390-99.

90) Cohen,G.H.,and Coon,G.A.(1953). Theoretical considerations of retarded control. Trans. ASME 75:827-34.

91) Cooper,K.E.,Edholm,O.G.,and Mottram,R.F.(1955). The blood flow in skin and muscle of the human forearm. J. Physiol. 128:258-67.

92) Cramp,D.G.,and Carson,E.R.(1981). The dynamics of short-term blood glucose regulation. In: Cobelli,C.,and Bergman,R.N.,(eds.), Carbohydrate Metabolism, pp349-68,John Wiley & Sons Ltd.,Chichester.

93) Crofford,O.B.(1975). Report of the National Commission on Diabetes to the Congress of the United States. United States Department of Health, Education, and Welfare Publication No.(NIH)67-1018, Government Printing Office, Washington, D.C.

94) Crone,C.(1965). Facilitated transfer of glucose from blood into brain tissue. J. Physiol. 181:103-13.

95) Cryer,P.E.,and Gerich,J.E.(1983). Relevance of glucose counterregulatory systems to patients with diabetes: critical roles of glucagon and epinephrine. Diabetes Care 6(1):95-99.

96) Csaky,T.Z.(1968). Intestinal Absorption and Malabsorption, Raven Press, New York.

97) Curry,D.L.,Bennett,L.L.,and Grodsky,G.M.(1968). Dynamics of insulin secretion bu the perfused rat pancreas. Endocrinology 83:572-84.

98) Davson,H.,and Spaziani,E.(1959). The blood-brain barrier and the extracellular space of the brain. J. Physiol. 149:135-43.

99) Dedrick,R.L.(1973). Animal scale-up. J. Pharmacokinet. Biopharm. 1:435-61.

100) DeFronzo,R.A.,Ferrannini,E.,Hendler,R.,Wahren,J.,and Felig,W.(1978). Influence of hyperinsulinemia, hyperglycemia, and the route of glucose administration on splanchnic glucose exchange. Proc. Natl. Acad. Sci. USA 75(10):5173-77.

101) DeFronzo,R.A.,Ferrannini,E.,and Wahren,J.(1979a). Regulation of hepatic glucose metabolism by intravenous insulin and glucose. (abstr.) Diabetes 28:379.

102) DeFronzo,R.A.,Tobin,J.D.,and Andres,R.A.(1979b). Glucose clamp technique: a method for quantifying insulin secretion and resistance. Am. J. Physiol. 237(3):E214-23.

103) DeFronzo,R.A.,Jacot,E.,Jequier,E.,Maeder,E.,Wahren,J.,and Felber,J.P. (1981a). The effect of insulin on the disposal of intravenous glucose. Diabetes 30:1000-7.

104) DeFronzo,R.A.,Alvestrand,A.,Smith,D.,Hendler,R.,Hendler,E.,and Wahren, J.(1981b). Insulin resistance in uremia. J. Clin. Invest. 67:563-68.

105) DeFronzo,R.A.,Binder,C.,Wahren,J.,Felig,P.,Ferrannini,E.,and Faber,K. (1981c). Sensitivity of insulin secretion to feedback inhibition by hyperinsulinaemia. Acta Endocr. 98:81-86.

106) DeFronzo,R.A.,Hendler,R.,and Simonson,D.(1982). Insulin resistance is a prominent feature of insulin-dependent diabetes. Diabetes 31:795-801.

107) DeFronzo,R.A.,Ferrannini,E.,Hendler,R.,Felig,P.,and Wahren,J.(1983). Regulation of splanchnic and peripheral glucose uptake by insulin and hyperglycemia in man. Diabetes 32:35-45.

108) DeLoecker,W.C.J.,and Prankard,T.A.J.(1961). Clin. Chim. Acta. 6:641-47.

109) De Meyts,P.,and Roth,J.(1975). Cooperativity in ligand binding: a new graphic analysis. Biochem. Biophys. Res. Commun. 66(4):1118-26.

110) De Pirro,R.,Fusco,A.,Spallone,L.,Magnatta,R.,and Lauro,R.: Insulin antibodies prevent insulin-receptor interactions. Diabetologia 19: 118-22.

111) Dietze,G.,Wicklmayr,M.,Hepp,K.,Bogner,W.,Mehnert,H.,Czempiel,H.,and Henftling,H.(1976). On gluconeogenesis of human liver: Accelerated hepatic glucose formation by increased precursor supply. Diabetologia 12:555-61.

112) Dixon,K.,Exon,P.D.,and Malins,J.M.(1975). Insulin antibodies and the control of diabetes. Q.J.Med. 176:543-53.

113) Dole,V.P.(1965). Energy storage. In: Renold,A.E.,and Cahill,G.F.,(eds.), Handbook of Physiology: Adipose Tissue, pp. 13-18, American Physiological Society, Washington, D.C.

114) Duckworth,W.C.(1979). Insulin degradation by liver cell membranes. Endocrinology 104(6):1758-64.

115) Dupre,J.,Curtis,J.,Unger,R.H.,Waddell,R.W.,and Beck,J.C.(1969). Effects of secretin, pancreozymin, or gastrin on the response of the endocrine pancreas to administration of glucose or arginine in man. J. Clin. Invest. 48:745-57.

116) Edelman,I.S.,and Leibman,J.(1959). Anatomy of body water and electrolytes. Am. J. Med. 27:256-77.

117) Eisentraut,A.,Ohneda,A.,Parada,E.,and Unger,R.H.(1968). Immunologic discrimination between pancreatic glucagon and glucagon-like immunoreactivity (GLI) in tissues and plasma. Diabetes 17 (suppl. 1): 321-22.

118) Elahi,D.,Andersen,D.K.,Brown,J.C.,Debas,H.T.,Hershcopf,R.J.,Raizes, G.S.,Tobin,J.D.,and Andres,R.(1979). Pancreatic alpha- and beta-cell responses to GIP infusion in normal man. Am. J. Physiol. 237(2):E185-91.

119) Elrick,H.,Stimmler,L.,Hlad,C.J.,Jr.,and Arai,Y.(1964). Plasma insulin response to oral and intravenous glucose administration. J. Clin. Endocrinol. Metab. 24: 1076-82.

120) Erdelyi,A.(1954). Tables of Integral Transforms I., McGraw-Hill, New York.

121) Fajans,S.S.,Floyd,J.C.,Jr.,Knopf,R.f.,and Conn,J.W.(1967). Effect of amino acids and proteins on insulin secretion in man. Recent Prog. Hormone Res. 23:617-62.

122) Fajans,S.S.,and Floyd,J.C.,Jr.(1972). Stimulation of islet cell secretion by nutrients and by gastrointestinal hormones released during ingestion. In: Greep,R.O.,and Astwood,E.B.,(eds.), Handbook of Physiology, Section 7: Endocrinology, Volume I. Endocrine Pancreas, pp. 473-94, American Physiological Society, Washington D.C.

123) Felber,J.P.,and Vannotti,A.(1964). Effects of fat infusion on glucose tolerance and plasma insulin levels. Med. Exptl. 10:153-6.

124) Felig,P.,and Wahren,J.(1971). Influence of endogenous insulin secretion splanchnic glucose and amino acid metabolism in man. J. Clin. Invest. 50:1702-11.

125) Felig,P.,Wahren,J.W.,and Hendler,R.(1975). Influence of oral glucose ingestion on splanchnic glucose and gluconeogenic substrate metabolism in man. Diabetes 24(5):468-75.

126) Felig,P.,Wahren,J.,and Hendler,R.(1976). Influence of physiologic hyperglucagonemia on basal and insulin-inhibited splanchnic glucose output in normal man. J. Clin. Invest. 58:761-65.

127) Fenn,W.D.,and Rahn,H.(eds.)(1965). Handbook of Physiology, Section 3 (Respiration) Volume III, American Physiological Society, pp979-1010, Washington D.C.

128) Ferrannini,E.,Wahren,J.,Felig,P.,and DeFronzo,R.(1980). The role of fractional glucose extraction in the regulation of splanchnic glucose metabolism in normal and diabetic man. Metabolism 29(1):28-35.

129) Field,J.B.,Rojdmark,S.,Harding,P.,Ishidi,T.,and Chou,M.C.Y.(1980). Role of liver in insulin physiology. Diabetes Care 3(2):255-60.

130) Fineberg,S.E.,and Schneider,S.H.(1982). Studies on the relationship between insulin concentrations and insulin action. Diabetes Care 5(3): 292-99.

131) Fineberg,S.E.,Galloway,J.A.,Fineberg,N.S.,and Goldman,J.(1983). Effects of species of origin, purification levels, and formulation on insulin immunogenicity. Diabetes 32:592-99.

132) Finkelstein,L.,and Carson,E.R.(1979). Mathematical Modeling of Dynamic Biological Systems, John Wiley & Sons Ltd., Chichester.

133) Fischer,U.,Jutzi,E.,Freyse,E.-J.,and Salzsieder,E.(1978). Derivation and experimental proof of a new algorithm for the artificial β-cell based on the individual analysis of the physiological insulin-glucose relationship. Endokrinologie 71:65-75.

134) Fischer,U.,Jutzi,E.,Bombor,H.,Freyse,E.-J.,Salzsieder,E.,Albrecht,G., Besch,W.,and Bruns,W.(1980). Assessment of an algorithm for the artificial β-cell using the normal insulin-glucose relationship in diabetic dogs and man. Diabetologia 18:97-107.

135) Fisher,M.,Sherwin,R.S.,Hendler,R.,and Felig,P.(1976). Kinetics of glucagon in man: effect of starvation. Proc. Natl. Acad. Sci. USA 73(5):1735-39.

136) Floyd,J.C.,Jr.,Fajans,S.S.,Conn,J.W.,Knopf,R.F.,and Rull,J.(1966a). Insulin secretion in response to protein ingestion. J. Clin. Invest. 45:1479-86.

137) Floyd,J.C.,Jr.,Fajans,S.S.,Conn,J.W.,Knopf,R.F.,and Rull,J.(1966b). Stimulation of insulin secretion by amino acids. J. Clin. Invest. 45: 1487-502.

138) Foa,P.(1972). The secretion of glucagon. In: Greep,R.,and Astwood,E., (eds.), Handbook of Physiology, Section 7: Endocrinology, Volume I. Endocrine Pancreas, pp. 261-78, Williams & Wilkins, Baltimore.

139) Foss,M.C.,Vlachokosta,F.V.,Cunningham,L.N.,and Aoki,T.T.(1982). Restoration of glucose homeostasis in insulin-dependent diabetic subjects. An inducible process. Diabetes 31:46-52.

140) Foster,R.O.(1970). The Dynamics of Blood Sugar Regulation, M.S. Thesis, Massachusetts Institute of Technology.

141) Foster,R.O.,Soeldner,J.S.,Tan,M.H.,and Guyton,J.R.(1973). Short term glucose homeostasis in man: a systems dynamic model. J. Dyn. Syst. Meas. Control 95:308-14.

142) Frohman,L.A.,Ezdinli,E.Z.,and Javid,R.(1967). Effect of vagotomy and vagal stimulation on insulin secretion. Diabetes 16:443-48.

143) Fromm,H.J.(1981). Mechanism and mode of regulation of brain hexokinase. In: Veneziale,C.M.,(ed.), The Regulation of Carbohydrate Formation and Utilization in Mammals, pp45-68, University Park Press, Baltimore.

144) Ganda,O.P.,and Soeldner,J.S.(1977). Genetic, acquired, and related factors in the etiology of diabetes mellitus. Arch. Intern. Med. 137: 461-69.

145) Ganda,O.P.(1983). Morbidity and mortality from diabetes mellitus: a look at preventable aspects. Am. J. Public Health 73(10):1156-58.

146) Garcia,C.E.,and Morari,M.(1982). Internal model control. 1. A unifying review and some new results. Ind. Eng. Chem. Process Des. Dev. 21(2): 308-23.

147) Gatewood,L.C.,Ackerman,E.,Rosevar,J.W.,and Molnar,G.D.(1968). Simulation studies of blood-glucose regulation: effect of intestinal glucose absorption. Comput. and Biomed. Research 2:15-27.

148) Gerich,J.E.,Langlois,M.,Noacco,C.,Karam,J.,and Forsham,P.H.(1973). Lack of glucagon response to hypoglycemia in diabetes: evidence for an intrinsic pancreatic alpha cell defect. Science 182:171-73.

149) Gerich,J.E.,Charles,M.A.,and Grodsky,G.M.(1974a). Characterization of the effects of arginine and glucose on glucagon and insulin release from the in vitro perfused rat pancreas. J. Clin. Invest. 54:833-41.

150) Gerich,J.E.,Langlois,M.,Noacco,C.,Schneider,V.,and Forsham,P.H. (1974b). Adrenergic modulation of pancreatic glucagon secretion in man. J. Clin. Invest. 53:1441-46.

151) Gerich,J.E.,Schneider,V.,Dippe,S.E.,Langlois,M.,Noacco,C.,Karam,J.H., and Forsham,P.H.(1974c). Characterization of the glucagon response to hypoglycemia in man. J. Clin. Endocrinol. Metab. 38(1):77-82.

152) Gerich,J.E.(1976a). Control of pancreatic IRG secretion in vivo. Metabolism 25(11):1437-41.

153) Gerich,J.E.,Charles,M.A.,and Grodsky,G.M.(1976). Regulation of pancreatic insulin and glucagon secretion. Ann. Rev. Physiol. 38:353-88.

154) Gerich,J.,Cryer,P.,and Rizza,R.(1980). Hormonal mechanisms in acute glucose counterregulation: the relative roles of glucagon, epinephrine, norepinephrine, growth hormone, and cortisol. Metabolism 29(11):1164-75.

155) Gerich,J.,Haymond,M.,Rizza,R.,Verdonk,C.,and Miles,J.(1981). Hormonal and substrate determinants of hepatic glucose production in man. In: Veneziale,C.M.,(ed.), The Regulation of Carbohydrate Formation and Utilization in Mammals, pp.419-57, University Park Press, Baltimore.

156) Gibson,J.G.,and Evans,W.A.(1937). Clinical studies of the blood volume. II. The relation of plasma and total blood volume to venous pressure, blood velocity rate, physical measurements, age and sex in ninety normal humans. J. Clin. Invest. 16:317-28.

157) Ginsberg,H.,and Rayfield,E.J.(1981). Effect of insulin therapy on insulin resistance in type II diabetic subjects: evidence for heterogeneity. Diabetes 30:739-45.

158) Gold,H.(1970). The effect of diabetes and insulin on liver glycogen synthetase activation. J. Biol. Chem. 245:903-905.

159) Gold,G.,Landahl,H.D.,Gishizky,M.L.,and Grodsky,G.M.(1982). Heterogeneity and compartmental properties of insulin storage and secretion in rat islets. J. Clin. Invest. 69:554-63.

160) Goldfine,I.D.(1978). Minireview, insulin receptors and the site of action of insulin. Life Sci. 23:2639-48.

161) Goldman, J., Baldwin, D., Rubenstein, A.H., Klink, D.D., Blackard, W.G., Fisher, L.K., Roe, T.F., and Schnure, J.J. (1979). Characterization of circulating insulin and proinsulin-binding antibodies in autoimmune hypoglycemia. J. Clin. Invest. 63:1050-1059.

162) Goodner,C.J.,Walike,B.C.,Koerker,D.J.,Ensinck,J.W.,Brown,A.,Chickadel, E.W.,Palmer,J.,and Kalnasy,L.(1977). Insulin, glucagon, and glucose exhibit synchronous, sustained oscillations in fasting monkeys. Science 195:177-79.

163) Gonene,B.,Goldman,J.,Baldwin,D.,Goldberg,R.B.,Ryan,W.G.,Blix,P.M., Schanzlin,D.,Fritz,K.J.,and Rubenstein,A.H.(1979). Metabolic control in diabetic patients: effect of insulin-secretory reserve (measured by plasma C-peptide levels) and circulating insulin antibodies. Diabetes 28:749-53.

164) Goriya,Y.,Kawamori,R.,Shichiri,M.,and Abe,H.(1979). The development of an artificial beta cell system and its validation in depancreatized dogs: the physiological resrtoration of blood glucose homeostasis. Med. Progr. Technol. 6:99-108.

165) Gottstein,U.,Bernsmeider,A.,and Sedlmeyer,I.(1963). Der Kohlenhydratstoffwechsel des menschlichen Gehirns. Klin. Wochschr. 41: 943-8.

166) Gray,R.S.,Scarlett,J.A.,Griffin,J,Olefsky,J.M.,and Kolterman,O.G. (1982). In vivo deactivation of peripheral, hepatic, and pancreatic insulin action in man. Diabetes 31:929-36.

167) Grayburn,J.,Harvey,R.,Jennings,R.,Dowsett,L.,and Hartog,M.(1975). Relationship between changes in serum cholecystokinin-pancreozymin and serum insulin after different stimuli. Diabetologia 11:35-38.

168) Grodsky,G.M.(1968). Insulin secretion from the perfused pancreas. Acta Diabetol. Lat. 5:239.

169) Grodsky,G.M.,Curry,D.,Landahl,H.,and Bennett,L.(1969). Further studies on the dynamic aspects of insulin release in vitro with evidence for a two-compartmental storage system. Acta Diabet. Lat. 6 (suppl. 1): 554-79.

170) Grodsky,G.M.,Landahl,H.,Curry,D.L.,and Bennett,L.L.(1970a). A two-compartmental model for insulin secretion. In: Camerini-Davalos,R., and Cole,H.S.,(eds.), Early Diabetes, pp. 45-50, Academic Press, New York.

171) Grodsky,G.,Landahl,H.,Curry,D.,and Bennett,L.(1970b). In vitro studies suggesting a two-compartmental model for insulin secretion. In: Falkner,S.,Hellman,B.,and Taljedal,B.,(eds), The Structure and Metabolism of Pancreatic Islets, pp409-20.

172) Grodsky,G.M.(1970c). Insulin and the pancreas. Vitam. Horm. 28:37-101.

173) Grodsky,G.M.(1972). A threshold distribution hypothesis for packet storage of insulin and its mathematical modeling. J. Clin. Invest. 51: 2047-58.

174) Grodsky,G.M.,Fanska,R.,and Schmid,F.G.(1973). Evaluation of the role of exogenous insulin on phasic insulin secretion. Diabetes 22:256-63.

175) Guest,G.M.,Mackler,B.,Graubarth,H.,and Ammentorp,P.A.(1953). Rates of utilization of glucose in erythrocytes and leucocytes. Am. J. Physiol. 172:295-300.

176) Guilbault,G.G.,and Lubrano,G.J.(1973). An enzymatic electrode for the amperometric determination of glucose. Anal. Chim. Acta 64:439-55.

177) Guilbault,G.G.(1982). Enzymatic glucose electrodes. Diabetes Care 5 (3):181-83.

178) Guyton,A.C.(1976). Textbook of Medical Physiology, Fifth Edition, Saunders and Co., Philadelphia.

179) Guyton,J.R.(1973). A Mathematical Model of Immediate Glucose Homeostasis, M.D. thesis, Harvard Medical School.

180) Guyton,J.R.,Foster,R.O.,Soeldner,J.S.,Tan,M.H.,Kahn,C.B.,Koncz,L., and Gleason,R.E.(1978). A model of glucose-insulin homeostasis in man that incorporates the heterogeneous fast pool theory of pancreatic insulin release. Diabetes 27:1027-42.

181) Hakanson,R.,Liedberg,G.,and Lundquist,I.(1971). Effect of vagal denervation on insulin release after oral and intravenous glucose. Experientia 27:460-61.

182) Harding,P.E.,Bloom,G.,and Field,J.B.(1975). Effect of infusion of insulin into portal vein on hepatic extraction of insulin in anesthetized dogs. Am. J. Physiol. 228(5):1580-88.

183) Harper,H.A.,Rodwell,V.W.,and Mayes,P.A.(1979). Review of Physiological Chemistry, Seventeenth Edition, Lange Medical Publications, Los Altos.

184) Harris,J.W.(1965). The Commonwealth Fund, Howard University Press, Cambridge, Massachusetts.

185) Harwood,R.(1960). Insulin-binding antibodies and "spontaneous" hypoglycemia. N. Engl. J. Med. 262:978-79.

186) Hayes,J.,Ardill,J.,and Buchanan,K.(1975). Gastrin and insulin secretion. Diabetologia 11:89-92.

187) Hentenyi,G.,and Norwich,K.(1974). Validity of the rates of production and utilization of metabolites as determined by tracer methods in intact animals. Fed. Proc. 33: 1841-8.

188) Heymsfield,S.B.,McManus,C.,Stevens,V.,and Smith,J.(1982). Muscle mass: reliable indicator of protein-energy malnutrition severity and outcome. Am. J. Clin. Nutr. 35:1192-99.

189) Hidaka,H.,Nagulesparan,M.,Klimes,I.,Clark,R.,Sasaki,H.,Aronoff,S.L., Vasquez,B.,Rubenstein,A.H.,and Unger,R.H.(1982). Improvement of insulin secretion but not insulin resistance after short term control of plasma glucose in obese type II diabetics. J. Clin. Endocrinol. Metab. 54:217-22.

190) Hillman,R.S.(1977). The Dynamics and Control of Glucose Metabolism, M.S. thesis, Massachusetts Institute of Technology.

191) Hilsted,J.,Madsbad,S.,Krarup,T.,Sestoft,L.,Christensen,N.J., Tronier, B.,and Galbo,H.(1981). Hormonal, metabolic, and cardiovascular responses to hypoglycemia in diabetic autonomic neuropathy. Diabetes 30:626-33.

192) Himmelstein,K.J.,and Lutz,R.J.(1979). A review of the applications of physiologically based pharmacokinetic modeling. J. Pharmacokin. et Biopharm. 7:127-45.

193) Himwich,H.E.,and Fazekas,J.F.(1937). The effect of hypoglycemia on the metabolism of the brain. Endocrinology 21:800-7.

194) Honey,R.N.,and Price,S.(1979). The determinants of insulin extraction in the isolated perfused rat liver. Horm. Metab. Res. 11:111-17.

195) Howell,S.L.,and Taylor,K.W.(1967). The secretion of newly synthesized insulin in vitro. Biochem. J. 162:922-7.

196) Howell,S.L.,Young,D.A.,and Lacy,P.E.(1969). Isolation and properties of secretory granules ffrom rat islets of Langerhans. III. Studies of the stability of the isolated beta granules. J. Cell Biol. 41:167-76.

197) Hultman,E.,and Nilsson,L.H.(1971). Liver glycogen in man. Effect of different diets and muscular exercise. In: Pernow,B.,and Saltin,B., (eds.), Muscle Metabolism During Exercise, pp.143-151, Plenum Press, New York-London.

198) Hultman,E.,Bergstrom,J.,and Roch-Norlund,A.E.(1971). Glycogen storage in human skeletal muscle. In: Pernow,B.,and Saltin,B.,(eds.), Muscle Metabolism During Exercise, pp.273-88, Plenum Press, New York- London.

199) Hunter,W.M.,and Sukkar,M.Y.(1968). Changes in plasma insulin levels during muscular exercise. J. Physiol. (London) 196:110P-12P.

200) Ichihara,K.,Shima,K.,Saito,Y.,Nonaka,K.,Tarui,S.,and Nishikawa,M. (1977). Mechanism of hypoglycemia observed in a patient with insulin autoimmune syndrome. Diabetes 26:500-506.

201) Insel,P.A.,Liljenquist,J.E.,Tobin,J.D.,Sherwin,R.S.,Watkins,P.,Andres, R.,and Berman,M.(1975). Insulin control of glucose metabolism in man. J. Clin. Invest. 55:1057-66.

202) Iverson,J.,and Miles,D.W.(1971). Evidence for a feedback inhibition of insulin secretion in the isolated perfused canine pancreas. Diabetes 20:1-9.

203) Iverson,J.(1973). Effectt of acetyl choline on the secretion of glucagon and insulin from the isolated perfused canine pancreas. Diabetes 22:381-87.

204) Jackson,R.A.,Peters,N.,Advani,U.,Perry,G.,Rogers,J.,Brough,W.H.,and Pilkington,T.R.E.(1973). Forearm glucose uptake during the oral glucose tolerance test in normal subjects. Diabetes 22(6):442-58.

205) Jacob,H.S.,and Jandl,J.H.(1964). Increased cell membrane permeability in the pathogenesis of hereditary spherocytosis. J. Clin. Invest. 43 (8):1704-20.

206) Jacot,E.,DeFronzo,R.A.,Jequier,E.,Maeder,E.,and Felber,J.P.(1982). The effect of hyperglycemia, hyperinsulinemia, and route of glucose administration on glucose oxidation and storage. Metabolism 31:922-30.

207) Jandl,J.H.(1965). Leaky red cells. Blood 26(3):367-82.

208) Jaspan,J.B.,and Rubenstein,A.H.(1977). Circulating glucagon. Plasma profiles and metabolism in health and disease. Diabetes 26(9):888-902.

209) Jazwinski,A.H.(1970). Stochastic Processes and Filtering Theory. Academic Press, New York-London.

210) Jeanrenaud,B.,aand Renold,A.E.(1959). Studies on rat adipose tissue in vitro. IV. Metabolic patterns produced in rat adipose tissue by varying insulin and glucose concentrations independently from each other. J. Biol. Chem. 234:3082-7.

211) Kaden,M.,Harding,P.,and Field,J.B.(1973). Effect of intraduodenal glucose administation on hepatic extraction of insulin in the anesthetized dog. J. Clin. Invest. 52:2016-28.

212) Kadish,A.H.(1963). Automation control of blood sugar: a sevomechanism for glucose monitoring and control. Trans. Am. Soc. Artif. Intern. Organs 9:363-7.

213) Kahn,C.R.(1978). Insulin resistance, insulin insensitivity, and insulin unresponsiveness: a necessary distinction. Metabolism 27: 1893-1902.

214) Kahn,C.R.(1979). The role of insulin receptors and receptor antibodies in states of altered insulin action. Proc. Soc. Exper. Biol. Med. 162: 13-21.

215) Kalant,N.,Leibovici,T.,Rohan,I.,and Ozaki,S.(1979). Interrelationships of glucose and insulin uptake by muscle of normal and diabetic man. Diabetologia 16:365-72.

216) Kappy,M.S.,and Plotnick,L.(1979). Studies of insulin binding in children using human erythrocytes in small amounts of blood. Diabetes 28:1001-5.

217) Karam,J.,Grasso,S.,Wegienka,L.,Grodsky,G.,and Forsham,P.(1966). Effect of selected hexoses, of epinephrine, and of glucagon on insulin secretion in man. Diabetes 15:571-78.

218) Karam,J.H.,Grodsky,G.M.,Ching,K.N.,Schmid,F.,Burrill,K.,and Forsham, P.H.(1974). "Staircase" glucose stimulation of insulin secretion in obesity. Measure of beta-cell sensitivity and capacity. Diabetes 23: 763-70.

219) Katz,J.,Golden,S.,and Wals,P.A.(1979). Glycogen synthesis by rat hepatocytes. Biochem. J. 180:389-402.

220) Katz,L.D.,Glickman,M.G.,Rapoport,S.,Ferrannini,E.,and DeFronzo,R.A. (1983). Splanchnic and peripheral disposal of oral glucose in man. Diabetes 32:675-79.

221) Kawamori,R.,Shichiri,M.,Goriya,Y.,Yamasaki,Y.,Shigeta,Y.,and Abe,H. (1978). Importance of insulin secretion based on the rate of change in blood glucose concentration in glucose tolerance assessed by the artificial beta cell. Acta. Endocrinol. 87:339-51.

222) Kawamori,R.,Shichiri,M.,Kikuchi,M.,Yamasaki,Y.,and Abe,H.(1980). Perfect normalization of excessive glucagon responses to intravenous arginine in human diabetes mellitus with the artificial beta-cell. Diabetes 29:762-65.

223) Kety,S.S.,Woodford,R.B.,Harmel,M.H.,Freyhan,F.A.,Appel,K.E.,and Schmidt,C.F.(1948). Am. J. Psychiatry 104:765-770.

224) Kleinbaum,J.,and Shamoon,H.(1983). Impaired counterregulation of hypoglycemia in insulin-dependent diabetes mellitus. Diabetes 32:493-8.

225) Kohen,E.,Kohen,C.,and Rabinovitch,A.(1983). Cell-to-cell communication in rat pancreatic islet monolayer cultures is modulated by agents affecting islet-cell secretory activity. Diabetes 32:95-98.

226) Kolterman,O.G.,Insel,J.,Sackow,M.,and Olefsky,J.M.(1980). Mechanism of insulin resistance in human obesity-evidence for receptor and post-receptor defects. J. Clin. Invest. 65:1273-84.

227) Kondo,T.,Ito,K.,Ohkura,K.,Ito,K.,and Ikeda,S.(1982). A miniature glucose sensor, implantable in the blood stream. Diabetes Care 5(3): 218-21.

228) Koppel,L.B.(1968). Introduction to Control Theory. Prentice-Hall, Inc., Englewood Cliffs, N.J.

229) Kraegen,E.W.,Campbell,L.V.,Meler,H.,Chia,Y.O.,and Lazarus,L.(1975). Clinical studies using an artificial endocrine pancreas. Aust. N.Z. J. Med. 5:390.

230) Kraegen,E.W.,Campbell,L.V.,Meler,H.,Chia,Y.O.,and Lazarus,L.(1977). Control of blood glucose in diabetics using an artificial pancreas. Aust. N.Z. J. Med. 7:280-86.

231) Kraegen,E.W.,Whiteside,R.,Bell,D.,Chia,Y.O.,and Lazarus,L.(1979). Development of a closed-loop artificial pancreas. Horm. Metab. Res. (suppl.) 8:38-42.

232) Kuku,S.F.,Jaspan,J.B.,Emmanouel,D.S.,Zeidler,A.,Katz,A.I.,and Rubenstein,A.H.(1976). Heterogeneity of plasma glucagon: Circulating components in normal subjects and patients with chronic renal failure. J. Clin. Invest. 58:742-50.

233) Kumar,D.(1979). Immunoreactivity of insulin antibodies in insulin-treated diabetes. Diabetes 28:994-1000.

234) Kurtz,A.B.,and Nabarro,J.D.N.(1980). Circulating insulin-binding antibodies. Diabetologia 19:329-34.

235) Lacy,P.E.,Howell,S.L.,Young,D.A.,and Fink,C.J.(1968). New hypothesis of insulin secretion. Nature 219:1177-9.

236) Lacy,P.E.,and Greider,M.H.(1972). Ultrastructural organization of mammalian pancreatic islets. In: Greep,R.O.,and Astwood,E.B.,(eds.), Handbook of Physiology, Section 7: Endocrinology, Volume I. Endocrine Pancreas, pp77-89, American Physiological Society, Washington D.C.

237) Landahl,H.D.,and Grodsky,G.M.(1982). Comparison of models of insulin release. Bull. Math. Biology 44(3):399-409.

238) Lang,D.A.,Matthews,D.R.,Burnet,M.,Ward,G.M.,and Turner,R.C.(1982). Pulsatile, synchronous basal insulin and glucagon secretion in man. Diabetes 31:22-26.

239) Langerlof,H.O.,Johansson,C.,and Ekelund,K.(1976). Human gastric and intestinal response to meals by a multiple indicator dilution method. Mount Sinai J. Med. 43:1-98.

240) Larner,J.,Cheng,K.,Galasko,G.,Huang,L.,Lawrence,J.,Walkenbach,R.J., Roach,P.J.,and DePaoli-Roach,A.A.(1981). Toward an understanding of the mechanism of action of insulin. In: Veneziale,C.M.,(ed.), The Regulation of Carbohydrate Formation and Utilization in Mammals, pp.1-44, University Park Press, Baltimore.

241) Lerner,H.,Giner,J.,Soeldner,J.S.,and Colton,C.K.(1981). Development of an implantable glucose sensor. Artificial Organs (suppl.) 5:743-8.

242) Lerner,H.,Soeldner,J.S.,Colton,C.K.,and Giner,J.(1982). Measurement of glucose concentration in the presence of coreactants with a platinum electrode. Diabetes Care 5(3):229-37.

243) Levine,R.,Goldstein,M.S.,Huddlestun,B.,and Klein,S.P.(1950). Action of insulin on the "permeability" of cells to free hexoses, as studied by its effect on the distribution of galactose. Am. J. Physiol. 163: 70-6.

244) Levine, R. (1984). Solfonylureas: background and development of the field. Diabetes Care 7(suppl. 1):3-7.

245) Lewandowski,J.J.,Szczepanska-Sadowska,E.,Krzymien,J.,and Nalecz,M. (1982). Amperometric glucose sensor: short-term, in vivo test. Diabetes Care 5(3):238-44.

246) Licko,V.,and Silvers,A.(1975). Open-loop glucose-insulin control with threshold secretory mechanism: analysis of intravenous glucose tolerance tests in man. Math. Biosciences 27:319-32.

247) Liljenquist,J.E.,Horwitz,D.L.,Jennings,A.S.,Chiasson,J.,Keller,U., and Rubenstein,A.H.(1978). Inhibition of insulin secretion by exogenous insulin in normal man as demonstrated by C-peptide assay. Diabetes 27:563-70.

248) Liljenquist,J.E.,Mueller,G.L.,Cherrington,A.D.,Perry,J.M.,and Rabinowitz,D.(1979). Hyperglycemia per se (insulin and glucagon withdrawn) can inhibit hepatic glucose production in man. J. Clin. Endocrin. Metab. 48(1):171-75.

249) Loreti,L.,Dunbar,J.C.,Chen,S.,and Foa,P.P.(1974). The autoregulation of insulin secretion in the isolated pancreatic islets of lean (obOb) and obese-hyperglycemic (obob) mice. Diabetologia 10:309-15.

250) Lui,G.,Coulston,A.,Chen,Y.-D.I.,and Reaven,G.M.(1983). Does day-long absolute hypoinsulinemia characterize the patient with non-insulin dependent diabetes mellitus? Metabolism 3:754-56.

251) Lundsguard,E.,Nielsen,N.A.,and Orskov,S.L.(1939). On the utilization of glucose and the formation of lactic acid in the isolated hind limb proparation. Skand. Arch. Physiol. 81:20-28.

252) Madison,L.L.,and Kaplan,N.(1958). The hepatic binding of I131-labeled insulin in human subjects during a single transhepatic circulation. J. Lab. & Clin. Med. 52(6):927.

253) Madison,L.L.,Combes,B.,Adams,R.,and Strickland,W.(1960). The physiological significance of the secretion of endogenous insulin into the portal circulation. III. Evidence for a direct immediate effect of insulin on the balance of glucose across the liver. J. Clin. Invest. 39:507-22.

254) Madison,L.L.,Mebane,D.,Lecocq,F.,and Combes,B.(1963). Physiological significance of the secretion of endogenous insulin into the portal circulation. V. The quantitative importance of the liver in the disposition of glucose loads. Diabetes 12:8-15.

255) Madison,L.(1969). Role of insulin in the hepatic handling of glucose. Arch. Intern. Med. 123:284-92.

256) Maher,T.D.,Tanenberg,R.J.,Greenberg,B.Z.,Hoffman,J.E.,Doe,R.P.,and Goetz,F.C.(1977). Lack of glucagon response to hypoglycemia in diabetic autonomic neuropathy. Diabetes 26:196-200.

257) Mahon,W.A.,Steinke,J.,McKhann,G.M.,and Mitchell,M.L.(1962). Measurement of I131-insulin and of insulin-like activity in cerebrospinal fluid in man. Metabolism 11(4):416-20.

258) Malaisse,W.J.,Malaisse-Lagae,F.,Lacy,P.E.,and Wright,P.H.(1967a). Insulin secretion by isolated islets in presence of glucose, insulin and anti-insulin serum. Proc. Soc. Exp. Biol. Med. 124:497-500.

259) Malaisse,W.,Malaisse-Lagae,F.,Wright,P.H.,and Ashmore,J.(1967). Effects of adrenergic and cholinergic agents upon insulin secretion in vitro. Endocrinology 80:975-8.

260) Malaisse,W.J.(1972). Hormonal and environmental modeification of islet activity. In: Greep,R.O.,and Astwood,E.B.,(eds.), Handbook of Physiology, Section 7: Endocrinology, Volume I. Endocrine Pancreas, pp.175-98, American Physiological Society, Washington D.C.

261) Mandarino,L.J.,and Gerich,J.E.(1984). Prolonged sulfonylurea administration decreases insulin resistance and increases insulin secretion in non-insulin-dependent diabetes mellitus: evidence for improved insulin action at a postreceptor site in hepatic as well as extrahepatic tissues. Diabetes Care 7(suppl. 1):89-99.

262) Mapleson,W.W.(1963). An electric analog for uptake and exchange of inert gases and other agents. J. Appl. Physiol. 18(1):197-204.

263) Matas,A.J.,Sutherland,D.E.R.,and Najarian,J.S.(1976). Current status of islet and pancreas transplantation in diabetes. Diabetes 25(9):785-95.

264) Matthews,D.R.,Naylor,B.A.,Jones,R.G.,Ward,G.M.,and Turner,R.C.(1983). Pulsatile insulin has greater hypoglycemic effect than continuous delivery. Diabetes 32:617-21.

265) Maybeck,P.S.(1982). Stochastic Models, Estimation and Control. Academic Press, New York.

266) Mayfield,R.K.,Sullivan,F.M.,Colwell,J.A.,and Wohltmann,H.J.(1983). Predicting insulin requirements for a portable insulin pump using the Biostator: evidence for reversible insulin resistance in poorly controlled type I diabetics. Diabetes 3:908-14.

267) McIntyre,N.,Holdsworth,C.D.,and Turner,D.S.(1965). Intestinal factors in the control of insulin secretion. J. Clin. Endocrinol. Metab. 25: 1317-24.

268) Mehlman,M.A.,Hanson,R.W.(eds.)(1971). In the Proceedings of a symposium on Recent Research in Diabetes - Intermediary and Drug Metabolism. Metabolism 20:27-99.

269) Meistas,M.,Vlachokosta,F.,and Aoki,R.(1984). Failure to reverse skeletal muscle insulin resistance in IDDM with artificial beta cell therapy. (In press.)

270) Miles,J.M.,Rizza,R.A.,Haymond,M.W.,and Gerich,J.E.(1980). Effects of acute insulin deficiency on glucose and ketone body turnover in man. Diabetes 29:926-30.

271) Menzel,R.,Besch,W.,Bruns,W.,Jahr,D.,Keilacker,H.,and Seidlen,I. (1981). Residual insulin secretion in insulin-dependent diabetics: its behavior during the course of diabetes and clinical importance. In: Irsigler,K.,Kunz,K.N.,Owens,D.R.,and Regal,H.,(eds.), New Approaches to Insulin Therapy, pp151-158, University Park Press, Baltimore.

272) Moody,A.J.(1972). Gastrointestinal glucagon-like immunoreactivity. In: Lefebvre,P.J.,and Unger,R.H.,(eds.), Glucagon: Molecular Physiology, Clinical and Therapeutic Implications, pp.319-41, Pergammom Press, Oxford.

273) Morgan,H.E.,Henderson,M.T.,Regen,D.M.,and Park,C.R.(1961). Regulation of glucose uptake in muscle. I. The effects of insulin and anoxia on glucose transport and phosphorylation in the isolated perfused heart of normal rats. J. Biol. Chem. 236:253-61.

274) Morgan,T.E.,Cobb,L.A.,Short,F.A.,Ross,R.,and Gunn,D.R.(1971). Effects of long-term exercise on human muscle mitochondria. In: Pernow,B.,and Saltin,B.,(eds.), Muscle Metabolism During Exercise, pp.87-109, Plenum Press, New York-London.

275) Morgan,L.M.(1979). Immunoassayable gastric inhibitory polypeptide: investigations into its role in carbohydrate metabolism. Annals Clin. Biochem. 16:6-14.

276) Mortimore,G.(1972). Influence of insulin on the hepatic uptake and release of glucose and amino acids. In: Steiner,D.,and Freinkel,N. (eds.), Handbook of Physiology, Section 7: Endocrinology, pp495-504, Williams & Wilkins, Baltimore.

277) Mortimore,C.H.,Turnbridge,W.M.G.,Carr,D.,Yeomans,L.,Lind,T.,Coy,D.H., Bloom,S.R.,Kastin,A.,Mallinson,C.N.,Besser,G.M.,Schally,A.V.,and Hall, R.(1974). Effects of growth hormone release-inhibiting hormone on circulating glucagon, insulin and growth hormone in normal, diabetic, acromegalic, and hypopituitary patients. Lancet I:697-701.

278) Mountcastle,V.B.(1974). Medical Physiology, Volume Two, Thirteenth Edition, C.V. Mosby Company, Saint Louis.

279) Munkgaard Rasmussen,S.,Heding,L.G.,Parbst,E.,and Volund,A.(1975). Serum IRI in insulin-treated diabetics during a 24 hour period. Diabetologia 2:151-58.

280) Murphy,J.R.(1960). Erythrocyte metabolism II. Glucose metabolism and pathways. J. Lab. Clin. Med. 55:286-302.

281) Mustaffa,B.E.,Daggett,P.R.,and Nabarro,J.D.N.(1977). Insulin binding in patients changed from conventional to highly purified insulins: an indicator of likely response. Diabetologia 13:311-15.

282) National Diabetes Advisory Board (1981). Treatment and control of diabetes: a national plan to reduce mortality and morbidity. Publication No.(NIH)81-2284, NIH, Bethesda, MD.

283) National Diabetes Data Group (1979). Classification and diagnosis of diabetes mellitus and other catagories of glucose intolerance. Diabetes 288:1039-57.

284) Nilsson,L.,Furst,P.,and Hultman,E.(1973). Carbohydrate metabolism of the liver in normal man under varying dietary conditions. Scand. J. Clin. Lab. Invest. 32:331-37.

285) Nilsson,L.,and Hultman,E.(1973). Liver glycogen in man - The effect of total starvation or a carbohydrate-poor diet followed by carbohydrate refeeding. Scand. J. Clin. Lab. Invest. 32:325-330.

286) Nordlie,R.C.(1981). Multifuncional glucose-6-phosphatase. In: Veneziale,C.M.,(ed.), The Regulation of Carbohydrate Formation and Utilization in Mammals, pp.291-314, University Park Press, Baltimore.

287) Oberhardt,B.J.,Fogt,E.J.,and Clemens,A.H.(1982). Glucose sensor characteristics for miniaturized portable closed-loop insulin delivery: a step toward implantation. Diabetes Care 5(3):213-17.

288) O'Connor,M.D.,Lahndal,H.,and Grodsky,G.M.(1980). Comparison of storage- and signal-limited models of pancreatic insulin secretion. Am. J. Physiol. 238:378-89.

289) Ohneda,A.,Parada,E.,Eisentraut,A.M.,and Unger,R.H.(1968). Characterization of circulating glucagon to intraduodenal and intravenous administration of amino acids. J. Clin. Invest. 47:2305-22.

290) Olefsky,J.M.(1981). Insulin resistance and insulin action. An in vitro and in vivo perspective. Diabetes 30:148-162.

291) Orci,L.,Malaisse-Lagae,F.,Ravazzola,M.,Rouiller,D.,Renold,A.E., Perrelet,A.,and Unger,R.H.(1975). A morphological basis for intercellular commonication between alpha- and beta-cells in the endocrine pancreas. J. Clin. Invest. 56:1066-70.

292) O'Sullivan,J.M.,and Mahan,C.M.(1964). Criteria for the oral glucose tolerance tesst in pregnancy. Diabetes 13:78-82.

293) O'Sullivan,J.M.(1970). Gestational diabetes and its significance. In: Camerini-Davalos,R.A.(ed.), Advances in Metabolic Disorders (suppl. 1), p339, Academic Press, New York.

294) O'Sullivan,J.B.,Charles,D.,and Dandrow,R.V.(1971). Treatment of verified prediabetes in pregnancy. J. Reproduc. Med. 7:21-4.

295) Palmer,J.P.,and Ensinck,J.W.(1975). Stimulation of glucagon secretion by ethanol-induced hypoglycemia in man. Diabetes 24:295-300.

296) Palmer,J.P.,Benson,J.W.,Walter,R.M.,and Ensinck,J.W.(1976). Arginine-stimulated acute phase of insulin and glucagon secretion in diabetic subjects. J. Clin. Invest. 58:565-70.

297) Park, B.N., Soeldner, J.S., and Gleason, R.E. (1974). Diabetes in remission: insulin secretory dynamics. Diabetes 23(7):616-23.

298) Patel,M.S.,Owen,O.E.,Goldman,L.I.,and Hanson,R.W.(1975). Fatty acid synthesis by human adipose tissue. Metabolism 24(2):161-73.

299) Patton,G.S.,Ipp,E.,Dobbs,R.E.,Orci,L.,Vale,W.,and Unger,R.H.(1977). Studies of pancreatic immunoreactive somatostatin (IRS) release. Proc. Natl. Acad. Sci. USA 74:2140-43.

300) Pelkonen,R.,Miettinen,T.A.,and Taskinen,M.R.(1968). Effect of acute elevation of plasma glycerol, triglyceride, and FAA levels on glucose utilization and plasma insulin. Diabetes 17:76-82.

301) Perley,M.J.,and Kipnis,D.M.(1967). Plasma insulin responses to oral and intravenous glucose: studies in normal and diabetic subjects. J. Clin. Invest. 46(12):1954-62.

302) Pernet,A.,Trimble,E.R.,Kuntschen,F.,Damoiseaux,P.,Assal,J.-Ph.,Hahn, C.,and Renold,A.E.(1984). Insulin resistance in type I (insulin-dependent) diabetes: depencence on plasma insulin concentration. Diabetologia 26:55-60.

303) Peters,J.P.,and VanSlyke,D.D.(1932). Gasometric methods for analysis of blood gases. In: Peters,J.P.,and VanSlyke,D.D., Quantitative Clinical Chemistry, Volume II Methods, p239, The Williams & Wilkins Company, Baltimore.

304) Peterson,R.A.,and Brown,J.C.(1978). Interaction of gastric inhibitory polypeptide, glucose, and arginine on insulin and glucagon secretion from the perfused rat pancreas. Endocrinology 103:610-15.

305) Pfeiffer,E.F.,Thum,Ch.,and Clemens,A.H.(1974). The artificial beta cell. A continuous control of blood sugar by external regulation of insulin infusion (glucose controlled insulin infusion system). Horm. Metab. Res. 6:339-42.

306) Pilo,A.,Ferrannini,E.,Biorkman,O.,Wahren,J.,Reichman,G.A.,Felig,P., and DeFronzo,R.A.(1981). Analysis of glucose production and disappearance rates following an oral glucose load in normal subjects: a double tracer approach. In: Cobelli,C.,and Bergman,R.N.,(eds.), Carbohydrate Metabolism, pp221-38,John Wiley & Sons Ltd., Chichester.

307) Pitts,R.F.(1974). Physiology of the Kidney and Body Fluids, Year Book Medical Publishers Incorporated, Chicago.

308) Polonsky,K.S.,and Rubenstein,A.H.(1984). C-peptide as a measure of the secretion and hepatic extraction of insulin. Pitfalls and limitations. Diabetes 33:486-94.

309) Porta,P.D.,Maiolo,A.T.,Negri,V.U.,and Rossella,E.(1964). Metabolism XIII:131-140.

310) Porte,D.,and Williams,R.(1966). Inhibition of insulin release by norepinephrine in man. Science 152:1248-50.

311) Porte,D.,Graber,A.,Kuzuya,T.,and Williams,R.(1966). The effect of epinephrine on immunoreactive insulin levels in man. J. Clin. Invest. 45:228-36.

312) Porte,D.(1967). A receptor mechanism for the inhibition of insulin release by epinephrine in man. J. Clin. Invest. 46:86-94.

313) Porte,D.,Jr.(1969). Synpathetic Regulation of insulin secretion. Its relation to diabetes mellitus. Arch. Internal Med. 123: 252-60.

314) Pozefsky,T.,Santis,M.R.,Soeldner,J.S.,and Tancredi,R.G.(1973). Insulin sensitivity of forearm tissues in prediabetic man. J. Clin. Invest. 52:1608-15.

315) Proietto,J.,Nankervis,A.,Aitken,P.,Caruso,G.,and Alford,F.(1983). Glucose utilization in type I (insulin-dependent) diabetes: evidence for a defect not reversible by acute elevations of insulin. Diabetologia 25:331-335.

316) Pryce,J.D.,Gant,P.W.,and Saul,K.J.(1970). Normal concentrations of lactate, glucose, and protein in cerebrospinal fluid, and the diagnostic implications of abnormal concentrations. Clin. Chem. 16(7): 562-5.

317) Rabinowitz,D.,and Zierler,K.L.(1962). Role of free fatty acids in forearm metabolism in man. Quantitated by use of insulin. J. Clin. Invest. 41(12):2191-97.

318) Rabinowitz,D.,Merimee,T.J.,Maffezzoli,R.,and Burgess,J.A.(1966). Patterns of hormonal release after glucose, protein, and glucose plus protein. Lancet 2:454-56.

319) Radziuk,J.,Norwich,K.,and Vranic,M.(1974). Measurement and validation of nonsteady state turnover rates with applications to the insulin and glucose systems. Fed. Proc. 33:1855-64.

320) Radziuk,J.,McDonald,T.J.,Rubenstein,D.,and Dupre,J.(1978). Initial splanchnic extraction of ingested glucose in normal man. Metabolism 27(6):657-69.

321) Radziuk,J.,and Inculet,R.(1983). The effects of ingested and intravenous glucose on forearm uptake of glucose and glucogenic substate in normal man. Diabetes 32(11):977-81.

322) Randle,P.J.,and Hales,C.N.(1972). Insulin release mechanisms. In: Greep,R.O.,and Astwood,E.B.,(eds.), Handbook of Physiology, Section 7: Endocrinology, Volume I. Endocrine Pancreas, pp219-35, American Physiological Society, Washington D.C.

323) Rasio,E.A.,Hampers,C.L.,Soeldner,J.S.,and Cahill,G.F.(1967). Diffusion of glucose, insulin, inulin, and Evans Blue protein into thoracic duct lymph of man. J. Clin. Invest. 46(6):903-10.

324) Rasio,E.A.,Mack,E.,Egdahl,R.H.,and Herrera,M.G.(1968). Passage of insulin and inulin across vascular membranes in the dog. Diabetes 17: 668-72.

325) Rasio,E.,Whichelow,M.J.,Butterfield,W.J.H.,and Hicks,B.H.(1972). Insulin fixation and glucose uptake by forearm tissues in response to infusions of physiologic amounts of insulin in nondiabetic subjects. Diabetologia 8:244-49.

326) Rasio,E.(1982). The capillary barrier to circulating insulin. Diabetes Care 5(3):158-61.

327) Raskin,P.,Fujita,Y.,and Unger,R.H.(1975). Effect of insulin-glucose infusions on plasma glucagon levels in fasting diabetics and nondiabetics. J. Clin. Invest. 56:1132-38.

328) Reach,G.,Jaffrin,M.Y.,and Desjeux,J.-F.(1984). A U-shaped bioartificial pancreas with rapic glucose-insulin kinetics. In vitro evaluation and kinetic modeling. Diabetes 33:752-61.

329) Reach,G.(1984). Bioartificial pancreas. Present status and future prospects. Biomed. Biochim. Acta 43(5):569-76.

330) Reaven,G.,and Miller,R.(1968). Study of the relationship between glucose and insulin responses to an oral glucose load in man. Diabetes 17:560-69.

331) Reaven,G.M.,Sageman,W.S.,and Swenson,R.S.(1977). Development of insulin resistance in normal dogs following alloxan-induced insulin deficiency. Diabetologia 13:459-62.

332) Reaven,G.M.,and Miller,R.G.(1979). An attempt to define the nature of chemical diabetes using a multidimentional analysis. Diabetologia 16: 17-24.

333) Reaven,G.M.(1984). Insulin secretion and insulin action in non-insulin-dependent diabetes mellitus: which defect is primary? Diabetes Care 7(suppl. 1):17-24.

334) Reichlin,S.(1983a). Somatostatin. N. Engl. J. Med. 309(24):1495-1501.

335) Reichlin,S.(1983b). Somatostatin. N. Engl. J. Med. 309(25):1556-63.

336) Revers,R.R.,Kolterman,O.G.,Scarlett,J.A.,Gray,R.S.,and Olefsky,J.M. (1984). Lack of in vivo insulin resistance in controlled insulin-dependent, type I, diabetic patients. J. Clin. Endocrinol. Metab. 58: 353-58.

337) Richter,G.J.,Luft,G.,and Gebhardt,U.(1982). Development and present status of an electrocatalytic glucose sensor. Diabetes Care 5(3):224-8.

338) Rizza,R.A.,and Gerich,J.E.(1978). Persistent effect of sustained hyperglucagonemia on glucose production in man. J. Clin. Endocrinol. Metab. 48(2):352-5.

339) Rizza,R.A.,Mandarino,L.J.,and Gerich,J.E.(1981). Dose-response characteristics for effects of insulin on production and utilization of glucose in man. Am. J. Physiol. 240:E630-39.

340) Robertson,R.P.,and Porte,D.,Jr.(1973). The glucose receptor: a defective mechanism in diabetes mellitus distinct from the beta adrenergic receptor. J. Clin. Invest. 52:870-76.

341) Robinson,J.R.(1967). Principles of renal physiology. In: Black,D.A.K., (ed.), Renal Disease, Blackwell Press, Oxford.

342) Rocha,D.M.,Faloona,G.R.,and Unger,R.H.(1972). Glucagon stimulating activity of twenty amino acids in dogs. J. Clin. Invest. 51: 2346-51.

343) Rodvell,M.(1972). Regulation of glucagon action at its receptor. In: Lefebvre,P.J.,and Unger,R.H.,(eds.), Glucagon: Molecular Physiology, Clinical and Therapeutic Implications, pp.61-75, Pergammom Press, Oxford, England.

344) Rojdmark,S.,Bloom,G.,Chou,M.C.Y.,and Field,J.B.(1978). Hepatic extraction of exogenous insulin and glucagon in the dog. Endocrinology 102:806-13.

345) Roth,J.,Lesniak,M.A.,Bar,R.S.,Muggeo,M.,Megyesi,K.,Harrison,L.C., Flier,J.S.,Wachslicht-Rodbard,H.,and Gorden,P.(1979). An introduction to receptors and receptor disorders. Proc. Soc. Exp. Biol. Med. 162:3-12.

346) Sacca,L.,Hendler,R.,and Sherwin,R.S.(1978). Hyperglycemia inhibits glucose production in man independent of changes in glucoregulatory hormones. J. Clin. Endocrin. Metab. 47(5):1160-63.

347) Sacca,L.,Sherwin,R.,Hendler,R.,and Felig,P.(1979). Influence of continuous physiologic hyperinsulinemia on glucose kinetics and counterregulatory hormones in normal and diabetic humans. J. Clin. Invest. 63:849-57.

348) Samols,E.,and Ryder,J.A.(1961). Studies on tissue uptake of insulin in in man using a differential immunoassay for endogenous and exogenous insulin. J. Clin. Invest. 40:2092-2102.

349) Samols,E.,Marris,G.,and Marks,V.(1965). Promotion of insulin secretion by glucagon. Lancet 2:415-17.

350) Samols,E.,Tyler,J.M.,and Marks,V.(1972). Glucagon-insulin interrelationships. In: Lefebvre,P.J.,and Unger,R.H.,(eds.), Glucagon: Molecular Physiology, Clinical and Therapeutic Implications, pp.151-73, Pergamom, Oxford, England.

351) San,K.Y.,and Stephanopoulos,G.(1984). Studies on on-line bioreactor identification. II. Numerical and experimental results. Biotechnol. Bioeng. XXVI:1189-1197.

352) Sando,H.,and Grodsky,G.M.(1973). Dynamic synthesis and release of insulin and proinsulin ffrom perifused islets. Diabetes 22:354-60.

353) Santiago,J.V.,Clemens,A.H.,Clarke,W.L.,and Kipnis,D.M.(1979). Closed-loop and open-loop devices for glucose control in normal and diabetic subjects. Diabetes 28:71-81.

354) Santis,M.R.,Lowrie,E.G.,Hampers,C.L.,and Soeldner,J.S.(1970). Diffusion of growth hormone into thoracic duct lymph in man. J. Clin. Endocr. 31:632-9.

355) Scarlett,J.A.,Gray,R.S.,Griffin,J.,Olefsky,J.M.,and Kolterman,O.G. (1982). Insulin treatment reverses the insulin resistance of Type II diabetes mellitus. Diabetes Care 5(4):353-63.

356) Schlichtkrull,J.,Brange,J.,Christiansen,A.H.,Hallunnd,O.,Heding,L.G., Jorgensen,K.H.,Munkgaard Rasmussen,S.,Sorensen,E.,and Volund,A.(1974). Monocomponent insulin and its clinical implications. Horm. Metab. Res. 5(suppl.):134-43.

357) Schultz,J.S.,Mansouri,S.,and Goldstein,I.J.(1982). Affinity sensor: a new technique for developing implantable sensors for glucose and other metabolites. Diabetes Care 5(3):245-53.

358) Scott,R.S.,Espiner,E.A.,Donald,R.A.,and Smith,J.R.(1978). Antibody binding of insulin in diabetic ketoacidosis. Diabetes 27:1151-55.

359) Segre,G.,Turco,G.L.,and Vercellone,G.(1973). Modeling blood glucose and insulin kinetics in normal, diabetic, and obese subjects. Diabetes 22:94-103.

360) Seltzer,H.S.,Allen,E.W.,Herron,A.L.,and Brenna,M.T.(1967). Insulin secretion in response to glycemic stimulus, relation of delayed initial release to carbohydrate intolerance in mild diabetes mellitus. J. Clin. Invest. 46:323-35.

361) Sen,A.K.,and Widdas,W.F.(1962). Determination of the temperature and pH dependence of glucose transfer across the human erythrocyte membrane measured by glucose exit. J. Physiol. 160:392-403.

362) Service,F.J.,Molnar,G.D.,Rosevear,J.W.,Ackerman,J.W.,Gatewood,L.C., and Taylor,W.F.(1970). Mean amplitude of glycemic excursions, a measure of diabetic instability. Diabetes 19:644-55.

363) Shakima,H.,and Ui,S.(1978). Glucose load diverts hepatic gluconeogenic product from glucose to glycogen in vivo. Am. J. Physiol. 235(4):E354-60.

364) Sharp,R.,Culbert,S.,Cook,J.,Jennings,A.,and Burr,I.M.(1974). Choligernic modification of glucose-induced biphasic insulin release in vitro. J. Clin. Invest. 53:710-16.

365) Sherwin,R.S.,Kramer,K.J.,Tobin,J.D.,Insel,P.A.,Liljenquist,J.E.,Berman, M.,and Andres,R.(1974). A model of the kinetics of insulin in man. J. Clin. Invest. 53:1481-92.

366) Shichiri,M.,Kawamori,R.,Goriya,Y.,Yamasaki,Y.,Nomura,M.,Hakui,N.,and Abe,H.(1983). Glycaemic control in pancreatectomized dogs with a wearable artificial endocrine pancreas. Diabetologia 24:179-84.

367) Shichiri,M.,Kawamori,R.,Hakui,N.,Yamasaki,Y.,and Abe,H.(1984). Closed-loop glycemic control with a wearable artificial endocrine pancreas. Variations in daily insulin requirements to glycemic response. Diabetes 33:1200-2.

368) Shima,K.,Tanaka,R.,Morishita,S.,Tarui,S.,Kumahara,V.,and Nishikawa, M.(1977). Studies on the etiology of "brittle diabetes." Relationship between diabetic instability and insulinogenic reserve. Diabetes 26: 717-25.

369) Shrago,E.,Glennon,J.A.,and Gordon,E.S.(1971). Comparative aspects of lipogenesis in mammalian tissues. Metabolism 20(1):54-62.

370) Silvers,A.,Swenson,R.,Farquhar,J.,and Reaven,G.M.(1969). Derivation of a three compartment model describing disappearance of plasma insulin-I131 in man. J. Clin. Invest. 48:1461-9.

371) Sjostrom,L.(1973). Fatty acid synthesis de novo in adipose tissue from obese subjects on a hypercaloric high carbohydrate diet. Scand. J. Clin. Lab. Invest. 32:339-49.

372) Skyler,J.S.(1984). Non-insulin-dependent diabetes mellitus: a clinical stategy. Diabetes Care 7(suppl. 1):118-29.

373) Soeldner,J.S.,Chang,K.W.,Aisenberg,S.,and Hiebert,J.M.(1973). Progress towards an implantable glucose sensor and an artificial beta cell. In: Urquhart,J.,and Yates,F.E. (eds.), Temporal Aspects of Therapeutics, pp181-207, Plenum Press, New York-London.

374) Soeldner,J.S.,and Park,B.N.(1977). Implications from oral glucose tolerance testing. In: Rose,L.I.,and Lavine,R.L.(eds.), New Concepts in Endocrinology and Metabolism, pp.107-24, Grune & Stratton, Inc.

375) Soeldner,J.S.(1981). Treatment of diabetes mellitus by devices. Am. J. Med. 70:183-94.

376) Soeldner,J.S.(1984). Joslin Research Laboratory, Boston, personal communication.

377) Sokolov,L.(1960). Metabolism of the central nervous system in vivo. In: Field,J.,Magoun,H.W.,and Hall,V.E.,(eds.), Handbook of Physiology, Section I: Neurophysiology, Volume III, pp1843-64, American Physiological Society, Washington D.C.

378) Solcia,E.,Capela,C.,Buffa,R.,Frigerio,B.,Usellini,L.,and Fontana,P. (1978). Endocrine cells of the gut and related growths. In: Bloom, S.R.,(ed.), Gut Hormones, pp.77-81, Churchill-Livingstone, Edinburgh.

379) Sols,A.,Salas,M.,and Vineula,E.(1964). Induced biosynthesis of liver glucoskinase. Adv. Enzyme Regul. 2:177-88.

380) Sorensen,J.T.,Colton,C.K.,Hillman,R.S.,and Soeldner,J.S.(1982). Use of a physiologic pharmacokinetic model of glucose homeostasis for assessment of performance requirements for improved insulin therapies. Diabetes Care 5(3):148-57.

381) Soskin,S.,Essex,H.E.,Herrick,J.F.,and Mann,F.C.(1938). The mechanism of regulation of the blood sugar by the liver. Am. J. Physiol. 124: 558-67.

382) Soskin,S.(1940). The liver and carbohydrate metabolism. Endocrinology 26:297-308.

383) Sparks,R.E.,Mason,N.S.,Finley,T.C.,and Scharp,D.W.(1982). Development, testing and modeling of an islet transplantation chamber. Trans. Am. Soc. Artif. Intern. Organs XXVIII:229-31.

384) Spector,W.S.(ed),(1956). Handbook of Biological Data. W.B. Saunders Company, Philadelphia.

385) Srikanta,S.,Ganda,O.P.,Eisenbarth,G.S.,and Soeldner,J.S.(1983a). Islet cell antibodies and beta cell function in monozygotic triplets and twins initially discordant for type I diabetes mellitus. N. Engl. J. Med. 308:322-25.

386) Srikanta,S.,Ganda,O.P.,Jackson,R.A.,Gleason,R.E.,Kaldany,A.,Garovoy, M.D.,Milford,E.L.,Carpenter,C.B.,Soeldner,J.S.,and Eisenbarth,G.S. (1983b). Type I diabetes mellitus in monozygotic twins: chronic progressive beta cell dysfunction. Ann. Intern. Med. 99:320-6.

387) Srikanta,S.,Ganda,O.P.,Gleason,R.E.,Jackson,R.A.,Soeldner,J.S.,and Eisenbarth,G.S.(1984). Pre-type I diabetes: linear loss of beta cell response to intravenous glucose. Diabetes 33:717-20.

388) Stephanopoulos,G.,and San,K.Y.(1984). Studies on on-line bioreactor identification. I. Theory. Biotechnol. Bioeng. XXVI:1176-1188.

389) Steiner,D.F.(1967). Evidence for a precursor in the biosynthesis of insulin. Trans. NY Acad. Sci. Ser. II 30:60-68.

390) Steiner,D.F.,Kemmler,W.,Clark,J.L.,Oyer,P.E.,and Rubenstein,A.H.(1972). The biosynthesis of insulin. In: Greep,R.O.,and Astwood,E.B.,(eds.), Handbook of Physiology, Section 7: Endocrinology, Volume I. Endocrine Pancreas, pp175-198, American Physiological Society, Washington D.C.

391) Steiner,D.F.,Kemmler,W.,Tager,H.S.,and Peterson,J.D.(1974). Proteolytic processing in the biosynthesis of insulin and other proteins. Federation Proc. 33:2105-115.

392) Swan,G.W.(1982). An optimal control model of diabetes mellitus. Bull. Math. Biol. 44(6):793-808.

393) Teorell,T.(1937). Kinetics of distribution of substances administered to the body. Arch. Int. Pharmacodyn. Ther. LVII:205-25.

394) Terris,S.,and Steiner,D.F.(1975). Binding and degradation of [125I]-insulin by rat hepatocytes. J. Biol. Chem. 21: 8389-98.

395) Terris,S.,and Steiner,D.F.(1976). Insulin binding and degradation in perfused rat liver. J. Clin. Invest. 57:885-96.

396) Thevenot,D.R.(1982). Problems in adapting a glucose-oxidase electrochemical sensor into an implantable glucose-sensing device. Diabetes Care 5(3):184-89.

397) Thorell,J.,Persson,B.,and Sterkey,G.(1966). Effect of fat inffusion on plasma glucose, FFA, glycerol and insulin levels during intravenous and oral glucose tolerance tests. (abstr.) Diabetologia 2(3):232.

398) Tiran,J.,Galle,K.R.,and Porte,D.Jr.(1975). A simulation model of extracellular glucose distribution in the human body. Ann. Biomed. Eng. 3:34-46.

399) Tiran,J.,Avruch,I.,and Albisser,A.M.(1979). A circulation and organs model for insulin dynamics. Am. J. Physiol. 237:E331-39.

400) Tiran,J.,Broekhuyse,H.,and Albisser,A.M.(1980). Glucose and insulin dynamics in the anaesthetized dog: a mathematical modeling study. Med. Progr. Technol. 7:183-92.

401) Tiran,J.,Yamasaki,Y.,and Albisser,A.M.(1981). A model study of canine glucose and insulin dynamics. In: Cobelli,C.,and Bergman,R.N.,(eds.), Carbohydrate Metabolism, pp329-47,John Wiley & Sons Ltd., Chichester.

402) Toffolo,G.,Bergman,R.N.,Finegood,D.T.,Bowden,C.R.,and Cobelli,C.(1980). Quantitative estimation of beta cell sinsitivity to glucose in the intact organism. Diabetes 29:979-90.

403) Unger,R.H.,Eisentraut,A.M.,McCall,M.S.,and Madison,L.L.(1961). Glucagon antibodies and an immunoassay for glucagon. J. Clin. Invest. 45:1280-88.

404) Unger,R.H.,Ohneda,A.,Aguilar-Parada,E.,and Eisentraut,A.M.(1969). The role of aminogenic glucagon secretion in blood glucose homeostasis. J. Clin. Invest. 48:810-22.

405) Unger,R.(1971). Glucagon and the insulin:glucagon molar ratio in diabetes and other catabolic diseases. Diabetes 20:834-38.

406) Unger,R.(1976). Diabetes and the alpha cell. Diabetes 25:136-51.

407) Unger,R.H.,and Dobbs,R.E.(1978). Insulin, Glucagon, and somatostatin secretion in the regulation of metabolism. Ann. Ref. Physiol. 40:307-43.

408) Unger,R.H.,Aguilar-Parada,E.,Muller,W.A.,and Eisentraut,A.M.(1970). Studies of pancreatic alpha cell function in normal and diabetic subjects. J. Clin. Invest. 49:837-48.

409) Unger,R.H.,and Orci,L.(1976). Physiology and pathophysiology of glucagon. Physiologic Reviews 56(4):778-826.

410) Urquhart,J.,and Keller,N.(1971). In situ and pilot organ perfusion techniques for the study of metabolic dynamics. In: Karolinska Symposia on Research Methods in Reproductive Endocrinology, 4th Symposium. Perfusion Techniques. pp. 9-25, Karolinska Institutet, Stockholm.

411) Vander,A.J.(1975). Renal Physiology, McGraw-Hill, Inc., New York.

412) Verdin,E.,Castillo,M.,Luyckx,A.S.,and Lefebvre,P.J.(1984). Similar metabolic effects of pulsatile versus continuous human insulin delivery during euglycemic, hyperinsulinemic glucose clamp in normal man. Diabetes 33:1169-74.

413) Waddel,W.R.,and Sussman,K.E.(1967). Plasma insulin after diversion of portal and pancreatic venous blood to vena cava. J. Appl. Physiol. 22 (4):808-12.

414) Wahren,J.,Felig,P.,Cerasi,E.,and Luft,R.(1972). Splanchnic and peripheral glucose and amino acid metabolism in diabetes mellitus. J. Clin. Invest. 51:1870-78.

415) Wahren,J.,Felig,P.,and Hagenfeldt,L.(1976). Effect of protein ingestion on splanchnic and leg metabolism in normal man and in patients with diabetes mellitus. J. Clin. Invest. 57:987-99.

416) Wall,J.,Steele,R.,DeBodo,R.,and Altszuler,N.(1957). Effect of insulin on utilization and production of circulating glucose. Am. J. Physiol. 189:43-50.

417) Weinless,N.L.,and Colton,C.K.(1983). A theoretical model for insulin secretory dynamics in a hybrid artificial pancreas. Ann. N.Y. Acad. Sci. 413:421-3.

418) Weir,G.C.,Samols,E.,Ranseur,R.,Day,J.A.,Jr.,and Patel,Y.C.(1977). Influence of glucose and glucagon upon somatostatin secretion from the isolated perfused canine pancreas (abstr.). Clin. Res. 25:403A.

419) Weller,C.,Linder,M.,Macaulay,A.,Ferrari,A.,and Kessler,G.(1960). Continuous in vivo determination of blood sugar in human subjects. Ann. N.Y. Acad. Sci. 87:658-68.

420) Whitton,P.D.,and Hems,D.A.(1975). Glycogen synthesis in the perfused liver of streptozotocin-diabetic rats. Biochem. J. 150:153-65.

421) Wick,A.N.,and Drury,D.R.(1953). Infuluence of glucose concentration on the action of insulin. Am. J. Physiol. 174:445-47.

422) Widdas,W.F.(1954). Facilitated transfer of hexoses across the human erythrocyte membrane. J. Physiol. 125:163-80.

423) Widdas,W.F.(1968). Membrane transport of sugars. In: Dickens,F.,Randle, P.J.,and Whelan,W.J., Carbohydrate Metabolism and Its Disorders, Volume 1, pp1-23, Academic Press, London.

424) Wilbrandt,W.(1961). Membrane Transport and Metabolism, Kleinzeller and Kotyk, New York.

425) Wilson,T.H.(1962). Intestinal Absorption, Saunders, Philadelphia.

426) Wilson,G.L.(1983). Factors affecting insulin secretion. Cellular Engin. Newsletter (October/November):3-6.

427) Windmuller,H.G.,and Spaeth,A.E.(1980). Respiratory fuels and nitrogen metabolism in vivo and in small intestine in fed rats. J. Biol. Chem. 255:107-12.

428) Wolfson,S.K.,Jr.,Tokarsky,J.F.,Yao,S.J.,and Krupper,M.A.(1982). Glucose concentration at possible sensor tissue implant sites. Diabetes Care 5(3):162-65.

429) Wrenshall,G.A.,Bogoch,A.,and Ritchie,R.C.(1952). Extractable insulin of pancreas. Diabetes 1(2):87-107.

430) Yki-Jarvinen,H.,and Koivisto,V.A.(1983). Effects of body composition on insulin sensitivity. Diabetes 32:965-69.

431) Yoffey,J.M.,and Courtice,F.C.(1970). Lymphatics, Lymph and the Lymphomyeloid Complex, Academic Press, New York-London.

432) Yue,D.K.,Baxter,R.C.,and Turtle,J.R.(1978). C-peptide secretion and insulin antibodies as determinants of stability in diabetes mellitus. Metabolism 27:35-44.

433) Zipper,H.,and Mawe,R.C.(1972). The exchange and maximal net flux of glucose across the human erythrocyte I. The effect of insulin, insulin derivatives and small proteins. Biochim. Biophys. Acta. 282:311-25.

APPENDIX A: Computer Source Program (Fortran 77)

```
C-------------------------------------------------------------------
C
C                MODEL OF GLUCOSE METABOLISM
C                     IN NORMAL MAN
C
C                LAST REVISION JUNE 20, 1984
C
C                     JOHN T. SORENSEN
C
C-------------------------------------------------------------------
C
C
C                          TABLE DEFINING VARIABLES:
C
C   CONSTANT                        DEFINITION
C
C   A              INVERSE TIME CONSTANT (MIN -1)
C   B              INVERSE TIME CONSTANT (MIN -1)
C   BGU            RATE OF BRAIN GLUCOSE UPTAKE (MG/MIN)
C   EGHGP          EFFECT OF GLUCOSE ON HGP
C   EGHGU          EFFECT OF GLUCOSE ON HGU
C   EGNHGP         EFFECT OF GLUCAGON ON HGP
C   EGNHGPI        INITIAL EFFECT OF GLUCAGON ON HGP
C   EGPGNR         EFFECT OF GLUCOSE ON PANCREATIC GLUCAGON RELEASE
C   EGPGU          EFFECT OF GLUCOSE ON PERIPHERAL GLUCOSE UPTAKE
C   EIHGP          EFFECT OF INSULIN ON HGP
C   EIHGPA         ASYMPTOTIC EFFECT OF INSULIN ON HGP
C   EIHGU          EFFECT OF INSULIN ON HGU
C   EIHGUA         ASYMPTOTIC EFFECT OF INSULIN ON HGU
C   EIPGNR         EFFECT OF INSULIN ON PANCREATIC GLUCAGON RELEASE
C   EIPGU          EFFECT OF INSULIN ON PERIPHERAL GLUCOSE UPTAKE
C   FICK           FRACTION INSULIN CLEARANCE KIDNEY
C   FICL           FRACTION INSULIN CLEARANCE LIVER
C   GAMMA          INSULIN TRANSFER RATE (U/MIN)
C   GNMCR          GLUCAGON METABOLIC CLEARANCE RATE (L/MIN)
C   GGA            RATE OF GUT ORAL GLUCOSE ABSORPTION (MG/MIN)
C   GGU            RATE OF GUT GLUCOSE UPTAKE (MG/MIN)
C   GIN            RATE OF INTRAVENOUS GLUCOSE INFUSION (MG/MIN)
C   H              INSULIN TRANSFER RATE CONSTANT (MIN -1)
C   HGP            HEPATIC GLUCOSE PRODUCTION RATE (MG/MIN)
C   HGPF           FASTING HEPATIC GLUCOSE PRODUCTION RATE (MG/MIN)
C   HGU            HEPATIC GLUCOSE UPTAKE RATE (MG/MIN)
C   HGUF           FASTING HEPATIC GLUCOSE UPTAKE RATE (MG/MIN)
C   KGE            RATE OF KIDNEY GLUCOSE EXCRETION (MG/MIN)
C   KIC            KIDNEY INSULIN CLEARANCE (MU/MIN)
C   LIC            LIVER INSULIN CLEARANCE RATE (MU/MIN)
C   PGNRN          RATE OF PANCREATIC INSULIN RELEASE (NORMALIZED)
C   PGU            RATE OF PERIPHERAL GLUCOSE UPTAKE (MG/MIN)
C   PGUF           FASTING RATE OF PERIPHERAL GLUCOSE UPTAKE (MG/MIN)
C   PIC            PERIPHERAL INSULIN CLEARANCE RATE (MU/MIN)
C   PIIR           RATE OF INTRAVENOUS INSULIN INFUSION (MU/MIN)
C   PIR            PANCREATIC INSULIN RELEASE RATE (MU/MIN)
C   PIRF           FASTING RATE OF PANCREATIC INSULIN RELEASE (MU/MIN)
C   PIRREF         INSULIN SECRETION RATE S(G) AT FASTING (U/MIN)
C   QVGA           HEPATIC ARTERY GLUCOSE VASCULAR FLOW RATE (DL/MIN)
C   QVGB           BRAIN GLUCOSE VASCULAR FLOW RATE (DL/MIN)
C   QVGG           GUT GLUCOSE VASCULAR FLOW RATE (DL/MIN)
C   QVGH           HEART GLUCOSE VASCULAR FLOW RATE (DL/MIN)
C   QVGK           KIDNEY GLUCOSE VASCULAR FLOW RATE (DL/MIN)
C   QVGL           LIVER GLUCOSE VASCULAR FLOW RATE (DL/MIN)
```

```
C   QVGP        PERIPHERAL GLUCOSE VASCULAR FLOW RATE (DL/MIN)
C   QVIA        HEPATIC ARTERY INSULIN FLOW RATE (L/MIN)
C   QVIB        BRAIN INSULIN VASCULAR FLOW RATE (L/MIN)
C   QVIG        GUT INSULIN VASCULAR FLOW RATE (L/MIN)
C   QVIH        HEART INSULIN VASCULAR FLOW RATE (L/MIN)
C   QVIK        KIDNEY INSULIN VASCULAR FLOW RATE (L/MIN)
C   QVIL        LIVER INSULIN VASCULAR FLOW RATE (L/MIN)
C   QVIP        PERIPHERAL INSULIN VASCULAR FLOW RATE (L/MIN)
C   RBCU        (HEART) RBC UPTAKE (MG/MIN)
C   TMGB        BRAIN GLUCOSE TRANSMEMBRANE EQUIL TIME (MIN)
C   TMGP        PERIPHERY GLUCOSE TRANSMEMBRANE EQUIL TIME (MIN)
C   TMIP        PERIPHERAL INSULIN TRANSMEMBRANE EQUIL TIME (MIN)
C   VGG         GUT GLUCOSE VOLUME (DL)
C   VGI         GUT INSULIN VOLUME (L)
C   VGN         GLUCAGON DISTRIBUTION VOLUME (L)
C   VIB         BRAIN INTERSTITIAL VOLUME (DL)
C   VIP         PERIPHERY INTERSTITIAL VOLUME (DL)
C   VKG         KIDNEY GLUCOSE VOLUME (DL)
C   VLG         LIVER GLUCOSE VOLUME (DL)
C   VKI         KIDNEY INSULIN VOLUME (L)
C   VLI         LIVER INSULIN VOLUME (L)
C   VVGB        BRAIN GLUCOSE VASCULAR VOLUME (DL)
C   VVGH        HEART GLUCOSE VASCULAR VOLUME (DL)
C   VVGP        PERIPHERY GLUCOSE VASCULAR VOLUME (DL)
C   VVIB        BRAIN INSULIN VASCULAR VOLUME (L)
C   VVIH        HEART INSULIN VASCULAR VOLUME (L)
C   VVIP        PERIPHERAL INSULIN VASCULAR VOLUME (L)
C   Y20R        LABILE INSULIN IN PANCREAS FOR G=0 MG/DL (U)
C   XM1         INSULIN RELEASE CONSTANT (DIMENSIONLESS)
C   XM2         INSULIN RELEASE CONSTANT (DIMENSIONLESS)
C
C
C-------------------------------------------------------------------
C
C                       INDEX DEFINITIONS:
C
C   INDEX                   DERIVATIVE VARIABLES
C
C   1           BRAIN VASCULAR GLUCOSE CONC. (MG/DL)
C   2           BRAIN INTERSTITIAL GLUCOSE CONC. (MG/DL)
C   3           HEART VASCULAR GLUCOSE CONC. (MG/DL)
C   4           KIDNEY GLUCOSE CONC. (MG/DL)
C   5           LIVER GLUCOSE CONC. (MG/DL)
C   6           PERIPHERY VASCULAR GLUCOSE CONC. (MG/DL)
C   7           PERIPHERY INTERSTITIAL GLUCOSE CONC. (MG/DL)
C   8           GUT GLUCOSE CONC. (MG/DL)
C   9           EFFECT OF INSULIN ON HGU (TIME DEPENDENT)
C   10          BRAIN VASCULAR INSULIN CONC. (MU/L)
C   11          HEART VASCULAR INSULIN CONC. (MU/L)
C   12          KIDNEY INSULIN CONC. (MU/L)
C   13          LIVER INSULIN CONC. (MU/L)
C   14          PERIPHERAL VASCULAR INSULIN CONC. (MU/L)
C   15          PERIPHERAL INTERSTITIAL INSULIN CONC. (MU/L)]
C   16          GUT INSULIN CONC. (MU/L)
C   17          EFFECT OF INSULIN ON HGP (TIME DEPENDENT)
C   18          PROVISIONARY FACTOR (DIMENSIONLESS)
C   19          INHIBITOR (DIMENSIONLESS)
C   20          LABILE INSULIN IN PANCREAS (U)
C   21          DECAYING EFFECT OF GLUCAGON ON HGP
C   22          NORMALIZED PLASMA GLUCAGON CONC.
```

```
C
C
C-------------------------------------------------------------
C
C                        NONDERIVATIVE VARIABLES
C
C   88          NONLINEAR EFFECT OF GLUCOSE ON PIR (DIMENSIONLESS)
C   87          ASYMPTOTIC PROVISIONARY FACTOR VALUE (DIMENSIONLESS)
C   85          INSULIN SECRETION RATE S(G) BEFORE NORMALIZATION (U/MIN)
C
C-------------------------------------------------------------
C
C                        RUNGE KUTTA INTEGRATION VARIABLES
C
C   T           SIMULATION TIME (MIN)
C   DT          TIME STEP (MIN)
C   N           NUMBER OF FIRST ORDER ODE'S
C   Y(1-N)      DERIVATIVE VARIABLES
C   F(I)        TIME DERIVATIVE OF Y(I)
C   Y(I,I>N)    NON-DERIVATIVE VARIABLES
C   NEWDT=      -1 (FIRST INTEGRATION CALL)
C               0  (INTERMEDIATE CALLS)
C               1  (FIRST CALL AT EACH NEW TIME STEP)
C   STIME       SIMULATION STARTING TIME (MIN)
C   FTIME       SIMULATION ENDING TIME (MIN)
C   CONSTANT(I) UNASSIGNED VARIABLES USED FOR INPUT TO PROGRAM
C               THROUGH COMMON STATEMENT
C
C-------------------------------------------------------------
C
C
      SUBROUTINE EQSIM
      COMMON T,DT,Y(98),F(98),STIME,FTIME,NEWDT,NEWRUN,N,
     *  IPR,ICD,ICN,TBREAK,PNEXT,TBACK,CONSTANT(30)
C
C
      REAL KGE,KIC,LIC
C
C   PARAMETERS - GLUCOSE MODEL
C
      IF(NEWDT.EQ.-1) THEN
      DATA QVGA,QVGB,QVGG,QVGH,QVGK/2.5,5.9,10.1,43.7,10.1/
      DATA QVGL,QVGP/12.6,15.1/
      DATA VIB,VIP,VKG,VGG,VLG/4.5,63.,6.6,11.2,25.1/
      DATA VVGB,VVGH,VVGP/3.5,13.8,10.4/
      DATA RBCU,GGU/10.,20./
      DATA BGU,HGUF,HGPF,PGUF/70.,20.,155.,35./
      DATA TMGB,TMGP/2.1,5.0/
C
C   PARAMETERS - INSULIN DISTRIBUTION
C
      DATA QVIA,QVIB,QVIG,QVIH,QVIK/.18,.45,.72,3.12,.72/
      DATA QVIL,QVIP/.9,1.05/
      DATA VKI,VLI,VGI/.505,1.14,.945/
      DATA VVIB,VVIH,VVIP/.265,.985,.735/
      DATA FICK,FICL,FICP/.30,.40,.15/
      DATA TMIP/20./
C
C   PARAMETERS - MODEL PANCREAS
C
```

```
      DATA A,B,XN,H/.048229,.93141,1.,.0079378/
      DATA Y20R,GAMMA/6.3294,.57493/
      DATA XM1,XM2/.007968,.106495/
C
C   PARAMETERS - GLUCAGON MODEL
C
      GNMCR=0.910
      VGN=VVIB+VVIH+VVIP+VKI+VLI+VIP*0.1
C
      ENDIF
C
C   INITIALIZE GLUCOSE MODEL
      IF(NEWDT.EQ.-1) THEN
C*** INPUT FASTING PERIPHERAL VENOUS BLOOD GLUCOSE CONC. (MG/DL)
      Y(6)=CONSTANT(20)/0.84
      Y(3)=Y(6)+PGUF/QVGP
      Y(4)=Y(3)
      Y(1)=Y(3)-BGU/QVGB
      Y(8)=Y(3)-GGU/QVGG
      Y(5)=(1./QVGL)*(QVGA*Y(3)+QVGG*Y(8)+HGPF-HGUF)
      Y(2)=Y(1)-(BGU*TMGB)/VIB
      Y(7)=Y(6)-(PGUF*TMGP)/VIP
      Y(9)=1.
      Y(17)=1.
      Y(21)=0.
C     STORE BASAL VALUES FOR FUTURE COMPUTATIONS
      Y3F=Y(3)
      Y5F=Y(5)
      Y7F=Y(7)
C
C   INITIALIZE INSULIN MODEL
C*** INPUT FASTING PERIPHERAL VENOUS PLASMA INSULIN CONC. (MU/L)
      Y(14)=CONSTANT(21)
      Y(11)=Y(14)/(1.-FICP)
      Y(10)=Y(11)
      Y(12)=Y(11)*(1.-FICK)
      Y(13)=(1./QVIL)*(QVIH*Y(11)-QVIB*Y(10)-QVIK*Y(12)-QVIP*Y(14))
      Y(16)=Y(11)
      Y(15)=Y(14)-((QVIP*TMIP)/(VIP*.1))*(Y(11)-Y(14))
      PIRF=(QVIL/(1.-FICL))*Y(13)-QVIG*Y(16)-QVIA*Y(11)
C     STORE BASAL VALUES FOR FUTURE COMPUTATIONS
      Y11F=Y(11)
      Y13F=Y(13)
      Y15F=Y(15)
C
C   INITIALIZE GLUCAGON MODEL
      Y(22)=1.
C
      ENDIF
C
C   GLUCOSE MODEL PHYSIOLOGIC FUNCTIONS
C
      IF(NEWDT.NE.0) THEN
C     KIDNEY GLUCOSE EXCRETION RATE KGE
      IF(Y(4).LT.460.) KGE=71.+71.*TANH(.011*(Y(4)-460.))
      IF(Y(4).GE.460.) KGE=0.872*Y(4)-330.
C     PERIPHERAL GLUCOSE UPTAKE
      EGPGU=Y(7)/Y7F
      EIPGU=7.035+6.51623*TANH(.33827*(Y(15)/Y15F-5.82113))
      PGU=EGPGU*EIPGU*PGUF
```

```
C       LIVER GLUCOSE METABOLISM
C        HEPATIC GLUCOSE UPTAKE
         EIHGUA=2.*TANH(.549*(Y(13)/Y13F))
         EIHGU=Y(9)
         EGHGU=5.6648+5.6589*TANH(2.4375*(Y(5)/Y5F-1.48))
         HGU=EIHGU*EGHGU*HGUF
C        HEPATIC GLUCOSE PRODUCTION
         EIHGPA=1.2088-1.138*TANH(1.669*(Y(13)/Y13F-.8885))
         EIHGP=Y(17)
         EGNHGPI=2.7*TANH(.388*Y(22))
         EGNHGP=EGNHGPI-Y(21)
         EGHGP=1.425-1.406*TANH(.6199*(Y(5)/Y5F-.4969))
         HGP=EGNHGP*EIHGP*EGHGP*HGPF
C
         ENDIF
C
C     INPUTS FOR MODEL SIMULATION STUDIES
C
         IF(NEWDT.NE.0) THEN
C
C        INPUT FOR INTRAVENOUS GLUCOSE INFUSION
         TIME1=-3.
         TIME2=0.
         IF(T.LT.TIME1) GIN=0.
         IF(T.GE.TIME1.AND.T.LT.TIME2) GIN=CONSTANT(1)
         IF(T.GE.TIME2) GIN=0.
C
C        INPUT FOR HYPERGLYCEMIC CLAMP
C        CALL HYCLAMP(Y(3),Y3F,Y(97),T,DT,NEWDT)
C
C        INPUT FOR INTRAVENOUS INSULIN INFUSION
C        PIIR=0.0
C        IF(T.GT.TIME1.AND.T.LT.TIME2) PIIR=CONSTANT(2)
C
C        INPUT FOR EUGLYCEMIC INSULIN CLAMP
C        CALL EUCLAMP(Y(3),Y3F,Y(97),PIIR,T,DT,NEWDT)
C
C        INPUT FOR 100G ORAL GLUCOSE TOLERANCE TEST
C        CALL XOGTT(GGA,PIR,PIRF,T,NEWDT)
C        (NOTE: MODEL PANCREAS OUTPUT PIR MUST BE DISABLED FOR OGTT)
C
C
         ENDIF
C
C    GLUCOSE MODEL MASS BALANCE EQUATIONS
C
         F(1)=(1./VVGB)*(QVGB*(Y(3)-Y(1))+(VIB/TMGB)*(Y(2)-Y(1)))
         F(2)=(1./VIB)*((VIB/TMGB)*(Y(1)-Y(2))-BGU)
         F(3)=(1./VVGH)*(QVGB*Y(1)+QVGL*Y(5)+QVGK*Y(4)+QVGP*Y(6)
     *     -QVGH*Y(3)-RBCU+GIN)
         F(4)=(1./VKG)*(QVGK*(Y(3)-Y(4))-KGE)
         F(5)=(1./VLG)*(QVGG*Y(8)+QVGA*Y(3)-QVGL*Y(5)+HGP-HGU)
         F(6)=(1./VVGP)*(QVGP*(Y(3)-Y(6))+(VIP/TMGP)*(Y(7)-Y(6)))
         F(7)=(1./VIP)*((VIP/TMGP)*(Y(6)-Y(7))-PGU)
         F(8)=(1./VGG)*(QVGG*(Y(3)-Y(8))-GGU+GGA)
C    TIME DEPENDENT LIVER GLUCOSE METABOLISM
         F(9)=(1./25.)*(EIHGUA-Y(9))
         F(17)=(1./25.)*(EIHGPA-Y(17))
         F(21)=(1./65.)*((EGNHGPI-1.)/2.-Y(21))
C
```

```
C   MODEL PANCREAS
C
        IF(NEWDT.NE.0) THEN
        Y(88)=(Y(3)**3.267)/(131.87**3.267+5.932*Y(3)**3.024)
        Y(87)=Y(88)**1.1141
C
C       INITIALIZE MODEL PANCREAS TO FIRST PASS GLUCOSE
        IF(NEWDT.EQ.-1) THEN
        Y(18)=Y(87)
        Y(19)=XN*Y(88)
        Y(86)=Y(88)-Y(19)
        IF(Y(86).LT.0.) Y(86)=0.
        Y(20)=(H*Y20R+GAMMA*Y(18))/(XM1*Y(87)+XM2*Y(86)+H)
        PIRREF=(XM1*Y(87)+XM2*Y(86))*Y(20)
        PIRF=(QVIL/(1.-FICL))*Y(13)-QVIG*Y(16)-QVIA*Y(11)
        ENDIF
C
        Y(86)=Y(88)-Y(19)
        IF(Y(86).LT.0.) Y(86)=0.
        Y(85)=(XM1*Y(87)+XM2*Y(86))*Y(20)
        PIR=(XM1*Y(87)+XM2*Y(86))*Y(20)*(PIRF/PIRREF)
        ENDIF
C
C       MODEL PANCREAS DERIVATIVE EQUATIONS
        F(18)=A*(Y(87)-Y(18))
        F(19)=B*(XN*Y(88)-Y(19))
        F(20)=H*(Y20R-Y(20))+GAMMA*Y(18)-Y(85)
C
C
C   INSULIN MODEL PHYSIOLOGIC FUNCTIONS
C
        IF(NEWDT.NE.0) THEN
C      KIDNEY INSULIN CLEARANCE
        KIC=FICK*QVIK*Y(11)
C      LIVER INSULIN CLEARANCE
        LIC=FICL*(QVIG*Y(16)+QVIA*Y(11)+PIR)
C      PERIPHERAL INSULIN CLEARANCE
        PIC=(1./((1.-FICP)/(FICP*QVIP)-(TMIP/(VIP*.1))))*Y(15)
        ENDIF
C
C
C   INSULIN MASS BALANCE EQUATIONS
C
        F(10)=(1./VVIB)*(QVIB*(Y(11)-Y(10)))
        F(11)=(1./VVIH)*(QVIB*Y(10)+QVIL*Y(13)+QVIK*Y(12)+
     *   QVIP*Y(14)-QVIH*Y(11)+PIIR)
        F(12)=(1./VKI)*(QVIK*(Y(11)-Y(12))-KIC)
        F(13)=(1./VLI)*(QVIA*Y(11)+QVIG*Y(16)-QVIL*Y(13)-LIC+PIR)
        F(14)=(1./VVIP)*(QVIP*(Y(11)-Y(14))+((VIP*.1)/TMIP)*
     *    (Y(15)-Y(14)))
        F(15)=(1./(VIP*.1))*(((VIP*.1)/TMIP)*(Y(14)-Y(15))-PIC)
        F(16)=(1./VGI)*(QVIG*(Y(11)-Y(16)))
C
C
C   GLUCAGON MODEL PHYSIOLOGIC FUNCIONS
        IF(NEWDT.NE.0) THEN
        EIPGNR=1.3102-0.61016*TANH(1.0571*((Y(11)/Y11F)-0.46981))
        EGPGNR=2.9285-2.095*TANH(4.18*((Y(3)/Y3F)-0.6191))
        PGNRN=EIPGNR*EGPGNR
        ENDIF
```

```
C
C   GLUCAGON MASS BALANCE EQUATION (DIMENSIONLESS)
C
        F(22)=(1./VGN)*(GNMCR)*(PGNRN-Y(22))
C
C   AUXILIARY OUTPUT VARIABLES
        IF(NEWDT.NE.0) THEN
        Y(50)=Y(6)*.84
        ENDIF
C
C
        RETURN
        END
```

```
C-------------------------------------------------
C
C       EUGLYCEMIC INSULIN CLAMP SUBROUTINE
C
C               NOV 15, 1984
C
C-------------------------------------------------
C
        SUBROUTINE EUCLAMP(GIN,Y3F,GINFUSE,PIIR,T,DT,NEWDT)
        GCLAMP=Y3F*.925
C       INSULIN INFUSION INPUT
        IF(T.LE.0.+DT/2.) PIIR=0.
        IF(T.GT.0.+DT/2.) PIIR=221.
        IF(T.GT.1.+DT/2.) PIIR=197.
        IF(T.GT.2.+DT/2.) PIIR=175.
        IF(T.GT.3.+DT/2.) PIIR=156.
        IF(T.GT.4.+DT/2.) PIIR=139.
        IF(T.GT.5.+DT/2.) PIIR=124.
        IF(T.GT.6.+DT/2.) PIIR=110.
        IF(T.GT.7.+DT/2.) PIIR=98.
        IF(T.GT.8.+DT/2.) PIIR=87.
        IF(T.GT.9.+DT/2.) PIIR=78.
        IF(T.GT.10.+DT/2.) PIIR=69.
        IF(T.GT.120.+DT/2.) PIIR=0.
C
C   GLUCOSE INFUSION ALGORITHM
        IF(NEWDT.EQ.-1) I12=0
        IF(NEWDT.EQ.-1) I11=-1
        IF(T.LT.0.+DT/2.) GO TO 112
        I11=I11+1
        IF(I11.EQ.50) THEN
           I12=I12+1
           QDEL=Q1
           Q1=GIN*.925
           SMDEL2=SMDEL1
           SMDEL1=SM
           FMDEL1=FM
           FM=(Y3F*.925)/Q1
           IF(I12.EQ.2) SMDEL2=280.
           IF(I12.EQ.3) SMDEL2=280.
           SM=SMDEL2*FM*FMDEL1
           SI=8.8667*(GCLAMP-Q1)+SMDEL2*FMDEL1*((Y3F*.925)/Q1)
           I11=0
        ENDIF
        IF(T.LT.4.+DT/2.) SI=0.
        IF(T.GE.4.+DT/2..AND.T.LT.10.+DT/2.) SI=140.
        IF(T.GE.10.+DT/2..AND.T.LT.15.+DT/2.) SI=175.
        GINFUSE=SI
        GO TO 113
112     GINFUSE=0.
113     CONTINUE
        RETURN
        END
```

```
C-----------------------------------------------------------------------
C
C          HYPERGLYCEMIC CLAMP INFUSION ALGORITHM
C
C                       DEC 27, 1984
C
C-----------------------------------------------------------------------
C
        SUBROUTINE HYCLAMP(GIN,Y3F,GINFUSE,T,DT,NEWDT)
C
C       GIN=ARTERIAL GLUCOSE CONC. (MG/DL)
C       GFAST=BASAL ARTERIAL GLUCOSE CONC. (MG/DL)
C       GINFUSE=GLUCOSE INFUSION RATE (MG/MIN)
C
C
        GFAST=Y3F*.925
        GCLAMP=GFAST+125.
        IF(T.LE.0.+DT/2.) PDOSE=0.
        IF(T.GT.0.+DT/2.) PDOSE=3059.
        IF(T.GT.1.+DT/2.) PDOSE=2470.
        IF(T.GT.2.+DT/2.) PDOSE=2000.
        IF(T.GT.3.+DT/2.) PDOSE=1588.
        IF(T.GT.4.+DT/2.) PDOSE=1353.
        IF(T.GT.5.+DT/2.) PDOSE=1118.
        IF(T.GT.6.+DT/2.) PDOSE=941.
        IF(T.GT.7.+DT/2.) PDOSE=765.
        IF(T.GT.8.+DT/2.) PDOSE=706.
        IF(T.GT.9.+DT/2.) PDOSE=647.
C**TEN MINUTE GLUCOSE VALUE USED TO ADJUST RATE
        IF(T.GT.10.-DT/2.) PDOSE=0.
C       IF(T.GT.10.+DT/2.) PDOSE=588.
C       IF(T.GT.11.+DT/2.) PDOSE=529.
C       IF(T.GT.12.+DT/2.) PDOSE=471.
C       IF(T.GT.13.+DT/2.) PDOSE=412.
C       IF(T.GT.14.+DT/2.) PDOSE=412.
C       IF(T.GT.15.+DT/2.) PDOSE=0.
C
        IF(NEWDT.EQ.-1) I12=0
        IF(NEWDT.EQ.-1) I11=-1
        IF(T.LT.0.-DT/2.) GO TO 112
        I11=I11+1
        IF(I11.EQ.50) THEN
         IF(I12.EQ.1) THEN
          SM=412.
          SMDEL1=412.
          FM=1.00
         ENDIF
           I12=I12+1
           QDEL1=Q1
           Q1=GIN*.925
           SMDEL2=SMDEL1
           SMDEL1=SM
           FMDEL1=FM
           FM=(GCLAMP-GFAST)/(Q1-GFAST)
           SM=SMDEL2*FM*FMDEL1
           SI=8.8667*(GCLAMP-Q1)+SM
           I11=0
        ENDIF
        GINFUSE=PDOSE+SI
        GO TO 113
```

```
112      GINFUSE=0.
113      CONTINUE
C
         RETURN
         END
```

```
C-----------------------------------------------------------------
C
C               100 G OGTT SIMULATION SUBROUTINE
C
C                       JUNE 1984
C
C-----------------------------------------------------------------
C
      SUBROUTINE XOGTT(GGA,PIR,PIRF,T,NEWDT)
      DIMENSION GGAIN(3000),PIRIN(3000)
C
C     READ IN GGA AND PIR FROM EXTERNAL FILES
      IF(NEWDT.EQ.-1) THEN
      OPEN(32,FILE='GGA',STATUS='OLD')
      OPEN(33,FILE='PIRIN',STATUS='OLD')
      DO 10 I=1,3000
      READ(32,1) GGAIN(I)
      READ(33,1) PIRIN(I)
1     FORMAT(9X,F12.5)
10    CONTINUE
      CLOSE(32,STATUS='SAVE')
      CLOSE(33,STATUS='SAVE')
      ENDIF
      PIR=PIRF
      IF(NEWDT.EQ.-1) ICOUNT=-1
      IF(T.GT.0.) THEN
      ICOUNT=ICOUNT+1
      GGA=GGAIN(ICOUNT)
      PIR=PIRIN(ICOUNT)*PIRF+PIRF
      ENDIF
C
      RETURN
      END
```

APPENDIX B: Summary Overview of the Glucose Metabolism Model of Guyton et al. (1978) Including the Modifications of Hillman (1977) for OGTT Simulation

In this section the mathematical model of Guyton et al. (1978) will be overviewed. For purposes of mathematical documentation, the model is presented in a tissue and organ compartmentalization format. A schematic diagram of the glucose model is presented in Figure B1. The mass balance equations for the glucose model were given by:

Glucose Model

Nervous System:
$$V_{NB}\frac{dG_{NB}}{dt} = Q_{NB}(G_{CB} - G_{NB}) + \frac{V_{NI}}{T_N}(G_{NI} - G_{NB}) - r^N_{RBC} \quad (B1)$$

$$V_{NI}\frac{dG_{NI}}{dt} = \frac{V_{NI}}{T_N}(G_{NB} - G_{NI}) - r_{CNS} \quad (B2)$$

Central Organs:
$$V_{CB}\frac{dG_{CB}}{dt} = Q_{NB}G_{NB} + Q_{PB}G_{PB} + Q_{LB}G_L + Q_{KB}G_K - Q_{CB}G_{CB} + \frac{V_{CI}}{T^G_C}(G_{CI} - G_{CB}) - r^C_{RBC} \quad (B3)$$

$$V_{CI}\frac{dG_{CI}}{dt} = \frac{V_{CI}}{T^G_C}(G_{CB} - G_{CI}) - r_{CEN} \quad (B4)$$

Periohery:
$$V_{PB}\frac{dG_{PB}}{dt} = Q_{PB}(G_{CB} - G_{PB}) + \frac{V_{CI}}{T^G_P}(G_{PI} - G_{PB}) - r^P_{RBC} \quad (B5)$$

$$V_{PI}\frac{dG_{PI}}{dt} = \frac{V_{PI}}{T^G_P}(G_{PB} - G_{PI}) - r_{PGU} \quad (B6)$$

Liver:
$$V_L\frac{dG_L}{dt} = Q_{LB}(G_{CB} - G_L) - r^L_{RBC} + r_{GNG} + r_{GBD} - r_{GSY} \quad (B7)$$

Kidney.
$$V_K\frac{dG_K}{dt} = Q_{KB}(G_{CB} - G_K) - r^K_{RBC} - r_{EXC} \quad (B8)$$

where the mathematical nomenclature employed in Figure B1 and Equations B1-B8

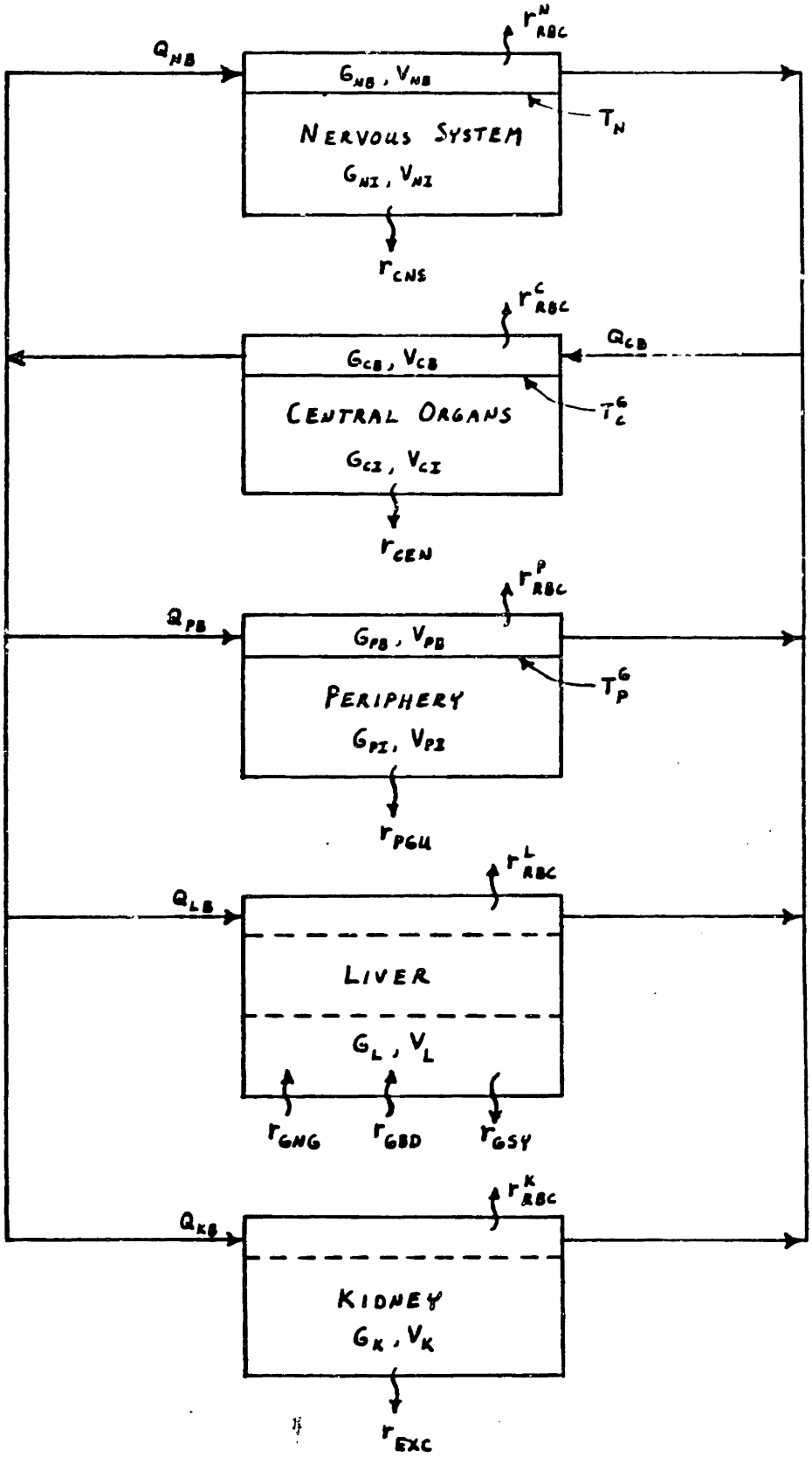

Fig. B1 Schematic diagram of the glucose model.

is defined as follows:

Variables: G = Glucose Concentration (mg/dl)
Q = Blood Flow Rate (dl/min)
V = Volume (dl)
T = Transcapillary Diffusion Time Constant (min)
r = Metabolic Source or Sink Rate (mg/min)
t = Time (min)

First Subscript or Superscript: Physiologic Compartment
N = Central Nervous System
C = Central Organs (heart, lungs, major blood vessels, and nonhepatic splanchnic organs)
P = Periphery (skeletal muscle and adipos tissue)
L = Liver
K = Kidney
G = Glucose Model

Second Subscript: Physiologic Subcompartment (if required)
B = Blood Space
I = Interstitial Fluid Space

Metabolic Rate Subscripts: RBC = Red Blood Cell Glucose Uptake
CNS = Central Nervous System Glucose Uptake
CEN = Central Organs Glucose Uptake
PGU = Peripheral Glucose Uptake
GNG = Liver Gluconeogenesis
GBD = Liver Glycogen Breakdown
GSY = Liver Glycogen Synthesis
EXC = Kidney Glucose Excretion

Numerical values for the glucose model physiologic parameters were as follows:

V_{NB} = 2 dl
V_{NI} = 2 dl
V_{CB} = 22 dl
V_{CI} = 35 dl
V_{PB} = 24 dl
V_{PI} = 70 dl
V_{L} = 20 dl
V_{K} = 6 dl

Q_{NB} = 7.25 dl/min
Q_{CB} = 58.0 dl/min
Q_{PB} = 24.65 dl/min
Q_{LB} = 14.5 dl/min
Q_{KB} = 11.6 dl/min

T_{N} = 0.2 min
T_{C}^{G} = 1.0 min
T_{P}^{G} = 5.0 min

Red blood cell uptake of glucose was assumed to occur at a total constant rate of 10 mg/min, which was divided among the various organ and tissue blood volume spaces according to their respective fractional contributions to the total blood volume:

r_{RBC}^{N} = 0.33 mg/min
r_{RBC}^{C} = 3.67 mg/min
r_{RBC}^{P} = 4.00 mg/min
r_{RBC}^{L} = 1.33 mg/min
r_{RBC}^{K} = 0.67 mg/min

r_{RBC} = 10.0 mg/min (constant)

In addition, glucose was taken up at a constant rate by the central nervous system and central organ tissues:

r_{CNS} = 100 mg/min (constant)
r_{CEN} = 20 mg/min (constant)

The rate of liver glycogen synthesis was modeled

$$r_{GSY} = A \times B \times r^{R}_{GSY} \quad \text{(B9)}$$

where r^{R}_{GSY} = Reference Rate of Liver Glycogen Synthesis
= 100 mg/min

and nonlinear multipliers "A" and "B" are shown in Figure B2. The liver glycogen synthesis rate was mediated by liver glucose concentration (multiplier B), liver interstitial insulin concentration (multiplier A), and changes in arterial blood glucose concentration which was used to account for modification of response during hypoglycemia. The rate of glycogen breakdown was given by

$$r_{GBD} = C \times D \times r^{B}_{GBD} \quad \text{(B10)}$$

where r^{B}_{GBD} = Basal Rate of Liver Glycogen Breakdown
= 100 mg/min

and multipliers "C" and "D" were given by the functions shown in Figure B3. The rate of liver gluconeogenesis (r_{GNG}) was modeled as a nonlinear function of liver interstitial insulin concentration and arterial blood glucose concentration as shown in Figure B4. Peripheral glucose uptake was mediated by changes in the peripheral interstitial glucose and insulin concentrations, modeled

$$r_{PGU} = E \times F \times r^{B}_{PGU} \quad \text{(B11)}$$

where r^{B}_{PGU} = Basal Peripheral Glucose Uptake Rate
= 30 mg/min

and multipliers "E" and "F" were computed from the nonlinear functions of Figure B5. All of the above dynamic metabolic sources and sinks for glucose

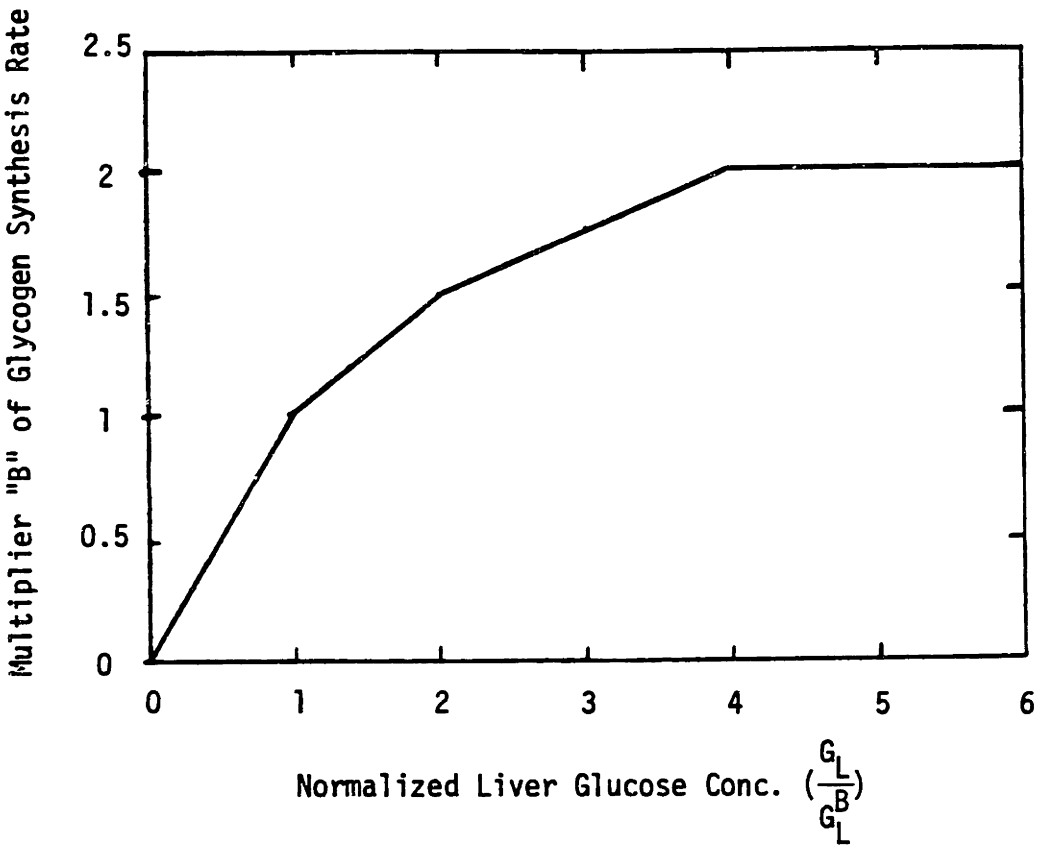

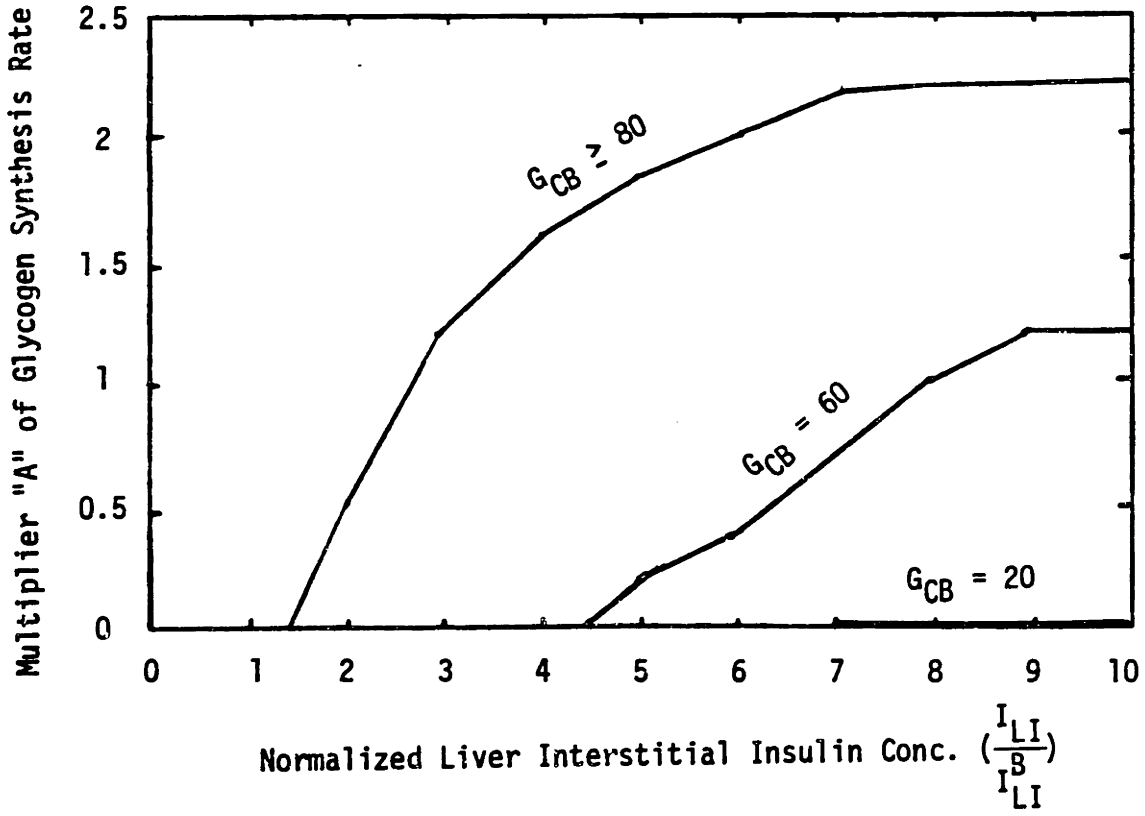

Fig. B2 Functions for computing rate of liver glycogen synthesis.

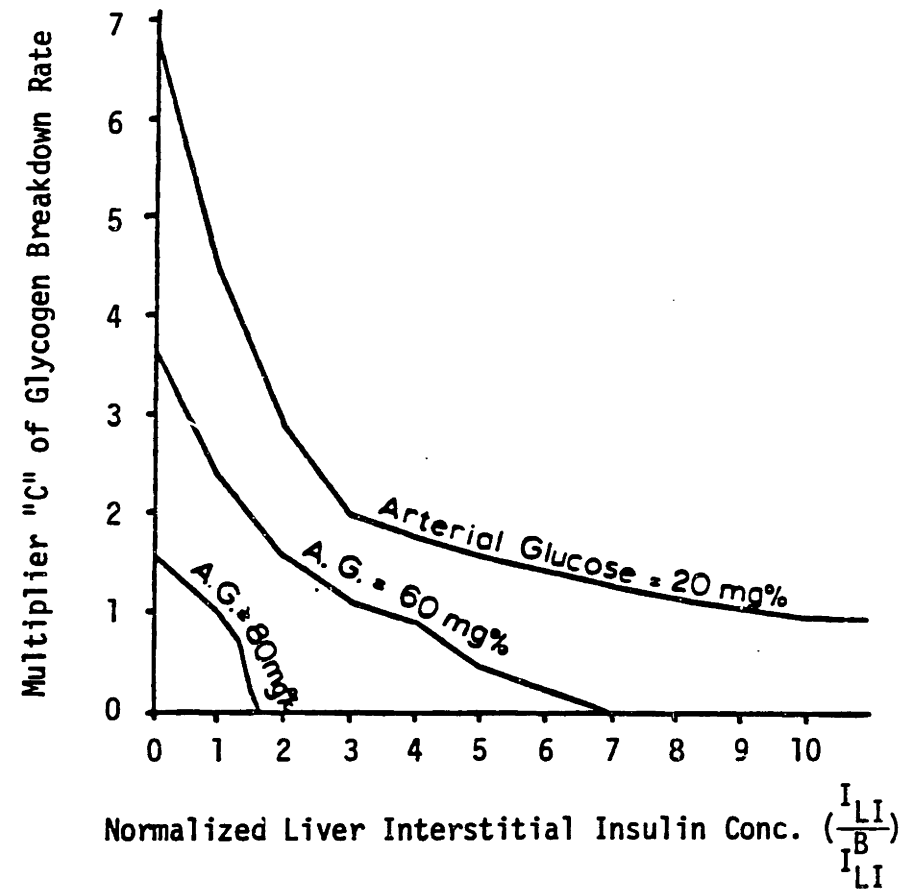

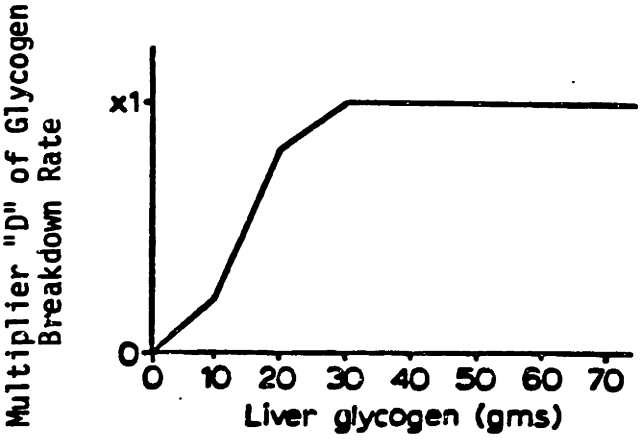

Fig. B3 Functions for computing rate of liver glycogen breakdown.

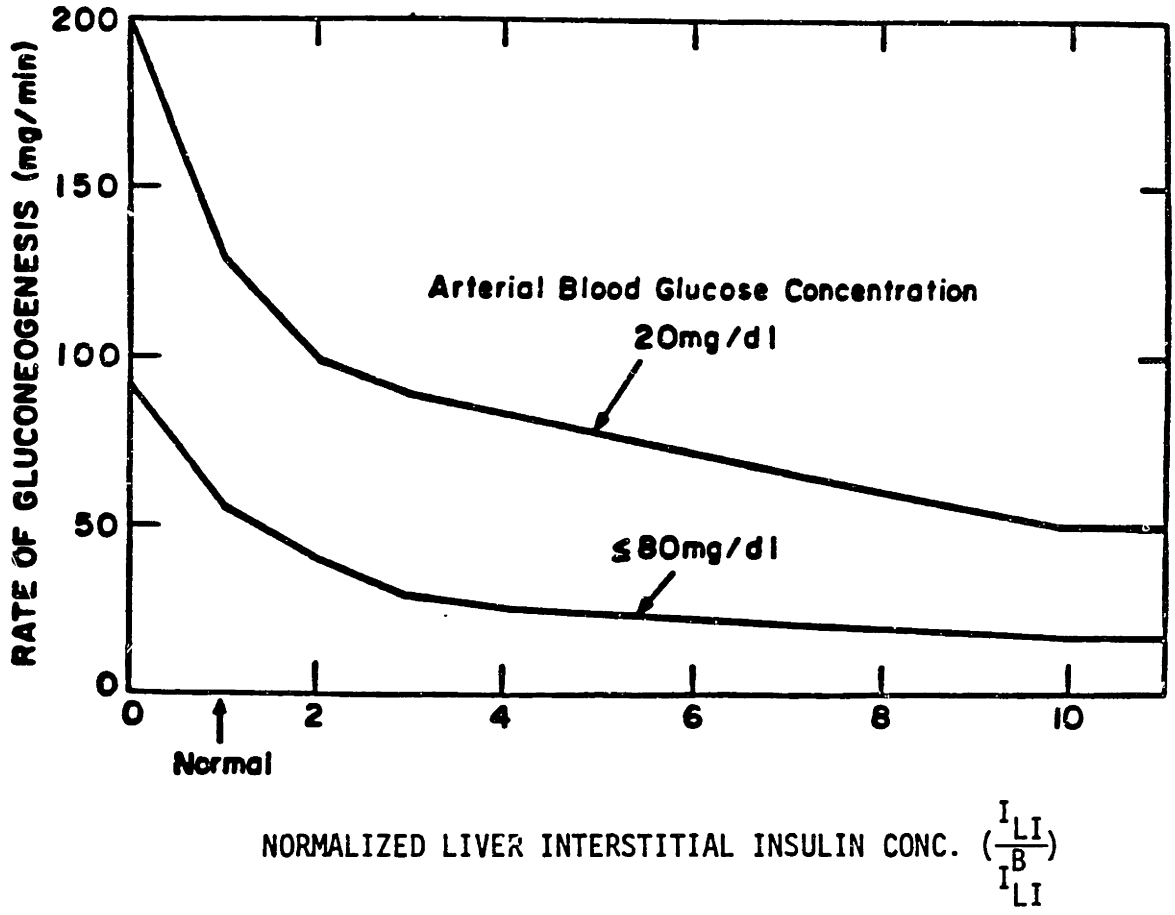

Fig. B4 Function for computing rate of liver gluconeogenesis.

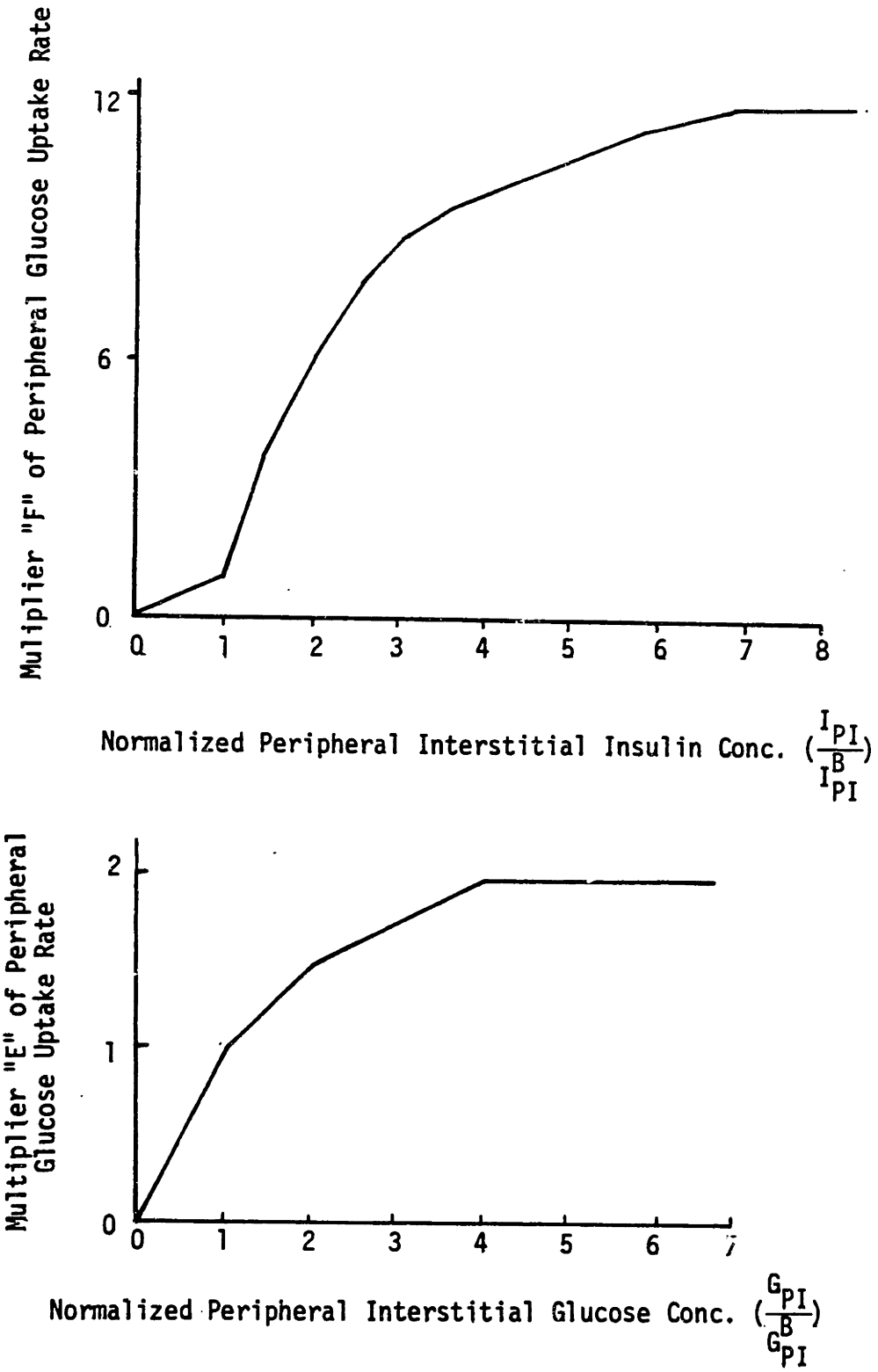

Fig. B5 Functions for computing the rate of peripheral glucose uptake.

in the glucose model formulation were introduced via a three-minute time delay representing the time required for regulatory mechanism activation. Finally, the rate of kidney glucose excretion as a function of the kidney glucose concentration was given by

$$r_{EXC} = \begin{cases} 0 & G_K \leq 180 \text{ mg/dl} \\ 1.278(G_K - 180) & G_K \geq 180 \text{ mg/dl} \end{cases} \quad \text{(B12)}$$

Initial conditions for the glucose model were as follows:

G_{NB} = 67.54 mg/dl

G_{NI} = 57.54 mg/dl

G_{CB} = 81.38 mg/dl

G_{CI} = 80.81 mg/dl

G_{PB} = 80.00 mg/dl

G_{PI} = 77.86 mg/dl

G_L = 92.32 mg/dl

G_K = 81.32 mg/dl

A schematic diagram of the insulin model is presented in Figure B6. The mass balance equations for the insulin model were given by:

Central Organs:
$$V_{CP}\frac{dI_{CP}}{dt} = Q_{PP}I_{PP} + Q_{LP}I_{LP} + Q_{KP}I_{KP} - Q_{CP}I_{CP} + \frac{V_{PI}}{T_C^I}(I_{CI} - I_{CP}) \quad \text{(B13)}$$

$$V_{CI}\frac{dI_{CI}}{dt} = \frac{V_{PI}}{T_C^I}(I_{CP} - I_{CI}) \quad \text{(B14)}$$

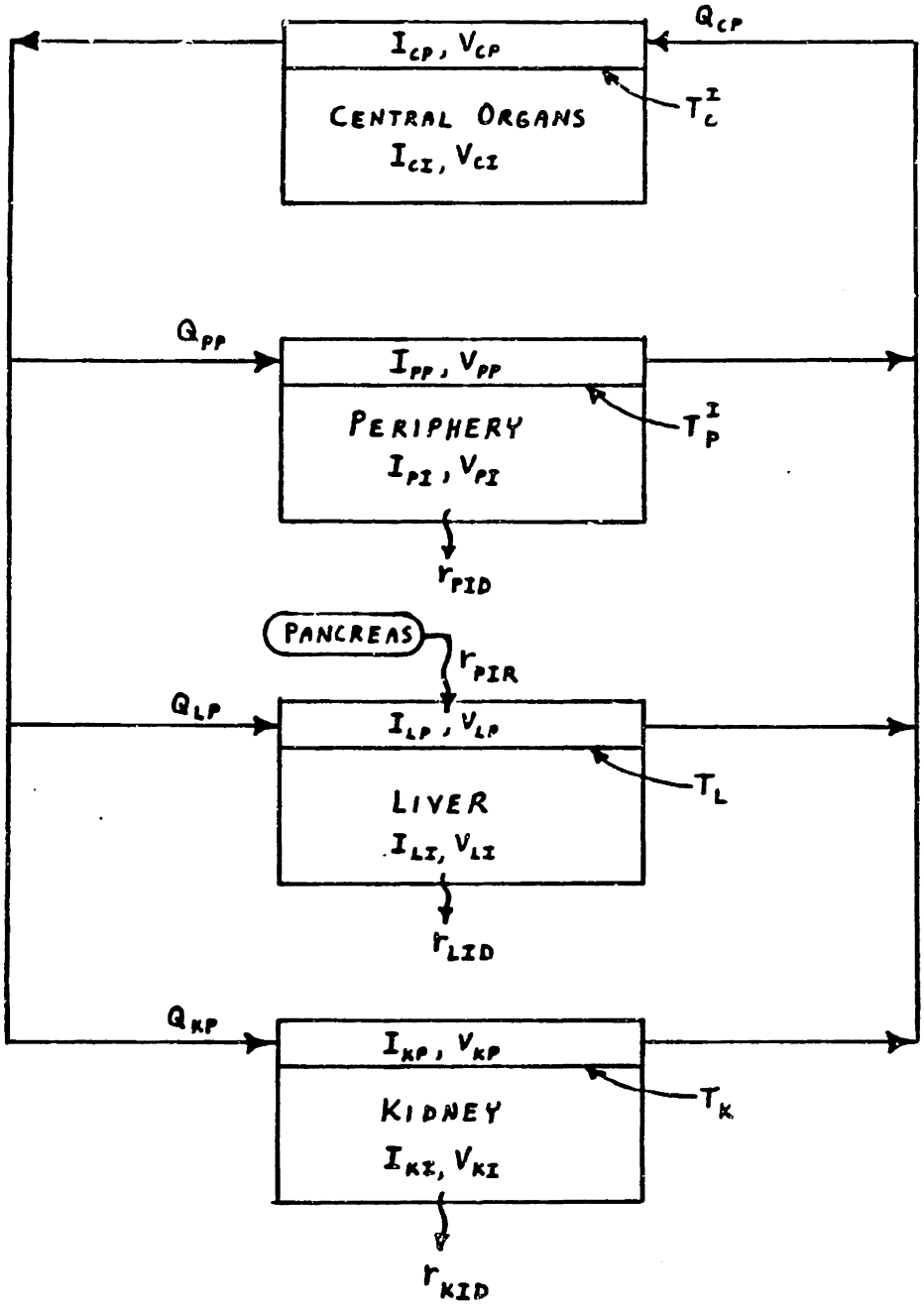

Fig. B6 Schematic diagram of the insulin model.

Periphery:
$$V_{PP}\frac{dI_{PP}}{dt} = Q_{PP}(I_{CP} - I_{PP}) + \frac{V_{PI}}{T_P^I}(I_{PI} - I_{PP}) \quad (B15)$$

$$V_{PI}\frac{dI_{PI}}{dt} = \frac{V_{PI}}{T_P^I}(I_{PP} - I_{PI}) - r_{PID} \quad (B16)$$

Liver:
$$V_{LP}\frac{dI_{LP}}{dt} = Q_{LP}(I_{CP} - I_{LP}) + \frac{V_{LI}}{T_L}(I_{LI} - I_{LP}) + r_{PIR} \quad (B17)$$

$$V_{LI}\frac{dI_{LI}}{dt} = \frac{V_{LI}}{T_L}(I_{LP} - I_{LI}) - r_{LID} \quad (B18)$$

Kidney:
$$V_{KP}\frac{dI_{KP}}{dt} = Q_{KP}(I_{CP} - I_{KP}) + \frac{V_{KI}}{T_K}(I_{KI} - I_{KP}) \quad (B19)$$

$$V_{KI}\frac{dI_{KI}}{dt} = \frac{V_{KI}}{T_K}(I_{KP} - I_{KI}) - r_{KID} \quad (B20)$$

where the mathematical nomenclature employed in Figure B6 and Equations B13-B20 is defined as follows:

Variables:
- I = Insulin Concentration (mU/l)
- Q = Plasma Flow Rate (l/min)
- V = Volume (l)
- T = Transcapillary Diffusion Time Constant (min)
- r = Metabolic Source or Sink Rate (mU/min)
- t = Time (min)

First Subscript or Superscript: Physiologic Compartment
- C = Central Organs (central nervous system, heart, lungs, major blood vessels, nonhepatic splanchnic organs)
- P = Periphery (skeletal muscle and adipose tissue)
- L = Liver
- K = Kidney
- I = Insulin Model

Second Subscript: Physiologic Subcompartment (if required)
- P = Plasma Space
- I = Interstitial Fluid Space

Metabolic Rate

Subscripts: PID = Peripheral Insulin Degradation
KID = Kidney Insulin Degradation
LID = Liver Insulin Degradation
PIR = Pancreatic Insulin Release

Numerical values for the insulin model physiologic parameters were as follows:

V_{CP} = 1.44 l	Q_{CP} = 3.05 l/min	T_C^I = 10 min
V_{CI} = 3.7 l	Q_{PP} = 1.48 l/min	T_P^I = 20 min
V_{PP} = 1.44 l	Q_{LP} = 0.87 l/min	T_L = 0.2 min
V_{PI} = 7.0 l	Q_{KP} = 0.70 l/min	T_K = 0.2 min
V_{LP} = 0.48 l		
V_{LI} = 0.40 l		
V_{KP} = 0.24 l		
V_{KI} = 0.20 l		

Insulin was degraded at a rate modeled as a linear function of the interstitial insulin concentrations in the liver, kidney, and periphery, respectively, given by

Liver: $$r_{LID} = r^B_{LID}\left(\frac{I_{LI}}{I^B_{LI}}\right) \quad \text{(B21)}$$

r^B_{LID} = Basal Liver Insulin Degradation Rate
= 17.6 mU/min

I^B_{LI} = Basal Liver Interstitial Insulin Concentration
= 11.76 mU/l

Kidney: $$r_{KID} = r^B_{KID}\left(\frac{I_{KI}}{I^B_{KI}}\right) \quad \text{(B22)}$$

r^B_{KID} = Basal Kidney Insulin Degradation Rate
= 3.18 mU/min

I^B_{KI} = Basal Kidney Interstitial Insulin Concentration
= 7.96 mU/l

Periphery: $$r_{PID} = r^{B}_{PID}\left(\frac{I_{PI}}{I^{B}_{PI}}\right) \quad \text{(B23)}$$

r^{B}_{PID} = Basal Peripheral Insulin Degradation Rate
= 1.16 mU/min

I^{B}_{PI} = Basal Peripheral Interstitial Insulin Concentration
= 12.0 mU/l

The heterogeneous fast pool model of pancreatic insulin release was used to compute the rate of pancreatic insulin release (r_{PIR}) as a function of arterial blood glucose concentration (G_{CB}). The mathematical equations for the heterogeneous fast pool pancreatic insulin release model, together with parameter values and initial conditions, were reviewed in the pancreatic insulin release section of the main text.

In order to simulate the 100g OGTT, Hillman (1977) modified the heterogeneous fast pool model of pancreatic insulin release to account for gut factor augmentation of insulin response to oral glucose. First, the rate of insulin transfer from the slow pool to the fast pool (r_{ISTF}) was potentiated through modification of the multiplying factor M_B in Equation 116 as shown in Figure B7. Second, the distribution of fast pool sites (θ) in Equation 122 was altered as shown in Figure B8. Finally, the rate of gut oral glucose absorption (r_{GAG}) for the 100g OGTT was modeled

$$r_{GAG}(\text{mg/min}) = \begin{cases} 0 & t \leq 3 \text{ min} \\ 800\left\{\sin\left[\left(\frac{t-3}{10-3}\right)\frac{\pi}{2}\right]\right\} & 3 < t \leq 10 \text{ min} \\ 800 & 10 < t \leq 30 \text{ min} \\ 800\left\{1 - \sin\left[\left(\frac{t-30}{240-30}\right)\frac{\pi}{2}\right]\right\} & 30 < t \leq 240 \text{ min} \\ 0 & 240 \text{ min} < t \end{cases} \quad \text{(B24)}$$

where the glucose input appeared as a source term in the liver glucose mass balance equation (B7).

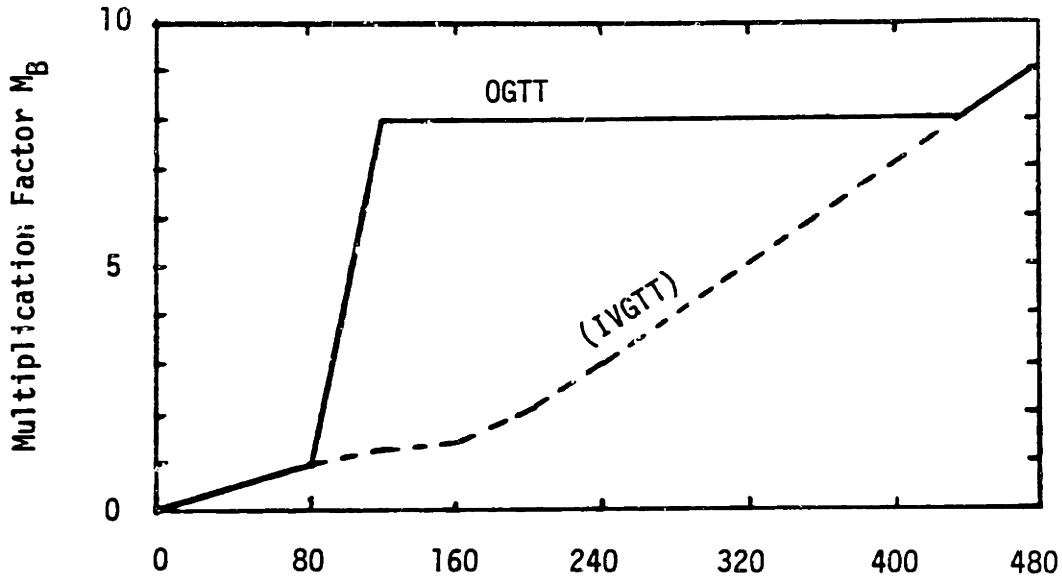

$$GMETC = 80\left(\frac{GMET}{GMET_{basal}}\right)$$

Fig. B7 OGTT modified multiplication factor for computing the effects of glucose on the rate of insulin transfer from the slow pool to the fast pool (r_{ISTF}) in the heterogeneous fast pool model of insulin release. (Compare with Fig. 43)

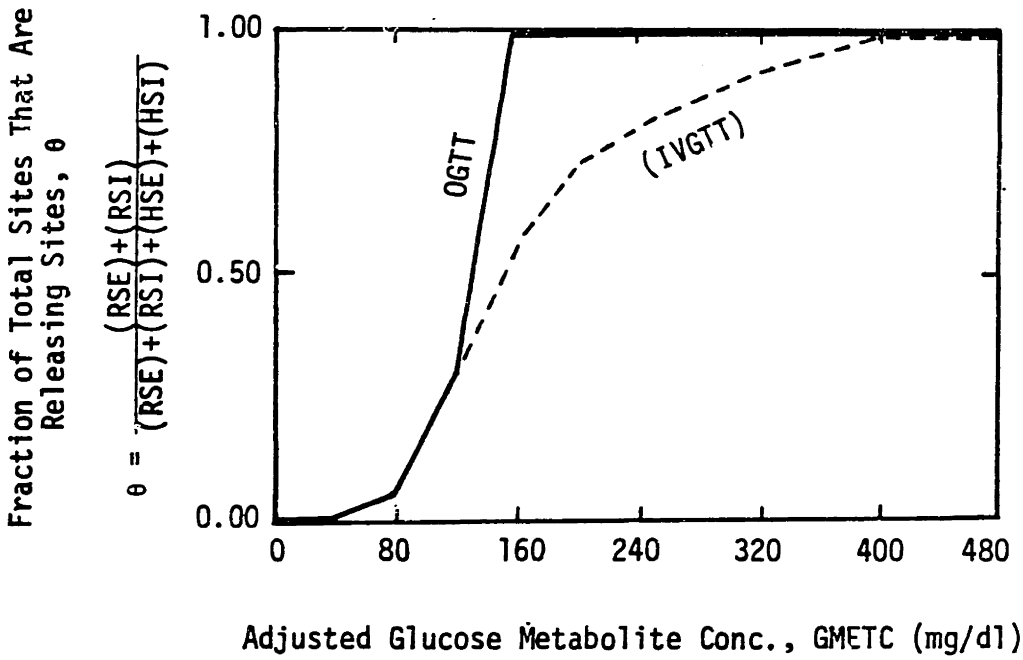

Fig. B8 OGTT modified effect of glucose metabolite concentration in the beta cell on the distribution of fast pool sites (θ) in the heterogeneous fast pool model of insulin release. (Compare with Figure 45)